

Glacial Ice as a Cryogenic Factor in the Periglaciation Zone of the Composed Rock Glacier Morenas Coloradas, Central Andes of Mendoza, Argentina

Dario Trombotto Liaudat
IANIGLA-CONICET, Mendoza, Argentina

Lucía Arena
Facultad de Matemática, Astronomía y Física, Universidad Nacional de Córdoba, Argentina

Giorgio Caranti
Facultad de Matemática, Astronomía y Física, Universidad Nacional de Córdoba, Argentina

Abstract

The present work focuses on the analyses of glacial ice from thermokarst in relict glacial and degraded Andean permafrost environments (4200 m a.s.l.) in order to reconstruct its environmental or paleoenvironmental history and to understand the processes that generated the Andean rock glaciers. The study area belongs to the Morenas Coloradas rock glacier, situated in the Cordón del Plata (at 33°S approximately), Central Andes, Mendoza, Argentina. An interpretation of the ice samples and an analysis of their internal and crystallographic characteristics is carried out in order to explain the geomorphological and cryogenic history of the landforms. The area of periglaciation—where cryogenic forms are generated—is studied thoroughly. Due to climatic oscillations, these periglacial areas may be identified by thermokarst. The degradation phenomenon helps to build new cryogenic forms like rock glaciers. Different possible environmental scenarios for the genesis of protoperiglacial landforms may be imagined.

Keywords: Central Andes of Mendoza; glacial ice; global warming; periglaciation zone; permafrost; rock glaciers.

Introduction

Rock glaciers, the typical Andean cryogenic mesoforms which characterize creeping mountain permafrost, contain different types of ice that interact with frozen cryosediments, that is to say with sediments of cryogenic origin. From a structural point of view, the types of constitutional ice generally observed are interstitial and segregation ice, but buried massive ice of sedimentary origin is also to be found (Shumskiy 1964, Haerberli & Vonder Mühl 1996). Areas with over 80% of ice (supersaturated permafrost) appear in the structure of the few drillings that have been carried out (Haerberli et al. 1988).

Interstitial ice is a superficial ice found in the first meters of depth in the rock glacier. This kind of ice depends on the diameter of the sedimentary pores which allow for an optimum nucleation of the ice (Van Vliet-Lanoë 1998) and correlates with the size of the particles which induce nucleation (Hobbs' ice, see Anderson et al. 1978), while segregation ice is the kind of ice that creates lenses or layers of few centimeters inside the frozen body (Shumskiy 1964, Trombotto et al. 1999).

But concerning the origin of the ice, periglacial ice is closely linked to different processes (e.g. percolation or regelation), various contributors (e.g. snow, graupel, harsch, or firn) or to other natural manifestations such as glaciers or nivodetritic avalanches. Sedimentary ice in periglacial domain is created mainly by the transformation of snow and graupel which percolate into the open structure of the cryosediments, although snow, harsch, and firn from Andean avalanches also play a decisive role in its creation. This material also incorporates to the frozen sedimentary body of

the rock glacier by percolation and burying of the latter under cryosediments. Another origin of the ice is the regelation of glacial ice, after a previous process of melting, which incorporates into the body of rock glaciers as periglacial ice, although the mechanism is fairly unknown.

A parallel process has been observed in the Andes of Mendoza for example, expressed by the fluxion of isolated ice bodies of glacial origin which, favoured by the slope, directly incorporate to the periglacial sedimentary bodies. This is the type of ice we are mostly concerned with in the present work and which shall be analysed and identified, because it contributes to the origin of periglacial landforms.

In general, macroscopical or large scale phenomena may be scientifically interpreted in function of microscopical parameters. In the case of the ice, and as has been shown

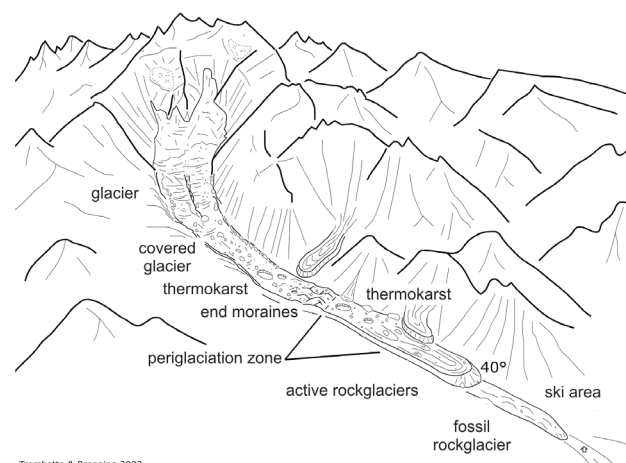


Figure 1. Periglaciation zone.

for glacial ice in thermokarst areas (Arena et al. 2005) microcrystallographical characteristics can be correlated with geomorphological characteristics of the environment in which the ice originated.

This work analyzes ice of a periglacial zone (Fig. 1), that is to say, an area that used to be glacial and in which periglacial or cryogenic landforms are being generated.

As glaciers retreat to higher altitudes, they leave a large quantity of still frozen morainic or cryogenic sediments behind. At the same time, islands of covered ice may remain. These types of ice, considered 'dead ice' by many authors, are key contributors or perfect natural cryogenic environments for the 'roots' or the genesis of debris rock glaciers. These processes indicate that at the Cordón del Plata, Mendoza, the periglacial level reaches down to 3600 m a.s.l. approximately (Fig. 1). This is a relatively low height considering that 'quasi continuous permafrost' at the same latitude exists only above a height of 4200 m a.s.l. (Trombotto 2000).

The present work also analyzes experimental samples in order to certify natural processes. In particular, microcrystallographical parameters are set up, which allow one to determine whether an ice sample belongs either to regenerated ice of the region close to the active layer, to thermokarst of cryogenic origin (degraded permafrost), or to ancient glacial ice. Moreover, correlations between the mentioned microscopical characteristics and the stress, directions samples underwent in thermokarst, are analyzed. Finally microscopical ice characteristics are linked with environmental and palaeoenvironmental processes.

Study Area

The study area is located in the Cordón del Plata, a mountain range of the Andes of Mendoza. The area is situated between 32°24'S and 33°39'S and 70°14'W and 70°46'W (Fig. 2). The area is glacierized. The Landsat 2000 image reveals glaciers, perennial snow patches, and also snow patches which are mostly considered to be temporary. The entire surface was figured to be 148 km², 119 km² of which correspond to rock glaciers (Trombotto 2003).

Geologically the Cordón del Plata is part of the Cordillera Frontal, limited in the W by the Argentine geological region called Cordillera Principal. In the Cordón del Plata graywacke prevails, sandstone conglomerates from the lower Carboniferous and volcanic rocks of the volcanic Variscian Association of Permian Age. A very important granitico-granodiorhyte batolite as intrusive is associated to the more recent Variscian tectogenesis. The Andean tectonic movement reactivated the entire area during the Tertiary, and it was particularly during that period that sedimentary rocks were deposited as sandstones and conglomerates (Fm Mariño and Mogotes). Three mountain chains may be distinguished in this area: La Jaula in the W, the Cordón del Plata in the central part, to the N and E after which the entire area is named, with El Plata as its highest peak (6310 m a.s.l.), and finally the Cordón Santa Clara in the SW. Taking into account the topographical line of 2000, the study area comprises a surface of approximately 2830 km².

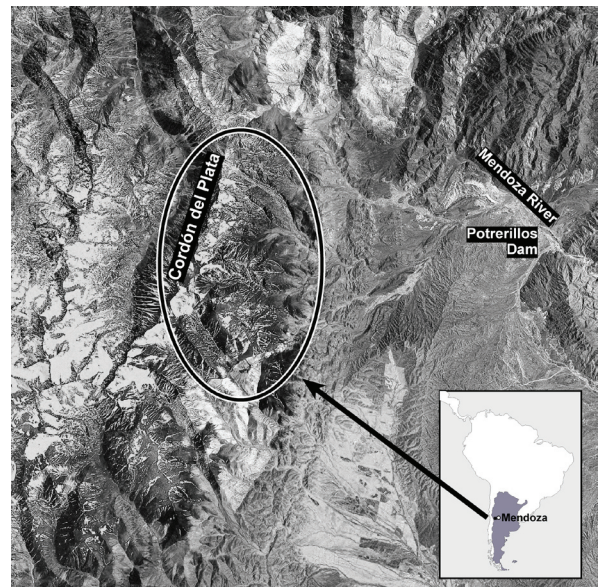


Figure 2. Study area.

The MAAT of the meteorological stations of Aguaditas (1972–1983) at a height of 2225 m a.s.l. and Vallecitos (1976–1985) at a height of 2500 m a.s.l. at its eastern flank are 7.7°C and 6°C respectively. The meteorological station Balcón I at 3560 m a.s.l. on the tongue of a rock glacier at Morenas Coloradas indicates a MAAT of 1.6°C and an annual precipitation between 500 mm (warm period April 2001–April 2002) and 630 mm (1991–1993). The vegetation ranges from shrubs to Andean tundra until 3600 m. Above this height and on rock glaciers vegetation is extremely scarce.

The analyzed ice samples come from a periglacial zone of the composed rock glacier Morenas Coloradas (with different superposed frozen cryoforms), an area with thermokarst and a detritic cover that varies in thickness between 60 and almost 150 cm. The samples were taken at a height of approximately 4200 m a.s.l. in a tributary valley which unites with the main valley, and where cryosediments meet with the main valley of the composed rock glacier.

Methodology

The natural samples were taken at a glacial valley and rock glacier which are being monitored and investigated at the IANIGLA (Institute of Snow and Ice Research and Environmental Studies) in Mendoza, Argentina, since the 1980s. The extraction of the samples is done by a simple procedure of cutting ice blocks in areas with visible ice. The samples were extracted from two different profiles taken from thermokarst walls perpendicular to each other, according to the imaginary axis of an ovoid (Fig. 3). Before cutting out ice blocks, surfaces were cleaned to a depth of 5 cm. For extraction, blocks or ice monoliths were confectioned in the ice wall. These blocks were carefully oriented according to two fundamental criteria. One is the zenith of the sample itself, in order to identify its positioning within the body of ice, and the other one is the magnetic N of the site, in

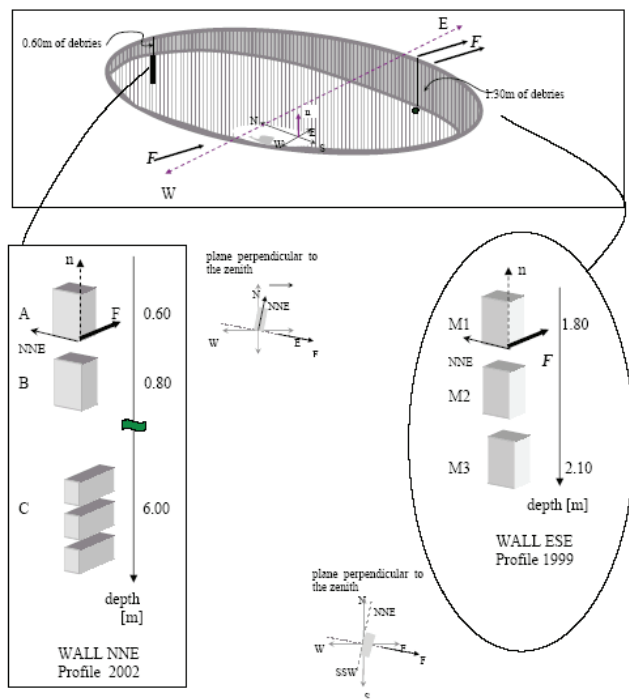


Figure 3. Sketch of thermokarst. F: principal stress, n: zenith.

order to be able to position the entire ice body sampled in the area. The samples were transported to the cold chamber of the LEGAN in Mendoza, where they were classified and preserved at -13°C .

Then thincuts were made of the ice samples, and plastic replicas were created at the University of Córdoba, Argentina. This technique complements the studies of the thincuts and helps to determine size and orientation of the ice crystals, dislocations as well as concentration, orientation and distribution of the bubbles inside the crystals. The method of plastic replication allows the detection of dislocations on the surface of the ice.

Thincuts were made using a xylotome Leitz, model 1400, adapted for ice cuts in the cold chamber. Thincuts were made in the cold chamber of the LEGAN Institute in Mendoza as well as at the University of Córdoba in Argentina. At the same time, laboratory tests of uniaxial statical isothermal compression of the ice core samples extracted from ice from below the base of the active layer of the thermokarst were carried out. These samples, treated in the laboratory, and those extracted from the ice cores and left in natural condition were crystallographically analyzed and compared to each other. It is the aim of these studies to establish a correlation between microcrystallographical and geomorphologically determined characteristics.

Analyzed Ice Characteristics

The most important components of the ice described in the present work are: (1) ice crystals: size and orientation of their C axis, (2) bubbles: areas with bubbles and areas without bubbles. Bubbles are classified into bubbles $>50\ \mu\text{m}$ and bubbles $<50\ \mu\text{m}$ and microbubbles, (3) defects and dislocations, and (4) presence of particles.

While for the study of the ice crystals (Table I) the size and orientation of their C axis were the important factors, in the case of the bubbles three different types were found and classified as follows:

- Two types of bubbles belong to microbubbles, with a diameter smaller than $0.1\ \text{mm}$
- Another type are macrobubbles with a diameter larger than $0.5\ \text{mm}$

In the first group, bubbles are distinguished according to whether their diameter is smaller than $50\ \mu\text{m}$ or larger than $50\ \mu\text{m}$. This distinction is important because size may influence the migration of the ice crystal edges. If the mean diameter of the bubbles is larger than $50\ \mu\text{m}$, it was observed that they do not impede or anchor the migration of the grain limit (Arena et al. 1997). The analysis of the bubbles (Table II) in the ice is very important because although some of them may abandon the edge of the grain without producing a remarkable effect, others, if they are small enough, anchor growth of the ice grain. In other cases bubbles of intermediate size may simply slow down their growth. Only at low temperatures and under the phenomenon of isothermal warming in the laboratory, for a long time (over one year), could it be observed that bubbles do not stop the growth of ice crystals.

There are two types of areas considered in the thincuts sections; one was called CB when it contained microbubbles and the other was called SB when it did not contain microbubbles (Table II).

In general (Nassello et al. 1992, Arena 1995) the mean size of ice crystals in areas with microbubbles is smaller, because these anchor the limits of the ice grains. This also occurs in areas with bubbles $>50\ \mu\text{m}$ and macrobubbles. It strikes the eye that the bubbles $<50\ \mu\text{m}$ are almost spherical while those $>50\ \mu\text{m}$ and macrobubbles are not, and that they can give clues about the main stress directions.

Regarding defects, the density of traces of dislocations holds information for us, for example about the forces of residual stress. The defects were classified into prismatical (P) and hexagonal (H) (Table III). The particles are mainly of mineral and cryogenic origin. They are the product of cryoweathering of cryosediments of glacial or periglacial origin.

Results

The microscopical characterization of glacial ice buried in a thermokarst at a height of $4200\ \text{m a.s.l.}$ which displayed ice visible to the naked eye, based on two ice profiles, is shown in the following tables. They summarize the most important results found in crystals, bubbles, and defects of the different analyzed ice samples.

Crystals

The mean size of the grains in an SB area generally increases with depth, except for the case of sample A. On the other hand, polycrystalline samples are more textured, that is to say they have a defined or particular texture which is more pronounced with growing depth of the profile.

Table 1. Crystals.

Sample	Characteristics	D [mm]		Orientation	
		SB	CB		
Profile I	M1	Top of profile, sedimentary ice	4.2	0.4	Random
	M2	naturally degraded ice zone (collapse)	5.8	nd	crystallographic axis C perpendicular to n
	M3	glacial ice, stress parallel to F	20	2.6	Crystallographic axis C parallel to F
Profile II	A	Top of the profile, naturally degraded ice zone (collapse)	4	0.4	Crystallographic axis C quasi perpendicular to n
	B	Top of the profile, naturally degraded ice zone (collapse)	2	0.3	Crystallographic axis C is 45° from n and NNE
	C	glacial ice	6	nd	Crystallographic axis C parallel to F

See Figure 1; D= mean diameter; SB= area without microbubbles; CB = area with microbubbles; nd = no data.

Table 2. Bubbles.

Sample	Bubbles					
	d [µm]		N _v [mm ⁻³]	Shape	Orientation	
	MBA	MBNA				
Profile I	M1	Nd	500	840	Spherical	Random
	M2	50	Nd	58	Spherical and elongated	25% elongated and parallel to F
	M3	10	Nd	23	Elongated	parallel to n
Profile II	A	20	1250	52	Elongated	parallel to n
	B	20	60	1080	Spherical	45° from n and NNE
					Elongated	45° from n and F
C	6	<50	465	Spherical	parallel to n	
				Elongated	parallel to n	

N_v = volumetric bubble density; d = mean bubble diameter; nd = no data; MBA = bubble <50 µm; MBNA = bubble >50 µm.

In M3 and C the crystals take a preferential orientation with the crystallographical axis C parallel to the direction of the flow, while at the top of the permafrost the bubbles appear coincidentally. Those crystals with a size of ≥0.5 cm suggest older age and a glacial origin. The latter are observed in samples taken at greater depth of the profiles.

Bubbles

For the understanding of Table 2 it is helpful to consider that:

- The mean size of the microbubbles which anchor the growth of grains (bubbles <50 µm) decrease with growing depth by a factor of 3 or more, except for sample A.
- The mean size of bubbles which do not anchor the growth of grains (bubbles >50 µm, macrobubbles) changes their shape from spherical to elongated with growing depth, except in the case of sample A.
- In profile I, elongated bubbles have their C axis parallel

Table 3. Defects and dislocations.

Sample	Defect density [x 10 ⁶ mm ⁻²]		
	Hexagonal plane	Prismatic plane	
Profile I	M1	2.1 ± 0.5	3.0 ± 1.4
	M2	1.5 ± 0.4	2.6 ± 0.8
	M3	1.5 ± 0.6	2.0 ± 0.1
Profile II	A	2.4 ± 0.7	5 ± 1
	B	0.7 ± 0.2	3 ± 1
	C	0.5 ± 0.2	3 ± 1

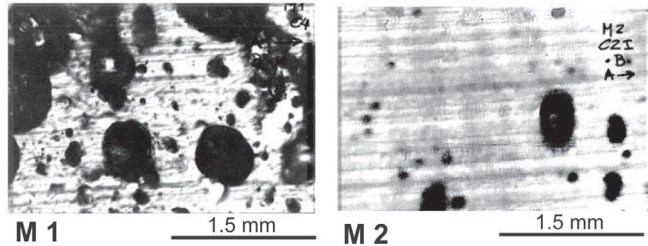


Figure 4. Ice thincuts of profile I (M1 and M2).

to “F”, which is the flow direction, in sample M2 (Fig. 4). This is not the case in sample M3 where the prevailing direction is parallel to n.

- In profile II, microbubbles are aligned with the zenith of the samples A and C, but they build an angle of 45° with the zenith of sample B.
- In the samples taken at greater depth, volumetrical density of the bubbles is greater in sample C (profile II) than in M3 (profile I).

Defects, dislocations, and particles

From Table 3 we may deduce that the samples indicate, in the sections analyzed with plastic replicas, that the density of patterns of chemical attack, expressing defects and dislocations, decreases with depth. As to the obtained particles, a lithological study has yet to be made, but it may be supposed that their origin is the local parental rock. In profile II, a majority of a diameter >20 µm prevails. It is assumed that this abundance must have had an important influence in slowing down the growth of the crystals.

Discussion

For reasons of climatic oscillations, ice covered areas express a degradation of glacial ice and formation of thermokarst. Thermokarst are holes or pits and when they are active they are usually filled with melting water, building tiny lakes, unfrozen only in summer. They are a typical characteristic of the irregular landscape of covered glaciers in the Andes of Mendoza. They are also found, less frequently though, on the surface of composed rock glaciers. This phenomenon of degradation of glacial ice contributes to a transformation of the area, making it part of a periglacial landscape. The ice partly melts and then freezes again in the matrix of the structures of periglacial forms.

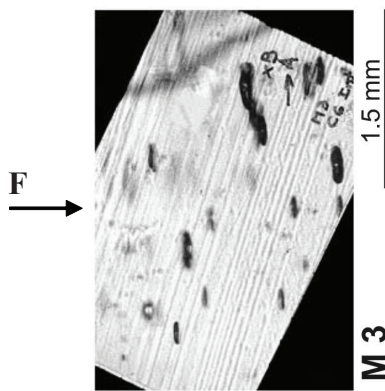


Figure 5. Ice thincut of profile I (M3).

Another important mechanism is the slow movement of small bodies of ice in the form of an “injection.” This process is associated with the existence of so-called “dead ice,” that is to say, bodies of ice without a connection with the glacier which generated them and which may continue to exist but withdrawn to much higher altitudes. The ice that remains locked in parallel, smaller, and colder valleys with less solar radiation, tends to flow or end up in main valleys with important rock glaciers or composed rock glaciers. In other words it favours periglacial genesis.

Comparing the two ice profiles made in 1999 (profile I) and 2002 (profile II) in a chosen thermokarst, it is easy to observe that M3 of profile I and C of profile II indicate the presence of glacial ice by analyzing the characteristics of their texture. Grains increase in size at growing depth, and their orientation follows the relict flow of the glacier, and the bubbles are elongated perpendicularly to F. In this sense, the C axes of the samples testify to the past glacial flow following the main direction of the stress (F). This way it is possible to prove that the samples taken at depth are correlated and have the pattern that corresponds to the stress of the main direction denominated F (Figs. 3, 5), and that they are of glacial origin.

On the other hand the decrease in the density of the defects indicates that the age of the samples increases with depth. The mean diameter of the bubbles also decreases with depth, following the same principle. Apparently the bubbles try to escape or move upwards, in the direction of n that is, responding to a temperature gradient in a direction normal to the site at the permafrost table. This would also explain the parallel alignment regarding n .

While sample M1 is not textured, M2 shows a texture. The first is indicating a genesis that is different from the second, possibly associated to the thick detritic cover of the profile which acts as an active layer. This ice is mainly of sedimentary origin, generated by solid precipitations which infiltrate and recrystallize, partly undergoing a liquid state in summer. The textured sample M2, with crystallographical axis C parallel to n , suggests an intervention of a different type of stress with an orientation that is perpendicular to the main stress and which may be due to the collapse phenomenon in connection with thermokarst formation. The shape and the orientation of the bubbles support this idea

(Fig. 4). On the other hand in the 2002 profile, sample A is textured, surprisingly with a diameter of grains superior to that of sample B which follows below, indicating most likely that the first sample has been exposed to a higher temperature than the samples of the rest of the thermokarst. This would be a case of degraded ice, a possible effect of local or global warming, and different from the characteristics mentioned above. The size, shape and orientation of the bubbles would also indicate a possible phenomenon of freezing. In addition a remarkable difference between samples A and M1 has to be pointed out, also reaffirmed by the low density of bubbles in sample A which was taken in 2002 and is interpreted as an increase of the mean temperature that affects and creates thermokarst. The special texture of sample B indicates a stress phenomenon geomorphologically observed in a thermokarst environment, which is growing at profile II. But what would be the origin of the ice of profile II? Is it glacial? This question arises when the proper characteristics of the different ice samples are defined. What existed before the ice suffered the variations described? The hypothesis is that it was glacial ice that grew with a sedimentary contribution on top, but that is being transformed and adapted to the present environmental conditions with warming. It would be interesting to reconsider the classification by Shumskiy (1964) according to the processes involved in ice formation.

Conclusions

The microscopical characterization presented in this work helps to classify three different types of ice in an area of periglaciation, or cryogenic processes, which interact with the rock glaciers and may be resumed as follows:

1. Massive ice of glacial origin, indicated by larger ice crystals with a preferential orientation, that is to say with the crystallographic C axis parallel to the flow direction; by elongated or ovoideal bubbles, with low density, also oriented towards the flow direction in some cases and by dislocations in the thincuts or plastic replicas which also indicate the flow direction; in some cases however, like C in profile II, the particles may limit the size of the crystals and influence the interpretation;

2. Sedimentary ice represented by small crystals and by almost spherical bubbles; like in the typical case of M1 and M2, with a high volumetrical density of bubbles and a larger mean diameter; and

3. Regenerated or degraded ice, which is monocrystalline, with bubbles of a large mean diameter but with low volumetrical density of bubbles. This ice is associated with the degradation of permafrost like in A and B of profile II.

On the other hand, as presumed, the layer of sediments has an important role in relation to the penetration of the external caloric wave which interacts with different types of subterranean ice. The phenomena are expressed microscopically and macroscopically.

In profile I, the external caloric wave is impeded and stopped by the thick layer of cryosediments accumulated perpendicularly to the F axis of the main flow and at lower height which interacts with the solid precipitation that falls

throughout the year and supports the aggradation of ice. However, this is not the case in profile II, where a much thinner layer of a thickness less than 1 m, allows much more external heat to enter and causes a regeneration or transformation of subterranean ice. In addition there are clear signals of collapse processes that preferably affect certain parts (profile II) of the thermokarst perimeter.

Evidently the chosen periglacial area is not in equilibrium, as inferred by the presence of active or reactivated thermokarst. These forms are supposed to be much older, probably from the Middle Holocene when a worldwide warming and a glacial inactivity were produced. This was also registered in South America (Röthlisberger 1986).

The changes caused by present warming, and which affect the structures of the ice, are also clearly observed in the microcrystalline results of the samples. The area of periglaciation extends altitudinally, but also affects lower heights for the contribution of more regenerated ice. It is an area with abundant "dead ice" that is integrating into periglacial forms such as rock glaciers. The "glacial flow" is kept up, hidden, discontinuous and slow, favoured by the inclination of the slopes of small colateral valleys.

The periglacial environment is growing or expanding upwards as glaciers disappear, are covered by sediments or are transformed into relict ice. Downwards, that means descending in height and slope downwards, the ice integrates into morainic or cryogenic sediments that fill up valleys and contributes to the formation of new rock glaciers or helps to maintain the existing rock glaciers in activity.

Different environmental situations may be analyzed on the basis of the conclusions. If the environment is considered as continually changing, the "dead ice," as if it were relict ice of glacial origin, does not persist in situ; it keeps flowing as has been pointed out above. This movement is proven by the microscopical characteristics of ice samples taken at great depth of the studied profiles. Sedimentary ice also incorporates into the massive ice in a process of aggradation. These types of ice merge from a periglacial environment in the existing periglacial forms that have been observed. The erroneously called "dead ice" partly disappears by degradation and sublimation, but partly plays an essential role for the evolution of periglacial forms at lower altitudes.

The phenomenon of ice aggradation would cease if the sedimentary or active layer was very thin and if the mean temperature of the thermokarst increased. These processes, the asymmetry and the deformation of the thermokarst, are represented in the landscape and are expressed in the microcrystallography of the ice, and they may be used as environmental indicators.

These studies allow the reconstruction of three environmental or paleoenvironmental scenarios: (1) old ice expressing its paleoenvironmental background, (2) ice indicating aggradation or degradation of the present permafrost environment, and (3) ice expressing geomorphological processes to be expected in the near future.

Acknowledgments

This work was carried out with the financing of project 4664 (PIP 1078/98) by CONICET: "Argentine General and Applied Geocriology." We would especially like to thank José Hernández (IANIGLA) for his permanent cooperation during fieldwork and his logistical support, and Sabine Herfert and Silvina Pereyra for their help with the English version.

References

- Anderson, D.M., Pusch, R. & Penner, E. 1978. *Physical and Thermal Properties of Frozen Ground. Geotechnical Engineering for Cold Regions* (Edited by Andersland & Anderson). McGraw-Hill Book Company: 37-102.
- Arena, L.E. 1995. *Crecimiento de grano en hielo puro*. Tesis doctoral FAMAF – Universidad Nacional de Córdoba, Argentina (inérita).
- Arena, L., Trombotto, D. & Caranti, G. 2005. Microscopical characterization of thermokarst ice from an area of Andean permafrost, Central Andes of Mendoza, Argentina. *2nd European Conference on Permafrost. Terra Nostra Heft 2005/2*, Potsdam, 55 pp.
- Arena, L.E., Nasello, O.B. & Levi, L. 1997. Effect of bubbles on grain growth in ice. *J. Phys. and Chem. B* Vol. 101, Nr. 32, 6109-6112.
- Haerberli, W., Huder, J., Keusen, H.-R., Pika, J. & Röthlisberger, H. 1988. Core Drilling through rock glacier-permafrost. *V International Conference on Permafrost, Trondheim. Proceedings Vol.2*, 937-942.
- Haerberli, W. & Vonder Mühl, D. 1996. On the characteristics and possible origins on ice in rock glacier permafrost. *Z Geomorph N.F.*, SB104: 43-57.
- Nasello, O.B., Arena, L.E. & Levi, L. 1992. Grain growth in pure ice, effects of mobile bubbles. *Phys. Chem. of Ice*, 422-427.
- Röthlisberger, F. 1986. *10000 Jahre Gletschergeschichte der Erde*. Verlag Sauerländer, Aarau, 416 pp.
- Shumskiy, P.A. 1964. *Part I, General Geocryology*. Chapter IX, *Ground (subsurface) Ice*. National Research Council of Canada, Techn. Translation 1130, 118 pp.
- Trombotto, D. 2000. Survey of cryogenic processes, periglacial forms and permafrost conditions in South America. *Revista do Instituto Geológico*, Vol. 21, Nr.1/2, São Paulo: 33-55.
- Trombotto, D. 2003. Mapping of permafrost and the periglacial environment, Cordon del Plata, Argentina. *8th International Conference on Permafrost*. Permafrost, Extended Abstracts, Reporting Current Research and New Information, Edited by W. Haerberli & D. Brandová, Zürich, 161-162.
- Trombotto, D., Buk, E. & Hernández, J. 1999. Rock glaciers in the Southern Central Andes (appr. 33° S.L.), Mendoza, Argentina: a review. *Bamberger Geographische Schriften* 19, Selbstverlag des Faches Geographie an der Universität Bamberg, Bamberg, 145-173.
- Van Vliet-Lanoë, B. 1998. Frost and soils: implications for paleosols, paleoclimates and stratigraphy. *Catena* 34, 157-183.

Increasing the Bearing Capacity of Pile Foundations by Using Thermostabilizers of Small Diameter in Cryolithozone of Russia

A.N. Tseeva

Yakutsk State Design and Research Institute for Construction, Yakutsk

R.M. Bayasan

VNIIGAS, LLC, InterHeatPipe, Moscow

G.P. Pustovoit

Department of Geocryology, Moscow State University, Moscow

A.P. Okoemova

Yakutagropromprojekt, Open Joint-Stock Company, Yakutsk

Abstract

Three case studies are presented to demonstrate the effect of *InterHeatPipes*, which are small-diameter thermostabilizers, under different permafrost conditions. The installation of the *InterHeatPipes* increases the bearing capacity of piled foundations and therefore provides increased building stability. Thermal disturbances caused by the installation of piles in warm saline permafrost required a quick heat extraction from the ground to provide the required bearing capacity of a multistory business centre in Yakutsk during construction. A series of thermostabilizers were installed that provided very fast ground cooling. Thermostabilizers were also installed to freeze unfrozen soil in the foundation of a nine-story residential building. The third example presents results of a power line tower foundation using thermostabilizers. Supports for power lines are critical because frost heave in warm permafrost often results in uneven lifts of the pile foundation resulting in tilted masts. Ground temperature measurements from the three examples demonstrate how thermostabilizers can be utilized to increase the bearing capacity of the soil.

Keywords: bearing capacity; permafrost; pile foundations; stability; thermostabilizer.

Introduction

Widespread saline and warm frozen grounds, and natural or human-induced taliks cause major problems in the construction of multistory buildings and engineered structures in permafrost environments. Pile foundations are affected by vertical frost heave and pull out forces. Such problems are recorded in Yakutsk, the oldest city among those with a population of more than 50,000 people built on permafrost. The geocryological conditions differ significantly from natural ones. Ground temperature regimes are extremely non-uniform within one construction site and talik zones are common under old buildings promoting permafrost thaw.

Future development of modern northern cities requires the construction of multistory buildings with increased foundation loads, both vertically and horizontally. Seasonal cooling devices in combination with local thermal insulation of the ground surface are efficient in increasing the bearing capacity of the ground for pile installation, freezing talik zones and providing stability of foundations against pull out forces, including frost heave forces. This paper presents the usage of *InterHeatPipe* thermostabilizers as cooling devices on two multistory buildings and a power line foundation.

Site Description

Business centre office building: Block B

The construction site for a new business centre is located in the centre of Yakutsk where previously one-story wooden

houses and public buildings were situated. The office building (block B) is 33.0 m x 40.5 m and is located in the centre of the new complex. It is a 13-story building capped by a two-story dome. Structurally, it represents a monolith reinforced concrete framework with a maximum pillar grid distance of 6.0 m x 7.5 m. During site investigations geocryological conditions were identified, characterized by low temperatures, which are typical for the centre of the city of Yakutsk, and high salinity of shallow soil layers. At the depth of zero annual amplitudes (10 m) the ground temperature varied between -3.4 and -5.2°C, with the lower temperatures measured in places with maximum ground salinity ($D_{\text{sal}} = 0.58\%$), and warm temperatures (-3.4°C) in places with minimum ground salinity ($D_{\text{sal}} = 0.13\%$).

According to the Russian construction code (1988) the calculations of the bearing capacity for pile foundations have to consider less favorable conditions: higher ground temperatures (-3.4°C) at a depth of 10 m, and the maximum depth of saline ground (5.5 m).

The geological section is represented by the following types of soils:

- 0–0.8 m: fill (medium and silty sand, construction waste);
- 0.8–5.5 m: silty sand with the some organic remains, saline;
- below 5.5 m: fine and silty sand of massive cryogenic texture, hard frozen.

Pile clusters of three or four piles combined were designed

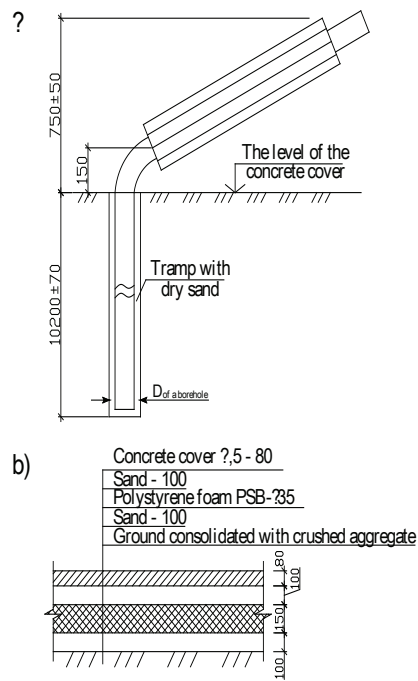


Figure 1. Schematics of the thermostabilizers (a) and the thermal insulation of the ground surface (b) for the business centre.

for the foundations depending on the loads. Square reinforced concrete piles measuring 40 cm x 40 cm were 10 m and 12 m long, and embedded into permafrost to depths between 8.8 m and 10.8 m. The piles were installed into boreholes with diameters larger than the piles. According to the design, borehole pockets should have been filled with cement and sand slurry. The calculated bearing capacities for the pile installation was 1620 kN and 2380 kN, for the 10 m and 12 m long piles, respectively. The calculated pile loads were 1300 kN and 1930 kN.

During the pile installation, water from the thawed layers close to the surface penetrated into the boreholes warming the ground so that the temperatures at 10 m depth increased -2.1 to -2.7°C . Inspections of the borehole grout showed that piles froze to the saline drilling mud but not to the cement and sand slurry. In addition, the temperatures were significantly higher than calculated. New calculations that considered in situ ground temperatures and salinity increase along the entire length of the piles showed that the bearing capacity of the installed piles was only 610 kN and 856 kN for the 10 m and 12 m long piles, respectively.

Nine-story residential building in the 29th city block in Yakutsk

Until late 1970s there was a lumber-processing plant located on the bank of the Zavodskaya river canal. Later the river canal was filled with lumber-processing waste. A zone of unfrozen ground with high content of organic material formed.

The site mainly consists of upper quaternary alluvial sediments represented by sandy and clayey deposits to a study depth of 26.3 m. Between a depth of 23.5 m and 25.7 m the top of Jurassic sediments formed by siltstones

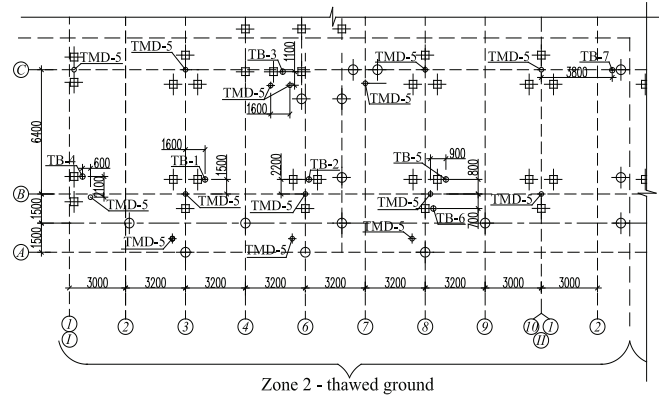


Figure 2. A section of the foundation scheme of the area with taliks of the 9-story residential building and the scheme of the thermostabilizers (TMD-5) and the location of boreholes (TB-1, 7).

were penetrated. The natural ground is overlain with a fill of sand, sandy loam and loam mixed with chip, bark, board chippings, logs; that is, all sorts of sawing wastes. The inclusions vary from rare to thick and are non-uniform in both horizontal and vertical direction. The thickness of the fill within the site is between 3.9 m and 9.4 m. Some loam sand lenses were also found. These layers are usually saline with organic inclusions. Below the fill the geological section is represented by sands of various ranges; that is, fine, silty, medium, and gravel sands.

Drilling in July/August 2006 revealed both frozen and thawed ground on the site. Thawed ground was penetrated in the active layer as well as at greater depths within the permafrost. Later are inter-permafrost taliks of different thicknesses and distribution. Thawed ground occupies about a third of the site. The origin of the inter-permafrost taliks is initially connected to a former river canal that formed a talik. The river canal was later filled with lumber processing wastes and the surface was leveled with fill, consisting of dry ground that resulted in deep freezing from the surface and a formation of shallow short-term frozen ground. Cast-in-place piles of 650 mm diameter and different lengths are designed for the foundations. The design also suggests that the lower part of the pile to be embedded in permafrost, as well as preconstruction ground freezing.

Power line supports

The site with supports for a power line is situated in the southwestern part of Yakutsk. According to the site investigations the active layer is represented by sandy loams and loams. The ground becomes liquid when it thaws. According to a frost heave parameter the sandy loam is referred to as a highly frost susceptible soil and the loam to an extremely frost susceptible soil.

The frozen ground is represented by silty, fine and medium sands. Ground temperatures measurements carried out in 2001 showed warm temperatures that are not typical for Yakutsk (-0.3 to -0.9°C at a depth of 10 m). The inclination of the support exceeded the maximum allowable values. The power line supports are sunk-drill piles (two piles under each foot)

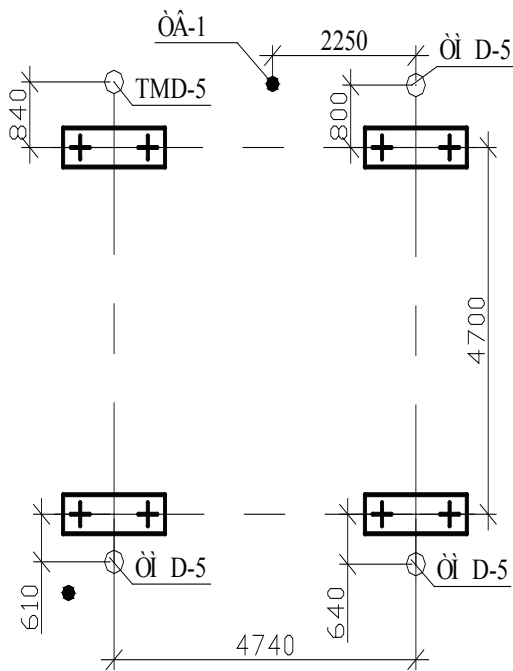


Figure 3. The scheme of the TMD-5 and location of temperature borehole TB-1 near the power line support No. 44.

with a 30 cm x 30 cm cross section and a length of 8 m.

Calculations of foundations showed their instability under vertical forces due to frost heave when the active layer refreezes. The power line supports are subjected to both compressing and pull out forces, therefore, the combination of pull out and vertical forces due to frost heave control heave and tilt of the foundations.

Techniques of Pile Bearing Capacity Increase

To provide the bearing capacity and stability of piles for engineering structures under the above-mentioned permafrost conditions ground temperature control was necessary. Seasonally cooling devices were widely used for heat extraction and to cool down ground temperatures. Thermopiles (Long 1963) and kerosene devices (Gapeyev 1969) are well known. Liquid seasonally cooling devices were used to refreeze thawed ground and to cool plastic frozen grounds (Biyarov et al. 1973), refrigerated piles were installed for multistory buildings in Mirny (Makarov et al. 1978), different types of thermosyphons and thermopiles were further used for numerous constructions in Alaska (Borjesson et al. 2007). In recent years *InterHeatPipe* thermostabilizers of small diameter are widely used for constructions in the Russian north (Lyazghin & Pustovoi 2001, Bayasan et al. 2002). Aluminum thermostabilizers, type TMD-5, with an equivalent diameter of 54 mm have the following advantages compared to other well-known seasonally cooling devices:

- low internal and external thermal resistance where the evaporator and the condenser are located;
- low temperature gradient along the length of the seasonally cooling device;

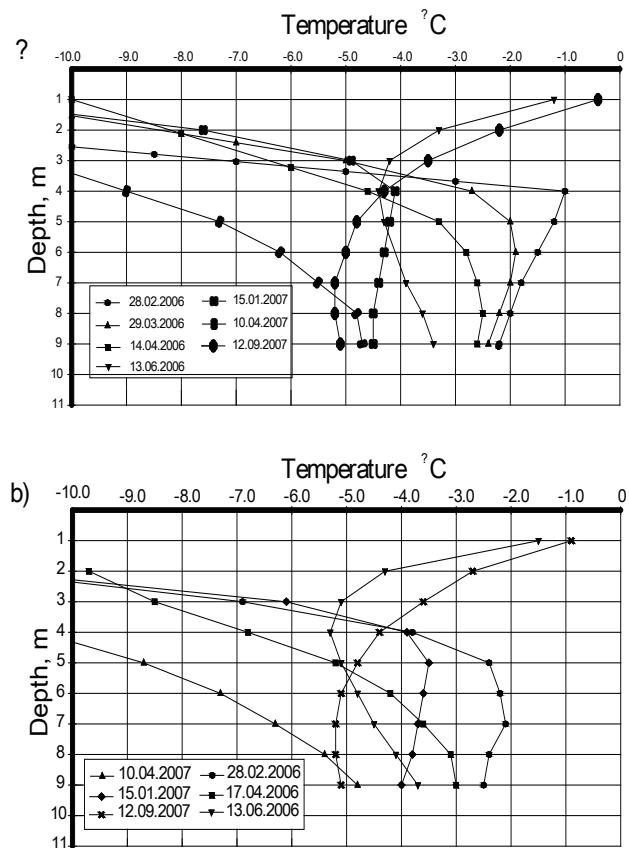


Figure 4. The ground temperatures near piles No. 52 (a) and No. 77 (b) of the business centre building after the installation of the thermostabilizers.

- high rate of freezing and effective cooling;
- short response time, which increases the period of active work of TMD-5 (1.0–1.5 months per season).

In addition to the seasonally cooling devices, the engineering design for ground thermal control includes the use of a thermal insulation. This was recommended and applied in all of the above-mentioned examples.

For the business centre office building, where the ground temperatures increase was recorded and the pile bearing capacity was exceeded, it was designed to install additional piles and to place thermostabilizers TMD-5. The condensators were tilted under the grid, in the centre of pile cluster. To decrease the depth of thawing and, consequently, to expand the adfreezing surface of the piles with the frozen ground the surface was protected with a thermal insulation foam (Fig.1).

Thermostabilizers for the 9-story residential building foundation were designed preliminary to refreeze the thawed ground. Piles will be loaded after the ground around them is frozen. The bearing capacity of the cast-in-place piles in a thawed zone was calculated considering the thawed state of the ground. An air space under the building allows cold air circulation, hence a gradual freezing of thawed ground and the maintenance of the frozen state.

Figure 2 shows a section of the foundation scheme for the area with inter-permafrost taliks where thermostabilizers were installed.

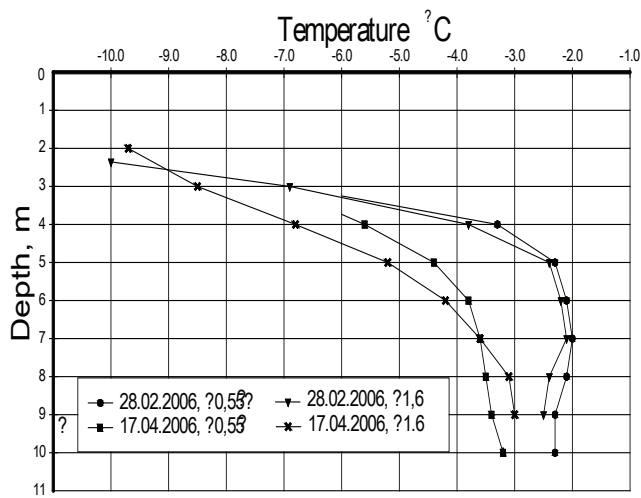


Figure 5. Ground temperature change after the installation of thermostabilizers located at different distances.

To prevent the failure of the power line supports, ground cooling by installing seasonally cooling devices was recommended. Thermostabilizers together with surface thermal insulation are provided to cool down the ground temperatures and to reduce the depth of seasonal thawing. This measure increases the adfreezing surface of the piles with the ground and decreases the surface of piles under the effect of vertical forces due to frost heave. The scheme of the TMD-5 installation is shown in Figure 3.

To measure the performance of the thermostabilizer and monitor ground temperatures boreholes were instrumented with thermistors. In addition, survey points were installed to measure support and foundation deformation.

The thermostabilizers for the business centre office building were installed in March 2006, those for a 9-story residential building in March 2007 and those near the power line supports in December 2006.

Results and Discussion

Figure 4 shows a set of ground temperatures beneath the business centre office building in two representative boreholes. TB-1 (near pile No. 52) is placed at the distance of 1.2 m, TB-2 (near pile No. 77) at the distance of 1.6 m from the TMD-5. Prior to the installation of the thermostabilizers (February 28, 2006) the temperatures at the tip of the pile (at the depth of 9 m) were between -2.2 and -2.5°C . At the same level the natural ground temperatures reached values between -3.4 and -4.2°C . Thermostabilizers were installed near pile No. 52 on March 15, 2006, and near pile No. 77 on March 26, 2006. The temperatures decrease as soon as the thermostabilizers had been installed. At the same time in upper permafrost layers (4–7 m) the temperature decrease was even more intensive and continued during the warm season (June 13, 2006)

Some temperature increase was recorded on January 15, 2007, but by the end of the cold season (April 10, 2007) the ground temperatures became much colder than on April 14, 2006 (after thermostabilizers worked for 20–30 days).

The end of a warm period (September for Yakutsk) is typical for the ground temperature regime. According to the temperature distribution on September 12, 2007, permafrost temperatures in both boreholes were low and nearly identical. As it has been stated above, thermistors were installed at a different distances from the thermostabilizers. Figure 5 shows the ground temperature decrease in two boreholes located at the distance of 0.55 m and 1.6 m from the thermostabilizers. Initial temperatures were almost similar and the thermostabilizers were installed on the same day. The figure further shows the intensive decrease in temperature where thermostabilizers were placed close (0.55 m) to the boreholes. However, such a tendency is not typical for the middle layers, which is probably affected by other factors, such as the composition, moisture content and salinity. These factors were not the subject of this investigation.

The data demonstrate that the proposed engineering design allowed the increase of considerably colder ground temperatures and a decrease in depth of seasonal thaw beneath the business centre office building. Ground temperatures lower than the calculated ones allowed the required bearing capacity of the soils and the transfer of calculated loads to piles.

Figure 6 shows typical diagrams of ground temperature changes for the 9-story residential building. As it was stated above, talik zones of different thickness were found below the building; thus ground temperatures were non-uniform. Figure 6a shows the temperature changes in borehole TB-1.

Ground temperatures along the entire depth of the borehole were positive at the end of a warm season (September 10, 2007), but by November 29, 2007, zero degree was recorded at depths below 3 m, and they stayed until January 24, 2008. Similar temperatures were observed in boreholes TB-2 and TB-4. Figure 6b presents the change in ground temperatures in borehole TB-5, where a talik was present at a depth of 7.5–9.5 m. According to the figure, ground cooling with the use of thermostabilizers resulted in subzero temperatures by December 5, 2007, and they continued to decrease (e.g., January 28, 2008). The figure further shows the peculiarities of refreezing thawed ground. Freezing of moist ground is characterized by the latent heat during phase change from water to ice. Therefore, the temperatures remain at about 0°C (the temperature of water freezing) before ground cooling continuous, which was observed in borehole TB-5. The data obtained demonstrate the efficiency of thermostabilizers when thawed soils are frozen under buildings.

The calculations for made-in-place piles of this building were made with consideration of thawed ground conditions. The purpose of installing thermostabilizers was to reach uniform ground temperatures and to avoid uneven settlements of the foundation. The design also requires the establishment of subzero temperatures before loading of the foundation may begin.

Thermostabilizers were installed near the foundations of each foot of power line supports, subjected to heave deformation. Figure 7 illustrates the change in ground temperatures after the thermostabilizers were installed in the ground under one of the supports.

Thermistors were installed in a borehole located at a

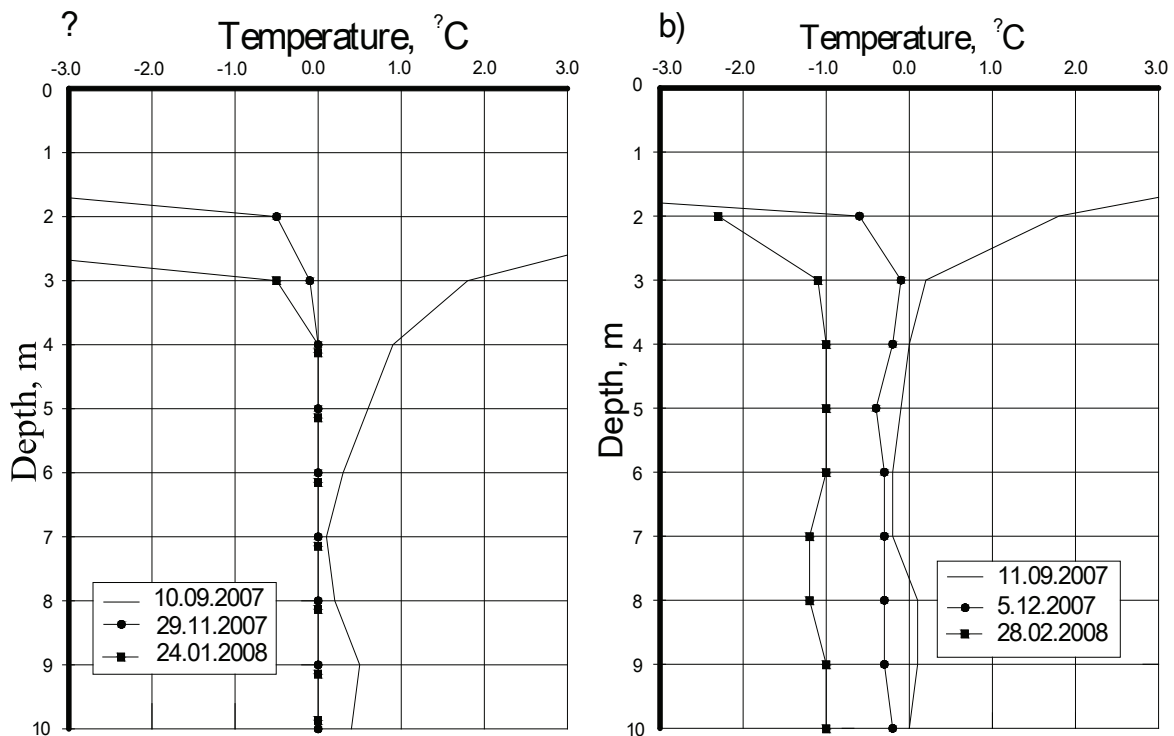


Figure 6. Ground temperature changes in boreholes TB-1 (a) and TB-5 (b) for the 9-story residential building.

rather large distance from the thermostabilizers (2.25 m). Nevertheless, the figure shows the decrease in temperature compared to the initial conditions. In addition to the temperature measurements, foundation deformations were monitored during the winter of 2006–2007, and no vertical deformations were noted for the two supports; that is, the reduction in ground temperature provided the necessary resistance of the foundations against the vertical forces of frost heave.

Conclusions

Small diameter *InterHeatPipe* thermostabilizers were installed under different structures in the city of Yakutsk to improve the ground-bearing capacity. In situ measurements of the temperature regimes of the ground cooled by the thermostabilizers allow for the following conclusions.

- Problems during the installation of the piles for a business centre office building resulted in warming ground temperatures and insufficient bearing capacity. Thermostabilizers and thermal insulation on the ground surface allowed the obtainment of calculated ground temperatures to decrease the depth of seasonal thaw and increase the bearing capacity of the pile foundation.
- Thermostabilizers used to freeze talik zones below a 9-story residential building showed their suitability and the dependency of the talik thickness on the period of temperature decrease.
- Thermostabilizers used to decrease ground temperatures and increase the resistance against vertical forces due to frost heave also eliminated uplift deformation of the pile foundations for a power line support.

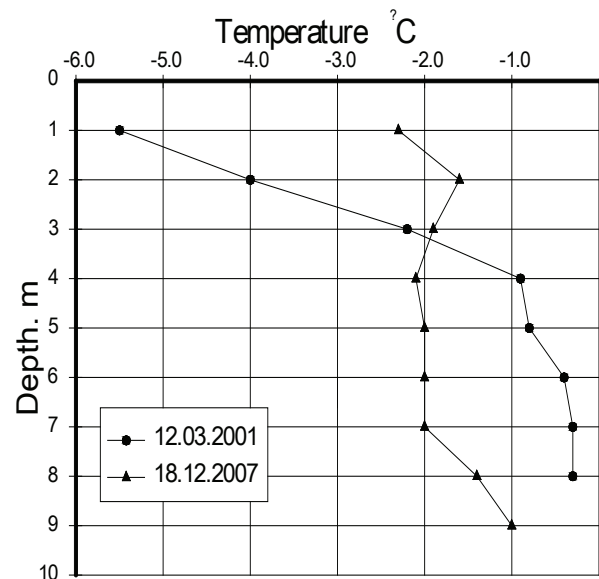


Figure 7. Ground temperatures before (2001) and after (2007) the installation of thermostabilizers the near power line support No. 44.

- The effectiveness of thermostabilizers depends on the initial ground conditions, properties, composition, and temperatures.
- The data obtained confirm the validity of engineering solutions by the use of seasonal cooling devices to increase the bearing capacity and stability of piles in permafrost.

Acknowledgments

The authors express their gratitude to the anonymous reviewers for their careful and thorough examination of the paper, constructive comments, and suggestions for the content change. Assistance with editing the English of the manuscript is greatly appreciated.

References

- Bayasan, R.M., Korotchenko, A.T. & Pustovoit, G.P. 2002. The probability, determinism and new technology in the problem of stability of perennially frozen bases. *Bases, Foundations and Soil Mechanics* 5: 26-31.
- Biyarov, G.F., Makarov, V.I. & Molochnikov, A.D. 1973. Liquing cooling units for freezing thawed ground and cooling plastically frozen ground for construction in areas with severe climate. *Proceedings of the Second International Conference on Permafrost, Yakutsk, June*: 195-199.
- Borjesson, B., Clarke, E.S., Miller, D., Musial, M., Shaw, S.R., Wyman, G.E., Yarmak, E. & Zarlring, J.P. 2007. *Permafrost Foundations. State of Practice*. Reston, Virginia: ASCE, 86 pp.
- Construction Code SNiP 2.02.04-88. 1991. *Bases and foundations on permafrost*. Gosstroy of the USSR. Moscow: APP CITP, 52 pp.
- Gapeyev, S.I. 1969. *Frozen Foundations Strengthening by Cooling*. Leningrad: Stroyizdat, 104 pp.
- Long, E.L. 1963. The Long Thermopile. *Proceedings of the First International Conference on Permafrost, Lafayette*: 487-491.
- Lyazgin, A.L. & Pustovoit, G.P. 2001. The stability of power line supports against frost heave under conditions of the north of Western Siberia. *Proceedings of the Second Conference of Geocryologists of Russia 4, Moscow*: 172-178.
- Makarov, V.I., Plotnikov, A.A. & Chumayevsky, B.F. 1978. Construction of Multi-Storey Buildings on Refrigerated Piles in the City of Mirny. *Proceeding of the Third International Conference on Permafrost, 1, Ottawa*: 820-825.
- Recommendations on Design and Calculation of Shallow Foundations in Frost Susceptible Ground*. 1985. Gosstroy, the N.V. Gersevanov VNIIOSP, Moscow, 59 pp.

Vegetation Response to Landslide Spreading and Climate Change in the West Siberian Tundra

N.G. Ukraintseva

Institute VNIIST (Institute of the Engineering and Construction of the Oil-Gas Pipeline), Russia

Abstract

Cryogenic landslides are widespread and well investigated in the sub-arctic tundra. On the Upper Pleistocene marine plains, active landslide process brings to the surface marine saline deposits saved by permafrost. The landslide-affected slopes present a system of morphologically expressed and often overlapping landslides of different age. Patterns of re-vegetation and “self-stabilization” of landslides as indicators of landslide age have been studied. Natural enrichment of the soil, water, and vegetation in many nutrients leads to anomalous productivity on landslide-affected slopes and to the expansion of high willow shrub to the north. Areas of near-surface distribution of marine saline deposits and old landslides are correlated to the area of high willow shrub tundra. Estimation of cryogenic landslide distribution north of Western Siberia has been studied using methods of landscape indications. Spreading of cryogenic landslides further to the north may be an indication of a warming tendency in the Arctic climate.

Keywords: cryogenic landslides; marine deposits; willow shrub.

Introduction

Special interest in studying the process of cryogenic sliding has arisen after a mass descent of landslides in many areas of the Russian and North American Arctic regions in 1988–1991. Landslide processes affect the surface of marine plains and terraces. The permafrost table serves as a “mirror” for sliding masses; therefore, the majority of researchers name them “cryogenic landslides” or “active-layer detachments” (Levkovicz 1990, Harry & Dallimore 1989, Leibman 1995, Poznanin 2001). The cryogenic landslides are developing on surfaces built of fine-grained marine sediments with high salinity. Outcropping of frozen salty marine sediments took place due to seasonal sliding of the thawed water-saturated ground over the permafrost table. This process leads to sediment desalinization and enrichment of the active layer with salts (Dubikov 2002, Leibman 1995, Ukraintseva et al. 2003).

The purpose of the present study is to estimate the distribution of cryogenic landslides in the north of the Western Siberia using methods of landscape indication.

Study Area and Methods

The basic area of research is the region of the Bovanenkovsky gas refinery (between the Mordyjaha and Naduyaha Rivers) and projected gas pipeline “Yamal Center” in western and central Yamal. The author’s research materials from the Peljatinsky gas refinery (Lake Pelyatka, southern Gudan) and the coast of the Yenisey Gulf (Shajtansky, western Taimyr) are used also.

The research station of “Vaskiny Dachi” is located in typical tundra of central Yamal. Since 1991, field groups from the Earth Cryosphere Institute of the Russian Academy of Sciences (Tyumen) have been studying cryogenic landslides (with participation of the author). The technique of field sampling and laboratory analysis of samples is described in the paper by Ukraintseva et al. (2003).



Figure 1. Study area: research station Vaskiny Dachi in central Yamal Peninsula is marked by the star.

In the area of the Bovanenkovsky gas field, 10 key sites within landscapes of IV, III, and II marine plains and terraces in the valleys of Nadujjaha, Seyaha, and Mordiyaha Rivers were explored. The large-scale landscape map of the Bovanenkovsky area was made using GIS-Technologies (Drozdov & Ukraintseva 2000). A method of landscape indication was applied to determine the relative age of landslides slopes (young and ancient) in each landscape.

The landscapes map of the north of Western Siberia published in 1991 (with scale 1:1,000,000) was used for extrapolation of the obtained data to all typical tundra. The legend of the landscape map of the Bovanenkovsky gas field was generalized and made consistent with the legend of the published map. This allowed the extrapolation of calculation results according to the principle of landscape analogies and estimation of a fraction of landslide slopes in landscape areas of typical (sub-arctic) tundra.

Spatial distribution various vegetation communities was evaluated using an analysis of the distribution of Nenets’

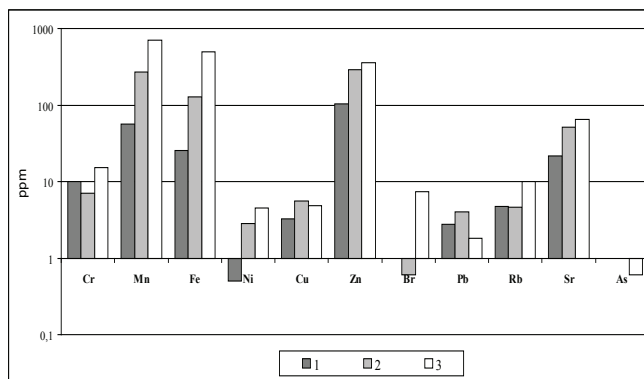


Figure 2. Trace element composition in various structural parts of willow. 1–willow trunk; 2–willow branches; 3–willow leaves.

names (toponyms) on topographic maps of northwestern Siberia with a scale of 1:1,000,000 (with insertion of several larger scale pieces).

Landslides in the Subarctic Tundra

Biogeochemical features of landslide-affected slopes

In the region of typical tundra where salted marine loams and clays lie close to a surface, cryogenic landslides of sliding are widespread on the Upper Pleistocene marine plains and terraces and have been studied in detail. Extended landslide slopes represent a system of morphologically expressed landslides of different ages quite often overlap each other. In comparison with background conditions, biogeochemical features of ecosystems of landslide slopes vary significantly. The main features of landslide processes in the regions of interest were described earlier:

- Mechanical displacement of land, mixing, and increase of heterogeneity (vertical and lateral) of granulometric structure of the active layer (Ukrainitseva & Leibman 2007);
- Periodic activation and recurrence of landslide descent, leading to change of a longitudinal profile of a slope and position of the permafrost table (Ukrainitseva et al. 2003);
- Destruction of topsoil layer and vegetation cover along the sliding surfaces, and burial of organic soils on the landslide bodies (Ukrainitseva & Leibman 2007);
- Desalination of the marine permafrost and enrichment of the soil-vegetation cover with dissolvable salts (mineral nutrients), accelerating “self-stabilization” process of the landslide-affected slopes (Ukrainitseva et al. 2003);
- Age of the landslides defined by the radiocarbon dating of buried organic matter, varies from 0–30 till 1500–2000 (Leibman et al. 2000).
- Increase of fertility of the soils enriched by nitrogen, potassium and organic matter: peat soils prevail in ancient landslide slopes with thickness of organic layer 20 cm or more (Ukrainitseva & Leibman 2007);
- Change of structure and increase of the phyto-mass storage on the surface of the landslide slopes represented by high willow shrubs (Ukrainitseva & Leibman 2000, Ukrainitseva 2004).

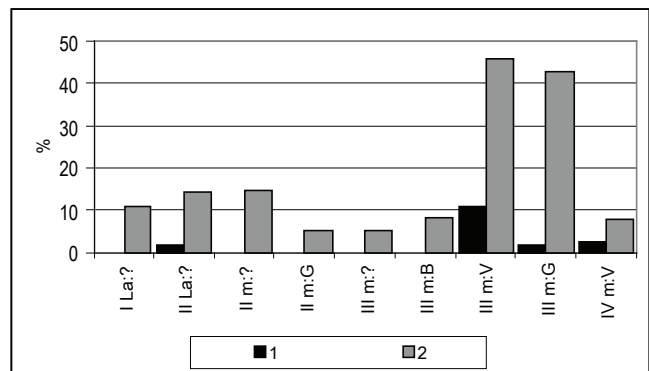


Figure 3. Landslide-affected slopes in structure of landscapes of the Bovankovskiy gas field (Melnikov & Grechishchev 2004). 1–young slopes; 2–old and ancient slopes.

The rich microelement structure of the substratum promotes zinc accumulation in leaves and trunks (Fig. 2), and raises the frost resistance of willow. Due to this, willows form steady communities in unusually high latitudes (up to 70°N, –72°N). This is confirmed by conclusions of other researchers who refer to willow bushes as pioneer plants which spread out into natural or human-caused bare soil tundra (Andreev 1970, Burn & Friele 1989, Geertsema & Pojar 2007, Matsuda et al. 1988, McKendrick 1987, Pospelova & Pospelov 2000, Rebristaya et al. 1995, Sturm et al. 2001, Ukrainitseva & Leibman, 2000).

The next step in research of the landslide processes is an estimation of their spatial distribution.

Landscape indicators of landslide-affected slopes

On large-scale aerial images, only young landslides (younger than 100 years old) can be detected. Old and ancient landslides are expressed weakly in morphological structure and do not have direct pattern on the image. For mapping of PLAITS on aerial images, the indirect method—the method of landscape indication based on studying of spatial and temporal variation of a vegetation cover—is applied.

In the investigated areas, the dominating community of hill tops and stable slopes is bush-grass-moss and bush-lichen-moss tundra—the background communities of typical tundra. The vegetation cover on the landslide slopes sharply differs from the background.

There are three basic stages of re-vegetation of landslides, and there are three gradations of landslide’ relative ages, respectively: young, old, and ancient (Ukrainitseva et al. 2003, Rebristaya et al. 1995). On *young* surfaces of landslides (10–15 years after a landslide occurred), bare soil sites alternate with pioneer meadow groupings of *Phippsia concinna*, *Tripleurospermum Hookerii*, etc. At the same time, some short bushes (willow, dwarf birch) still remain on young landslides; mosses degrade and wilt, and pioneer plants (cereals, a sedge, a horsetail) appear. On *old* landslides (from 100–300 till 1000 years old), the second stage of re-vegetation is observed—meadow communities with participation of mosses and active renewal of a willow (0.3–1 m height). And finally, associations of *Salix glauca* and *S. lanata* (height: 1.5–2 m) are characteristic for *ancient* landslides (from 1000

Table 1. Landslide slope area in typical tundra of Western Siberia.

Regions	Area, km ²	Fraction of area in the zone %	Fraction of landslide slopes in the area %	Fraction of landslide slopes in the zone %
11	4946	4,94	20,28	1,00
12	19337	19,31	30,19	5,83
13	18103	18,07	1,83	0,33
14	8767	8,75	31,92	2,79
15	3063	3,06	0,46	0,01
16	13500	13,48	15,92	2,15
17	20764	20,73	9,54	1,98
18	11677	11,66	19,11	2,23
Total	100161	100,00	-	16,32

to 2000 years old (Leibman et al. 2000)—sparse moss-grass willows on surfaces of sliding and dense grass-moss willows on landslide bodies. High willows occupy the most area on the landslide slopes.

Successive stages of re-vegetation of landslides determine choice of landscape indicators. Two last stages of landslide re-vegetation are poorly distinguishable on aerial images, merging together and creating a small grey texture of bush communities. Thus, the landscape indicators of old and ancient landslides (older than 100–300 years) are high willows (an index *6n*), and modern young landslides are identified by pioneer meadow communities with bare soil surfaces (an index *6p*).

Distribution of landslide-affected slopes on the Bovanenkovsky gas field

On a large-scale landscape map of the Bovanenkovsky gas field (Drozdov & Ukraintseva 2000), the relative age of landslide slopes (young and ancient) in the structure of each landscape is calculated. The maximum distribution of landslide slopes is characteristic for large-hill thermodenudation areas of III marine plain (III m: V = about 57%). The fraction of young landslides from the total area of landslide slopes for all districts does not exceed 20–30% that indicates some attenuation of process (Fig. 3).

Landslide slopes in typical tundra

The map of natural complexes of northwestern Siberia (scale 1:1,000,000) published in 1991 was used for extrapolation of the received data on all typical tundra. In the region of typical tundra, eight landscape areas are allocated, for each of which the histogram of morphological structure—a percentage of landscape and land area—is determined. This allowed extrapolation of results of calculations by a principle of landscape analogies. The legend for a landscape map of the Bovanenkovsky gas field was generalized and is made consistent with a legend of the published map.

Evaluation of the distribution of landslide slopes in typical tundra of western Siberia is presented in Table 1.

Areas of landslide processes occupy more than 16% of a total area of typical tundra zone. It is a high percentage, considering that landslides occur only in the most elevated locations. The

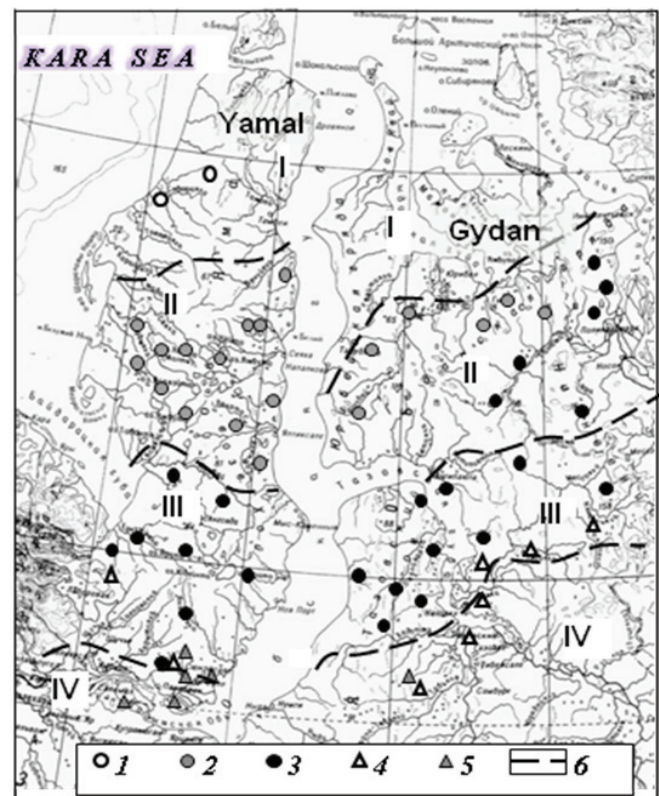


Figure 4. Nenets toponymics (denominations) on the West Siberian topographical map. 1—*pyasyada, tartsya* (nude); 2—*nero, nerka, neruta* (willow shrub, willow canopy, *Salix* sp.); 3—*pae, paya* (alder shrub, *Alnus fruticosa*); 4—*kharv* (larch, *Larix sibirica*); 5—*khadita* (fir, *Picea obovata*); 6—limits of subzones. Zone and subzone: I—arctic tundra; II—typical (subarctic) tundra; III—southern (low) tundra; IV—forest-tundra.

maximum activity of landslide development—over 30% of the area—is characteristic for central Yamal (area 12) and western Gudan (area 14), where hilly sites (V) consisting of permafrost marine loam and clay with salinity over 0.5% (Dubikov 2002) prevail. Landslide slopes occupy about 15–20% of the area of Western Yamal (area 11), Gydansky ridge (area 16), and Tanamo-Yenisey valley (area 18). The structure of these areas almost does not concede to the first two, but the fraction of sand covering salted marine clay increases. The fraction of landslide slopes is minimal in low, strongly boggy, mainly sandy areas (A) with widely-developed river network: east Yamal (area 13), valleys of the rivers Juribej (area 15) and Tanama (area 17) on Gudan Peninsula.

Willow tundra in Nenets toponymics

The main feature of toponymics of the Nenets people living in the Far North in severe climatic conditions is their deep penetration into nature. To survive in tundra, every Nenets knows (notices) seasonal rhythms of nature and is able to predict the approach of sharp changes of weather and extreme natural phenomena by monitoring the behavior of animals or the state of the vegetation. Figure 4 shows zone borders from the map of northwestern Siberia and the distribution of Nenets toponymics characterising the vegetative cover.

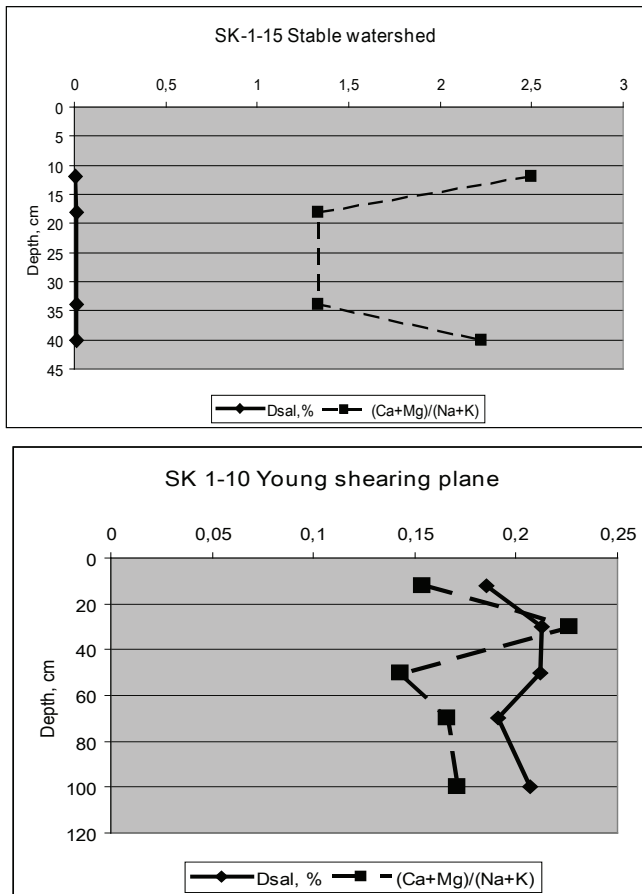


Figure 5. Salinity and cation ratio in active layer profiles on Cape Shaitansky, Western Taimyr. Top panel–stable watershed; bottom panel–young shearing plane.

Thus, the typical terms for the Arctic tundra are *pyasyada* (bald) and *tartsya* (nude). In typical tundra, the names *nero*, *nerka*, *neruta*, and *neromo* (willow shrub, willow canopy) are very common. Borders of southern tundra are underlined by various names with a root base of *pae* or *payu*, corresponding to alder shrubs. The northern limit in the spread of these names on the Yamal Peninsula is the lower part of River Juribej. And it was 40 km from the mouth of Juribej, where the first and the most northern curtains of alder shrubs have been observed on the aerial images.

Toponymic areas repeat outlines of natural zones and subzones, being a little displaced to the north. In the eastern (Priensejsky) part of the region, the warming effect of the Yenisey River accounts for the especially considerable displacement of toponymic area of alder and larch to the north.

Toponymic areas of alder shrubs and tree species are not in the focus of the present study of landslide slopes distribution. They are shown on the map to illustrate high correlation of Nenets' toponymics to the nature laws. The alder shrub is not an indicator of subzones in southern tundra since it grows mainly in valleys of the rivers (dependent sites). Willow tundra, on the contrary, is widespread on the watersheds (independent sites) where they can be the indicator of ancient landslide activity (Ukrainitseva 2004).

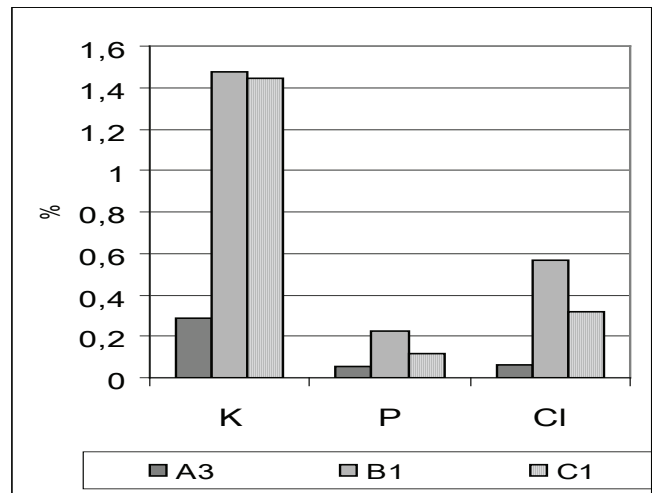


Figure 6. Potassium, phosphorous, and chlorine in grasses on Cape Shaitansky. A3–stable site; B1–shearing plain; C1–landslide body.

Landslides in the Arctic Tundra

Cryogen landslides with glide faces formed by the roof of the salty marine permafrost are widespread on the Yamal and Gudan Peninsulas, on the Taimyr coast of the Yenisey Gulf (from Dixon to Cape Shaitansky), as well as on the islands of the Canadian Archipelago (Ukrainitseva et al. 2004, Harry & Dallimore, 1989, Lewkowicz et al 1990). Bare landslide surfaces with salt outcrops are well observed and overgrown with pioneer grasses and herbs with halophytes (vegetation cover varies from 10% to 80%). Landslide age being estimated by vegetation development ranges from a few to several dozen years.

Cryogen landslides are studied in Yenisey Gulf near Cape Shaitansky. The salinity and marine cation ratio (Dubikov 2002) in active layer witnesses the marine origin of sediments (Fig. 5). A joint plot of vertical distribution of salinity and cation ratio clearly illustrates the degree of diagenetic transformation of the marine deposits. On the young shearing plane, the saline marine clay got into the active layer only recently, and its desalination is still in the initial stage. The values of clay salinity on the young shearing plane profile (Fig. 5, bottom panel) are close to 0.2%, which is higher than cation ratio values (salinity curve is to the right from the cation ratio curve). The active layer of stable watershed and slopes was long-term flushed due to drainage and precipitation during the warm seasons of the year. In these areas, the salinity of the active layer is close to zero (Fig. 5, top panel), and the salinity curve is to the left from the cation ratio curve.

Grasses growing on the shearing plain and landslide bodies were considerably more enriched with chlorine, phosphorous, and potassium relative to stable areas, therefore marking leaching of these elements in stable conditions (Fig. 6).

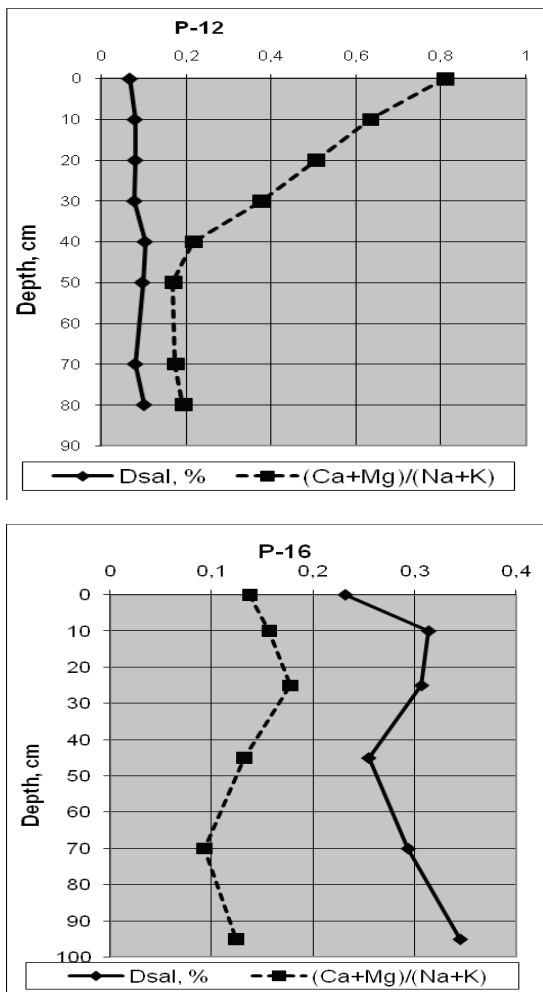


Figure 7. Salinity and cation ratio in active layer profiles on Pelyadkinsky gas field, Southern Gydan. Top panel—young shearing plane; bottom panel—the same shearing plane after repeated landslide event.

Landslides in the Low (Southern) Tundra

The 10–20-year-old landslide events have been studied in 2003–2005 in the Pelyatkinsky gas field located in southern tundra. Salinity and ratios of continental and marine cations also showed the initial marine origin of the sediments in these areas (Fig. 7). Unlike typical and arctic tundra, landslide events in southern tundra bring already significantly diagenetically reworked marine sediments to the active layer (Fig. 7, top panel); thus, cryogen sliding in these areas can be traced by thick layers of diagenetically reworked deposits. After repeated landslide events on the same slope in 2004, the saline marine layer has been exposed at the surface (Fig. 7, bottom panel). As a result, the saline marine permafrost lies twice as deep compared to modern thaw-depth: at 2.5 m depth or even deeper.

The slope is overgrown with low dwarf birch and undershrub-moss tundra. Despite the long-term desalination process, chlorine content is still higher in horsetail and willow leaves inhabiting shearing plains and landslide bodies as compared to the stable background surface (Fig. 8).

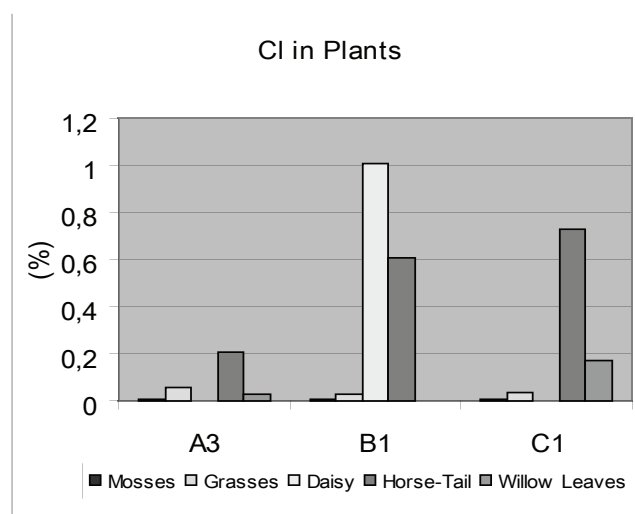


Figure 8. Chlorine in plants. For sites, see comments to Figure 6.

Conclusions

In the arctic tundra, young cryogenic landslides formed by the roof of the saline marine permafrost are widespread. Bare landslide shearing planes with salt outcrops are well observed and overgrown with pioneer grasses and herbs with halophytes. Landslide age estimated from vegetation development ranges from a few to several dozen years.

In the typical (subarctic) tundra, cryogenic landslides are mostly widespread and extensively investigated. Areas of cryogenic landslide slopes have been evaluated using the landscape indicator technique, and they occupy close to 16% of the total area of the subzone. The cryogenic landslide process is the leading landscape-forming process in the typical tundra of western Siberia.

Maximum landslide activity (more than 50% of the area) is characteristic for the elevated plains of central Yamal and western Gydan, formed by permafrost marine loam and clay with 0.5% salinity and higher. The fraction of young landslide slopes (10–100 years old) is estimated not to exceed 5–30%. This is an indication of the gradual decay of landslide processes in these areas.

In the southern (low) tundra, cryogenic landslides have been active since the Holocene Hypsithermal (7000–8000 years ago). At the present time, the desalination process of landslide slopes is finished. The slopes are covered with thick mosses and high willow shrubs partially replaced by dwarf birch. Thick layers of old diagenetically reworked deposits containing a mixture of iron-enriched and buried organic-enriched sediments might be the only indicators that cryogenic sliding took place on these hill slopes.

Thus, during the Holocene, landslide processes slowly moved further north, causing the consequent spread of willow communities with high bio-productivity to the north. Southern tundra (at present the process is finished) formed 5000–8000 years ago; typical tundra (active process, widespread high willows), 2000–0 years ago; and arctic tundra (the beginning stage, young landslide slopes with

grass cover and sparse willow restoration), 20–30 years ago. The indicator of the final stage of the landslide process is the replacement of high willow shrubs by typical zonal vegetation with a thick lichen-moss-litter layer.

Therefore, the presented study has demonstrated that the dynamic process of cryogen sliding caused by increase of heat, moisture, and seasonal thaw-depth is moving to the north. This can be considered as an additional indication of the global warming tendency in the arctic climate.

Acknowledgments

The author is grateful to Elena Korobova and Tatiana Smirnova for assistance in paper preparation, and to the crew of the research vessel “Akademik Boris Petrov” who participated in the fieldwork. The author also acknowledges A. Savichev, S. Sorokin, and R. Grishina for chemical analyses of samples.

References

- Andreev, V.N. 1970. Some geographical laws in the distribution of above-surface phytomass in tundra zone in connection with progress to the north of tree-shrubs vegetation. In: *Biological Basis of Nature Usage in the North*. Syktyvkar: Komi Publisher (in Russian).
- Burn, C.R. & Friele, P.A. 1989. Geomorphology, Vegetation Succession, Soil Characteristics and Permafrost in Retrogressive Thaw Slumps near Mayo, Yukon Territory. *Arctic* 42(1): 31-40.
- Geertsema, M. & Pojar, J.J. 2007. Influence of landslides on biophysical diversity—A perspective from British Columbia. *Geomorphology* 89(1): 55-69.
- Drozov, D.S. & Ukraintseva, N.G. 2000. *The map of natural geocryosystem of Bovanenkovo gas field (landscape map)*. E.S. Melnikov (ed.). Earth cryosphere Institute SB RAS.
- Dubikov, G. I. 2002. *Structure and a cryogenic structure of frozen thicknesses of Western Siberia*. Moscow: GEOS, 246 pp.
- Harry, D.G. & Dallimore, S.R. 1989. Permafrost, Ground Ice and Global Change in the Beaufort Sea Coastlands. Moscow: GEOS 3, 48-53.
- Leibman, M.O. 1995. Preliminary results of cryogenic landslides study on Yamal Peninsula, Russia. *Permafrost and Periglacial Processes* 6: 259-264.
- Leibman, M.O., Arhegova, I.B., Gorlanova, L.A. & Kizyakov, A.I. 2000. Stages of cryogenic landslides on Yugorsky and Yamal Peninsulas. *Earth Cryosphere* IV(4): 67-75 (in Russian).
- Leibman, M.O. & Egorov, I.P. 1996. *Climatic and Environmental Controls of Cryogenic Landslides, Yamal, Russia. Landslides*. Rotterdam: Balkema Publishers, 1941-1946.
- Lewkowicz, A. 1990. Morphology, frequency and magnitude of active-layer detachment slides, Fosheim peninsula Ellesmere Island, N.W.T., Permafrost-Canada. *Proceedings of the Fifth Canadian Permafrost Conference*, Quebec: Collection Nordicana, 54.
- Matsuda, K. et al. 1988. Observations of Geomorphic and Vegetational Changes Caused by Thermal Erosion of an Involved Hill in Tuktoyaktuk, N.W.T., Canada. In: *Characteristic of the massive ground ice body in the Western Canadian Arctic related to paleoclimatology, 1984-1985*. Hokkaido: Inst. Low Temp. Sci., Hokkaido Univ.
- McKendrick, Jay D. 1987. Plant Succession on Disturbed Sites, North Slope, Alaska, U.S.A. *Arctic and Alpine Research* 19 (4): 554-565.
- Melnikov, E.S. (ed.). 1991. *Map of natural geosystem of the North Western Siberia*. 1:1,000,000. Novosibirsk: Map Publishing House, 6 sheets.
- Melnikov E.S. & Grechishthev S.E. 2002. *Permafrost and Development of Oil and Gas Regions*. Moscow: GEOS, 402 pp.
- Pospelova, E.B. & Pospelov, I.N. 2000. Relic high shrub communities near the northern border (the central part of Byrranga mountains, Taymyr Peninsula). *Novosti Akademii nauk, seriya geographicheskaya*, (4): 92-97.
- Poznanin, V. L. 2001. Morphology, the mechanism of formation and dynamics active-layer detachments on the central Yamal. In: *Problems of environment and natural resources*. Moscow: VINITI (2), 78-92.
- Rebristaya, O.V., Khitun, O.V., Chernyadyeva, I.V. & Leibman, M.O. 1995. Dynamics of vegetation on the cryogenic landslides at the central part of Yamal Peninsula. *Botanical Journal* 80(4): 31-48 (in Russian).
- Sturm, M., Racine, C. & Tape, K. 2001. Increasing shrub abundance in the Arctic. *Nature* 411: 546-547.
- Ukraintseva, N.G. & Leibman, M.O. 2000. Productivity of willow-shrub tundra in connection with landslide activity. In: *30th Arctic Workshop, March 15-19 2000*. Boulder, CO USA: INSTAAR, University of Colorado, 150-152.
- Ukraintseva, N.G., Streletskaya, I.D., Ermokhina, K.A. & Yermakov, S.Yu. 2003. Geochemical properties of plant-soil-permafrost system at landslide slopes, Yamal, Russia. In: M. Phillips, S.M. Springman & L.U. Arenson (eds.), *Proceedings of the Eighth International Conference on Permafrost, Zurich, Switzerland, July 20-25, 2003*: 1149-1154.
- Ukraintseva, N.G. 2004 Spreading of cryogenic landslides in typical tundra subzone of Western Siberia. In: Moscow, GEOS (ed.), *Sergeevsky chteniya* (6): 211-214
- Ukraintseva, N.G., Shuvalova, E.M. & Smetanin, N.N. 2005. Cryogenic landslides in the area of Bovanenko gas field: spread, peculiarities, consequence. *Proceedings of the 3th Conference of the Russian Geocryologist. Moscow, 1–3 July 2005*. Moscow: MSU. V.2, teil 3, 178-185 (in Russian).
- Ukraintseva, N.G. & Leibman, M.O. 2007. Cryogenic landslides (active-layer detachments) and fertility of tundra soils on Yamal Peninsula, Russia. *Proceedings of the First North American Landslide Conference Vail, Colorado, June 3–8, 2007*: 1605-1615. Conference CD.

Permafrost Occurrence in Southernmost South America (Sierras de Alvear, Tierra del Fuego, Argentina)

Marcos Valcárcel-Díaz

Department of Geography, University of Santiago de Compostela, Santiago de Compostela, Spain

Pedro Carrera-Gómez

Department of Geography, University of Santiago de Compostela, Santiago de Compostela, Spain

Ramón Blanco-Chao

Department of Geography, University of Santiago de Compostela, Santiago de Compostela, Spain

Augusto Pérez-Alberti

Department of Geography, University of Santiago de Compostela, Santiago de Compostela, Spain

Abstract

Several lines of evidence indicate that permafrost is present at elevations above ca. 775 m a.s.l. in the Mount Alvear region of the Sierras de Alvear, Fuegian Andes, Argentina. Ground temperatures recorded to depths of 1.3 m in sorted circles remain near 0°C in late summer and suggest perennial frozen ground at a depth of approximately 1.5 to 2 m. Three active rock glaciers occur in the upper Alvear Valley. On the flat surface to the east of the Alvear Glacier, sorted circles are located in the centres of poorly-defined polygons. The latter are interpreted to reflect either joint widening in underlying bedrock or thermal-contraction cracking in bedrock. Collectively, this evidence suggests the presence of permafrost on the higher summits of the Fuegian Andes.

Keywords: Argentina; Fuegian Andes; ground thermal regime; mountain permafrost; rock glacier.

Introduction

The distribution and characteristics of mountain permafrost in the southernmost Andes are, to date, poorly known. This contribution provides both geomorphological and instrumental (ground temperature records) evidence for the occurrence of permafrost in the high levels of the Sierras de Alvear, Tierra del Fuego, Argentina (Fig. 1). The central sector of the Fuegian Andes is characterized by the presence of a wide variety of cryogenic landforms related to ground freezing and/or to nivation activity (e.g., frost-heaved clasts, patterned ground, debris lobes, clast pavements, and protalus ramparts) (Valcárcel-Díaz et al. 2006), and to permafrost occurrence (rock glaciers). According to Corte (1997), the lower limit of permafrost in the Fuegian Andes is located at 900 m a.s.l.

The research presented in this contribution has focused on an unnamed summit and the upper Alvear Valley (54°40'S, 68°02'W), both located ca. 2.5 km to the E of Mount Alvear and the Eastern Alvear Glacier, at elevations ranging from 775 to 1077 m a.s.l. The summit is a nearly flat, clast-covered surface with occasional rock outcrops. The upper Alvear Valley shows steep slopes and is bounded by an arête and a near-vertical rock wall. The bedrock is composed of Late-Jurassic basalts, porphyrites, and slates (Olivero & Martinioni 2001). Southern Tierra del Fuego climate is cold-temperate and wet (Tuhkanen 1992). Air temperature measured from January 2005 to January 2006, at 1050 m a.s.l. near the upper col of the Alvear Valley was -2°C. No precipitation data are available for these mountains. Snowfalls are frequent and may take place year-round, even during summer. Strong and persistent winds blow on the



Figure 1. Location of the Sierras de Alvear.

summit area, where gusts exceeding 140 km/h have been recorded. Vegetation cover is extremely scarce and is limited to communities of lichens and mosses.

Geomorphological Observations

A geomorphological survey, focused on the identification of potentially active landforms indicative of permafrost, was carried out in the summit area and the upper Alvear Valley.

The nearly flat summit is almost entirely covered by a sheet of rock rubble, composed of basalt and porphyrite angular clasts, overlying solid bedrock. The thickness of the rubble sheet is roughly estimated to exceed 1 m. However, small outcrops of bedrock occur, showing evidence of widespread and intense mechanical weathering. Poorly defined polygons, 4 to 5 m wide, delimited by shallow furrows or trenches 30 to 50 cm deep, have developed in the underlying bedrock. Small depressions or stone pits have formed in the intersections of the furrows. Sorted circles (“stony earth circles”), composed of an exterior border of coarse clasts enclosing an inner sector of sands, silts, and isolated larger clasts, occur in the centers of the polygons (Fig. 2). The latter are interpreted to reflect either joint or fracture widening in underlying bedrock or thermal-contraction cracking of the bedrock. Although it has yet to be proven if the polygons are presently active, the inner nonsorted circles show present-day activity related to seasonal freezing.

Three rock glaciers occur at the foot of the northwestern ridge of the upper Alvear Valley. According to shape, one is complex, the second is lobate, and the third is tongue-shaped. All of them are of reduced dimensions, but nevertheless, seem to be presently active. As the tongue-shaped rock glacier is better-developed than the others, the geomorphological survey was conducted on it. This is a small, talus-derived rock glacier 150 m long, 70 m wide, and 22 m high (Fig. 3). It is located at the foot of a southwest-facing, near-vertical rock wall, and it extends downwards to 775 m a.s.l. The root area grades into a steep talus slope (mean gradient is 36°). It is predominantly composed of angular, slate blocks, embedded in finer debris, and it is directly connected with its source area. The shales that form the rock wall are densely jointed and foliated, being highly susceptible to frost weathering and favoring talus production. Under present climatic conditions, talus production is considerable. Transport of debris from the talus to the root area of the rock glacier seems to be steady. This landform shows some of the features stated by Barsch (1996) as to be distinctive of active rock glaciers, e.g., steep front and side slopes (mean gradient is 38°), and exposure of fine, light-colored, unweathered material in the front and side slopes.

Methods

A shallow borehole equipped with thermistor probes was set up in the summit area. The aim was to get temperature records that could prove the occurrence of permafrost. Due to logistical problems, a similar borehole could not be drilled in the tongue-shaped rock glacier of the upper Alvear Valley.

The borehole is 2 cm in diameter, and it was made in the centre of a nonsorted circle located at 1057 m. a.s.l. (Fig. 2), using a battery-powered drill. Drilling was mainly conducted through a thick layer of frost-weathered rock rubble, up



Figure 2. Oblique aerial view of nonsorted circles and polygons developed on the summit surface. Arrow indicates shallow borehole site.



Figure 3. View of the tongue-shaped rock glacier of the upper Alvear Valley. Arrows indicate the front slope of the complex rock glacier.

to a depth of 130 cm. Further deepening of the drill hole was impeded by the presence of solid bedrock. Thermistor probes were fixed with adhesive tape to a wooden rod 1.5 cm in diameter. The rod was then inserted into the drill hole, and the probes were installed at depths of 1, 5, 10, 20, 35, 70, 100, and 130 cm. Only the records corresponding to the probes located at depths of 1, 70, and 130 cm will be discussed in this paper. Temperature probes have a resolution of 0.03°C and an accuracy of $\pm 0.25^\circ\text{C}$. Data were read and stored hourly using “U12” multi-channel data loggers (from Onset Computer Corp.).

The time span covered by the temperature records extended from mid-February 2006 to the end of January 2007.

Results

Figure 4 shows the temperature curves obtained from the shallow borehole of the summit. Ground temperature evolution at the surface (1 cm depth) is mainly characterized by the occurrence of short-term fluctuations throughout

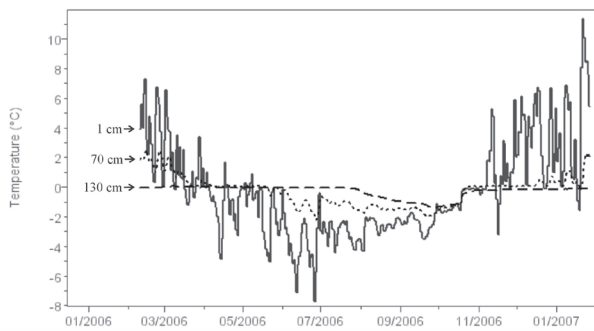


Figure 4. Temperature curves displaying daily mean values, obtained at depths of 1, 70, and 130 cm in the shallow borehole of the summit.

the year, including winter. The mean temperature of the recording period was -0.3°C . Minimum temperature occurred in early winter (end of June) and was -7°C . Temperature at the end of the winter (mid-September) was slightly below -3°C . Seasonal freezing extended from early April to early November and was interrupted on three occasions by daily above zero fluctuations. The end of the seasonal freezing (period from mid-October to early November) was characterized by an increase in temperature, attaining a nearly constant value close to 0°C , probably due to snow melting and heat transfer by percolating melt water. Daily frost mainly takes place during late spring and summer.

The evolution of ground temperature at a depth of 70 cm during the seasonal freezing period, shows a general trend similar to that at 1 cm depth. Surface daily fluctuations have been filtered at this depth, and the mean temperature was -0.28°C . Similar to the upper thermistor, the minimum temperature occurred in early winter (end of June) and in this case was -2.3°C . Seasonal freezing was not interrupted and extended from mid-May to early November. Two zero curtains occurred immediately before (from mid-April to mid-May) and after (from the end of October to mid-December) the seasonal freezing period.

Ground temperature at a depth of 130 cm continuously remained below 0°C , except from a short period of 20 days with positive values (from early to mid-March), in which a maximum temperature of 0.05°C was attained. The mean temperature was -0.28°C , and the minimum temperature occurred in early spring (end of September) and was -1.39°C . Short-term temperature fluctuations have been completely filtered at this depth, and only the annual cooling and warming cycle is observed.

Discussion

Evidence of the occurrence of perennial frozen ground in the summit area is provided by the temperature records obtained in the shallow borehole. Ground temperature at a depth of 1.3 m remained subzero almost year-round (mean temperature was -0.28°C), except for a short period in late summer (from early to mid-March), when it experienced slightly above 0°C values.

Winter short-term fluctuations observed in the surficial level of the borehole suggest the presence of a thin snow cover. The summit is swept by persistent and strong winds, limiting snow cover build-up. Direct exposure to the cold atmosphere throughout winter takes place, allowing deep frost penetration into the ground. Bearing this evidence in mind, permafrost is estimated to occur at depths below ca. 1.5–2 m in the summit area.

The occurrence of permafrost in the upper Alvear Valley can only be inferred from the geomorphological evidence of activity observed in rock glaciers.

It is difficult to establish the lower altitudinal limit of the permafrost belt with the currently available data. However, if we consider the active rock glaciers of the upper Alvear Valley as permafrost indicators, then we can propose the approximate lower limit of discontinuous permafrost. This limit is roughly indicated by the elevation reached by rock glacier fronts (Barsch 1996). In our case, the lower limit of discontinuous permafrost would be at ca. 800–775 m a.s.l. Patches of sporadic permafrost could exist at lower elevation in particularly suitable topoclimatic locations.

The suggested limit is lower than that proposed by Corte (1997), who estimated the lower limit of permafrost in the mountains of Tierra del Fuego to be at 900 m a.s.l.

Conclusions

Preliminary observations suggest the occurrence of permafrost at 1057 m. a.s.l. in the unnamed summit located to the E of Mount Alvear and the Eastern Alvear Glacier, at depths below ca. 1.5–2 m. However, a longer time series from the summit borehole is needed to obtain definitive results.

The lower limit of the discontinuous permafrost in the studied area is tentatively placed at ca. 800–775 m a.s.l., according to the elevation reached by the front of active rock glaciers.

Further research is needed in order to gain a better understanding about mountain permafrost distribution and characteristics in the Sierras de Alvear. Proposed future work comprises geoelectric surveys and the drilling and equipment of new shallow boreholes (particularly in the rock glaciers of the the upper Alvear Valley).

Acknowledgments

The authors want to thank Professor Hugh M. French for his help and valuable suggestions during the 2007 field season. Thanks are also due to Mr Luis Lavado, helicopter pilot, for his logistical support. Two anonymous reviewers provided valuable comments that helped to improve the initial version of the paper. Their advice is greatly appreciated. This research has been funded by the Ministerio de Educación y Ciencia (Spain) projects CGL2004-03380/BOS and POL2006-09071, and it is a contribution to the International Polar Year.

References

- Barsch, D. 1996. *Rockglaciers. Indicators for the Present and Former Geoecology in High Mountain Environments*. Berlin: Springer-Verlag, 331 pp.
- Corte, A. 1997. *Geocriología. El Frío en la Tierra*. Mendoza, Ediciones Culturales de Mendoza, 398 pp.
- Olivero, E.B. & Martinioni, D.R. 2001. A review of the geology of the Argentinian Fuegian Andes. *Journal of South American Earth Sciences* 14: 175-188.
- Tuhkanen, S. 1992. The climate of Tierra del Fuego from a vegetation geographical point of view and its ecoclimatic counterparts elsewhere. *Acta Botanica Fennica* 145: 1-64.
- Valcárcel-Díaz, M., Carrera-Gómez, P., Coronato, A., Castillo-Rodríguez, F., Rabassa, J. & Pérez-Alberti, A. 2006. Cryogenic landforms in the Sierras de Alvear, Fuegian Andes, Subantarctic Argentina. *Permafrost and Periglacial Processes* 17(4): 371-376.

Appearance of Heinrich Events on Pollen Plots of Late Pleistocene Ice Wedges

Alla C. Vasil'chuk

Geography Department, Lomonosov's Moscow University, Moscow, Russia

Yurij K. Vasil'chuk

Geography and Geology Departments, Lomonosov's Moscow University, Moscow, Russia

Abstract

The palynological characteristics of large ice wedges and surrounding syngenetic yedoma sediments at three locations in the Lower Kolyma River Valley in northeast Yakutia are presented. AMS ^{14}C dating of micro-organic and pollen concentrates from the ice wedges reveal sharp oscillations of pollen and spore spectra, and permit correlation of these rhythms with Heinrich events. The variability of global, regional, and local pollen components in yedoma sediments linked with periodical rhythms is discussed.

Keywords: ice wedge; Heinrich events; pollen; Yakutia.

Introduction

Coolings of the North Atlantic Ocean associated with Heinrich events appeared throughout the various natural systems at global and regional scales. For example, traces of Heinrich events are recorded in sediments of Lake Baikal as variations in diatoms and Fe(II)/Fe(III) ratios (Grygar et al. 2006), and maximum terminal position of glaciers in the Swiss and Austrian Alps (Ivy-Ochs et al. 2006). Regional response of Siberian landscapes linked to the North Atlantic's thermohaline circulation is indicated by oxygen-isotope analysis of syngenetic ice wedges and by pollen data from well-dated cross-sections of ice-wedge complexes. Simulation of Late Pleistocene circulation (Sarnthein et al. 2002, Lowe et al. 2006) shows that there was positive feedback for the northern Eurasian region. We suppose that Heinrich Events were characterized as times of low summer temperatures. Hence pollen spectra could be potential archives of Heinrich Events. Pollen is well preserved in ice-wedge ice because of low temperatures, the stable conditions of this closed system and the low microbial activity. ^{14}C dating of fossil pollen grains contained in ground ice could therefore provide new information about past environments. The pollen concentration in ice wedges is very similar to those of Arctic ice caps: approximately 10 to 1000 grains/l. As with Arctic ice caps (Bourgeois 2000), the pollen assemblages from ice wedges in arctic and subarctic tundra comprise a high percentage of far-travelled pollen, primarily tree pollen. The regional tundra pollen input is essential also, and the local pollen contribution is very small. The penecontemporaneous pollen grains and spores are also found in ice wedges (Vasil'chuk et al. 2003, 2005a, b, Vasil'chuk 2005, 2007).

To interpret the pollen variations in ice wedges and their host sediments we apply Yu.Vasil'chuk's (1992) multistage model of large syngenetic ice-wedge ice formation. The ice wedges develop as large pulses of subaqueous deposition alternate with subaerial conditions of ice-wedge growth. The main water source for ice wedges is snowmelt water during the subaerial stage and mixtures of snowmelt, river or lake water during the subaqueous stage. Water enters frost

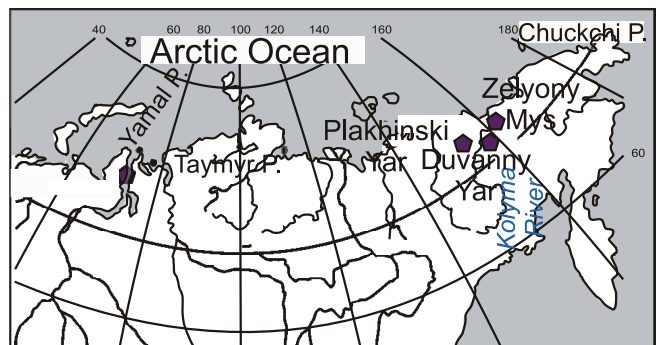


Figure 1. Location of ice-wedge sections in the Lower Kolyma River area of northeast Yakutia: Duvanny Yar, Plakhinskii Yar, and Zelyony Mys.

cracks in spring, when snow melting and flooding take place. During the subaqueous stage "reworked" pollen and spores may enter into ice wedges.

Regional Setting

The locations of the study sites in the Lower Kolyma River area of northeast Yakutia are shown in Figure 1. Vertical cross-sections through ice-wedge complexes were examined at Duvanny Yar, (69°N, 158°E); at Plakhinskii Yar, on the left bank of the Stadukhinskaya stream (68°40'N, 160°17'E); and At Zelyony Mys (70°N, 160°E), in northern taiga near the boundary with forest tundra. The mean winter air temperature is -22°C. This sequence with a depth of 22–24 m is especially valuable for palaeogeographical reconstruction because of the abundance of multistage ice wedges. The dominance of herb immature pollen indicates a very short vegetation period.

Results and Discussion

The Plakhinskii Yar exposure reveals syngenetic permafrost sediments with thick ice wedges. Here we present the results of a palynological study of ice wedges (16 samples) and the surrounding sediments (30 samples).

The pollen plot from sediments is dated by ^{14}C from 26 to 11 kyr BP, and the ice wedges are dated from 17 to 11 kyr (Fig. 2).

The sediments are characterized by a dominance of immature herb pollen (55.8–97.0%). Two intervals of very short vegetation periods are identified on the pollen plot: 24–21 kyr BP (9–12 m) and 17–11 kyr BP (3–6 m).

Larix pollen is found at a depth of 6.3 m in the sediments and also in the ice wedge at a depth of 8.2–8.8 m. The difference may be the depth of frost cracking at that time.

Every maximum of immature pollen comes before a local maximum of *Artemisia* and *Pinus pumila*. The pollen spectra of ice wedges show regional vegetation changes from 14 to 17 kyr; i.e., during the first Heinrich event. The *Artemisia* maximum (36.6%) coincides with a local maximum of immature pollen (42.2%) and a minimal amount of *Betula nana* pollen.

In the upper part of the plot the *Artemisia* content decreases and *Poaceae* increases together with *Selaginella sibirica* and *Pinus pumila*.

There are three development stages of vegetation cover. The first stage is single *Larix* trees, *Betula* sect. *Nanae* and *Poaceae-Artemisia* grass tundra. The second stage is the maximum development of herbaceous nival meadows (a very short vegetation period) with *Artemisia*. The third stage is grassland tundra.

Because the ^{14}C dates approximately correlate with H1, we suggest that pollen phase changes indicate this global climatic change. The structure of H2, according to ^{14}C -dates (21–23 kyr BP), can be followed only in the pollen plot of the sediments. The indicator of most extreme conditions is the maximum immature pollen, comes before the local *Artemisia* maximum (Vasil'chuk 2005, 2007).

The *Zelyony Mys* 36 m exposure of ice wedges occurs in loamy syngenetic sediments. There is no organic material in the upper 10 m. The lower 26 m consist of three layers of high and low peat content. Large ice wedges have shoulders at levels of peaty layers. The tops of small ice wedges are located at the level of the shoulders. The cryogenic structure is caused by subaqueous conditions of sedimentation and subaerial freezing of the sediment, together with peaty layers and ice-wedge growth (Vasil'chuk 1992).

According to the ^{14}C -dates, the duration of the subaerial stage is about 2–3 kyr, and that of the subaqueous one is about 1–1.5 kyr. From 37 to 27 kyr BP there were three subaerial periods. Gophers' holes mark subaerial horizons, when ice wedges grew in width. Seeds from the holes are dated at 30.5 and 32.8 kyr.

Figure 3 shows the results of a palynological study of ice wedges (11 samples) and the surrounding sediments (45 samples). The pollen plot of the sediments is dated by ^{14}C from 36–38 to 22–23 kyr BP, and the ice wedges date from 27 to 13 kyr. Every maximum of immature pollen corresponds with a local maximum of *Selaginella sibirica* and a local minimum of *Pinus pumila*. Most *Varia* is represented by *Brassicaceae* and *Rosaceae*. The seeds and pollen of *Potentilla nivea* L., *Draba cinerea* Adam., *Ranunculus repens* L., are found in

gophers' holes at a depth of 5–15 m (Vasil'chuk 2005).

Simultaneous changes in both local and regional components indicate regional or global changes of seasonal vegetation conditions. Maxima of *Pinus sibirica* are located immediately under peaty layers. Peaty layers contain high concentrations (up to 26%) of shrub pollen, mainly *Betula* sect. *Nanae*. But shrub remains have not been found.

There are three rhythms in the pollen plot of sediments, expressed by variations of local and regional components. At the base of the lower rhythm, the maximum percentages of *Selaginella sibirica* (about 40%) are replaced with maximum percentages of *Artemisia* (14.2%), *Poaceae* (16.4%) and *Betula* sect. *Nanae* (18.1%).

The most unfavorable conditions (very short vegetation season) are recorded by maximum percentages of unmatured pollen in the peaty layer at a depth of 24–22 m. The peat contains "reworked" organic material, as indicated by inverted ^{14}C dates. There is no penecontemporaneous pollen, but the content of coal particles is about 250%. Then the percentages of unmatured herb pollen decreases from 87 to 19%. Simultaneously there are increases in the content of *Pinus sylvestris* (21%) and *Betula* sect. *Nanae*. (19%) together with twin peaks of *Selaginella sibirica* (37–41%).

We suggest that sediments at a depth of 22 m accumulated at the erosion level caused by H3, about 29–27 kyr BP.

The next rhythm has another structure. The peak of *Betula* sect. *Nanae* (22.5%) is replaced with a maximum of *Pinus sylvestris* (19.8%), *Selaginella sibirica* (29.2%) and a very low content of *Poaceae*. This "suggests an" increase of the accumulation rate of sediments at the thermal minimum and subsequent improvement of vegetation season conditions.

Due to difference of the scales between the plots of sediment and ice wedges, we can look after regional changes of pollen rain of this rhythm at the pollen plot of the ice wedge. The maximum *Poaceae* and *Selaginella sibirica* is replaced by a *Pinus sylvestris* peak continuous with maximum percentages of *Varia* at a depth of 20–18 m. According AMS- ^{14}C dates of ice and the similar variations of regional components, we suggest that this rhythm coincides with H2 (about 23 kyr BP).

In the upper part of the pollen plot, *Pinus sylvestris* pollen disappears. The same variation of pollen is observed as at Plakhinskii Yar, and is correlated with H2. The *Artemisia* maximum is replaced by a peak of immature *Varia* pollen. The content decreases and *Poaceae* increases together with *Selaginella sibirica* and *Pinus pumila*. The final stage of H2 is absent in the ice-wedge record.

In the *Duvanny Yar* exposure large syngenetic ice wedges occurred in a 55 m thick section of loam (Fig. 4). The wedges are up to 3–3.5 m wide in the bottom of the cross-section, and up to 1.0–1.5 m wide in the upper part.

On the basis of more than 50 ^{14}C conventional dates of the host sediments we conclude that ice-wedge formation occurred from 37 to 17 kyr BP (Fig. 4). The age of the beginning of sediment accumulation is confirmed by a ^{14}C date of 31,200 yr BP from ice-wedge ice at a height about 6 m above sea level (Fig. 3), as well as by AMS ^{14}C dating of

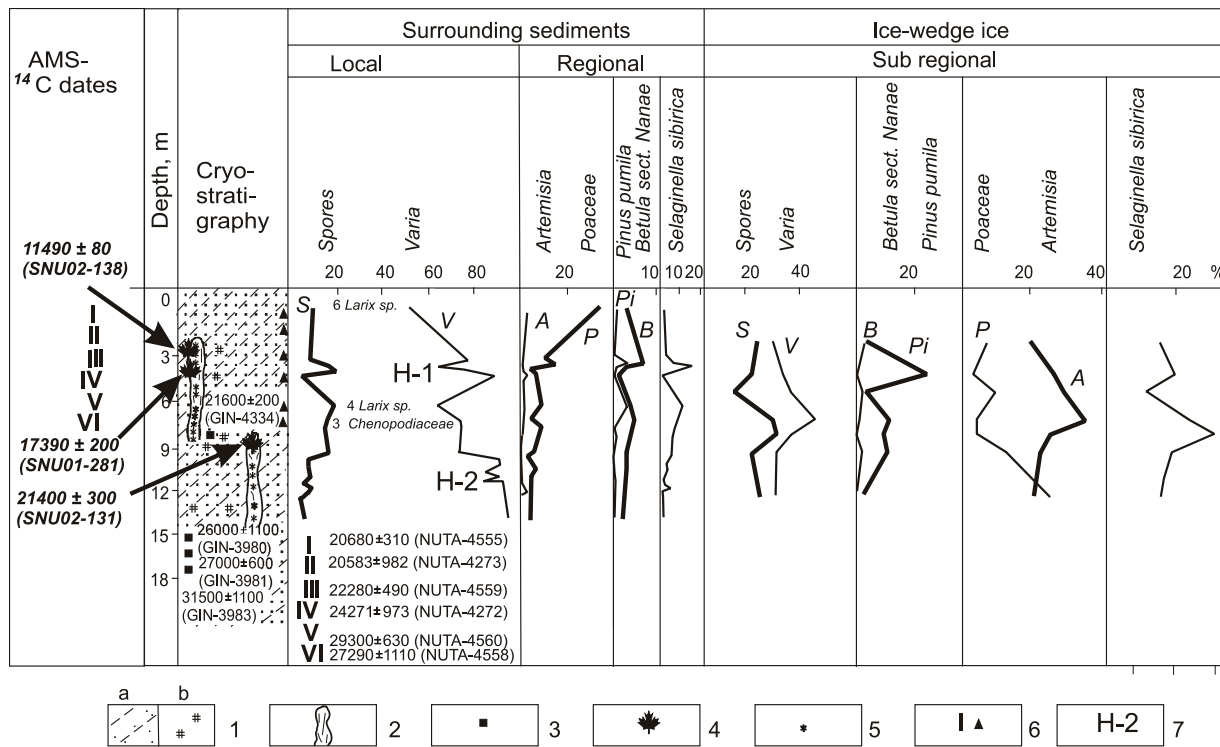


Figure 2. Pollen and spores plot of Plakhinskii Yar ice-wedge cross-section (after Vasil'chuk 2007 with corrections): 1 – sediments: a – sandy loam, b – peat remains in edoma sediments, 2 – large syngenetic ice wedges 3 – sampling point in surrounding sediments for radiocarbon dating; 3–4 sampling point of for AMS radiocarbon dating; 3–of micro organic from ice-wedge ice 4 – of pollen concentrate from ice-wedge ice, 5 – 6 – sampling point for palynological analysis: 5 – from surrounding sediments, 6 – from ice-wedge ice; 7 - a cold phase of Heinrich events on pollen curve. Latin letters near to pollen curves indicate first letter of the name of the appropriate plant. NUTA – radiocarbon dates of Fukuda et al. (1997).

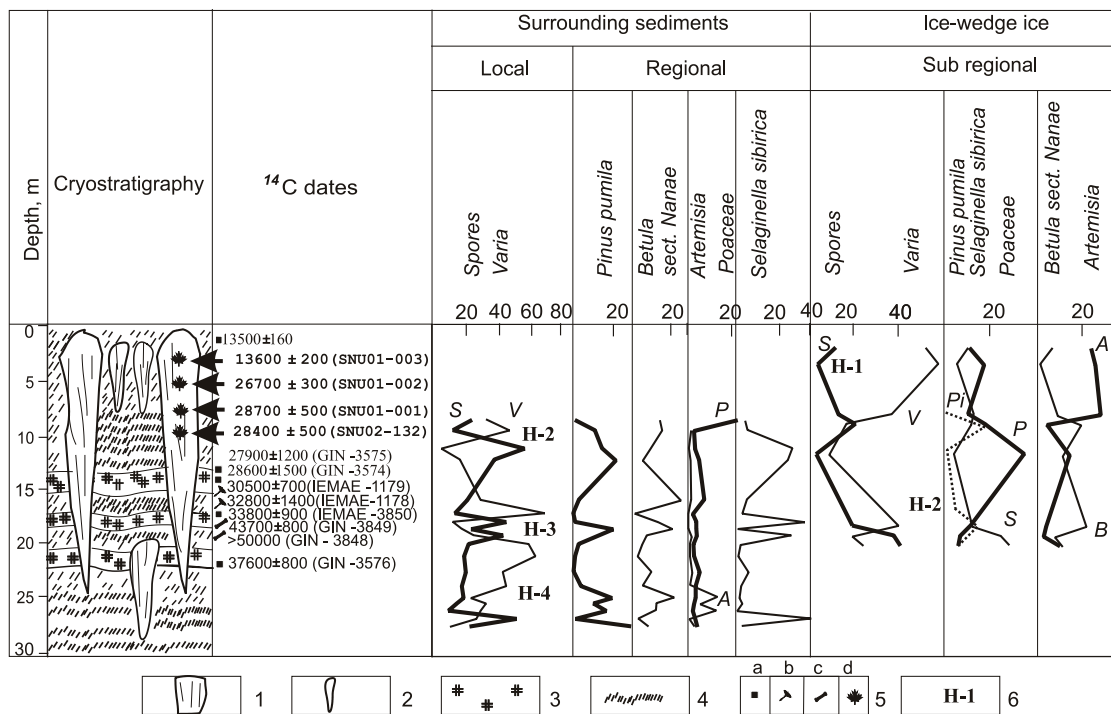


Figure 3. Pollen and spores plot of the Zelyony Mys ice-wedge cross-section: 1 – large syngenetic ice wedge 2 – small buried ice wedge 3 – peat remains; 4 – sandy loam; 5 – sampling point for ¹⁴C dating: a – rootlets, b – seeds, c – bones; d – micro organic remains ≤ 200µm; 6 – cold phase of Heinrich events on pollen curve. Latin letters near the pollen curve indicate first letter of the name of the appropriate plant.

separate fractions of plant organic material separated using a microscope from samples of mixed plant detritus.

Here we present the results of a palynological study of sediments (93 samples) and their contained ice wedges (23 samples). The pollen plot of sediments dated by ¹⁴C is from 31 to 14 kyr BP. The ice wedges have been dated from 25 to 14 kyr BP (Vasil'chuk 2007, Vasil'chuk & Vasil'chuk 1998, Vasil'chuk et al. 2004).

A main feature of the Duvanny Yar pollen plot is the stable ratio between local components. This suggests that sediment accumulation took place during stable local conditions. Various herbs and *Selaginella sibirica* represent local vegetation. Minimal salt concentrations correspond to high percentages of *Varia* and *Poaceae*, whereas maximum salt concentration corresponds with a peak of *Selaginella sibirica*.

Larix pollen is found in ice wedges, indicating that larch

occurred as isolated trees in that vegetation community. The three small peaks of *Artemisia* percentages (4.5–5.1%) indicate short-term dry periods. It is possible to assume that the sediment at the depth of 15–19 m accumulated at 27–29 kyr BP and corresponds to H3. It is also possible to correlate an increase of *Poaceae* with a warm phase, and a subsequent maximum of *Artemisia* with H2 (21–23 kyr BP). In the upper part of the plot is observed a typical distribution of the components for H1 (16.5–14 kyr BP).

Pollen spectra of ice wedges demonstrate regional peculiarities of two rhythms of vegetation cover changes. The lower one, at a depth of 11.6–21 m, is similar to the lower rhythm of the ice-wedge plot of Zelyony Mys. The maximum spores percentages correspond with the *Poaceae* peak, which is replaced by *Artemisia* and then by *Varia* peak. We equate this rhythm with H2 (21–23 kyr BP).

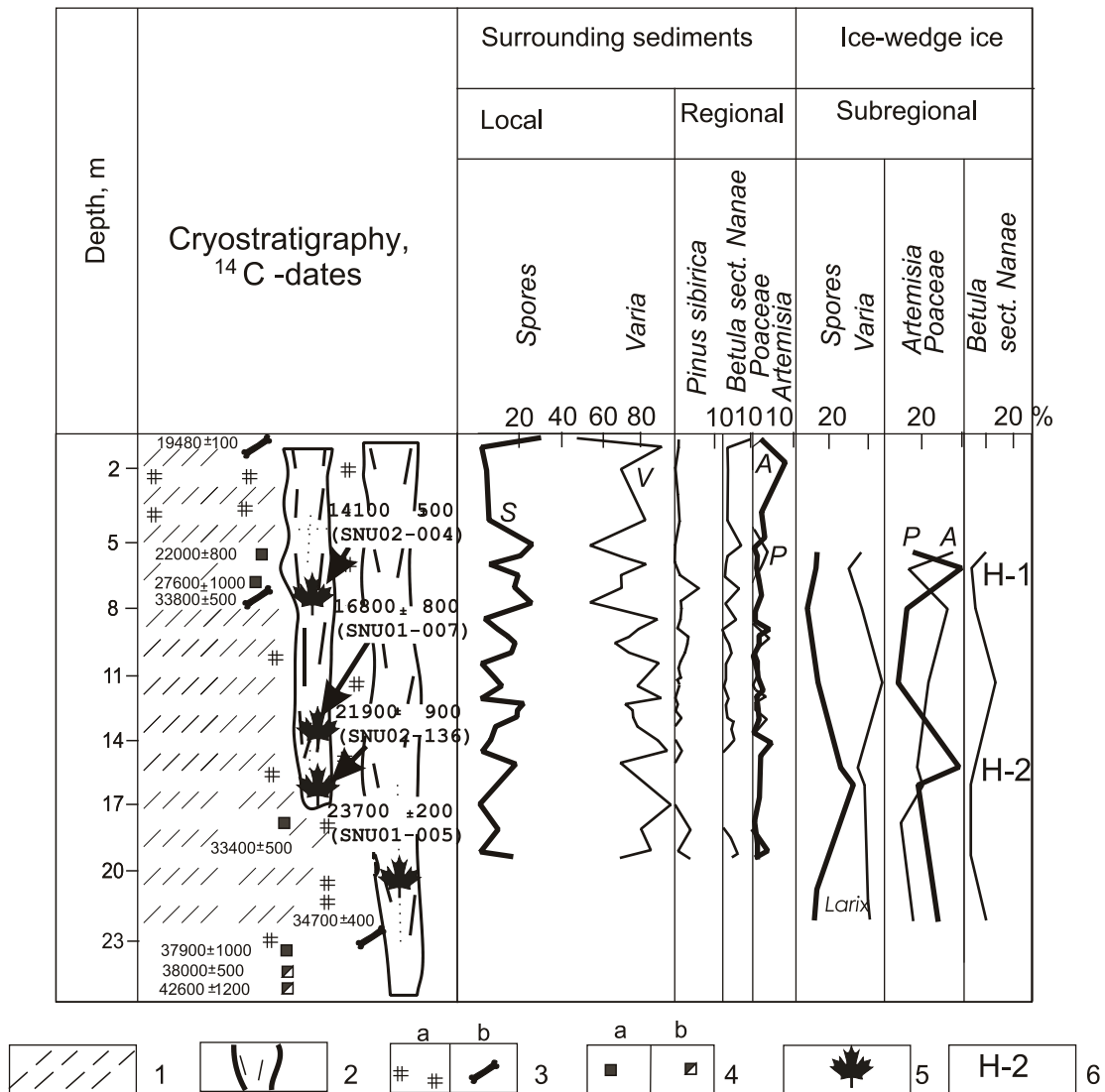


Figure 4. Pollen and spores plot of Duvanny Yar ice-wedge cross-section (after Vasil'chuk 2007 with corrections): 1 – sandy loam; 2 – large syngenetic ice wedge; 3-a – plant remains and peat, b – bones; 4 – sampling point for radiocarbon dating: a – rootlets, b – branches; 5 – sampling point from ice-wedge ice: for AMS ¹⁴C dating, of pollen concentrate; 6 – a cold phase of Heinrich events on pollen curve. Latin letters near to pollen curves indicate first letter of the name of the appropriate plant.

The structure of upper rhythm (11.6–5.5 m) is similar to variations of the main components observed in ice wedges of Plakhinskii Yar. The fluctuations of the contents of *Poaceae* and *Artemisia* pollen are opposite. The *Betula* sect. *Nanae* peak follows *Artemisia*. This rhythm corresponds to H1 (16.5–14 kyr BP).

Changes of vegetation cover are found at the same time intervals. They may correspond with Heinrich events (Bond et al. 1997, Veiga-Pires et al. 1999, Vidal et al. 1999, Ivy-Ochs et al. 2006, Parnell et al. 2007, Sepulchre et al. 2007). Every event has a specific appearance.

H1 is divided into three phases on the basis of pollen plots of the syngenetic sediments and ice wedges. The first pollen phase corresponds to relatively high temperatures and normal humidity, nival meadows and Pleistocene mesic tundra with a mosaic of shrubs and trees (*Betula* and *Larix*).

The second phase corresponds to low temperatures during the vegetation growth season, a very short vegetation season, low humidity and a maximum distribution of nival meadow vegetation (*Varia* and *Selaginella sibirica* or *Bryales*). The regional pollen rain is characterized by a prevalence of *Artemisia* pollen. The third phase corresponds to relatively high temperatures and increased humidity. *Poaceae* and *Varia* are prevalent and *Pinus pumila* pollen is represented in the regional pollen rain.

H2 is expressed by a change of a combination of peaks of *Poaceae* and *Selaginella sibirica*, by maximum immature pollen of *Varia* and then by the appearance of *Pinus sylvestris* pollen. This rhythm in the Lower Kolyma plain was asymmetrical.

The warm phase before the thermal minimum was relatively dry and long in comparison with the thermal minimum stage. A difference between the local and regional pollen rain was observed. The maximum distribution of vegetation of nival meadows took place simultaneously with the appearance of *Pinus* pollen.

H3 is characterized by consecutive changes of local peaks of *Betula* sect. *Nanae*, *Poaceae* and *Artemisia* and the disappearance of *Pinus pumila*.

H4 is characterized by an absolute maximum of *Selaginella sibirica*, then a sharp decrease of the total concentration of pollen and then twin peaks of *Poaceae* and *Artemisia* and *Betula* sect. *Nanae* percentages growth.

These sharp oscillations of pollen and spores caused by global changes are recorded in other pollen plots of polygonal ice-wedge complexes of northern Eurasia. It is possible to find millennial scale events in Holocene ice-wedge complexes also as manifestations of a pervasive millennial-scale climate cycle operating independently of the glacial-interglacial climate state (Bond et al. 1997).

Acknowledgments

The authors are grateful to H. Jungner, J. van der Plicht and J.-C. Kim for ¹⁴C dating of pollen and micro inclusions in ice-wedge ice and organic material in host sediments.

Dr. Julian Murton kindly commented on and greatly

improved the original manuscript.

The work is partially financed by Russian Foundation for Basic Research (grants 05–05–64814 and 07-05-01100).

References

- Bond, G., Showers, W., Cheseby, M., Almasi, P., deMenocal, P., Priore, P., Cullen, H., Hajdas, I. & Bonani, G. 1997. A pervasive millennial-scale cycle in North Atlantic Holocene and glacial climates. *Science* 278: 1257–1266.
- Bourgeois, J.C. 2000. Seasonal and interannual pollen variability in snow layers of arctic ice caps. *Review of Palaeobotany and Palynology* 108(1-2): 17–36.
- Fukuda, M., Nagaoka, D. et al. 1997. Radiocarbon dating results of organic materials obtained from Siberian permafrost areas. Reports of Institute of Low Temperature Science. Sapporo. Hokkaido University: 17–28.
- Grygar, T., Kadlec, J., Pruner, P., Swann, G., Bezduka, P., Hradil, D., Lang, K., Novotna, K. & Oberhänsli, H. 2006. Paleoenvironmental record in Lake Baikal sediments: environmental changes in the last 160 ky. *Palaeogeography Palaeoclimatology Palaeoecology* 237: 240–254.
- Ivy-Ochs, S., Kerschner, H., Kubik, P.W. & Schluchter, C. 2006. Glacier response in the European Alps to Heinrich Event 1 cooling: the Gschnitz stadial. *Journal of Quaternary Science* 21(2): 115–130.
- Lowe J.A., Gregory J.M., Ridley J., Huybrechts P., Nicholls R.J. & Collins M. 2006. The role of sea-level rise and the Greenland ice sheet in dangerous climate change: implications for the stabilisation of climate. In: J. Schellnhuber, W. Cramer, N. Nakicenovic, T. Wigley & G. Yohe (eds.), *Avoiding Dangerous Climate Change*. Cambridge: Cambridge University Press, 29–36.
- Parnell, J., Bowden, S., Andrews, J.T. & Taylor, C. 2007. Biomarker determination as a provenance tool for detrital carbonate events (Heinrich events?): Fingerprinting Quaternary glacial sources into Baffin Bay. *Earth and Planetary Science Letters* 257(1-2): 71–82.
- Sarnthein, M., Kennett, J.P., Allen, J.R.M., Beer, J., Grootes, P., Laj, P., McManus, J., Ramesh R. & SCOR-IMAGES Working Group 117. 2002. Decadal-to-millennial-scale climate variability chronology and mechanisms: summary and recommendations. *Quaternary Science Reviews* 21(10): 1121–1128.
- Sepulchre, P., Ramstein, G., Kageyama, M., Vanhaeren, M., Krinner, G., Sanchez-Goni, M.-F. & d'Errico, F. 2007. H4 abrupt event and late Neanderthal presence in Iberia. *Earth and Planetary Science Letters* 258: 283–292.
- Vasil'chuk, A.C. 2005. *Pollen spectra formation features in permafrost areas of Russia*. Moscow: Moscow University Press, 247 pp.

- Vasil'chuk, A.C. 2007. *Palynology and chronology of polygonal ice wedge complexes in Russia permafrost area*. Ed.: Member of the Russian Academy of Natural Sciences, Professor Yuriy K.Vasil'chuk. Moscow: Moscow University Press, 488 pp.
- Vasil'chuk, A.C., Kim, J.-C. & Vasil'chuk, Yu.K. 2003. First radiocarbon dating of pollen and spores from syngenetic ice-wedge ice. *Proceedings of the Eighth International Conference on Permafrost, Zurich, Switzerland, 21–25 July 2003*: 1167-1172.
- Vasil'chuk, A., Kim, J.-Ch. & Vasil'chuk, Yu. 2005a. AMS ^{14}C dating of pollen concentrate from Late Pleistocene ice wedges from the Bison and Seyaha Sites in Siberia. *Radiocarbon* 47(2): 243-256.
- Vasil'chuk, A.C., Vasil'chuk, Yu.K. Kim, J.-Ch., van der Plicht J. & Sulerzhitsky, L.D. 2005b. Appearance of Heinrich events in radiocarbon dated pollen and spores diagrams of ice-wedge ice and its surrounding Edoma sediments of Kolyma River. *Terra Nostra. 2nd European Conference on Permafrost. June 12-16, 2005. Potsdam, Germany. Abstracts*. AWI: 28-29.
- Vasil'chuk, Yu.K. 1992. *Oxygen isotope composition of ground ice application to paleogeocryological reconstructions* (in Russian, with English the contents, all figure captions and appropriate summary). Theoretical Problems Department, Russian Academy of Sciences and Moscow University publ., Moscow. V. I, 420 pp.; V. II, 264 pp.
- Vasil'chuk, Yu.K. & Vasil'chuk, A.C. 1998. ^{14}C and ^{18}O in Siberian syngenetic ice wedge complexes. *Radiocarbon* 40(2): 883-893.
- Vasil'chuk, Yu.K., van der Plicht, J., Jungner, H., Sonninen, E. & Vasil'chuk, A.C. 2000. First direct dating of Late Pleistocene ice-wedges by AMS. *Earth and Planetary Science Letters* 179(2): 237-242.
- Vasil'chuk, Yu.K., Kim, J.-C. & Vasil'chuk, A.C. 2004. AMS ^{14}C dating and stable isotope plots of Late Pleistocene ice-wedge ice. *Nuclear Instruments and Methods in Physics Research. Section B: Beam Interactions with Materials and Atoms* 223-224: 650-654.
- Veiga-Pires, C.C. & Hillaire-Marcel, C. 1999. U and Th isotope constraints on the duration of Heinrich events H0 – H4 in the southeastern Labrador Sea. *Paleoceanography* 14(2): 187-199.
- Vidal, L., Schneider, R.R., Marchal, O., Bickert, T., Stocker, T.F. & Wefer, G. 1999. Link between the North and South Atlantic during the Heinrich events of the glacial period. *Climate Dynamics* 15(12): 909-919.

Dansgaard-Oeschger Events on Isotope Plots of Siberian Ice Wedges

Yurij K. Vasil'chuk and Alla C. Vasil'chuk

Geology and Geography Department, Lomonosov's Moscow University, Moscow, Russia,

Abstract

Hydrogen and oxygen isotope records with a resolution of 100–200 years were obtained from ice-wedge ice at four locations in Siberia. Micro-organic inclusions and pollen concentrates from ice wedges allowed precise AMS radiocarbon dating of the isotope records and comparison with GISP2 and GRIP ice cores. Separate Dansgaard-Oeschger events are distinguished within the ice-wedge ice and correlated with the Greenland ice cores.

Keywords: Dansgaard-Oeschger events; ice wedge; radiocarbon; stable isotope.

Introduction

Isotope records of Siberian ice wedges have become available from 50 sequences of syngenetic permafrost sediments of northern Eurasia (Vasil'chuk 1992, 2006). Late Pleistocene and Holocene syngenetic ice wedges have been studied throughout the Yamal Peninsula to the Chukotka and Magadan regions, and from northern Yakutia to the Aldan and Vilyui River valleys and to the Chara depression (Trans-Baikal Region) (Vasil'chuk 1992). At first we inferred a local origin for dramatic cyclic oscillations of stable isotope values within ice-wedge ice. However, the first radiocarbon dates of micro inclusions, alkaline extract and pollen concentrate directly in ice-wedge ice (Vasil'chuk 1992, 2006, Yu. Vasil'chuk et al. 1999, 2000, 2001, 2004, Vasil'chuk & Kotlyakov 2000) have fixed stable isotope curves of ice wedges onto a ^{14}C scale, allowing us to evaluate the duration of the oscillations.

A variety of multi-millennial oscillations from ice wedges with a dominant periodicity of ca. 1.5 kyr was obtained. Several parameters of ice-wedge isotope curves show some correlation with the GISP2 and GRIP $\delta^{18}\text{O}$ records (Dansgaard et al. 1993, Grootes et al. 1993, Jouzel et al. 2007), although not all of the same amplitude or frequency. Such changes might be associated with the response of winter temperatures in Siberia to freshwater anomalies in the North Atlantic, which dramatically reduce the transport of the meridional overturning cell. This paper addresses this question with ice wedge records dated by ^{14}C AMS. Four ice-wedge complexes are located in Yakutia, and one is in northwest Siberia. This enables us to follow the changes depending on longitude and distance from the Atlantic.

Regional Setting

We present several cross-sections with syngenetic ice wedges studied in detail. The Seyaha cross-section is located in typical tundra of northwest Siberia. Sections at Duvanny Yar, Plakhinskii Yar and Bison are located in forest tundra in the Lower Kolyma River Valley in northeastern Yakutia, and one at Mamontova Gora is located in taiga in Central Yakutia (Fig. 1). The ice wedges of these cross-sections have been dated directly by ^{14}C AMS.

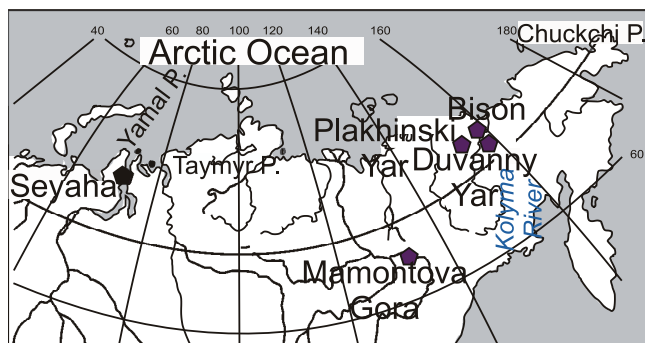


Figure 1. Location of Siberia ice wedge sections: Seyaha cross-section ($70^{\circ}10'\text{N}$, $72^{\circ}34'\text{E}$, Yamal Peninsula, northwest Siberia), Duvanny Yar (69°N , 158°E , Lower Kolyma River, northeast Yakutia), Plakhinskii Yar ($69^{\circ}40'\text{N}$, $160^{\circ}17'\text{E}$, Lower Kolyma River, northeast Yakutia), Bison ($68^{\circ}15'\text{N}$, $150^{\circ}45'\text{E}$) (Lower Kolyma River, northeast Yakutia).

Dating Strategy

Many parts of cross-sections from modern permafrost areas can be dated by ^{14}C ; however, date-inversions are common in permafrost, and this requires a special study.

In Arctic regions inversion of dates on different fractions of organic material is more likely the rule than an exception (Vasil'chuk & Vasil'chuk 1997). Contamination by old material is the main problem in ^{14}C dating of permafrost sediments because of the low decay rate of organic material and repeated re-deposition of old organic material (Nelson et al. 1988). The search for the most reliable subject for dating is a prominent part in a dating strategy for syngenetic permafrost sediments. So we suppose that the youngest ^{14}C date from a number of dates of various fractions of the same sample or from the same layer is the most reliable method for determining the apparent age of syngenetic permafrost sediments and ice wedges.

Several different fractions were dated in the ice wedges, including organic micro-inclusions, alkali extracts and pollen concentrates. The micro-inclusions most likely originated from contemporaneous plant material and in most cases provided the youngest dates. Alkali extracts were older than micro-inclusions, with the difference between them ranging from 1100 years to more than 7900 years. It is evident that

there is a correlation between ^{14}C -dates of pollen concentrate and re-deposited pollen and spores content. The youngest date corresponded to the minimum amount of re-deposited pollen and spores. This indicates a high probability of old organic contamination in organic material within permafrost. In a case like that it is impossible to calibrate AMS dates from ice-wedge complexes. So the comparison of ice-wedge isotope profiles with GRIP and GISP curves is approximate and the correlations could be done with shifts of 1500–2000 years.

However, in such a case where pollen concentrate from syngenetic ice wedges was relatively free from organic particles and contained well-preserved pollen and spores of typical Late Pleistocene tundra plants (dwarf birch and especially thin-walled pollen such as *Salix* or *Liliaceae*), the pollen concentrate ^{14}C date was the youngest (Vasil'chuk et al. 2005). The youngest numbers of ^{14}C AMS dates are utilized for dating of isotope profiles. The majority of them are the dates of micro-organic material; some dates are from pollen concentrate (Fig. 2, Table 1). In any case, the youngest date was picked as a base of ^{14}C scale.

AMS dating of ice wedges confirms the vertical stratification of ice-wedge ice, that is, where younger ice is located above older ice (i.e., syngenetic accumulation).

Results

Hydrogen and oxygen isotope records from ice-wedge ice with a resolution of 100–200 years were obtained from well-dated Siberian cross-sections. In each case the isotope profile was sampled along the axis of a single ice wedge.

1. Seyaha cross-section: the $\delta^{18}\text{O}$ values range from -25.0 to -20.4‰ (modern ice wedge $\delta^{18}\text{O}$ values range from -19.0 to -17‰). Direct ^{14}C AMS dates of micro-inclusions from ice are from 14,700 to 20,900 yr BP.
2. Duvanny Yar cross-section: $\delta^{18}\text{O}$ values range from -32.7 to -28.7‰ (modern ice wedge $\delta^{18}\text{O}$ values range from -24 to -27‰). Direct ^{14}C AMS dates of micro-inclusions from ice are from 14,100 to 25,900 yr BP.
3. Plakhinskii Yar cross-section: $\delta^{18}\text{O}$ values range from -34.7 to -28.7‰ (modern ice wedge $\delta^{18}\text{O}$ values range from -24 to -27‰). Direct ^{14}C AMS dates of micro inclusions from ice are from 11,400 to 21,400 yr BP.
4. Bison cross-section: $\delta^{18}\text{O}$ values range from -33.79 to -28.7‰ (modern ice wedge $\delta^{18}\text{O}$ values range from -24 to -27‰). Direct ^{14}C AMS dates of micro inclusions and pollen from ice are from 26,400 to 32,600 yr BP.
5. Mamontova Gora cross-section: the $\delta^{18}\text{O}$ values range from -29.0 to -25.4‰ (modern ice wedge $\delta^{18}\text{O}$ values range from -19.0 to -17‰). Direct ^{14}C AMS dates of micro inclusions from ice are from 18,900 to 13,900 yr BP. ^{14}C dating of stable isotope records from the ice-wedge ice shows millennial scale changes of isotope composition. These oscillations can be compared with Greenland ice-sheet records. The plots from each ice-wedge system could be separated into episodes correlating with Dansgaard-Oeschger events lasting

1–2.5 kyr (Fig. 2). AMS ^{14}C dates of the ice yields the age of the stable isotope shift.

The key points for the comparison of the ice-wedge ice record are found at the GISP2 and GRIP $\delta^{18}\text{O}$ records as positive shifts at the stable isotope curves.

The large $\delta^{18}\text{O}$ oscillations recorded in the Seyaha ice-wedge ice are ^{14}C dated to between 20,900 and 14,000 yr BP (Fig. 2a). A positive shift of $\delta^{18}\text{O}$ values of almost 4‰ and then a negative one of 4.2‰ from 17 to 15 m depths (dated about 17–15 kyr BP) in ice-wedge ice corresponds to a warm oscillation of D/O event 1 in the Greenland record: the Bølling and Allerød episodes.

Detailed AMS dating of Bison ice-wedge ice is based on 6 micro-organic dates and 5 pollen concentrate dates, allowing selection of the youngest dates from 32,600 up to 26,400 yr BP (Fig. 2b). The stable isotope record of this cross-section can be compared with some parts of the GISP2 ice core. Several episodes can be correlated with from 3 to 7 D/O events lasting 1–2 kyr. However, the shift of $\delta^{18}\text{O}$ values in this section is negligible (from -33.2 up to -32‰). This fact could be caused by reduced climatic response on global changes.

Similar to the Seyaha stable isotope profile, a significant oscillation of $\delta^{18}\text{O}$ values is observed in the upper part of Plakhinskii Yar ice-wedge ice record, which is ^{14}C dated 21,400–11,400 yr BP (Fig. 2c). A positive shift of $\delta^{18}\text{O}$ values of almost 4‰ and then a negative one of 3.5‰ from 4.5 to 1.5 m depths (dated about 15–11.5 kyr BP) in ice-wedge ice corresponds to D/O event 1 and possibly D/O event 2.

Oscillating $\delta^{18}\text{O}$ values are observed in the middle part of Duvanny Yar ice-wedge ice record, which is ^{14}C dated 23,700–14,100 yr BP (Fig. 2e). A positive shift of $\delta^{18}\text{O}$ values of about 4‰ and then a negative one in ice-wedge ice corresponds to D/O event 1. A second oscillation in underlying ice dated about 22,000–23,000 yr BP probably corresponds with to D/O event 2.

The 3‰ oscillation of $\delta^{18}\text{O}$ values in the Mamontova Gora ice-wedge ice is dated about 14,000–15,000 yr BP (Fig. 2f). It may correspond to D/O event 1.

Discussion and Conclusions

Ice-wedge ice originates from snow. Such ground ice is a natural archive of climatic changes. There are some differences, however, between the palaeotemperature interpretation of ice cores and ice-wedge ice. Ice cores are repositories of past precipitation.

One of the backbones of ice-core palaeoclimate reconstructions is the use of δD and $\delta^{18}\text{O}$ stable isotopes in the ice, which have classically been interpreted as indicating local to regional temperature (Dansgaard 1964).

The tritium concentration is low in all ice samples. It does not exceed 1.5 TU, indicating the absence of any exchange processes of Late Pleistocene ice-wedge ice with the external environment and high preservation of primary properties of ice-wedge ice, including its isotope characteristics.

The starting point for the analysis is to decide on criteria for defining DO events and determining the transition times.

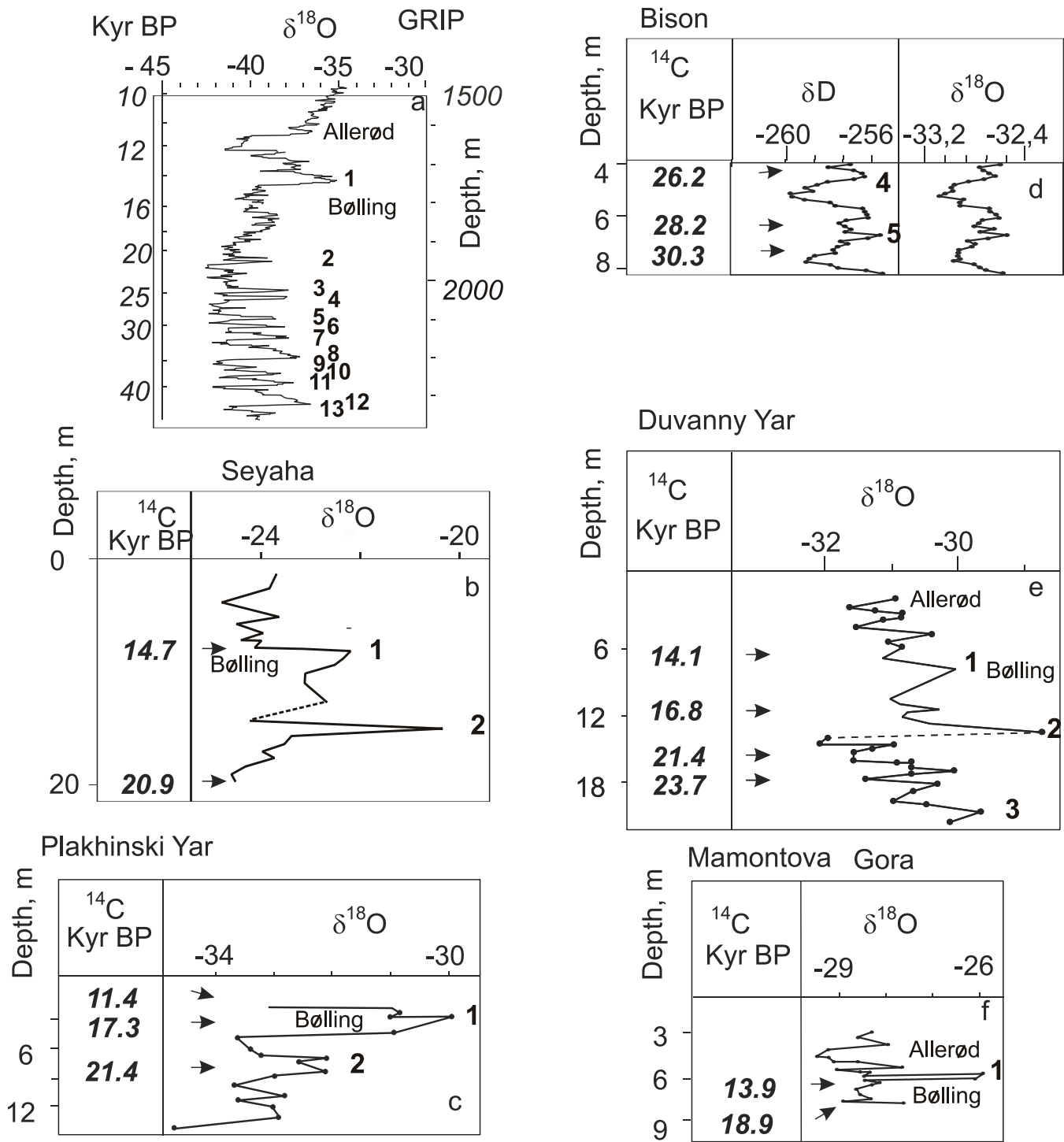


Figure 2. Comparison of Dangaard-Oeschger events of Siberian ice-wedge ice: a – fragment of GRIP ice core (Dansgaard et al. 1993); b – Seyaha cross-section, Yamal Peninsula; c – Plakhinski Yar, Lower Kolyma River; d – Bison, Lower Kolyma River; e – middle part of Duvanny Yar; Lower Kolyma River; f – Mamontova Gora, Aldan River. Numbers – suggested number of D/O event.

The “canonical” numbered DO events were identified visually (Dansgaard et al. 1993). Schulz (2002) defined the DO events from a positive 2 permil anomaly in the 12 kyr highpass filtered isotope signal. By that DO9 is disregarded. Rahmstorf (2003) defined a criterion for increase of 2 permil within 200 years on the 2 m sampled record (approx. 100 years lowpass). In this way DO9 is omitted and an event

“A” in the Allerød period is included. Alley et al. (2001) use a bandpass procedure by which 43 events in the glacial period were defined. Ditlevsen et al. (2005, 2007) defined first upcrossings of an upper level following upcrossings of a lower level as a criterion. In this way the critical dependence on the (arbitrary) lowpass filter and crossing levels is to a large extent avoided (Ditlevsen et al. 2005). Using this

Table 1. Direct AMS radiocarbon dates of organic micro inclusions from Siberian ice wedge.

Field number	Depth, m	AMS ¹⁴ C data BP	Lab. Number	δ ¹³ C, ‰
<i>Seyakha ice-wedge complex</i>				
363–YuV/27	1,8	14550 ± 100	GrA-10538	–25.7
363–YuV/87	12.0	14720 ± 100	GrA-10539	–26.3
363–YuV/125	20.6	20960 ± 140	GrA-10536	–26.1
<i>Plakhinsii Yar ice-wedge complex</i>				
311–YuV/6	3.9	13130 ± 130	SNU02-129	–23.3
311–YuV/18	3.9	11490 ± 80	SNU02-130	–30.4
311–YuV/21	4.5	17390 ± 200	SNU01-281	–40.4
311–YuV/29	8.6	21400 ± 300	SNU02-131	–25.9
<i>Bison ice-wedge complex</i>				
378–YuV/90	4.0	29500 ± 500	GrA-16802	–26.5
		26200 ± 300*	SNU02-147	
378–YuV/101	6.3	30430 ± 1500	GrA-12893	–26.1
378–YuV/100	7.6	32600 ± 700	GrA-16808	–26.1
		28200 ± 600*	SNU02-150	
378–YuV/102	7.6	30750 ± 550	GrA-16804	–26,2
		35600 ± 800*	SNU02-124	
378–YuV/103	7.6	30350 ± 550	GrA-16807	–26,3
<i>Mamontova Gora ice-wedge complex</i>				
335–YuV/24	2.6	17040 ± 100	SNU01-283	–31.5
335–YuV/27	3.2	19800 ± 600	SNU01-284	–40.9
335–YuV/33	5.0	19050 ± 180	SNU01-285	–29.8
335–YuV/13	5.7	16190 ± 250	SNU02-142	–22.9
335–YuV/12	5.9	13950 ± 200	SNU02-141	–23.1
335–YuV/5	6.9	18400 ± 400	SNU02-140	–32.4
335–YuV/2	7.2	18900 ± 200	SNU02-139	–26.8
<i>Duvanny Yar ice-wedge complex</i>				
320–YuV/15	7.0	14100 ± 500	SNU02-004	–30.3
320–YuV/17	11.6	20100 ± 1400	SNU02-137	–24.1
320–YuV/8	13.0	16800 ± 800	SNU01-007	–46.7
320–YuV/3	16.3	25800 ± 300	SNU01-006	–35.4
320–YuV/2	16.8	21900 ± 900	SNU02-136	–37.8

* AMS ¹⁴C dating of pollen concentrate

criterion several additional DO events are identified, such as DO2, which is split into two separate events.

The sampling of ice-wedge ice for isotope analysis with a vertical interval of 10–15 cm and a horizontal interval of 3–5 cm corresponds to a resolution of 60–100 years according to layer counting and ¹⁴C AMS dating. The isotope records of ice wedges are shorter in comparison with Greenland ice cores. Moreover, ice-wedge records may contain gaps when ice-wedge formation stopped.

Having ¹⁴C dated organic micro-inclusions in ice-wedges we can attempt to compare their stable isotope records with such records in polar ice. In the GRIP ice core, δ¹⁸O values from 35 to 25 kyr BP range from –38‰ to –43‰ (Dansgaard et al. 1993) This is a factor of two higher than that in simultaneous Bison ice wedges (from –33.25 to –32.40‰). Such sharp excursions could be caused by Atlantic ice cover changes, especially in summer, whereas winter conditions were much more stable. The 100-year resolution of the Bison ice wedge isotope record shows changes of mean

winter temperatures of the air. A number of matching points can be identified between the GRIP core and two fragments of ice wedges in Bison (see Fig.2). It is enough to identify similar sequences of major and minor events in the interval 35–25 kyr BP as in GRIP.

The d_{exc} values differ from those inherent in modern snow, d_{exc} – about 10‰. It is supposed that there was a difference in the mode of evaporation above the oceans during the Late Pleistocene, confirming the earlier data on small d_{exc} values for Late Pleistocene ice-wedge ice in comparison with Late Pleistocene Antarctic ice (Jouzel et al. 2007). Slight isotope variations of Bison ice-wedge ice do not give sufficient evidence for division into warm and cold periods from 25 to 35 kyr BP.

Late Quaternary climate instability implies rapid, closely linked changes in the Earth's environmental systems: hydrosphere, atmosphere, cryosphere and biosphere. Ice-wedge ice is one of the natural archives reflecting climatic changes. Direct AMS ¹⁴C dating of ice-wedges enabled

comparison of their stable isotope contents with those in polar ice. Ice wedges, however, cover a shorter time span than ice cores. By means of AMS ^{14}C -dating, paleoenvironmental proxies from ice wedges can be "stacked".

Variations of stable isotope ratios in ice wedges are similar to those in the ice cores. The range of $\delta^{18}\text{O}$ values from ice-wedge ice is about 2‰, indicating precipitation during wintertime and mean winter temperatures. In polar ice cores $\delta^{18}\text{O}$ is proportional to the difference between the mean annual temperature of the air above the inversion layer from which it was precipitated and the temperature of the precipitation source region. Atlantic ice cover changes especially in summer, whereas winter conditions were much more stable.

Several other ice-wedge sections have previously been analyzed (Vasil'chuk et al. 2005, Vasil'chuk 2006). At Zelyony Mys (69°N, 160°E, Lower Kolyma River) the ^{14}C dates range from 13,600 to 28,400 yr BP, and $\delta^{18}\text{O}$ values range from -34.1 to -29.4‰. At Mamontova Gora (64°N, 134°E, Aldan River) the ^{14}C dates range from 13,900 to 18,400 yr BP, and $\delta^{18}\text{O}$ values range from -29.4 to -25.9‰. At Phoenix (68°34'N, 158°34'E, Magadan Region) the youngest ^{14}C date is 11,000 yr BP, and $\delta^{18}\text{O}$ varies from -32.2 to -32.6‰ at the top to -24.9‰ at the bottom.

The most negative isotopic shifts are observed between 16.5–14 and 11–12 kyr BP. They demonstrate that a single spectral peak (indicating a ~1500 yr cycle) is characteristic of the records in both the Greenland ice sheet and Siberian ice wedges.

Especially interesting is the coincidence of D-O events 1 and 2 with distant ice-wedge sequences at Seyaha and Duvanny Yar.

Diverse palaeoclimatic evidence, including marine sediment data, pollen profiles, and glacial snow line data, indicates that the effects of at least some events were felt on a global scale (Broecker 1993). Recently well-dated curves with identifiable D-O events have been obtained for the last 10–60 kyr. Dansgaard-Oeschger events are described in the southern Aegean Sea (Geraga et al. 2005), by coccolithophores from the Gulf of Cadiz (NE Atlantic) and Alboran Sea (W Mediterranean) (Colmenero-Hidalgo et al. 2004), in bottom sediments in the Okhotsk Sea (Goldberg et al. 2005), and in the northern area of the East China Sea (Ijiri et al. 2005). Isotope records of Siberian ice wedges also demonstrate millennium scale oscillations (Vasilchuk et al. 2004). Stable oxygen and hydrogen isotope analysis of the ice in combination with adequate radiocarbon dates is one of the best tools available to obtain palaeotemperature information for the last 40 thousand years.

Several episodes lasting 1–2.5 kyr can be distinguished in isotope plots from each ice-wedge system. The AMS dates yields a precise age of the observed stable isotope shift. The ice-wedge records for northern Siberia are consistent in providing a chronological framework for this region. A ~1500 yr cycle characterizing both the Greenland ice sheet and Siberian ice wedges is observed.

Acknowledgments

The authors are grateful to Prof. H.Jungner, Dr. J. van der Plicht and Prof. J.-C.Kim for ^{14}C dating of pollen and micro inclusions in ice-wedge ice and organic material in host sediments, Prof. M.Geyh, Dr. W.Papesch, Prof. D.Rank and E.Sonninen for stable isotope analyses, and Dr. J.Murton for improvements to the final text.

The work is partially financed by Russian Foundation for Basic Research (grants 05–05–64814 and 07-05-01100).

References

- Alley, R.B., Anandakrishnan, S. & Jung, P. 2001. Stochastic resonance in the North Atlantic. *Paleoceanography* 16: 190-198.
- Broecker, W.S. 1993. *The glacial world according to Wally*. Palisades: Lamont-Doherty Earth Observatory of Columbia University. 318 pp.
- Colmenero-Hidalgo, E., Flores, J.-A., Francisco, J. Sierro, F.J., Ángeles Bárcena, M., Löwemark, L., Schönfeld, J. & Grimalt, J.O. 2004. Ocean surface water response to short-term climate changes revealed by coccolithophores from the Gulf of Cadiz (NE Atlantic) and Alboran Sea (W Mediterranean). *Palaeogeography, Palaeoclimatology, Palaeoecology* 205(3–4): 317-336.
- Dansgaard, W. 1964. Stable isotopes in precipitation. *Tellus* 16(4):436-468.
- Dansgaard, W., Johnsen, S.J., Clausen, H.B., Dahl-Jensen, D., Gundestrup, N.S., Hammer, C.U., Hvidberg, C.S., Steffensen J.P., Sveinbjornsdottir A.E., Jouzel, J. & Bond, G. 1993. Evidence for general instability of past climate from a 250-kyr ice-core record. *Nature* 364(6434): 218-220.
- Ditlevsen, P.D., Kristensen, M.S. & Andersen, K.K. 2005. The Recurrence Time of Dansgaard-Oeschger Events and Limits on the Possible Periodic Component. *Journal of Climate* 18: 2594-2603.
- Ditlevsen, P.D., Andersen, K.K. & Svensson, A. 2007. The DO-climate events are probable noise induced: statistical investigation of the claimed 1470 years cycle. *Climate of the Past* 3: 129-134.
- Geraga, M., Tsaila-Monopolis, S., Ioakim, C., Papatheodorou G. & Ferentinos, G. 2005. Short-term climate changes in the southern Aegean Sea over the last 48,000 years. *Palaeogeography, Palaeoclimatology, Palaeoecology* 220(3–4): 311-332.
- Goldberg, E.L., Gorbarenko, S.A., Shaporenko, A.D., Bosin, A.A., Leskov, V.Yh. & Chebykin, E.P. 2005. Instability of last glacial climate from SRXFA data for bottom sediments in the Okhotsk Sea. *Nuclear Instruments and Methods in Physics Research Section A: Accelerators, Spectrometers, Detectors and Associated Equipment* 543(1): 284-287.

- Grootes, P.M., Stuiver, M., White, J.W.C., Johnsen, S. & Jouzel, J. 1993. Comparison of oxygen isotope records from the GISP2 and GRIP Greenland ice cores. *Nature* 366(6454): 552-554.
- Ijiri, A., Luejiang Wang, L., Oba, T., Kawahata, H., Huang, C.-Y. & Huang, C.-Y. 2005. Paleoenvironmental changes in the northern area of the East China Sea during the past 42,000 years. *Palaeogeography, Palaeoclimatology, Palaeoecology* 219(3-4): 239-261.
- Jouzel, J., Masson-Delmotte, V., Cattani, O., Dreyfus, G., Falourd, S., Hoffmann, G., Minster, B., Nouet, J., Barnola, J. Chappellaz, M.J., Fischer, H. et al. 2007. Orbital and Millennial Antarctic Climate Variability over the Past 800,000 Years. *Science* 317: 793-796.
- Nelson, R.E., Carter, L.D. & Robinson, S.W. 1988. Anomalous radiocarbon ages from a Holocene detrital organic lens in Alaska and their implications for radiocarbon dating and paleoenvironmental reconstructions in the Arctic. *Quaternary Research* 29(1): 66-71.
- Rahmstorf, S. 2003. Timing of abrupt climate change: A precise clock. *Geophysical Research Letters* 30(10): 1029-1032.
- Raisbeck, G.M., Yiou F., Jouzel, J. & Stocker, T.F. 2007. Direct north-south synchronization of abrupt climate change record in ice cores using beryllium 10. *Climate of the Past Discussions* 3: 755-769. www.clim-past-discuss.net/3/755/2007/
- Schulz, M. 2002. On the 1470-year pacing of Dansgaard-Oeschger warm events. *Paleoceanography*. 17(2): 1014 – 1023.
- Vasil'chuk, A., Kim, J.-Ch. & Vasil'chuk, Yu. 2005. AMS ¹⁴C Dating of Pollen Concentrate from Late Pleistocene Ice Wedges from the Bison and Seyaha Sites in Siberia. *Radiocarbon*. 47(2): 243-256.
- Vasil'chuk, Yu.K. 1992. *Oxygen isotope composition of ground ice application to paleogeocryological reconstructions* (in Russian, with English the contents, all figure captions and appropriate summary). Theoretical Problems Department, Russian Academy of Sciences and Moscow University publ., Moscow, V. 1, 420 pp., V. 2, 264 pp.
- Vasil'chuk, Yu.K. 2006. *Ice wedge: Heterocyclity, Heterogeneity, Heterochroneity*. Moscow: Moscow University Press: - 404 pp.
- Vasil'chuk, Yu.K. & Vasil'chuk, A.C. 1997. Radiocarbon dating and oxygen isotope variations in Late Pleistocene syngenetic ice-wedges, northern Siberia. *Permafrost and Periglacial Processes* 8(3): 335-345.
- Vasil'chuk, Yu.K., van der Plicht, J., Jungner, H. & Vasil'chuk, A.C. 1999. AMS-dating of Late Pleistocene and Holocene syngenetic ice-wedges. *Eighth International Conference on Accelerator Mass Spectrometry, Abstracts, Palais Auersperg, Vienna, Austria, 6–10 September*: 141.
- Vasil'chuk, Yu.K. & Kotlyakov, V.M. 2000. *Principles of Isotope Geocryology and Glaciology. A Comprehensive Textbook*. Moscow University Press. 616 pp.
- Vasil'chuk, Yu.K., van der Plicht, J., Jungner, H. & Vasil'chuk, A.C. 2000. AMS-dating of Late Pleistocene and Holocene syngenetic ice-wedges. *Nuclear Instruments and Methods in Physics Research. Section B: Beam Interactions with Materials and Atoms* 172: 637-641.
- Vasil'chuk, Yu.K., Vasil'chuk, A.C., Rank, D., Kutschera, W. & Kim, J. 2001. Radiocarbon dating of $\delta^{18}\text{O}$ – δD plots in Late Pleistocene ice – wedges of the Duvanny Yar (Lower Kolyma River, northern Yakutia). *Radiocarbon* 43(2B): 541-553.
- Vasil'chuk, Yu.K., Kim, J.-C. & Vasil'chuk, A.C. 2004. AMS ¹⁴C dating and stable isotope plots of Late Pleistocene ice-wedge ice. *Nuclear Instruments and Methods in Physics Research. Section B: Beam Interactions with Materials and Atoms* 223-224: 650-654.
- Vasil'chuk, Yu.K., Kim, J.-Ch., van der Plicht, J., Papesch, W. & Vasil'chuk, A.C. 2005. AMS-dating Dansgaard-Oeschger events in Siberian ice-wedge ice. *Tenth International Conference on Accelerator Mass Spectrometry. AMS-10. Conference Agenda & Abstracts, Berkeley, California, September 5–10, 2005*: 35-36.

Active Layer Monitoring in West Siberia Under the CALM II Program

A.A. Vasiliev

Earth Cryosphere Institute SB RAS, Tyumen, Russia

M.O. Leibman

Earth Cryosphere Institute SB RAS, Tyumen, Russia

N.G. Moskalenko

Earth Cryosphere Institute SB RAS, Tyumen, Russia

Abstract

Active-layer monitoring in northern West Siberia started in 1972 at the Nadym site. Sites at Marre-Sale polar station in 1978 and Vaskiny Dachi polygon followed in 1991. Measurements are obtained within dominating landscape units and aimed at establishing active layer and ground temperature changes in various bioclimatic zones and landscapes. In 1993 the CALM (Circumpolar Active Layer Monitoring) project was launched, and monitoring began on the 100 x 100 m CALM grids at Nadym and Vaskiny Dachi and 1000 x 1000 m grid at Marre-Sale. The focus was on the active-layer dynamics in connection to climate change. Results obtained at the CALM grids, as well as at previously established sites and transects, facilitate estimation of the main factors involved in active-layer dynamics on various landscape units of the Tundra and Northern Taiga bioclimatic subzones under climate fluctuations. Results reveal that active-layer depth in mires is very sensitive to climate changes, while peatlands are least sensitive.

Keywords: active layer; climate change; ground temperature; monitoring; northern taiga; typical tundra.

Introduction

The northern part of the West Siberian lowland is characterized by relatively flat topography, variable drainage, marine and continental climate, and well developed latitudinal zonality (Melnikov 1983). Northern West Siberia is divided into three bioclimatic subzones according to the thermal and moisture balances: northern taiga, forest-tundra, and tundra. Surficial geology is dominated by sandy-clayey Pleistocene deposits. Permafrost distribution is continuous north of 67°N and discontinuous south of this latitude.

Active layer monitoring in northern West Siberia has been ongoing at the Nadym site (Northern Taiga subzone) since 1972, at Marre-Sale since 1978, and at the Vaskiny Dachi site since 1991 (both in Typical Tundra subzone, coastal and inland localization) (Fig. 1). The Marre-Sale and Vaskiny Dachi research sites are in the continuous permafrost zone, while permafrost distribution at Nadym is discontinuous.

Active layer/landscape interrelations are largely controlled by the composition and moisture content of the constituent soils. The maximum active layer is characteristic of sands, especially in recent blowouts that lack vegetative cover and are well drained. In the northern taiga, the maximum active layer may also occur in mires and dry tundra with peaty hummocks. The minimum active layer is found at the sites with relatively thick organic cover, mainly on fine-grained soils in poorly drained environments.

Observations are performed at environmentally homogeneous sites 10 x 10 m in size and along transects several hundred meters long that cross dominant landscape units (Table 1). Active-layer and permafrost temperatures are measured in boreholes up to 10 m deep at the same sites. Studies are aimed at establishing active-layer and ground temperature changes in bioclimatic subzones and landscape units within the context of climate change.

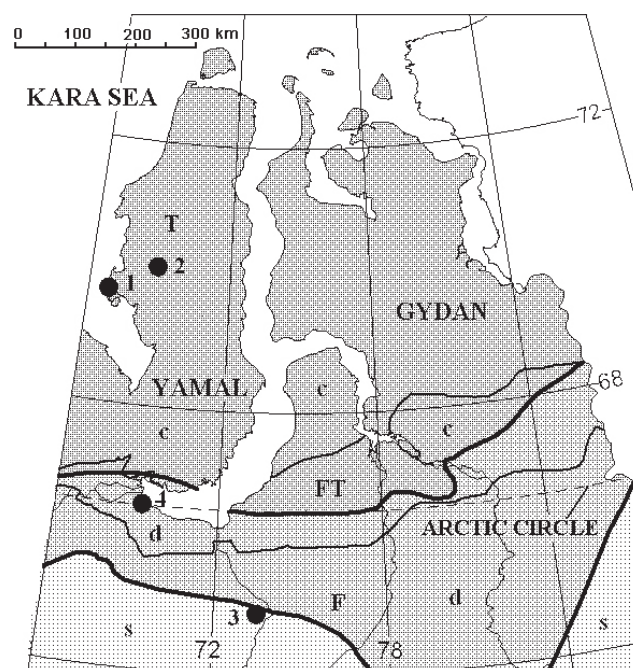


Figure 1. Location of the Marre-Sale (1), Vaskiny Dachi (2), and Nadym (3) research sites, and Salekhard weather station (4). Permafrost zones: c – continuous, d – discontinuous, s – sporadic.

In 1993–1995, observations following the protocol of the CALM (Circumpolar Active Layer Monitoring) project started on the 100 x 100 m CALM grids at Nadym and Vaskiny Dachi and on 1000 x 1000 m at Marre-Sale. The primary focus was on the active-layer dynamics in connection to climate change (Brown et al. 2001). The active layer studies within the framework of the CALM project were conducted for a number of years both on CALM sites, and on additional grids and profiles (Table 1).

Table 1. Metadata summary for CALM grid and additional grids and transects.

Research site	Observation unit	Unit size, m	Years of record
Marre-Sale	CALM grid (R3*), borehole 2 m deep	1000x1000	1995-2007
	Grid 1, borehole 10 m deep	10x10	1978-2007
	Grid 17, borehole 10 m deep	10x10	1978-2007
	Grid 36, borehole 10 m deep	10x10	1987-2007,
Vaskiny Dachi	CALM grid (R5*), borehole 2 m deep	100x100	1993-2007, 1999-2007
	Transect boreholes 5-10 m deep	320	1989-2006 1989-1993
Nadym	CALM grid (R1*), borehole 2 m deep	100x100	1997-2007
	transects 5x200 m	1000	1972-2007
	18 grids,	10x10	1972-2007
	boreholes 10 m deep		

* CALM grid numbers are given as in (Brown et al. 2001).

Methods

Northern West Siberian north is known for wide distribution of saline marine deposits, and thus measuring the active layer in this area is not trivial. The salinity of clay in the active layer in the Typical Tundra subzone may be as high as 1.6% (Leibman & Streletskaya 1997). Some parts of the slope were subjected to landsliding that removed washout deposits to expose saline clay. Salinity in the active layer strongly correlates with the age of a landslide event (Ukrainitseva et al. 2000).

In fine-grained soils mechanical strength changes gradually with decreasing unfrozen water content. When clayey soil is saline, the changes are much less apparent. At the same time, the freezing point departs from zero. Thermal measurements to determine the 0°C temperature position, when compared to insertion of a metal probe, show that in clayey soils the probe is inserted to a depth of 5 cm to 25 cm deeper than that of the 0°C isotherm depth (Leibman 1998); by comparison, Mackay (1977) measured a difference of 23 cm in early summer. In sand and silt the probe insertion can be even less than the 0°C isotherm depth due to higher mechanical resistance of the sandy-silty thawed layer. The probe can be inserted into the clay to a depth where ground temperatures are -0.5°C to -1.0°C according to our measurements (-0.6°C to -0.9°C in Mackay 1977).

CALM protocol (Brown et al. 2001) was applied from 1993–1995. Replicate thaw-depth measurements were performed using a metal probe in late August or early September, when the depth of seasonal thaw was close to maximum. The measurement error for the probe is about 1 cm. At the same time, in aeolian sands of the Marre-Sale grid in the warmest years the active layer depth may exceed the probe length (>160 cm). At Vaskiny Dachi, measurement

error can be large owing to the presence of saline soils. In warm years thaw depth (or depth of penetration) at some Vaskiny Dachi probing points exceeds the probe length (180 cm) in the clayey active layer with the surface recently exposed by landsliding (Leibman 1998). Accordingly in this study, observations from such probing points were eliminated from calculations to better follow the interannual dynamics of active layer depth. The thaw index was calculated using monthly averages from weather records at the nearest meteorological stations.

A landscape survey was performed at each site based on the classification suggested in Melnikov et al. (1983). Determined were: structure of vegetative complexes and coverage as suggested in Moskalenko (1999); organic layer thickness by direct field measurements in similar areas adjacent to the probing point; density, moisture content, and chemical properties of soils, grain size, water content by volumetric weighting, and ionic analysis in water extraction. Geochemical tests were performed at Vaskiny Dachi to locate probing points with erroneous measurements due to recent landsliding.

Most of these methods were used since the 1970s and were improved within the framework of the CALM project. Measuring along the transects and within the landscape units started in the 1970s. Transects were set to cross the majority of the landscape units according to the results of a landscape survey. This approach is most common in the geocryological surveys in Russia, allowing us to extrapolate key site monitoring data to regions of similar landscape structure. This method helps when using remotely sensed imagery to map parameters not directly measured from space.

Climate

According to the climate zoning of the Russian Arctic (Prick 1971), the northern West Siberian lowland belongs to the Eastern region of the Atlantic sector of the Arctic Ocean. This region is subject to the strong impact of circulation processes from the mid-latitudes, specifically the Icelandic depression, and is subdivided into three zones. The northern tundra subzone of northern Yamal and Gydan peninsulas is characterized by marine arctic climate. The middle zones of typical and southern tundra of the Yamal, Gydan, and Tazovsky peninsulas are territories with marine sub-Arctic climate. The southern zone of forest-tundra and northern taiga is of moderate-continental climate.

The most important climatic parameters affecting permafrost dynamics are air temperature and snow cover depth. Northern West Siberia, due to climatic zoning mentioned above, is characterized by highly variable mean annual air temperature. At the Kara sea coast, mean annual air temperature decreases from -7.6°C on the southwestern coast of the Kara sea (Ust-Kara weather station, 69°12'N, 65°07'E) up to -11.3°C on the northeastern coast of Gydan (Gyda weather station, 70°53'N, 78°31'E) (Temperature of air and soils 1966). Inland there are few weather stations with short-term records. Within the study area, the southernmost

inland station is Nadym, with the highest mean annual air temperature (-5.7°C). Calculations based on the short-term air temperature records show that the mean annual air temperature at Central Yamal decreases eastward, with a minimum at the main watershed of Yamal and at Vaskiny Dachi as low as -9°C (Belopukhova et al. 1989). At Marre-Sale the weather station mean annual air temperature is about -8°C .

Permafrost dynamics, including that of the active-layer depth, is linked to air temperature fluctuations. It is generally accepted that climate warming has been observed during the last 30–35 years (Pavlov 2003). Warming is more intensive inland, while along the coasts it is less expressed (Pavlov & Malkova 2005).

Figure 2 shows a time series of the mean annual air temperature at the West Siberian weather stations Salekhard, Marre-Sale, and Nadym. One can see that starting in the 1970s, there is a mean annual air temperature increase. Warming is rather synchronous across the entire region, though with local deviations. However, the degree differs. According to estimates by Pavlov & Malkova (2005) for northern West Siberia maximum warming is noted on the Tazovsky peninsula (Nadym area), exceeding 1.5°C . The least warming is in northern Yamal (0.7°C).

In analyzing long-term records for diurnal air temperature we noted that in the past 25 years in the tundra zone, the warm period has increased by 5–6 days, while in the northern taiga it increased by 15–17 days. The duration of the cold period decreased accordingly.

The thermal regime of permafrost is strongly affected by the thickness and regime of snow accumulation. In Marre-Sale the average perennial snow depth is 20–30 cm, while at Nadym it is as high as 50–60 cm, with year to year deviation. Total snow thickness tends to increase northward in West Siberia.

Results and Discussion

Results of active layer measurements at the monitoring sites located on the dominant landscape units are presented as Figures 3 and 4. The graphs show that active layer dynamics generally follow the sum of positive air temperatures, or thawing degree-days (DDT). However, one can see that short-term active layer records cannot characterize real trends in active layer evolution due to the oscillating nature of active layer dynamics. Still, it is apparent from the time series that all the landscape units show a tendency to increase over time since the 1970s until the recent. Trends of active-layer deepening within similar landscape units in the typical tundra are of smaller magnitude compared to the northern taiga. In the peatlands, active-layer changes are small, while in the mires and wet tundra they are much higher (Vasiliev et al. 2003, Melnikov et al. 2004). The same climate warming in the northern taiga is two times greater compared to the typical tundra.

Climate warming affects ground temperature, so permafrost reaction to climate change can be expressed in

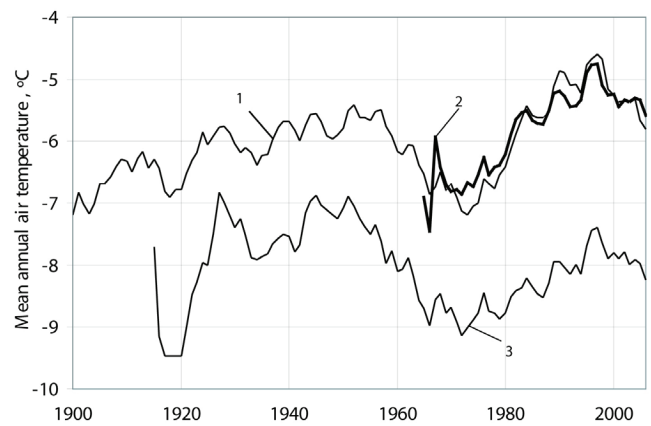


Figure 2. Ten-year moving averages of mean annual air temperature for Salekhard (1), Nadym (2), and Marre-Sale (3) weather stations.

mean annual ground temperature dynamics. In northern West Siberia the depth of zero annual temperature amplitude is about 10 m, the depth of most boreholes at the research sites. Results from the Marre-Sale and Nadym borehole temperature measurements, collected under conditions of changing climate at a depth of ~ 10 m, are shown in Figure 5. These traces also show oscillations that are similar to those for the active-layer depth. However, the mean annual ground temperature increase is more clearly marked since the 1970s. It is especially well observed at the Nadym site. At this station, in peatlands, the mean annual ground temperature rose from -0.9°C to -0.1°C . In the mires the mean annual ground temperature rose from -0.3°C to -0.1°C . Thus, in the discontinuous permafrost zone of the West Siberian northern taiga, recent climate warming has already caused a critical ground temperature increase approaching entire permafrost degradation.

In the typical tundra subzone, a ground temperature increase is observed as well. As snow cover here is less thick and its impact is not very pronounced, ground temperature shows a strong correlation with air temperature (Fig. 6). As a first approximation, the linear trend is applied. The slope of the straight-line approximation differs for each landscape unit. We suppose that the slope trend characterizes the annual ground temperature response of a particular landscape unit to climate fluctuations. The maximum slope is typical of flat peatlands, whereas the minimum slope is typical of mires. All other landscape units are characterized by intermediate values of annual ground temperature versus annual air temperature.

Conclusions

The study of permafrost reaction to climate change through active-layer depth dynamics was initiated within the framework of the CALM program. The response to climate changes of dominant landscape units in typical tundra and northern taiga subzones, as manifested by the active-layer depth, is evaluated quantitatively.

The active layer depth in mires is very sensitive to climate

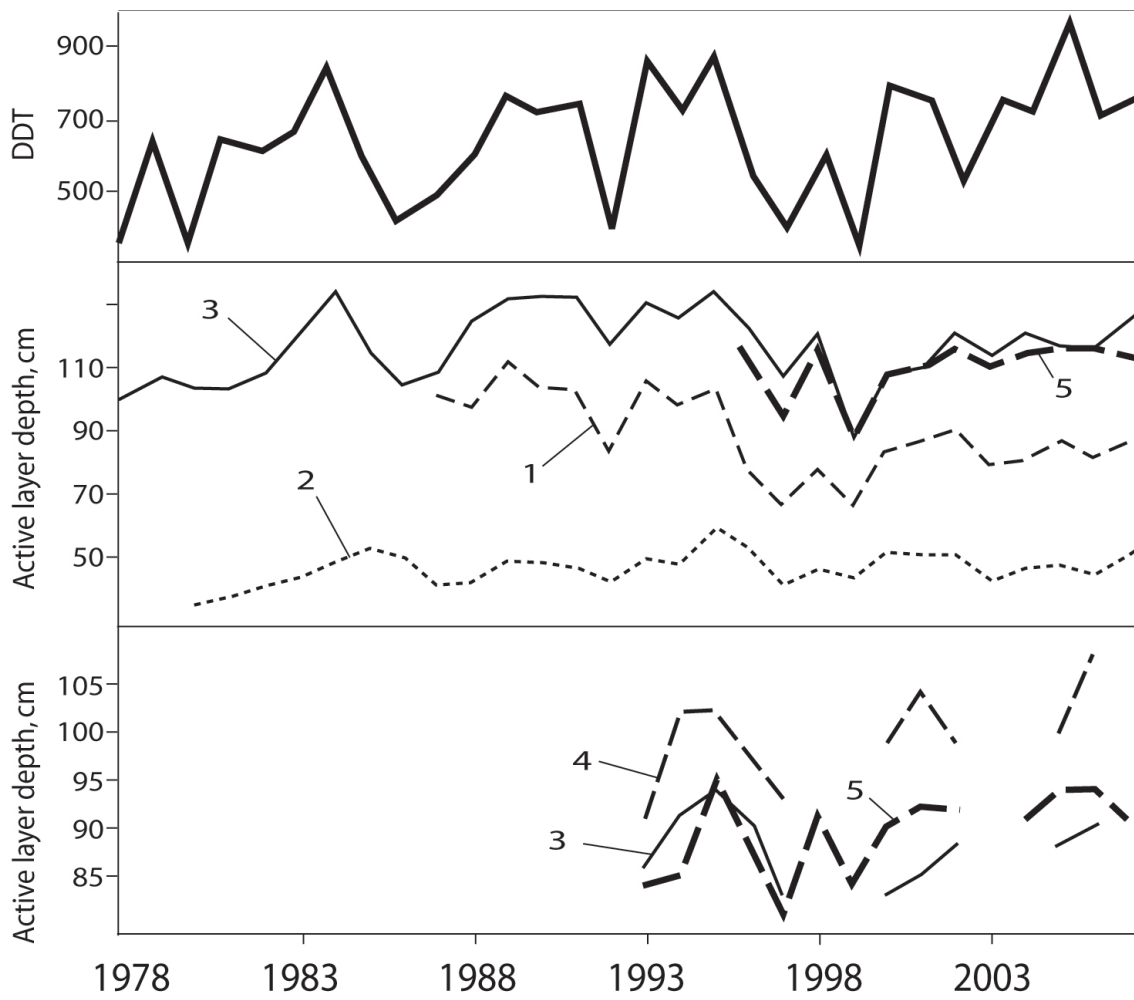


Figure 3. Time series of thaw index (DDT, upper pane), and average active layer depths on the dominating landscape units and CALM grid average in Marre-Sale (middle pane) and Vaskiny Dachi (lower pane): 1, mire; 2, peatland; 3, wet tundra; 4, dry tundra; 5, CALM grid average.

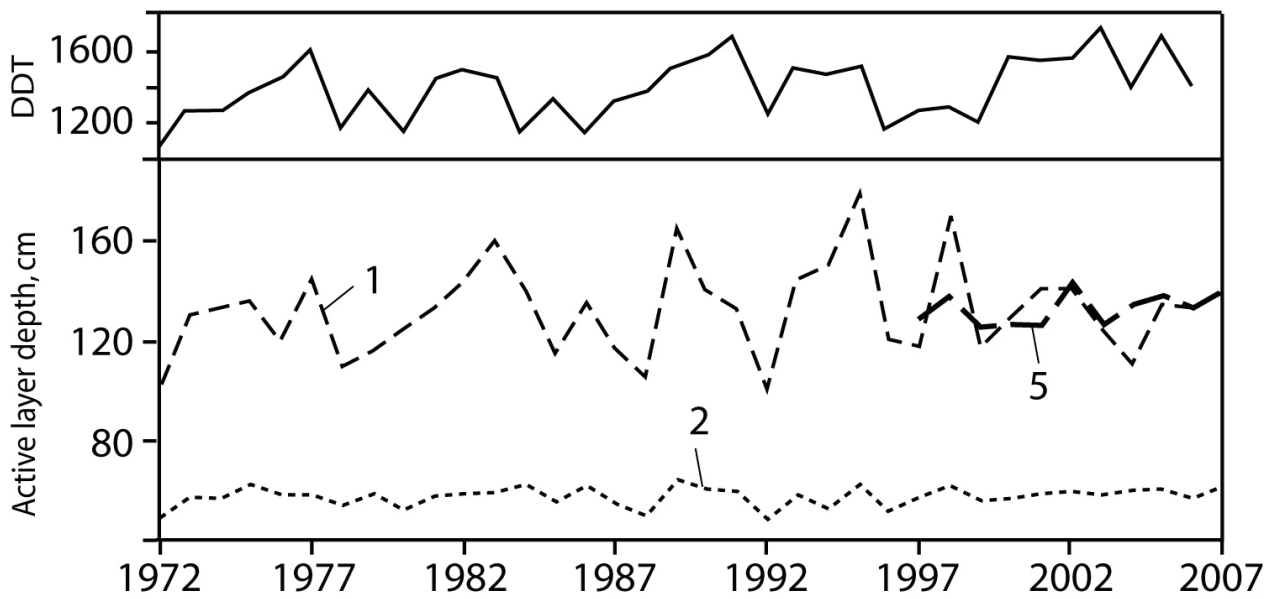


Figure 4. Time series of DDT (upper pane), and average active layer depths (lower pane) on the dominating landscape units and CALM grid average in Nadym area: 1, mire; 2, peatland; 5, CALM grid average.

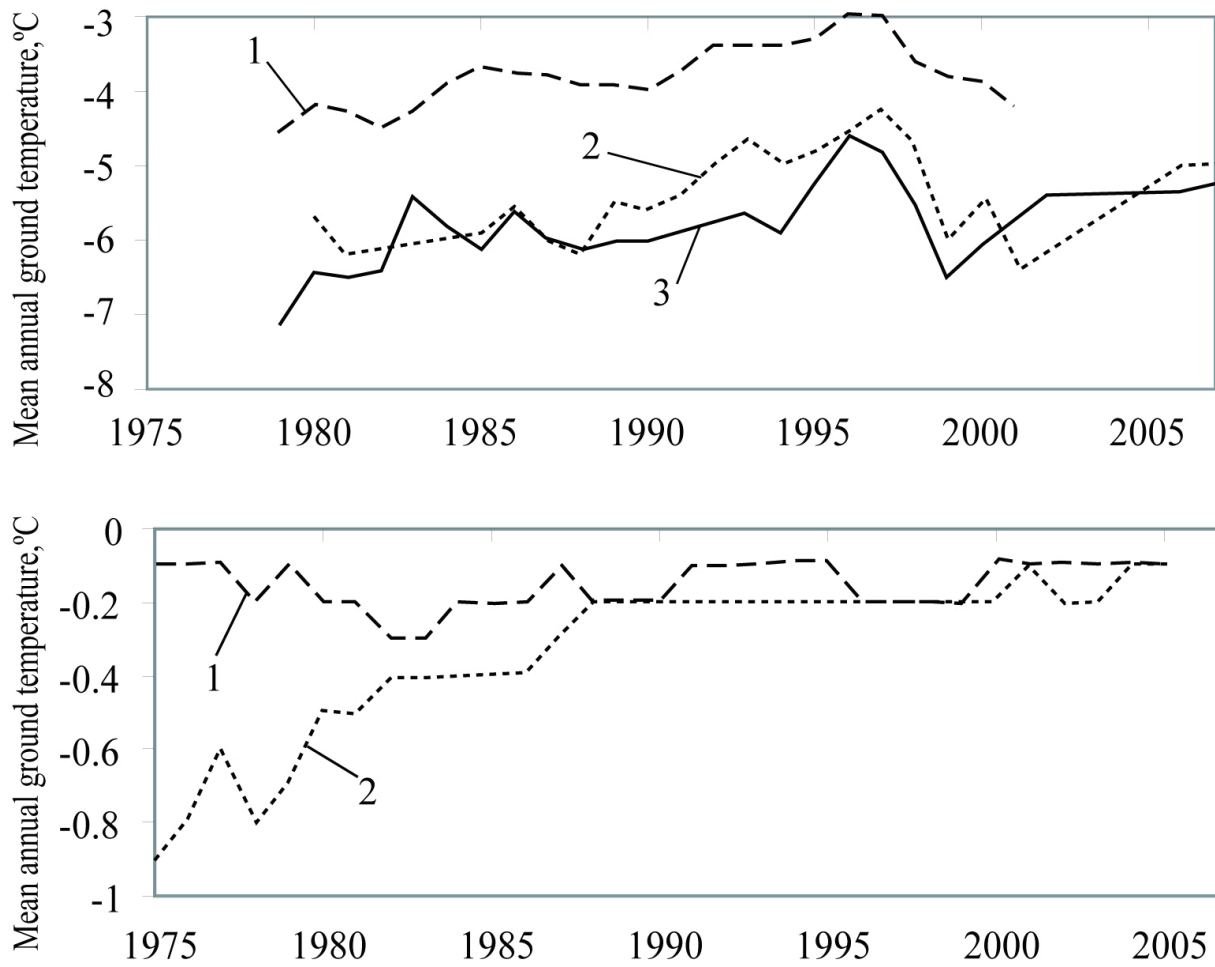


Figure 5. Time series of average ground temperature (depth of ~10 m) at Marre-Sale (upper pane) and Nadym (lower pane) sites: 1, mire; 2, peatland; 3, wet tundra.

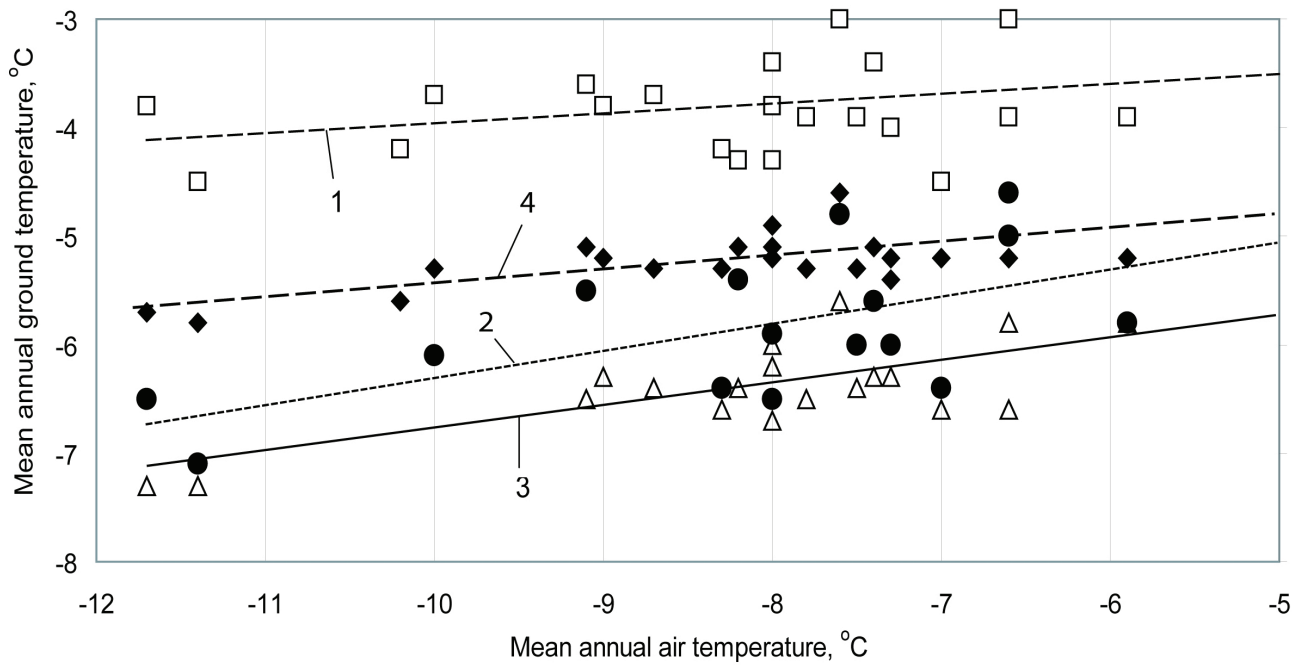


Figure 6. Correlation of mean annual air and ground temperature in Marre-Sale: 1, mire; 2, peatland; 3, wet tundra; 4, dry tundra.

change, while peatlands are least sensitive. And vice versa, the average annual ground temperature of permafrost changes considerably in the peatlands, while only minor changes are noted in mires. The landscape response to climate change expressed through the active layer is opposite to the response expressed through the average annual ground temperature.

Thus, analysis of the monitoring data allows us to conclude that the reaction of permafrost landscapes in northern West Siberia to climate change can develop in two directions. For some landscape units maximum increase of the active-layer depth is observed under the minimum change of mean annual ground temperature. For other landscapes with maximum change of mean annual ground temperature, minimum change of the active layer depth is characteristic. We cannot expect coincidence of both parameter maxima or minima within any environment.

Acknowledgments

This study was supported by the U.S. National Science Foundation (Grant # OPP-9732051), and Russian Academy of Sciences, Siberian Branch (Program of Fundamental Research SB RAS “Evolution of natural and Technogenic Geosystems in Cryolithozone”).

References

- Belopukhova, E.B., Leibman, M.O. & Tkacheva, L.A. 1989. Impact of climatic parameters on the ground temperature and active-layer depth on Yamal Peninsula. In: *Engineering Investigations for Construction in Yakutian Republic*. Yakutsk: GOSSTROI RSFSR, 111-112 (In Russian).
- Brown, J., Hinkel, K.M. & Nelson, F.E. 2001. The Circumpolar Active Layer Monitoring (CALM) program: research designs and initial results. *Polar Geography* 24: 165-258.
- Melnikov, E.S. (ed.) 1983. *Landscapes of permafrost zone in the West Siberian gas province*. Novosibirsk: Nauka, 185 pp. (in Russian).
- Melnikov, E.S., Leibman, M.O., Moskalenko, N.G. & Vasiliev, A.A. 2004. Active layer monitoring in West Siberia. *Polar Geography* 28(4): 267-285.
- Pavlov, A.V. 2003. Permafrost-climate changes in the Russian North: observations, prediction. *Transactions of RAS, Geographic Series* 6: 22-29 (in Russian).
- Pavlov, A.V. & Malkova, G.V. 2005. *Contemporary Changes of Climate in Northern Russia*. Novosibirsk: Academic Publishing House “GEO,” 54 pp. (in Russian).
- Pavlov, A.V. & Moskalenko, N.G. 2002. The thermal regime of soils in the North of Western Siberia. *Permafrost and Periglacial Processes* 13(1): 43-51.
- Prick, Z.M. 1971. Climatic zoning of the Arctic. In: *Transactions of AARI 304*: Leningrad, 72-84 (in Russian).
- Leibman, M.O. 1998. Active layer depth measurements in marine saline clayey deposits of Yamal Peninsula, Russia: procedure and interpretation of results. *Permafrost. Seventh International Conference, June 23-27, 1998, Proceedings, Yellowknife, Canada-1998*: 635-639.
- Leibman, M.O. & Streletskaya, I.D. 1997. Land-slide induced changes in the chemical composition of active-layer soils and surface-water runoff, Yamal Peninsula, Russia. In: I.K. Iskandar, E.A. Wright, J.K. Radke, B.S. Sharratt, P.H. Groenevelt & L.D. Hinzman (eds.), *Proceedings of the International Symposium on Physics, Chemistry, and Ecology of Seasonally Frozen Soils, Fairbanks, Alaska, June 10-12, 1997*. CRREL Special Report 97-10, CRREL, Hanover: 120-126.
- Mackay, J.R. 1977. Probing for the bottom of the active layer. Report of activities, Part A; *Geological Survey of Canada*, Paper 77-1A: 327-328.
- Moskalenko, N.G. 1999. *Anthropogenic Vegetation Dynamics of Cryolithozone Plains*. Novosibirsk: Nauka, 280 pp. (in Russian).
- Temperature of air and soils. 1966. In: *Reference Book of USSR Climate* 24 (II). Leningrad: Gidrometeoizdat, 404 pp. (in Russian).
- Ukrainitseva, N.G., Leibman, M.O. & Streletskaya, I.D. 2000. Peculiarities of landslide process in saline frozen deposits of central Yamal, Russia. In: E. Bromhead, N. Dixon & L.-L. Ibsen (eds.) *Landslides. Proceedings of VIII International Symposium on Landslides* 3, London: Thomas Telford, 1495-1500.
- Vasiliev, A.A., Moskalenko, N.G. & Brown, J. 2003. A new approach for interpreting active layer observations in the context of climate change: a West Siberian example. In: *Proceedings, Eighth International Conference on Permafrost Zurich, Switzerland, July 21-25 2003, Extended Abstracts*: 169-170.

Relation Between Soil Temperature and Late 20th Century Climatic Change in Yakutia

I.S. Vasiliev

Melnikov Permafrost Institute, SB RAS, Yakutsk, Russia

Abstract

This report presents analysis of the relationships of mean annual soil temperature at a depth of 1.6 m to air freezing index and snow depth, based on data from 40 weather stations in Yakutia. These relationships are discussed for the regional groups distinguished on the basis of linear trends in soil temperature. In the high-latitude lowland regions showing a negative trend, the decrease in mean annual soil temperature, with the freezing index remaining stable, is attributed to the persistence of snow cover long after the onset of positive air temperatures retarding soil warming, rather than to the increased snow depth and density. In the regions with a positive trend, the increase in mean annual soil temperature is caused by the weakening of the Asian anticyclone in winter. In the mountainous regions, soil temperatures are determined by local temperature-controlling factors, showing a decrease in cold landscapes and an increase in warm landscapes.

Keywords: freezing index; mean annual soil temperature; snow depth; trend.

Introduction

Changes in mean annual air temperature in the high latitudes of the Northern Hemisphere have been analyzed during the last 30 years by many investigators, using various approaches (Climate Change 1990, Ghil & Vautard 1991, Zhang & Osterkamp 1993, Pavlov 1994, 1997, Drozdov & Lugina 1996, Varlamov & Skachkov 1996, Balobaev 1997, Zukert & Zamolodchikov 1997, GavriloVA & Cherdonova 1997, Varlamov et al. 1998, Fedorov and Svinoboev 2000, Gedalof & Smith 2001, Harris 2002, 2005, and others).

Along with assessing the changes in air temperature, it is important to determine the responses of near-surface

permafrost, particularly upper soil layers, to climatic variation. Pavlov (1997) reported data from several sites near Igarka and Vorkuta, indicating an increase in the mean annual permafrost temperatures to a depth of 10 m. Other studies also indicate a warming trend in ground temperature in Russia, on the North Slope of Alaska, along the Arctic coasts of Canada, and in the Northern Hemisphere as a whole (Osterkamp & Romanovsky 1999, Gilichinsky et al. 2000, Chudinova et al. 2001, 2003, Izrael et al. 2002, 2006, Frauenfeld et al. 2004, 2006, Smith et al. 2003). For Yakutia, it was shown previously (Vasiliev 1999) that linear trends in soil temperature at 1.6 m were of opposite sign in different regions (Fig. 1), which were provisionally grouped into three zones based on the character of soil temperature variation (Fig. 2).

This report presents analysis of the relationships of mean annual soil temperature at a depth of 1.6 m ($T_{m 1.6}$) to air freezing index ($\sum_{at} < 0$) and snow depth (h_s).

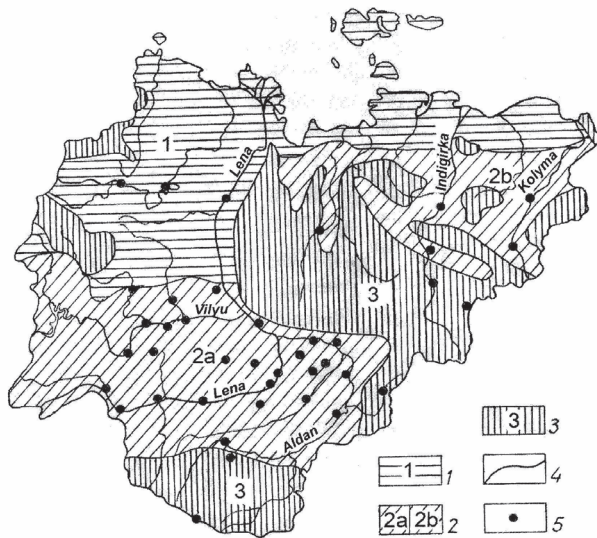


Figure 1. Map showing the location of soil temperature measurement sites and the regional groups identified based on linear trends: 1 – regions with negative trends; 2(a, b) – regions with positive trends; 3 – mountainous regions with opposing trends; 4 – group boundaries; 5 – weather stations.

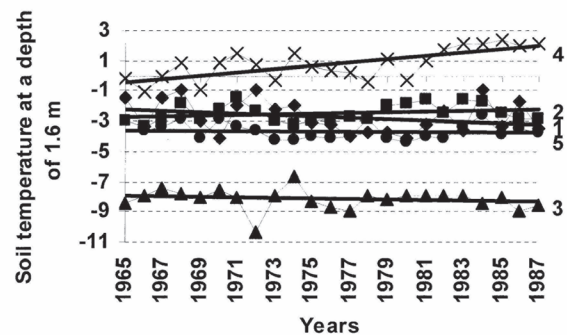


Figure 2. Variations and linear trends of mean annual soil temperature at 1.6 m for the Jarjan (1), Pokrovsk (2), Predporozhnaya (3), Gorelyy (4) and Nagornyy (5) weather stations.

Method

Regular instrumental measurements of soil temperature have been made in Yakutia since 1931. Soil temperature records of various lengths are available from 50 weather stations. However, the relocation of sites and the discontinuance of measurements introduce inhomogeneities into the temperature series. Of the 50 stations, only 16 continue to make soil temperature observations, 12 stations were closed by 1987, 9 stations by 1989 and 3 by 1994. Moreover, in the 1970s–1980s, instruments were relocated at 12 stations. Only homogeneous data sets from the same sites can provide a general picture of how the parameters under discussion have varied in the region. Therefore, soil temperature records from 40 weather stations for only the period from 1965 to 1987 have been used in the present study. Data on air freezing index and snow depth, which are compared to soil temperature, cover the same period (Fig. 3).

Results

Relations between $T_{m1.6}$, $\sum_{at} < 0$ and h_s have been analyzed for the three regional groups distinguished in the previous study: (1) northern plains with a negative trend of $T_{m1.6}$; (2a) southwestern and central plains and (2b) northeastern plains and intermontane depressions, where $T_{m1.6}$ shows a steady increasing trend; and (3) mountains, exhibiting either stable or opposing $T_{m1.6}$ trends.

1. The northern plains with a negative trend of $T_{m1.6}$ include the tundra and north-taiga areas of western Yakutia and the tundra areas of eastern Yakutia (see Fig. 2, line 1). Air freezing indices were temporally stable at most stations of the region (Fig. 3, plot 1a), while snow depths slightly increased during the study period. The linear trend in h_s is 0.14–0.36 cm per year (Saskylakh, Sukhana and Siktyakh stations). At Jarjan, no trend is noted, although some increase in h_s occurred in the 1980s (Fig. 3, plot 1b). In the northernmost areas, increased snow depth is known to have a cooling effect on the soil thermal regime (Dostovalov & Kudryavtsev 1967, p. 252). The negative effect of snow cover in these regions can be due to three main reasons. First, snow density increases from south to north up to 0.2–0.3 g/cm³ in mid winter and to 0.35–0.4 g/cm³ in late winter. The high snow densities are caused by strong winds with speeds increasing to 20 m/s during snow storms. The frequency of storm winds is 20–40 days/yr in northern Yakutia, increasing to 60–80 days/yr on the Arctic islands. It is known that the higher that snow density is, the lower is the insulating effect of snow cover, even with increased thickness. Second, snow cover disappears as late as mid-June in northern Yakutia and late June on the Arctic islands, and the duration of the snow-covered season is 230–240 days in the north and 290–300 days on the Arctic islands. Under these severe climatic conditions, snowmelt occurs very slowly after air temperatures rise above 0°C, thus retarding soil warming. This 2–3 week delay results in a decrease in mean annual permafrost temperature. Third, it is a common knowledge that the snow cover of long duration increases the albedo and this also has a negative effect on

mean annual ground temperature. With no changes in $\sum_{at} < 0$, the decrease in $T_{m1.6}$ therefore appears to result from the persistence of snow cover long after the onset of positive air temperatures retarding soil warming, rather than to the increased snow depth and density. The soils in northern Yakutia showed a rise in the early 1980s, while according to Pavlov (1997) the mean annual soil temperatures in northern West Siberia began warming a decade earlier. Although Jarjan records indicate a negative linear trend of temporal $T_{m1.6}$ variation (see Fig. 2, plot 1), its extremely low values (–4°C) occurred at $\sum_{at} < 0 = -6000$ degree-day/year or lower and $h_s = 20$ cm or less (see Fig. 4, plots 1a and 1b).

2a. In western Yakutia, winters have become milder with a decrease in $\sum_{at} < 0$ at 3–9 degree-day/year. According to the graphical relationship, h_s increased at a trend of 0.18–1.18 cm/year (Berdigestyakh and Vilyuisk stations). In Central Yakutia, where h_s shows temporal stability, winters also tend to become milder, resulting in increased $T_{m1.6}$. This is attributed to the general weakening of the Asian anticyclone. The plot constructed from the Pokrovsk weather station data indicates that $T_{m1.6}$ increases to –1.3°C at $\sum_{at} < 0 = -5300$ degree-day/year and $h_s = 40$ cm and decreases to –3.4°C at $\sum_{at} < 0 = -5700$ and $h_s < 30$ (Fig. 4, plots 2a and 2b). In southwestern Yakutia, trends toward lower $\sum_{at} < 0$ and greater h_s , resulting in increased $T_{m1.6}$, suggest stronger winter advection in the westerlies.

2b. The northeastern plains of the north-taiga zone and the major intermontane depressions also show a positive trend in $T_{m1.6}$. Winters became much warmer throughout the region, where $\sum_{at} < 0$ decreased at a rate of 13.6–27 to 59 degree-day per year (Batagai, Srednekolymsk, Delyankir and Ust-Moma). During winter, these areas are predominantly under the influence of the Asian anticyclone and the cyclones bringing precipitation from the Pacific Ocean (Kazurova 1961, Gavrilova & Cherdonova 1997). Because the winter snow cover is thin, its insulating effect is small. At the same time, a decrease in h_s of 0.13–0.4 cm per year is observed in the region (Batagai and Zyrianka stations). The reduction of $\sum_{at} < 0$ is accompanied by an increase in $T_{m1.6}$ despite a tendency toward thinner h_s , which can also be explained by the instability or lesser influence of the Asian anticyclone.

3. In the mountainous regions, the changes in $\sum_{at} < 0$ suggest a warming throughout the region during winter. Decreasing trends of 13.6–15.9 degree-day/year in $\sum_{at} < 0$ and 0.09–0.36 cm/year in h_s are found. The plot for the Predporozhnaya weather station (Fig. 4, plots 3a and 3b) indicates that $T_{m1.6}$ varies inter-annually from –6.7 to –10.3°C, when $\sum_{at} < 0$ increases from –6500 to –6600 degree-day/year and h_s decreases from 35 to 10 cm. $T_{m1.6}$ shows a closer relationship to h_s than to $\sum_{at} < 0$. At this site characterized by relatively cold winter temperatures, cooling of $T_{m1.6}$ is associated with the decreasing trend in already shallow snow depth.

In the northern and central parts of the Aldan Plateau, the increase in $T_{m1.6}$ is directly related to the reduction of $\sum_{at} < 0$ and the increase in h_s . At the Gorelyy weather station, a trend of $T_{m1.6}$ was 0.09°C per year during the period from 1966 to 1985 (Fig. 2, line 4). The linear relationship for this site

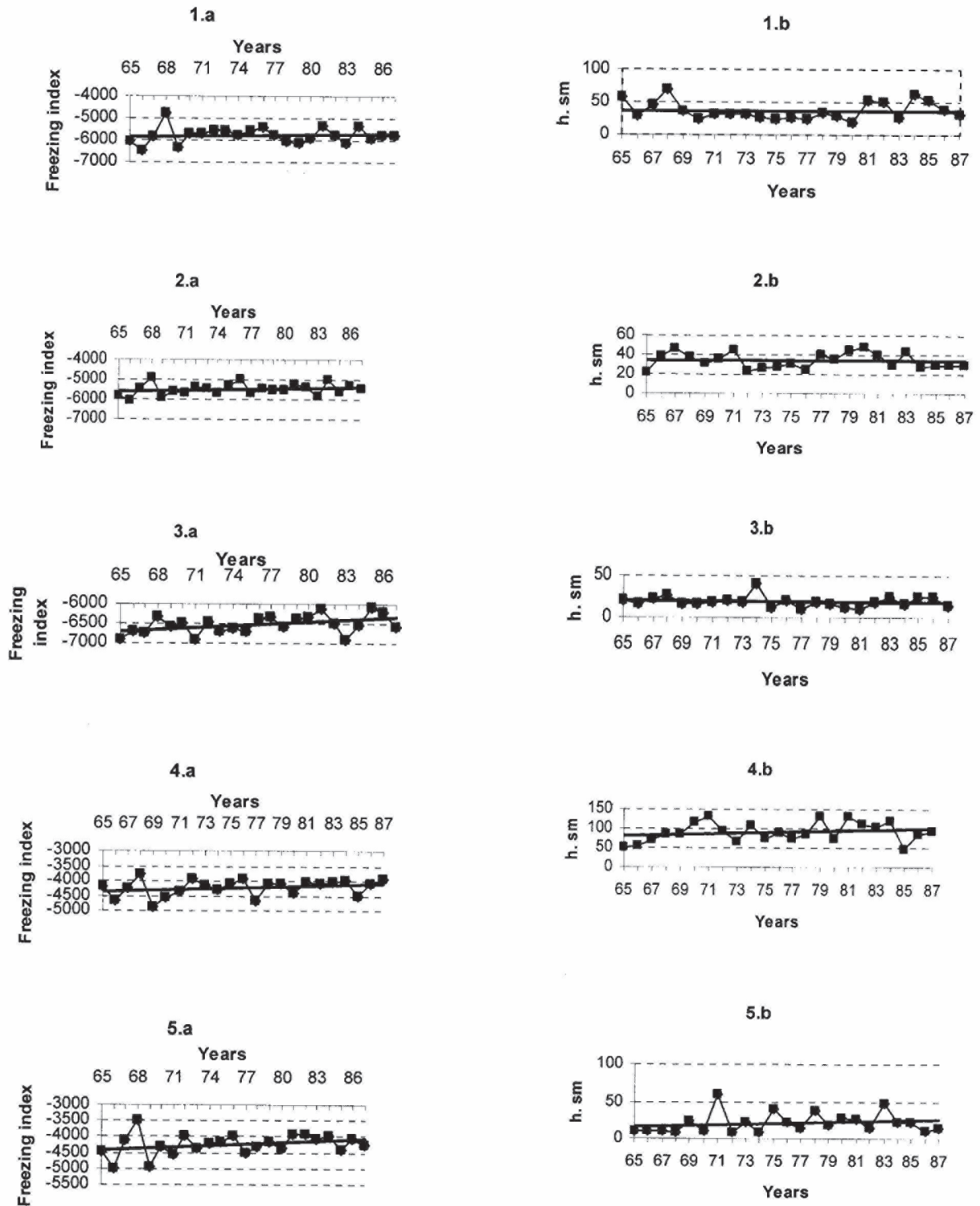


Figure 3. Variations of mean annual freezing index (a) and snow depth (b) for the same station (see Fig. 1).

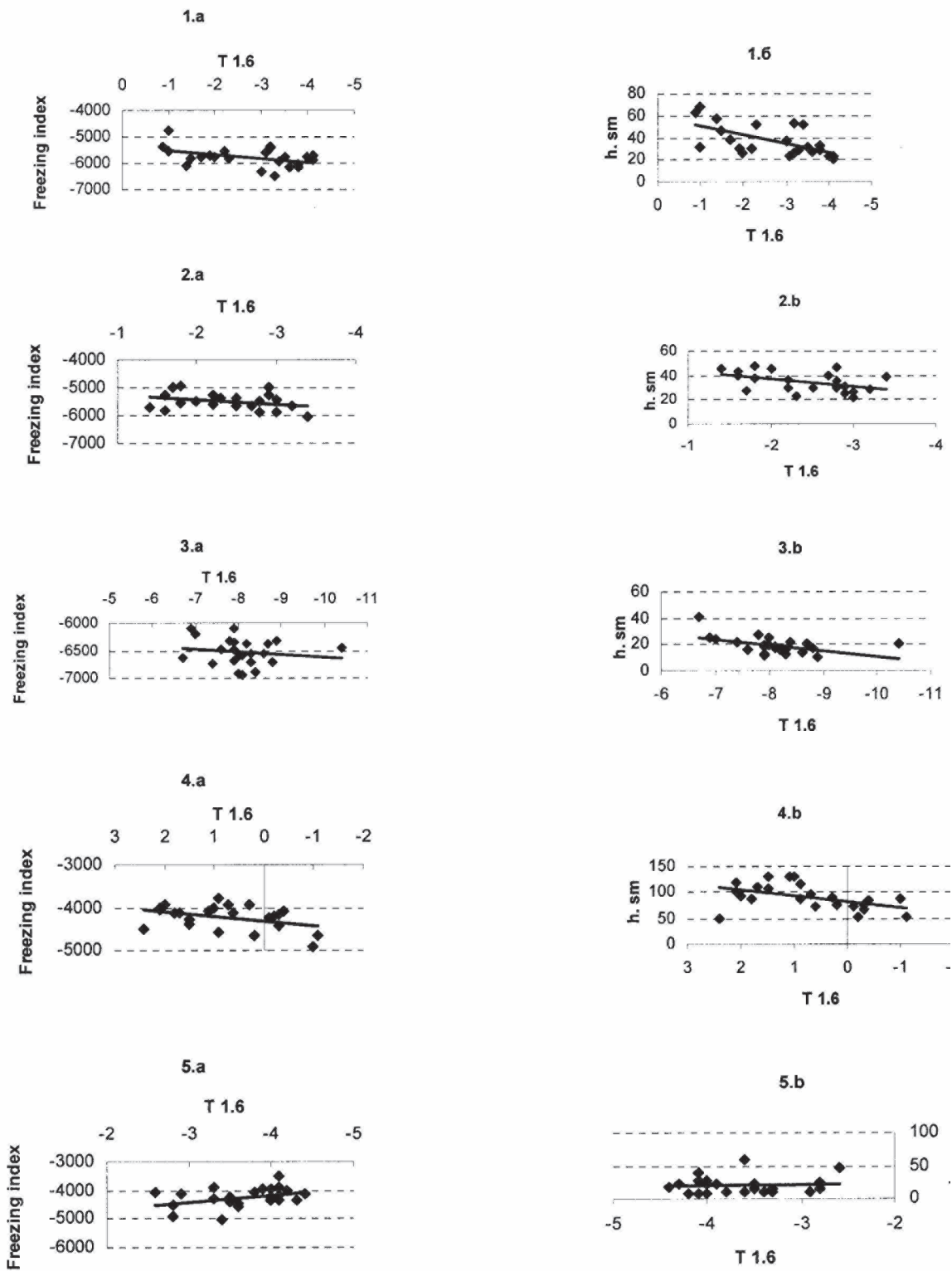


Figure 4. Relation of mean annual soil temperature variation at 1.6 m to air freezing index (a) and snow depth (b) for the same stations (see Fig. 2).

shows that $T_{m1.6}$ increases from -1 to $+2.4^{\circ}\text{C}$ with changes in $\sum_{at} < 0$ from -4400 to -4000 degree-day/year and in h_s from 70 to cm (Fig. 4, plots 4a and 4b).

In the southernmost part of Yakutia, on the northern megaslope of the Stanovoy Range, $T_{m1.6}$ is found to be temporally stable exhibiting a very slight negative trend (0.01°C per year) at Nagornyy (Fig. 2, line 5). Comparison of $T_{m1.6}$ with $\sum_{at} < 0$ variation (Fig. 4, plot 5a) leads to the misleading conclusion that $T_{m1.6}$ decreases with decreasing $\sum_{at} < 0$. The slight progressive decrease in $T_{m1.6}$ with positive trends in $\sum_{at} < 0$ and h_s (see Fig. 4, plot 5b) is attributed to the persistence of snow cover long after the onset of positive air temperatures, because the station is located at a relatively high elevation (861 m a.s.l.) on a north-facing slope. Besides, the Timplon valley narrows here to 800 m, while shortly downstream it is $2\text{--}2.5$ km wide, resulting in strong local winds which can also cause significant soil cooling. Thus, in the mountainous regions, some decrease in $\sum_{at} < 0$ and increase in h_s do not lead to an increase in $T_{m1.6}$.

Conclusions

- In the northern regions of Yakutia, the decreasing trend in $T_{m1.6}$, with the freezing index remaining stable, appears to be due to the persistence of snow cover long after the onset of positive air temperatures retarding soil warming, rather than to the increased snow depth and density.

- In the north of Yakutia, a recent rise of $T_{m1.6}$ occurred in the early 1980s, while in northern East Siberia an increase was observed since the early 1970s.

- In the middle-taiga areas of western and central Yakutia, in the north-taiga areas of eastern Yakutia, and in the intermontane basins, the increase of $T_{m1.6}$ is attributed to the instability or lesser influence of the Asian anticyclone. In southwestern Yakutia, it is caused by stronger advection of the westerlies.

- In the mountains, $T_{m1.6}$ variation under present climate are largely determined by local temperature-forming factors, showing a decrease in cold landscapes and an increase in warm landscapes.

References

- Balobaev, V.T. 1997. Global changes of the Earth's climate and permafrost (in Russian). *Nauka i Obrazovanie* 2(6): 82-90.
- Chudinova, S.M., Bykhovets, S.S., Fedorov-Davydov, D.G., Sorokovikov, V.A., Gubanov, V.S., Barry, R.G. & Gilichinsky, D.A. 2001. Response of temperature regime of Russian north to climate changes during second half of XX century (in Russian). *Kriosfera Zemli* V(3): 63-70.
- Chudinova, S.M., Bykhovets, S.S., Fedorov-Davydov, D.G., Sorokovikov, V.A., Barry, R., Zhang, T. & Gilichinsky, D.A. 2003. Features of soil warming versus recent climate warming in Russia (in Russian). *Kriosfera Zemli* VII(3): 23-30.
- Climate Change. 1990. The IPCC Scientific Assessment. Report of Working Group I of the International Panel on Climate Change. New York: Cambridge Univ. Press, 364 pp.
- Dostovalov, B.N. & Kudryavtsev, V.A. 1967. *Permafrost Science (Obshchee merzlotovedenie)* (in Russian). Moscow: Izd-vo Moskovskogo Universiteta, 404 pp.
- Drozdov, O.A. & Lugina, K.M. 1996. Non-uniformity of climate variation effects in the sectors and zones of the Northern Hemisphere (in Russian). *Vestnik St.-Petersburgskogo Universiteta* 1(7): 44-57.
- Fedorov, A.N. & Svinoboev, A.N. 2000. Changes in near-surface air temperature in the Republic of Sakha (Yakutia). In: *Climate and Permafrost: Integrated Investigations in Yakutia (Klimat i merzlota: kompleksnye issledovania v Yakutii)* (in Russian). Yakutsk: Permafrost Institute Press, 68-75.
- Frauenfeld, O.W., Zhang, T. & McCreight, J.L. 2006. Northern Hemisphere freezing/thawing index variations over the 20th century. *Int. J. Climatol.* 27: 4763.
- Frauenfeld, O.W., Zhang, T., Barry, R.G. & Gilichinsky, D.A. 2004. Interdecadal changes in seasonal freeze and thaw depths in Russia. *J. Geophys. Res.*, 109, D05101, doi 10.1029/2003JD004245.
- Gavrilova, M.K. & Cherdonova, V.S. 1997. Pacific atmospheric circulation processes in Yakutia. *Proceedings of International Workshop on Energy and Water Cycle in GAME-Siberia, 1995: Research Report of JHAS (3)*. Nagoya, 9-12.
- Gedalof, Z. & Smith, D.J. 2001. Interdecadal climate variability and regime-scale shifts in Pacific North America. *Geo. Res. Lett.* 28: 1515-1518.
- Ghil, M. & Vautard, R. 1991. Interdecadal oscillations and the warming trend in global time series. *Nature* 350: 324-327.
- Gilichinsky, D.A., Bykhovets, S.S., Sorokovikov, V.A., Fedorov-Davydov, D.G., Barry, R.G., Zhang, T., Gavrilova, M.K. & Alekseeva, O.I. 2000. Use of the data of hydrometeorological survey for century history of soil temperature trends in the seasonally frozen and permafrost areas of Russia (in Russian). *Kriosfera Zemli* IV(3): 59-66.
- Harris, S.A. 2002. Global heat budget, plate tectonics and climatic change. *Geografiska Annaler* 84A: 1-10.
- Harris, S.A. 2005. Thermal history of the Arctic Ocean environs adjacent to North America during the last 3.5 Ma and a possible mechanism for the cause of the cold events (major glaciations and permafrost events). *Progress in Phys. Geography* 29(4): 218-237.
- Izrael, Y.A., Pavlov, A.V. & Anokhin, Y.A. 2002. Permafrost evolution related to current global climatic change (in Russian). *Meteorologia i Hidrologia* 1: 22-34.
- Izrael, Y.A., Pavlov, A.V., Anokhin, Y.A., Myach, L.T. & Shershtyukov, B.G. 2006. Statistical evaluation of variations of climate parameters in the Russian permafrost zone (in Russian). *Meteorologia i Hidrologia* 5: 27-38.

- Kazurova, N.S. 1961. Synoptic processes in Yakutia in different seasons and their brief characterization. In: *Issues of Yakutia Geography (Voprosy geografii Yakutii)* (in Russian). Yakutsk: Knizn. izd-vo, 19-26.
- Osterkamp, T. E. & Romanovsky, V.E. 1999. Evidence for warming and thawing of discontinuous permafrost in Alaska. *Permafrost and Periglacial Processes* 10: 17-37.
- Pavlov, A.V. 1994. Prediction of permafrost evolution in relation to global change of contemporary climate. In: *Current Issues in Hydrogeology, Engineering Geology and Ecology (Sovremennye problemy gidrogeologii, inzhenernoy geologii i ekologii)* (in Russian). Moscow: VSEGINGEO, 135-151.
- Pavlov, A.V. 1997. Permafrost and climate monitoring in Russia: methodology, observational results and prediction (in Russian). *Kriosfera Zemli* 1(1): 47-58.
- Smith, S.I., Burgess, M.M. & Taylor, A.E. 2003. High Arctic permafrost observatory at Alert, Nunavut – analysis of a 23 year data set. *Proceedings of the Eighth International Conference on Permafrost, Zurich, Switzerland, 21-25 July, 2003*: 1073-1078.
- Varlamov, S.M., Kim, E.S. & Han, E.C. 1998. Recent temperature variations in East Siberia and the Russian Far East (in Russian). *Meteorologia i Gidrologia* 1: 19-28.
- Varlamov, S.P. & Skachkov, Y.B. 1996. Spatiotemporal variability of climatic elements. In: V.T. Balobaev, M.K. Gavrilova, & A.N. Fedorov (eds.), *The Influence of Climate on Permafrost Landscapes in Central Yakutia (Vlianie klimata na merzlotnye landshafty Centralnoi Yakutii)* (in Russian). Yakutsk: Permafrost Institute Press, 11-36.
- Vasiliev, I.S. & Torgovkin, Y.I. 1996. The influence of climate on temperature and thickness of thawing soils. In: V.T. Balobaev, M.K. Gavrilova, & A.N. Fedorov (eds.), *The Influence of Climate on Permafrost Landscapes in Central Yakutia (Vlianie klimata na merzlotnye landshafty Centralnoi Yakutii)* (in Russian). Yakutsk: Permafrost Institute Press, 37-45.
- Vasiliev, I.S. 1992. Changes in climate elements and active layer thickness in western Yakutia. In: *Natural Resource Management in Permafrost Regions (Ratsionalnoe prirodopolzovanie v kriolitozone)* (in Russian). Moscow: Nauka, 43-46.
- Vasiliev, I.S. 1999. Response of soil temperatures to recent climatic variations (in Russian). *Meteorologia i Gidrologia* 2: 98-104.
- Zhang, T. & Osterkamp, T.E. 1993. Changing climate and permafrost temperatures in the Alaskan Arctic. *Proceedings of the Sixth International Conference on Permafrost, Beijing, China. July 5-9. Vol. 1*, 783-788.
- Zukert, N.V. & Zamolodchikov, D.G. 1997. Long-term trends of air temperature and precipitation in Russian tundra zone (in Russian). *Meteorologia i Gidrologia* 1(1): 47-58.

Approaches to Allocation of Terrain Complexes (Landscapes) in the Areas of Thermokarst Development

Alexandra Veremeeva

*Institute of Physicochemical and Biological Problems in Soil Science, Russian Academy of Sciences,
Pushchino, Moscow Region, Russia*

Stanislav Gubin

*Institute of Physicochemical and Biological Problems in Soil Science, Russian Academy of Sciences,
Pushchino, Moscow Region, Russia*

Abstract

Evaluation of organic matter content and the amount of greenhouse gases released in polar areas of Northern Yakutia, as well as the study of polar landscape stability in the face of climate warming, now demand systematization of the data on landscape structure of the Northern Yakutia lowlands. In this study, such systematization is performed on the basis of classifying and mapping major terrain complexes in the northern Kolyma Lowlands.

Keywords: global warming; landscape; mapping; permafrost; terrain complex; thermokarst.

Introduction

Active research in the Kolyma Lowlands started in the late 1950s. The greatest interest in this territory lies in the peculiarities of its formation during the Pleistocene. A considerable number of publications are devoted to the origin and stratigraphy of the Pleistocene deposits, Pleistocene flora and fauna, and to general paleo-reconstructions.

Since the 1990s, the Kolyma Lowland has become a key region for studies of possible permafrost degradation, which can be triggered by global warming. Degradation of permafrost is likely to be followed by significant release of methane and carbon dioxide (Rivkina et al. 1996, Rivkina et al. 2006, Walter et al. 2006). To answer the questions triggered by these studies, it is necessary to calculate the quantity of organic matter and amount of greenhouse gases released from it, and then to forecast future development of thermokarst. This, in turn, demands conducting studies of modern landscapes and systematization of present day concepts of the terrain structure. Detailed landscape studies for the northern Kolyma Lowland have not yet been implemented. To fill this gap, we set a task to define and distinguish the major landscapes types (Terrain Complexes) of the northern Kolyma Lowland, to classify them, to identify patterns of their distribution, and to map them using Geographic Information Systems for acquiring the desired parameters.

Objects and Methods of Research

Objects of research

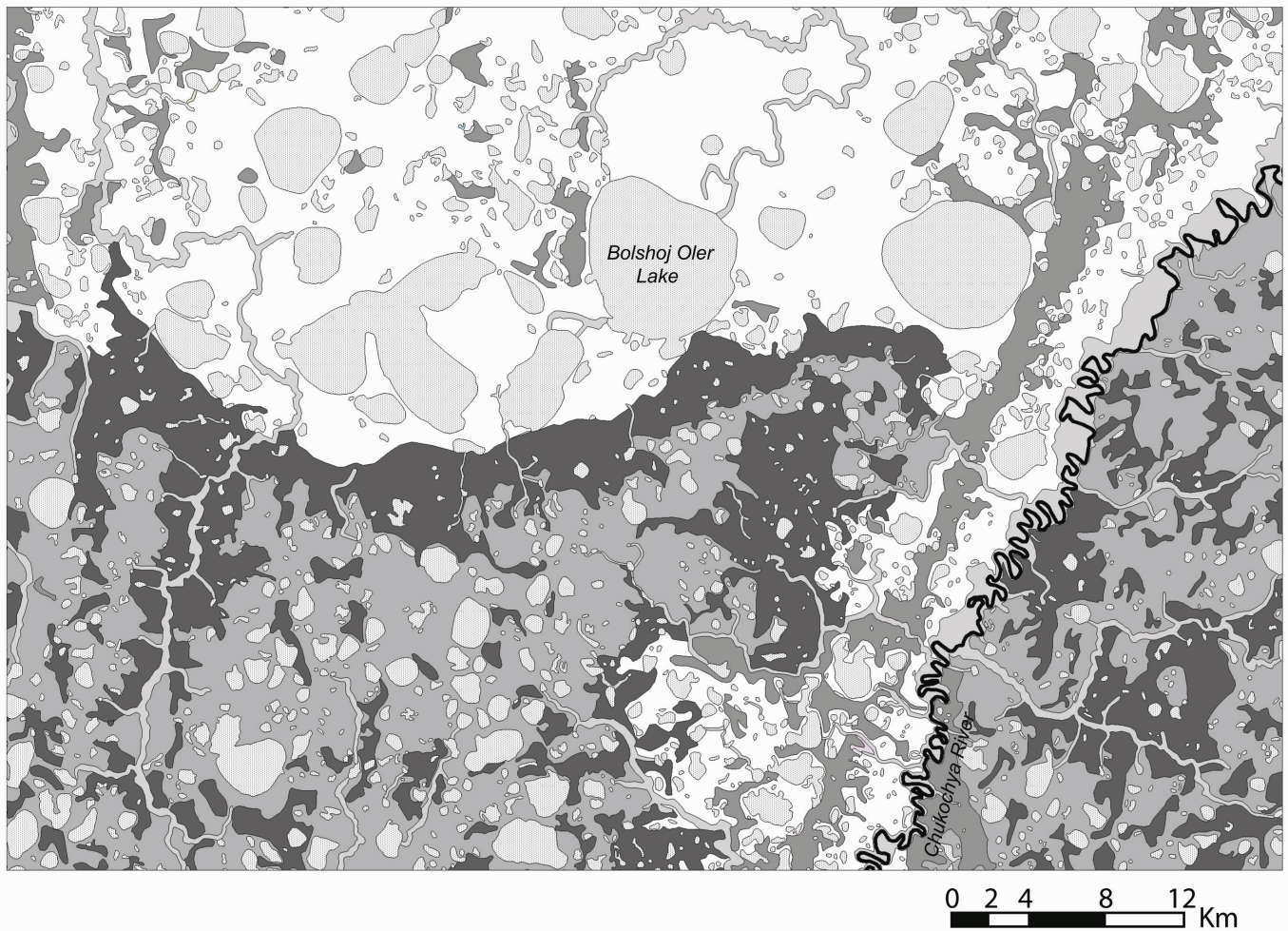
Our investigations are based on field data, collected during expeditions to this region (1980-2000), the studies of A.N. Fedorov (Fedorov 1991), and the permafrost-landscape map of Yakutian ASSR at 1:2500000 scale edited by P.I. Melnikov (1991). After analysis of field data, existing maps and publications, we selected the key study region for our research, which is a 6500 km² area in the Kolyma Lowlands located between the Alazeya River and Chukochoya River in

their middle flows (central coordinate is 69°30'N, 156°0'E). The region is located within the continuous permafrost zone; it belongs to the Alazeya-Kolyma lake-thermokarst province (Fedorov 1991). Comparison of the key region structure with the structure of other Northern Yakutia lowland areas shows that it is typical and reflects major patterns of tundra landscape development in the Holocene impacted by active thermokarst processes.

The key study region is characterized by flat and gently sloping thaw-lake depressions (thaw-lake basins), and the remnants of the Late Pleistocene surface formed by ice-rich deposit with polygonal ice wedges (named in the literature *Ice Complex* or *yedoma*). Based on paleogeographical data, we presume that during the Pleistocene the region was a flat plain underlain by ice-rich silts with ice wedges. At the Late Pleistocene-Holocene boundary, the active structural change began as a result of climate warming. Under the impact of thermo-erosional and thermokarst processes, the Ice Complex areas have been reduced, and they now represent different stages of thermokarst evolution. Some surfaces (relatively high elevation yedoma remnants) have not yet been reworked by thermokarst and have the thickest strata with ice wedges. Other surfaces have been partly reworked, and some have been transformed into thaw-lake basin depressions due to thawing of ground ice.

Methods of research

Allocation and mapping of landscapes first requires the determination of the basin mapping unit. A.N. Fedorov recommended distinguishing the hierarchy of local territorial geosystems on the basis of identifying leading factors among different characteristics, and considers the resulting boundaries to be absolute (Fedorov 1991). Another approach is suggested by Gr.A. Isachenko (Isachenko & Reznikov 1996, Isachenko 1998), who distinguish within a particular landscape different types of units characterized by relatively stable parameters:



Type of terrain	Index	Depth of permafrost table (m)	Sediments	Absolute elevations, m	Prevailing soils	Dominant type of vegetation
1. Drained surface of Yedoma remnants (gradient 0-15°) with initial forms of developing thermokarst (High Yedoma)		0.5-0.6	Ice-rich Late Pleistocene silts with polygonal ice wedges (Ice Complex)	40-80	Cryosols, gleysols	Gramineous-dryas, sedge-herbaceous shrub-moss
2. Slightly drained surface of Yedoma remnants (gradient 0-10°), with initial forms of developing thermokarst (Low Yedoma)		0.4-0.5	Ice-rich Late Pleistocene silts with polygonal ice wedges and overlaid with taberal deposits (thawed and refrozen sediments)	20-40	Gleysols histosols	Sedge-Herbaceous shrub-moss
3. Waterlogged flat surface with polygonal nano- and mesorelief, and numerous small lakes (Upper thaw-lake depressions)		0.2-0.4	Ice-rich lacustrine-alas deposits of thaw-lake basins with partially remained polygonal ice wedges	20-40	Gleysols histosols	Sedge-cotton grass, Herbaceous shrub- moss
4. Heavily waterlogged flat surface with polygonal nano- and mesorelief, and numerous lakes (Low thaw-lake depressions)		0.2-0.3	Ice-rich lacustrine-alas deposits of thaw-lake basins	10-30	Histosols, Gleysols	Sedge-moss
5. River valleys complex (with terraces)		0.3-0.8	Fluvial silty-sandy deposits	0-20	Fluvisols, histosols	Moss-shrub, Sedge-moss

Figure 1. Portion of terrain complexes map of the key study region.

1. similar position in relief (single meso-scale landform);
2. similar composition and cryogenic structure of sub-surface layers;
3. similar drainage conditions.

These characteristics determine the hydrographical network, distribution of lakes and bogs, soils and vegetation. They also define the so-called “rigid design” of the territory, which acts as a reference frame for study of long-term (hundreds of years) processes of landscapes development (Isachenko & Reznikov 1996). This approach corresponds to our tasks including the forecasting of terrain evolution at the onset of global warming.

Figure 1 shows the landscape map based on topographic maps of 1:200000 scale and confronted with Landsat 7 ETM+ satellite images. For charting, we used MapInfo 7.0 and ArcView 3.2. Topographic maps of 1:200000 scale are most useful for our task because they show every substantial roughness while, at the same time, make it possible to cover large territories. Another important property of this scale is its comparativeness with existing satellite images.

Results

On the basis of Isachenko's (1998) approach, we have distinguished five major types of terrain complexes in the key region: high yedomas, low yedomas, upper thaw-lake depressions, low thaw-lake depressions and river valleys. We have charted the digital landscape map of the key region at a 1:200,000 scale (Fig. 1). Analysis of the map shows that the largest part of the territory is the interstream area between the Alazeya River and the Chukochya River. In the north is located an extensive low thaw-lake depression. It is filled with many lakes (as large as 50 km²); the surface is flat so the drainage is limited. Within the depression only small remnants (not larger than 4 km²) of low yedoma are still preserved. Only along the major river valleys are vast remnants of low yedoma present, some of them as large as 50 km². Southward the territory of upper thaw-lake basins is located. There are a number of high yedoma remnants found here (with areas not larger than 6 km²). Large areas of yedoma are adjacent to river valleys and low thaw-lake depressions. The right bank of the Chukochya River is also an upper thaw-lake basin, where large areas of high yedoma are preserved (up to 60 km²). The latter are being drained by tributaries of the Chukochya River. The presence of vast high yedoma here is associated with exposed Oler sequence deposits containing low ice content and lacking polygonal ice wedges (Sher 1971). Thus, it determines the greater ruggedness of the surface and therefore the better drainage of the territory.

Table 1 shows that most common types of terrain complexes are thaw-lake depressions formed due to thawing ice wedges. They occupy 64.8% of the territory. The area of low and upper thaw-lake basins is 34.8% and 30.0%, respectively, of the total area of the key region. The area occupied by lakes in the upper and lower thaw-lake depressions makes up 21.5% and 29.3%, respectively, of the terrain complex area. High

Table 1. Areas occupied by terrain complexes and lakes.

Terrain complexes	Area of terrain complex (with lakes), sq km	Percentage of total area, %	Area of lakes, sq km	Percentage of total area of terrain complex, occupied by lakes, %
High Yedoma	1181.0	18.1	63.5	5.4
Low Yedoma	548.7	8.4	17.8	3.2
Upper thaw-lake depressions	1956.6	30.0	420.0	21.5
Low thaw-lake depressions	2274.3	34.8	665.8	29.3
River valleys	567.1	8.7	18.0	3.2
Total classified area	6527.7	100	1185.1	18.2

Table 2. Distribution of different groups of lakes (number and square) within separate terrain complex.

Groups of lakes	Number	In % of total lake number for terrain complex	Area, sq km	In % of total lake area	In % of terrain complex area
High Yedoma					
<0.1 km ²	204	56.4	11.1	17.4	0.9
0.1–1 km ²	151	41.7	38.4	60.5	3.2
>1 km ²	8	2.2	14.0	22.1	1.2
Low Yedoma					
<0.1 km ²	60	58.3	3.0	16.7	0.5
0.1–1 km ²	41	39.8	9.5	53.2	1.7
>1 km ²	3	2.9	5.3	30.0	1.0
Upper thaw-lake depressions					
<0.1 km ²	551	45.8	29.7	7.1	1.5
0.1–1 km ²	563	46.8	185.9	44.3	9.5
>1 km ²	90	7.5	204.4	48.7	10.4
Low thaw-lake depressions					
<0.1 km ²	373	42.1	22.0	3.3	1.0
0.1–1 km ²	408	46.1	133.2	20.3	5.9
>1 km ²	104	11.8	502.6	76.4	22.1
River valleys					
<0.1 km ²	78	60.5	4.1	22.8	0.7
0.1–1 km ²	49	38.0	10.3	57.1	1.8
>1 km ²	2	1.6	3.6	20.2	0.6

and low yedomas occupy about 26.5% of the territory, and the lake percentage of terrain complexes is 5.4 and 3.2%, respectively.

Lakes are classified according to the area on three groups within each terrain complex: large (>1 km²), medium (0.1 to 1 km²) and small (<0.1 km²) (Table 2).

Lakes with areas of more than 1 km² occur sporadically within yedomas, and medium lakes predominate here by total area. Small lakes, which existence is connected with the initial stages of thermokarst development, prevail by number. Within the high yedoma terrain complex are found small thermokarst depressions, filled by medium lakes. Large lakes dominate in low thaw-lake basins. They occupy 22.1% of the area of low thaw-lake basins and 76% of summarized area of lakes within this landscape. In upper thaw-lakes basins, areas of large and medium lakes are comparable (10.4 and 9.5% respectively). It demonstrates the potential of increasing the area of medium lakes from climate warming and thawing of polygonal ice wedges.

Conclusions

Allocated terrains (all types except river valleys) represent different stages in the regional development. High yedoma are the remnants of the Late Pleistocene surface. At the end of Pleistocene and the beginning of the Holocene at 12 kyr BP (Schirmeister et al. 2002), as a result of climate warming the active modeling of initial landscape and the formation of vast thaw-lake basins had begun. The most active stage of thermokarst development, characterized by maximum total area occupied by thaw-lake basins (present upper thaw-lake depressions), took place 7–5 kyr BP (Kachurin 1961, Grosse 2005). A substantial proportion of thaw-lake basins formed during this time later underwent further development from thermokarst and thermo-erosional process, especially at watershed locations. On that part of the region where thermokarst processes ceased or stopped, low yedomas were formed with partly melted polygonal ice wedges overlain by tabular deposits.

The next stage of active thermokarst development and formation of low thaw-lake basins took place in the late Holocene 3000–700 years ago (Baulin et al. 1967, Chekhovskiy & Shamanova 1976).

The present age is characterized by climate cooling (Schirmeister et al. 2002), which is confirmed by the absence of track of thermokarst activation during the past 50 years (Voskresenskiy 2001). More than 80% of the initial Late Pleistocene plains are modeled by thermokarst and thermo-erosional processes. Slopes of yedomas and thaw-lake depressions are gradually flattening and overgrowing by vegetation. The total portion of thaw-lake basins area in the region of research is 18.2%. It is commensurable with other regions with Ice Complex: Bykovskiy Peninsula (lower course of river Lena – 14.4%, (Grosse 2005), and the Barrow Peninsula (Alaska) – 22% (Hinkel et al. 2003).

In case the global warming scenario is realized, the most stable areas will be low thaw-lake depressions because at these areas polygonal ice wedges have already melted out, and peat layers with a thick moss mat formed at the surface protects the permafrost substrate from incoming warmth.

Upper thaw-lake basins are subject to partial surface modeling in case of the onset of global warming. Polygonal ice wedges, although partly melted, still exists here; activation

of thermokarst and thermo-erosional processes causes further melting and an increase of lake areas is likely.

Even more unstable during climate warming by thermokarst activation will be yedomas. Low yedomas will be more stable than high yedomas because polygonal ice wedges in low yedomas are located deeper, the peat and moss mat is thicker, and permafrost is more resistant to thermokarst (waterlogged areas are more frequent here).

High yedomas are the most unstable areas and are highly susceptible to thermokarst and thermo-erosional processes because polygonal ice wedges are very close to the surface, which in turn is characterized by free drainage. Peat and vegetation are uncommon and don't provide thermal insulation.

The information obtained about terrain structure and terrain complex distribution and evolution patterns helps to forecast thermokarst development in the northern Yakutia coastal lowlands at the onset of global warming.

This study is the first stage of northern Kolyma Lowland landscapes research. We consider it as a basis for other studies of northern coastal lowlands of Yakutia.

References

- Baulin, V.V., Belopukhova, E.B., Dubikov, G.I. & Shmelev, L.M. 1976. *Geocryological conditions of Western Siberia Lowland*. Moscow: Nauka Press, 214 pp (in Russian).
- Chekhovskiy, A.L. & Shamanova, I.I. 1976. Forming of taliks under the thermokarst lakes of Western Siberia. *Proceedings of PNIIS*. Moscow, 49: 64-73 (in Russian).
- Fedorov A.N. 1991. *Permafrost landscapes of Yakutia: method of allocation and problems of mapping*. Yakutsk, Russia, 140 pp. (in Russian).
- Grosse, G. 2005. *Characterisation and evolution of periglacial landscapes in Northern Siberia during the Late Quarternary – Remote sensing and GIS studies*. Dissertation. Potsdam, 126 pp.
- Hinkel, K.M., Eisner, W.R., Bockheim, J.G., Frederick, E.N., Peterson, K.M. & Dai, X. 2003. Spatial extent, age, and carbon stocks in drained thaw lake basins on the Barrow Peninsula, Alaska. *Arctic, Antarctic and Alpine Research* 35: 291-300.
- Isachenko, Gr.A. 1998. *Field landscape research methods and landscape-ecology mapping*. St.-Petersburg State University Press, 112 pp. (in Russian).
- Isachenko, Gr.A. & Reznikov, A.I. 1996. *Taiga of the European Russia north-west: landscape dynamics*. St.-Petersburg State University Press, 140 pp. (in Russian).
- Kachurin, S.P. 1961. Thermokarst on USSR territory. Moscow, Academy of Science Press, 291 pp. (in Russian).
- Permafrost-landscape map of Yakutian ASSR of 1:2500000 scale. 1991. Edited by Melnikov P.I. Moscow, 2 pp. (in Russian).

- Rivkina, E.M., Kraev, K.V., Krivushin, K.S., Laurinavichus, K.S., Fyodorov-Davydov, D.G., Kholodov A.L., Shcherbakova, V.A. & Gilichinskyy, D.A. 2006. *Methane in permafrost of Northeastern Arctic. Cryosphere of Earth* 3: 23-42 (in Russian).
- Rivkina, E.M. & Gilichinskyy, D.A. 1996. Methane as a paleoindicator for genesis and dynamics of frozen layers. *Lithology and Minerals* 4: 183-193 (in Russian).
- Schirmermeister, L., Siegert, C., Kuznetsova, T., Kuzmina, S., Andreev, A.A., Kienast, F., Meyer, H. & Bobrov, A. 2002. Paleoenvironmental and paleoclimatic records from permafrost deposits in the Arctic region of Northern Siberia. *Quaternary International* 89: 97-118.
- Sher, A.V. 1971. *Mammals and Stratigraphy of the Pleistocene of the Extreme Northeast of the USSR and North America*. Moscow: Nauka Press, 310 pp. (in Russian).
- Voskresensky, K.S. 2001. *Modern relief forming processes at plains of North of Russia*. Moscow State University Press, Geographic Department, 260 pp. (in Russian).
- Walter, K.M., Zimov, S.A., Chanton, J.P., Verbyla, D. & Chapin III, F.S. 2006. Methane bubbling from Siberian thaw lakes as a positive feedback to climate warming. *Nature*. V (443): 71-75.

Numerical Studies of Permafrost Effects on Groundwater Flow

Patrik Vidstrand

Chalmers University of Technology, Gothenburg, Sweden

Jens-Ove Näslund

Swedish Nuclear Fuel and Waste Management Company, Stockholm, Sweden

Juha Hartikainen

Helsinki University of Technology, Espoo, Finland

Abstract

Despite the inferred present global warming trend, future climate during the long life-span of a nuclear waste repository could well include periods of permafrost development in all of Sweden. The occurrence of permafrost in soil and bedrock can alter significantly surface boundary conditions that affect groundwater recharge and discharge as well as the deeper circulation of groundwater in the bedrock presently investigated for the potential to accommodate nuclear waste. Within the safety assessments, generic studies on deep groundwater circulation in the presence of permafrost have been conducted. The present study includes a compilation of future permafrost scenarios and their implications on the groundwater flow. The results suggest that for a location where unfrozen taliks are present, sporadic permafrost will reduce while continuous permafrost will enhance groundwater flow. The study, although generic in character, is conclusive on the importance of permafrost in controlling both local and regional groundwater flow systems.

Keywords: climate scenario; groundwater flow; permafrost; taliks.

Introduction

Over the life-span of relevance for a nuclear waste geological repository, climate models predict future climatic situations that result in permafrost development, glacial conditions, and changes in shoreline elevation with possibilities for both elevated and submerged situations. Conditions of permafrost as surface boundary cause changes within the subsurface environment in hydrogeological properties as well as in the hydrogeochemistry.

Permafrost is defined as ground that is at or below 0°C for at least two consecutive years (French 1996). This definition has the implication that permafrost does not necessarily need to be frozen ground. However, the greatest impact on the subsurface hydrology from permafrost is the phase change related to the freezing of water. Frozen water creates an almost impervious stratum, which inhibits groundwater recharge but also the possibility of discharge, highlighting the possibility of high groundwater pressure beneath the permafrost (McEwan & de Marsily 1991, Boulton et al. 1993, Haldorsen & Heim 1999). One possible change due to permafrost is a re-organization of the regional as well as local groundwater flow regimes caused by the occurrence of frozen and nonfrozen areas within the ground.

This study mainly addresses the possible effects of different upper boundary conditions. The different scenarios considered are based on climate scenarios for the Forsmark site in Northern Uppland, Sweden; with special attention to the SFR geological repository for low and intermediate radioactive substances.

Even though the study is a hydrogeological flow study, it was not intended to create a realistic representation of the “true” groundwater flow situation. The purpose was instead to provide a safety analysis with quantification of, and

uncertainty indicators for, the possible effects of different upper boundary conditions. Overall, the strategy was to use simplified models in the simulation of scenario cases to provide the safety analysis with relative flux values and uncertainty ranges.

Site Description

The site for this study is found in the Forsmark area in Northern Uppland, on the east coast of Sweden; some 200 km northwest of Stockholm. The site is one of the candidate sites for siting a nuclear waste deep geological repository in Sweden, but also hosts an active repository for low and intermediate nuclear waste (SFR).

The corrected precipitation in Forsmark for the measurement period August 1, 2003, to July 31, 2004, was



Figure 1. Location of the study area.

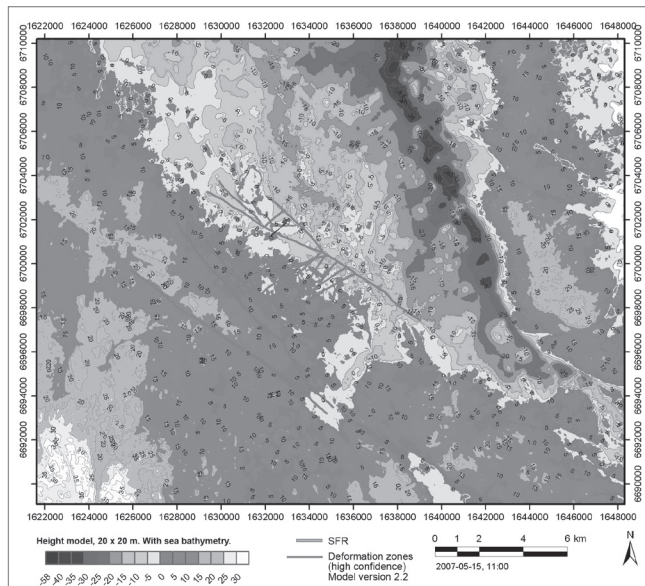


Figure 2. Local topography of the SFR region and the high confidence large-scale deformation zones as defined in the site investigation program.

630 mm. The total “potential evapotranspiration” as reported in Lindborg (2005) was 472 mm for the same period. These numbers are in alignment with the long-term statistics from the Swedish Meteorological and Hydrological Institute (SMHI) for nearby stations as reported in Larsson-McCann et al. (2002). Based on these numbers, the net precipitation and the ground hydraulic properties indicate an excess of water in order to keep the groundwater table close to the surface. A permafrost environment may be significantly dryer as compared to present day conditions. However, the topography and geology at the site support a groundwater table close to the surface even if the net recharge is decreased to only one tenth. Hence, it is justified to assume a fully saturated subsurface and a groundwater table close to the surface as well as a prescribed pressure boundary condition at the surface also during permafrost conditions.

The local topography of the SFR region and the high-confidence large-scale deformation zones as defined in the site investigation programme is presented in Figure 2.

Future Climate and Permafrost Development

Climate-related changes, such as changes in shoreline elevation and development of permafrost and ice sheets, are the most important naturally occurring external factors affecting a nuclear waste repository in a time perspective from tens to hundreds of thousands of years.

It is not possible to predict the evolution of the climate in a 100,000-year time perspective with enough confidence for a safety assessment. However, the extremes within which the climate of Sweden may vary can be estimated with reasonable confidence. Within these limits, characteristic climate-related conditions of importance for repository safety can be identified. The conceivable climate-related conditions can be represented as *climate-driven process domains* (Boulton

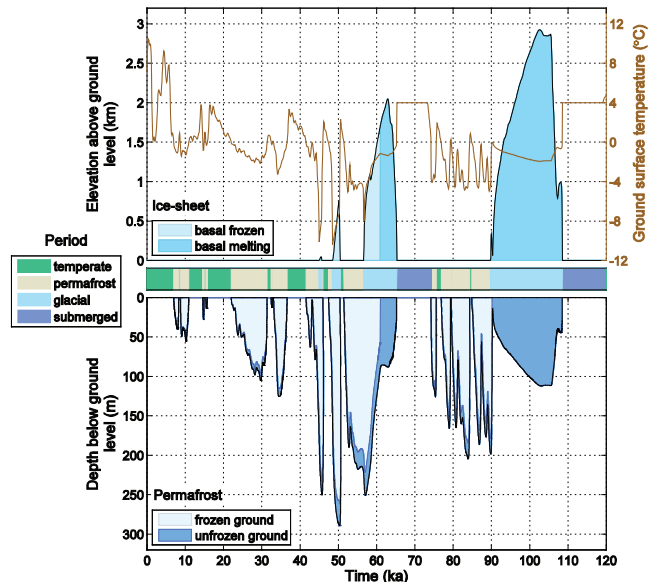


Figure 3. A climate scenario for the Forsmark region, including prevailing climate domains and climate related variables for a timeframe of 120,000 years in the future.

et al. 2001) where such a domain is defined as a *climatically determined environment in which a set of characteristic processes of importance for repository safety appear*. In the following, these climate-driven process domains are referred to as *climate domains*.

The identified relevant climate domains are named as

- The temperate domain
- The permafrost domain
- The glacial domain

The purpose of identifying climate domains is to create a framework for the assessment of issues of importance for repository safety associated with particular climatically determined environments that may occur in Sweden. If it can be shown that a repository fulfills the safety requirements independent of the prevailing climate domain, and the possible transitions between them, then the uncertainty regarding their exact timing in the future is less important. In addition to these climate domains, it is necessary to consider the periods for which the site is submerged by the Baltic Sea.

Figure 3 shows an example of a future scenario at Forsmark in a 120,000-year time frame in the future (SKB 2006). The scenario based on the evolution of the last glaciation, the Weichselian, and involves all the three climate domains. The permafrost domain is defined as periglacial regions that contain permafrost. It is a cold region without the presence of an ice sheet. The permafrost can occur in sporadic, discontinuous, or continuous forms. Regions belonging to the permafrost domain are not necessarily the same as regions with a climate that *supports* permafrost; i.e., as long as permafrost is present and not underlying an ice sheet, the region is defined as belonging to the permafrost domain, regardless of the prevailing temperature at the ground surface. Thereby, the climate in the permafrost domain can be warm diminishing permafrost. This way of defining the

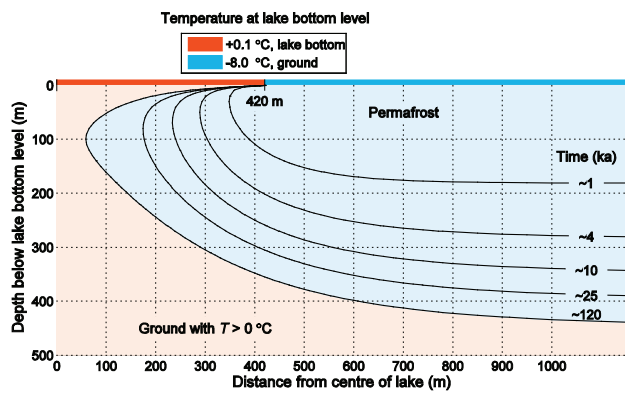


Figure 4. Evolution of permafrost in the vicinity of a circular lake of radius of 420 m at Forsmark when a constant lake bottom temperature of +0.1°C, and a constant ground temperature of -8°C at lake bottom level are assigned.

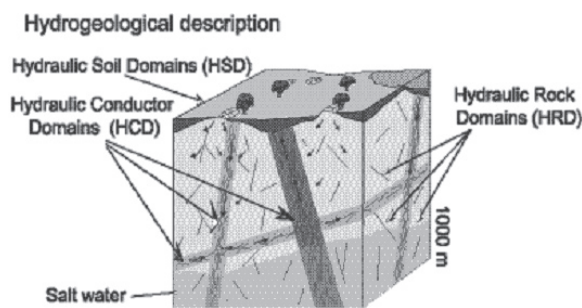


Figure 5. The Quaternary deposits and the crystalline bedrock are divided into separate hydraulic domains named the Hydraulic Soil Domains (HSD), Hydraulic Rock Mass Domains (HRD), and Hydraulic Conductor Domains (HCD). Within each domain, the hydraulic properties are represented by mean values or by spatially distributed statistical distributions (after Rhén et al. 2003).

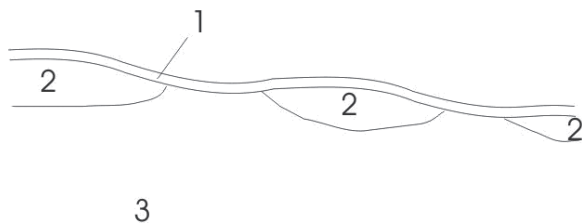


Figure 6. Illustration of conceptual model when permafrost is present.

domain is used because the presence of permafrost is more important for the safety function of the repository than the actual temperature at the ground surface. In general, the permafrost domain has a climate colder than the temperate domain and warmer than the glacial domain.

Large water bodies affect permafrost development and the presence of taliks. A talik can exist beneath a water body when its bottom temperature remains above the freezing point. Figure 4 demonstrates that an open talik can survive beneath a circular shallow lake, if its radius is greater than the thickness of ambient permafrost (SKB 2006).

Hydrogeological Numerical Flow Modeling

Basis

The computer code DarcyTools has been developed for simulations of groundwater flow and mass transport in porous and fractured media; the code uses continuum equations. Detailed descriptions of the concepts, methods, and equations of DarcyTools are documented in Svensson et al. (2004).

The modeling methodology used in this study followed SKB’s system approach for hydrogeological modeling (Rhén et al. 2003), which herein is much simplified. This approach divides the geosphere into three types of Hydraulic Domains, representing the Quaternary deposits, or Hydraulic Soil Domain (HSD), the fracture zones (HCD), and the rock mass between the fracture zones (HRD) (Fig. 5).

This study was conducted in two dimensions, even though such an approach is not necessarily well suited to the representation of fracture systems. Also, the study did not concentrate on a surface hydrology and, hence, did not include any soil cover (soil domain). The bedrock is in principle assumed to be a homogeneous porous medium with isotropic characteristics.

Common to all cases is no-flow boundary conditions on the lateral (side) boundaries and at the bottom for the sake of simplicity; sensitivity studies where the lateral boundaries were specified as hydrostatic showed no change in the results. The model is a fresh water model. The upper boundary is a spatially distributed specified pressure boundary assessed for the different surface conditions (climate domains); i.e., the groundwater table is fixed close to or at the ground surface. All simulations are steady-state.

All assigned hydrogeological properties are homogeneous within their specified model domains (Fig. 6):

- Unfrozen bedrock [3] (deep bedrock) has a hydraulic conductivity of $3 \cdot 10^{-8}$ m/s;
- Frozen bedrock [2] (permafrost) has a hydraulic conductivity of $3 \cdot 10^{-14}$ m/s;
- An active layer [1], if present, has a hydraulic conductivity of $3 \cdot 10^{-4}$ m/s.

An active layer is present for all cases with assumed maximum infiltration capacity. Sensitivity to less available water has been tested where the active layer is removed and replaced with no-flow bodies along the surface boundary.

Reference case

These results are considered to be a representation of the present-day conditions. However, the simulations are a simplification in terms of conceptual model as well as flow dimensions and hydrogeological properties.

For simulations of the reference case, the hydraulic conductivity was specified as a homogeneous value of $3 \cdot 10^{-8}$ m/s. The upper boundary has a prescribed pressure at ground surface, which mimics a case of maximum infiltration (groundwater recharge). The regional topographic gradient is 3 m per km, but applies in combination with a more local gradient created by a sinusoidal surface with a wavelength of 5 km and amplitude of 10 m. Further, the groundwater throughout the domain is taken to be fresh water.

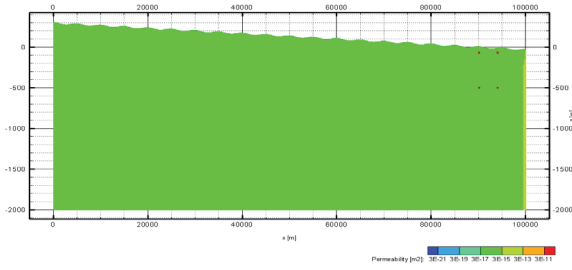


Figure 7. Permeability structure of the reference case. The four dots in the right upper model domain corner indicate the locations for synthetic repositories through which the flow is investigated.

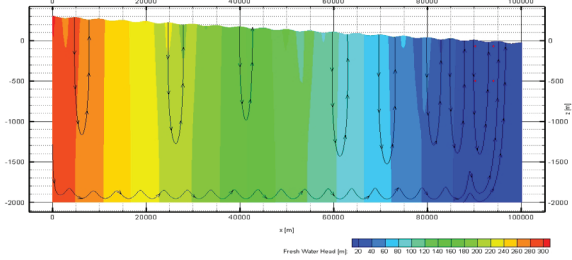


Figure 8. Fresh water heads of the steady-state solution of the reference case.

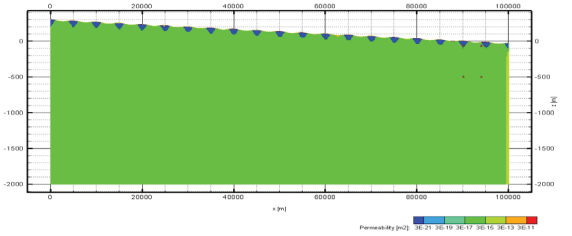


Figure 9. Conceptual model for the case of sporadic permafrost.

Figure 8 presents the fresh water head of the steady-state solution of the reference case. The head situation along with the illustrative streamlines indicates the strong influence of the local topographic gradient. However, these results are strongly dependent on the shape of the local topography; for a case with only a regional gradient the flow also is regional with discharge only in the sea. A smaller local topographic variation yields more regional flow as compared with the reference case. These effects also affect the magnitude of the flux and were hence the subject of the sensitivity study presented below.

It should be noted that regions located beneath sea elevation (zero m altitude) all have a fresh water head of zero independent of where the sea bottom is located.

Permafrost cases

The sporadic permafrost case is illustrated below (Fig. 9). The maximum depth of permafrost is 100 m. The chosen maximum permafrost depth is used since it is adequate for illustration purposes.

The continuous permafrost case is illustrated below (Fig. 10). The maximum depth of permafrost is again due to illustrative reasons set to 100 m. Open taliks are located

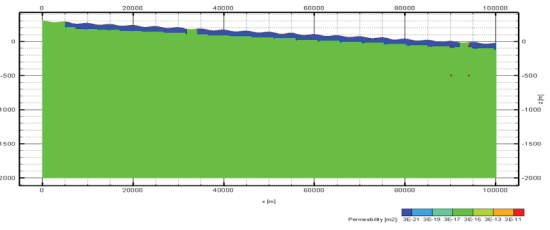


Figure 10. Conceptual model for the case of continuous permafrost.

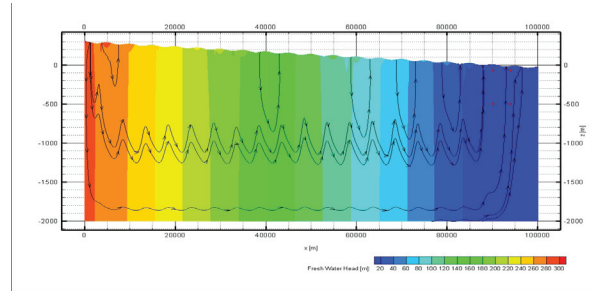


Figure 11. Fresh water heads of the steady-state solution for the sporadic permafrost case.

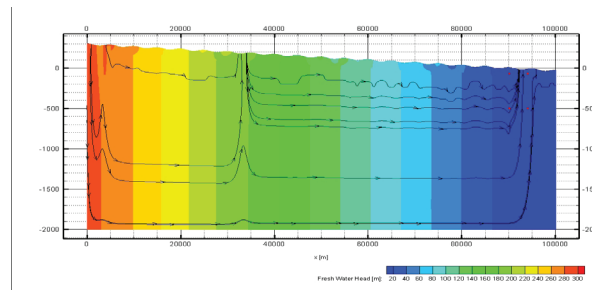


Figure 12. Fresh water heads of the steady-state solution for the continuous permafrost case.

between the extensive areas of permafrost.

Figure 11 presents the fresh water head of the steady-state solution of the maximum infiltration case for sporadic permafrost. The maximum infiltration case is conducted with a fully saturated active layer on top of all frozen regions. The head situation along with the illustrative streamlines indicates the influence of the patches of frozen ground on the regional flow.

Figure 12 presents the fresh water head of the steady-state solution of the maximum infiltration case for continuous permafrost. The head situation along with the illustrative streamlines indicates the strong influence of the open taliks and of the regional topographical gradient. The flow is from one open talik toward the next, downstream, open talik. The results further indicate that a talik located along the regional gradient acts as a discharge location but also, at the same time, recharges water into the system.

Discussion

Two different groundwater flow scenarios involving the presence of permafrost have been studied. These are (1) a sporadic permafrost distribution, in which the groundwater

within local topographic highs is frozen, and (2) a continuous permafrost distribution, in which extensive permafrost exists all over the model domain, only locally bypassed by open taliks (i.e., unfrozen regions in the permafrost).

The sporadic permafrost produces a situation where the regional groundwater flow becomes more important and the flow driven by local topographical differences becomes less important. This yields a smaller total flow for the sporadic permafrost scenario as compared with the reference case.

The continuous permafrost case yields an increase in the water flux all over a talik where discharge of water is occurring; a situation where a talik contains regions of both recharge and discharge is possible according to the conceptual model used, but is more likely to occur in regional up-stream locations than at the location of SFR repository. However, after emerging from the sea by shoreline displacement, when permafrost first is encountered, the location of SFR will be on a hill side. The location is more on the shaded side and hence it is possible for it to have early permafrost development. Hence the location may become frozen relatively early. However, the location of the shoreline when the first permafrost arrives is not well determined, and for a situation in which the SFR is still beneath water at that time, a talik could be formed above it. A sensitivity test of the location of the measurement volume within a talik indicates that a continuous permafrost situation could enhance the water flux through the facility by up to one order of magnitude.

The continuous permafrost situation may have a smaller impact, if the amount of available water is small, an effect different from that found in the sporadic permafrost case. A situation with less available water is mimicked by replacing the active layer with no-flow bodies (frozen) along the surface boundary. However, the decrease of flow in a dry scenario is not so large that it counteracts the effect of a talik in increasing the flow.

Even though it was not an investigated issue of the study it is, as expected, clear that for both the sporadic and continuous permafrost cases the total flow of groundwater through the model domain is decreased as compared to the reference case. This effect is most dominant when no active layer is part of the simulations. However, as described above this does not by necessity mean that the flow through the investigated generic repository volume is decreased.

In relation to thermal permafrost simulations, it should be noted that for most simulated episodes of possible future permafrost the frozen groundwater has reached a depth exceeding that of the SFR repository. If the ground surrounding the repository is frozen, the groundwater flow becomes negligible, but other problems arise, such as possible failures of the buffer material.

Conclusions

The upper boundary conditions have a significant impact on the groundwater flow in the geosphere. Permafrost and the development from sporadic permafrost to continuous permafrost yield increased groundwater flows in unfrozen parts of the domain. The increase is one order of magnitude

or less. In the permafrost, the flow is negligible.

The characteristic of the surface in regard to being a recharge or discharge area affects the results. In general, a discharge area will experience an increase in groundwater flow under changed conditions.

Acknowledgments

The economic support for this work provided by the Swedish Nuclear Fuel and Waste Management Company (SKB) and Bergab is greatly acknowledged.

Further, the review work by Professor M. Thorne, Professor L.O. Ericsson, and Dr. J-O Selroos of the main report published by SKB is acknowledged. The main report could be downloaded from www.skb.se under Publications (Hydrogeological flux scenarios at Forsmark, R-07-63).

The anonymous reviewer is acknowledged for improving the clarity of the paper.

References

- Boulton, G.S., Kautsky, U., Morén, L. & Wallroth, T. 2001. *Impact of Long-Term Climate Change on a Deep Geological Repository for Spent Nuclear Waste*. SKB TR-99-05, Stockholm, Sverige: Svensk Kärnbränslehantering AB.
- Boulton, G.S., Slot, T., Blessing, K., Glasbergen, P., Leijnse, T. & van Gijssel, K., 1993. Deep circulation of groundwater in overpressured subglacial aquifers and its geological consequences. *Quaternary Science Review* 12(9): 739-745.
- French, H.M., 1996. *The Periglacial Environment*, 2nd ed.. Addison Wesley Longman Limited.
- Haldorsen, S. & Heim, M. 1999. An arctic groundwater system and its dependence upon climatic change: An example from Svalberg, *Permafrost and Periglacial Processes* 10(2): 137-149.
- Larsson-McCann, S., Karlsson, A., Nord, M., Sjögren, J., Johansson, L., Ivarsson, M. & Kindell, S. 2002. *Meteorological, Hydrological and Oceanographical Information and Data for the Site Investigation Program in the Communities of Östhammar and Tierp in the Northern Part of Uppland*. SKB TR-02-02. Stockholm, Sverige: Svensk Kärnbränslehantering AB.
- Lindborg, T. (ed.) 2005. *Description of Surface Systems Preliminary Site Description Forsmark Area – Version 1.2*. SKB R-05-03. Stockholm, Sverige: Svensk Kärnbränslehantering AB.
- McEwan, T. & de Marsily, Gh. 1991. *The Potential Significance of Permafrost to the Behaviour of a Deep Radioactive Waste Repository*. SKI Technical Report 91:8. Stockholm, Sweden: Swedish Nuclear Power Inspectorate.
- Rhén, I., Follin, S. & Hermansson, J. 2003. *Hydrogeological Site Descriptive Model – a Strategy for its Development During Site Investigations*. SKB R-03-08. Stockholm, Sverige: Svensk Kärnbränslehantering AB.

- SKB, 2006. *Climate and Climate-related Issues for the Safety Assessment SR-Can*. SKB TR-06-23. Stockholm, Sverige: Svensk Kärnbränslehantering AB.
- Svensson, U., Kuylenstierna, H-O. & Ferry, M. 2004. *DarcyTools Version 2.1. Concepts, Methods, Equations and Demo Simulations*. SKB R-04-19, Stockholm, Sverige: Svensk Kärnbränslehantering AB.

Geomorphological Observations of Permafrost and Ground-Ice Degradation on Deception and Livingston Islands, Maritime Antarctica

Gonçalo Vieira

Centre of Geographical Studies, University of Lisbon, Portugal

Jerónimo López-Martínez

Autonomous University of Madrid, Spain

Enrique Serrano

Department of Geography, University of Valladolid, Spain

Miguel Ramos

Department of Physics, University of Alcalá de Henares, Spain

Stephan Gruber

Department of Geography, University of Zurich, Switzerland

Christian Hauck

University of Karlsruhe, Germany

Juan José Blanco

Department of Physics, University of Alcalá de Henares, Spain

Abstract

The Antarctic Peninsula is experiencing one of the fastest increases in mean annual air temperatures (ca. 2.5°C in the last 50 years) on Earth. If the observed warming trend continues as indicated by climate models, the region could suffer widespread permafrost degradation. This paper presents field observations of geomorphological features linked to permafrost and ground-ice degradation at two study areas: northwest Hurd Peninsula (Livingston Island) and Deception Island along the Antarctic Peninsula. These observations include thermokarst features, debris flows, active-layer detachment slides, and rockfalls. The processes observed may be linked not only to an increase in temperature, but also to increased rainfall, which can trigger debris flows and other processes. On Deception Island some thermokarst features may be related to anomalous geothermal heat flux from volcanic activity.

Keywords: active layer; Antarctic; debris flow; permafrost; thermokarst.

Introduction

The Antarctic Peninsula is experiencing the strongest warming signal in the Southern Hemisphere, with mean annual air temperatures (MAAT) increasing ca. 3°C since 1951 (Marshall et al. 2002, Meredith & King 2005, Turner et al. 2005). However, the region of strongest warming is limited in area, with the highest increases near Faraday/Vernadsky Stations and lesser increases near the northern tip of the Peninsula and the Orcadas Islands (King & Comiso 2003, Turner et al. 2007). Global Climate Model (GCM) projections for 2001–2100 suggest that the strongest warming will extend into the Antarctic continent, with values even greater than those expected on the Antarctic Peninsula (Chapman & Walsh 2007).

The strong atmospheric warming in the Antarctic Peninsula region has had a substantial effect on glaciers in the last few decades, especially on ice-shelves along the eastern coast (Scambos et al. 2003). The collapse of Larsen-B in 2002 is the most well-known example, but the retreat of mountain and outlet glaciers has been also reported. On Livingston Island (Hurd Peninsula) glaciers have been retreating and equilibrium-line elevations increasing (Ximenis et al. 1999, Molina et al. 2007).

Permafrost is central to the carbon cycle and to the climate system, especially due to CH₄ and CO₂ release following permafrost degradation in organic-rich sediments (Anisimov et al. 1997, Osterkamp 2003). The active-layer thickness and dynamics are also important factors in polar ecology. Since most exchanges of energy, moisture, and gases between the atmospheric and terrestrial systems occur through the active layer, its thickening has important ramifications on geomorphic, hydrologic and biological processes (Nelson & Anisimov 1993). Furthermore, permafrost degradation can cause terrain instability and increase geomorphological hazards and damage to infrastructures. According to the International Panel on Climate Change (IPCC), regions underlain by permafrost have been reduced in extent, and a warming of the ground has been observed in many areas (Anisimov et al 2001, Lemke et al 2007). Permafrost is, therefore, recognized by the (World Climate Research Programme/World Meteorological Organization (WCRP/WMO) as a key element of the Earth System in which research efforts should focus. However, compared with the Arctic, very little is known about the distribution, thickness, and properties of permafrost in Antarctica. The scarcity of data on Antarctic permafrost is reflected in the last IPCC

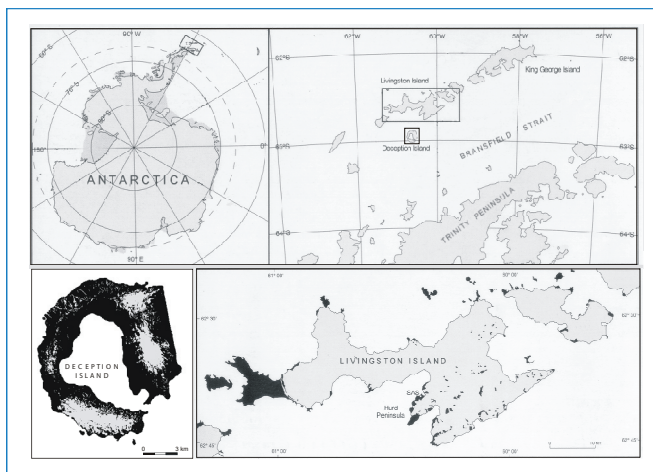


Figure 1. Location of Deception and Livingston Islands in the Antarctic.

report (Lemke et al. 2007) where it is not even mentioned. The main problem is the limited network of boreholes for monitoring permafrost temperatures and the paucity of active-layer monitoring sites. Turner et al. (2007) mention a reduction in permafrost extent in the Antarctic Peninsula region.

In general, increasing air temperatures will have a direct influence on ground-temperature regimes and, therefore, on permafrost and ground ice. A major consequence of warming of the lower atmosphere is an increase in active-layer thickness, which induces permafrost degradation and amplifies the rates of geomorphic processes. As a consequence, thermokarst features are prone to occur in ice-rich and unconsolidated sediments, active-layer detachment slides and debris flows on sloping ground, and an increase in rockfall activity may occur in rocky terrain.

The northerly location of the Antarctic Peninsula region and the oceanic setting result in a milder and moister climate than in the interior of the Antarctic continent. The northern Antarctic Peninsula is roughly located between the MAAT isotherms of -1 to -8°C at sea level and, therefore, the northern tip of the Peninsula and especially the South Shetland islands are close to the environmental limits of permafrost occurrence (Bockheim 1995). If the observed warming trend continues, as indicated by climate models, the region might suffer widespread permafrost degradation.

Monitoring of ground temperatures is essential for assessing the reaction of permafrost to global change, but in remote areas the drilling and maintenance of boreholes is problematic. Geomorphological surveying enables identification of the processes related to permafrost degradation and provides important information for assessing the influence of climate change on ground temperatures. However, other techniques are needed, such as geophysical surveying, monitoring of active-layer depths, micrometeorological measurements, and modelling to achieve a more complete overview of the response of permafrost to regional warming.

This paper joins together inputs from two groups researching in the South Shetlands. The group of the

Autónoma de Madrid and Valladolid universities (i.e., Serrano & López-Martínez 2000, Smellie et al. 2002, Serrano 2003) has been focusing on geomorphological surveying and mapping of the periglacial processes in the South Shetlands (Fig. 1). The group at the universities of Alcalá de Henares, Lisbon, Zurich, and Karlsruhe (Ramos & Vieira 2003, Vieira & Ramos 2003, Ramos et al. 2007, Hauck et al. 2007) has been monitoring ground temperatures and modelling spatial distribution of permafrost. In this paper a synthesis of observations on geomorphic processes that are seemingly related to permafrost and ground-ice degradation from Hurd Peninsula (Livingston Island) and Deception Island is presented. The next step is a geomorphological and climatological monitoring programme, which is planned to start in 2008–09.

Climate of the South Shetlands

The climate of the South Shetlands is cold-oceanic at sea level with frequent summer rainfalls and a moderate annual temperature range. Mean annual air temperatures are close to -2°C at sea level and average relative humidity is very high, ranging from 80 to 90% (Simonov 1977, Rakusa-Suszczewski 1993). The weather conditions are dominated by the influence of the polar frontal systems, and atmospheric circulation is variable, with the possibility of winter rainfall occurring as far south as Rothera Station (Turner et al. 2007). Temperature data from Hurd Peninsula recorded by our group for the period of 2003–05 at 20 m a.s.l. show values comparable to those at Arctowski Station on King George Island. From April to November average daily temperatures stay generally below 0°C and from December to March temperatures are generally slightly above 0°C . Two contrasting seasons in terms of freezing and thawing are, therefore, defined. At 275 m a.s.l. on Reina Sofia Hill the recorded mean annual air temperatures were of ca. -4.2°C . This corresponds to a lapse rate of $-0.8^{\circ}\text{C}/100\text{ m}$ and to a freezing season that is about one month longer than at sea level. The climate on Deception Island is similar to Hurd Peninsula.

Geomorphological Setting and Permafrost Distribution

Deception Island

Deception Island is an active stratovolcano with a large collapsed caldera; the most recent eruptions occurred in 1967, 1969, and 1970 (Smellie et al. 2002). In some places there are fumaroles and ground temperature anomalies from continued volcanic activity. Mean annual air temperature at sea level is close to -2°C . The volcano rim rises to 539 m a.s.l. at Mount Pond, and the island is glaciated to a large extent. As a result of recent eruptions, the island has been covered by volcanic ash and debris, and many of the glaciers remain ash-covered today. Pyroclastic deposits covered snow, and buried snow is still present at some sites. The pyroclastic deposits are very porous and insulating, and give rise to a thin active layer, which varies from 30 to 90 cm in thickness.



Figure 2. Thermokarst bumpy terrain in Deception Island (arrow).

On lower valley slopes, exposures of fossil snow (buried-ice) with perennially frozen ice-cemented volcanic debris on top can be observed, testifying to post-eruption aggradation of permafrost. At these sites, ice-cemented permafrost also occurs under the buried-ice layer.

Buried-ice is widespread on Deception Island, especially along the lower slopes, and ice-cemented permafrost occurs down to sea level. Geophysical surveying and trenches show that the permafrost inside the caldera thins near sea level and is absent on beaches near the shore.

Hurd Peninsula (Livingston Island)

Hurd Peninsula is comprised of mountainous terrain and is located on the southern coast of Livingston Island. About 90% of the island is glaciated, with ice-free areas occurring at low altitude, generally on small peninsulas with rugged relief. Our study focused on ice-free areas of the northwestern part of Hurd Peninsula in the vicinity of the Spanish Antarctic Station Juan Carlos I. The bedrock is a low-grade metamorphic turbidite sequence with alternating layers of quartzite and shales; conglomerates and breccias occur in some areas (Miers Bluff Formation). Dolerite dykes and quartz veins are frequent (Arche et al., 1992), with the surficial lithology being very heterogeneous (Pallàs 1996).

The geological setting on Hurd Peninsula is substantially different to that of Deception Island. On the former, bedrock outcrops are prevalent, with only a thin cover of diamictite. Therefore, studying permafrost distribution is much more complex than at Deception, since frozen bedrock is very difficult to identify without a good network of boreholes. Observations from boreholes and geophysical surveying (Electrical Resistivity Tomography and Refraction Seismics Tomography) will allow a first insight into permafrost distribution, and a dense network of boreholes is planned for installation in 2007/08.

The observations indicate that continuous permafrost is present in diamictite and bedrock at least at 275 m a.s.l. At 115 m a.s.l. permafrost probably occurs only at some locations and seems to be controlled by late-lying snow patches. At this altitude in diamictite deposits, during summer, the ground thaws at least down to 1 m depth. On Hurd Peninsula, the



Figure 3. Thermokarst hollows in Deception Island.

limit between continuous and discontinuous permafrost in bedrock is probably located between these two altitudinal limits, 115 and 275 m a.s.l. However, it is possible that at 115 m the active layer is thicker than 1 m. At 35 m a.s.l. ground temperature data indicate that permafrost may be absent in bedrock, or that the active layer is thicker than 2.3 m.

Ice-cored sediments are widely distributed on Hurd Peninsula and occur down to sea level. These are likely of glacial origin, but in several cases still show active deformation giving origin to rockglaciers, mostly of the protalus or moraine-derived types.

Permafrost and Ground-Ice Degradation Features

Thermokarst

Thermokarst features have been observed at different sites on Deception Island. Two types of features occur, including thermokarst bumpy terrain and thermokarst hollows.

Bumpy terrain consists on a series of depressions with a small depth/width ratio that cover the terrain continuously (Fig. 2). They appear on the upper parts of the slopes inside the caldera. Preliminary observations suggest that they are more frequent on slopes below 100–150 m a.s.l.

Bumpy terrain is related to the thaw of buried-ice derived from buried snow patches. It is not yet clear if the depressions are solely the consequence of atmospheric warming or if they relate to a dynamic situation mainly induced by the thinning of the insulating layer of pyroclastic material being eroded. The thinning of the sedimentary cover, which is stronger in upper sector of the slopes, induces a decrease of the thermal insulation of the buried-ice layer, allowing for thawing. On the lower slope, the sedimentary cover is thickest due to the accumulation of material transported from upslope. There, a permafrost layer above the buried-ice layer can be observed which is probably linked to an increasing insulation effect due to sediment accretion.

Thermokarst hollows are features of decimetric to metric size and occur isolated or in small groups (Fig. 3). Their depth/width ratio is larger than the bumpy terrain, but they were not studied in detail yet. They appear in flat or



Figure 4. Debris-flow tracks in a talus slope on Hurd Peninsula (Livingston Island).



Figure 5. Debris flows depositing over the surface of the Las Palmas Glacier in Hurd Peninsula (Livingston Island).

gentle sloping terrain. No trenches were excavated, nor was geophysical surveying conducted in these features. They are probably related to localized degradation of massive ice. Their origin is not clear yet, since they can result from a climatic influence, but may also relate to changes in ground heat flux due to the volcanic activity. Geophysical surveying of these thermokarst hollows will be conducted in 2007/08.

Debris flows

Sub-aerial present-day debris-flow activity is a geomorphic process that has been poorly analysed in the literature for maritime Antarctica. Recent debris-flow tracks and deposits have been observed at several sites both on Livingston (Vieira & Ramos 2003) and Deception Islands (Figs. 4, 5, 6). Debris-flow activity is initiated by the saturation of surface unconsolidated material that flows along a channel in the slope, reworking the slope material.

In several mountain regions in the northern hemisphere an increase or altitudinal change in debris-flow activity has been linked to permafrost degradation (Jomelli et al. 2004). In maritime Antarctica, the widespread distribution of permafrost, together with the mountainous terrain and its proximity to the climatic limits of permafrost, a similar consequence of increasing air temperatures is to be expected.



Figure 6. Debris flow tracks in Deception Island.



Figure 7. Active layer detachment slide on Deception Island.

However, rainfall episodes may also be a triggering mechanism for debris flows. The lack of monitoring data does not allow us to precisely define the origin of the debris-flow activity and, therefore, in 2008/09 a monitoring programme for debris-flows will be implemented.

On Deception Island debris-flow tracks are widespread, at least in the inner slopes of the caldera. These are erosional slopes built up of volcanoclastic material. The debris flows form on the upper parts of the slopes and seem to be related to permafrost degradation, since this area is also at a similar geomorphological setting to the bumpy terrain features. The tracks are tens to a few hundred metres long. The predominantly gravely grain-size of the slope material and moderate slope angle limit the downslope movement of the flow; therefore, the debris generally does not contribute significantly to the valley floors. In the 2007/08 campaign a systematical mapping of the debris-flow tracks will be conducted in order to detect their spatial pattern and controlling factors.

On Hurd Peninsula several debris-flow tracks have been

observed and one of them is known to have occurred in late spring. Debris flows on Hurd affect mainly talus slopes and lateral moraines. Due to the steep slope angles and slope length they reach more than a hundred metres in length and have been observed being deposited on top of glaciers (Fig. 5).

Active-layer detachment slides

Active-layer detachment slides form from the presence of an impermeable frozen layer at depth. Several small slides of metric dimension have been observed affecting the surface of the ice-cored moraine of the Argentine lobe of Hurd glacier in January 2000 and are related to the degradation of the ice-rich till on the very steep inner slope of the moraine. Other ice-cored moraines near sea level have been detected using electrical resistivity tomography and refraction seismics tomography and they can be subject to these processes of degradation in the near future if the current climate trend continues.

On Deception Island small detachment slides were also found on steep slopes. The mass movements were under 40 m² in area (Fig. 7).

Rockfalls

Rockfalls in the mountain permafrost zone have been pointed out as a consequence of permafrost degradation, especially relating to the melting of ice filling rock wall fractures (Davies et al. 2001, Kaab et al. 2005, Gruber & Haeberli 2007). Rockfalls occur on both Hurd Peninsula and Deception Island; however, without proper monitoring it is difficult to access the influence of permafrost degradation on their origin.

Conclusions

The South Shetland Islands are a privileged area to study climate change and its effects on landscape dynamics. Permafrost is widespread and occurs down to sea level. On Deception Island permafrost is continuous throughout most of the area, but on the Hurd Peninsula continuous permafrost likely occurs only above ca. 150 m a.s.l. In the same area discontinuous and sporadic permafrost exist down to sea level, especially in the form of ice-cored moraines and rock glaciers. The mean annual air temperatures at sea level are close to -2°C, positioning the archipelago near the climatic limit of permafrost. This fact, together with the warming that affects the Antarctic Peninsula region should be responsible for permafrost degradation.

This paper describes landforms and geomorphic processes related to permafrost and ground-ice degradation that seem to result from climate change. Where ground-ice occurs, thermokarst hollows, bumpy terrain, and active-layer detachment slides have been found. The first occurs on flat or gentle sloping ground and the latter on moderate to steep slopes. Debris-flow activity was observed to be widespread on slopes of both. Their genesis has still to be assessed, since they can be linked either to ground warming or to heavy

rainfall events. On Deception Island heat flux anomalies caused by volcanic activity can also generate permafrost degradation features. These anomalies are of small areal extent and their locations are known.

The observations presented here are preliminary and constitute a starting point for a new approach that will emphasize monitoring of geomorphological activity in order to detect the influence of climate change on present-day processes. Another interesting issue to be analysed is the control of changing geothermal heat fluxes on permafrost degradation in Deception Island and to assess on the possibility of using permafrost degradation features as indicators of changes in volcanic activity.

Acknowledgments

This study was conducted as part of the project PERMAMODEL within the Spanish Antarctic Program CICYT (CGL2004-20896-E/ANT). This research is included in the IPY project ANTPAS – Antarctic and Sub-Antarctic Permafrost, Soils and Periglacial Processes. G. Vieira was funded by the Fundo de Apoio à Comunidade Científica (FCT) and Fundação Calouste Gulbenkian.

References

- Anisimov, O. A., Shiklomanov, N. I. & Nelson, F.E. 1997. Global warming and active layer thickness: results from transient general circulation models. *Global and Planetary Change* 15: 61-67.
- Arche, A., López-Martínez, J. & Martínez de Pisón, E. 1992. Sedimentology of the Miers Bluff Formation, Livingston Island, South Shetland Islands, in *Recent Progress in Antarctic Earth Science*, edited by Y. Yoshida et al., 357-362, Terrapub., Tokyo.
- Bockheim, J.G. 1995. Permafrost distribution in Southern circumpolar region and its relation to the environment: a review and recommendations for further research. *Permafrost and Periglacial Processes* 6, 27-45.
- Chapman, W.L. & Walsh, J.E. 2007. A synthesis of Antarctic temperatures. *Journal of Climate* 20(16): 4096-4117.
- Davies, M.C.R., Hamza, O. & Harris, C. 2001. The effect of rise in mean annual temperature on the stability of rock slopes containing ice-filled discontinuities. *Permafrost and Periglacial Processes* 12: 137-144
- Gruber, S. & Haeberli, W. 2007. Permafrost in steep bedrock slopes and its temperature-related destabilization following climate change. *Journal of Geophysical Research* 112.
- Hauck, C., Vieira, G., Gruber, S., Blanco, J. & Ramos, M. 2007. Geophysical identification of permafrost in Livingston Island, Maritime Antarctica. *Journal of Geophysical Research* 112.
- Jomelli, V., Pech, V.P., Chochillon, C. & Brunstein, D. 2004. Geomorphic Variations of Debris Flows and Recent Climatic Change in the French Alps. *Climatic Change* 64(1-2): 67-102.

- Kaab, A., Reynolds, J.M. & Haeberli, W. 2005. Glaciers and permafrost hazards in high mountains. In: U.M. Huber, H.K.M. Bugmann, & M.A. Reasoner (eds.). *Global Change and Mountain Regions – An overview of current knowledge*: 225-234.
- King, J.C. & Comiso, J.C. 2003. The spatial coherence of interannual temperature variations in the Antarctic Peninsula. *Geophysical Research Letters* 30(2): 1040.
- Lemke, P., Ren, J., Alley, R.B., Allison, I., Carrasco, J., Flato, G., Fujii, Y., Kaser, G., Mote, P., Thomas, R.H. & T. Zhang, 2007. Observations: Changes in Snow, Ice and Frozen Ground. In: S. Solomon, D. Qin, M. Manning, Z. Chen, M. Marquis, K.B. Averyt, M. Tignor & H.L. Miller (eds.) *Climate Change 2007: The Physical Science Basis. Contribution of Working Group I to the Fourth Assessment Report of the Intergovernmental Panel on Climate Change*. Cambridge, UK & New York, NY: Cambridge University Press.
- Marshall, G.J., Lagun, V. & Lachlan-Cope, T.A. 2002. Changes in Antarctic Peninsula tropospheric temperatures from 1956 to 1999: A synthesis of observations and reanalysis data. *International Journal of Climatology* 22: 291–310.
- Meredith, M.P. & King, J.C. 2005. Rapid climate change in the ocean west of the Antarctic Peninsula during the second half of the 20th century. *Geophysical Research Letters* 32.
- Molina, C.; Navarro, F.J.; Calvet, J. García-sellés, D. & Lapazaran, J.J. 2007. Hurd Peninsula glaciers, Livingston Island, Antarctica, as indicators of regional warming: Ice-volume changes during the period 1956–2000. *Annals of Glaciology* 46: 43-49.
- Nelson, F.E. & Anisimov, O.A. 1993. Permafrost zonation in Russia under anthropogenic climate change. *Permafrost and Periglacial Processes* 4(2): 137-148.
- Osterkamp, T.E. 2003. Establishing Long-term permafrost observatories for active-layer and permafrost investigations in Alaska: 1977-2002. *Permafrost and Periglacial Processes* 14: 331-342.
- Pallàs, R. 1996. *Geologia de l'illa de Livingston (Shetland del Sud, Antàrtida). Del Mesozoic al Present*. PhD thesis, Universitat de Barcelona.
- Ramos, M. & Vieira, G. 2003. Active layer and permafrost monitoring in Livingston Island, Antarctic. First results from 2000 and 2001. In: M. Phillips, S.M. Springman & L.U. Arenson (eds.), *Permafrost. Proceedings of the Eight International Conference on Permafrost, 21-25 July 2003, Zurich, Switzerland*: 929-933.
- Rakusa-Suszczewski, S. 1993. *The maritime Antarctic coastal ecosystem of Admiralty Bay*. Department of Antarctic Biology. Polish Academy of Sciences, Warsaw.
- Scambos, T.A., Hulbe, C. & Fahnestock, M.A. 2003. Climate-induced ice shelf disintegration in the Antarctic Peninsula. *Antarctic Research Series* 79: 79-92.
- Serrano, E. 2003. Paisaje natural y pisos geoecológicos en las áreas libres de hielo de la Antártida Marítima (Islas Shetland del Sur). *Boletín de la A.G.E.* 35: 5-32.
- Serrano, E. & López-Martínez, J. 2000. Rock glaciers in the South Shetland Islands, Western Antarctica, *Geomorphology* 35: 145-162.
- Smellie, J.L., López-Martínez, J. et al. 2002. *Geology and geomorphology of Deception Island*. BAS Geomap Series Sheets 6-A and 6-B, 1:25 000. Cambridge: British Antarctic Survey.
- Simonov, I.M. 1977. Physical geographic description of Fildes Peninsula (South Shetland Islands). *Polar Geography* 1: 223-242.
- Turner, J., Colwell, S.R., Marshall, G.J., Lachlan-Cope, T.A., Carleton, A.M., Jones, P.D., Lagun, V., Reid, P.A. & Iagovkina, S. 2005. Antarctic climate change during the last 50 years. *International Journal of Climatology* 25: 279-294.
- Turner, J., Overland, J.E. & Walsh, J.E. 2007. An Arctic and Antarctic perspective on recent climate change *International Journal of Climatology* 27(3): 277-293.
- Ximenis, L., Calvet, J., Enrique, J., Corbera, J., Fernández de Gamboa, C. & Furdada, G. 1999. The measurement of ice velocity, mass balance and thinning-rate on Johnsons Glacier, Livingston Island, South Shetland Islands, Antarctica. *Acta Geologica Hispanica* 34(4): 403-409.
- Vieira, G. & Ramos, M. 2003. Geographic factors and geocryological activity in Livingston Island, Antarctic. Preliminary results. In: M. Phillips, S.M. Springman & L.U. Arenson (eds.), *Permafrost. Proceedings of the Eight International Conference on Permafrost, 21–25 July 2003, Zurich, Switzerland*: 1183-1188.

Effect of Wildfire and Fireline Construction on the Annual Depth of Thaw in a Black Spruce Permafrost Forest in Interior Alaska: A 36-Year Record of Recovery

Leslie A. Viereck

University of Alaska Fairbanks, Fairbanks, Alaska

Nancy R. Werdin-Pfisterer

University of Alaska Fairbanks, Fairbanks, Alaska

Phyllis C. Adams

US Forest Service, Pacific Northwest Research Station, Portland, Oregon

Kenji Yoshikawa

University of Alaska Fairbanks, Fairbanks, Alaska

Abstract

Maximum thaw depths were measured annually in an unburned stand, a heavily burned stand, and a fireline in and adjacent to the 1971 Wickersham fire. Maximum thaw in the unburned black spruce stand ranged from 36 to 52 cm. In the burned stand, thaw increased each year to a maximum depth of 302 cm in 1995. In 1996, the entire layer of seasonal frost remained, creating a new active layer depth at 78 cm. An unfrozen soil zone (talik) remained between the two frozen layers until 2006 when the entire profile remained frozen. Permafrost returned to the burned site by the formation of a layer of seasonal frost that remained frozen through subsequent years. The fireline displayed a similar pattern with a maximum thaw of 266 cm in 1995 and the establishment of a continuous frozen layer at 69 cm, but the upper frozen layer became discontinuous after several years.

Keywords: active layer; boreal forest; disturbance; fire effects; permafrost.

Introduction

The 1971 Wickersham fire burned 6313 ha in an open black spruce (*Picea mariana* [Mill.] BSP) forest underlain with permafrost in the boreal forest of interior Alaska. As a part of the fire suppression effort, 113 km of fireline were constructed with heavy equipment which removed most of the organic layer and resulted in an increase in depth of thaw. This fire provided an opportunity for long-term studies of the effects of fire and fireline construction on the rate and pattern of permafrost degradation and subsequent recovery. The annual thawing of the active layer in undisturbed vegetation at the site was also documented and vegetation change following the fire was observed. This is one of the longest records of annual active layer measurements in the boreal forest of North America (Brown et al. 2000). Initial results of this study were reported 12 years after the fire (Viereck 1982) and again 33 years after the fire (Viereck et al. 2004).

When wildfire burns through a northern black spruce forest, there is usually a subsequent increase in soil temperature and depth of thaw due largely to reduction in organic layer depth and subsequent loss of thermal insulation (Van Cleve & Viereck 1981, Mackay 1995, Swanson 1996, Burn 1998). Reduced heat loss from decreased evapotranspiration and a lowering of the surface albedo after wildfires also contribute to higher ground surface temperature and an increase in active layer thickness (Mackay 1995, Burn 1998, O'Neill et al. 2002).

We hypothesized that a continuous increase in the active layer would occur initially at the burned site, followed by the

return of a shallow active layer by a gradual freezing back from the lower depth (Fig. 1).

This long-term study presents results of 36 years of annual measurements of the active layer in a burned black spruce site, a fireline in which the organic layer was removed, and in an adjacent undisturbed black spruce forest underlain by ice-rich permafrost. The purpose of this paper is to compare annual depth of thaw among these three sites and to document the recovery of vegetation, soil organic layers, and permafrost after fire and fireline construction.

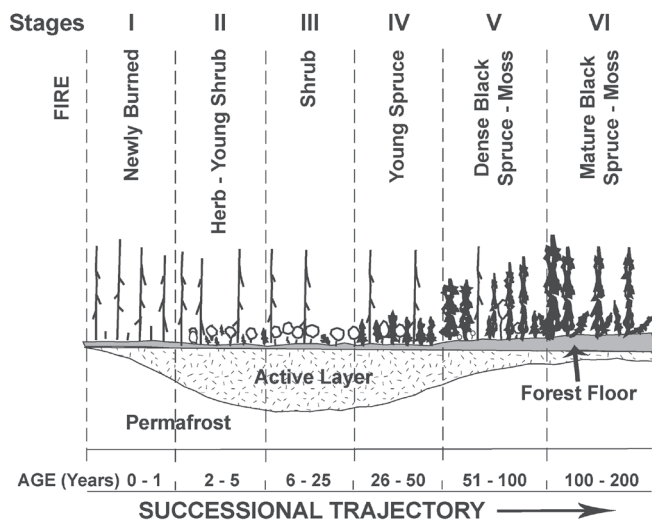


Figure 1. Succession model showing vegetation and active layer changes in a burned black spruce stand. Model modified from Van Cleve & Viereck (1981).

Methods

Study area

The Washington Creek Fire Ecology Research Area, located 50 km northwest of Fairbanks in interior Alaska (65°10'N, 147°54'W, 335 m elevation), was established to study the effects of the June 1971 Wickersham fire. The fire was ignited by lightning and burned 6313 ha in an open black spruce stand underlain by permafrost (Viereck & Dyrness 1979).

The vegetation prior to the fire was a 100- to 150-year-old open black spruce/lichen stand with a moss-derived organic layer 25 to 30 cm thick. The burn severity was originally classified as heavy, but later reduced to moderate. All of the trees and above-ground parts of the mosses, lichens, herbs, and shrubs were killed by the fire, but below-ground parts of some herbs and shrubs remained alive. Approximately one third (10 to 15 cm) of the organic layer was removed by the fire (Viereck & Dyrness 1979). At the time of the fire (June 24–30), the organic layer would have been thawed to only 20 to 30 cm. The soil is in the Saulich series with an active layer that varied from 40 to 50 cm.

Climate

Continuous climate records are not available from the site; the long-term weather record was obtained from the Weather Bureau's Fairbanks airport site. The Fairbanks record was compared with short-term climate studies at the Wickersham site. These include weather records kept at the study site from November 1971 to September 1980 and at the adjacent Washington Creek Fire Ecology Research site from January 1977 to September 1999.

From these records, we have estimated that the mean annual temperature at the Wickersham site is 1°C to 2°C colder than at the Fairbanks airport. Summer months tend to be cooler than Fairbanks, but winter months are warmer because of the lack of a cold inversion layer present during extreme cold spells in Fairbanks (Viereck 1982). The air temperatures at the Fairbanks airport have risen considerably during the period of this study (Hinzman et al. 2006). Since air temperatures at other weather stations in interior Alaska have also risen (Osterkamp & Romanovsky 1999), air temperatures at the Wickersham site are likely to have warmed, but there are no recent measurements to confirm this.

Maximum snow depths for each year at the Fairbanks airport are reported here. Based on only two winters of snowfall records available from the Wickersham fire (1977 and 1980), snow accumulation at the study site is usually about 25 cm greater than in Fairbanks (Viereck 1982).

Experimental design

A 25 m wide fireline was constructed up and down the slope between a heavily burned black spruce stand and an unburned stand, which before the fire was continuous and very similar to the stand that was burned. Most but not all of the organic layer was removed by the bulldozers in the construction of the fireline.

Three study sites were established in: 1) the heavily burned stand, 2) the fireline where vegetation and organic material were removed down to the frozen layer, and 3) the adjacent unburned black spruce stand that served as a control to compare the fireline and burned areas. At each site, 10 permanent probe points were established at 2 m intervals across the slope and perpendicular to the fireline. Maximum thaw depths were measured annually from 1971 to 2006 at each sample point using a metal probe.

A permanent transect of fixed points at 1 m intervals was established across the fireline from the burned stand on the north side to the unburned stand on the south side. At the center of this transect were ten poles that were used as probe sites to obtain the average thaw for the fireline. Across the entire width of the fireline, active layer depths were measured annually. Levels to the soil surface of the transect were made with a theodolite at intervals of three to five years, and changes in surface level relative to a fixed point were measured. Using these surface levels, it was possible to plot the profile of the surface and the depth of the active layer annually across the transect.

In 2002, a 6.5 m deep borehole was drilled in the burned site and a string of thermistors installed at 25 and 50 cm intervals to record temperatures. These temperatures have been logged both manually and with a logger at intermittent periods between 2002 and the present.

Vegetation

The vegetation of each of the sites was recorded at varying intervals. In the early years of the study, the vegetation of the burned and unburned stands was determined with a 20-plot system (Viereck 1982). In 1980, 1995, and 2004, vegetation of the burned, unburned, and fireline sites was measured by plots centered on the ten active layer probe sites. Moss, lichen, herb, and shrub percent cover was measured in 1 m² plots centered on the probe poles. Shrub cover was measured on 4 m² circular plots centered on the probe poles. Tree density and diameters were measured on larger circular plots.

Organic layer thickness

The thickness of the organic layer was originally measured in the 20 vegetation plots in the burned and unburned stands. Organic layer thickness of the fireline transect was assumed to be negligible at the beginning of the study. Organic layer thickness was remeasured along the probe lines in 1980, 1995, and 2004.

Results

Vegetation

The general vegetation type is a black spruce/moss/lichen community (*Picea mariana* / feathermoss / *Cladonia*—open needleleaf forest community) (Viereck 1982). Previous to the fire, the vegetation consisted of an open canopy of black spruce with an average diameter of 5.2 cm at 1.3 m height, a density of 1240 trees/ha and 45% canopy cover. In 1971, the age of most of the trees was 70 years, but there were a few scattered trees of 135 to 140 years in the stand. There

was an open tall shrub layer of *Salix pulchra* and *Betula glandulosa* and a low shrub layer of *Ledum groenlandicum* and *Vaccinium vitis-idaea*. The moss and lichen layer was made up primarily of *Pleurozium schreberi* and scattered *Sphagnum* species, and several species of *Cladonia* and *Peltigera* (Viereck 1982).

Unburned control site: Vegetation data recorded in 1980, 1995, and 2004 at the control site showed that the stand did not change significantly during that period and was similar to that recorded in 1971. Cover of the black spruce canopy was 22% in 2004. There was an open tall shrub layer of 8% mostly of *Salix pulchra* and *Betula glandulosa* and a low shrub layer of 47% *Ledum groenlandicum* and *Vaccinium vitis-idaea*. The moss and lichen layer of 95% cover was made up primarily of *Sphagnum girgensohnii*, *Pleurozium schreberi* and *Cladonia rangiferina*.

Burned site: Revegetation was slow for the first 9 years following the fire, probably as a result of the 10 to 20 cm organic layer that remained after the fire and provided a poor seedbed for invading pioneer species (Viereck 1982). Early revegetation was primarily from roots and underground rhizomes that had survived the fire. *Equisetum sylvaticum* and *Calamagrostis canadensis* and an occasional *Epilobium angustifolium* provided nearly 70% cover by 1980. Early successional mosses, *Ceratodon purpureus* and *Polytrichum juniperinum*, covered 35% of the surface. A few black spruce seedlings had become established, but provided less than 1% cover.

From 1980 to 2004, development of the site toward a mature black spruce stand continued at a somewhat faster pace. Black spruce reestablished with a cover of 17%. The tall shrub cover of *Betula glandulosa* and *Salix pulchra* reached 12%, while a low shrub layer primarily of *Ledum groenlandicum* and *Vaccinium vitis-idaea* developed a cover of 40%. The herbaceous layer of 55% cover is still dominated by *Equisetum sylvaticum* with some scattered clumps of *Calamagrostis canadensis*. The moss layer with 55% cover is still dominated by *Polytrichum juniperinum*, but feather mosses have developed a combined cover of 20%. Although *Ceratodon purpureus* has disappeared from the stand, the first small clumps of *Sphagnum* species (<1% cover) are now present in the stand. There has not been a significant return of any lichens to the stand after 36 years.

Fireline site: Invasion of herbaceous species and shrubs by seed was rapid in the first nine years after the fireline construction because of the exposed mineral soil and the wet condition of the surface. Herbaceous species of wet habitats accounted for nearly all of the 52% herbaceous cover. Since 1980, the herbaceous cover has been reduced drastically to 31% in 1995 and 18% in 2004. Tall shrub cover was nearly constant at 33% to 36% from 1980 to 2004. The moss layer changed dramatically throughout the 36-year period. Total moss cover dropped from 75% in 1980 to 44% in 2004. As of 2004, no lichens had established on the fireline. Although a few black spruce seedlings established near the edge of the fireline transect in the first few years following the fire, they had achieved a cover of only 4% by 2004.

Organic layer thickness

Unburned control site: The study area, situated on Saulich silt loam soils, originally had a combined organic layer thickness of 25 to 30 cm at the time of the fire (Viereck 1982). The profile was comprised of decaying mosses and litter (O1 and O2 layers). The organic layer of the unburned control stand was measured again in 1980 and 1995. The organic layer consisted of mosses and peat, formed primarily of *Sphagnum*. The average thickness of these layers was 33 cm, ranging from 16 to 45 cm.

Burned site: In the burned stand, the fire removed an average of 10 cm of the organic layer, although depths were variable (Viereck 1982). In 1980, the organic layer consisted of a 0 to 3 cm thick moss layer overlying a 1 to 2 cm layer of dark humus. By 1995, the organic layer consisted of 3 cm of mosses, primarily *Polytrichum* species, overlying 5 cm of dry, decaying mosses and the previously developed 2 cm layer of humus for a total organic layer of 10 cm. In 2004, the organic layer still consisted of 3 cm of moss, but the decaying moss layer had decreased to 3 cm and the humus layer had increased to 6 cm, for a total organic layer of 12 cm.

Fireline site: The irregular organic layer of the fireline is difficult to characterize. Although most of the organic layer was removed by the fireline construction, pockets and areas of the original humus layer remained. The surface of the fireline remained very wet, and several semi-aquatic mosses and *Sphagnum* species developed quickly. By 1980, the organic layer consisted of approximately 5 cm of live and decaying mosses overlying 4 to 5 cm of humus, for a total organic layer of 9.3 cm. The overall organic layer thickness was less in 1995 with a small decrease in both the moss and the humus layers. However, by 2004, the overall organic layer had increased to 12 cm. Although the humus layer had decreased since 1995, a fibrous layer of decayed sedges and grasses had developed to account for the increase.

Active layer thickness

The primary objective of this study was to document the changes in the annual depth of thaw (the active layer) following the 1971 fire (Fig. 2).

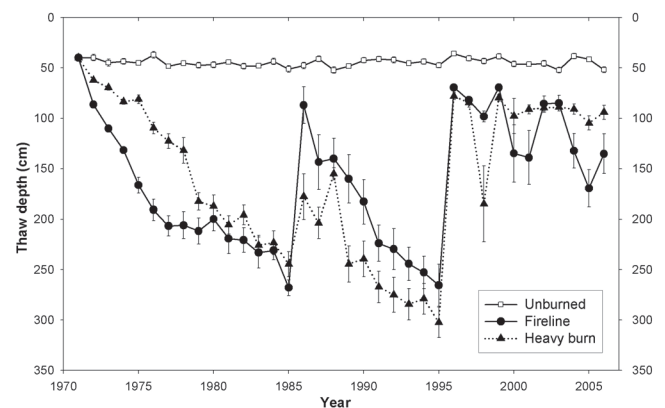


Figure 2. Maximum thaw depth of an unburned black spruce stand, a burned black spruce stand, and a fireline from 1971 to 2006. Values represent the mean ($n = 10$) and standard error.

Unburned control site: Maximum thaw ranged from 36 cm in 1996 to 52 cm in 1988, 2003, and 2006. The average thaw depth over the 36-year period was 45 cm. There was a tendency for deeper thaws to be associated with higher snowfall the previous winter and higher thawing degree days the following summer. For example, the minimum thaw depth of 36 cm in 1996 followed a previous cold winter with low snowfall through the month of January.

Burned site: Annual maximum thaw depth increased rapidly in the first 14 years following the fire to a maximum depth of 245 cm in 1985. In 1986, however, seasonal frost remained in 3 of the 10 probe sites resulting in an average thaw of 178 cm. An upper layer of frozen soil remained at some of the probe sites for the next 2 years resulting in an average thaw of only 155 cm in 1988. These upper layers melted out completely in 1990 and the depth of thaw continued to increase to 302 cm in 1995. In 1996, following a winter with light snow and cold temperatures, the upper seasonal frost layer remained at all 10 probe sites, giving an average thaw of only 78 cm. This upper layer has remained frozen, except in 1998 when 4 of the probe sites reached the bottom thaw layer of over 300 cm, to give an average thaw depth of 185 cm. From 1998 to 2006, the upper layer has remained frozen, and the thaw depth has ranged from 80 to 105 cm.

Mean annual temperatures and snow depths from the Fairbanks International Airport (Fig. 3) show that the two summers when seasonal frost first remained (1986 and 1996)

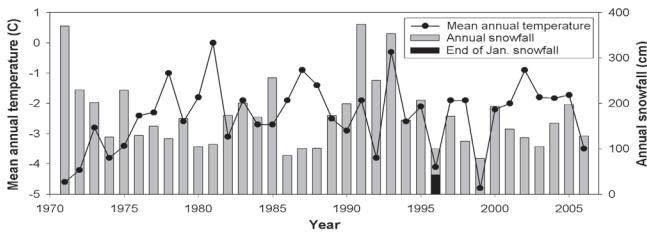


Figure 3. Mean annual temperature and mean annual snowfall for Fairbanks, Alaska from 1971 to 2006.

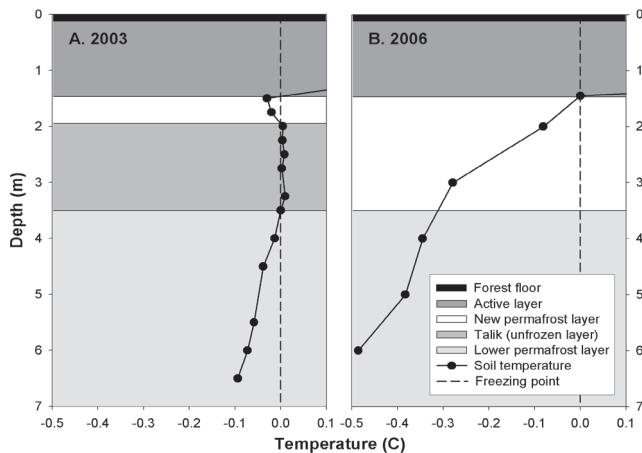


Figure 4. Soil temperature profiles from the burned site borehole, A) 2003 profile shows a new frozen layer approximately 50 cm thick extending from 1.4 to 1.9 m below the active layer, B) 2006 profile shows complete freezing of the talik and new permafrost extending 1.45 m below the present active layer.

followed winters of low snowfall. In addition, 1996 had a below average mean annual temperature.

Fireline site: For the first 25 years following the fire, the thaw depth under the fireline followed much the same pattern as the burned site. There was an annual increase in thaw depth from 1971 to a maximum of 268 cm in 1985. In 1986, the upper layer of seasonal frost remained frozen across the entire fireline. For the next six years, the upper seasonal frost layer began to thaw, and the number of probe points that penetrated through to the lower frozen layer increased from three in 1987 to all ten of the probe points in 1992, when the thaw depth approached the pre-1986 level. This condition continued until 1995 when a thaw depth of 266 cm was recorded.

In 1996, a winter of light snow and below average temperatures (Fig. 3) resulted in a seasonally frozen layer that persisted throughout the following summer. The average depth of thaw in 1996 was only 69 cm. Unlike the burned area, the shallow layer of frozen soil did not remain along the probe line. From 1997 through 2006, there was an increase in the number of probe points that reached the pre-1996 level. By 2006, only 2 points along the probe line had thaw depths less than 100 cm, and the average thaw depth of all 10 points was 135 cm.

At this time, it is impossible to predict if the upper frozen layer will continue to melt or if a light snow year with cold temperatures, such as occurred in 1996 and 2006, will result in the reestablishment of a continuous upper frozen layer.

Borehole profile

The thickness of the upper frozen layer was impossible to determine using our probing method. In 2002, we drilled a 6.5 m deep borehole in the burned site near the probe line and installed a series of thermistors to obtain temperatures throughout the soil profile.

A temperature profile from the borehole during the period of maximum thaw in September of 2003 (Fig. 4A) shows an active layer of 1.4 m. The new frozen layer was approximately 50 cm thick and extended from 1.4 to 1.9 m below the current active layer. This new permafrost layer divided the active layer and the talik formation. The talik temperatures were very close to 0°C. Below 3.4 m, the temperatures of the original permafrost layer decreased to -0.1°C at the bottom of the borehole (6.5 m). The lower permafrost depth stabilized at 3.5 to 4.0 m, and an unfrozen soil zone (talik) remained between the two frozen layers. However, in September of 2006, the temperature profile (Fig. 4B) shows the disappearing talik layer. The permafrost temperature at 6 m depth is more than 0.3°C colder after 3 years. The new permafrost development, since 1996, accelerated the refreezing of the talik layer. As a result of the three years of permafrost aggradations, the ground temperature profile is becoming similar to the pre-fire thermal conditions.

Fireline cross section

To better understand the changes in thaw depth across the fireline, cross sections of the fireline were measured

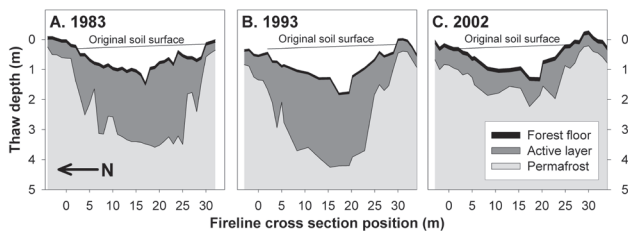


Figure 5. Cross section of the fireline in A) 1983, B) 1993, and C) 2002, showing considerable lowering of the original surface, and the reestablishment of permafrost in an uneven band across the entire fireline.

periodically during the 36 years of the study. Changes prior to 1980 are described by Viereck (1982). Figure 5 shows the cross section in 1983; 1993, when thaw was near the maximum; and 2002, the most recent cross section where the new layer of seasonal frost had persisted.

Surface: Figure 5 shows a considerable lowering of the surface level over time through subsidence and erosion. In 1983 (Fig. 5A), the surface lowered about 1 m through erosion and subsidence with slightly more on the northern side of the fireline. By 1993 (Fig. 5B), a small intermittent stream that formed from water captured upslope in the fireline had created a ditch that was approximately 75 cm deeper than the surrounding surface. The 2003 profile of the surface (Fig. 5C) shows that there has been some filling of the ditch and a slight rise in the surface of the fireline, which may be the result of vegetation buildup, deposition, and expansion due to the refreezing of water into ice in the newly frozen upper layer.

Depth of thaw: The cross sections in Figure 5 show that the depth of maximum annual thaw and the reestablishment of permafrost occur in an uneven band across the fireline. In 1983 (Fig. 5A), the deepest thaw occurs near the middle of the fireline beneath the small stream. There is a very steep rise of the permafrost on the south side of the fireline, due perhaps to the shading of that side of the fireline by trees to the south. The cross section in 1993 (Fig. 5B) shows that the thaw is fairly even across the middle of the fireline and rises sharply on both edges to the level of the active layer in the adjacent undisturbed vegetation. By 2002 (Fig. 5C), the upper surface of the newly developed permafrost is uneven, but in general follows the surface layer.

Estimated fireline cross section: Figure 6 illustrates a conceptual fireline cross section during the late 1990s and early 2000s, when the upper zone of permafrost (newly established in 1996) was intact. It shows the surface of the fireline, lowered through erosion and subsidence, and the uneven surface of the new upper frozen layer. The base of this layer is estimated from the measured thickness in the burn site (approximately 150 cm) at a similar period. Below this is an unfrozen layer of talik that is surrounded above and below by the permafrost in the adjacent unburned area. For the base of the talik, we have used the depth of thaw taken in 1995 when the thaw was at its deepest. Below the talik is the zone of permafrost that was there before the fire and reaches an unknown depth.

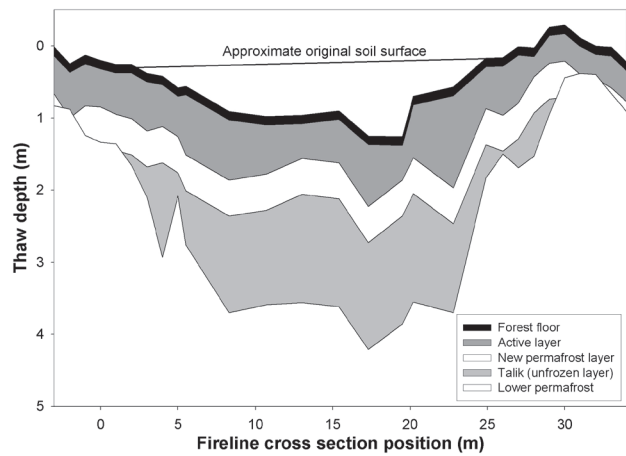


Figure 6. Conceptual fireline cross section during the period (1996–2003) that the upper zone of newly established permafrost was intact.

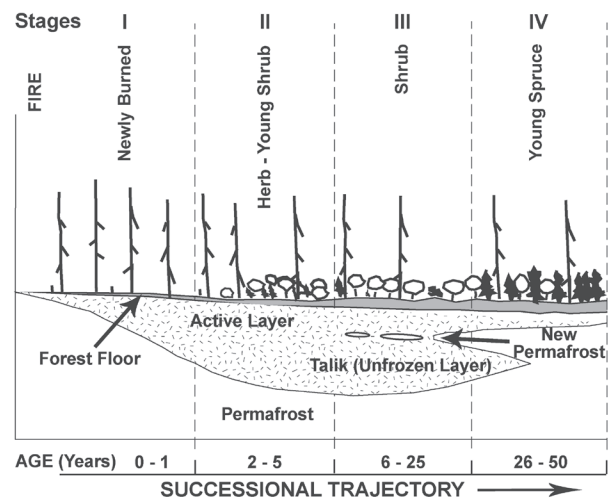


Figure 7: Successional changes observed in vegetation and the active layer at the burned site following the Wickersham fire.

Conclusion

Long-term observations such as those made on active layer and vegetation changes over the last 36 years at the Wickersham fire site are extremely valuable for developing an understanding of the effects of fire and fireline construction in the boreal forest of Alaska. We originally hypothesized that a shallow active layer would return to the burned site by a gradual freezing back from the lower depth (Fig. 1). We expected to observe a continuous increase in the active layer to a maximum depth during the first 30 to 50 years after the fire. Next, a gradual decrease in the active layer was expected to return the active layer to its approximate pre-fire depth 100 years following the fire. Other long-term measurements of active layer recovery following wildfire in the southern Yukon Territory (Burn 1998) and near Inuvik, N.W.T., Canada (Mackay 1995) reported that permafrost aggraded upward in a return to pre-fire conditions.

Surprisingly, a layer of seasonal frost formed at the Wickersham burned site that eventually remained frozen throughout the entire year and continued to remain frozen for

the next ten years (Fig. 7). The active layer did increase for the first 25 years following the fire as originally hypothesized. However, an upper layer of seasonal frost remained frozen 17 years after the fire and then became discontinuous for the next 10 years. Since 1996, the seasonal frost layer has remained frozen. This created a new permafrost layer with an active layer of 90 cm and an unfrozen talik layer between the upper and the lower frozen layers. This new permafrost layer accelerated the refreezing of the talik layer, and by 2006, the talik layer disappeared (Fig. 4B) and the permafrost has returned to the pre-fire thermal conditions.

Another important observation of this study is that under present climate conditions, permafrost is reforming at the Wickersham fire site on the burned stand but not on the fireline. The increased maximum thaw depth pattern for the two sites is similar, with a maximum thaw of 266 cm for the fireline and 302 cm for the burned site in 1995 (Fig. 2). Also, the development of an upper frozen zone in 1986 and 1996 was similar. The difference on the fireline is that the upper frozen zone has become intermittent, but it may be rejuvenated by another cold snowless year.

In addition to the permafrost differences at the burned and fireline sites, there is a significant difference in rate of vegetation recovery between the burned area and the fireline. The vegetation of the burned area is beginning to have many features of the original black spruce stand, whereas the fireline has remained very different with few features and species of the original stand.

Acknowledgments

This work was funded by the Bonanza Creek Long Term Ecological Research program (funded jointly by the National Science Foundation and USDA Forest Service, Pacific Northwest Research Station).

References

- Brown, J., Hinkel, K.M. & Nelson, F.E. 2000. The Circumpolar Active Layer Monitoring (CALM) Program: Research designs and initial results. *Polar Geography* 24(3): 166-254.
- Burn, C.R. 1998. The response (1958-1997) of permafrost and near-surface ground temperatures to forest fire, Takhini River valley, southern Yukon Territory. *Canadian Journal of Earth Sciences* 35: 184-199.
- Hinzman, L.D., Viereck, L.A., Adams, P.C., Romanovsky, V.E. & Yoshikawa, K. 2006. Climate and permafrost dynamics of the Alaskan boreal forest. In: Chapin, F.S. III, Oswood, M.W., Van Cleve, K., Viereck, L.A. & Verbyla, D.L. (eds.), *Alaska's Changing Boreal Forest*. New York: Oxford University Press, 39-61.
- Mackay, J.R. 1995. Active layer changes (1968 to 1993) following the Forest-Tundra Fire near Inuvik, N.W.T., Canada. *Arctic and Alpine Research* 27(4): 323-336.
- O'Neill, K.P., Kasischke, E.S. & Richter, D.D. 2002. Environmental controls on soil CO₂ flux following fire in black spruce, white spruce, and aspen stands of interior Alaska. *Canadian Journal of Forest Research* 32: 1525-1541.
- Osterkamp, T.E. & Romanovsky, V.E. 1999. Evidence for warming and thawing of discontinuous permafrost in Alaska. *Permafrost and Periglacial Processes* 10: 17-37.
- Swanson, D.K. 1996. Susceptibility of permafrost soils to deep thaw after forest fires in interior Alaska, U.S.A., and some ecologic implications. *Arctic and Alpine Research* 28(2): 217-227.
- Van Cleve, K. & Viereck, L.A. 1981. Forest succession in relation to nutrient cycling in the boreal forest of Alaska. In: West, D.C., Shugart, H. & Botkin, D.B. (eds.), *Forest Succession Concepts and Application*. New York: Springer Verlag, 185-211.
- Viereck, L.A. 1982. Effects of fire and firelines on active layer thickness and soil temperatures in interior Alaska. *Proceedings of the Fourth Canadian Permafrost Conference, Calgary, Alberta, March 2-6, 1981*: 123-135.
- Viereck, L.A. & Dyrness, C.T. 1979. Ecological effects of the Wickersham Dome fire near Fairbanks, Alaska. USDA Forest Service, Pacific Northwest Forest and Range Experiment Station. General Technical Report PNW-90, 71 pp.
- Viereck, L.A., Werdin, N.R., Yoshikawa, K. & Adams, P.C. 2004. Effect of wildfire and fireline construction on the annual depth of thaw in a black spruce-permafrost forest in interior Alaska: a 33-year record. *International Boreal Forest Research Association Conference, Fairbanks, Alaska, May 3-7, 2004*: poster presentation.

Investigation of the Permafrost Environment for Pile Installation at Fort Wainwright, Alaska

Ted S. Vinson

Professor (Emeritus), Department of Civil Engineering, Oregon State University, Corvallis, Oregon, USA

Abstract

During 2004, 516 piles were driven to -18 m (59 ft) for housing units on Fort Wainwright, Alaska. Nearly 93% of the piles encountered permafrost compared to the contractor's estimate of 15%. Owing to the substantial difference between the actual and estimated number of piles that encountered permafrost, an investigation was undertaken to determine if the prediction of the percentage of piles that would encounter permafrost could have been improved prior to pile driving. Very limited data was available. No borings within 100 m (330 ft) of the housing units were advanced to a depth of 18 m (59 ft). Notwithstanding this fact, a topographic surface was generated using commercially available mapping software from four borings which encountered permafrost and six borings advanced to 14.5 m (47.5 ft) in thawed material at the project site. When the building footprints were projected on the predicted surface, it was estimated that greater than 80% of the piles would encounter permafrost.

Keywords: degrading permafrost; mapping; pile driving; topographic surface.

Introduction

During the period July 6 to October 16, 2004, 516 piles were driven as foundation elements for four housing units on Fort Wainwright, Alaska. The piles were driven to a design tip elevation of -18 m (-59 ft) on an approximate two hectare (five acre) tract to the west of an existing housing complex on Alsace Loop. A total of 129 piles were driven at each housing unit (i.e., 4 units x 129 piles per unit = 516 piles). The 2-cm (8-in.) diameter piles were driven with a hardened steel driving shoe welded to the pile tip to prevent damage during high driving resistance. Of the 516 piles driven, 479 piles experienced high driving resistance when permafrost (typically frozen sand and/or gravel) was encountered at depths ranging from 6 to > 15 m (19 to > 50 ft). When permafrost was encountered, it required a substantial change in the installation procedure. Specifically, the pile was cut, a tricone (or roller) drilling bit was inserted in the pipe pile, a hole was advanced (i.e., predrilled) to the pile tip elevation or beyond, the cut section of the pile was welded back onto the pile, and the pile was driven through the permafrost to the design tip elevation. Of the 479 piles encountering permafrost, 24 were completed without predrilling, 362 required one predrilling operation and 93 required two predrilling operations.

Nearly 93% of the piles at the four housing units, designated as Buildings C, D, F, and H, encountered permafrost. The pile foundation contractor, based on a "conventional" interpretation of the pre-bid boring logs, estimated 15% of the piles would encounter permafrost. More specifically, the contractor noted "Six of the forty (40) test borings in or near the four buildings where pile foundations were specified indicated the existence of permafrost" Consequently, $[6/40] \times 100\% = 15\%$ of the piles would encounter permafrost.

Owing to the substantial difference between the estimated compared to the actual number of piles that encountered permafrost, an investigation was undertaken to determine if

the prediction of the permafrost surface and the percentage of piles that would encounter permafrost could have been improved prior to pile driving. The results of the investigation are reported herein.

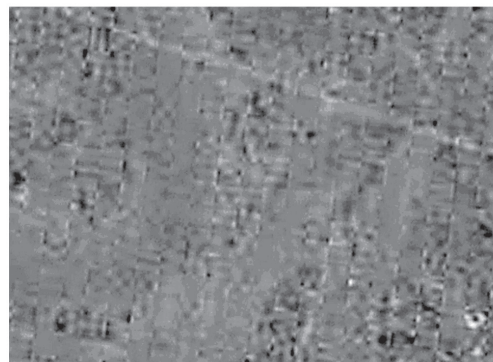
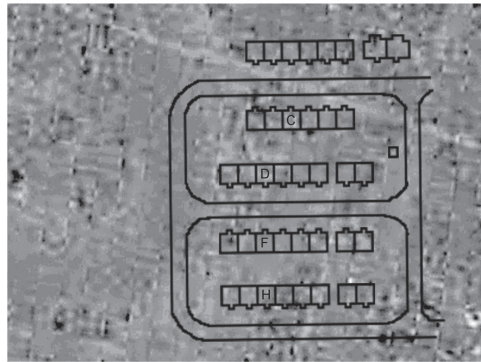
Geologic Conditions, History of Surface Disturbance and Modification, Boring Logs

Fort Wainwright is situated in the Tanana River Valley, to the south and east of Fairbanks, on the broad floodplain of the Tanana and Chena Rivers. The Tanana basin was filled through alluvial processes with deposits of silt, sand, and gravel, in excess of 180 m (590 ft) deep near the Tanana River. A mantle of 1–5 m of aeolian silt to silty fine sand may overlie these alluvial deposits in the Fort Wainwright area. At the project, site there is a silt-to-silty sand layer of approximately 1–5 m (3–16 ft) depth overlying clean sand and/or gravel to a depth greater than approximately 16 m (53 ft) (maximum boring depth).

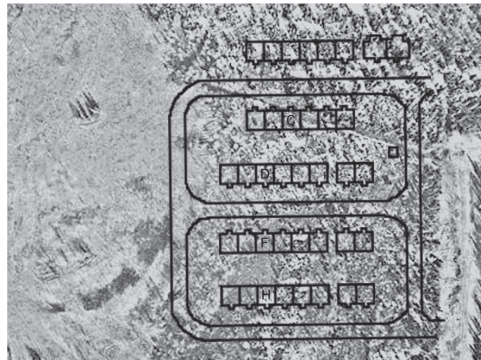
Fairbanks and Fort Wainwright are in a discontinuous permafrost zone. The occurrence and characteristics of permafrost in a discontinuous zone can vary dramatically. On Fort Wainwright moss-dominated black spruce forests on lowlands or lower slopes are generally underlain by permafrost. Romanovsky (2006) reports the typical thickness of permafrost around Fairbanks is about 50 meters (165 ft), but varies between a few meters to 150 m (490 ft) and more.

Removal of the vegetative cover in an area underlain by permafrost will cause the permafrost to degrade. Pewe & Reger (1983) report that past surface disturbances have increased the depth of permafrost in the Fairbanks area by 7–12 m (23–40 ft). Linell (1973) reported that on a research site in the Fairbanks area underlain by frozen silt, when the trees and brush were removed, the permafrost level, initially at -1.1 m (-3.6 ft), degraded to -4.7 m (-15.4 ft) after 26

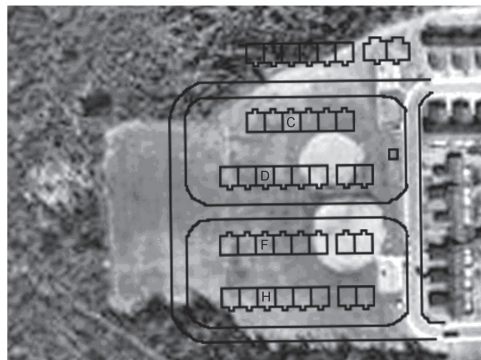
1949



1983



1993



2001

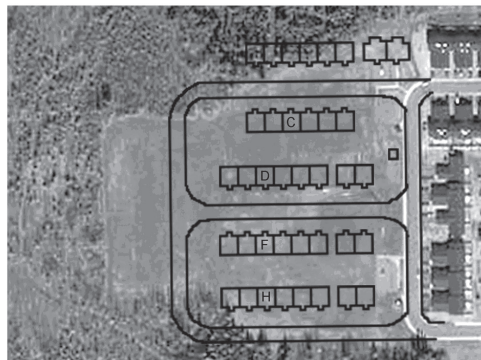


Figure 1. Comparison of 1949, 1983, 1993, and 2001 airphotos of the project site. The left frames show the project site with the building structures and roads superimposed. The right frames are without building structures and roads. North is at the top of the photographs.

years. In the same study, when the trees, brush, and surface vegetation were removed, the permafrost level degraded to -6.7 m (22 ft) after 26 years. Studies by the Defense Mapping Agency Hydrographic/Topographic Center (1978) indicate that permafrost at Fort Wainwright in cleared areas occurs at 8–13 m (26–43 ft) below the ground surface. Cleared areas were defined as areas where surface vegetation has been removed. It is apparent from past studies in the Fairbanks area that the amount and rate of degradation is dependent on a number of factors.

The preceding reported thaw depth estimates are based on conduction as the heat transfer mode. Convective heat transport associated with groundwater flow will cause thawing of permafrost. Conduction and convection heat transfer modes acting in concert have resulted in permafrost thawing in the Fairbanks and Fort Wainwright area greater than the values noted above.

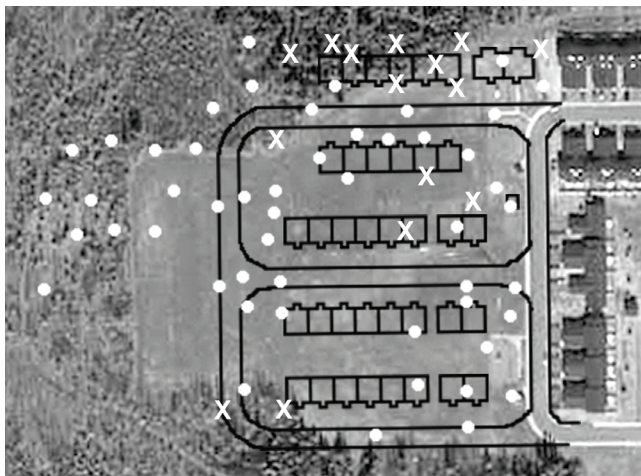


Figure 2. Schematic of borings, buildings, and roads on the 2001 airphoto. Circles indicate permafrost thawed to a depth greater than the boring was advanced; X indicates permafrost was encountered.

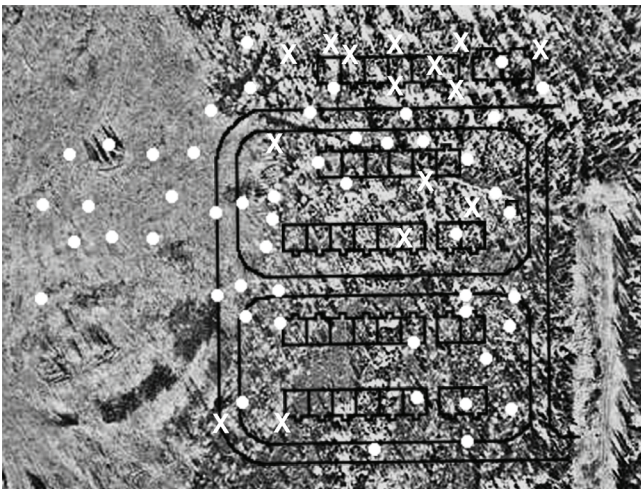


Figure 3. Schematic of borings, building, and roads on the 1983 airphoto. Circles indicate permafrost thawed to a depth greater than the boring was advanced; X indicates permafrost was encountered. The similarity in the surface vegetation over the project site is apparent.

Fort Wainwright (formerly Ladd Field) was established in 1939. Figure 1 shows 1949 and 1983 airphotos of the project site in which the surface vegetation and trees prior to surface disturbance and modification are clearly visible. It is apparent that significant surface disturbance did not occur on the project site prior to 1983. Considering the character of the vegetation, it is likely the project site was completely underlain by permafrost at a relatively shallow depth prior to surface disturbances. Based on boring logs presented in the March 2003 Geotechnical Report for the project, in “Black spruce woods with moss on the ground” permafrost occurred at a depth of less than 1 m (3.3 ft). Evidence of a substantial change in surface cover is shown in the 1993 airphoto taken approximately two years after construction activities were initiated for a housing complex on Alsace Loop to the east of the project site. The 2001 airphoto shows the likely site condition when the geotechnical investigation was conducted at the project site (2002–2003). The central portion of the site was a recreational facility (e.g., softball fields and playground). An old excavation was present at the mid-eastern portion of the site. There was evidence that a large portion of the site was graded in the past. It was reported that the open areas are fill material.

The boring logs for the project site provide evidence of permafrost degradation in the 10- to 12-year period from the early 1990s to 2002–2003. The boring locations are shown in Figure 2 overlain on the 2001 airphoto of the site.

Following a review of the boring logs in the general vicinity of Buildings C, D, F, and H, 17 borings were advanced through thawed material to a depth of approximately 7 m (23 ft). The correct interpretation of the 17 boring logs is that permafrost has degraded to a depth of at least 7 m (23 ft) at the location of the borings. It cannot be assumed that permafrost is absent at these locations or permafrost has thawed to a depth of 18 m (59 ft) (i.e., design depth of pipe pile). Six borings were advanced to a depth of approximately 14.5 m (47.5 ft), indicating that permafrost had degraded to a depth of at least 14.5 m (47.5 ft) at these locations. Three borings which were in the “footprints” of Buildings C, D, and H, indicated permafrost was present at depths of 1.5, 6.5, and 9.5 m, respectively. A fourth boring west of Building C indicated permafrost at a depth of 14.2 m (46.6 ft). Figure 3 shows the boring locations superimposed on the 1983 airphoto. As previously noted, there was very little difference in the character of the surface vegetation

Table 1. Borings in the footprint and close proximity of Buildings C, D, F, and H.

Building	Borings in Building Footprint	Borings within 10 m of Building Footprint	Total Number of Applicable Borings
C	1	5	6
D	1	2	3
F	1	1	2
H	1	1	2

from 1949 (and likely much earlier) up to the initiation of construction activities at the project site in the early 1990s. This implies that permafrost was very likely at a relatively shallow depth over most of the project site prior to the early 1990s.

The number of borings in the footprint and close proximity of Buildings C, D, F, and H is given in Table 1. It is apparent that very limited data is available to estimate the permafrost surface beneath the buildings. Furthermore, and equally significant, is the fact that no borings within 100 m (330 ft) of any proposed building were advanced to the tip elevation of the pipe piles (18 m, 59 ft).

Use of Pile Driving Records to Plot Topographic Map of Permafrost Surface

The driving record for the 479 piles which experienced high driving resistance when permafrost (typically frozen sand and/or gravel) was encountered at depths ranging from 6 to >15 m (20 to >50 ft) may be used to create a topographic map of the surface of the permafrost at the project site. Each pile location was assigned an X and Y coordinate. The Z coordinate is the depth at which permafrost was encountered during pile driving. A topographic surface is produced using a surface generation algorithm. A contour map can be plotted on the topographic surface or projected to the ground surface. The topographic surface and contour map shown in Figure 4 is believed to be an accurate depiction of the actual permafrost environment at the site. The irregular character of the surface and depth of thaw strongly suggests that both conduction and convection heat transport processes are occurring at the project site. Figure 5 presents the contour map together with the footprints of Buildings C, D, F, and H. It is apparent that permafrost at a depth of 18 m (59 ft) underlies all of Buildings C and D, and 85+% of Buildings F and H. This is in excellent agreement with the occurrence of permafrost at a depth of 18 m (59 ft) or less from the pile driving records.

Comparison of Permafrost Surface at Site to the Record provided by Boring Logs

Figure 6 shows a contour map of the depth to permafrost from the pile driving record and the locations of borings advanced in the area. Borings which encountered permafrost and borings advanced in thawed material are shown. The number adjacent to the boring locations indicates either the depth to permafrost or the maximum depth to which thawed material was encountered. By comparing the depths shown adjacent to the borings to the contour intervals it is possible to establish if the boring logs indicated a site condition that was different than the conditions actually encountered. For the fifteen borings that were inside the boundary of the contour map, there are no apparent contradictions. At the locations where 12 borings were advanced to an approximate 7 m (23 ft) depth and thawed ground was reported, permafrost was encountered at a greater depth during the pile driving

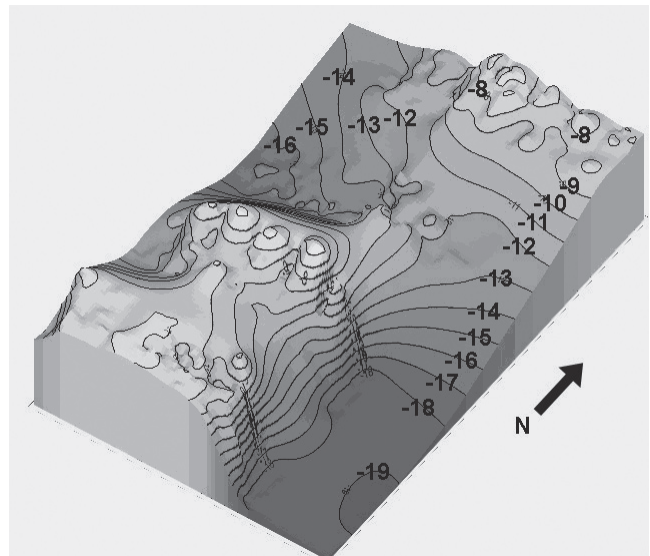


Figure 4. Topographic surface of permafrost based on the pile driving records. The irregular character of the surface strongly suggests that conduction and convection heat transport processes are occurring at the project site. The depth in meters is shown on the contour lines.

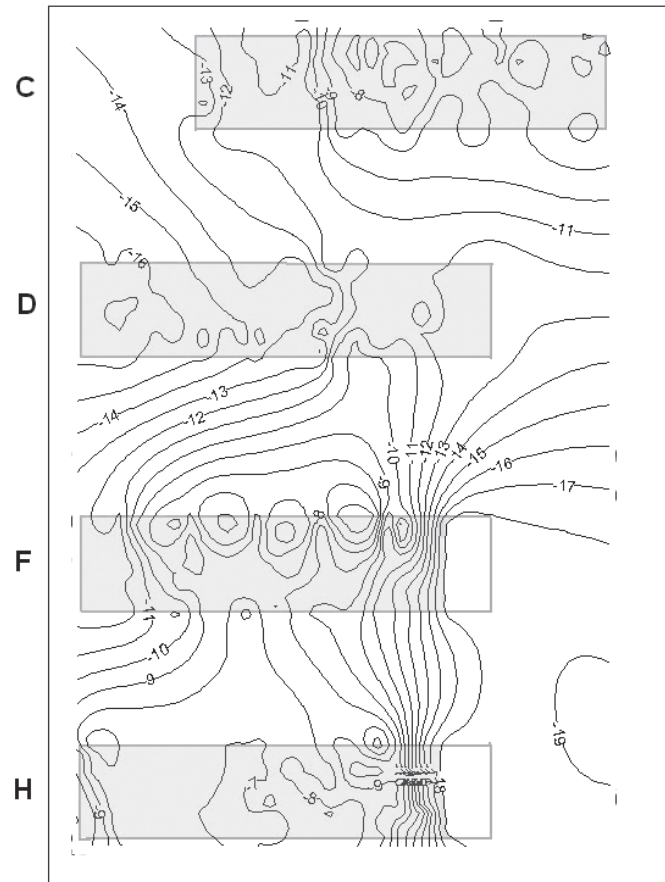


Figure 5. Contour map together with the footprints of Buildings C, D, F, and H. The shaded area represents the occurrence of permafrost at a depth of 18 m (59 ft) or less. It is apparent that permafrost at a depth of 18 m (59 ft) underlies all of Buildings C and D, and 85+% of Buildings F and H. The depth in meters is shown on the contour lines.

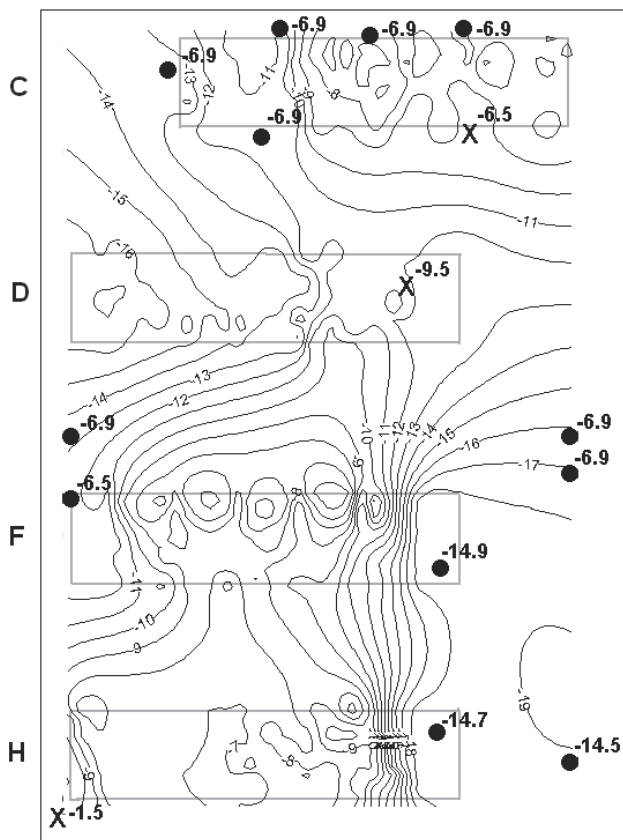


Figure 6. Contour map of the depth to permafrost from the pile driving record. Circles indicate permafrost thawed to a depth greater than the boring was advanced; X indicates permafrost was encountered during the pile-driving operation at the approximate depth indicated by the borings. The number adjacent to the boring location indicates either the depth (m) to permafrost or the maximum depth to which thawed material was encountered. North is at the top of the figure.

operation. For the three borings that indicated permafrost would be encountered at a specific location, permafrost was encountered during the pile-driving operation at the approximate depth indicated by the borings. An assertion of a “Differing Site Condition” is without merit.

Use of Boring Logs to Plot Topographic Map of Permafrost Surface

A topographic surface of the permafrost may be predicted from the boring logs provided in the contract documents. Figure 7 shows a surface produced using 4 borings which encountered permafrost at the project site together with 6 borings advanced to approximately 14 m (46 ft) in thawed material. For the borings advanced to approximately 14 m (46 ft), it was assumed that permafrost was at a depth of 20 m (66 ft). The predicted surface is in very good general agreement with the actual surface (see Fig. 4). A very satisfactory topographic surface can be generated from the boring logs with one of three commonly used topographic mapping algorithms considered in the investigation (i.e., Kriging, linear equations, and inverse distance). A fourth method (i.e., triangulation) was less satisfactory. When the building footprint is projected on the topographic surface

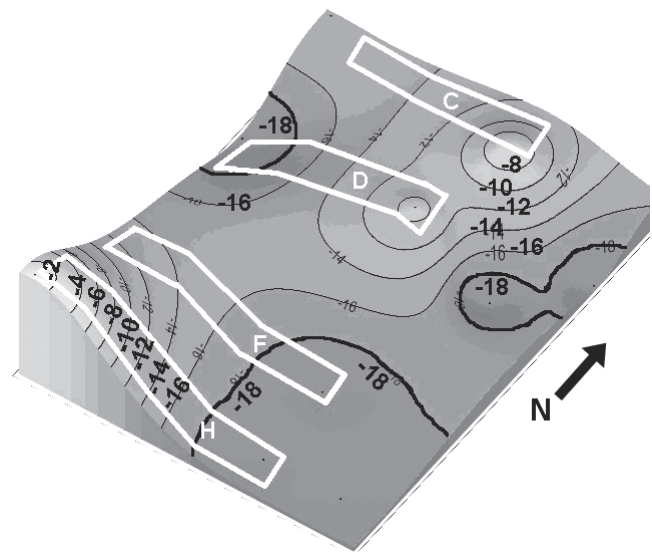


Figure 7. Topographic surface developed from boring logs with the Kriging surface mapping algorithm. The -18 m (59 ft) elevation is shown as a bold contour line. A distortion of the building footprint occurs when it is projected on the topographic surface, and the footprint no longer appears to be rectangular or at the correct distance from adjacent structures.

and the area inside the building footprint with permafrost at a depth of 18 m (59 ft) or less is noted, it represents the area over which permafrost would be encountered during pile driving. To estimate the area it is convenient to display the permafrost surface contour map with the footprint of the buildings (Fig. 8). It is apparent from Figure 8 that all of Building C is underlain by permafrost at a depth less than or equal to 18 m and approximately 90%, 70%, and 70% of the piles in Buildings D, F, and H, respectively, would be underlain by permafrost at a depth less than or equal to 18 m. Based on the results presented in Figure 8, a reasonable estimate of the piles that would encounter permafrost at a depth less than or equal to 18 m would be greater than 80%.

Summary and Conclusions

It is highly probable that the entire housing unit project site was underlain by permafrost at a shallow depth prior to the establishment of Fort Wainwright. Permafrost degradation was initiated when surface disturbance and modification occurred (primarily) in the early 1990s.

It is apparent that very limited data was available to estimate the depth of permafrost beneath the buildings. No borings within 100 m (330 ft) of the housing units were advanced to a depth of 18 m (59 ft). Notwithstanding these facts, it is possible to generate a topographic surface of the permafrost using commercially available software and the 4 borings which encountered permafrost at the project site, together with 6 borings advanced to approximately 14 m (46 ft) in thawed material. For the borings advanced to approximately 14 m (46 ft), it was assumed that permafrost was at a depth of 20 m (66 ft). When the building footprints are projected on the predicted topographic surface, and the

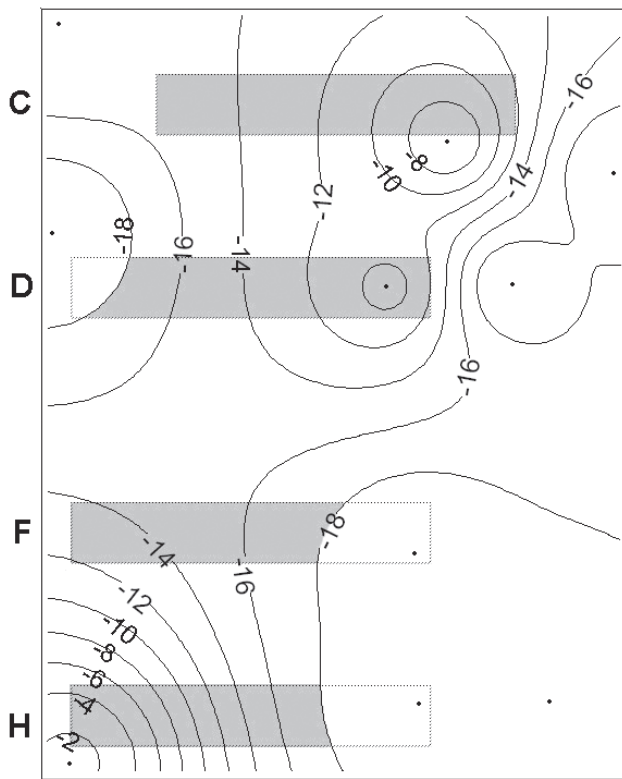


Figure 8. Contour map with emphasis on the -18 m permafrost surface elevation. The shaded area represents the occurrence of permafrost at a depth of 18 m (59 ft) or less. All of Building C is underlain by permafrost at a depth less than 18 m and approximately 90%, 70%, and 70% of the piles in Buildings D, F, and H, respectively, would be underlain by permafrost at a depth of 18 m (59 ft) or less. Based on the results, a reasonable estimate of the piles that would encounter permafrost at a depth less than or equal to 18 m would be approximately 80%. North is at the top of the figure.

area inside the building footprints with permafrost at a depth of 18 m (59 ft) or less is noted, a reasonable estimate of the piles that would encounter permafrost would be greater than 80%. The predicted surface compares very favorably with the actual surface plotted from the 479 piles that encountered permafrost.

It is neither logical nor reasonable in the permafrost environment in which the piles were to be installed at Fort Wainwright to conclude that 15% would encounter permafrost. The possibility that permafrost could exist over the entire project site at a depth less than 18 m (59 ft) should have been anticipated. Studies relating to degrading permafrost in the Fairbanks area have been reported in the scientific and engineering literature for more than three decades. Based on available information, it is without precedent that permafrost in the Fairbanks area at an initial depth of 1 m would degrade to a depth of 18 m (59 ft) in 10 to 12 years (with conduction as the heat transfer mode; in the absence of convective heat transport, e.g., groundwater flow).

The logs of the borings advanced in the thawed materials do not confirm the *nonexistence* of permafrost. Prior to surface disturbance and modification, permafrost was

present over nearly the entire project site at a very shallow depth. The permafrost did not disappear in the 10- to 12-year period following surface disturbance and modification. To correctly interpret the likely subsurface conditions at the project site the permafrost must be thought of as a surface that is changing with time and not a feature that is present or exclusively absent even in a discontinuous permafrost zone.

Acknowledgments

Steve Young, Corvallis, Oregon, assisted in the data reduction, and executed the software used to perform the topographic mapping. Charles Wilson and Greg Carpenter, U.S. Army Corps of Engineers, Anchorage, Alaska, provided information related to the geotechnical conditions at the site. Miles Illichmann, U.S. Army Corps of Engineers, Fairbanks, Alaska, provided the photographs shown herein and valuable insight into the history of the project site. Steve Pinnell and Blake Marchand, Pinnell Busch, Inc., Portland, Oregon, reviewed the project report written by the author that is the basis for this paper. The contribution of these individuals is gratefully acknowledged.

References

- Defense Mapping Agency Hydrographic/Topographic Center. 1978. Fort Wainwright, Alaska, Terrain Analysis, prepared for the Terrain Analysis Center, U.S. Army Engineer Topographic Laboratories, Fort Belvoir, Virginia, September.
- Linell, K.A. 1973. Long-term effects of vegetative cover on permafrost stability in an area of discontinuous permafrost. *Proceedings of the Second International Conference on Permafrost, Yakutsk, USSR, July 13-28, 1973*: 688-693.
- Pewe, T.L. & Reger, R.D. (Eds.) 1983. Guidebook to permafrost and Quaternary geology along the Richardson and Glenn Highways between Fairbanks and Anchorage, Alaska. *Proceedings of the Fourth International Conference on Permafrost, Fairbanks, Alaska, July 18-22, 1983*: Guidebook 1.
- Romanovsky, V.E. 2006. How rapidly is permafrost changing and what are the impacts of these changes? Arctic Theme Page, National Oceanic and Atmospheric Administration.

Stone Polygons in Southern Colorado, USA: Observations of Surficial Activity 1975–2004

John D. Vitek

Office of Graduate Studies & High Altitude Research Program (HARP), Texas A&M University, College Station, TX, USA

Netra Raj Regmi

HARP & Geology & Geophysics Department, Texas A&M University, College Station, TX, USA

Daniel Humbolt

Electrical & Computer Engineering, Texas A&M University, College Station, TX, USA

John R. Giardino

HARP, Geology & Geophysics Department, Geography Department, & Water Management & Hydrological Sciences Program, Texas A&M University, College Station, TX, USA

Abstract

Small stone polygons occupy a depression at 3865 m in the Sangre de Cristo Mountains, southern Colorado, USA. Vertical photographs were collected between 1975 and 2004 to document natural change on the surface of these polygons. Over time, the stones in the core region of these small polygons moved in multiple directions rather than directly toward the edges of the polygons. Clearly, movement results from freeze-thaw forces in three-dimensions within the polygons and from forces generated by water freezing in the stone gutters. Smaller polygons formed within the larger unit. Some stones observed in 1975 disappeared by 2004, essentially moved into the edges of the polygon and rotated such that identification becomes difficult. Measured horizontal displacements reached 29 cm, although the average is 7.4 cm for all stones. Maps of change and vectors of motions reveal the dynamic aspects of three dimensional forms subjected to intense freeze-thaw in an alpine environment.

Keywords: displacement; frost processes; repeat photography; stone polygons.

Introduction

Stone polygons, forms of patterned ground that are common in arctic and alpine areas, are generally attributed to intense freeze-thaw processes (Washburn 1956). In the years since Washburn's comprehensive review, numerous researchers have reported on many aspects of patterned ground in various locations (Washburn 1979, French 1996, Hallet et al. 2004) and attributed them to numerous processes of formation. Additional research will be cited with specific information as this paper is developed rather than simply listing them in this introduction. Vitek (1983) reported on seven years of surficial activity observed on stone polygons found in a small depression in glacial till at 3865 m in the Blanca Massif of the Sangre de Cristo Mountains in south-central Colorado. This paper extends the record of those initial observations to 30 years. In total, observations were made 22 times from 1975–2004. On several occasions, observations could not be obtained because the stone polygons in the 850 m² depression in a cirque were underwater from snowmelt and precipitation.

Since the site was first observed in 1975 until the last visit in 2004, standing water during the growing season is a major deterrent to grasses occupying the depression. Occasionally small tufts of grass appear but seldom do they survive the harsh winters. The lack of vegetation suggests that frost processes are not impeded and readily move stones around the surfaces of the polygons. The site is very remote, a five hour hike from the nearest road, and is not on any marked trail, nor would a causal hiker venture into this area because

of the lack of access to high peaks, i.e. those above 4300 m .a.s.l. Aside from an occasional small animal print embedded in the center of a polygon, the site has been virtually undisturbed. Every effort was made during photography to retain the site as undisturbed.

This paper presents observations, analyses of these observations, and discusses the forces involved in creating these stone polygons and movements of stones in the center of several polygons. How these observations relate to published research will be described in the discussion section along with suggestions for future research at this site. Whereas these observations represent changes in a surficial plane, stone polygons are three-dimensional phenomena. Within the centers of these small polygons, smaller polygons have been observed; they form either from desiccation drying or are the remnants of frost polygons left over from winter. Movement vectors reveal that motion is possible in many directions rather than just toward the edges of the polygons. We present only total change from 1975–2004 in this paper rather than the incremental changes that are possible with the data that have been collected. Greater detail will be published in a subsequent paper.

Study Area

The Sangre de Cristo Mountains are located in south-central Colorado (Fig. 1). Extensively glaciated during the Pleistocene, the Blanca Massif portion of the range contains numerous sites with patterned ground. Large stone polygons (Vitek & Tarquin 1984, Berta 1988, Vopata et al. 2006) are

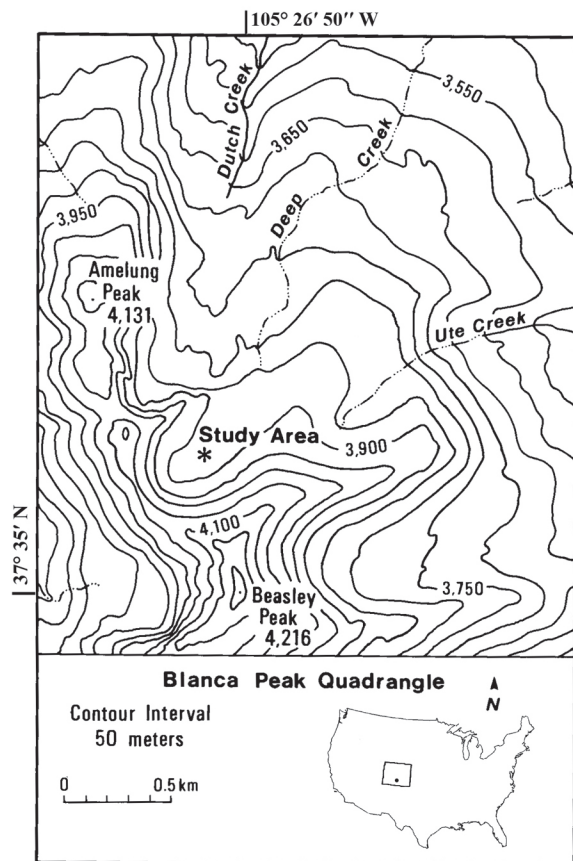


Figure 1. Location of the study area in southcentral Colorado.

prevalent in numerous locations above the tree line, including sites on ridges above 3900 m a.s.l. The location of these stone polygons, shown on an aerial photograph (Fig. 2), is precisely $37^{\circ}36'27.89''\text{N}$, $105^{\circ}26'54.51''\text{W}$, with these values read from an image on Google Earth[®]. At approximately 180 m above the tree line, the climatic conditions of the site can be classified as alpine tundra, but exact temperature and moisture conditions have not been monitored. When the site was first observed in 1975, it was covered by water. Within several weeks after the initial observation, however, the water evaporated and/or infiltrated through the glacial till (the frost table or permafrost may have lowered sufficiently to allow the water to drain) and revealed the stone polygons that have been photographed since 1975 (Fig. 3).

Methodology

Repeat photography is a viable technique for observing surficial change (Graf 1985, Kull 2005). In some instances changes occur rapidly, but some changes occur so slowly that photographic records can be used to confirm change. Over the years, every effort was made to take these handheld photographs at approximately the same time of day to keep shadows constant. Colored slides and black-and-white photographs were collected on every trip to the site. The same Pentax camera was used for all black-and-white photography, and two different Nikons were used to record colored slides of the polygons. A 50 mm lens was used on

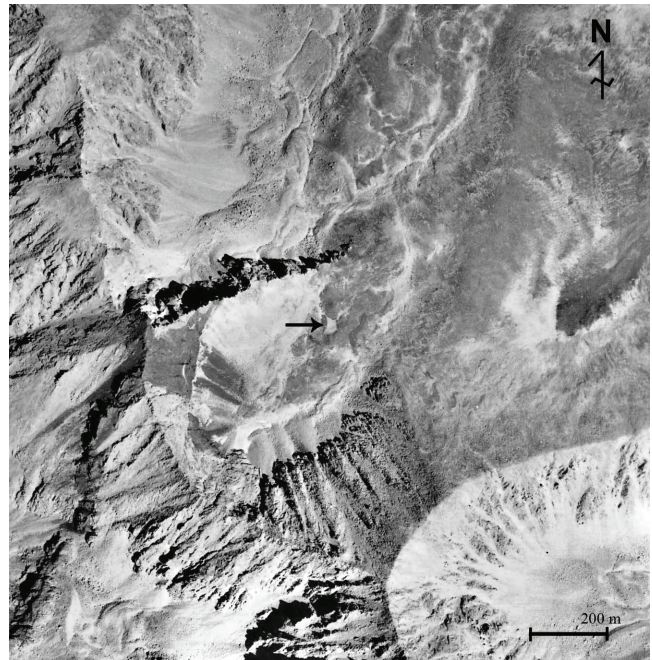


Figure 2. August 31, 1974, aerial photograph of the study area.



Figure 3. July 31, 2004, ground view of the study site with colleagues for scale.

both cameras. In 2004, digital images were acquired of the site in addition to traditional film medium. A steel ruler was positioned in every photograph to provide a consistent scale. J. Vitek took the photographs in every year but one. In this manner, any variation in the distance from the camera to the surface of a polygon was minimized.

The analyses for Vitek (1983) required making maps of the locations of stones from photographic prints and overlaying a map from one year over the photograph of the next year to detect change. The process was slow and only as accurate as the cartographic representation of the photographic image. Minor scale changes were made during the photographic process to create images that could be compared.

Fast forward into the twenty-first century and high speed computing. Digital images can be processed with software and provide a wealth of data about surficial change that occurs between two sets of imagery. ERSI ArcGIS 9.0[®]

is used to digitize, analyze, and layout the stone polygon images of 1975 and 2004. Identifiable structures and features on the largest stones found around the edges of the polygons were recognized and were used in the geo-referencing process. The structures chosen are mainly mafic inclusions, fractures, stone edges and stone corners. Geo-referencing of the images was done in the same coordinate system (UTM, Zone 13 N) and the same spatial extent. The scales of all the geo-referenced images are defined according to the metal scale placed on a stone polygon and measured during photography in 1975. After geo-referencing, all the boundaries of the stones were mapped as polygons. For each stone in 1975, a point, primarily the edges of the stone, and polygon centroids were marked and tracked to positions in the 2004 image. The magnitudes and directions of the movement of these points are represented by vector lines. The lengths of these vector lines and area of the polygons were calculated. Finally, the stone polygons from both dates and the vectors of movement were overlaid and the layouts of stone movement were created. The position of a stone in 2004 can be visually linked to its position in 1975. We believe that computer-generated and compared images yield results that are significant because images that are compared can be aligned more precisely than with manual mapping.

All images were converted to digital images for these analyses because of the ease of comparing such images. Although the stone polygons were not disturbed during the observation period, individual stones are lost only because we could no longer positively identify them at a new location. For the purpose of this paper, we chose to compare several images from 1975 against the images of the same sites collected in 2004. An initial assumption that the large stones forming the edges of the polygons do not move was easily discredited. Some large stones that formed the edges of the polygons have moved, but the analyses considered such changes in calculating the movement of the stones in the centers of the polygons for this paper.

Observations

We never knew before making the trek from the base camp at 3110 m to the site at 3865 m if the depression in which the stone polygons formed would contain water or would be dry. Water over the stone polygons excluded photographic data being collected on individual stone polygons. Often, water was observed in the gutters between polygons but below the level of the centers. During dry summers, water completely disappeared from this site. We can assume that water was lost to evaporation as well as drainage into the till once it was no longer frozen. The annual depth of frost penetration is unknown and no information exists on permafrost in this area. A trench dug to a meter in depth in August of 1983 revealed a frozen surface. Whether the ice survived until the next summer is unknown.

A site visit in March of 1978 was made to assess the conditions of the depression in late winter. Interestingly, lacustrine ice over the site had already begun to thaw, but



Figure 4. Photograph of site D taken on August 6, 1975. Metal scale is 150 mm.



Figure 5. Photograph taken of site D on July 31, 2004. Metal scale is 150 mm.

needle ice, isolated patches of lacustrine ice, and frozen centers were observed in several polygon centers that were exposed above the level of the lacustrine ice. Stones on the surfaces of the polygons, therefore, are subjected to more forces than the simple freeze-thaw introduced into the till by temperature fluctuations. The variety of forces at work will be evaluated in the discussion section. No effort was made to visit the site during the winter because the depth of snow was impassable in the main valley and the total distance and time to walk to the site doubled in such severe conditions.

For this paper, the same four-stone polygon centers presented in Vitek (1983) are re-assessed. Photographic data also exist for 12 additional stone polygons and will be used in conjunction with a complete analysis of this site at a later date. Figure 4 is a photograph of site D collected on August 6, 1975, and Figure 5 is the same sited on July 31, 2004. Scanning and comparing these two images generates Figure 6. Figure 7 shows the vectors of motion for stones in polygon D using the center of each stone as the position of reference.

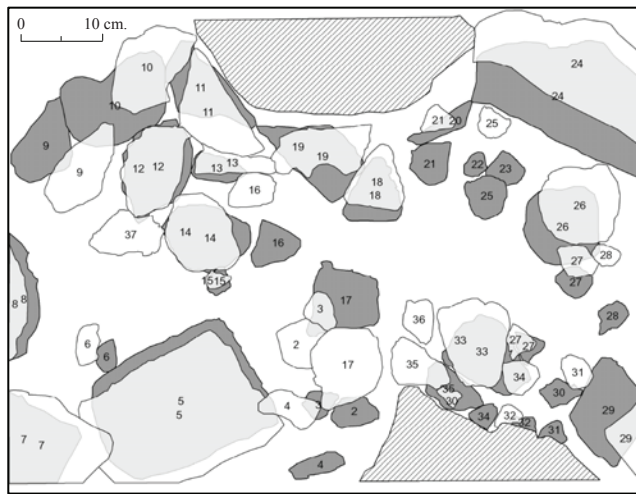


Figure 6. Map of stone movements at site D observed from 1975–2004. Gray tone is 1975 position; white is 2004. Stripe is a stable stone from 1975–2004.

Results

Observing this site over 30 years reveals how slowly freeze-thaw processes operate in an alpine environment to rearrange the surficial appearance of the polygons. Given that the site has been free of glaciers since the end of the Pleistocene, approximately 11,000 years have been available for various freezing processes to reorganize the till left behind by the glacier. The absence of trees at this elevation and the current absence of grass and other alpine plants in the depression allows frost processes to be active. In close proximity to the depression with active stone polygons, large relict stone polygons (Vitek & Tarquin 1984) probably ceased to develop once grass was able to stabilize the centers of the polygons. Grass was observed growing over some stone gutters between the relict polygons. The frequent presence of water in this depression (probably for a significant amount of time each year), therefore, is the primary reason why the site remains active and free of vegetation.

Stones in the centers of the polygons were identified in 1975 and mapped using the system discussed in the Methodology section. Table 1 is a comparative summary of the observations made in four centers of stone polygons that were photographed in 1975 and 2004. Perhaps the most important observation in Table 1 is the number of stones that could not be easily identified in 2004 compared to the initial positions in 1975. Movement of a stone plus rotation often makes it impossible to conclude the fate of a particular stone. Such stones are reported as “lost” and the amount of movement cannot be calculated. Even if the stone is resting with others along the edges of the polygon, it was considered “lost” if precise identification was not possible. The number of “lost” stones may be minimized when a comparison is made between every photograph available for each site, a total of 22 iterations being possible. Movement of an individual stone ranged from only the slightest degree of movement to 29 cm in one instance (polygon C) with the

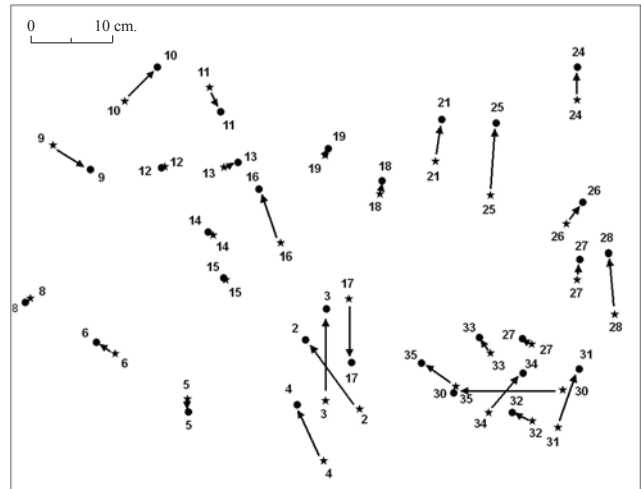


Figure 7. The amount and direction of movement of stones in polygon D, 1975–2004.

Table 1. Summary of measurements for 1975–2004.

Site	N (1975–2004)*	Mean Disp.	SD	Range
A	57 – 36	7.69 cm	4.53	1.0 – 16 cm
B	40 – 27	7.67 cm	5.78	1.8 – 19.9 cm
C	52 – 23	8.65 cm	7.99	1.0 – 29 cm
D	37 – 30	5.59 cm	3.89	1.0 – 15.7 cm

* N is the number of stones observed in 1975 and those relocated in 2004; Mean Disp. is the mean displacement observed; and SD is the standard deviation.

average distance moved for all stones that were re-identified in 2004 being 7.4 cm. Figure 6 shows the position of stones in polygon D in 1975 and 2004, respectively. If all stones could be located, we believe that the average distance moved would significantly increase.

The level of analysis possible is a function of the size of stone selected and whether it can be relocated during the next time period, or in this case, after 30 years. Many stones were deemed too small to trace even yearly because when rotation occurred positive identification was difficult, if not impossible. Moreover, assumptions about the direction of movement (toward the edge of the polygon) are not correct in that stones were moved toward the center of the polygon as observed in every polygon. No stone was physically identified by lifting it from the site. Interpretation to relocate a stone was based on viewing each site in color, and black-and-white images. If one were to continue the study, perhaps some type of marker could be added to each stone without disturbing it.

On a yearly average basis, stone movement is about 0.25 cm. Hence, years of observation really are necessary to detect significant change in the arrangement of stones in stone polygons. Whereas this focus has been on the visual changes in the surface, essentially a plane, the centers of

stone polygons are three dimensional because sorting over the history of the feature has concentrated fine material (sand, silt and clay) in the core and stones were noticeably absent in the center of the core of one polygon that was excavated. Other research has shown how stone polygons function as three-dimensional systems such that stones are sorted to the surface and edges of the polygon. This concept is expanded in the discussion section.

Discussion

In the 25 years since the fourth Permafrost Conference was held in Fairbanks, significant contributions have been made to the literature on patterned ground. Detailed measurements by Hallet (1998) of motion within sorted circles demonstrated how frost processes operate. Hallet's instrumented efforts from 1983–1997 on Spitsbergen represent the best effort to interpret change in patterned ground at a low elevation, high latitude location. He measured vertical heave, the rapid settling of fines, a preferential subsidence of borders, and was able to conclude that convection occurred in the sorted circles. He observed that a small residual difference in displacement remains after each full-year cycle and over time pattern evolves. Gleason et al. (1986) demonstrated that sorted patterned ground can arise from density-driven Rayleigh free convection in water saturated soils that are frozen. With the presence of water in the alpine depression that we studied, observations confirmed that a small average yearly displacement is capable of sorting material given sufficient time. An ample supply of water is transformed into ice (needle, lacustrine, and ground), thereby, generating re-occurring forces that transform till into sorted stone polygons.

Kessler & Werner (2003) developed a numerical model to explain how stones and soil self-organize in polar and high alpine environments to create patterned ground. They demonstrated that frost heave can act in a number of different orientations within the surface based upon the nature of the material encountered. Lateral sorting and stone domain squeezing are the feedback mechanisms that develop stone polygons. They stated that polygons are enhanced by rapid freezing. At our alpine site, the centers of the stone polygons can be squeezed as frost penetration occurs from the surface and through the sides (gutters) given that ample air spaces are prevalent in the stone gutters between centers. If water occupies these gutters, however, the centers will be squeezed by water freezing within the gutter and material in the core of the stone polygons will, therefore, freeze from the surface and the sides. How the water in the stone gutters (and subsequently ice) contacts the core material of the stone polygon will definitely impact how the core freezes and how much heaving occurs. Hence, the presence or absence of water in the depression during the dominant freeze-thaw periods (fall and spring) will have a significant impact on the forces generated in the till. Fowler & Noon (1997) noted that differential frost heave depends on the soil heaving characteristics and the rate of frost penetration. Observations

at our site suggests that the rate of frost penetration will be extremely variable because of the variation in the sizes of stones that formed the gutters and the sides of the polygons in addition to the size of stones on the surface and the sediment composition of the core. In actuality, every site will exhibit such variability and, thereby, complicate formulation of models to replicate the processes involved in formation. Without precise temperature and moisture values for the site, including the presence or absence of water during freezing, one can only hypothesize about the frost processes that contribute to stone motion from the forces generated by freezing and thawing.

Fang & Hager (2002) believe that the stones represent large sources of noise in a non-linear reaction-diffusion type of model. Regardless of the model used, the variability of the sizes of stones in the centers and in the gutters of stone polygons complicates any model because nothing is uniform in any setting with stone polygons. The role of differential frost heave (Peterson & Krantz 2003) is dependent upon heat transfer in the system. The variable sizes of the stones in the till in this depression create complexities that would be difficult to model. Penetration of the freezing plane in three dimensions is very irregular and would result in thrusts and heaves in multiple directions. These forces are reflected in the observation of stones moving in the multiple directions in the centers of the polygons not just toward the edges.

Ugolini et al. (2006) assessed how fines were segregated in the development of patterned ground. They mentioned that airborne fines, plus those produced by weathering, contribute to the core of fine material segregated by frost processes. We believe that fines at this site can be attributed, in part, to aeolian transport because sand dunes occur in the San Luis Valley immediately west of the site. Detailed analyses of the silts and clays would be necessary to confirm the source of the fines in the centers of the polygons. Although radiocarbon techniques have been used to date patterned ground (Jeong 2006), no efforts were made to date these stone polygons. The absence of lichens on stones within the depression also provides an indication of the dynamic nature of the site. Vitek & Tarquin (1984) observed and measured lichens found on large inactive stone polygons nearby that indicated the stones in the gutters were stable for at least 2500 years based upon a growth rate curve for lichens from another location in Colorado (Benedict 1979).

Gleason et al. (1986) observed that the depth of the active layer at the onset of convection corresponded to the depth of sorting. Holness (2003) reported similar relationships for sorted circles in the maritime Subantarctic. Convection cells may account for certain features of the circles, including regularity of form morphology, but differential frost heave contributes to movement within the circles. He noted that increasing frost penetration was highly correlated with the distance between fine centers and also the depth of sorting. At our site, the short distances between centers suggests shallow depth of sorting, perhaps a function of the thin till layer over the bedrock surface of this glacial cirque.

Conclusions

Stone polygons are common in arctic and alpine areas in which freeze-thaw processes dominate. Observing one site on 22 occasions over 30 years yields information about the rate at which the surface is changing. Although 30 years is less than 0.27% of the total time since deglaciation, these observations do demonstrate change. For some stones in the system, change is significant whereas it is not for others. We also observed secondary polygons forming within the fines of the cores and we observed stones on the surface moving in directions other than toward the edges of the polygons. Whereas repeat photography of the surface of the centers reflects two-dimensional change, forces acting on these polygons do so in three dimensions – the surface and through the sides (the gutters). Variability between each polygon is a function of how these forces act at each site. Whereas the average total movement of the stones observed was 7.4 cm from 1975–2004, the average yearly rate of motion was only 0.25 cm for stones relocated in 2004. The passage of time, however, makes change easier to detect.

To increase the complexity of the study would require significant resources for instruments and transportation to the site in all seasons. We believe that the data collected thus far provide a unique glimpse of the two-dimensional changes that can occur. Additional research on this unique alpine site in southern Colorado is possible because it has not been disturbed.

Acknowledgments

Friends who made the five-hour hike to the site to assist with data collection include Mark Vitek, Mark Gregory, Marshall Cossman, Phil Ward, Lance Salisbury, Pam Tarquin, and Ellen Rose. Our sincere thanks for your help.

References

- Benedict, J.B. 1979. Fossil ice wedges polygons in the Colorado Front Range: Origin and significance. *Geol. Soc. Am. Bull.* 90:173-197.
- Berta, S. 1988. Three-dimensional characteristics of stone polygons in a periglacial environment. *Abstracts with Programs, Geol. Soc. Am.* 20(7): 184.
- Fang, M. & Hager, B.H. 2002. Stone polygons: self-organization assisted by noise. *AGU Abstracts* #U72B-0018.
- Fowler, A.C. & Noon, C.G. 1997. Differential frost heave in seasonally frozen soils. *Proceedings on the International Symposium on Physics, Chemistry, and Ecology of Frozen Soils*. Special Report-Corps of Engineers, US Army CRREL, 247-252.
- French, H.M. 1996. *The Periglacial Environment*. Second Edition. London: Longman, 341 pp.
- Gleason, K.J., Krantz, W.B., Caine, N., George, J.H. & Gunn, R.D. 1986. Geometrical aspects of sorted patterned ground in recurrently frozen soils. *Science* 232: 216-220.
- Graf, W.L. 1985. Geomorphic measurements from ground-based photographs. In: A.F Pity (ed.), *Geomorphology Themes and Trends*. Totowa, NJ: Barnes & Noble, 211-225.
- Hallet, B. 1998. Measurement of soil motion in sorted circles, Western Spitsbergen. *Proceedings of the Seventh International Conference on Permafrost, Yellowknife, Canada, June 23-27, 1998*: 415-420.
- Hallet, B., Putkonen, J., Sletten, R. S. & Potter, N.J. 2004. Permafrost process research in the U.S. since 1960. *Developments in Quaternary Science* 1: 127-145.
- Holness, S.D. 2003. Sorted circles in the maritime Subantarctic, Marion Island. *Earth Surface Processes and Landforms* 28(4): 337-347.
- Jeong, G.Y. 2006. Radiocarbon ages of sorted circles on King George Island, South Shetland Islands, West Antarctica. *Antarctic Science* 18(2): 265-270.
- Kessler, M.A. & Werner, B.T. 2003. Self-organization of sorted patterned ground. *Science* 299: 380-383.
- Kull, C.A. 2005. Historical landscape repeat photography as a tool for land use change research. *Norsk Geografisk Tidsskrift* 59:253-268.
- Peterson, R.A. & Krantz, W.B. 2003. A mechanism for differential frost heave and its implications for patterned-ground formation. *Journal of Glaciology* 49(164): 69-80.
- Ugolini, F.C., Corti, G. & Certini, G. 2006. Pedogenesis in the sorted patterned ground of Devon Plateau, Devon Island, Nunavut, Canada. *Geoderma* 136: 87-106.
- Vitek, J.D. 1983. Stone polygons: observations of surficial activity. *Proceedings of the Fourth International Conference on Permafrost*, National Academy Press, Washington, DC: 1326-1331.
- Vitek, J.D. & Tarquin, P. 1984. Characteristics of relict stone polygons, Sangre de Cristo Mountains, Colorado, USA. *Zeitschrift fuer Geomorphologie* 28(4): 455-465.
- Vopata, J., Aber, J.S. & Kalm, V. 2006. Patterned ground in the Culebra Range, southern Colorado. *Emporia State Research Studies* 43(1): 8-21.
- Washburn, A.L. 1956. Classification of patterned ground and review of suggested origins. *Geological Society of America Bulletin* 67: 823-865.
- Washburn, A.L. 1979. *Geocryology*. London: Edward Arnold, 406 pp.

Transformations of Cryogenic Structure of Frozen Clay Soils at Shear

S.S. Volokhov

Faculty of Geology, Moscow State University, Vorobiev Gory, 119899, Moscow, Russia

Abstract

This report presents research results regarding the process of ice segregation in frozen clay soils at shear under creep conditions. It is demonstrated that the process of ice segregation takes place in the shearing area only at the stage of frozen soil failure and is related to crack formation during shear. When soils were subjected to continuous creep deformation, no increase in ice content was observed. It is concluded that the formation of a film of ice within the soil shear surface has a strengthening effect.

Keywords: creep; failure shear; migration; moisture; segregation.

Introduction

Transformation of cryogenic structure of frozen soils at shear is the subject of works by Vyalov (1959), Tsytoich (1975), Roggensack & Morgenstern (1978), Yershov et al. (1981), Chuvilin et al. (1994), and others. It is demonstrated by Roggensack & Morgenstern (1978) that as a result of shear of frozen clay samples at a constant deformation velocity of frozen clay samples at temperatures from -1°C to -1.5°C , ice schliers are formed in the shearing area orientated along the shear planes. Similar results are obtained in Yershov et al. (1981) and Chuvilin et al. (1994) under shear tests of bentonite, polymineral, and kaolinite clays in creep conditions at a temperature of -3°C . Moreover, Savigny & Morgenstern (1986) reported a growth of new ice lenses in ice-rich soils along shear surfaces at triaxial compression. This research is far from being complete. The issue of the nature of unfrozen water migration and of ice segregation in the shearing area is still of present interest.

Scientific literature contains evidence of the fact that unfrozen water migration may result from changing of the pore geometry and the interfacial energy of soil particles at formation of dislocations, microfractures, and other defects (Sakharov 1994, Komarov 1999). This suggests that unfrozen water migration and ice segregation at shear in frozen soils happens due to formation of microfractures when shearing stress exceeds the long-term strength; i.e., in divergent creep conditions, at deformation velocities comparable with unfrozen water migration velocities. Verifying this hypothesis is the subject of the present research.

Research Methods

Kaolinite clay (Chelyabinsk), polymineral clay (Gzhel), and loam (Yamal) were tested. The tests were performed on samples of soils of disturbed structure. The samples of frozen soils were prepared in work rings from a soil paste, consolidated for 2 days under a step load increasing until it reached 0.2 MPa, cooled for 4 h at a temperature of 0°C , and frozen for one day in a low-temperature cabinet (-30°C). They were then maintained at the experiment temperature (-3°C or -1°C) for one day. The values of total moisture content and density of the samples were, respectively, 37%–

38% and 1.68 g/cm³ for kaolinite clay, 30% and 1.86 g/cm³ for polymineral clay, and 29%–30% and 1.85 g/cm³ for loam. The samples were of cylindrical form and had a diameter of 71.4 mm and a height of 35–37 mm.

Single-plane shear apparatus PRS (Fig. 1) designed by NIIOSP (Sadovsky 1967) was used for shear tests on frozen soils. The test scheme is shown on Figure 2. The research was carried out at constant shear loads in conditions of convergent and divergent creep. In convergent creep cases the duration of the experiments was up to 30 days, and in divergent creep cases the samples were brought to failure. The tests were carried out at normal load of 0.1 MPa with double replication. The experiments were performed in a refrigerating chamber NKR at temperatures -3°C and -1°C maintained within the accuracy of $\pm 0.1^{\circ}\text{C}$. One of the two tested samples was used for studying the transformation of cryogenic structure, the other one for studying the changes in the total moisture content of the frozen soil.

Research on cryogenic structure of soil samples was performed by means of an optical microscope. Distribution of the total moisture content along the height of the samples was determined by division into 12 layers, each about 3 mm thick. Each layer was then divided by two cutting rings of different diameter into three areas: the edge area, the intermediate area, and the central area (Fig. 3). For

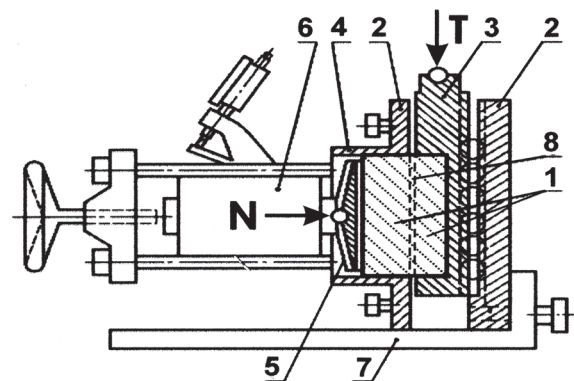


Figure 1. Single-plane shear apparatus PRS. 1 – sample of frozen soil, 2 – shear cell, 3 – mobile carriage, 4 – work rings, 5 – lateral stamp, 6 – dynamometer, 7 – supporting plate, 8 – apparatus clearance. N – normal load, T – shear load.

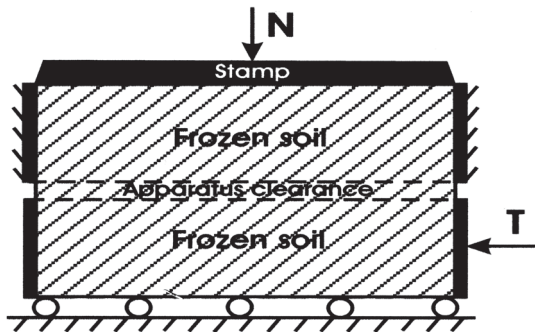


Figure 2. Scheme of shear test. N – normal load, T – shear load.

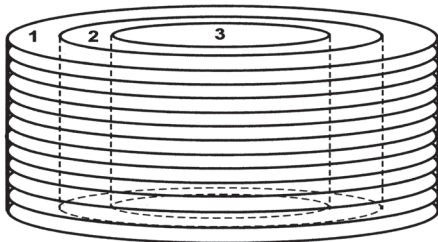


Figure 3. Scheme of frozen samples cutting. 1 – the edge area, 2 – the intermediate area, 3 – the central area.

each of them, a curve of total moisture content distribution according to sample height was plotted. Comparison was made between the tested samples and of samples which had not undergone shear.

Research Results

In order to verify the hypothesis stated above regarding the nature of ice segregation in the shearing zone, analysis was undertaken of transformation of cryogenic structure and of moisture content in frozen soils which had undergone constant loads, both being under the value of the limit of long-term shear strength and exceeding this value. Thus, the tests were performed under convergent creep and divergent creep conditions. In the latter case, the samples were brought to failure.

The results of this research are demonstrated with the kaolinite clay example. Tests of polymineral clay and loam samples had similar results.

An example of the initial cryogenic structure of frozen kaolinite clay samples at a temperature of -3°C before the shear test is demonstrated in Figure 4. In general, the samples had a massive cryogenic texture, with ice pocket and air bubble inclusions. Increase of ice content from the centre of the samples to their peripheral areas is indicated. The soil in the centre of the samples was more solid, almost without ice inclusions. Detached ice schliers parallel to the exterior surfaces of the samples could be seen in the edge areas. The patterns of the initial total moisture content distribution are demonstrated on Figure 5. The diagrams show that moisture content increased from the central part of the sample towards the edges. It was connected with moisture migration at soil freezing.

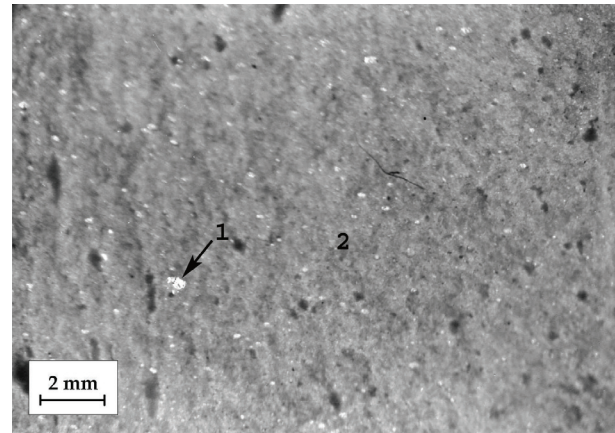


Figure 4. Initial cryogenic structure of cross section of frozen kaolinite clay samples before the shear test. Temperature -3°C . 1 – ice, 2 – mineral skeleton.

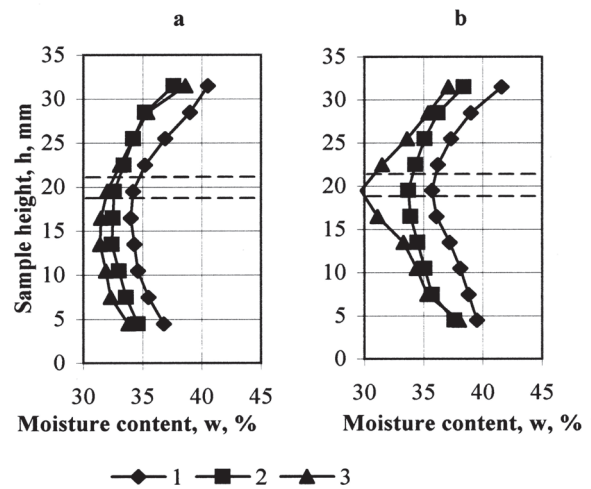


Figure 5. Initial total moisture content distribution in the samples of frozen kaolinite clay. 1 – in the edge area, 2 – in the intermediate area, 3 – in the central area. Dashed lines show a position of apparatus clearance.

Tests were performed on frozen kaolinite clay samples at the temperature -3°C , by means of constant shear loads of 0.5 and 0.45 MPa. The shear load of 0.5 MPa corresponded to the limit of long-term shear strength achieved by step-stress tests. When a shear load of 0.5 MPa was applied, sample failure was achieved in 29 days. At that load, the transient creep stage lasted for about 7 days. When the load of 0.45 MPa was applied, convergent creep was observed for 29 days. A duplicate test of the samples under the load of 0.5 MPa was carried out, with an interruption after 7 days, i.e., in the end of the transient creep stage.

The results showed that increase of the total moisture content (Fig. 6c) and formation of ice schliers in the shearing area (Fig. 7c) was observed only in the samples brought to failure. In this case, the schliers originated at the lateral surface, in the zone of apparatus clearance, and had an angle to it equal to approximately 45° . The moisture increased by 3%–5% in the upper edge area of the samples.

In convergent creep conditions, and at the transient stage

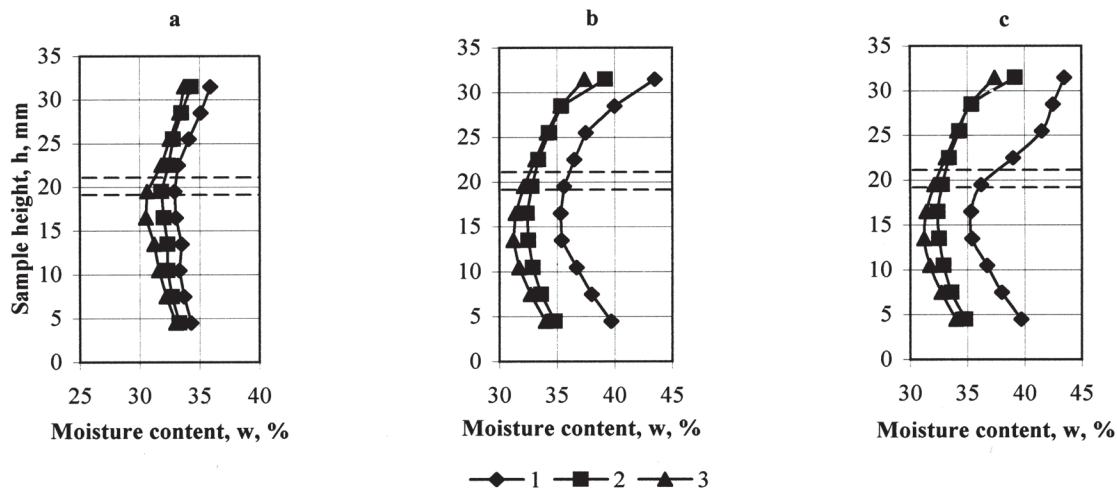


Figure 6. Total moisture content distribution in frozen kaolinite clay samples after shear tests under shear loads: a – 0.45 MPa (29 days), b – 0.5 MPa (7 days), c – 0.5 MPa (29 days). Temperature -3°C . 1 – in the edge area, 2 – in the intermediate area, 3 – in the central area. Dashed lines show a position of apparatus clearance.

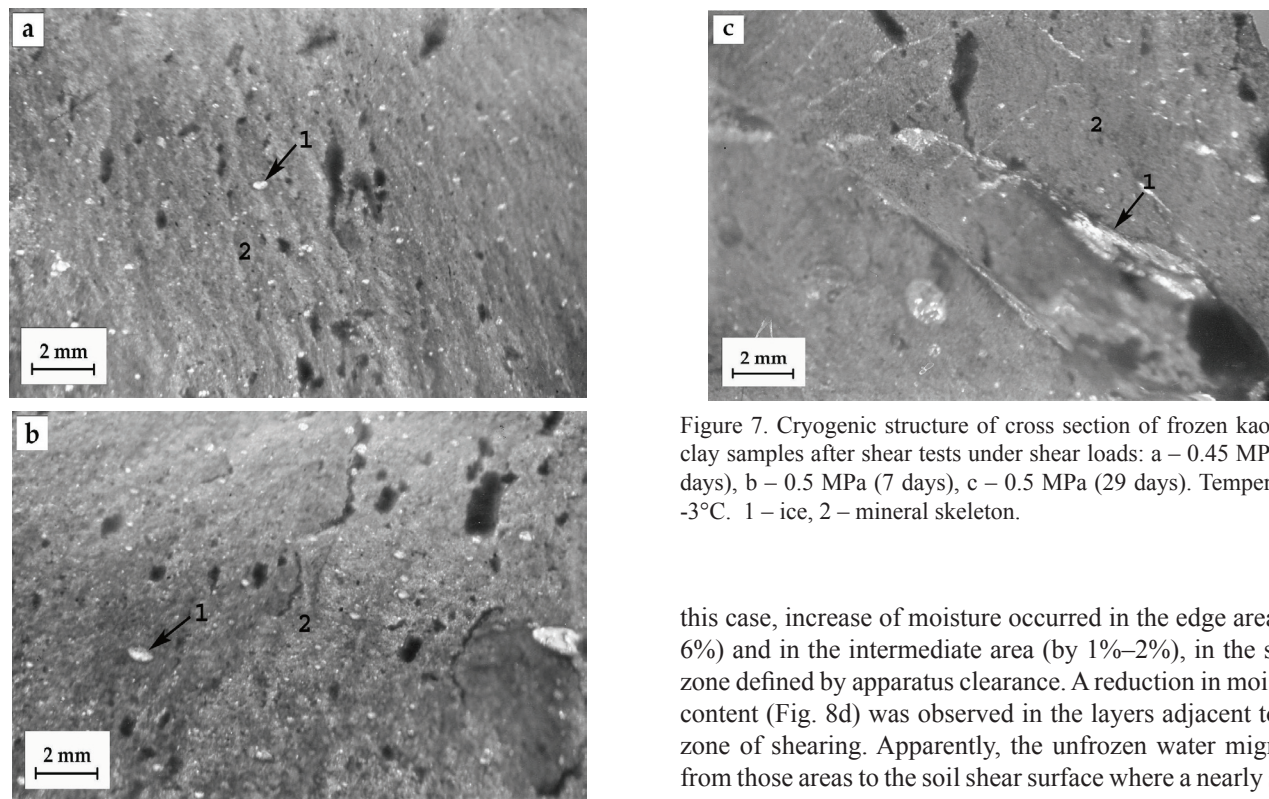


Figure 7. Cryogenic structure of cross section of frozen kaolinite clay samples after shear tests under shear loads: a – 0.45 MPa (29 days), b – 0.5 MPa (7 days), c – 0.5 MPa (29 days). Temperature -3°C . 1 – ice, 2 – mineral skeleton.

at divergent creep, no changes in the moisture distribution along the height of the samples (Fig. 6a, b) or in the cryogenic structure (Fig. 7a, b) of the frozen soil occurred. Thus, redistribution of moisture and formation of schliers in the shearing area took place only at the stages of steady-state creep and progressing flow; i.e., at the stage of sample failure.

The tests of frozen kaolinite clay were also done at the temperature of -1°C , under constant shear loads of 0.1, 0.3, and 0.4 MPa, and under a step load increasing until it reached 0.4 MPa. The tests lasted for 18 to 21 days. Failure of samples was achieved only under constant shear load of 0.4 MPa. In

this case, increase of moisture occurred in the edge area (by 6%) and in the intermediate area (by 1%–2%), in the shear zone defined by apparatus clearance. A reduction in moisture content (Fig. 8d) was observed in the layers adjacent to the zone of shearing. Apparently, the unfrozen water migrated from those areas to the soil shear surface where a nearly solid layer of ice (Fig. 9) was formed. At lower loads (0.1 and 0.3 MPa) and at a step load increasing up to 0.4 MPa, convergent creep was observed and no changes in the cryogenic structure or total moisture content were recorded (Fig. 8a, b, c). As the work of Volokhov (2005) demonstrates, under shear tests of kaolinite clay at the temperature of -3°C , the shear surface does not coincide with the plane of the shear apparatus clearance but has an angle of gradient to it equal to about 45° , originating at the lateral surface of the samples and reaching their frontal surface. Here, displacement of a conical-shaped part of the sample takes place, overthrusting the other part of the sample (Fig. 10a). At the temperature of -1°C , the soil shear zone is arc-shaped confined to the clearance of the apparatus (Fig. 10b). It appears from this

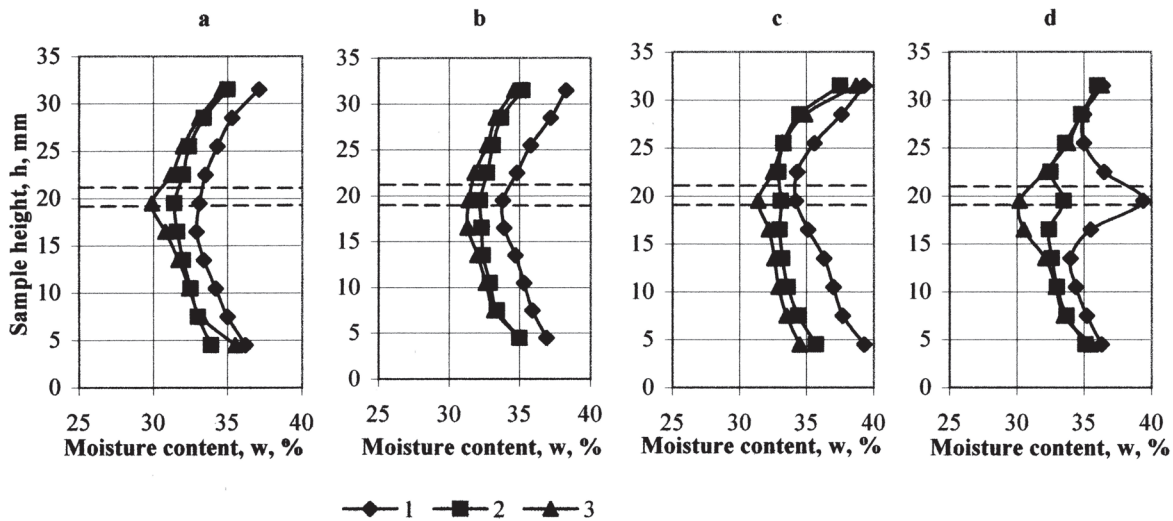


Figure 8. Total moisture content distribution in frozen kaolinite clay samples after shear tests under shear loads: a – 0.1 MPa, b – 0.3 MPa, c – a step load increasing until it reached 0.4 MPa, d – 0.4 MPa. Temperature -1°C. 1 – in the edge area, 2 – in the intermediate area, 3 – in the central area. Dashed lines show a position of apparatus clearance.

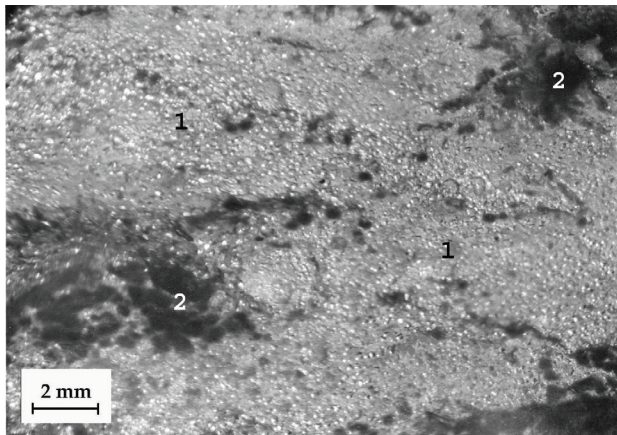


Figure 9. Cryogenic structure of soil shear surface of the frozen kaolinite clay sample. Temperature -1°C. 1 – ice, 2 – mineral skeleton.

that the aforementioned changes in the cryogenic structure and in moisture content of frozen kaolinite clay occur in the zone of soil shear dislocation.

Thus, this research has provided the following results.

1. In convergent creep conditions, no changes in the cryogenic structure or in distribution of the total moisture content occur. Ice segregation and an increase of total moisture content happen only in divergent creep conditions; i.e., under failure of samples.

2. In divergent creep conditions, ice segregation occurs in the shear area only at the stages of steady-state creep and progressing flow; i.e., at the stage of frozen soil failure. It is not recorded at the transient creep stage.

3. In all of the cases, ice segregation is confined not to the clearance plane of the shear apparatus, but to the shear surface within the soil, irrespective of its alignment in relation to the clearance of the shear apparatus. In this soil shear surface, an ice film develops.

4. Maximal increase of the total moisture content of frozen

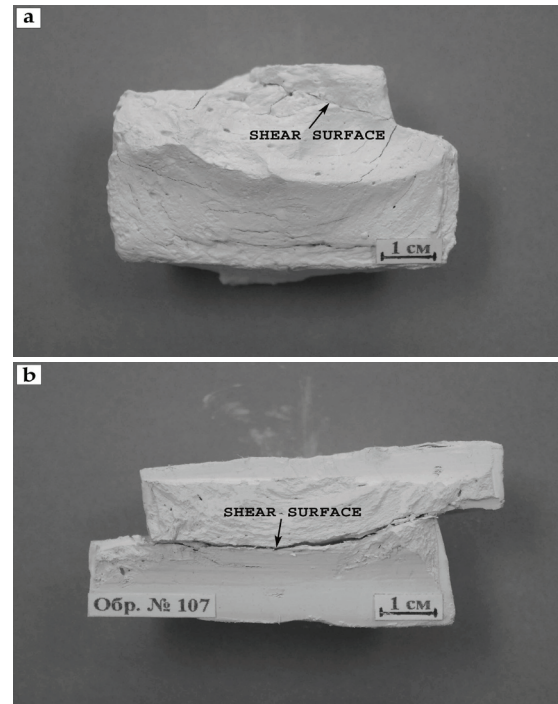


Figure 10. Character of failure of frozen kaolinite clay samples at temperatures: a – 3°C, b – 1°C.

soils and formation of ice schliers at shear is characteristic for the edge area of the samples. As for the central area of the samples, such changes are not present.

Analysis of Results

The results achieved allow conclusions to be drawn concerning the nature of unfrozen water migration and of ice segregation in the shearing area. Changes in the cryogenic structure and in moisture content of frozen clay samples occurred only at the failure stage and their confinement to the sample shear surface suggests that processes of unfrozen

water migration to the shearing area and ice segregation in it are related to formation of microfractures at the failure stage. Formation of cracks in the soil is accompanied by formation of new surfaces and increase of interfacial energy of the mineral or ice components of frozen soil. It can cause unfrozen water migration from the areas having lower specific interfacial energy to the microfractures with high values of specific interfacial energy; i.e., under the effect of thermodynamic water potential gradient. Continuous deformation of frozen soil under steady-state creep and progressing flow, and the formation of new microfractures must provide for inflow of unfrozen water to the shearing area from adjacent areas of soil. Freezing of excessive water in the microfractures results in formation and growth of ice schliers there.

Apparently, the described process can go on provided that the unfrozen water migration velocity and the velocity of microfracture formation are commensurate. This is possible at rather low strain rates during frozen soil failure stages, provided that the duration of the stages is significant.

Verification of the hypothesis on the leading role of crack formation in the process of ice segregation at shear is based on the fact that this process occurs mainly in the edge area of the samples and does not affect their central area. This may be related to the fact that shearing of samples begins at the lateral surface at low crack formation velocities. The central area of the samples remains unaffected by the failure process. Therefore, unfrozen water has time to migrate to the shearing zone, filling the cracks in the edge area and freezing there. Advance of the cracks to the central area of samples occurs at high strain rates so that moisture has no time to migrate into them; therefore no changes in the cryogenic structure and in moisture content of the samples takes place in this area of the samples. This process is possible only within a certain range of strain rates at the stage of frozen soil failure.

The conclusion can be made regarding the role of ice segregation in forming of frozen soil strength. Ice schliers appearing in the cracks serve to bond cracks, preventing their advancement and decelerating frozen soil failure. If this process did not occur, frozen soil would be destroyed faster. Consequently, it plays a strengthening role.

Acknowledgments

The work was carried out with the financial support of RFFR RAS (project № 05-05-64310).

References

- Chuvilin, E.M., Roman, L.T., Tsyrendorjjeva, M.D. & Degasyuk, V.N. 1994. Experimental study of structural and textural transformations in frozen rocks during shear. *Geoecology* 3: 69-75.
- Komarov, I.A. 1999. *Thermodynamic of Freezing and Frozen Disperse Grounds. Doctoral Dissertation, Abstract*. Moscow: Lomonosov Moscow State University Press, 52 pp.
- Roggensack, W.D. & Morgenstern, N.R. 1978. Direct shear tests on natural fine-grained permafrost soils. *Proceedings of the Third International Conference on Permafrost, Edmonton, Alberta, Canada, July 10-15, 1978*: 729-735.
- Sadovsky, A.V. 1967. Determination of adfreezing strength of soil with concrete by method of plane shear. In: *Works of the Nord Department of SRI Bases*. Syktyvkar 3: 70-79.
- Sakharov, I.I. 1994. Structural and textural transformations in freezing rocks and their relation to moisture migration processes. *Geoecology* 1: 56-64.
- Savigny, K.W. & Morgenstern, N.R. 1978. Creep behavior of undisturbed clay permafrost. *Canadian Geotechnical Journal* 23(4): 515-526.
- Tsytovich, N.A. 1975. *The Mechanics of Frozen Ground*. Washington DC: Scripta Book Company, 426 pp.
- Vialov, S.S. 1959. *Rheological Properties and Bearing Capacity of Frozen Soils*. Moscow: Izdatelstvo Akademii Nauk SSSR, CRREL Translation, Hanover, NH, 219 pp.
- Volokhov, S.S. 2005. The character of frozen clay soils failure at shear. *Proceedings of the Third Russian Conference on Geocryology, MSU, Moscow, June 1-3*: 27-32.
- Yershov, E.D., Lebedenko, Y.P., Yershov, V.D. & Kondakova, O.A. 1981. Migration of moisture and segregation ice exudation in frozen soils under strain gradient during shear. *Engineering Geology* 6: 104-112.

PERMOS – A Comprehensive Monitoring Network of Mountain Permafrost in the Swiss Alps

Daniel S. Vonder Mühl

PERMOS Coordination Office, University of Zurich and SystemsX.ch, ETH Zurich, Switzerland

Jeannette Noetzli

PERMOS Coordination Office, Glaciology, Geomorphodynamics and Geochronology, Department of Geography, University of Zurich, Switzerland

Isabelle Roer

PERMOS Coordination Office, Glaciology, Geomorphodynamics and Geochronology, Department of Geography, University of Zurich, Switzerland

Abstract

Permafrost Monitoring in Switzerland (PERMOS) has been built up since the early 1990s. After a 6-year pilot phase starting in 2000, PERMOS has taken root. In 2007, all potential PERMOS elements were evaluated based on the criteria and categorised into (A) approved element, (B) element subject to verification in the next two years, and (C) no PERMOS element. The concept “PERMOS 2007” was updated and adapted accordingly. All approved elements will fulfill defined technological and methodological standards. Hence, in 2010, PERMOS will be a sound, sustainable observation network with two types of PERMOS stations: (1) drill sites building the basis of the monitoring network, and (2) kinematic sites, where systematic observations of permafrost geomorphodynamics are performed, allowing for an integral assessment of the permafrost state in the Swiss Alps. PERMOS is presently active in four regions: Upper Engadine, Bernese Oberland, Matter Valley, and “Quatre Vallées.”

Keywords: active layer; monitoring; mountain permafrost; permafrost temperature; rock glacier creep velocity.

Introduction

PERmafrost MONitoring Switzerland (PERMOS) has taken root and passed from first steps in the 1990s (Haeberli et al. 1993) through its pilot phase (2000–2006) (Vonder Mühl et al. 2001, 2004) and has now reached its implementation phase (2007–2010).

Low-latitude high-altitude mountain permafrost is governed mainly by climate conditions, in particular mean annual air temperature but also snow precipitation. Climate change therefore has an impact on mountain permafrost that is also an important indicator for environmental changes. According to IPCC assessments (IPCC 2007), circumpolar but also mountain regions will be affected much more strongly than the global average. Therefore, the Global Terrestrial Network for Permafrost (GTN-P) that is currently being established within the worldwide climate-monitoring program (GCOS/GTOS) of the World Meteorological Organization (WMO) and others (FAO, UNEP, UNESCO, ICSI) increases in importance. PERMOS is one early component of GTN-P. Moreover, it complements the glacier monitoring network in Switzerland, which was already established towards the end of the 19th century.

In contrast to glaciers and snow, systematic scientific investigation of Alpine permafrost only was started in the early 1970s by the Barsch group of the University of Basel. Since the late 1980s and after the drilling through the Murtèl-Corvatsch rock glacier in 1987 (Haeberli et al. 1988; Vonder Mühl & Haeberli 1990), a number of Swiss institutes started performing research on low-latitude mountain permafrost.

An important and valuable contribution was the EU-funded project PACE (Permafrost and Climate in Europe; Harris et al. 2003). These various activities formed the basis for establishing PERMOS, which officially started in 2000 under the umbrella of the Swiss Academy of Sciences (SAS) with support of the Federal Office for Environment (FOE) for a pilot-phase which ended in 2006.

As for the four years from 2007 to 2010, the Federal Office for Environment, the Swiss Academy of Sciences, and the Federal Office for Meteorology signed a contract to implement PERMOS within the responsible federal monitoring structures in Switzerland. This means that after an evaluation, the PERMOS-approved sites will be updated to a technological and methodological standard, and a 50% position is financed for coordination and reporting.

Goals and Strategy

The main goal of PERMOS is to document the state of permafrost in the Swiss Alps on a long-term basis, and hence, temporal permafrost variations. In fact, this is perfectly complementary to the glacier monitoring network. The Cryosphere Commission of the Swiss Academy of Sciences is presently setting up an integral cryosphere monitoring concept which includes all relevant parts of the Alpine cryosphere: snow, glaciers, and permafrost.

As simple as this task is to formulate, as difficult it is to implement. In contrast to glaciers and snow, permafrost is invisible. Moreover, permafrost characteristics change within short distances in low-latitude mountain regions such

Table 1. “Priorities for GGD” according to the IPA- resolution of August 1995 (Hegginbottom 1995, p 13).

PARAMETER*	APPLICATIONS				
	Process understanding	Engineering design	GCM validation	Change detection	Impact evaluation
Geometry					
Permafrost extent	M	H	H	H	M
Permafrost thickness (shallow†)	H	H	H	H	H
Permafrost thickness (deep†)	M	M	L	H	L
Active layer thickness	H	H	M	H	H
Ground ice extent	H	H	M	M	H
Lateral /vertical displacement	H	H	L	H	H
Thermal State					
Temperature (shallow†)	H	H	H	H	H
Temperature (deep †)	M	M	M	H	L
Properties (Soil/Rock)					
Moisture content (water/ice)	H	H	M	H	H
Bulk density	H	H	H	L	L
Texture	H	H	L	M	M
Chemistry (water/ice)	M	M	L	M	M
Trace gases	H	L	H	M	M

* Site descriptions include location, geology, geotechnical properties, vegetation, etc.
 † Metadata includes techniques, equipment, precision, post-processing, data ownership, etc.
 † For permafrost thickness and temperature, the demarcation between “shallow” and “deep” is taken as the local depth of zero annual amplitude.
 H, M, L = High, moderate, or low priority.

as the Alps. The observed parameters were chosen according to the “Priorities for Global Geocryological Database (GGD),” released by the IPA resolution in August 1995 (Hegginbottom 1995, Table 1). The strategy has been set up in a pragmatic way; PERMOS is based on infrastructure (equipped drillings, ground surface temperature sites, and observation of permafrost creep at various rock glaciers) that was established within research projects. New and explicit PERMOS sites will be placed only after available and existing stations are updated to a common standard. New stations will be located in regions where gaps occur. Ideally, each climate region of the Alps is covered by four PERMOS stations.

Pilot Phase (1990s–2006)

The pilot phase aimed to (1) ensure continuation of established time series, (2) check, improve, and adapt observations, and (3) propose a monitoring concept that allows maintenance over decades.

Initial PERMOS observations

In 1999, three items were defined to be observed during the pilot phase:

- (1) borehole measurements (temperature, deformation)
- (2) lower boundary of permafrost distribution (BTS)
- (3) aerial photographs to document surface characteristics

After three years, first corrections were made based on gained experiences of the monitoring and ongoing research projects: (a) drill sites will be complemented by permanent electrodes to regularly record Electrical Resistivity Tomographies (ERT) following the principles according to Hauck and Vonder Mühl (2003); (b) it turned out that the annual lower boundary of permafrost distribution could not be determined by combining the bottom temperature of the snow cover (BTS) and ground surface temperature (GST). Consequently, permafrost pattern is determined in

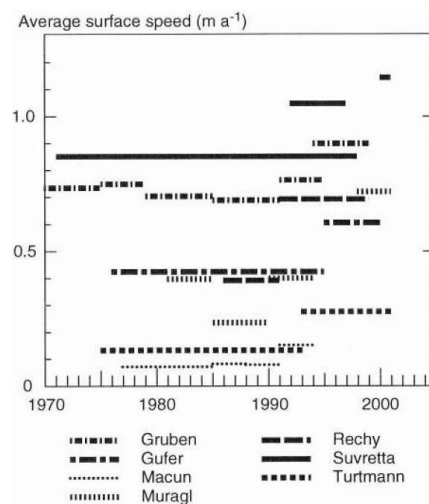


Figure 1. Creep velocities of seven rock glaciers determined by photogrammetry (Kääb et al. 2006). Note the marked variations, e.g., of Muragl rock glacier.

few areas every 10 years only. In addition, GST sites were complemented with a number of single-channel-temperature-loggers mounted in steep walls (Gruber et al. 2003); (c) Creep processes and behaviour of alpine rock glaciers are only poorly understood so far. However, recent studies (Kääb et al. 2006, Roer 2003) indicate that creep velocities vary considerably (see Fig. 1). Arenson et al. (2002) report even annual variations. Therefore, creep velocity of selected rock glaciers shall be determined by photogrammetry and geodetic surveys.

Types of PERMOS Sites

Following the adaptations and in discussing the monitoring results, it was decided to focus on two types of PERMOS sites: drill sites and kinematic sites.

Drill sites

Each drill site of PERMOS shall be composed of:

- One or several borehole(s) that is (are) at least some 15 m deep, equipped with a thermistor string attached to a data logger. Sensors are recommended to be at the following depths [m]: 0.0, 0.4, 0.8, 1.2, 1.6, 2.0, 2.5, 3.0, 4.0, 5.0, 7.0, 9.0, 11, 13, 15, 20, 25, 30, 40, 50, 60, 70, 80, 85, 90, 92, 94, 96, 98, 100 with temporal interval of 6 hours down to 5 m depth, farther down, once every day.
- Snow thickness and air temperature shall be measured as a minimum for climate parameters.
- Geophysical monitoring consists of at least 20 fixed installed electrodes to regularly record ERTs.
- Single-channel-temperature loggers recording ground surface temperatures in at least 15 spots with (flat and oblique) and without (steep rock walls) a snow cover in winter in the region (distributed at various altitude, exposure, locality within a few kilometers).

Kinematic sites

Rock glacier creep is observed either by photogrammetry using aerial photos, by geodetic survey, or differential GPS. Each rock glacier is equipped individually according to the applied methodology and movement pattern.

PERMOS 2007–2010

The updated concept was discussed, elaborated, and approved by the PERMOS community. A comprehensive evaluation of each potential PERMOS element was conducted in 2007.

Evaluation and applied criteria

During the pilot phase, each potential monitoring element was included and, to a limited amount, financially supported. While at the beginning of the pilot phase only few sites were available, the number increased. Consequently, each potential element was evaluated according to various criteria. Approved elements shall be recorded for the next several decades. The base line was to continue rather few elements on a standardized high quality and technology level and to omit redundancies.

The following set of criteria was elaborated within the expert Cryosphere Commission SAS:

- (a) Relevance towards the overall aim to document the permafrost state in the Swiss Alps;
- (b) Importance towards society and politics; i.e., contribution to understanding issues related to environment, climate change, and natural hazards;
- (c) Importance for research and academic education;
- (d) Feasibility in terms of accessibility.

In addition, time series were assessed according to length and temporal resolution, quality (accuracy, gaps), site characteristics, representativeness, accessibility, contribution to the GHOST tier structure (Cilhar et al. 1997), additional parameters available, and particular remarks.

The evaluated elements were allocated to one of the following categories:

(A) PERMOS approved: the element will be recorded for the next several decades, and a large part will be funded by PERMOS. The site will be updated to the technological and methodological standard.

(B) Retention: the element is part of PERMOS. Particular requirements and open questions are addressed. The element will be re-evaluated in 2009.

(C) Rejected: the element is rejected and no longer financially supported by PERMOS. It is up to the institution to continue the time series.

Network in 2007

In the evaluation, all drill sites that are not fully equipped according to the above-mentioned composition were B-rated, and similarly most “GST sites.” Within the updated concept, these two elements will be merged into one “drill site” until 2010. Presently, PERMOS consists of 9 A-rated drill sites, 9 A-rated GST sites, which will be updated and transferred

into “standard PERMOS drill sites.” All B-rated elements (6 drill sites, 3 GST sites, and 5 kinematic sites) are subject to additional installation or further strategical aspects and a re-evaluation in 2009 (see Table 2). Figure 2 shows the geographical distribution of the elements in 2007.

PERMOS Partners

A comprehensive monitoring network must be set up among interested partners from academia and administration. Academia provides the permafrost know-how and the link to ongoing research projects, while administration is responsible for monitoring and provides political links.

The pilot phase allowed for setting up a concept with parameters and elements that could be adapted according to gained experiences and new research results. After some 15 years, PERMOS complements the Swiss glacier monitoring network and Swiss snow observation, data of which all are being compiled to contribute to cryological monitoring.

In general, funding institutions are skeptical to invest in monitoring programs, since they cannot fund “infinite” long-term projects. Also, universities cannot carry such programs, since their core activities are research and education. However, both research funding institutions and universities were key to setting up PERMOS. Research projects funded by the Swiss National Science Foundation (SNSF) and the European Commission, and from ETH Zurich and SFISAR Davos also, have established important milestones without which PERMOS would not exist. Still, the maintenance of the elements is being carried by the university institutes and has been supported since 2000 by the financing partners.

In fact, the success of PERMOS is based on a go-together of the academic institutions involved in permafrost research in Switzerland and the financial support of the SAS: University of Zurich (coordination), ETH Zurich, SFISAR Davos, the Universities of Berne, Fribourg, Lausanne, and the Academia Engadina Samedan.

This, in turn, triggered the commitment of the authorities, which are officially in charge of climate and environmental monitoring: the Federal Office for Environment (FOE) and the Federal Office for Climatology (MeteoSwiss).

Monitoring Results

Most important results from monitoring consist of comparing elements from one time interval to another. However, many details of involved processes that are modeled are based on data provided by monitoring sites. In particular, numerical and statistical models are calibrated using one part of monitoring data. It is therefore neither possible nor intelligent to distinguish or separate permafrost monitoring and research.

PERMOS drill sites are located in different terrain and lithologies. Murtèl-Corvatsch is a rock glacier site with a coarse, blocky surface layer and permafrost below the active layer consisting of almost pure ice. The Schilthorn drill site is on schist bedrock with a shallow weathered clay-rich debris layer of some decimeters in thickness. The same climate

Table 2. PERMOS elements 2007.

<i>(1) Drill sites and GST sites</i>		
Name	borehole	GST
Flüela	A	A
Lapires	A	A
Murtèl-Corvatsch	A	A
Schafberg / Mt Barba Peider	A	A
Schilthorn	A	A
Gentianes	A/B	C
Matterhorn	A/B	C
Stockhorn	A/B	A
Tsaté	A/B	C
Arolla / Mt. Dolin	B	B
Dreveuneuse	B	C
Gemsstock	B	C
Les Attelas	B	C
Muragl	B	C
Jungfrau	B/C	A
Alpage de Mille / Aget	C	A
Gemmi	C	A
Réchy	C	B
Yettes Condjà	C	B

(2) Kinematic sites

Name	air photo	terrestr
Gemmi-Furggentälti	A	yes
Gruben	A	no
Muragl	A	yes
Murtèl	A	no
Réchy	A	yes
Gianda Grischa	B	no
Gross Gufer	B	no
Turtmann Grueo1	B	yes
Yettes Condjà	B	yes
Suvretta	B/C	no

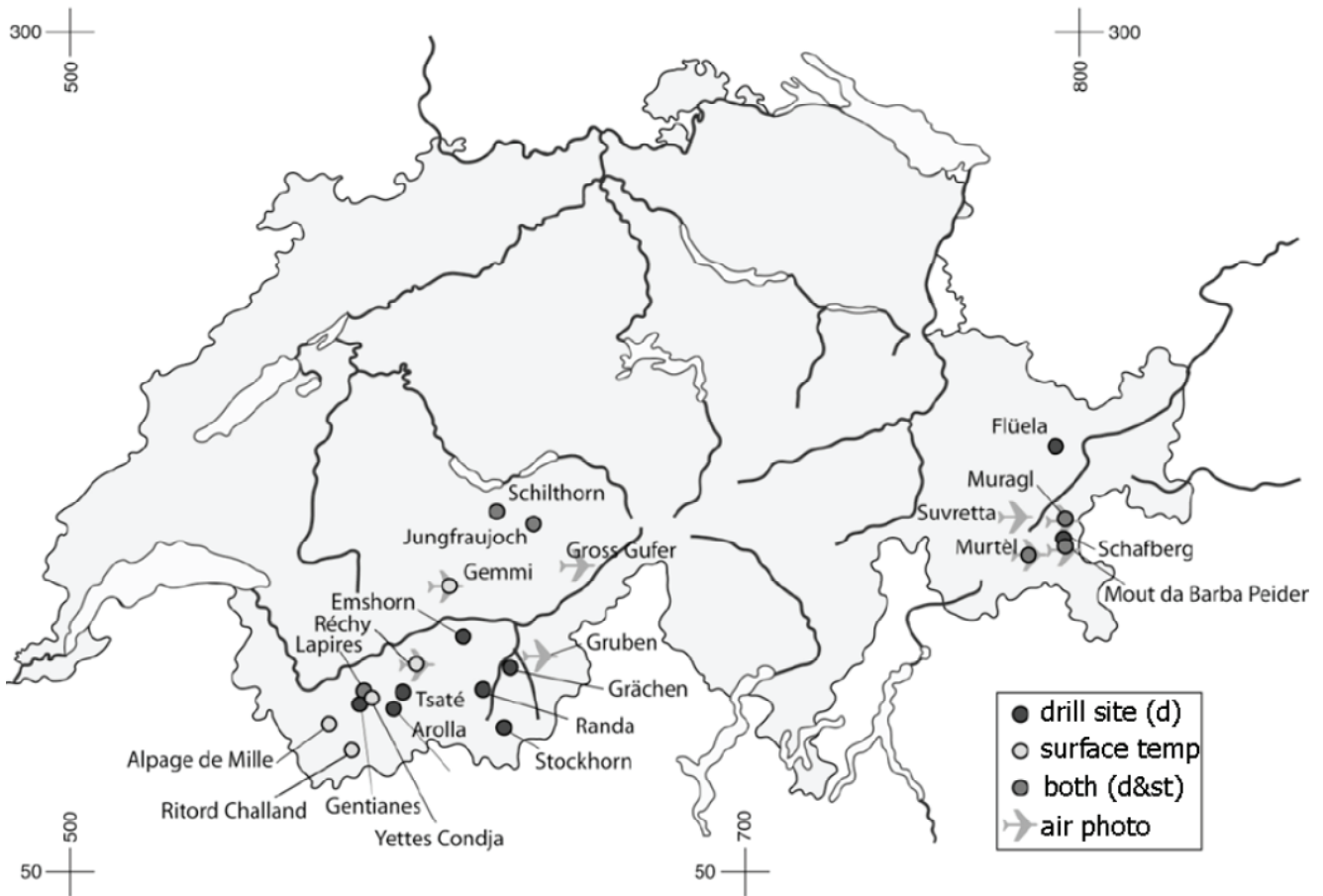


Figure 2. PERMOS sites in 2007 where different parameters are measured.

signal causes different reactions of the thermal regime at such different locations.

Process understanding

In winter 2006/2007, snow cover was only thin, and mean monthly temperatures were 1°C to 3°C warmer than normal. Permafrost temperatures were influenced differently: in steep walls where snow cannot accumulate, air temperatures caused a warming. At permafrost sites with usually a significant snow cover, lacking snow led to a cooling of subsurface temperatures.

Active layer

The thickness of the active layer is mainly influenced by summer weather conditions. Recorded in summer 2003 was an active layer almost twice as thick as in the years before and afterwards (Fig 2). Within PERMOS, maximal active layer thicknesses and the corresponding date are recorded. Several PERMOS sites are integrated into the CALM network (Brown et al. 2000).

Permafrost temperatures

Permafrost temperatures at about 10 m depth are

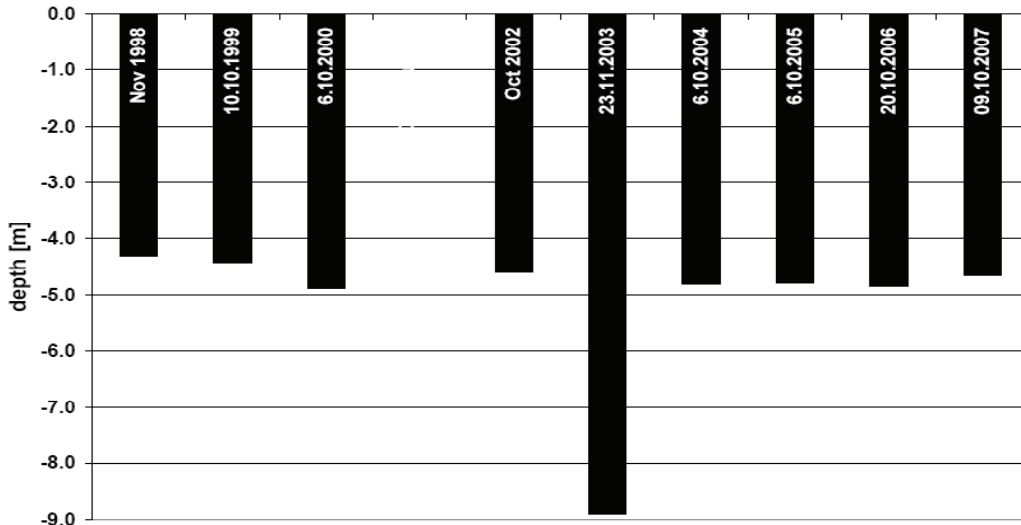


Figure 3. Depth and date of the active layer thickness at borehole Schilthorn 51/1998. In the extremely warm summer 2003 permafrost thawed down to almost 9 m.

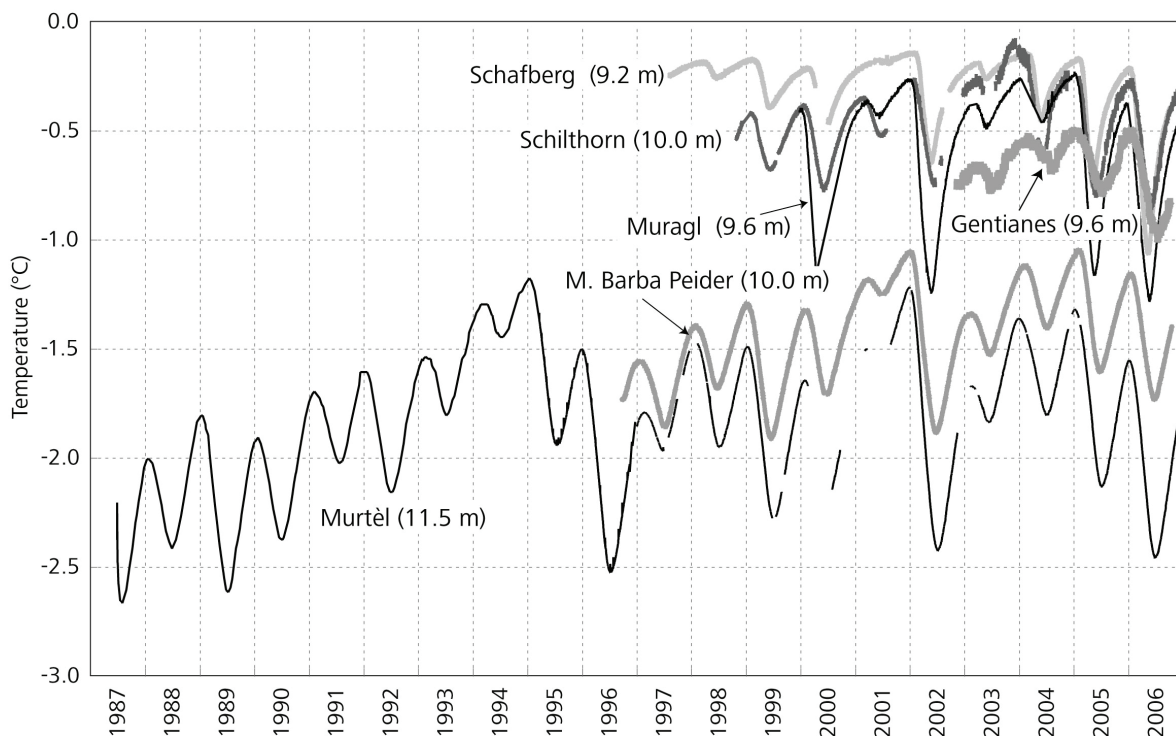


Figure 4. Permafrost temperature of a number of PERMOS elements at about 10 m depth.

characterized by a nice sinusoidal shape and a phase lag of about half a year. High frequency “noisy” parts of the temperature signal are largely filtered out, and differences of the various localities are damped as well. Therefore, these graphs are used for comparison of the various drill sites and also to determine region-specified trends.

Figure 4 shows a compilation of temperatures at about 10m depth from a number of drill sites, all located on flat or oblique terrain with a snow cover in winter. At these sites, snow characteristics govern mainly thermal regime.

Conclusions

A comprehensive monitoring network must be set up among interested partners from academia and administration. Academia provides the permafrost know-how and the link to ongoing research projects, while administration is responsible for monitoring and provides political links.

The pilot phase allowed for setting up a concept with parameters and elements that could be adapted according to gained experiences and new research results. After some 15 years, PERMOS has found its place by complementing the Swiss glacier monitoring network and Swiss snow observation, data of which all are being compiled to contribute to cryological monitoring.

Acknowledgments

Obviously, PERMOS as a monitoring program involves many contributors and depends on key persons that support the efforts, and on financial support. The Swiss Academy for Sciences (SAS), the Federal Office for Environment (FOE), and the Federal Office for Climatology (MeteoSwiss) finance PERMOS based on a signed contract. Equally important are the contributions of the academic institutions, providing synergies from research and education projects.

References

- Arenson, L.U., Hoelzle, M. & Springman, S.M. 2002. Borehole deformation measurements and internal structure of some rock glaciers in Switzerland. *Permafrost and Periglacial Processes* 13: 117-135.
- Brown, J., Nelson, F.E. & Hinkel, K.M. 2000. The circumpolar active layer monitoring (CALM) program research designs and initial results. *Polar Geography* 3: 165-258.
- Cihlar, J., Barry, T.G., Ortega Gil, E., Haeberli, W., Kuma, K., Landwehr, J.M., Norse, D., Running, S., Scholes, R., Solomon, A.M. & Zhao, S. 1997. *GCOS/GTOS plan for terrestrial climate-related observation. GCOS 32, version 2.0.* WMO/TD-796, UNEP/DEIA/TR, 97-7.
- Gruber, S., Hoelzle, M. & Haeberli, W. 2004. Rock wall temperatures in the Alps - modeling their topographic distribution and regional differences, *Permafrost and Periglacial Processes* 15(3): 299-307.
- Haeberli, W., Huder, J., Keusen, H.-R., Pika, J. & Röthlisberger, H. 1988. Core drilling through rock glacier-permafrost. *Proceedings of the Fifth International Conference on Permafrost, Trondheim, Norway*, 2: 937-942.
- Haeberli, W., Hoelzle, M., Keller, F., Schmid, W., Vonder Mühll, D. & Wagner, S. 1993. Monitoring the long-term evolution of mountain permafrost in the Swiss Alps. *Proceedings of the Sixth International Conference on Permafrost, Beijing, China*, 1: 214-219.
- Harris, C., Vonder Mühll, D., Isaksen, K., Haeberli, H., Sollid, J.L., King, L., Holmlund, L., Dramis, F., Guglielmin, M. & Palacios, D. 2003. Warming permafrost in European mountains. *Global and Planetary Change* 39: 215-225.
- Hauck, C. & Vonder Mühll, D. 2003. Inversion and interpretation of 2-dimensional geoelectrical measurements for detecting permafrost in mountainous regions. *Permafrost and Periglacial Processes* 14(4): 305-318.
- Heginbottom, J.A. 1995. Report of the IPA Data Workshop. *Frozen Ground* 18: 12-13.
- IPCC. 2007: Climate change 2007: impacts, adaptation and vulnerability. *Contribution of Working Group II to the Fourth Assessment Report of the Intergovernmental Panel on Climate Change.* M.L. Parry, O.F. Canziani, J.P. Palutikof, P.J. van der Linden & C.E. Hanson (eds.), Cambridge, UK: Cambridge University Press, 976 pp.
- Käab, A., Frauenfelder, R. & Roer, I. 2006. On the response of rockglacier creep to surface temperature variations. *Global and Planetary Change*.
- Roer, I. 2003. Rock glacier kinematics in the Turtmanntal, Valais, Switzerland - observational concept, first results and research perspectives. *Proceedings of the Eighth International Conference on Permafrost, Zürich, Switzerland*, 2: 971-975.
- Vonder Mühll, D. & Haeberli, W. 1990. Thermal characteristics of the permafrost within an active rock glacier (Murtèl/Corvatsch, Grisons, Swiss Alps). *Journal of Glaciology* 36(123): 151-158.
- Vonder Mühll, D., Delaloye, R., Haeberli, W., Hoelzle, M. & Krummenacher, B. 2001. Permafrost Monitoring Switzerland PERMOS - 1. *Jahresbericht 1999/2000, Glaciological Report (Permafrost) of the Glaciological Commission (GC) of the Swiss Academy of Sciences (SAS)* 1: 32 pp.
- Vonder Mühll, D., Nötzli, J., Makowski, K. & Delaloye, R. 2004. Permafrost in Switzerland 2000/2001 and 2001/2002. *Glaciological Report (Permafrost) of the Glaciological Commission (GC) of the Swiss Academy of Sciences (SAS)* 2/3: 80 pp.

Methane Cycle in Terrestrial and Submarine Permafrost Deposits of the Laptev Sea Region

Dirk Wagner, Katharina Koch

Alfred Wegener Institute for Polar and Marine Research, Research Unit Potsdam, Potsdam, Germany

Andreas Gättinger

Helmholtz Zentrum München-German Research Center for Environmental Health, Neuherberg, Germany

André Lipski

Universität Osnabrück, Abteilung Mikrobiologie, Osnabrück, Germany

Abstract

Permafrost environments within the Siberian Arctic are natural sources of the climate-relevant trace gas methane. In order to improve our understanding of present and future carbon dynamics in high latitudes, we studied the activity and biomass of the methanogenic communities in terrestrial and submarine permafrost deposits. For these investigations, permafrost cores of Holocene and Late Pleistocene age were drilled in the Laptev Sea region. A high CH₄ concentration was found in the upper 4 m of the Holocene deposits, which correlates well with the methanogenic activity and biomass. Even the incubation of core material at -3°C and -6°C showed a significant CH₄ production (range: 0.04–0.78 nmol CH₄ h⁻¹ g⁻¹). The results indicated that the methane in permafrost deposits originated from modern methanogenesis by cold-adapted methanogenic archaea. Microbial-generated methane in permafrost sediments is, so far, an underestimated factor for future climate development.

Keywords: Laptev Sea; methane; methanogenesis; permafrost deposits; phospholipid biomarker; psychrophiles.

Introduction

The Arctic plays a key role in Earth's climate system, as global warming is predicted to be most pronounced at high latitudes and because one third of the global carbon pool is stored in ecosystems of the northern latitudes. Global warming will have important implications for the functional diversity of microbial communities in these systems. It is likely that temperature increases at high latitudes will stimulate microbial activity and carbon decomposition in Arctic environments, and accelerate climate change by increasing trace gas release (Melillo et al. 2002, Zimov et al. 2006). Currently, the functioning of microbial communities and their impact on changing environmental conditions are not adequately understood, and the potential methane release from frozen sediments is not adequately quantified.

Methane is chemically very reactive and more efficient in absorbing infrared radiation than carbon dioxide. Estimates of methane emissions from arctic and sub-arctic wetlands range between 10 and 39 Tg a⁻¹, or between 2.2 and 8.6% of global methane emissions (Bartlett & Harriss 1993, Cao et al. 1998). Methane, as a powerful greenhouse gas, contributes to about 20% of global warming (IPCC 2001).

In general, temperature is one of the most important variables regulating the activity of microorganisms. The growth potential, as well as the molecular, physiological and ecological aspects of microbial life at low temperatures, has been investigated in many studies (e.g., Gounot 1999, Wagner 2008). Certain key processes of the methane cycle are carried out exclusively by highly specialised microorganisms such as methanogenic archaea and methane oxidising bacteria. The microbial methane production (methanogenesis) in

the active layer of permafrost is the terminal step during the anaerobic decomposition of organic matter, while the methane oxidation is the primary sink for methane in Arctic wetlands (Wagner et al. 2005).

However, there are only a few studies investigating the geochemistry and microbiology of permafrost deposits, which were mainly done in Siberia and Canada. Direct bacterial counts in the order of 10⁷ to 10⁸ were reported for permafrost deposits from Northeast Siberia (Rivkina et al. 1998). Shi and colleagues (1997) found viable bacteria in permafrost sediments up to 3 million years in age in the Kolyma-Indigirka lowlands. Most of the isolated bacteria showed mesophilic growth characteristics. In contrast, the minimum temperature for growth of permafrost bacteria was recently calculated to be -20°C (Rivkina et al. 2000). Furthermore, molecular life markers and low numbers of methanogens were found in the Mallik gas hydrate production research well (Colwell et al. 2005, Mangelsdorf et al. 2005). However, methanogenic activity could not be detected in the permafrost sediments using radiolabelled ¹⁴C-substrates.

For the understanding and assessment of recent and future carbon dynamics in high latitudes, we have to answer the question: "What will happen to the carbon stored in permafrost, in the event of a climate change?" From this view point, we studied the methane concentration, the quantity and quality of organic matter, and the activity, biomass and diversity of methanogenic communities in permafrost deposits of the Laptev Sea region.

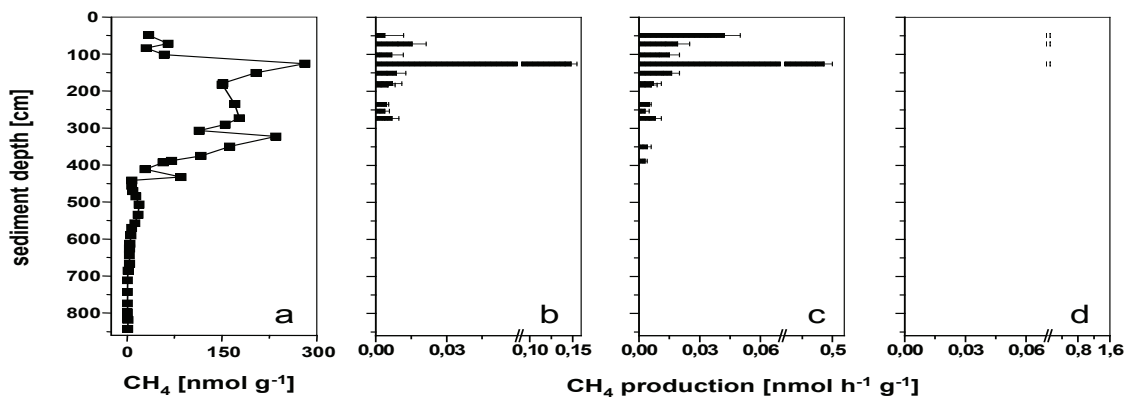


Figure 1. Vertical profiles of methane concentration (a), and methane production rates determined at 5°C without any additional substrate (b), with acetate (c) with hydrogen (d) as methanogenic substrates.

Study Sites

Within the scope of long-term studies on carbon dynamics in the Siberian Arctic, several expeditions were carried out by the Alfred Wegener Institute for Polar and Marine Research.

The Holocene permafrost core was drilled during the LENA 2001 expedition on the main study site Samoylov Island (72°22'N, 126°28'E, Pfeiffer & Grigoriev 2002). Samoylov, with the Russian-German Research Station, is located in the active part of the Lena Delta (Hubberten et al. 2006). The Lena Delta lies at the Laptev Sea coast between the Taimyr Peninsula and the New Siberian Islands. Continuous permafrost, which occurs throughout the investigation area, extends to depths of about 100–300 m (Yershov 1998), with active layer thicknesses between 30 and 60 cm depth.

The submarine permafrost cores of Late Pleistocene age were recovered in the framework of the COAST expedition from the western Laptev Sea along a transect running perpendicular to the coastline (Rachold et al. 2007). The Laptev Sea region is characterised by an arctic continental climate with low mean annual air temperature of about -15°C and low summer precipitation of <198 mm. Further details of the study sites were described previously in Wagner et al. (2003) and Rachold et al. (2007).

Drilling of Permafrost Deposits

The drilling of an 850 cm long core was carried out with a portable gasoline powered permafrost corer without using drilling fluid to avoid microbiological contamination of the permafrost samples. A mixing of the permafrost sediments was not observed due to the frozen state of the core material. The individual core segments, which were up to 50 cm in length, were placed immediately after removal from the corer into plastic bags and stored at about -8°C in the permafrost cellar of the Research Station Samoylov. After drilling of the core, the borehole temperature was monitored with a string of 9 thermistors. The cores were transported in a frozen state to Potsdam, Germany. During transport, the temperatures in the containers were monitored by micro data loggers. The storage temperature in the Potsdam laboratory was -22°C.

Core segments were split along their long axis into two halves under aseptic conditions with a diamond saw in an ice laboratory at -22°C. Afterwards, one half of the core was cleaned with a sterile knife for lithological and geocryologically descriptions. Subsequently, one half was cut into segments of about 10–30 cm length according to the lithology and the geocryology. Small pieces (approx. 10 g) of each sub-sample were taken for analysing the methane concentration in the frozen sediments. The remaining material of each sub-sample was thawed at 4°C and homogenized under anoxic and sterile conditions for analysis of the sediment properties and the microbial activities and biomarkers. Sub-samples for the different analyses were placed into sterile plastic Nalgene boxes. Separated samples were used directly for the experiments (methane concentration, methane production rates, and biomarker analysis) or were freeze-dried for the organic carbon analyses. The second half of the core is kept as an archive in the ice core storage at the Alfred Wegener Institute.

Methanogenesis in Terrestrial Permafrost

Our results show significant amounts of methane in the first four meters of frozen sediments (up to 282 nmol CH₄ g⁻¹ sediment, Late Holocene, 5000 yr BP until today) and only trace amounts of methane in the bottom section of the core (0.4–19 nmol CH₄ g⁻¹ sediment; Middle Holocene, 9000–5000 yr BP; and Early Holocene, 11500–9000 yr BP; Fig. 1a). Different amounts of methane in different aged permafrost deposits from northeastern Eurasia were reported by Rivkina & Gilichinsky (1996). They detected methane in modern (Holocene) and old permafrost deposits (Middle and Early Pleistocene, 1.8–0.78 mill. yr BP), but not in Late Pleistocene ice complexes (ice rich permafrost, 130000–11500 yr BP). They concluded from their findings that methane cannot diffuse through permafrost sections. If methane is unable to diffuse through permafrost from deeper deposits, it must either be entrapped during the deposition of the sediments or originate from recent methane production by methanogenic archaea (methanogenesis) in the frozen ground.

The analyses of methane production in selected sediment samples at 5°C, revealed activity only in permafrost layers with significant concentrations of methane (upper 4 m of the sediments; Fig. 1b). An important finding from the activity analyses is that no methane production was detectable in the bottom part of the permafrost section (>4 m) characterized only by traces of methane. This was also the case after addition of acetate or H₂/CO₂ as energy and carbon source (Fig. 1c, d). This indicates that the absence of methanogenesis does not depend on deficiency of methanogenic substrates in the Middle and Early Holocene deposits. Methane was only found in permafrost sediments with verifiable methane production activity.

The investigation of phospholipids as molecular biomarkers for *Bacteria* (PLFA) and *Archaea* (PLEL) shows a vertical profile with the same trend as the methane concentration. Specifically, significant amounts of phospholipids were determined in the upper Late Holocene deposits (<4 m sediment depth), which correlates ($r = 0.632$, $P = 0.05$) with the highest amount of methane (Fig. 2). In contrast, the biomarker concentrations in the Middle and Early Holocene permafrost sediments (>4 m sediment depth) drastically decreased to values below 10 nmol g⁻¹ sediment, which corresponds with the detected traces of methane. Phospholipids are compounds of cell membranes that rapidly degraded after cell death (Harvey et al. 1986, White et al. 1979). They are regarded as appropriate biomarkers for viable microorganisms (e.g., Ringelberg et al. 1997, Zelles 1999). Therefore, the positive correlation of methane concentration with viable bacteria and archaea gives us the first strong evidence of recent methanogenesis under in situ conditions in permafrost deposits.

Although only a few psychrophilic strains of methanogenic archaea have been isolated, there are some indications of methanogenic activity in cold permafrost environments (Kotsyurbenko et al. 1993, Ganzert et al. 2006). However, the incubation of permafrost samples from 45–63 cm depth at sub-zero temperatures with acetate and hydrogen as methanogenic substrates, indicated a relatively high methane production rate under permafrost temperature conditions. At a temperature of -3°C, a significant increase in methane production was found, which rose linearly to headspace concentrations of about 1000 ppm (with acetate) and 2500 ppm (with hydrogen) during 300 h after the initiation of the experiment. At a temperature of -6°C, methanogenesis was lower; however, after a lag phase of about 300 h, a significant increase to 200 ppm (with acetate), and 500 ppm (with hydrogen) within 200 h, was observed. The calculated activity of methanogenic archaea with hydrogen reached values of 0.78 ± 0.31 nmol CH₄ h⁻¹ g⁻¹ and 0.14 nmol CH₄ h⁻¹ g⁻¹ at incubation temperatures of -3°C and -6°C, respectively. This was 2.5 and 3.5 times higher compared to the activity with acetate (0.31 ± 0.04 nmol CH₄ h⁻¹ g⁻¹ and 0.04 ± 0.01 nmol CH₄ h⁻¹ g⁻¹) at the corresponding temperatures.

The quality of organic carbon is a limiting factor in the microbial metabolism process. Our results reveal a high organic carbon content (on average 2.4%) for the Holocene

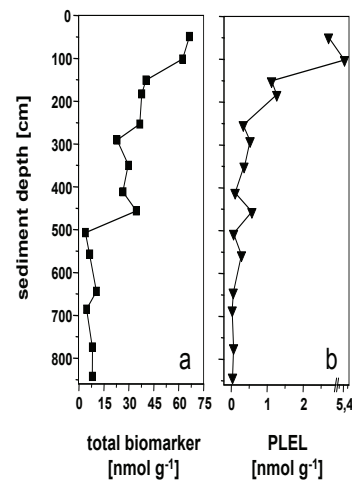


Figure 2. Vertical profiles of total lipid biomarkers (a) and phospholipid ether lipids (PLEL, b) within the Holocene permafrost core.

permafrost deposits (Table 1). However, the quantity of organic matter in permafrost ecosystems provides no information on the quality, which determines the availability of organic compounds as energy and carbon sources for microorganisms (Hogg 1993, Bergman et al. 2000). For this purpose, the humification index (HIX), which is a qualitative parameter, can give suitable information with regard to microbial metabolism. Wagner and colleagues (2005) demonstrated that the availability of organic carbon in permafrost soils decreased with increasing HIX. This is in agreement with the present study. It was shown for the permafrost sequence that the HIX increased continuously with depth. This indicates that the organic carbon is less available for microorganisms with depth because of the higher degree of humification. Consequently, at this point, we can summarize that the zone with significant concentrations of methane and activity of methanogenic microorganisms is characterized by the highest concentration of high quality organic carbon.

In contrast to the results of the soil-ecological variables (methane production activity, PLEL biomarker concentration, TOC, HIX), we do not achieve any hint for a possible entrapment process of methane during sedimentation, which was deduced from data of paleoclimate research carried out in the same study area (Andreev et al. 2004, Andreev & Klimanov 2005).

More than 20 percent of the terrestrial Arctic is characterized by ice rich permafrost (Zhang et al. 1999). Large areas, mainly dominated by continuous permafrost, exist in Siberia with thicknesses up to 900 m (Yershov 1998). The present study revealed that considerable parts of these cold habitats are recent sites of methane production, probably catalyzed by specific cold-adapted methanogenic archaea. This increasing reservoir of climate-relevant trace gases becomes of major importance against the background of global warming which could result from a thawing of

permafrost area up to 25% until 2100 (Anisimov et al. 1999) and subsequent disposal of the methane reservoirs into the atmosphere. Additionally, the results show that an increase of the permafrost temperature would lead to substantial rise in microbiologically-produced methane in the frozen ground. This would further strengthen the contribution of permafrost to the atmospheric methane budget.

Table 1. Borehole temperature, total organic carbon (TOC), and humification index (HIX, dimensionless) of the Holocene permafrost deposits from Samoylov Island.

Depth [cm]	T [°C]	TOC [%]	HIX
49	-1.9	4.82	3.71
72		2.50	5.74
84		3.64	5.33
102	-4	4.47	6.39
126		4.91	5.47
151		4.01	3.80
179		2.63	5.62
183	-7.4	3.42	6.64
235		n.d.	6.88
254		2.54	5.69
273		1.65	8.13
291		3.11	6.95
307	-9.4	0.87	0.68
323		1.88	6.08
350		2.11	6.83
375		2.49	8.01
389		n.d.	8.07
393	-12.5	n.d.	7.65
412		1.19	6.42
433		1.57	7.06
442		2.46	8.34
456		2.90	n.d.
471		3.00	7.65
485		2.54	8.10
507	-12.8	1.85	n.d.
534		2.27	8.25
557		2.49	8.70
570		2.65	7.80
590	-12.7	2.52	6.65
613		2.39	9.20
626		1.92	8.42
644		1.51	9.10
667		1.85	9.08
686		0.96	9.58
712		0.61	9.23
743		1.25	11.29
774		1.04	8.38
798	-11.5	1.69	9.11
819		1.97	9.46
843		2.56	8.42

n.d. = not detected

Methanogenesis in Submarine Permafrost

Coastal erosion and sea level rise created the shallow shelf of the Laptev Sea whose bottom is formed by the formerly terrestrial permafrost (Rachold et al. 2007). Flooding of the cold (-5 to -15°C) terrestrial permafrost with relatively warm (-0.5 to -2°C) saline sea water changed the system profoundly and resulted in a warming of the permafrost. Therefore, we consider submarine permafrost as a natural laboratory for studying the impact of environmental changes on permafrost habitats.

First results obtained from submarine permafrost deposits of the Laptev Sea shelf revealed methane concentrations of up to 284 nmol CH₄ g⁻¹ sediment (Fig. 3a). Highest methane values were found in the layers with the highest amount of organic carbon (up to 9%). Extremely low δ¹³CH₄ values of -75 ‰ indicated active methanogenesis in this zone (Knoblauch, pers. com.). According to the studies of Rivkina & Gilichinsky (1996), who did not find any significant amounts of methane in Late Pleistocene permafrost sediments, it can be concluded that our findings in submarine permafrost are also a result of recent methanogenesis. This interpretation is supported by first data of DNA-based analyses of methanogenic communities in the sediments, which revealed a higher diversity and abundance of methanogens within the core segment with the highest amount of methane (Fig. 3b).

Conclusions

This work shows, for the first time, that methanogenic archaea do not only survive in permafrost habitats, but also can be metabolically active under in situ conditions. Due to the sub-0°C experiments and the in situ temperatures of permafrost sediments, we can conclude that the methanogenic community is dominated by psychrotolerant or even psychrophilic microorganisms. Despite this adaptation to cold environments, we show that a slight increase of the temperature can lead to a substantial increase of methanogenic activity. In the event of degradation of terrestrial or submarine permafrost sediments, this would lead to an extensive expansion of the methane deposits with subsequent impacts on total methane emissions. A future in-depth characterization of the metabolism of these cold-adapted methanogens will reveal biotic and abiotic factors which influence the methane production activity of these organisms.

Methane of microbial origin in perennially frozen deposits probably represents an unconsidered source for the global methane budget. Methane release to the atmosphere from frozen ground is mediated by ongoing permafrost degradation through enhanced thermokarst formation and accelerated coastal erosion in the Arctic. Although the change in permafrost conditions by global warming is examined in the framework of several international projects (e.g., ACD: Arctic Coastal Dynamics, CALM: Circumpolar Active Layer Monitoring), these investigations should be linked more closely with microbiological process studies and biodiversity research. Microbial parameters important

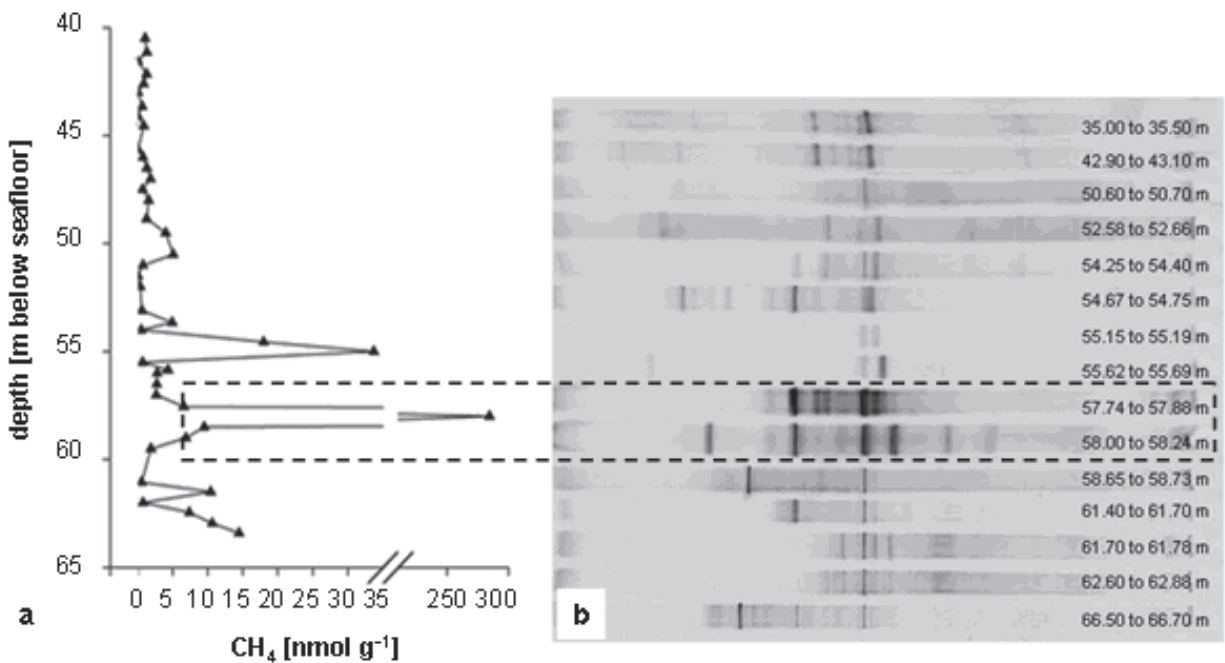


Figure 3. Vertical profiles of methane concentration (a), and DGGE fingerprinting of 16S rRNA genes (b) amplified from the submarine permafrost sediments (between 35.0 and 66.7 m depth).

for the assessment of the carbon turnover (e.g., cell numbers, activities, biodiversity and stability of microbial communities) should be analysed at observation areas in the Arctic, where long-term ongoing monitoring programs are undertaken. The evaluation of microbiological data and their correlation with climatic and geochemical results represents the basis for the understanding of the role of permafrost in the global system, in particular feedback mechanisms related to material fluxes and greenhouse gas emissions in the scope of a warming Earth.

Acknowledgments

The authors wish to thank the Russian-German field parties during the expeditions LENA 2001 and COAST, especially Dimitri V. Melnitschenko (Hydro Base Tiksi), Dimitry Yu. Bolshiyarov (Arctic and Antarctic Research Institute) and Waldemar Schneider (Alfred Wegener Institute for Polar and Marine Research) for their logistic support as well as Volker Rachold (IASC, formerly AWI) and Eva Pfeiffer (University of Hamburg, formerly AWI) for their leadership of the expeditions COAST and LENA 2001, respectively.

References

- Andreev, A. & Klimanov, A. 2005. Late-Glacial and Holocene in Chapter 5 East Siberia (based on data obtained mainly in Central Yakutia). *Geological Society of America Bulletin* 382: 98-102.
- Andreev, A., Tarasov, P., Schwamborn, G., Ilyashuk, B.P., Ilyashuk, E.A., Bobrov, A.A., Klimanov, V.A., Rachold, V. & Hubberten, H.W. 2004. Holocene paleoenvironmental records from Nikolay Lake, Lena River Delta, Arctic Russia. *Palaeogeography, Palaeoclimatology, Palaeoecology* 209: 197-217.
- Anisimov, O.A., Nelson, F.E. & Pavlov, A.V. 1999. Predictive scenarios of permafrost development under conditions of global climate change in the XXI century. *Earth Cryology* 3: 15-25
- Bartlett, K.B. & Harriss, R.C. 1993. Review and assessment of methane emissions from wetlands. *Chemosphere* 26: 261-320.
- Bergman, I., Klarqvist, M. & Nilsson, M. 2000. Seasonal variation in rates of methane production from peat of various botanical origins: effects of temperature and substrate quality. *FEMS Microbiology Ecology* 33: 181-189.
- Cao, M., Gregson, K. & Marshall, S. 1998. Global methane emission from wetlands and its sensitivity to climate change. *Atmospheric Environment* 32: 3293-3299.
- Colwell, F.S., Nunoura, T., Delwiche, M.E., Boyd, S., Bolton, R., Reed, D.W., Takai, K., Lehman, R.M., Horikoshi, K., Elias, D.A. & Phelps, T.J. 2005. Evidence of minimal methanogenic numbers and activity in sediments collected from the JAPEX/JNOC/GSC et al. Mallik 5L-38 Gas Hydrate Production Research Well. In: S.R. Dallimore & T.S. Collett (eds.), Scientific Results from Mallik 2002 Gas Hydrate Production Research Well Program, Mackenzie Delta, Northwest Territories, Geological Survey of Canada, Microbiology section, Canada Bulletin 585: 1-11.
- Ganzert, L., Jurgens, G., Münster, U. & Wagner, D. 2006. Biodiversity of methanogenic archaea in permafrost environments of the Laptev Sea coast. *FEMS Microbiology Ecology* 59: 476-488.
- Gounot, A.M. 1999. Microbial life in permanently cold soils. In: R. Margesin & F. Schinner (eds.), *Cold-Adapted Organisms*. Berlin: Springer, 3-16.

- Harvey, H.R., Fallon, R.D. & Patton, J.S. 1986. The effect of organic matter and oxygen on the degradation of bacterial membrane lipids in marine sediments. *Geochimica et Cosmochimica Acta* 50: 795-804.
- Hogg, E.H. 1993. Decay potential of hummock and hollow Sphagnum peats at different depths in a Swedish raised bog. *Oikos* 66: 269-278.
- Hubberten, H.W., Wagner, D., Pfeiffer, E.M., Boike, J. & Gukov, A.Yu. (2006) The Russian-German research station Samoylov, Lena Delta – a key site for polar research in the Siberian arctic. *Polarforschung* 73: 111-116.
- IPCC 2001. Climate change 2001: The scientific basis. Contribution of the working group I to the third assessment report of the Intergovernmental Panel on Climate Change. J.T. Houghton, Y. Ding, D.J. Griggs, M. Nogner, P.J. van der Linden, X. Dai, K. Maskell & C.A. Johnson. (eds.), Cambridge, New York: Cambridge University Press, 881.
- Kotsyurbenko, O.R., Nozhevnikova, A.N. & Zavarzin, G.A. 1993. Methanogenic degradation of organic matter by anaerobic bacteria at low temperature. *Chemosphere* 27: 1745-1761.
- Mangelsdorf, K., Haberer, R.M., Zink, K.-G., Dieckmann, V., Wilkes, H. & Horsfield, B. 2005. Molecular indicators for the occurrence of deep microbial communities at the JAPEX/JNOC/GSC et al. Mallik 5L-38 Gas Hydrate Production Research Well. In: S.R. Dallimore & T.S. Collett (eds.) *Scientific Results from Mallik 2002 Gas Hydrate Production Research Well Program, Mackenzie Delta, Northwest Territories*. Geological Survey of Canada, Microbiology section. Canada Bulletin 585: 18-29.
- Melillo, J.M., Steudler, P.A., Aber, J.D., Newkirk, K., Lux, H., Bowles, F.P., Catricala, C., Magill, A., Ahrens, T. & Morriseau, S. 2002. Soil warming and carbon-cycle feedbacks to the climate system. *Science* 298: 2173-2176.
- Pfeiffer, E.M. & Grigoriev, V. (eds.). Russian-German Cooperation System Laptev Sea 2000: The Expedition Lena 2001. *Reports on Polar Research* 426, 186 pp.
- Rachold, V., Bolshiyarov, D.Y., Grigoriev, M.N., Hubberten, H.-W., Junker, R., Kunitsky, V.V., Merker, F., Overduin, P. & Schneider, W. 2007. Nearshore arctic subsea permafrost in transition. *EOS* 88: 149-156.
- Ringelberg, D.B., Sutton, S. & White, D.C. 1997. Biomass, bioactivity and biodiversity: microbial ecology of the deep subsurface: analysis of ester-linked phospholipid fatty acids. *FEMS Microbiology Reviews* 20: 371-377.
- Rivkina, E.M., Friedmann, E.I., McKay, C.P. & Gilichinsky, D. 2000. Metabolic activity of permafrost bacteria below the freezing point. *Applied Environmental Microbiology* 66: 3230-3233.
- Rivkina, E.M. & Gilichinsky, D.A. 1996. Methane as a paleoindicator of the dynamics of permafrost deposits. *Limnology and Mineral Resources* 31: 396-399.
- Rivkina, E.M., Gilichinsky, D., Wagener, S., Tiedje, J., Shcherbakova, V. & McGrath, J. 1998. Biochemical activity of anaerobic microorganisms from buried permafrost sediments. *Geomicrobiology* 15: 187-193.
- Shi, T., Reeves, R., Gilichinsky, D. & Friedmann, E.I. 1997. Characterization of viable bacteria from Siberian permafrost by 16S rDNA sequencing. *Microbial Ecology* 33: 167-179.
- Wagner, D., Kobabe, S., Pfeiffer, E.-M. & Hubberten H.-W. 2003. Microbial controls on methane fluxes from a polygonal tundra of the Lena Delta, Siberia. *Permafrost Periglac. Process.* 14: 173-185.
- Wagner, D. 2008 Microbial communities and processes in Arctic permafrost environments. In: P. Dion & C.S. Nautiyal (eds.), *Microbiology of Extreme Soils. Soil Biology* 13, Berlin: Springer, 133-154.
- Wagner, D., Lipski, A., Embacher, A. & Gattinger, A. 2005. Methane fluxes in extreme permafrost habitats of the Lena Delta: effects of microbial community structure and organic matter quality. *Environmental Microbiology* 7: 1582-1592.
- White, D.C., Davis, W.M., Nickels, S., King, J.D. & Bobbie, R.J. 1979. Determination of the sedimentary microbial biomass by extractible lipid phosphate. *Oecologia* 40: 51-62.
- Yershov, E.D. 1998. *General geochronology*. Cambridge: Cambridge University Press, 580 pp.
- Zelles, L. 1999. Fatty acid patterns of phospholipids and lipopolysaccharides in the characterisation of microbial communities in soil: a review. *Biology and Fertility of Soils* 29: 111-129.
- Zhang, T., Barry, R.G., Knowles, K., Hegnibottom, J.A. & Brown, J. 1999. Statistics and characteristics of permafrost and ground-ice distribution in the Northern Hemisphere. *Polar Geography* 2: 132-154.
- Zimov, S.A., Schuur, E.A.G. & Chapin III, F.S. 2006. Permafrost and the global carbon budget. *Science* 312: 1612-1613.

Importance of Glacier-Permafrost Interactions in the Preservation of a Proglacial Icing: Fountain Glacier, Bylot Island, Canada

Pablo A. Wainstein

Department of Geography, University of Calgary, Alberta, Canada

Brian J. Moorman

Department of Geography, University of Calgary, Alberta, Canada

Ken Whitehead

Department of Geography, University of Calgary, Alberta, Canada

Abstract

Fountain Glacier is hydrologically unique in the Canadian Arctic for the large perennial icing in its proglacial valley. It is hypothesized that the icing holds information on the glacier hydrology and the role permafrost has on the overall hydrological system. A spring first observed in 1991, down valley from the glacier, is thought to be supplied by pressurized subglacial water. Aerial and geophysical surveys have been used in conjunction with thermal-hydrological modeling to study the spring's stability and longevity of the icing. Results indicate that there is a well established temporal relationship between changes experienced by the glacier and the icing. It is suggested that the relationship between glacier and permafrost, is an unstable equilibrium, where the glacier drives the system out of equilibrium by altering the proglacial hydraulic conditions as it retreats, whereas the growth of permafrost restores the system back to a new hydro-thermal balance.

Keywords: Bylot Island; glacial hydrology; glacier; GPR; icing; naled.

Introduction

A major issue in glacial hydrology is to determine the way water flows in the glacial environment and the interactions it has with the surrounding ground, which are mainly controlled by the local hydrology, geology and topography.

However, in the High Arctic, where the permafrost is continuous, the interaction between the flow of glacial meltwater and the surrounding ground is mainly governed by temperature. Subzero temperature regimes promote the formation of permafrost and cold glacier ice fringes which, frozen to the glacial bed, act as effective water barriers, enabling the storage of pressurized subglacial flow.

Icings and associated features are often observed on proglacial floodplains in the High Arctic. These occur where water, flowing through a network of subglacial and intra-permafrost passages, comes to the surface and freezes in layers. Studies have pointed out that water could mainly come from two sources: (1) subglacial long-term storage; or (2) interconnected supraglacial or marginal ice dammed lakes (Pollard et al. 1999, Hodgkins 2004). It has been commonly accepted that the formation of some icings are related to polythermal glaciers, such as Fountain Glacier on Bylot Island, that have a temperate base, under which water can be stored in a network of interconnected cavities (Pollard et al. 1999, Yde & Knudsen 2005). However recent research by Hodgkins et al. (2004) has presented evidence supporting the existence of icings in front of Scott Turnerbreen Glacier in Svalbard, believed to be a cold based glacier.

Field observations suggest that the icing in front of Fountain Glacier is a perennial feature that partially degenerates throughout the melt season as a result of thermal

and hydraulic erosion. However, once the ablation season is over and air temperatures become negative, a delicate hydrostatic and thermal balance enables its regeneration by allowing an uninterrupted liquid water supply throughout the winter.

This paper describes the glacier-permafrost interactions that lead to the preservation of a proglacial icing on Bylot Island, Canada; and proposes that subglacial water storage is responsible for supplying water to the icing through a proglacial talik. Additionally, it is suggested that the slow overall thinning of the proglacial icing is directly related to the retreat and thinning of Fountain Glacier.

Study Area

Bylot Island (Fig. 1a) is located at the eastern margin of the Canadian Arctic, north of Baffin Island, at approx 73°N, 78°W. It is roughly 180 km in length and 100 km in width; with a 4,500 km² icefield covering the centre of the island.

Even though the island has been studied by a few authors (e.g., Zoltai et al. 1983, Moorman 1998, 2000a, b, 2003, Irvine-Fynn 2004, Fortier & Allard 2004) it is still considerably unexplored.

Mountain areas are composed mainly of crystalline Canadian Shield bedrock, while the lowlands that receive the flowing glaciers mainly consist of poorly consolidated sandstone and mudstone of Cretaceous-Tertiary age.

The climate of Bylot Island can be considered as an arctic desert. It has a mean annual temperature of -15°C, a mean annual precipitation of 225 mm and the average local snow depth was measured to be less than 80 cm near the terminus of Fountain Glacier (Moorman & Michel 2000a, b,

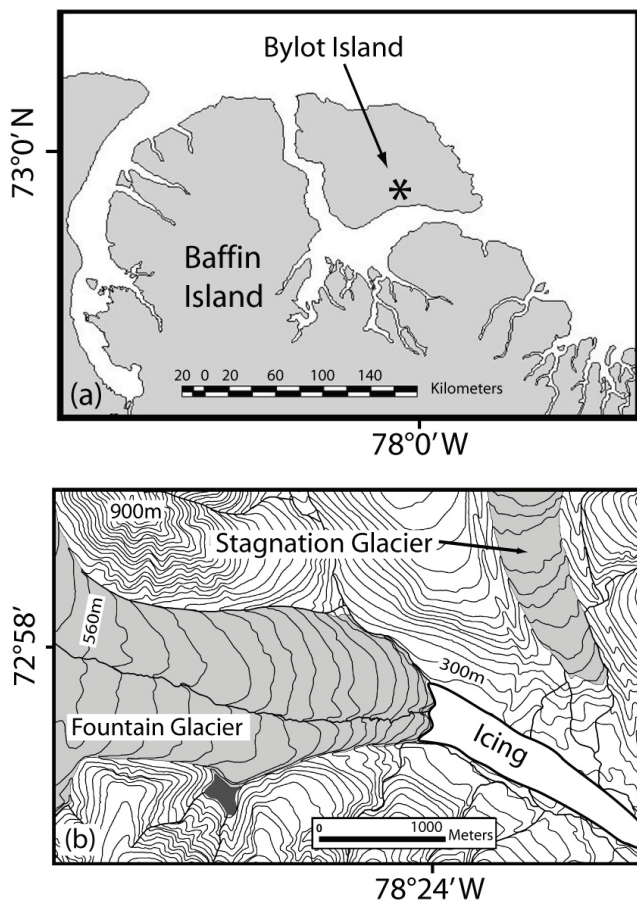


Figure 1. (a) Location of Bylot Island on the northern edge of Baffin Island, Canadian Arctic and (b) topography of the study area in the region of Fountain and Stagnation Glaciers.

Moorman 2003). The island is located in a zone of continuous permafrost (Zoltai et al. 1983) with estimated thicknesses being between 200 and 400 m (Moorman 2003). The coupled action of the strong presence of permafrost and the low precipitation makes the hydrology highly dependent on glacial conditions (i.e., ice melt and dynamics). The island's air and ground temperature regimes directly influence the preservation of hydrologic features in ice, ice cored moraines and proglacial plains. Klassen (1993) and McCuaig (1994) have presented evidence suggesting that Bylot Island has not experienced glacial advances in more than 40,000 years. Its glaciers currently show signs of retreat from their Neoglacial maximum at the end of the Little Ice Age.

Field observations were carried out on the lower ablation zone of Fountain Glacier and the adjacent section of the icing located on its proglacial plains (Fig. 1b).

Methodology

Glacial retreat and thinning

The quantification of the retreat and thinning of Fountain Glacier was obtained through the comparison of the following images and Digital Elevation Models (DEM):

- Aerial photographs obtained in 1958 and 1982

were georeferenced using a second order polynomial, and resampled to a standard pixel size of 5 m.

- A CV580 radar image was acquired over the area of interest in May 1995 by the Canada Centre for Remote Sensing. This image was already terrain-corrected and had a pixel resolution of 5 m.

- A 15 m-resolution orthorectified panchromatic Landsat ETM image was obtained in 2001.

All four images were re-sampled to UTM zone 17X, NAD 83 and given a pixel size of 5 m. Vectors were then drawn representing the position of the glacier snout on each of the four dates.

- A 5 m gridded DEM was generated for the lower part of Fountain Glacier from 20 m contours available as a vector layer from the 1:50,000 Canvec vector coverage, derived from the 1982 photography.

- A second DEM was generated from DGPS positions obtained in the summer of 2007.

The 2007 DEM was then subtracted from the 1982 DEM to establish the amount of thinning which has occurred over the ablation zone of Fountain Glacier over the last 25 years.

Icing thinning

Ground Penetrating Radar (GPR) surveys were carried out on the proglacial icing in front of Fountain Glacier during the summer of 2007. Transverse survey lines were established all over the extent of the icing following a zigzag pattern. Additionally, a longitudinal line was surveyed through the middle section of the icing in order to tie the transverse profiles together.

Survey lines were conducted using a Pulse Ekko Pro GPR System (Sensors and Software) with 200 MHz antennas in parallel broadside configuration. The profiles were acquired in continuous mode using a 400V transmitter and a stacking of 16, which allowed an average step size of 12 cm. A Garmin GPS receiver was connected to the GPR unit allowing the continuous acquisition of positional data while the radar profile was collected. Radar data was then filtered for low frequency signal saturation and enhanced with an Automatic Gain Control (AGC).

A Common Mid Point (CMP) survey was also acquired in order to determine the wave propagation velocity for the icing ice and convert time-based profiles to depth.

The base of the icing was delineated using ReflexW software and a contour map of the icing showing ice thickness was then generated.

Based on GPR surveys conducted in 1993 with a Pulse Ekko IV System (200MHz antennas), Moorman & Michel (2000) produced an ice thickness map of the proglacial icing. Both maps were compared and a contour map was generated showing the changes in ice thickness over the period from 1993 to 2007.

Spring activity and location

The spring activity and location was determined through the comparison of:

- Image extracted from an aerial video shot in 1991.

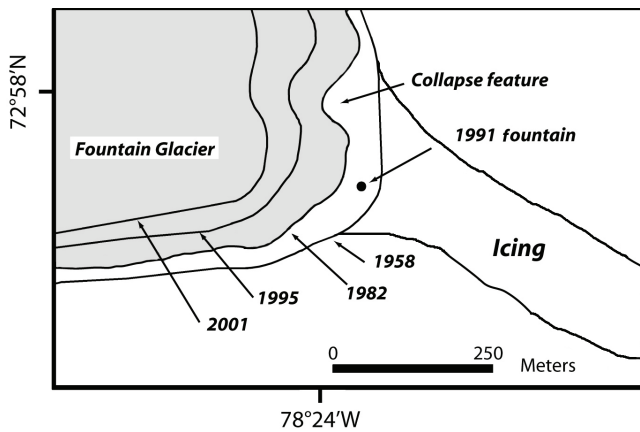


Figure 2. Temporal variation of Fountain Glacier's terminus. The retreat rate has increased considerably since 1982 when a collapse feature on the northern half of the snout was first observed.

- Georeferenced aerial photograph acquired in 1982.
- Icing map created by Moorman & Michel (2000) in 1993.
- Field observations conducted in 1991, 1993, 1994, 1995, 1999, 2001, 2003 and 2007.

Glacial Behavior

Fountain Glacier (Fig. 1b) has a total catchment area of 72 km² (Walter 2003). The glacier is 16 km long, its elevation ranges from 255 m a.s.l. to 1758 m a.s.l. and its average surface slope is 5.5° (Walter 2003).

The snout of Fountain Glacier terminates in a 20–30 m cliff face overlooking the proglacial plain where the icing is situated. It is flanked by vegetated moraines which tend to be considerably smaller than the ones surrounding neighboring glaciers, such as Stagnation Glacier.

The glacier's surface is generally smooth, with few moulins and crevasses, characteristic of polythermal glaciers subjected to subzero temperature regimes. As such, the superficial hydrology of Fountain Glacier mainly consists of marginal streams and a deeply incised meandering channel in the lower 3 km of the ablation area that discharges a large percentage of the supraglacial meltwater. This deeply cut and strongly meandering supraglacial stream is an indication that some hydraulic features are reoccupied annually (e.g., Moorman & Michel 2000a).

Although the glacier's englacial and subglacial hydrology has not been thoroughly studied, signs of preserved englacial conduits have been observed by Ground Penetrating Radar (GPR) surveys and corroborated with field observations on the glacier's margins. Radar profiles have also shown areas of higher concentration of noise, interpreted as water-rich temperate ice towards the base of the glacier. Although there were no observations of subglacial channels flowing from Fountain Glacier in 2007, continuous water chemistry measurements showed that water turbidity considerably increased towards the end of June, suggesting the beginning of the emergence of subglacial flow.

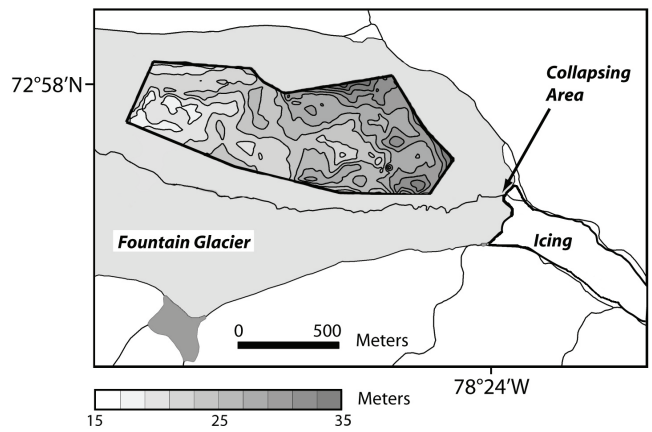


Figure 3. Contour map showing the thinning experienced by Fountain Glacier during the last 25 years (1982–2007). Contour interval is 2 m. The glacier's outline corresponds to its 1982 position.

Even though the proglacial plains are reworked seasonally by meltwater erosion, there are a few signs of high water pressure events. A roughly 5 m-high, water-transported boulder was deposited on the southern side of the proglacial plain between field observations made in 1996 and 1999. These observations support the hypothesis that Fountain Glacier may sporadically exhibit water outbursts as a result of the sudden release of subglacially stored pressurized water. This affects the area's morphology, including the permafrost that surrounds the glacier terminus.

Until recently (since the Little Ice Age) the glacier has not presented marked retreats, slowly losing mass via ice melting and sublimation only during the short ablation summer period. However, this appears to have changed in the last few years. The terminus has shown important signs of activity, retreating about 60 m between 1958 and 1982, giving an average retreat rate of about 2.5 m per year over this period (Fig. 2).

Between 1982 and 1995, it retreated about 80 m, which gives an average retreat rate of about 6 m per year. On average, the retreat rate has more than doubled in speed over a period of 13 years. Between 1995 and 2001 the glacier receded 60 m more at an average rate of 10 m per year. Although imagery is not yet available for 2007, preliminary field observations support the hypothesis that this trend will continue and that the rate of retreat is still increasing.

During the period 1958 and 1982, a collapse feature began to develop in the northern half of the glacier's snout very close to the effluent point of the incised supraglacial stream shown in Figure 1b. Before the collapse, the glacier's snout showed a mild slope ramp, characteristic of undisrupted termini. The collapse feature is clearly shown by a distinct curve in the contour lines representing the glacier's position in 1982. The collapse feature has become more predominant throughout the years, severely increasing the snout's slope.

The long-observed equilibrium of Fountain Glacier has not only been disrupted by recession but also by thinning (Fig. 3).

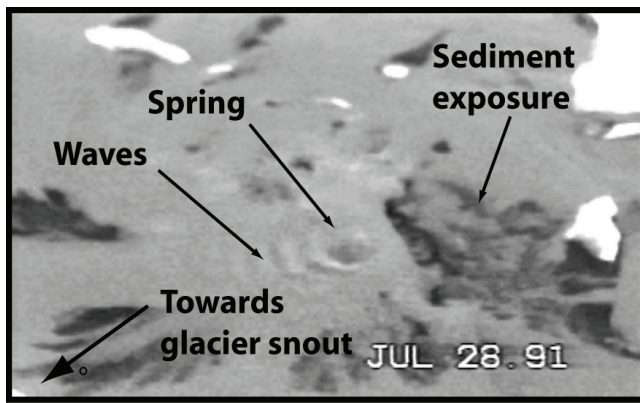


Figure 4. Image extracted from a video shot during a helicopter flight over the proglacial plains of Fountain Glacier in 1991. Note the spring activity shown by the presence of concentric waves on the water surface.

Although there is insufficient data to determine the thinning rates over the last 50 years, the comparison of the 1982 DEM and field observations collected during 2007 shows that the upper surveyed area had thinned by around 15–20 m, while the section nearest the snout showed the greatest thinning, typically between 25 and 30 m. On average Fountain Glacier appears to have thinned between 0.6 and 1.2 m per year over the last 25 years.

Icing and Spring Activity

Fountain Icing is a proglacial icing located at an elevation of approximately 260 meters above sea level. It presents well developed candle ice and is considerably debris free. The icing extends for over 11 km from the terminus of Fountain Glacier down valley until the margins of Sirmilik Glacier; although aerial photographs show that only the section closest to Fountain Glacier (500 m wide by 1.2 km long) has had perennial ice cover since 1948 (Moorman & Michel 2000b). This last section presents a valley bottom profile characteristic of outwash plains, with some areas emerging through the icing surface. The sub-icing topography varies considerably and is continuously being reworked by water erosion during the melting season.

As in glaciers, field observations show that meltwater tends to concentrate in channels that grow bigger at the expense of smaller ones. As such, the icing has historically presented a main supra-icing channel that drains the majority of the meltwater. Aerial and field photographs show that this channel was located on the north side of the icing until the glacier collapse feature began to develop. Some time before 1999, when the collapse feature was big enough and the glacier's terminus ramp had become steepened, this main drainage channel shifted towards the southern side of the icing. The prevalence of drainage channels on the margins of the icing has promoted a dome shape surface recognized by Moorman & Michel (2000b).

During the fall and winter, when freezing temperatures prevail, the icing is rebuilt. Field observations conducted during early June and late August show that even though the

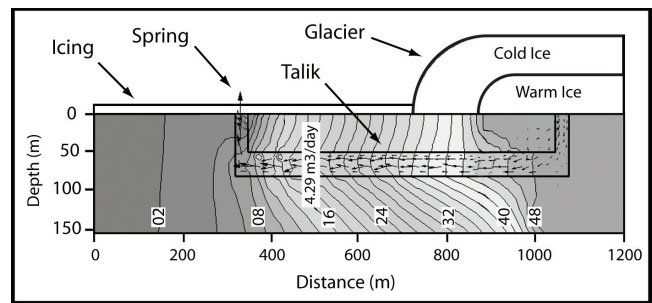


Figure 5. Thermal hydrological modeling of the generation and preservation of the proglacial icing. The model shows a stable liquid water flow through the proglacial talik after 10 years of modeling iterations. The talik is 30 m thick and the spring is located at approximately 300 m from the glacier terminus which is the maximum attainable distance for the talik to be preserved. Contour lines represent hydraulic head with an interval of 2 m.

icing is significantly eroded by the end of one melting season, it is totally replenished by the beginning of the subsequent one. By the end of the ablation season, superficial water flow rapidly decreases leaving only groundwater sources as an option for the icing to regenerate.

Fountain Glacier, originally named B26, got its unofficial name from the presence of a fountain, first observed during over flights in 1991 (Fig. 4). The spring emerged strongly at a distance of roughly 50 meters from the glacier's terminus, flooding the proglacial plains, which at that time promoted the partial erosion of the icing that covered the proglacial valley.

It is hypothesized that pressurized subglacial storage is responsible for supplying water to the icing through a proglacial talik that connects the glacier to the spring, promoting the regeneration of the icing during the freezing winter. Simplified finite element thermal-hydrological models support the hypothesis that liquid water may indeed flow, even under harsh arctic winter conditions, by means of a proglacial talik, which is preserved unfrozen by the heat produced by pressurized flowing water. Although the model shows that the talik begins a slow freeze-back process after some time, high water pressure episodes such as the one that occurred in 1991 cause a thermal enlargement of the talik (Fig. 5).

Aerial photograph comparison suggests that the icing did not extend all the way to the terminus of the glacier before 1991 (Moorman & Michel 2000) when the spring was first observed. However, field observations conducted in 1993 determined that the area flooded by the spring activity in 1991 had become covered by icing ice, and that an ice blister had developed in the former location of the fountain. Marks of small supra-icing streams radiating out were observed (Fig. 6). The ceasing of the spring activity, the development of the collapse feature on the glacier snout and an increasingly consistent glacial retreat appear to have occurred around the same time. From this time onwards the icing has thinned considerably.

The thinning of the icing allowed the exposure of what is

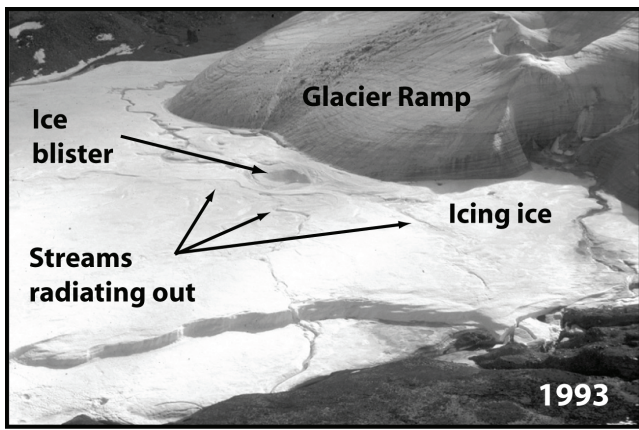


Figure 6. Oblique aerial photograph showing the ice blister adjacent to the terminus of Fountain Glacier. A series of radiating streams have been presumably fed by water flowing from a spring under the blister.

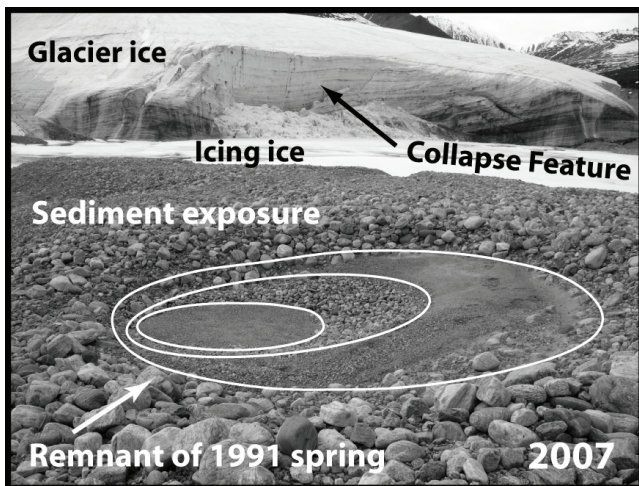


Figure 7. Circular feature embedded in a sediment exposure in front of Fountain Glacier. The feature has been interpreted as the remnants of the spring observed in 1991 which resulted in the icing blister observed in 1993.

inferred to be the remnants of the spring observed in 1991. Figure 7 shows a circular sediment feature embedded in a sediment exposure located in the same area where the spring was observed. In fact, its position taken by GPS closely aligns with the position presented by the map created in 1993 by Moorman & Michel (2000b). The remnant feature consists of three well-sorted sediment rings devoid of fines. Additionally, marks of incipient channels radiating out from the circular feature were observed. As such, based on its location, sediment characteristics and morphology, it has been concluded that the feature is in fact the remnants of the spring observed in 1991.

The subtraction between the ice thicknesses measured by Moorman & Michel (2000b) in 1993 and those obtained in the summer of 2007 reveals a considerable thinning of the icing, by almost 10 m in some areas (Fig. 8). These areas are included within the zones of perennial ice, and as such it is suggested that the icing's thinning is the result of the closure of the spring that once supplied liquid water year

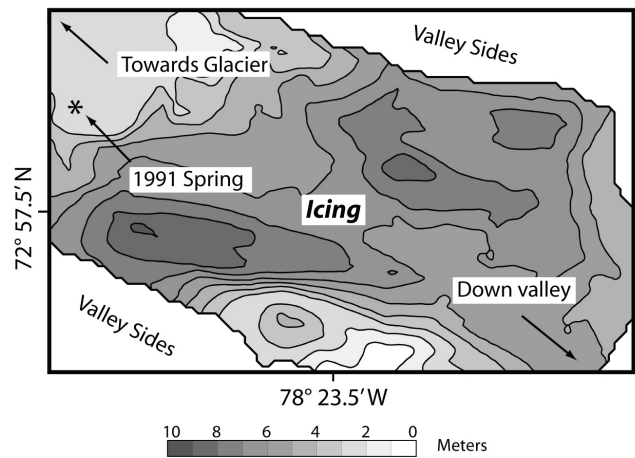


Figure 8. Contour map showing the thinning experienced by the Fountain Glacier Icing during the last 15 years (1993–2007). Contour interval represents 1 m of change in the ice thickness.

round. The total volume lost is 507,075 m³ over a surveyed area of 94,813 m², giving an average thinning of 5.3 m.

It is worth noting that even though the icing has experienced a considerable overall thinning, it is still being rebuilt every winter. This supports the idea that another routing for groundwater has been established, presumably closer to the glacier.

Discussion and Conclusions

The growth and preservation of the Fountain Glacier icing depends on the balance between the glacial system and the surrounding permafrost. Field observations show there is a well established temporal relationship between changes experienced by the glacier and the icing.

The cold impermeable margin of Fountain Glacier results in the year round pressurized storage of liquid water used in the regeneration of the proglacial icing. It was observed that after the collapse of the terminus, the winter spring flow was dramatically reduced, resulting in the thinning of the perennial icing.

The hydrology and dynamics of Fountain Glacier have a considerable effect on the characteristics and response of the proglacial talik responsible for connecting the subglacial environment with the proglacial plain. Figure 9 illustrates a conceptual model that links the reaction of the icing and permafrost systems to the retreat and collapse of Fountain Glacier. It is suggested that the icing is rebuilt by water running through a proglacial talik which needs to remain unfrozen in order to deliver the necessary water year round.

Preliminary results from thermal-hydrological modeling of the proglacial talik suggest that there is a maximum distance between the glacier snout and the point of water expulsion (spring) that can be attained if the talik is to remain unfrozen. The talik is kept unfrozen as a result of a balance between the energy extracted by the subzero air temperature regime and the incoming energy produced by the friction of the pressurized water flow through the sediments (Fig. 5).

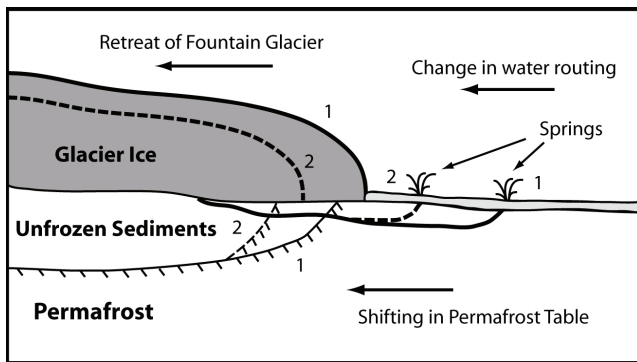


Figure 9. Schematic diagram showing changes in icing and permafrost table as a result of variations in glacial dynamics. (1) Shows the old equilibrium position whereas (2) is the new equilibrium attained.

As such, the retreat and collapse of the glacier terminus exposes a new portion of the proglacial plain to cold air temperatures, altering the talik energy balance, resulting in freeze back and reduction of the spring activity. However, field observations show that the icing is replenished every winter; supporting the hypothesis that a new water routing is readily established as the system attains a new equilibrium position.

It is suggested that the relationship between the two systems, glacier and permafrost, is an unstable equilibrium, where changes in the behavior of either of the two will have considerable effects on the characteristics of the icing. The glacier is considered the dominant factor able to drive the icing out of equilibrium by altering the hydraulic conditions needed to maintain an open talik. Permafrost is the secondary factor that promotes talik freezeback upon the retreat of the glacier, leading to a decrease of water flow through the talik. This hydro-thermal disturbance results in abandonment of the portion of the talik furthest from the glacier terminus. It appears that the closest portion of the talik is preserved, enabling the establishment of a new spring. As such, glacier retreat will promote the up-valley movement of the spring, maintaining a constant distance between the point of water emergence and the glacier snout.

The remotely-sensed data, field observations and finite element modeling demonstrate how the preservation of the icing is a function of the balance between hydrological and thermal regimes that change over a number of time scales. In the short term, seasonal variations in water pressure result from changes in summer temperatures and glacial discharge; that subsequently control the seasonal accretion and erosion of the icing. Over the longer term, glacial retreat and thinning affects the glacier's hydrology and the proglacial subsurface thermal regime. This alters the talik thermal equilibrium at the decadal scale and results in shifts in the spring equilibrium location and discharge.

Finally, steady state thermal disequilibrium (resulting from the gradual talik freezeback) and short high-water pressure events results in intermittent hydrological changes that can affect the icing over the short, medium or long-term.

Acknowledgments

This work was supported by the Natural Sciences and Engineering Research Council of Canada (NSERC) through a research grant held by Dr. Brian Moorman, by the Polar Continental Shelf Project (PCSP), and Alberta Ingenuity.

References

- Fortier, D. & Allard, M. 2004. Late Holocene syngenetic ice-wedge polygons development, Bylot Island, Canadian Arctic Archipelago. *Canadian Journal of Earth Sciences* 41: 997-1012.
- Hodgkins, R., Tranter, M. & Dowdeswell, J. A. 2004. The characteristics and formation of a High-Arctic proglacial icing. *Geografiska Annaler* 86: 265-275.
- Irvine-Fynn, T.D.L. 2004. *A non-invasive investigation of polythermal glacial hydrology: Stagnation Glacier, Bylot Island, Nunavut, Canada*. M.S. Thesis. Calgary: Department of Geography, University of Calgary, 389 pp.
- Klassen, R.A. 1993. *Quaternary Geology and Glacial History of Bylot Island, Northwest Territories*. Ottawa, Ontario: Geological Survey of Canada, 93 pp.
- McCuaig, S.J. 1994. *Glacial chronology of the South Bylot and Salmon River lowlands, NWT, using erratic dispersal patterns, cosmogenic dating and lichenometry*. M.S. Thesis. Ottawa, Ontario: Carleton University, 140 pp.
- Moorman, B.J. 1998. *The development and preservation of tabular massive ground ice in permafrost regions*. Ph.D. Thesis. Ottawa, Ontario: Carleton University, 308 pp.
- Moorman, B.J. & Michel, F.A. 2000a. The burial of ice in the proglacial environment on Bylot Island, Arctic Canada. *Permafrost and Periglacial Processes* 11(3): 161-175.
- Moorman, B.J. & Michel, F.A. 2000b. Glacial hydrological system characterization using ground-penetrating radar. *Hydrological Processes* 14(15): 2645-2667.
- Moorman, B.J., Robinson, S.D. & Burgess, M.M. 2003. Imaging periglacial conditions with ground-penetrating radar. *Permafrost and Periglacial Processes* 14(4): 319-329.
- Pollard, W., Omelon, C., Andersen, D. & McKay, C. 1999. Perennial spring occurrence in the Expedition Fiord area of western Axel Heiberg Island, Canadian High Arctic. *Canadian Journal of Earth Sciences* 36: 105-120.
- Walter, F.S.A. 2003. *Glacier fluctuations and glacier hypsometry on Bylot Island, Nunavut, Canada, using remote sensing methodology*. M.S. Thesis. Calgary: Department of Geography, University of Calgary, 159 pp.
- Yde, J.C. & Knudsen, N.T. 2005. Observations of debris-rich nales associated with a major glacier surge event, Disko Island, West Greenland. *Permafrost and Periglacial Processes* 16: 319-325.
- Zoltai, S.C., McCormick, K.J. & Scotter, G.W. 1983. *A natural resources survey of Bylot Island and adjacent Baffin Island, Northwest Territories*. Ottawa: Parks Canada, 176 pp.

Isolation and Identification of Cold-Adapted Fungi in the Fox Permafrost Tunnel, Alaska

Mark P. Waldrop

United States Geological Survey, Geologic Division, Menlo Park, CA, USA

Richard White III

United States Geological Survey, Geologic Division, Menlo Park, CA, USA

Thomas A. Douglas

Cold Regions Research and Engineering Laboratory, Fort Wainwright, AK, USA

Abstract

Permafrost microbiology is important for understanding biogeochemical processes, paleoecology, and life in extreme environments. Within the Fox, Alaska, permafrost tunnel, fungi grow on tunnel walls despite below freezing (-3°C) temperatures for the past 15,000 years. We collected fungal mycelia from ice, Pleistocene roots, and frozen loess. We identified the fungi by PCR, amplifying the ITS region of rRNA and searching for related sequences. The fungi within the tunnel were predominantly one genus, *Geomyces*, a cold-adapted fungi, and has likely “contaminated” the permafrost tunnel from outside. We were unable to obtain DNA or fungal isolates from the frozen loess, indicating fungal survival in permafrost soils can be strongly restricted. *Geomyces* can degrade complex carbon compounds, but we are unable to determine whether this is occurring. Results from this study suggest *Geomyces* may be an important colonizer species of other permafrost environments.

Keywords: Fox tunnel; fungi; *Geomyces*; ice wedge; loess; permafrost.

Introduction

The permafrost tunnel near Fox, Alaska, was constructed in the early 1960s to examine mining, tunneling, and construction techniques in permafrost. The tunnel was constructed, and continues to be maintained, by the U.S. Army Cold Regions Research and Engineering Laboratory. The tunnel consists of ice-cemented loess, massive ice, and ice wedges that have been dated from 12 kbp to 40 kbp. The permafrost present in the tunnel is syngenetic with multiple exposures of primary and secondary ice features (Bray et al. 2006, Shur et al. 2004). Fungal growth has been observed on the interior walls. The interior walls, ice wedges, and hanging roots within the tunnel are covered with white fungal mycelia all year. Although the temperature in the permafrost tunnel has remained below freezing (approximately -3°C) for at least the past 15,000 years (Katayama et al. 2007) microbial activity is still present. The tunnel is also very dry and there is no evidence of liquid water. As a consequence, the organisms that grow in the tunnel must be adapted to cold and dry environments.

Observational evidence, such as fungal growth appearing from drilled holes and nails, suggests that the fungal organisms were contaminants brought in from outside the tunnel either from air contamination or on sampling equipment. Fungal growth was observed not only on the loess-rich interior walls, but mycelia often completely carpeted ice wedges. The widespread nature of the fungi throughout the tunnel suggests that it can be transported by air currents. It may also be possible that the fungi occurs on ice surfaces and around drill holes because it is moisture-limited. When a hole is drilled, ice-cemented material is exposed and immediately

starts to melt and then sublimate. Therefore, when a hole is drilled, moisture is liberated, and fungal growth at these sites should be possible.

Our research objective was to determine the identity of the fungal organism(s) covering the interior walls and ice wedges of the permafrost tunnel. Understanding their taxonomy could help us understand the microbiology of permafrost environments and determine the range of environmental parameters in which the some fungi can grow. A secondary objective was to determine whether the identified organisms have important characteristics related to biogeochemical processes or human health.

Methods

Soil sampling

To determine the identity of the fungal organisms throughout the permafrost tunnel and on different substrates, five samples were collected from interior walls, hanging roots, and ice wedges. Three samples were taken from the interior walls by scraping the fungus gently with the end of a sterile plastic centrifuge tube. When doing this it was common for loess particles to enter the tube (Figs. 1a, b, d). One sample was taken from an ice wedge in the ceiling in the side corridor (winze) of the tunnel (Fig. 1c). The mycelial “mat” was covering the ice wedge and was easily collected with tweezers and placed in a sterile centrifuge tube (Fig. 1c). The fourth sample was taken from a root hanging from the ceiling of the main adit where the adit and winze separate near the entrance (Fig. 1e). The root was covered in mycelia and the root was broken off with tweezers and placed in a sterile centrifuge tube. The tubes were frozen that same

day and later transported to the USGS in Menlo Park for isolation and molecular characterization. We also sampled loess samples from the wall using a serrated metal drill corer (keyhole corer) that had been sterilized using ethanol. In the lab, we further attempted to minimize any potential contamination by scraping of the exterior of the core with sterile razor blades and sampling the interior of the frozen loess core. Carbon and nitrogen concentrations of loess were quantified on oven-dried material (105°C, 48 h) on a Carlo Erba C/N analyzer.

Soil preparation

Soil or fungal flocs were weighed out into 2 ml microcentrifuge tubes (Eppendorf Inc., Westbury, NY) in 0.5 g increments. Under sterile technique, 1.5 ml of DNase/RNase free water (Eppendorf Inc., Westbury, NY) was added to the soil samples or fungal mat. The soil slurry was vortexed for 10 minutes. The slurry was then centrifuged at 10,000 rpm for 1 minute. The supernatant was then serially diluted 10-fold, 100-fold and 1000-fold. These serial dilutions were then plated onto standard potato dextrose agar plates (Difco Inc., Lawrence, KS). As a control the wet soil from the previous step and the dry soil from the original sample were also plated onto potato dextrose agar plates (Difco Inc., Lawrence, KS).

Growth conditions

Plates of each dilution were grown at 0, 4, 20, and 37°C in the dark for 28–31 days. Fungal growth did not occur at 20 or 37°C but did occur at 0 and 4°C. Fungal isolates that appeared on the 4°C plates were isolated onto fresh potato dextrose plates. This step of removing isolates from plates took another 2–3 months of replica plating until there was no difference in isolate morphology. Pure cultures were tested for pH sensitivity at various pHs ranging from 2–8 on potato dextrose agar (Difco Inc., Lawrence, KS) over a period of one month. Growth was only observed at pH 5 and 6.

DNA isolation

Single isolates were removed from agar plates by scraping, placed in liquid nitrogen, and homogenized with a mortar and pestle. DNA was isolated from the homogenized samples following gram-positive bacteria DNA isolation protocol from a Purelink Genomic DNA mini kit (Invitrogen Inc., Carlsbad, CA). There was no fungal protocol with this kit. The isolated DNA was quantified using a standard Picogreen dsDNA assay (Invitrogen Inc., Carlsbad, CA). We also attempted to extract DNA from loess samples in bare (no mycelia) areas using a Powersoil DNA extraction kit (Mo Bio, Inc.), but agarose gel electrophoresis and the picogreen dsDNA assay showed that there was no measurable DNA in the extract. PCR was also tried but was not successful.

PCR conditions

Fungal DNA from isolates was amplified using ITS1-ITS4 primers in a PCR reaction using 0.5 to 1.0 µl of genomic fungal DNA. BSA at a final concentration of 1 µg/ml was



Figure 1a. Fungi on tunnel walls where previous core samples had been taken (sample FG1).

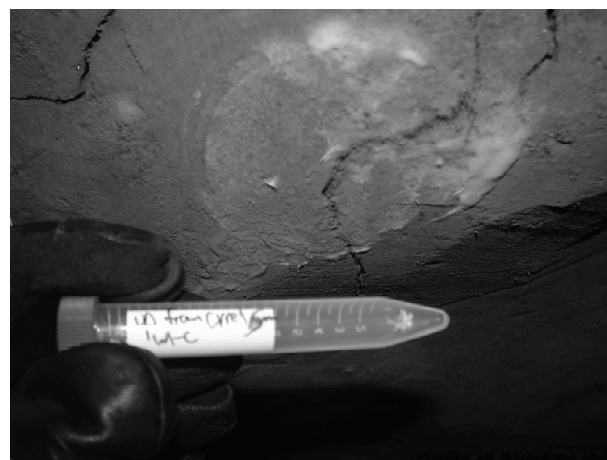


Figure 1b. Sample taken from tunnel ice-cemented loess wall (sample FG2).



Figure 1c. Fungal mycelia carpeting ice wedge (sample FG3).

used to bind to common PCR inhibitors. Thermocycler parameters were an initial melting step 95° (10 minutes one cycle), followed by 40 cycles of 95° (1 minute), 53° (30s), and 72° (1 minute). PCR was concluded with a long extension step of 72° (10 minutes), and then the PCR reactions were placed in the -20°C freezer.



Figure 1d. Fungal mycelia on a loess wall where a previous core had been collected (sample FG5).



Figure 1e. Fungi taken from alder tree root hanging from ceiling (sample FG6)

Sequence analysis

Amplified DNA was sequenced at a commercial lab (MClab, San Mateo, CA), and results were imported into Geneious software (Biomatters Ltd., New Zealand). Sequences were examined for quality and Blast searched on the NCBI database. The three best matches were recorded.

Restriction analysis

Restriction analysis was performed on the PCR products in order to determine if the sequences were of the same or different organisms. PCR products were digested overnight with the enzyme *CFO1*. BSA was added at a concentration of 10 $\mu\text{g}/\mu\text{l}$ to aid in enzymatic digestion. Digests were then run on a 3% gel for 90 min at 75 volts, with a 100 bp ladder (NEB Inc, Ipswich, MA), and negative controls. The gel was stained in ethidium bromide, rinsed for 20 min, and digitally photographed on a UV light table.

Results and Discussion

White mycelia are present on tunnel walls, ice wedges, and plant roots within the permafrost cave near Fox,

Alaska, (Figs. 1a–f). The fungal organisms sampled and isolated from multiple locations within the Fox permafrost tunnel were all of the same genus, *Geomyces*. Two of the organisms were identified as *Geomyces pannorum*, while three other samples were closely associated with *Geomyces* strain FMCC-4 (Table 1). Restriction digests of the PCR products produced different restriction patterns for most of the organisms (Fig. 2). The restriction patterns for sample FG1 and FG2 were the only two samples to be identical to each other. Except for FG1 and FG2, all samples had unique restriction patterns, indicating that they had slightly different DNA sequences. Therefore, although they were all the same genus, they differed at the species or strain level.

The physiology of *Geomyces* is such that it is very well adapted to growth in the cold, dark, and dry conditions of the permafrost tunnel. Fungi are generally well suited for growing in dry habitats due to their hyphal growth form and unique forms of osmoprotection. Additionally, *Geomyces* is one of only a few fungal organisms known for growth below freezing, which would be a necessity for any organism living within this frozen environment (Ozerskaya et al. 2005, Panikov & Sizova 2007). *Geomyces* was not capable of growth at 20°C or above, but grew well, albeit slowly, at 4°C. *Geomyces* is considered to be a psychrotrophic fungi, which is an organism that can grow at 0°C, but its optimum growth rate is above 20°C. (Gilichinsky et al. 2005, Robinson 2001). Our results indicate that our isolates could not grow at 20°C or above, and therefore they should be considered psychrophilic fungi.

Geomyces is a commonly observed fungi in boreal and arctic ecosystems that can survive in permafrost environments due to its ability to grow at cold temperatures, its ability to withstand moisture stress and high salt tolerance (Lydolph et al. 2005, Robinson 2001). *Geomyces* has the ability to break down keratin, a compound contained within hair and nails, as well as cellulose, present in plant tissues (Friedrich et al.). Because *Geomyces* is a keratinolytic fungi, it has been used as an indicator of the presence of ancient megafauna (due to the presence of hair and nails in some permafrost). The use of *Geomyces* as an “indicator species” is supported by this study because of the visible presence of ancient megafauna (generally bones) contained within the Pleistocene loess deposits (Willerslev et al. 2004). Cellulose may also be present in this permafrost environment due to the visible presence of plant roots, although *Geomyces* appeared no more dense on plant roots than on the loess tunnel walls.

Geomyces appeared to be capable of much more extensive growth on ice wedges compared to either roots or ice-cemented loess walls (compare Fig. 1c with others). The growth forms of *Geomyces* differed between the ice wedge and the permafrost tunnel walls. *Geomyces* often formed thin brittle mycelial sheets over the entire surface of the ice wedge that could be easily sampled with a small metal instrument. The ice wedges were dark in color and exhibited elevated DOC dissolved organic carbon concentrations (18.4 to 68.5 ppm; Douglas & Cai, unpublished data) which is probably a strong source of carbon substrate for the fungi.

Table 1. Identification of four fungal isolates taken from the interior of the Fox permafrost tunnel. BLAST results matched with the 18S rRNA gene, partial ITS1, 5.8S rRNA, ITS2, and 28S partial sequence.

Sample	Source	Colony Description	Best Identity	Homology	E score	Accession number
FG1	Loess wall	White to yellow colored, spiked hairy circular arrangement	1. <i>Geomyces</i> sp. BC7	94%	4e-156	DQ317337
			2. <i>Geomyces</i> sp. LC-03-010	94%	2e-154	DQ402527
			3. <i>Geomyces pannorum</i> strain VKM	94%	2e-154	DQ189224
FG2	Loess wall	White, pink to light rust colored powdery small circular arrangement	1. Uncultured fungus clone	86%	3e-70	EF434070
			2. Uncultured fungus clone	86%	3e-70	EF433976
			3. <i>Geomyces</i> sp. FMCC-4	86%	3e-70	DQ499474
FG3	Ice wedge	White to gray colored, smooth, hairy, powdery, linearly arranged	1. Uncultured fungus clone	97%	0.0	EF434070
			2. Uncultured fungus clone	97%	0.0	EF433976
			3. <i>Geomyces</i> sp. FMCC-4	97%	0.0	DQ499474
FG5	Loess wall	White, smooth colonies, powdery, linearly arranged	1. <i>Geomyces pannorum</i> strain 857	99%	0.0	DQ189229
			2. <i>Geomyces pannorum</i> strain 2236	99%	0.0	DQ189228
			3. <i>Geomyces pannorum</i> strain VKM	98%	0.0	DQ189224
FG6	Plant root	White, smooth colonies, powdery, linearly arranged	1. <i>Geomyces pannorum</i> strain VKM	94%	0.0	DQ189229
			2. <i>Geomyces pannorum</i> strain VKM	94%	0.0	DQ189228
			3. <i>Geomyces</i> sp. BC-7	94%	0.0	DQ317337

On ice-cemented loess walls, *Geomyces* tended to have a spotty distribution. Growth was generally circular emanating from previously sampled areas, and the mycelia could not be easily sampled without breaking off loess particles from the walls. The growth of *Geomyces* on loess walls tended to be associated with disturbance or points of contamination, where people would, for example, place nonsterile sampling instruments on their surface. The loess walls had carbon and nitrogen concentrations of 2.75% and 0.25%, respectively, and had moisture contents ranging from 18 to 55%. Root samples were not examined for nutrient content, but organic tissues can generally range from 40 to 50% carbon and 1 to 5% N. Therefore, these substrates had enough C and N for microbial growth.

Surprisingly, no other genus of organism except *Geomyces* was isolated from the tunnel. It is possible that given our growth conditions for isolation, we selected for this organism, although we attempted isolation at multiple pH and temperature ranges. This does not preclude other organisms from being present in the tunnel, but it is a strong indication that all of the organisms visible within the tunnel are *Geomyces*. Restriction analysis showed that we isolated several species or strains of *Geomyces*. Although all of our isolates were of the same genus, restriction analysis showed that there were slight differences in their ITS or ribosomal sequences (Fig. 2). It is likely the fact that the isolated *Geomyces* fungi is common in boreal soils, can grow well at cold temperatures, and can be easily dispersed in air that allows it to be the dominant (or only) fungal organism visibly present on the walls of the permafrost tunnel.

We also attempted to isolate DNA from the ice-cemented loess walls in order to compare the fungal DNA present within the loess to the isolates. However, we were either

unsuccessful at extracting DNA or the concentration of DNA within the ice-cemented loess walls was so low that we could not measure it, even using sensitive fluorometric techniques. We have been successful at extracting DNA from surface permafrost loess samples (1 m below the soil surface in boreal forests), which leads us to conclude that DNA concentrations within the tunnel loess walls were so low as to be unquantifiable. Our inability to extract DNA from loess in the Fox tunnel may have been due to the fact that few organisms survive frozen conditions for long periods of time (Panikov & Sizova 2007), and DNA quality in frozen soils is reduced over millennia (Willerslev et al. 2004).

We suspect that *Geomyces* in the Fox tunnel is a contaminant from outside the tunnel, rather than an organism that was present in the extant permafrost that has begun to grow on disturbed tunnel walls. *Geomyces* is a common soil organism associated with black spruce (Filion et al. 2004) and therefore is probably very prevalent in the surrounding environment. *Geomyces* growth is observed primarily around sampling holes, metal nails, and areas where the soil has been disturbed by human activity. This could have been caused by using nonsterile tools during sampling. Alternatively, small amounts of soil moisture that are released upon sampling the frozen walls (heat produced by friction between sampling equipment and wall) would permit water-limited fungi to grow rapidly in disturbed areas. The door to the Fox permafrost tunnel is often open and there is good air circulation through the tunnel. Therefore, it would be possible for organisms to contaminate the tunnel from outside.

There are some minor human health aspects to consider with regard to *Geomyces*. It is considered an indoor mold that reduces the air quality within some buildings. It is also found

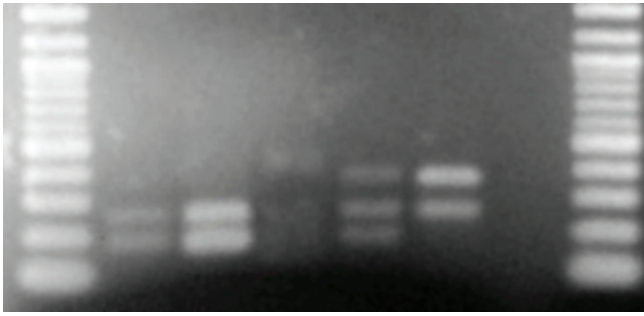


Figure 2. Restriction analysis of PCR products of the four isolates. Lanes 1 and 8 are 100 bp ladders. From left to right the samples in each lane are FG1, FG2, FG3, FG5, FG6, and a negative control.

in household dust, damp walls, and archived paper such as in libraries. It is not considered dangerous. However, one variety of *Geomyces*, *Geomyces pannorum* var *pannorum* is suspected in creating slight skin and nail infections (Bloom et al. 2007).

Cold-adapted fungi and biogeochemical cycling

Carbon and nitrogen cycling within thawed permafrost soils is an important area of global change research (Zimov et al. 2006). This study highlights two factors that make permafrost environments unique microbiologically which, in turn, are important for biogeochemical cycling.

First, results from the permafrost tunnel and permafrost studies at the ground surface indicate that fungal abundance in permafrost soils is very low (Gilichinsky et al. 2005, Waldrop et al., unpubl.). Microbial diversity in permafrost soil is also likely to be restricted because fewer organisms are able to withstand frozen temperatures for long periods of time. Therefore, as permafrost soils thaw, what will be the fungal organisms that enter into this new biological niche? Likely it will be cold-adapted organisms not unlike *Geomyces* in this study. Therefore, the study of cold-adapted fungi in C and N cycling is an important area of future research.

Secondly, the temperature response of microbial activity in cold permafrost environments with low fungal diversity may have to be carefully evaluated. Normally, microbial activity increases with temperature, but cold-adapted fungi, such as *Geomyces*, may have faster growth rates and enzyme activities at low temperatures than at higher temperatures (Robinson 2001). An area of further study will be to determine the fungal organisms that act as primary colonizers of permafrost soils as they thaw. Could low microbial diversity in permafrost soils affect the efficiency or rate of biogeochemical processes as permafrost soils thaw? Given that soil microorganisms mediate biogeochemical cycles and the lack of data on permafrost microbiology, there is certainly a strong research need in this area.

Acknowledgments

I would like to acknowledge the U.S. Army Cold Regions Research and Engineering Laboratory for sampling assistance.

References

- Bloom, E., Bal, K., Nyman, E., Must, A. & Larsson, L. 2007. Mass spectrometry-based strategy for direct detection and quantification of some mycotoxins produced by *stachybotrys* and *aspergillus* spp. in indoor environments. *Applied and Environmental Microbiology* 73: 4211-4217.
- Bray, M.T., French, H.M. & Shur, Y. 2006. Further cryostratigraphic observations in the CRREL permafrost tunnel, Fox, Alaska. *Permafrost and Periglacial Processes* 17: 233-243.
- Filion, M., Hamelin, R.C., Bernier, L. & St-Arnaud, M. 2004. Molecular profiling of rhizosphere microbial communities associated with healthy and diseased black spruce (*picea mariana*) seedlings grown in a nursery. *Applied and Environmental Microbiology* 70: 3541-3551.
- Gilichinsky, D., Rivkina, E., Bakermans, C., Shcherbakova, V., Petrovskaya, L., Ozerskaya, S., Ivanushkina, N., Kochkina, G., Laurinavichuis, K., Pecheritsina, S., Fattakhova, R. & Tiedje, J.M. 2005. Biodiversity of cryopegs in permafrost. *FEMS microbiology ecology* 53: 117-128.
- Katayama, T., Tanaka, M., Moriizumi, J., Nakamura, T., Brouchkov, A., Douglas, T.A., Fukuda, M., Tomita, F. & Asano, K. 2007. Phylogenetic analysis of bacteria preserved in a permafrost ice wedge for 25,000 years. *Applied and Environmental Microbiology* 73: 2360-2363.
- Lydolph, M.C., Jacobsen, J., Arctander, P., Gilbert, M.T.P., Gilichinsky, D.A., Hansen, A.J., Willerslev, E., & Lange, L. 2005. Beringian paleoecology inferred from permafrost-preserved fungal DNA. *Applied and Environmental Microbiology* 71: 1012-1017.
- Ozerskaya, S.M., Ivanushkina, N.E., Kochkina, G.A., Fattakhova, R.N. & Gilichinsky, D.A. 2005. Mycelial fungi in cryopegs. *International Journal of Astrobiology* 3: 327-331.
- Panikov, N.S. & Sizova, M.V. 2007. Growth kinetics of microorganisms isolated from Alaskan soil and permafrost in solid media frozen down to -35 degrees C. *FEMS Microbiology Ecology* 59: 500-512.
- Robinson, C.H. 2001. Cold adaptation in arctic and antarctic fungi. *New Phytologist* 151: 341-353.
- Shur, Y., French, H.M., Bray, M.T. & Anderson, D.A. 2004. Syngenetic permafrost growth: Crystallographic observations from the CRREL tunnel near Fairbanks, Alaska. *Permafrost and Periglacial Processes* 15: 339-347.
- Willerslev, E., Hansen, A.J. & Poinar, H.N. 2004. Isolation of nucleic acids and cultures from fossil ice and permafrost. *Trends in Ecology & Evolution* 19: 141-147.
- Zimov, S.A., Schuur, E.A.G. & Chapin, F.S. 2006. Permafrost and the global carbon budget. *Science* 312: 1612-1613.

A Web-Based Arctic Geobotanical Atlas and a New Hierarchy of Maps of the Toolik Lake Region, Alaska

D.A. Walker, H.A. Maier, and E.M. Barbour

Alaska Geobotany Center, Institute of Arctic Biology, University of Alaska Fairbanks, AK 99775, USA

Abstract

Accurate maps of arctic terrain at multiple scales are needed for spatial analyses, modeling and monitoring of permafrost responses to a changing climate. A new *Arctic Geobotanical Atlas* (AGA) is a web-based multi-scale (plant-to-planet) collection of geobotanical maps and supporting data. A new set of geobotanical maps focuses on the area around the University of Alaska's Toolik Lake Research Field Station in the vicinity of Toolik Lake Alaska, and includes the Upper Kuparuk River region (published at 1:63,360 scale), the Toolik Lake area (published at 1:20,000 scale), and a map of a 1.2-km² intensive research grid on the south side of the Toolik Lake (published at 1:5000 scale). We present an overview of the AGA and descriptions of the new maps and mapping methods.

Keywords: GIS; geomorphology; NDVI; remote-sensing; tundra; vegetation.

Introduction

Vegetation distribution is a key variable for predicting the thickness of the active layer and other properties related to permafrost. Most importantly the vegetation mat acts as an insulating blanket above the mineral soil and prevents deep heat penetration in the summer (Walker et al. 2003). Vegetation maps of CALM grids are being used for modeling active layer depths at local scales within 1-km areas (Nelson et al. 1998), and a vegetation map of the entire Kuparuk River basin was used to model regional scale patterns of active layer depth (Nelson et al. 1997, Hinzman et al. 1998). The vegetation is also strongly related to snow distribution (Evans et al. 1989), another variable that strongly influences permafrost temperatures (Zhang et al. 1997). Maps of

vegetation at several scales would be highly useful for monitoring and modeling active layer and permafrost temperatures at site and regional scales.

The Arctic Geobotanical Atlas

The Arctic Geobotanical Atlas (AGA) is a web-based archive of geobotanical maps that is being developed to aid such studies and other studies that require detail spatial information of the vegetation and other geobotanical information at several scales. The term "geobotany" refers to the science of the relationship of plants to the Earth (Rübel 1927).

The AGA contains a hierarchy of maps and supporting data at seven scales ranging from 1:10 scale (1 m² plots) of local areas near Toolik Lake and Imnavait Creek, Alaska to 1:7,500,000 scale for the entire Arctic (Fig. 1). Diverse geobotanical themes include vegetation, geology, topography, landforms, lake cover, and surficial geomorphology. Students and researchers can view thematic maps and download the data by several methods including a map server and SwathViewer software developed at the Geographic Information Network of Alaska (GINA), or they can explore the Arctic using Google Earth. They can also view and print out pdf versions of the original published maps. The map legends are linked to extended descriptions and photographs of the map units.

Other features of the AGA include: (1) an *image library* with photos of the various map units and plant species mentioned in the atlas; (2) a *map catalog* whereby users can select maps according to region of interest, scale of interest, theme or topic of interest, or year of interest; (3) a *glossary* with links to scientific terms used in the atlas; (4) a *bibliography* linked to pdf versions of the references; and (5) a *supporting data* section with links to the original plot-level vegetation and soils data used to describe the map units. The AGA currently includes maps and data from the following projects:

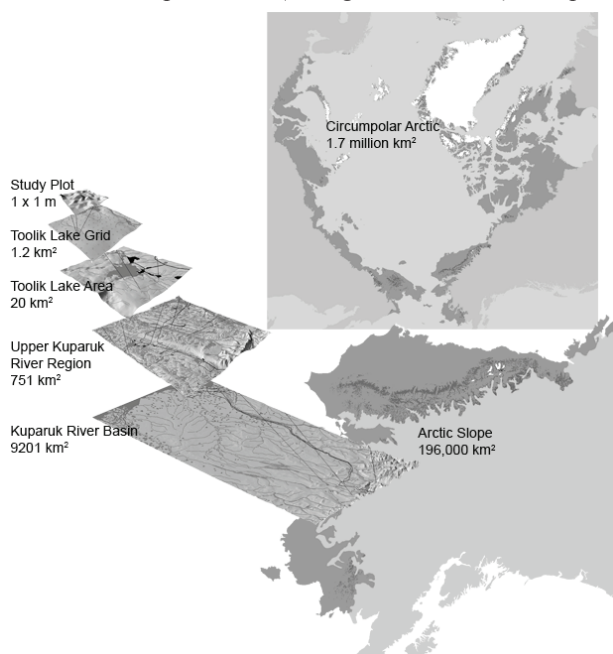


Figure 1. Hierarchy of digital elevation models for the Toolik Lake region in the AGA. Geobotanical maps of the upper Kuparuk River, Toolik Lake area, and Toolik Lake grid are presented in this paper.

Circumpolar Arctic Vegetation Map (CAVM)

The CAVM covers the global region north of the arctic treeline. It contains maps and descriptions of the vegetation, bioclimate subzones, floristic provinces, topography, landscapes, lake cover, substrate pH, and plant biomass. This section also contains an area analysis of the map by bioclimate subzones and countries (CAVM Team 2003, Walker et al. 2005).

Alaska Arctic Tundra Vegetation Map (AATVM)

The AATVM is a plant community-level map of Arctic Alaska derived from the CAVM. It portrays the dominant plant communities across all of Arctic Alaska, in contrast to the physiognomic-level mapping of the CAVM (Raynolds et al. 2006).

Toolik Lake/upper Kuparuk River basin hierarchy of maps

The Toolik Lake Field Station is a flagship US Arctic Observatory. The upper Kuparuk River basin is a key region for terrestrial arctic research associated with the station. Numerous maps have been prepared to support the research in the area, including that of the Arctic Long-Term Ecological Research (LTER) program and the Department of Energy’s R4D studies at Imnavait Creek (Reynolds & Tenhunen 1996). Several maps in the region have been published previously,

including geobotanical maps of the Imnavait Creek study areas (Walker & Walker 1996), a Landsat-derived vegetation map of the entire Kuparuk River watershed (Muller et al. 1998) and a Star3i digital elevation model of the entire Kuparuk River watershed (Nolan 2003). Here we present the maps of upper Kuparuk River region, the Toolik Lake area, and the Toolik Lake research grid (see Fig. 1).

New Maps of the Toolik Lake Area

A new set of geobotanical maps of three areas in the vicinity of the Toolik Lake Research Station have been added to the AGA. A portion of the maps will also be published as a map sheet in the Biological Papers of the University of Alaska (Walker & Maier 2008 in review). The new maps include the Upper Kuparuk River region (Fig. 2, 3) (published at 1:63,360 scale), a map of the 20 km² area surrounding Toolik Lake (Fig. 4) (published at 1:20,000 scale), and a map of a 1.2-km² intensive research grid on the south side of the Toolik Lake (Fig. 5) (published at 1:5000 scale).

Maps of the upper Kuparuk River region

The 751-km² upper Kuparuk River region has terrain typical of the southern Foothills of the Brooks Range, including landscapes affected by three major glacial events

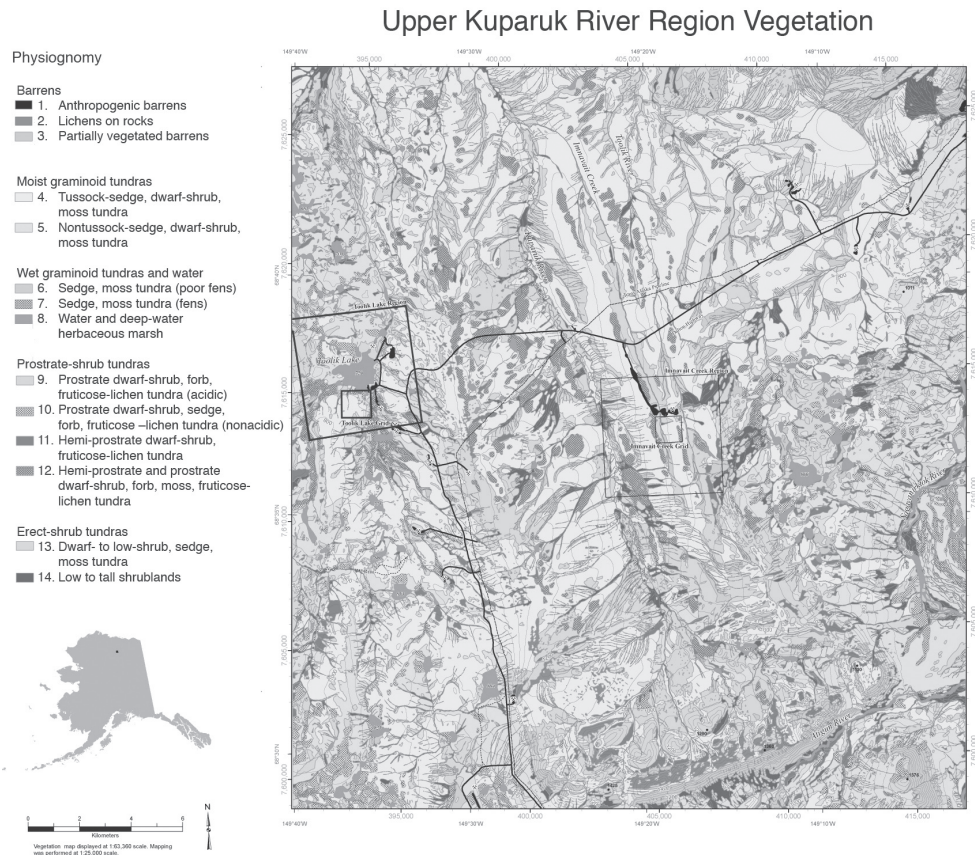


Figure 2. Vegetation of the upper Kuparuk River region. The color version of the map published at 1:63,360 scale has an expanded legend that includes dominant plant communities with GIS codes, typical microsites where each vegetation map unit is found, and area summaries for each map unit (Walker and Maier 2008). A color version also can be found at <http://www.arcticatlas.org/>. The black rectangles on the vegetation map delineate the boundaries of the Toolik Lake Area, and Toolik Lake Grid (Figs. 4, 5). The location of the mapped area is shown at actual scale as the small black rectangle on the inset map of Alaska.

(Hamilton 2003). The region includes the Toolik Lake and the Imanvait Creek research areas and a stretch of the Dalton Highway and Trans-Alaska Pipeline from the Galbraith Lake airstrip to Slope Mountain. A black and white rendition of the vegetation map of this region is shown in Figure 2.

The vegetation portrayed on the map is derived from a geobotanical database of the region. The base map for the geobotanical map was a 1:25,000-scale black-and-white orthophoto-topographic map that was prepared especially for the mapping project by Vexcel Corp., Denver, CO, in 1994 from stereo pairs of 1:60,000-scale 9 x 9-inch color-infrared aerial photographs that were obtained by NASA in 1982. The base map was prepared without ground-control points, but was registered as closely as possible to the 1:63,360 USGS map of the region. Vegetation and other geobotanical features were mapped by photo-interpretation onto 1:25,000-scale enlargements of the 1982 NASA aerial photographs.

No formal accuracy assessment was performed, but 320 of the map polygons representing 3.2% of the total map polygons, and about 16% of the total map area were checked on the ground during helicopter-assisted transects in 1994.

Geobotanical variables coded for each map polygon included: primary vegetation, secondary vegetation, tertiary vegetation, landform, surface deposit, primary surficial geomorphology, and secondary surficial geomorphology. (Secondary and tertiary types are subdominant types that cover more than 30% of a map polygon.) The geobotanical map was made using methods and legends specially developed for northern Alaska (Walker et al. 1980, 1986, 1989). The geographic information system (GIS) was developed using Arc/Info software and followed the integrated terrain-unit mapping approach (Dangermond & Harnden 1990). The resulting geobotanical maps were presented at conferences in 1996 (e.g., Walker & Walker 1996), but remained unpublished until now. In 2007 the map boundaries were modified to register with a recent digital elevation model (DEM) of the Kuparuk River region (Nolan 2003) and a 1989 SPOT image of the region. The legends were also modified to better fit the hierarchy of maps in the *Arctic Geobotanical Atlas*.

The vegetation of the region was studied and mapped as part of the Arctic Long-Term Ecological Research (LTER) project at Toolik Lake (Walker et al. 1994, Walker & Walker 1996), and the Department of Energy R4D (Response, Resistance, Resilience and Recovery of vegetation from Disturbance) project at Imnavait Creek (Walker & Walker 1996).

Fifty-seven plant communities and land-cover types were recognized during the mapping of the upper Kuparuk River region and are designated by the numeric GIS codes that are included in the expanded legend (not shown here). These were grouped into the 14 physiognomic map units shown on the map, which are compatible with the Circumpolar Arctic Vegetation Map (CAVM Team et al. 2003) and the Alaska Arctic Tundra Vegetation Map (Raynolds et al. 2006). Photos and explanations of the geobotanical mapping units and the

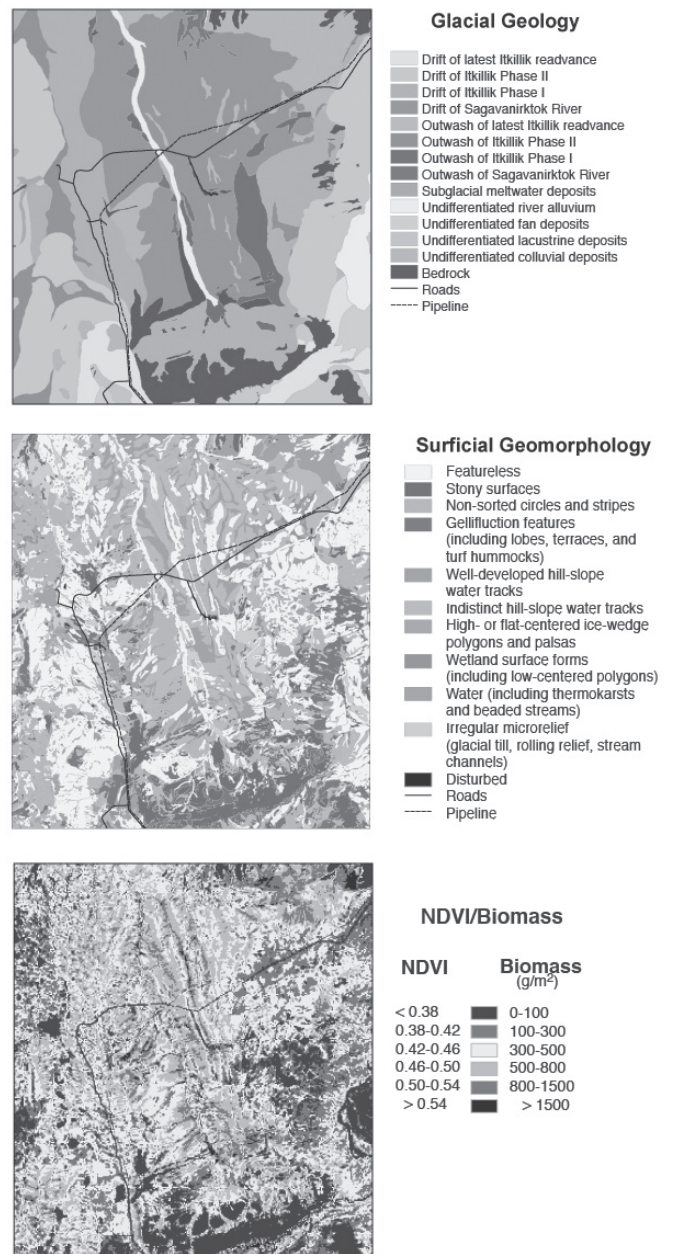


Figure 3. Glacial geology (derived from Hamilton 2003), surficial geomorphology, and NDVI/biomass (derived from Shippert et al. 1995) maps of the upper Kuparuk River region. Color versions can be found at <http://www.arcticatlas.org/>.

supporting field data and metadata can be found on the AGA web site <http://www.arcticatlas.org/>.

The other maps on the front side of the published map sheet include a false color-infrared satellite image derived from the French SPOT (Système Probatoire d'Observation de la Terre) satellite (not shown), glacial geology (Hamilton 2003), surficial geomorphology, and a map of greenness and biomass as portrayed by the Normalized Difference Vegetation Index (NDVI) (Shippert et al. 1995) (Fig. 3), all published at 1:226,576 scale.

Toolik Lake Area Vegetation

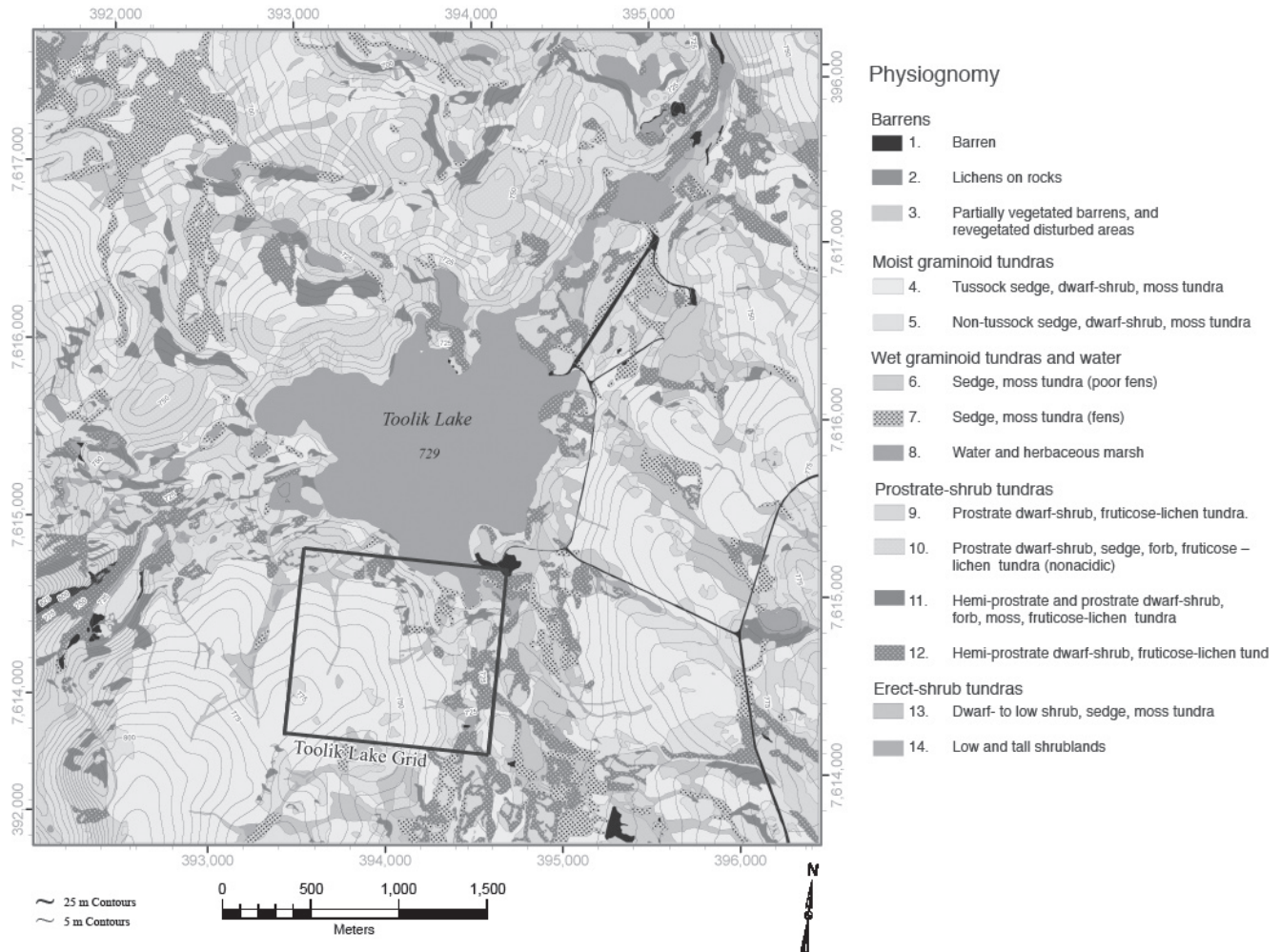


Figure 4. Vegetation map of the Toolik Lake region. The black rectangle delineates the boundary of the Toolik Lake Grid (Fig. 5). A color version can be found at <http://www.arcticatlas.org/>.

Maps of the Toolik Lake area and grid

The reverse side of the published map sheet shows more detailed vegetation maps of the 20 km² area centered on Toolik Lake (Fig. 4) and a 1.2 km² intensive research grid on the south side of Toolik Lake (Fig. 5). The Toolik Lake map includes terrain that stretches from the Dalton Highway on the east side of Toolik Lake to Jade Mountain on the west. It includes the Toolik Lake Field Station, the old pipeline construction camp pad and airstrip on the northeast side of the lake, and the primary terrestrial research areas on the south, west, and east side of the lake, as well as several smaller research lakes in the immediate vicinity of Toolik Lake. The area contains surfaces that were glaciated during the Late Pleistocene during the Itillik I and Itillik II glaciations.

The vegetation legend for the Toolik Lake area (Fig. 4) is essentially the same as for the map of the Upper Kuparuk River region but the map shows more detail corresponding to the variations in terrain. Fifty-one landcover and vegetation types were recognized in the field and later grouped into the 14 physiognomic units on the map. The units portray the physiognomy (dominant plant growth forms) of the major

plant communities in each mapped polygon.

The map of the Toolik Lake Grid (Fig. 5) focuses on the 1.1 km² research grid on the south side of Toolik Lake. This area is one of the principal intensive research areas at the Toolik Lake Field Station. It includes many experimental research sites where long-term measurements are being made, such as snow-fence study sites and greenhouse experimental sites. The grid was constructed in 1989 to provide geographic referencing for the experimental plots and to provide a sampling scheme for periodic measurements of snow, active layer, and the plant communities.

Sixty-five plant communities were recognized in the field and were then grouped into the 25 units appearing on the map. The vegetation units are primarily at the plant-community level (compared to the physiognomic level for the maps of the Upper Kuparuk River Region and the Toolik Lake region).

Details of the methods for both maps, including sources for aerial photos, orthophoto topographic map, and the other geobotanical variables that were mapped are in the Arctic Geobotanical Atlas <http://www.arcticatlas.org/>.

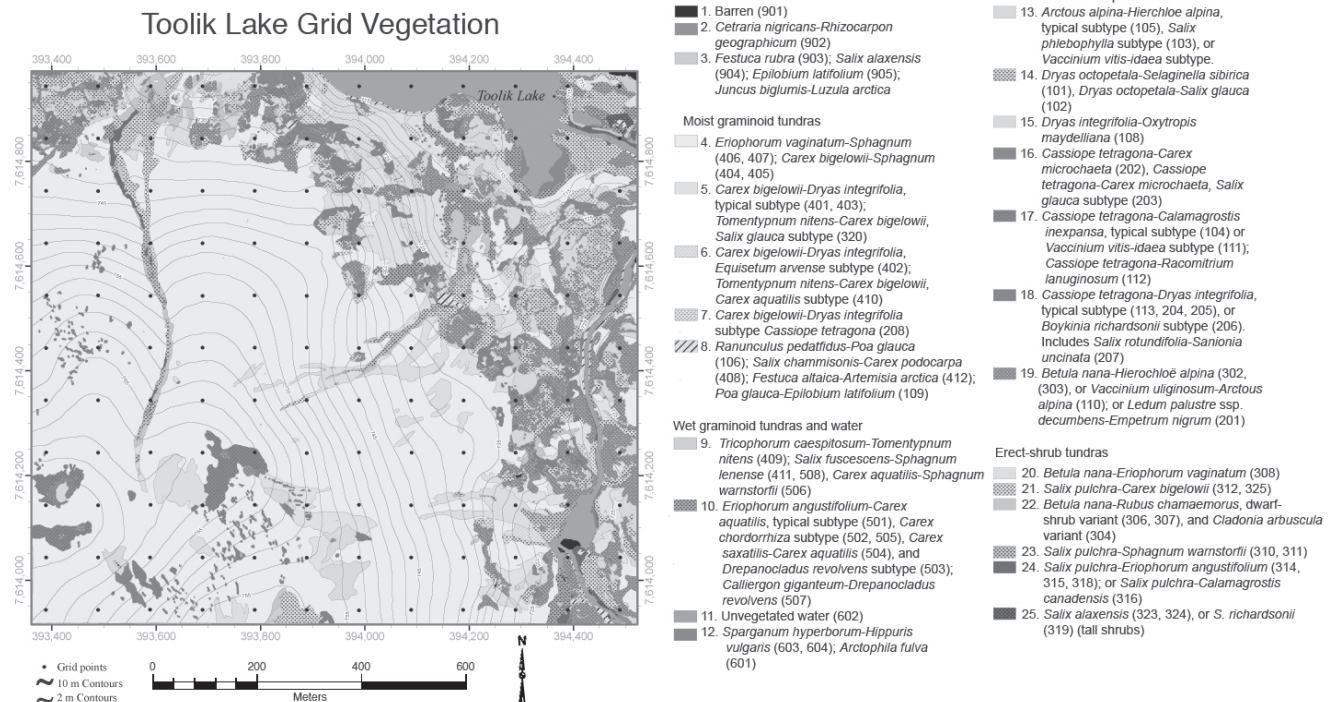


Figure 5. Vegetation map of the Toolik Lake grid. The grid points are spaced at 100-m intervals. A color version can be found at <http://www.arcticatlas.org/>. The grid is also a component of the Circumpolar Active Layer Monitoring (CALM) program (Brown et al. 2000).

Conclusion

The maps presented here lend themselves well to permafrost-related studies because of the long history of permafrost and active-layer studies in the Toolik Lake region (e.g., Osterkamp 2003, Reynolds et al. 2008 in press, Romanovsky et al. 2008, Walker et al. 2003, 2008 in press) and the clear need to conduct such studies in areas with detailed maps of vegetation, topography, and other terrain information at a variety of scales. Maps at similar scales to those presented here have been extensively for active layer studies and modeling in northern Alaska (Nelson et al. 1997, 1998, Hinzman et al. 1998). The hierarchic nature of the map legends allows results of plot-level studies conducted at Toolik Lake to be extrapolated to much broader regions up to and including the circumpolar tundra region.

Acknowledgments

The maps and website were developed at the Alaska Geobotany Center in the Institute of Arctic Biology and in collaboration with other groups at the University of Alaska Fairbanks, including: Water and Environmental Research Center, Geographic Information Network of Alaska, and Toolik Lake Field Station. Many people have helped in the production of the AGA including Nancy Auerbach, Andrew Balser, Jason Grimes, Tom Heinrichs, Julie Knudson, Leanne Lestak, Corinne Munger, Martha Reynolds, Lael Rogan, Dan Stahlke, and Scott Vockeroth. Funding for the mapping and the AGA came from the Toolik Lake LTER project, the DOE R4D program, and NSF Grants ARC-0425517, ARC-0225517, and ARC-0531180.

References

- Brown, J., Hinkle, K.M. & Nelson, F.E. 2000. The circumpolar active layer monitoring (CALM) program: research designs and initial results. *Polar Geography* 24: 165-258.
- CAVM Team. 2003. *Circumpolar Arctic vegetation map*. 1:7,500,000. Conservation of Arctic Flora and Fauna (CAFF) Map No. 1. Anchorage, Alaska. U.S. Fish and Wildlife Service.
- Dangermond, J. & Harnden, E. 1990. Map data standardization: A methodology for integrating thematic cartographic data before automation. *ARC News* 12: 16-19.
- Evans, B.M., Walker, D.A., Benson, C.S., Nordstrand, E. A. & Petersen, G.W. 1989. Spatial interrelationships between terrain, snow distribution and vegetation patterns at an arctic foothills site in Alaska. *Holarctic Ecology* 12: 270-278.
- Hamilton, T.D. 2003. *Glacial Geology of Toolik Lake and the Upper Kuparuk River Region*. Biological Papers of the University of Alaska No. 26. Fairbanks, AK: University of Alaska Printing Services.
- Hinzman, L.D., Goering, D.J. & Kane, D.L. 1998. A distributed thermal model for calculating soil temperature profiles and depth of thaw in permafrost regions. *Journal of Geophysical Research—Atmospheres* 103: 28,975-28,991.

- Muller, S.V., Walker, D.A., Nelson, F., Auerbach, N., Bockheim, J., Guyer, S. & Sherba, D. 1998. Accuracy assessment of a land-cover map of the Kuparuk River basin, Alaska: considerations for remote regions. *Photogrammetric Engineering & Remote Sensing* 64: 619-628.
- Nelson, F.E. & Hinkle, K.M. 1998. Active-layer thickness in north central Alaska: Systematic sampling, scale, and spatial autocorrelations. *Journal of Geophysical Research—Atmospheres* 103: 28,963-28,973.
- Nelson, F.E., Shiklomanov, N.I., Mueller, G.R., Hinkle, K.M., Walker, D.A. & Bockheim, J.G. 1997. Estimating active-layer thickness over a large region: Kuparuk River Basin, Alaska. *Arctic, Antarctic, and Alpine Research* 29: 367-378.
- Nolan, M. 2003. Distribution of the Star3i DEM of the Kuparuk River watershed (on CD-ROM). Boulder, CO: Joint Office of Scientific Support.
- Osterkamp, T.E. 2003. Establishing long-term permafrost observations for active layer and permafrost investigations in Alaska 1977-2002. *Permafrost and Periglacial Processes* 14: 331-342.
- Raynolds, M.K., Walker, D.A. & Maier, H.A. 2005. *Alaska Arctic vegetation map*, Scale 1:4,000,000. Conservation of Arctic Flora and Fauna (CAFF) Map No. 2. Anchorage, AK: U.S. Fish and Wildlife Service.
- Raynolds, M.K., Walker, D.A., Munger, C.A., Vonlanthen, C.M. & Kade, A.N. 2008, in press. A map analysis of patterned-ground—vegetation relationships along a North American Arctic transect. *Journal of Geophysical Research—Biogeosciences*.
- Reynolds, J.F. & Tenhunen, J.D. (eds.) 1996. *Landscape Function and Disturbance in Arctic Tundra*. Berlin: Springer-Verlag.
- Romanovsky, V.E., Marchenko, S.S., Daanen, R., Sergeev, D.O. & Walker, D.A. 2008. Soil climate and frost heave along the permafrost/ecological North American Arctic transect. *Ninth International Conference on Permafrost, Fairbanks, Alaska, June 29-July 3, 2008* (this proceedings).
- Rübel, E. 1927. Ecology, plant geography, and geobotany; their history and aim. *Botanical Gazette* 84: 428-439.
- Shippert, M.M., Walker, D.A., Auerbach, N.A. & Lewis, B.E. 1995. Biomass and leaf-area index maps derived from SPOT images for Toolik Lake and Imnavait Creek areas, Alaska. *Polar Record* 31: 147-154.
- Walker, D.A., Binnian, E., Lederer, N.D., Nordstrand, E. & Webber, J. 1989. Terrain, vegetation and landscape evolution of the R4D research site, Brooks Range Foothills Alaska. *Holarctic Ecology* 12: 238-261.
- Walker, D.A., Epstein, H.E., Gould, W.A., et al. 2008 in press. Biocomplexity of small patterned-ground features along the North American Arctic Transect. *Journal of Geophysical Research - Biogeosciences*.
- Walker, D.A., Everett, K.R., Webber, P.J. & Brown, J. 1980. *Geobotanical Atlas of the Prudhoe Bay Region, Alaska*. CRREL Report 80-14. U.S. Army Cold Regions Research and Engineering Laboratory.
- Walker, D.A., Jia, G.J., Epstein, H.E., Raynolds, M.A., Chapin III, F.S., Copass, C.D., Hinzman, L., Knudson, J.A., Maier, H., Michaelson, G.J., Nelson, F., Ping, C.L., Romanovsky, V.E. & Shiklomanov, N. 2003. Vegetation-soil-thaw-depth relationships along a low-arctic bioclimate gradient, Alaska: synthesis of information from the ATLAS studies. *Permafrost and Periglacial Processes* 14: 103-123.
- Walker, D.A. & Maier, H.A. 2008. *Geobotanical Maps in the Vicinity of the Toolik Lake Field Station, Alaska*. Biological Papers of the University of Alaska, No. 28.
- Walker D.A., Raynolds M.K., Daniëls F.J.A., et al. 2005. The circumpolar Arctic vegetation map. *Journal of Vegetation Science* 16: 267-282 + appendices.
- Walker, D.A., & Walker, M.D. 1996. Terrain and vegetation of the Imnavait Creek Watershed. In: J.F. Reynolds & J.D. Tenhunen (eds.), *Landscape Function and Disturbance in Arctic Tundra*. Berlin: Springer-Verlag, 73-108
- Walker, D.A., Weber, P.J., Walker, M.D., Lederer, N.D. & Meehan, R.H. 1986. Use of geobotanical maps and automated mapping techniques to examine cumulative impacts in the Prudhoe Bay Oilfield, Alaska. *Environmental Conservation* 13: 149-160.
- Walker, M.D., Walker, D.A. & Auerbach, N.A. 1994. Plant communities of a tussock tundra landscape in the Brooks Range Foothills, Alaska. *Journal of Vegetation Science* 5: 843-866.

Lake Modification in a Permafrost Region, the Colville River Delta, Alaska

H. Jesse Walker

Louisiana State University, Baton Rouge, USA

Abstract

The Colville River Delta, like most deltas of the world, contains a variety of lakes. They range in size from small ponds (less than 0.0125 km² in area) that occupy low-centered ice-wedge polygons to large lakes (five of which are larger than 2.0 km²) that occupy abandoned river channels. As the delta's distributaries migrate, they not only destroy ice wedges and the polygons the ice wedges helped create, but also tap lakes causing them to drain. After tapping, lakes become sedimentary traps and subject to rapid fill. Not all tapping is the result of the river, because the lakes themselves (especially the larger ones) tend to expand with time due to the physical and thermal erosion of their banks. Lake expansion into an ice-wedge polygonal field results in the melting of adjacent ice wedges, the production of an inverted relief and a serrated lake border.

Keywords: delta; erosion; flooding; ice wedge; lakes; permafrost

Introduction

The North Slope of Alaska extends from the crest of the Brooks Range northward to the Arctic Ocean. It is a part of the area dominated by continuous permafrost and has a surface much of which is covered with lakes and ice-wedge polygons. It drains into the Arctic Ocean via a number of rivers, the longest of which is the Colville River (Fig. 1). At its mouth the Colville has constructed a delta that is about 600 km² in area (Fig. 2). The delta supports a variety of forms many of which are similar to their counterparts in more temperate regions. However, most of these deltaic forms are impacted by snow, ice, and permafrost in addition to the typical processes, such as those caused by wind and river flow, dominating elsewhere.

The Delta's Lakes

Unlike on the general tundra surface of the North Slope where oriented lakes are common, the delta has a highly varied lake system. The delta's lakes range in size from small ponds to those that are more than 2 km² in area (Fig. 3) and in shape from circular and rectangular to sinuous and elongated. They vary in depth from a few centimeters to more than 10 m. Those that are deeper than 2 m usually do not freeze to the bottom during winter and have a permafrost-free zone (talik) beneath them. The delta's lakes vary in age from newly formed to some that have lasted hundreds

of years, and they also vary in genesis from those formed in association with ice-wedge polygons and sand dunes to those resulting from river channel migration.

Basically all of the delta's lakes are ephemeral because of the continuous migration of the delta's distributaries which not only aids in the creation of lakes but inevitably leads to their destruction.

The types and distribution of lakes within the Colville Delta

The lakes and ponds of the delta exhibit a variety of types including ice-wedge polygons, abandoned channels, terrace flank depressions, and ice-scour holes (Dawson 1975). The most common are those ponds that occupy low-centered polygons. They are present on most surfaces except newly deposited areas such as sandbars and mudflats. Many of the delta's lakes fit into the thaw-lake category in that they

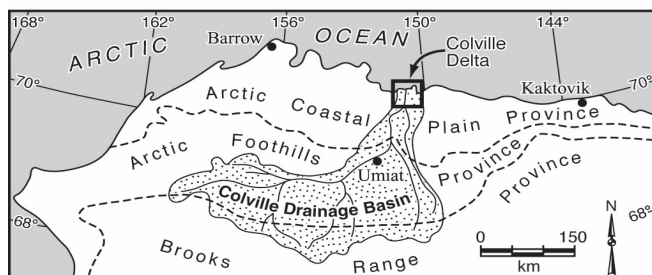


Figure 1. Regional map of the North Slope, Alaska, showing the Colville River Basin and Delta.

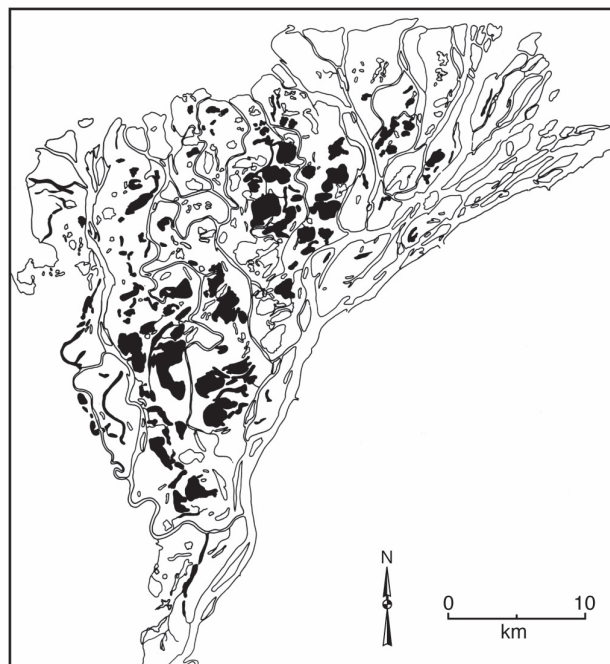


Figure 2. The Colville River Delta showing lake distribution. Those lakes subject to flooding are in black.

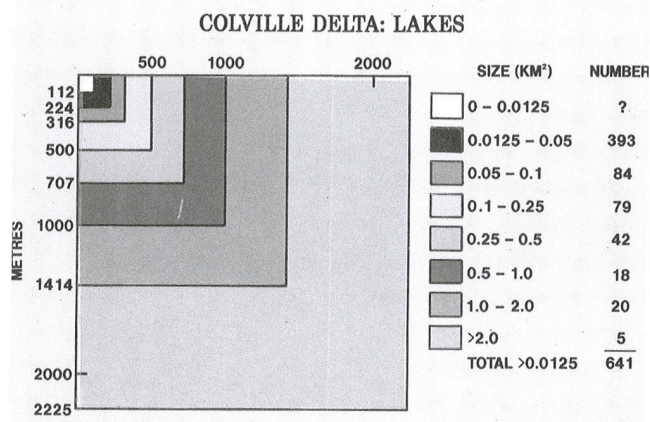


Figure 3. The numbers and sizes of lakes in the Colville River Delta.

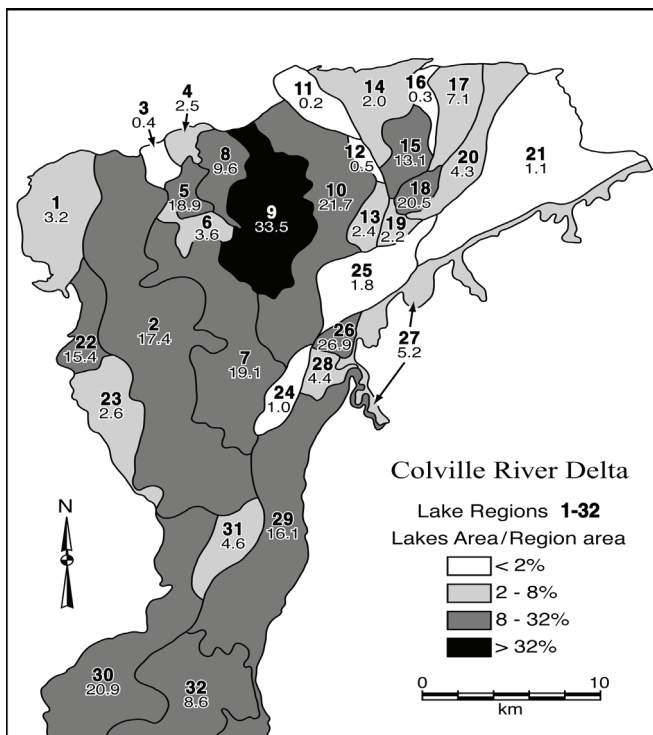


Figure 4. A regional map of the Delta's lakes with percentage of surface area occupied by lakes with areas more than 0.0125 km².

exhibit subsidence following the thawing of permafrost (Hopkins 1949, Jorgenson & Shur 2007).

Although the most distinctive characteristic of the delta is often considered to be its lakes, there is great variation in their occurrence within the delta (Fig. 4). The area with the most lake coverage is a north-south band through that part of the delta impacted by meandering distributaries, whereas the least coverage is especially in the northeast part of the delta which is characterized by braided drainage.

Perched Ponds and the Active Layer

One of the characteristics of permafrost is that it prohibits percolation and thus, under the right conditions, can serve as an aquiclude. The Colville River Delta with its varied relief

provides a number of situations where perching can occur. The best examples are found within sand dune complexes throughout much of the delta. However, in a sense, the ponds present in low-centered polygons (especially those near a river channel) are perched in that they are perennial lakes with a surface level lying at an elevation above what would be the normal level of the water table in a permafrost-free environment.

Within the Colville Delta, local relief is more varied within sand dune complexes than elsewhere. Further, the delta is an ideal location for the formation of dunes because of the extensive sandbars that form along its channels. This is especially true of the main channel on the east side of the delta. Because the prevailing wind is from the northeast, dunes are best developed in left-bank locations. Dunes nearest the river channel tend to be active, whereas those away from the bank are usually stable and are covered with vegetation. Stabilized dunes, over time, become rounded and smooth, a type of relief that does not favor pond formation. Active dunes on the other hand have a varied relief that often provides ideal conditions for pond formation.

The dunal systems of the delta provide two types of perching: inter-dune and intra-dune ponds. Inter-dune ponds form between dune ridges, whereas intra-dune ponds form within dune ridges. During several field seasons in the 1960s and 1970s, detailed studies of inter-dune ponds were made (Walker & Harris 1976).

The pond selected for repetitive measurements (including active layer thickness and water stage and temperature) is near a field camp on Putu Channel, 3 km north of the head of the delta (Fig. 5). Putu Pond, as we named it, lies in an elliptical basin that is about 96 m long and 31 m wide (Fig. 6, 7). The pond at its maximum extent, which occurs during the snowmelt period, has an area of about 300 m² and a depth of 1.3 m. The lowest edge of the basin is about 6 m above the mudflat of Putu Channel, an ideal perching situation. The vegetation in the basin includes a variety of aquatic plants, moss, grasses, flowering plants, and willows that are up to 2 m tall. However, the steep sides of the dune are vegetation free and composed of coarse-textured sand.

During most of the year the area is blanketed with snow, which in the basin itself is several meters thick. The lake freezes to the bottom, and the active layer is frozen for some 7 to 8 months. Although wind, even during winter, removes snow from the crest of the dune, the snow in the basin remains intact until snowmelt begins. The rate of snowmelt varies; snow in the willows lasts much longer than it does elsewhere in the basin. Measurements indicated that active layer thaw began almost immediately after snowmelt exposed the surface. The actual deepening of the active layer varied mainly because of the nature of the vegetation cover (Fig. 8).

Once the active layer begins to thaw, percolation occurs through the coarse sand that makes up the riverbank. Thus during the short summer period, the lake not only lost water to evaporation but also to percolation. However, the lake was sufficiently deep so that it has never dried up.

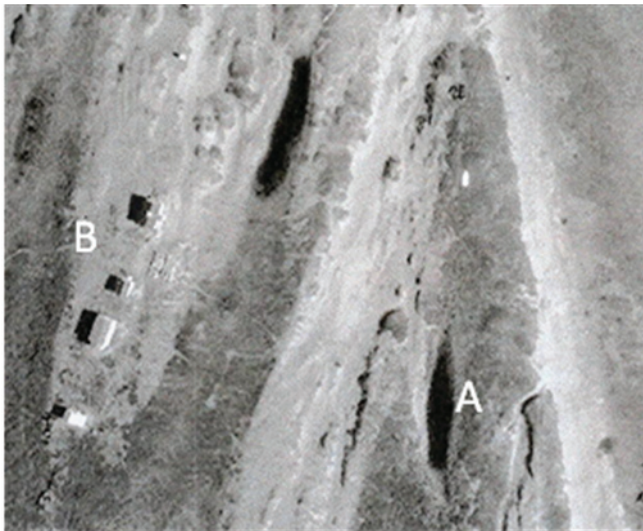


Figure 5. Air photograph of perched lakes in sand dunes at Camp Putu. A. Lake Putu, B. Research cabins.



Figure 6. Ground-level photograph of Lake Putu. Scale is shown in Figure 7.

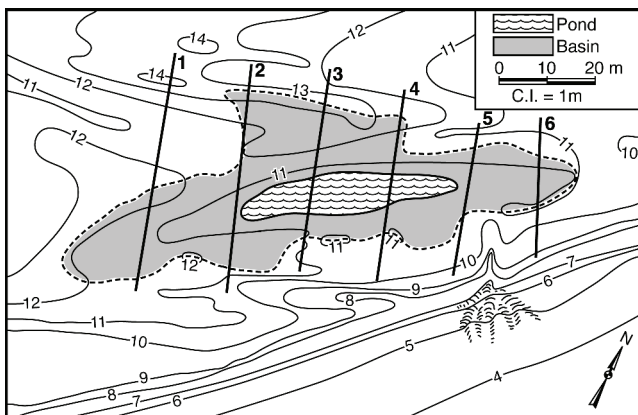


Figure 7. Map showing characteristics of Lake Putu. Lines 1 – 6 are basin transects.

Although perched ponds are less common in stabilized dunes than in active dunes, a few can be found in the delta (Fig. 9). It is not known what initiated the pond illustrated in Figure 9; however, some such ponds begin as blowouts, possibly when ground squirrel dens have been enlarged by bears. Once initiated, thermal degradation increases the pond's depth due to subsidence.

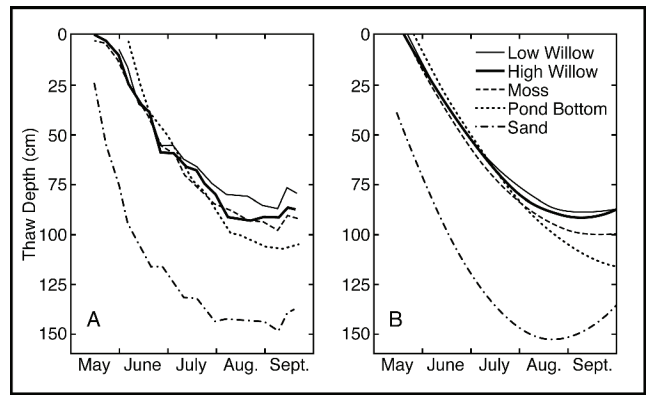


Figure 8. Seasonal development of active layer during 1973 of Lake Putu. A. Actual measurements, B. Calculated trends.

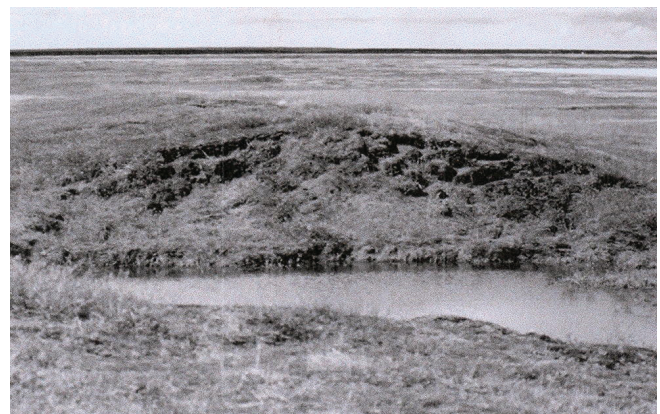


Figure 9. Photograph of intra-dune pond.

Ice Wedges and Lake Expansion

Many of the lakes in the Colville Delta are bordered by ice-wedge polygons which are subject to erosion by wind-generated waves, ice scour, and temperature-induced thaw. These processes are much less active than those accompanying a flooding river so that lake-bank retreat, even in the larger lakes, is relatively small. Another difference is that the eroded or thawed materials from a lake's shoreline remain in the lake. In Figure 10, the importance of wind-wave erosion is demonstrated by the repetitive saw-like form of the irregular shoreline. The predominating northeast wind causes wave action, which thermally erodes the ice-wedge polygons along the shoreline. The resulting form contrasts with that of the relatively smooth channel shoreline (Fig. 10).

Many of the low-center polygons that surround lake basins have water levels that are lower than lake levels. When the ice wedges facing the lakes melt and the ridges around the polygons collapse, lake water invades creating an inverted relief with a highly irregular bench around the lake margin (Fig. 11).

Expansion of lakes by physical and thermal erosion frequently results in the elimination of barriers between adjacent lakes so that they join. The resulting combination often produces a lake that has an irregular shape.

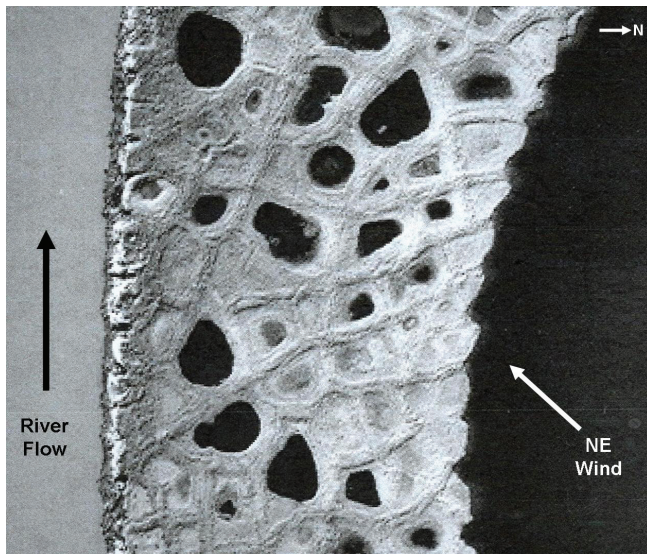


Figure 10. A 1981 air photograph of the upper Nechelik Channel and an adjacent lake illustrating the contrast between river and lake shorelines.

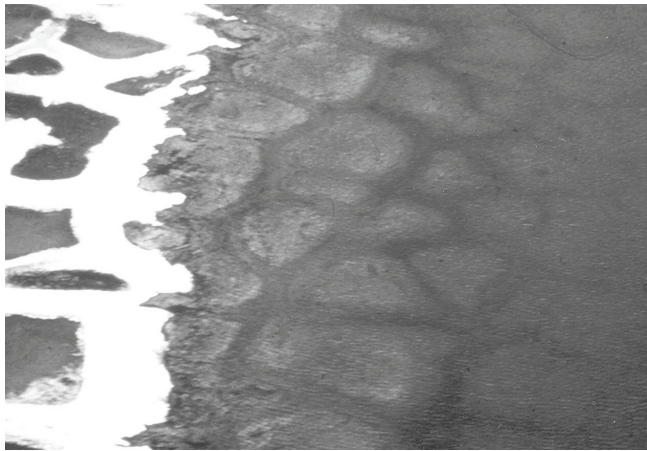


Figure 11. Photograph of the inversion of shoreline relief as ice wedges melt.



Figure 12. Photograph of the erosion and drainage of ice-wedge polygons.

Lake Tapping

One of the most distinctive changes in delta morphology occurs because of the tapping or breaching of lakes by migrating river channels. An examination of the delta's

shorelines in 1971 (Ritchie & Walker 1974) showed that 59% are erosional, 35% are depositional, and 6% are neutral. Rates of retreat vary from an average of a fraction of a meter to two or more meters per year (Walker et al. 1987). In the process not only are the materials of which the banks are composed removed, but any ponds or lakes that the banks previously protected are breached. If the river banks are high and the lakes (usually ice-wedge polygons) are perched at the top above floodwater level, bank erosion, especially via ice wedges, causes the ponds to drain (Fig. 12). Often within peat banks, ice-wedge melting progresses inward from the bank, draining additional ponds (see McGraw, this Proceedings).

Once tapping occurs, lake drainage follows and the former lake level, if the lake bottom is below the level of the river, subsequently fluctuates with river stage. It then serves as a settling basin and begins to fill with the sediment transported into it by the river. The coarsest material is deposited near the lake entrance, and the fines are spread throughout the lake basin. The nature of the deposition is such that the lake basin becomes segmented as it fills. As the river continues to erode lakeward, the entrance channel is enlarged and the near-river deposits begin to be eroded.

Another morphologic/hydrologic change that occurs with lake tapping is the creation of a scour hole at the entrance to the lake. These scour holes as well as lake morphology changes are illustrated in the discussion below of Lake Nanuk (Polar Bear), Lake Tuttut (Caribou), and Lake 35.

Within the delta there are examples of virtually every stage in the life history of tapped lakes from those recently tapped to those nearing complete destruction.

Lake Nanuk and Lake Tuttut

Lake Nanuk (Polar Bear Lake) and Lake Tuttut (Caribou Lake) were two of the delta's largest lakes until they were tapped by migrating river channels (Roselle 1988). Lake Nanuk faced the Nechelik Channel whereas Lake Tuttut, which is just east of Lake Nanuk, faced Sakoong Channel. It is not known just when Lake Nanuk was tapped, but it was probably in the late 1930s or 1940s based on the width of the entrance channel and the smallness of the lake delta displayed on 1948 photographs. In contrast, however, Lake Tuttut was tapped in 1971 at the time a field crew was working in the delta (Fig. 13).

Subsequent to tapping, two major events occurred: the lakes began to fill with sediment and the entrances began to enlarge. Because Lake Nanuk faces a channel that carries (at least during flood) some 25% of the delta's discharge it is filling at a much more rapid rate than Lake Tuttut whose facing channel only carries about 2% (Arnborg et al. 1966). Although the low-water stage of Lake Tuttut displays extensive bottom material, most of it is the result of the fact that it was sufficiently shallow to begin with so that once drainage occurred bottom materials became exposed.

In 1962, depth measurements were made by boat in Lake Nanuk between its southern- and northern-most points, a condition that today, because of this shallow depth, would be

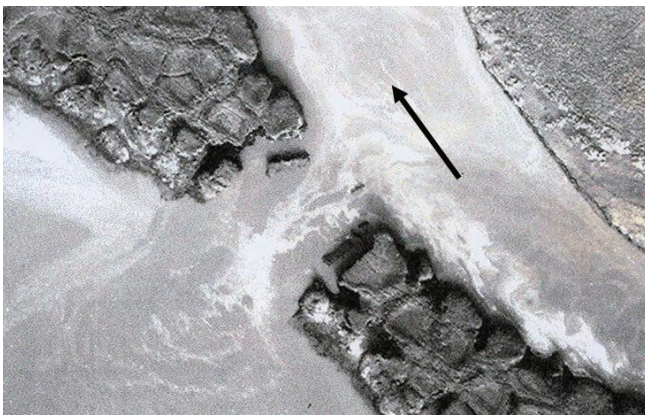


Figure 13. Photograph of Lake Tutnut entrance.

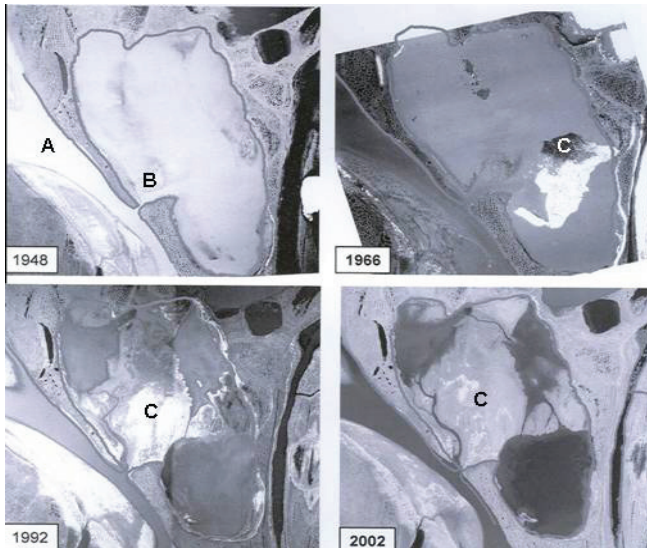


Figure 14. The depositional sequences in Lake Nanuk from 1949 to 2002. A. River channel, B. Lake entrance, C. Lake deposits.

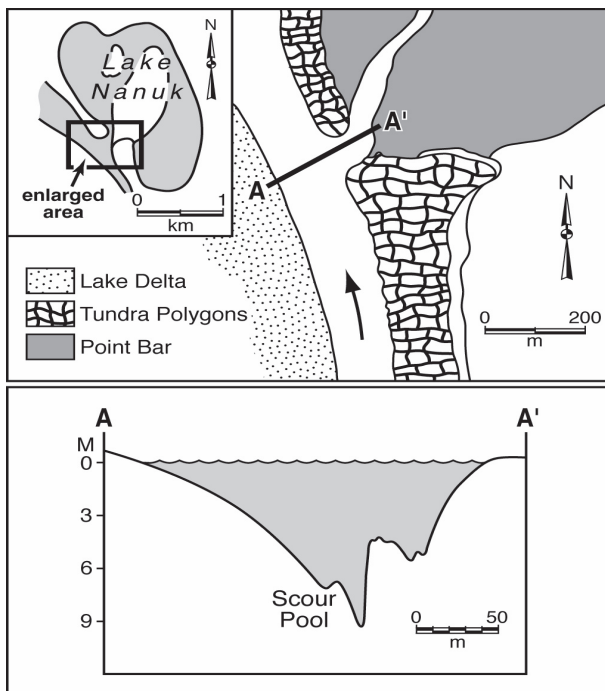


Figure 15. Scour hole at Lake Nanuk's entrance.

impossible (Fig. 14). In addition to showing the amount of fill that has occurred during the past 70 or so years, Figure 14 also shows the evolution of the entrance (also exit) channel with time. Such a long, winding channel is a typical feature of tapped lakes after they begin to fill. The channel in Lake Tutnut shows the same feature.

Upon tapping, lakes, most of which have levels some 2 m above normal river level, drain rapidly enlarging the opening and developing a scour hole at their mouths (Fig. 15).

Lake 35

Lake 35 (the number given the lake in a catalog of lakes made in the 1970s) is located in the northcentral part of the delta (Walker 1978). The changes that have occurred through the tapping of Lake 35 are among the most distinctive changes to have happened in the delta in the last century. The changes include not only the development of a scour hole, the exposure of shallow bottom areas, the creation of a lake delta, and widening of the inlet (outlet), but also the addition of other lakes to the system and the rearrangement of river channel flow. These changes are diagrammed in Figure 16. The locations of the changes that are discussed below are indicated by the letters A, B, and C in Figure 16:1.

When the first air photos of the delta were made, Lake 35 and its adjacent lakes were essentially distinct and not impacted by the river, even during flood stage (Fig. 17). The exact dates of the initiation of various events are unknown because their recognition depends on the dates of photo coverage or field observation. Although, in 1949 there was some overflow and percolation along ice wedges between some of the lakes, the first major change was the tapping of Lake 35 a few years before 1970. By 1971 a small delta had formed, and at low water a bench was visible along both the south and north sides of the lake.

By 1981 (Fig 16:2) the adjacent lakes were all connected by irregular water courses through ice-wedge polygons as

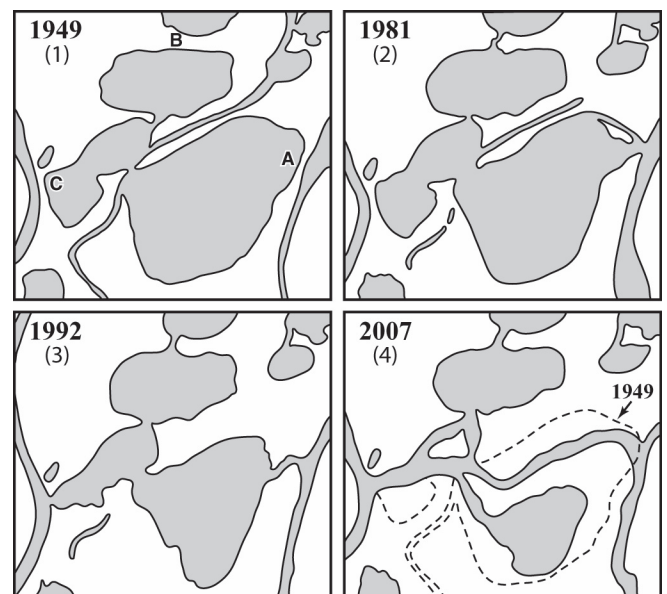


Figure 16. The modification of Lake 35 between 1949 and 2007, explanation in the text.

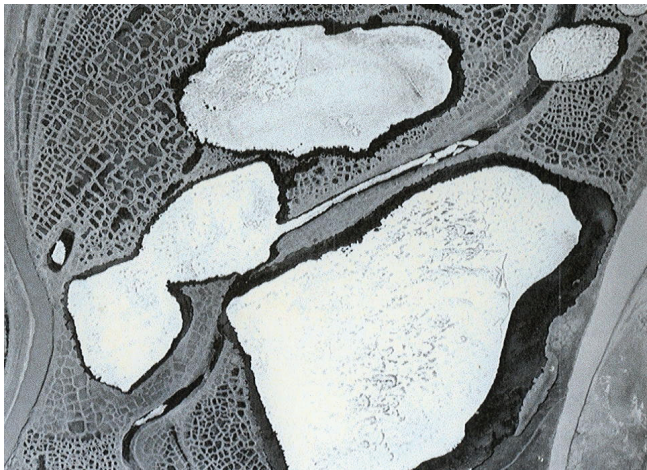


Figure 17. Lake 35 prior to tapping (See Fig. 16:1 A).

exampled at Figure 16:1 B, the lakes were still distinctive, the exposed shore areas around Lake 35 had expanded, and Lake 35's delta had shifted northward.

Eleven years later (Fig. 16:3) tapping had occurred at location C. It appears that, in this case, much of the erosion that caused the rupture was the result of floodwaters flowing through Lake 35 from east to west. Further, by this time, deposition in Lake 35 had reduced the actual water surface to less than half its original size.

The impact of this flow from east to west continued to increase so that by 2007 (Fig. 16:4), Lake 35 had become channelized. Because so much water and sediment was now being carried toward the west, the original distributary that caused the initial tapping some 40 years earlier ceased flowing north at low stage.

Conclusions

Although there are other types of lakes and ponds in the delta, such as those formed as toeheads at channel bifurcation points, the most distinctive relationships between permafrost and ice wedges with lakes are those associated with perching and ice-wedge polygons and with the processes of riverbank and lake bank erosion.

Lake tapping not only alters a lake's morphology, but also, through deposition, creates ideal conditions for former taliks to become frozen and for new sets of ice-wedge polygons to develop.

Acknowledgments

The research for this paper, which is based in part on field work conducted in the Colville River Delta since 1961, was supported by a number of organizations both financially and logistically. Included are: ONR, AINA, the North Slope Borough, the town of Nuiqsut, ARCO, Conoco Phillips, ABR, and Louisiana State University. To all of them, I extend my thanks. The assistance of Molly McGraw, Clifford Duplechin, and Mary Lee Eggart, and the suggestions made by two anonymous reviewers are much appreciated.

References

- Arnborg, L., Walker, H.J. & Peippo, J. 1966. Water discharge in the Colville River, 1962. *Geografiska Annaler* 48: 195-210.
- Dawson, A.G. 1975. *Landforms of the Colville River Delta, Alaska, as Interpreted from Aerial Photographs*. Unpublished thesis, Louisiana State University, 93 pp.
- Hopkins, D.M. 1949. Thaw lakes and thaw sinks in the Imuruk lake area, Seward Peninsula, Alaska. *Journal of Geology* 57: 119-131.
- Jorgenson, M. T. & Shur Y. 2007. Evolution of lakes and basins in northern Alaska and discussion of the thaw lake cycle. *Journal of Geophysical Research-Earth Surface* 112 (F2): F02S17.
- McGraw, M. 2008. The degradation of ice wedges in the Colville River Delta and their role in pond drainage. *Proceedings of the Ninth International Conference on Permafrost*, Fairbanks, Alaska.
- Ritchie, W. & Walker, H. 1974. Riverbank forms of the Colville River Delta. In: J.C. Reed & J.E. Sater (eds.), *The Coast and Shelf of the Beaufort Sea*. Washington, D.C.: The Arctic Institute of North America, 545-562.
- Roselle, D.L. 1988. *Morphology and sedimentation of Arctic tapped lakes*. Unpublished thesis, Louisiana State University, 109 pp.
- Walker, H.J. 1978. Lake tapping in the Colville River Delta, Alaska. In: R.J.E. Brown, *Proceedings, Third International Conference on Permafrost*. Ottawa, National Research Council of Canada, 233-238.
- Walker, J., Arnborg, L. & Peippo, J. 1987. Riverbank erosion in the Colville Delta, Alaska. *Geografiska Annaler* 69A: 61-70.
- Walker, H. & Harris, M. 1976. Perched ponds: An arctic variety. *Arctic* 29: 223-238.

Submarginal Glaciotectonic Deformation of Pleistocene Permafrost

Richard Waller

Research Institute for the Environment, Physical Sciences & Applied Mathematics, Keele University, Staffordshire, U.K.

Julian Murton

Department of Geography, University of Sussex, Brighton, U.K.

Colin Whiteman

School of Environment and Technology, University of Brighton, Brighton, U.K.

Abstract

Recent advances in our understanding of glacier-permafrost interactions provide an alternative hypothesis to interpret Pleistocene glaciotectonic sequences in regions where permafrost no longer exists. Instead of necessarily forming under unfrozen subglacial conditions, some glaciotectonic sequences may have formed by submarginal deformation of warm, partially-frozen permafrost. An example from North Norfolk, U.K., suggests that an ice sheet during Marine Isotope Stage 12 advanced across permafrost terrain, deforming it beneath the margin. Such a scenario can help explain some features whose formation under unfrozen conditions is problematic, including (1) the substantial thickness of the deforming layer and (2) the preservation of stratified intraclasts. Accordingly, glacial geologists should remain open to the possibility of glacier-permafrost interactions when interpreting glacial sequences. Such a re-interpretation could have major implications for reconstructing basal thermal regimes and modeling palaeo-ice sheets.

Keywords: basal thermal regime; eastern England; glacier-permafrost interaction; glaciotectonic deformation; Pleistocene permafrost.

Introduction

Whilst the ability of glaciers to deform their substrates has long been recognized (Lamplugh 1911), the glaciological significance of glaciotectonic deformation was not fully appreciated until the late 1970s (e.g., Boulton & Jones 1979). Since then, numerous papers have inferred the process at many Pleistocene localities and demonstrated its widespread occurrence beneath former continental ice masses (e.g., Hart et al. 1990, Clark 1994, Benn & Clapperton 2000). In addition, it has been invoked to explain states of fast ice flow (e.g., Hart & Smith 1997, Truffer et al. 2000), ice streaming (Alley et al. 1986), high sediment fluxes (Dowdeswell & Siegert 1999), and the creation of distinctive glacial landforms and sediments (Boulton 1987, Benn & Evans 1996).

The majority of this research has assumed that sediment deformation only occurs beneath warm-based ice, when subglacial sediments are unfrozen and water-saturated. This stems from the widespread assumption that basal processes are inactive at subfreezing temperatures (e.g., Paterson 1994) and by inference that cold-based glaciers are slow moving and geomorphologically ineffective (Kleman 1994). Recent research has demonstrated, however, that cold-based glaciers can slide over and deform their beds (Echelmeyer & Zhongziang 1987, Cuffey et al. 1999) and therefore actively erode and deposit (Atkins et al. 2002). This conclusion is supported by work in high-latitude Pleistocene glacial environments where thick sequences of deformed permafrost provide evidence of extensive glacier-permafrost interaction beneath former ice sheets (Mackay et al. 1972, Astakhov et al. 1996, Murton et al. 2004).

Whilst the implications of glacier-permafrost interactions are being explored within glaciology (e.g., Cutler et al. 2000), little attempt has been made to consider their

potential implications for interpreting Pleistocene glacial sequences. But if we consider deformation under partly-frozen conditions as an alternative hypothesis, it may help to explain features difficult to reconcile with deformation under entirely unfrozen conditions.

We suggest here that submarginal deformation of permafrost can help to explain key aspects of the well-known glaciotectonic sequences of North Norfolk, U.K.

Processes and Products of Subglacial Sediment Deformation

Whilst the importance of subglacial sediment deformation is widely acknowledged by glaciologists and glacial geologists, the identification of an appropriate flow law for subglacial tills remains elusive and controversial. To date, four flow laws have been applied to subglacial sediment rheology: (1) linear viscous, (2) non-linear viscous, (3) non-linear Bingham, and (4) Coulomb-plastic (Kavanaugh and Clarke 2006). Models one to three consider tills as viscous fluids. In model one, the strain rate is linearly related to the shear stress, and the till viscosity is independent of porewater pressure. Models two and three are both non-linear, with porewater pressure determining the till's shear resistance, and the latter incorporating a yield strength determined by the Mohr-Coulomb failure criterion (Boulton & Hindmarsh 1987). Model 4 differs from the first three models in that it treats tills as plastic materials, with no permanent deformation occurring until a yield strength (again based on the Mohr-Coulomb failure criterion) is surpassed, after which they experience infinite strains. The choice of flow law is highly significant, as it represents a key control on the dynamic behavior of glaciers and ice sheets. However, there is currently conflict between the strong evidence for

the Coulomb-plastic model derived from studies at modern-day glaciers and the geological evidence for the viscous fluid models, illustrated by contrasting deformation profiles.

Initial research at modern-day glaciers suggested that subglacial tills behaved like viscous fluids, with both field measurements (Boulton & Hindmarsh 1987) and geophysical data (Alley et al. 1986) suggesting that subglacial sediments deformed pervasively in layers several metres thick. Subsequent work, however, has favoured a Coulomb-plastic rheology, with new observations and borehole measurements suggesting that subglacial sediment deformation is restricted to thin shear zones only a few tens of centimetres thick (e.g., Iverson et al. 1995; Engelhardt & Kamb 1998; Fuller & Murray 2002). For example, recent work by Kavanaugh & Clarke (2006) at the Trapridge Glacier, British Columbia, concluded that the Coulomb-plastic model provided the closest match to the field instrument records. The model, in turn, predicted a deformation depth of 0.35 m, in close accordance with the measured depth of ~0.3 m.

Geological evidence has also been widely employed, both to infer the existence of subglacial sediment deformation beneath former ice sheets and to reconstruct the sediment deformation profile. Cited evidence includes a range of structures that belie varying amounts and styles of deformation involving both ductile and brittle failure (see Hart 1995, Boulton et al. 2001, & Evans et al. 2006 for lengthier reviews). At low strains, folds are commonly developed where compression occurs on the up-glacier flank of an obstacle. As shear strains increase, the folds are progressively attenuated and boudinaged, which can generate a tectonically-laminated deposit, which in turn can later be re-folded. The shearing can affect pre-glacial materials to generate glaciectonites (Banham 1977). Ultimately, high strain deformation can homogenize sediments and form so-called deformation tills (Benn & Evans 1996); in this case, clast fabrics (van der Meer 1993, Hart 1994) and micro-scale structures provide the only evidence of the sediment's strain history, although the ability of the former to infer strain history remains controversial (Benn 2007).

Geological evidence has frequently been used to infer pervasive deformation within a deforming layer several metres thick (e.g., Hart et al. 1990, Alley 1991), supporting a viscous fluid model of till rheology. But such a conclusion is increasingly difficult to reconcile with the results of field-based investigations at modern-day glaciers. Whilst this paradox has been used to argue that subglacial deformation is less extensive or deep-seated than originally thought (e.g., Piotrowski et al. 2001), this paper considers an alternative hypothesis, that the geological evidence may instead indicate subglacial deformation under contrasting thermal conditions.

Glaciotectonic Deformation of Permafrost

The deforming-bed model was originally limited to the situation where warm-based glaciers overlie thawed beds (see Alley 1991). Consequently, ice-sheet models commonly include the boundary condition that basal velocities are zero where the temperature of the basal ice falls below the pressure melting

point (e.g., Payne 1995). There is growing evidence, however, that this assumption is not universally applicable. Echelmeyer & Zhongxiang (1987), for example, found that over 60% of the surface motion of the cold-based Urumqi No. 1 Glacier in China was accommodated via the deformation of ice-rich subglacial sediment with an effective viscosity two-orders of magnitude lower than the overlying ice. This demonstrates the ability of glaciers to couple with subglacial permafrost.

Permafrost that has never thawed since it was overridden and deformed by Pleistocene ice sheets provides an important touchstone for interpreting glaciotectonic sequences in regions where permafrost no longer exists. Previous work has highlighted evidence for glacier-ice thrusting near the northwest limit of the Laurentide ice sheet in western Arctic Canada (Mathews & Mackay 1960, Mackay et al. 1972), and for a deformable bed of permafrost beneath the southern Kara ice sheet in western Siberia (Astakhov et al. 1996). More recently, we have detailed the stratigraphy and glaciotectonic structures of permafrost in the Tuktoyaktuk Coastlands of western Arctic Canada (Murton et al. 2004). Several important observations arise from these studies.

First, the thickness of glaciotectonically-deformed permafrost is substantial. Astakhov et al. (1996) reported thicknesses of tens of metres from the western Yamal Peninsula and the lower Yenisei region, and Murton et al. (2004) reported thickness of at least 5–20 m from the Tuktoyaktuk Coastlands (Fig. 1a, 1b). Second, ductile deformation of warm, ice-rich materials is inferred from recumbent and S-shaped folds, sand lenses and layers (Fig. 1c), whereas there is less evidence for brittle failure in the form of pinch-and-swell structures and ice-filled tension gashes. Third, submarginal erosion of permafrost is indicated by (1) incorporation of rafts of massive ice (Fig. 1d) and smaller ice clasts into frozen glaciectonite (Fig. 1b), and (2) angular unconformities (décollement surfaces) beneath the glaciectonite (Fig. 1a). Adjacent layers of frozen silt, clay, and sand have deformed around some ice clasts, giving the latter the misleading appearance of 'dropstone-like' structures. Overall, the permafrost was probably warm, ice-rich, and contained limited amounts of liquid water – a type of easily deformable permafrost termed 'plastic frozen ground' (Tsyrovich 1975).

A Reconsideration of the Glaciotectonic Sequences of North Norfolk

The coastal cliffs of northeast Norfolk exhibit a complex sequence of glacial sediments (e.g., Lee et al. 2004). Banham (1968, 1977, 1988) recognized evidence for glaciotectonic processes, a conclusion supported by Hart & Boulton (1991), Hart & Roberts (1994), and, in part, by Lunkka (1994); the latter author also recognized evidence for subaqueous processes. Lunkka's conclusions, and those of Roberts and Hart (2005), probably reflect the influence of Eyles et al. (1989), who interpreted the whole sediment pile in glaciomarine terms. Eyles et al.'s interpretation, however, has received little support, and Roberts and Hart (2005) have re-affirmed their view that the 'Laminated Diamict' at West Runton is

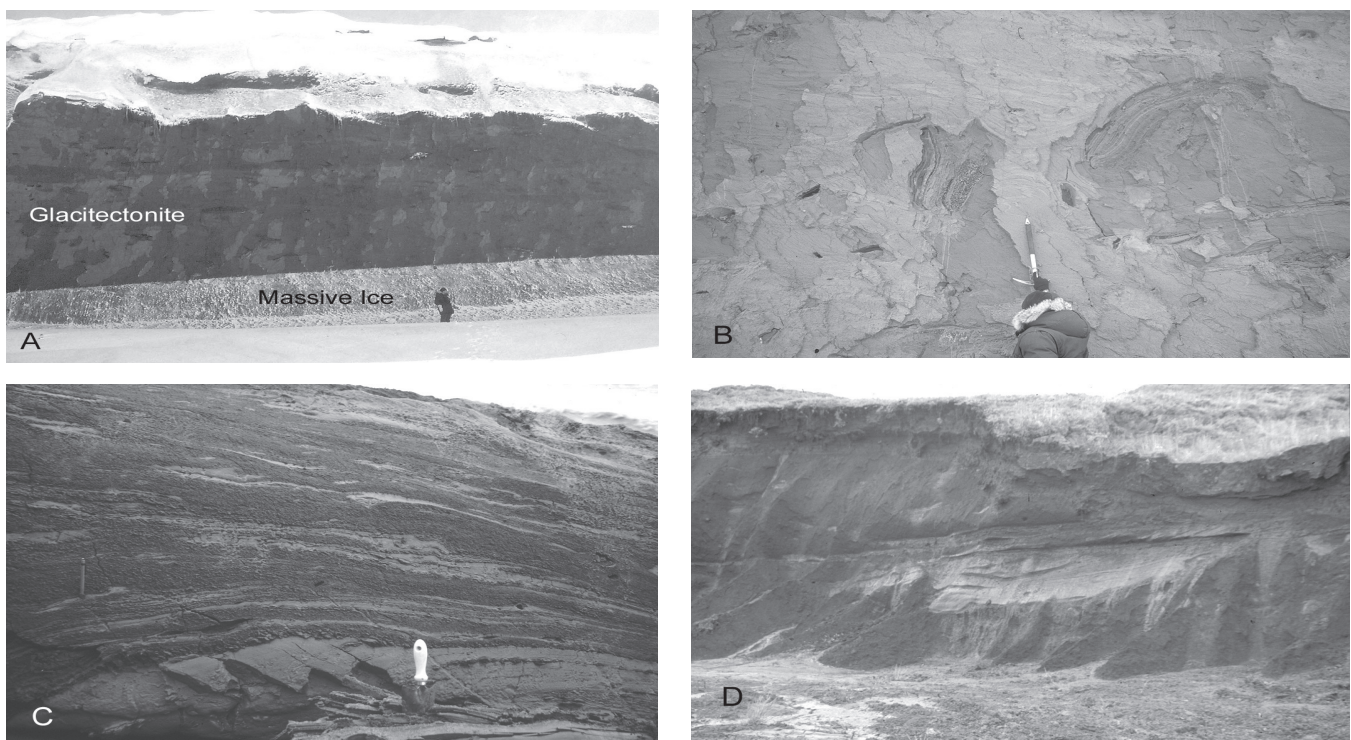


Figure 1. Glaciectonically-deformed permafrost in the Canadian Arctic: (A) frozen glaciectonite above massive ice at Pullen Island - note intervening angular unconformity ($69^{\circ}46'25''\text{N}$, $134^{\circ}24'18''\text{W}$, figure for scale), (B) close-up of chaotically-orientated and deformed sand lenses and ice clasts at Pullen Island (figure for scale), (C) sand lenses and fold noses between silty clay at North Head ($69^{\circ}43'22''\text{N}$, $134^{\circ}26'08''\text{W}$), (D) raft of massive ice (~ 14 m long) within frozen glaciectonite at Liverpool Bay ($69^{\circ}50'10''\text{N}$, $129^{\circ}20'12''\text{W}$).

essentially a subglacially-deformed sediment package, although the primary depositional process of some of the sediment may have been subaqueous. They recognize two types of stratified diamict, Type 1 and Type 2. While both types of laminae are said to be the product of “primary extensional glaciectonism, with ductile, intergranular pervasive shear and brittle shear, ... the lateral continuity of Type 2 laminae and the presence of dropstone-like structures supports a primary subaqueous origin with secondary subglacial deformation” (p. 123). Preservation of Type 2 laminae is attributed to “low strain at the lower interface of the deforming bed” (p. 138). In an earlier iteration of this material (Roberts and Hart in Lewis et al. 2000), these authors noted that the presence of ice wedge pseudomorphs implied subaerial permafrost conditions during the onset of glaciation.

Remarkably, none of the work mentioned above has paid significant attention to the existence of pre-glacial permafrost. Wedge-shaped structures do occur at several horizons in the pre-glacial sediments (West 1980), but many are small and isolated, and both Worsley (1996) and Preece (2000) have questioned their permafrost origin. They could be hydrofractures, water-escape structures or soft-sediment deformations. Nevertheless, the largest wedge-shaped structures in these sediments possess convincing ice wedge-pseudomorph characteristics associated with permafrost (Whiteman 2002). They extend downwards from the upper surface of the pre-glacial sediments and have been correlated to the widespread, Anglian periglacial soil-stratigraphic-unit known as the Barham Soil (Rose et al. 1985). There can be

no doubt that cold permafrost subject to thermal contraction cracking was an integral component of the Norfolk landscape prior to glaciation. Less certain are the thickness, ice content, and temperature of the permafrost.

We suggest that submarginal deformation occurring under partially-frozen conditions at temperatures close to, but slightly below, the pressure melting point (“warm permafrost”) represents an alternative hypothesis for interpreting the glaciectonic sequences of North Norfolk. This hypothesis may elucidate some features that are hard to explain if the substrate was entirely unfrozen:

First, the prevailing model of an unfrozen deforming layer ≤ 15 m thick (Hart et al. 1990) appears increasingly at odds with observations from modern glaciers that suggest that even under thick ice, deformation is restricted to layers a few tens of cm thick or at most, 1–2 m thick (Engelhardt & Kamb 1998). Whilst the incremental stacking of thin, deforming layers at the ice margin might create a thick sequence of deformed sediments (e.g., Evans & Hiemstra 2005, Benediktsson et al. in press), this cannot account for the size and coherence of the structural features observed at West Runton, for example. In contrast, the presence of a thick and pervasively-deformed sequence (Fig. 2a) is entirely consistent with deformation at subfreezing conditions, as documented by the authors in the western Canadian Arctic (Murton et al. 2004) and by Astakhov et al. (1996) in Western Siberia.

Second, the streamlined sand lenses at West Runton (Fig. 2b, c, e, g, Hart et al. 1990, Lunkka 1994) are difficult to reconcile with high-strain deformation under unfrozen

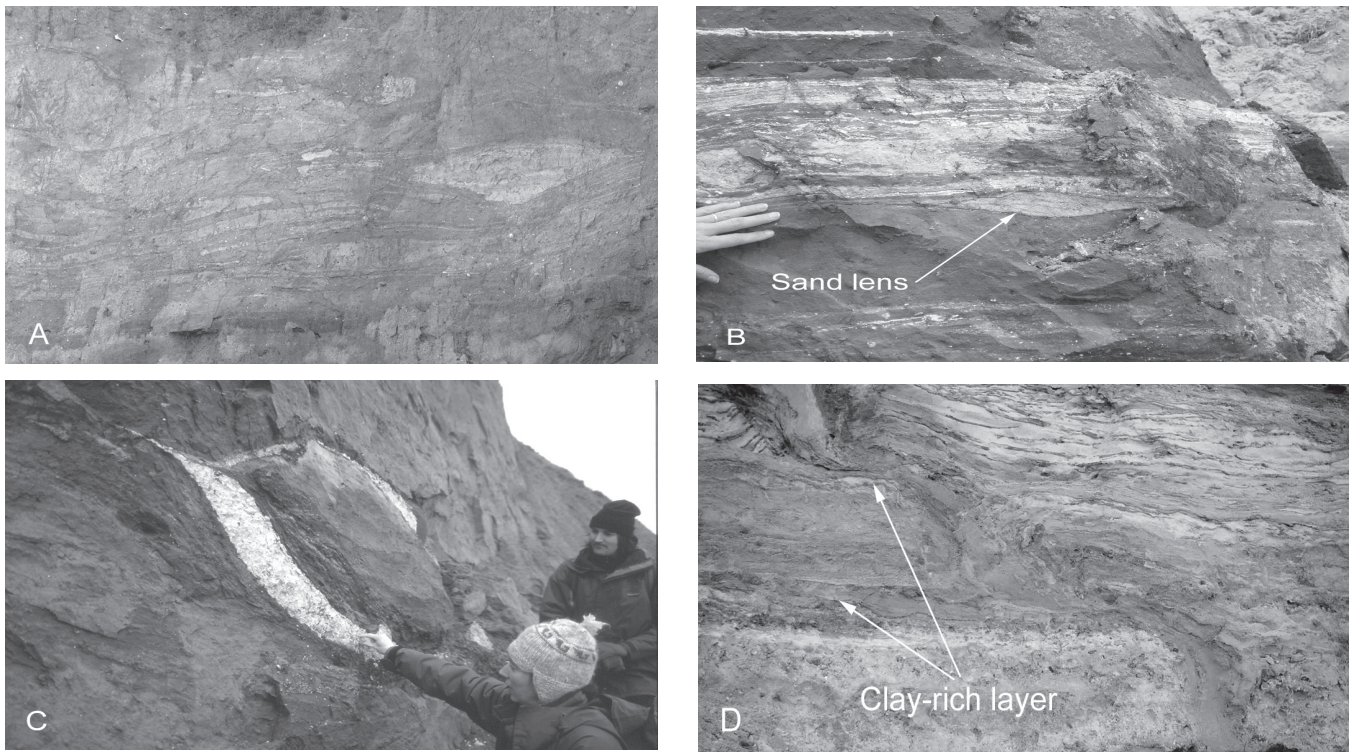


Figure 2. Glaciotectionic features in Northern Norfolk: (A) streamlined lenses, pods and folds at Weybourne ($52^{\circ}56'25''\text{N}$, $1^{\circ}08'42''\text{E}$, area depicted ~ 10 m across), (B) stratified and streamlined sand lens at West Runton ($52^{\circ}56'25''\text{N}$, $1^{\circ}15'21''\text{E}$, hand for scale), (C) streamlined sand lens surrounded by chalk, West Runton (figures for scale), (D) sheared ice wedge pseudomorph, West Runton (area depicted ~ 0.8 m across).

conditions. If the fine-grained till surrounding the sand lenses experienced high porewater pressures, then the lenses could not have been well drained and therefore able to act as more resistant masses. Also, it is difficult to envisage how they could have remained intact as they lacked any cohesion (see also Piotrowski et al. 2001). In contrast, the survival of recognizable intraclasts within an actively deforming till, and the associated rheological heterogeneity, are easy to explain if deformation takes place at temperatures below, but close to, the pressure melting point. The presence and quantity of liquid water, and therefore the mechanical properties of frozen ground at these relatively warm temperatures, are strongly grain-size dependent (Williams & Smith 1989). Consequently, if such a sequence was overridden by ice, deformation would occur preferentially within the fine-grained till matrix (which contains liquid water), whilst the sand intraclasts should remain frozen and largely intact. This prediction is consistent with field observations of subglacially-deformed permafrost in the western Canadian Arctic, showing streamlined and occasionally boudinaged sand lenses within a pervasively deformed till matrix (Murton et al. 2004, Fig. 2c). Menzies (1990) has similarly argued that undeformed, sand intraclasts within a deformation till in Ontario, Canada must have been frozen when deformation took place, producing a “block-in-matrix” mélange.

Observation of a sheared ice wedge pseudomorph at West Runton provides additional evidence for a grain-size-related variation in rheology. The pseudomorph has been displaced by several centimeters where it transects clay-rich layers, whilst those parts situated within sand-rich layers have not

been substantially deformed (Fig. 2d). This is consistent with the findings of Astakhov et al. (1996), who found deformation within permafrost sequences to be restricted to ice-rich or clay-rich layers.

Finally, the deformed permafrost hypothesis is consistent with the pre-glacial history of the region. There is extensive evidence that the area was characterized by permafrost conditions immediately prior to glaciation. Therefore, the ice would have initially advanced over frozen ground, probably warming it from cold to warm permafrost. Cutler et al. (2000) have modeled interactions between the Green Bay lobe of the southern Laurentide Ice Sheet and pre-existing permafrost and concluded that glacier-permafrost interactions would have persisted for 80–200 km up-glacier of the margin, and could have remained intact for up to a few thousand years beneath the advancing ice.

Discussion

With recent research suggesting that subglacial permafrost has been more widespread than previously thought (Cutler et al. 2000) and that glaciers can couple with ice-rich materials (Astakhov et al. 1996, Bennett et al. 2004, Murton et al. 2004), it seems highly likely that there should be evidence of this process within the geological record.

At present, the alternative hypothesis advocated in this paper remains speculative. Whilst there is clear evidence for deformation under subfreezing conditions in high-latitude regions where permafrost has remained intact, we currently lack any sedimentological criteria with which to recognize

glacier-permafrost interactions in areas where the permafrost has subsequently thawed. More detailed investigation of the origin and significance of undeformed intraclasts within pervasively deformed sequences might provide a useful starting point as a research avenue amenable both to field and laboratory testing.

If such criteria, capable of distinguishing between deformation under unfrozen and partly-frozen conditions can be developed, then the potential applications are highly significant. They could enable the basal boundary conditions of past ice sheets to be reconstructed on the basis of geological evidence, thereby providing an opportunity to independently test the predictions both of numerical ice-sheet models and geomorphological inverse models.

Conclusions

Recent research indicates that subglacial sediment deformation and erosion can remain active at subfreezing temperatures, allowing some glaciers to couple with and deform permafrost beneath their margins. Submarginal deformation of past permafrost may explain some problematic features of the glaciotectionic sequences in North Norfolk, previously attributed to deformation of an unfrozen substrate. Deformation under subfreezing conditions should be considered as an alternative hypothesis elsewhere, particularly in ice-marginal settings where pre-glacial permafrost is known to have occurred. It is hoped that further research on the products of glacier-permafrost interactions will help to identify geological criteria for distinguishing between deformation of permafrost and that of unfrozen materials.

References

- Alley, R.B. 1991. Deforming-bed origin for southern Laurentide till sheets? *Journal of Glaciology* 37: 67-76.
- Alley, R.B., Blankenship, D.D., Bentley, C.R. & Rooney, S.T. 1986. Deformation of till beneath Ice Stream B, Antarctica. *Nature* 322: 57-59.
- Astakhov, V.I., Kaplyanskaya, F.A. & Tarnogradsky, V.D. 1996. Pleistocene permafrost of West Siberia as a deformable glacier bed. *Permafrost & Periglacial Processes* 7: 165-191.
- Atkins, C.B., Barrett, P.J. & Hicock, S.R. 2002. Cold glaciers erode and deposit: evidence from the Allan Hills, Antarctica. *Geology* 30: 659-662.
- Banham, P.H. 1968. A preliminary note on the Pleistocene stratigraphy of northeast Norfolk. *Proceedings of the Geologists' Association* 79: 507-512.
- Banham, P.H. 1977. Glacitectonites in till stratigraphy. *Boreas* 6: 101-105.
- Banham, P.H. 1988. Polyphase glaciotectionic deformation in the contorted drift of Norfolk. In: D. Croot (ed.), *Glaciotectonics: Forms and Processes*. Balkema, Rotterdam: 27-32.
- Benediktsson, Í.Ö., Möller, P., Ingólfsson, O., van der Meer, J.J.M., Kjær, K.H. & Krüger, J. In press. Instantaneous end moraine and sediment wedge formation during the 1890 glacier surge of Brúarjökull, Iceland. *Quaternary Science Reviews*.
- Benn, D.I. 2007. Interpreting glacial sediments. In: P.G. Knight (ed.), *Glacier Science and Environmental Change*. Oxford: Blackwell Publishing, 434-439.
- Benn, D.I. & Clapperton, C.M. 2000. Pleistocene glaciotectionic landforms and sediments around central Magellan Strait, southernmost Chile: evidence for fast outlet glaciers with cold-based margins. *Quaternary Science Reviews* 19: 591-612.
- Benn, D.I. & Evans, D.J.A. 1996. The recognition and interpretation of subglacially-deformed materials. *Quaternary Science Reviews* 15: 25-32.
- Bennett, M.R., Waller, R.I., Midgley, N.G., Huddart, D., Gonzalez, S., Cook, S.J. & Tomio, A. 2003. Subglacial deformation at subfreezing temperatures? Evidence from Hagafellsjökull-Eystri, Iceland. *Quaternary Science Reviews* 22: 915-923.
- Boulton, G.S. 1987. A theory of drumlin formation by subglacial sediment deformation. In: J. Menzies & J. Rose (eds.), *Drumlin Symposium*. Rotterdam: Balkema, 25-80.
- Boulton, G.S. & Jones, A.S. 1979. Stability of temperate ice caps and ice sheets resting on beds of deformable sediment. *Journal of Glaciology* 24: 29-42.
- Boulton, G.S. & Hindmarsh, R.C.A. 1987. Sediment deformation beneath glaciers: rheology and geological consequences. *Journal of Geophysical Research* 92: 9059-9082.
- Boulton, G.S., Dobbie, K.E. & Zatsepin, S. 2001. Subglacial sediment deformation beneath glaciers and its coupling to the subglacial hydraulic system. *Quaternary International* 86: 3-28.
- Clark, P.U. 1994. Unstable behaviour of the Laurentide ice sheet over deforming sediment and its implications for climate change. *Quaternary Research* 41: 19-25.
- Cuffey, K.M., Conway, H., Hallet, B., Gades, A.M. & Raymond, C.F. 1999. Interfacial water in polar glaciers, and glacier sliding at -17°C . *Geophysical Research Letters* 26: 751-754.
- Cutler, P.M., MacAyeal, D.R., Mickelson, D.M., Parizek, B.R. & Colgan, P.M. 2000. A numerical investigation of ice-lobe/permafrost interaction around the Southern Laurentide Ice Sheet. *Journal of Glaciology* 46: 311-325.
- Dowdeswell, J.A. & Siegert, M.J. 1999. Ice-sheet numerical modeling and marine geophysical measurement of glacier-derived sedimentation on the Eurasian Arctic continental margins. *Geological Society of America Bulletin* 111: 1080-1097.
- Echelmeyer, K. & Zhongxiang, W. 1987. Direct observation of basal sliding and deformation of basal drift at subfreezing temperatures. *Journal of Glaciology* 33: 83-98.
- Engelhardt, H. & Kamb, B. 1998. Basal sliding of Ice Stream B, West Antarctica. *Journal of Glaciology* 44: 223-230.
- Evans, D.J.A. & Hiemstra, J.F. 2005. Till deposition by glacier sub-marginal, incremental thickening. *Earth Surface Processes & Landforms* 30: 1633-1662.

- Evans, D.J.A., Phillips, E.R., Hiemstra, J.F. & Auton, C.A. 2006. Subglacial till: Formation, sedimentary characteristics and classification. *Earth-Science Reviews* 78: 115-176.
- Eyles, N., Eyles, C.H. & McCabe, A.M. 1989. Sedimentation in an ice-contact subaqueous setting: the mid-Pleistocene "North Sea Drifts" of Norfolk, UK. *Quaternary Science Reviews* 8: 57-74.
- Fuller, S. & Murray, T. 2002. Sedimentological investigations in the forefield of an Icelandic surge-type glacier: implications for the surge mechanism. *Quaternary Science Reviews* 21: 1503-1520.
- Hart, J.K. 1994. Till fabric associated with deformable beds. *Earth Surface Processes & Landforms* 19: 15-32.
- Hart, J.K. 1995. Subglacial erosion, deposition and deformation associated with deformable beds. *Progress in Physical Geography* 19: 173-191.
- Hart, J.K., Hindmarsh, R.C.A. & Boulton, G.S. 1990. Styles of subglacial glaciotectionic deformation within the context of the Anglian ice sheet. *Earth Surface Processes & Landforms* 15: 227-241.
- Hart, J.K. & Boulton, G.S. 1991. The interrelations of glaciotectionic and glaciodepositional processes within the glacial environment. *Quaternary Science Reviews* 10: 335-350.
- Hart, J.K. & Roberts, D.H. 1994. Criteria to distinguish between subglacial glaciotectionic and glaciomarine sedimentation, I. Deformation styles and sedimentology. *Sedimentary Geology* 91: 191-213.
- Hart, J.K. & Smith, 1997. Subglacial deformation associated with fast ice flow, from the Columbia Glacier, Alaska. *Sedimentary Geology* 111: 117-197.
- Iverson, N.R., Hanson, B., Hooke, R.LeB. & Jansson, P. 1995. Flow mechanism of glaciers on soft beds. *Science* 267: 80-81.
- Kavanaugh, J.L. & Clarke, G.K.C. 2006. Discrimination of the flow law for subglacial sediment using in situ measurements and an interpretation model. *Journal of Geophysical Research* 111: F01002, doi:10.1029/2005JF000346.
- Kleman, J. 1994. Glacial landforms indicative of a partly frozen bed. *Journal of Glaciology* 40: 255-264.
- Lamplugh, G.W. 1911. On the shelly moraine of the Sefstrom glacier and other Spitsbergen phenomena illustrative of the British glacial conditions. *Proceedings of the Yorkshire Geological Society* 17: 216-241.
- Lee, J.R., Booth, S.J., Hamblin, R.J.O., Jarrow, A.M., Kessler, H., Moorlock, B.S.P., Morigi, A.N., Palmer, A., Pawley, S.J., Riding, J.B. & Rose, J. 2004. A new stratigraphy for the glacial deposits around Lowestoft, Great Yarmouth, North Walsham and Cromer, East Anglia, UK. *Bulletin of the Geological Society of Norfolk* 53: 3-60.
- Lewis, S.G., C.A. Whiteman & R.C. Preece (eds). 2000. *The Quaternary of Norfolk and Suffolk: Field Guide*. London: Quaternary Research Association.
- Lunkka, J.P. 1994. Sedimentation and lithostratigraphy of the North Sea Drift and Lowestoft Till Formations in the coastal cliffs of northeast Norfolk, England. *Journal of Quaternary Science* 9: 209-233.
- Mathews, W.H. & Mackay, J.R. 1960. Deformation of soils by glacier ice and the influence of pore pressure and permafrost. *Royal Society of Canada Transactions* LIX, Series III, Section 4: 27-36.
- Mackay, J.R., Rampton, V.N. & Fyles, J.G. 1972. Relic Pleistocene permafrost, western Arctic, Canada. *Science* 176: 1321-1323.
- Menzies, J. 1990. Sand intraclasts within a diamicton mélange, southern Niagara Peninsula, Ontario, Canada. *Journal of Quaternary Science* 5: 189-206.
- Murton, J.B., Waller, R.I., Hart, J.K., Whiteman, C.A., Pollard, W.H. & Clark, I.D. 2004. Stratigraphy and glaciotectionic structures of permafrost deformed beneath the northwest margin of the Laurentide Ice Sheet, Tuktoyaktuk Coastlands, Canada. *Journal of Glaciology* 49: 399-412.
- Payne, A.J. 1995. Limit cycles in the basal thermal regime of ice sheets. *Journal of Geophysical Research* 100(B3): 4249-4263.
- Paterson, W.S.B. 1994. *The Physics of Glaciers* (3rd Ed.). Oxford: Pergamon Press, 480 pp.
- Piotrowski, J.A., Mickelson, D.M., Tulaczyk, S., Krzyszkowski, D. & Junge, D.W. 2001. Were deforming subglacial beds beneath past ice sheets really widespread? *Quaternary International* 86: 139-150.
- Preece, R.C. 2000. Molluscan evidence for differentiation of interglacials within the 'Cromerian Complex'. *Quaternary Science Reviews* 20: 1643-1656.
- Roberts, D.H. & Hart, J.K. 2005. The deforming bed characteristics of a stratified till assemblage in north East Anglia, UK: investigating controls on sediment rheology and strain signatures. *Quaternary Science Reviews* 24: 123-140.
- Rose, J., Allen, P., Kemp, R.A., Whiteman, C.A. & Owen, N. 1985. The early Anglian Barham Soil in southern East Anglia. In: J. Boardman (ed.), *Soils and Quaternary Landscape Evolution*. Chichester: Wiley, 197-229.
- Truffer, M.A., Harrison, W.D. & Echelmeyer, K.A. 2000. Glacier motion dominated by processes deep in underlying till. *Journal of Glaciology* 45: 213-221.
- Tsytoovich, N.A. 1975. *The Mechanics of Frozen Ground*. Washington DC: Scripta Book Company, 426 pp.
- van der Meer, J.J.M. 1993. Microscopic evidence of subglacial deformation. *Quaternary Science Reviews* 12: 553-587.
- West, R.G. 1980. *The Pre-glacial Pleistocene of the Norfolk and Suffolk Coasts*. Cambridge: Cambridge University Press, 203 pp.
- Whiteman, C.A. 2002. Implications of a Middle Pleistocene ice-wedge cast at Trimmingham, Norfolk, Eastern England. *Permafrost and Periglacial Processes* 13: 163-170.
- Williams, P.J. & Smith, M.W. 1989. *The Frozen Earth: Fundamentals of Geocryology*. Cambridge: Cambridge University Press, 306 pp.
- Worsley, P. 1996. On ice-wedge casts and soft sediment deformations. *Quaternary Newsletter* 78: 1-7.

Simulations of Present Arctic Climate and Future Regional Projections

John E. Walsh

International Arctic Research Center, University of Alaska Fairbanks

Abstract

Projections of changes in permafrost require credible projections of the atmosphere that overlies terrestrial regions containing permafrost. The critical atmospheric variables for permafrost are surface air temperature and precipitation, especially snowfall. In this study, global climate models used in the Intergovernmental Panel on Climate Change (IPCC) Fourth Assessment Report are ranked on the basis of their simulations of regional Arctic temperature, precipitation and sea level pressure. When evaluated by the root-mean-square error relative to an atmospheric reanalysis, the models that perform best over the pan-Arctic and broader Northern Hemisphere domains are generally found to have the smallest errors over permafrost areas (e.g., Alaska). However, even the highest ranking model has some areas in which its simulations are problematic. The changes of temperature and precipitation projected by the highest ranking models are generally larger than the changes projected by the other models used by the IPCC.

Keywords: Arctic; climate; climate models; permafrost; temperature.

Introduction

Global climate models are the most widely used tools for projections of climate change over the timescale of a century. The periodic assessments by the Intergovernmental Panel on Climate Change (IPCC) have relied heavily on global model simulations of future climate driven by scenarios of increasing greenhouse gas concentrations. The global model simulations show a polar amplification of the greenhouse-driven warming and of other variations in climate (Serreze & Francis 2006, Wang et al. 2007), although the ratio of the models' projected changes to the natural variability is not necessarily greater in the Arctic than in lower latitudes (Kattsov & Sporyshev 2006).

Given the likelihood that the Arctic will experience greater climate changes than most other regions over the next century, the credibility of the model simulations of Arctic climate becomes a key issue when, for example, atmospheric simulations are used to drive projections of changes in permafrost. The absence of databases for validation of future climate simulations increases the importance of evaluations of models' ability to simulate recent climate, for which syntheses of observational data are available.

Greenhouse-driven climate change largely represents a sensitivity to forcing, i.e., the radiative forcing associated with carbon dioxide, methane, water vapor and other radiatively active gases, as well as associated changes in cloudiness. Hence the models' sensitivity to forcing is an essential consideration in assessing the credibility of climate projections. While changes in the radiative forcing associated with increasing greenhouse gases have thus far been relatively small (only a few Watts per square meter, IPCC 2007), a far more potent change in forcing occurs each year through the seasonal cycle of solar radiation. In the present paper, we place the models' ability to capture the *seasonal cycle* of present-day climate at the core of a strategy for evaluating the models' simulation of Arctic climate. Our evaluation is motivated by regional applications of the

climate model output in the Arctic, specifically in the regions such as Alaska and Greenland where permafrost may be vulnerable to a warming climate. These regions have surface states that can be fundamentally altered by relatively small climate changes of temperature and precipitation, especially during the cold season when precipitation determines the depth and density of the snowpack that insulates the soil.

Models and Methodology

Our evaluation is based on the 20th-century simulations by the fifteen of the models used in the Fourth Assessment Report (AR4) of the Intergovernmental Panel on Climate Change (IPCC, 2007). For those models with ensembles of 20th-century simulations, only one (the first archived) simulation is used. Also, output from about seven additional models that were added to the IPCC archive after this study began is not included here. The output used here consists of the monthly grids of surface air temperature and precipitation for 1958–2000, which is a subperiod of the 20th-century simulations by these models and is also the period spanned by the validation fields (see below). The models are listed in Chapman & Walsh (2007, their Table 1). Most of the model simulations were begun in the 1800s and continued through 2000 with prescribed greenhouse gas concentrations and, in some cases, estimated sulfate aerosols and variable solar forcing (see discussion in Wang et al. (2007)). The simulations were continued through the 21st century with forcing prescribed from the IPCC's greenhouse scenarios (A2, A1B, B1, etc.). For the evaluation performed in this study, we use the output from the 20th-century simulations.

The IPCC model output is compared here against the European Centre for Medium-Range Weather Forecasts (ECMWF) Re-Analysis, ERA-40, which directly assimilates sea level pressure (SLP) observations and some air temperature observations into a reanalysis product spanning 1958–2000. Precipitation is computed by the model used in the data assimilation. The ERA-40 is one of the most consistent and

Table 1: Summary of performance rank derived from the models' RMSE for three variables: temperature, precipitation and sea level pressure over three domains: Alaska, pan-Arctic (60-90°N) and the Northern Hemisphere extratropics (20-90°N). An integrated rank, defined as the sum of ranks over the three domains and the three variables, is included in the right-most column.

Overall Rank	Model										
1	MPI ECHAM5	13	1	1	5	3	3	1	1	1	29
2	GFDL CM2.1	6	3	5	2	1	2	5	4	2	30
3	MIROC 3.2	2	4	3	7	6	8	10	3	5	48
4	UKMO HADCM3	11	8	6	3	2	9	4	6	7	56
5	CCCMA 3.1	12	11	10	4	8	2	8	2	4	61
6	GFDL CM2.0	6	9	14	1	10	6	4	8	4	62
7	MRI CGM2.3.2A	11	13	7	6	5	4	2	11	6	65
8	CNRM CM3	1	5	5	12	12	13	7	12	11	78
9	NCAR CCSM3	8	2	2	9	8	7	15	15	13	79
10	INMC 3.0	7	6	10	10	13	12	9	7	9	83
11	NCAR PCM1	14	13	14	8	5	10	6	5	12	87
12	CSIRO MK3.0	6	14	12	11	11	5	11	9	9	88
13	IPSL CM4	11	7	12	13	9	11	14	11	15	103
14	GISS E R	6	10	10	14	14	15	13	14	14	110
15	IAP_FGOALS1_0_G	15	15	15	15	15	14	12	13	10	124

accurate gridded representations of these variables available, and it compares favorably with other reanalyses of the Arctic (Bromwich et al. 2007). It is therefore, a logical choice for observational analyses from which we determine the model biases of late-twentieth-century surface air temperatures, precipitation and SLP. (Data and documentation for the ERA-40 can be found online at <http://www.ecmwf.int/research/era/Products>.) While the ERA-40 reanalysis was performed at T106 (~125 km) resolution with 60 levels, we use the version of the output archived on a 2.5° latitude x 2.5° longitude grid for compatibility with the climate model output. This grid resolution, to which the various model grid configurations were interpolated, is typical of the resolution of the global climate models.

To facilitate GCM intercomparison and validation against the reanalysis data, all monthly fields of GCM temperature, precipitation and SLP are interpolated to the common 2.5° × 2.5° latitude–longitude ERA-40 grid. Our evaluation of the models' simulated fields uses monthly, seasonal, and annual climatological means for the late-twentieth-century period 1958–2000.

The core statistic of our validation is the root-mean-square error (RMSE) evaluated from the differences between ERA-40 and each model for each grid point and calendar month. In all cases, the differences are between climatological means for the 1958–2000 period. The RMSE calculations are performed for each of the fifteen models, for each calendar month, and area-weighted for each of three domains: Alaska, the “pan-Arctic” polar cap (60–90°N) and a middle-high latitude “Northern Hemisphere” domain (20–

90°N). The Alaska domain is contained within the Arctic and Northern Hemisphere domains (except for a small portion of southeastern Alaska), so the results for the various domains are not independent. The reason for our choice of the three overlapping domains is that, although our primary interest is in the models' performance for a region that contains permafrost (Alaska), the simulation of present-day and future climate in Alaska will depend on the simulation of regions from which weather systems move toward Alaska. In particular, the larger-scale circulation over much of the Northern Hemisphere influences Alaska via advection and teleconnections, so credible simulations of future changes will depend on the models' ability to capture the large-scale circulation of the pan-Arctic and Northern Hemisphere domains.

As a seasonally inclusive measure of the models' success in simulating the regional and larger-scale climates, we sum the RMSE values over the 12 calendar months. In this respect, we are evaluating the models' ability to simulate the seasonal cycle and hence the models' sensitivities to the cycle of solar forcing. While success in capturing this sensitivity does not guarantee a realistic sensitivity to greenhouse gas forcing (infrared radiation), one may view a climate model's ability to respond to seasonally varying solar radiation as a prerequisite for a realistic response to perturbations of infrared radiation.

After summation of the regional mean RMSEs over the 12 calendar months, the sums are used to rank the models. The model with the smallest 12-month sum of the RMSE is ranked #1 for that variable and region, while the model

with the largest 12-month sum of the RMSE is ranked #15. The ranks can then be summed over different variables and/or different domains, depending upon a user’s priorities for variables and regional emphasis. The raw RMSE values for individual months also enable users to assess the utility of a particular model for a particular month or season.

Results

Present climate

This paper’s main objective is an identification of the models that are most successful at simulating the seasonal cycle of the climates of Alaska and the Arctic. Information on the variables most relevant to permafrost is contained in Figures 1 and 2, which show the 12-month mean RMSEs of the different models, arranged in order of increasing RMSE, for the surface air temperature (Fig. 1) and precipitation (Fig. 2). Each figure contains a separate display for the three domains discussed earlier: (a) Alaska, (b) the pan-Arctic, 60–90°N, and (c) the extratropical Northern Hemisphere 20–90°N. It is apparent from these figures, especially Figure

1 for temperature, that the models vary widely in their ability to capture the seasonal climates of Alaska. For example, the yearly averaged RMSE of temperature over Alaska varies from 2.9°C in MPI-ECHAM5 to 11.0°C in IAP-FGOALS. The range for the pan-Arctic domain (60–90°N) is even greater, from 2.9°C to 13.6°C. While the ranges are smaller for the other variables, the RMSEs still vary across the models by nearly a factor of two for precipitation and by more than a factor of two for sea level pressure. Similar ranges are found for the larger domains, i.e., the pan-Arctic and hemispheric polar caps.

A noteworthy feature of Figures 1 and 2 is the tendency for some models to rank highly for both Alaska and the larger domains, although there are exceptions. Table 1 provides a synthesis of the model performance based on the RMSE metric. This table ranks the models from 1 (smallest RMSE) to 15 (largest RMSE) for each variable and domain. As in Figures 1 and 2, these ranks are based on RMSEs summed over all twelve calendar months, so they incorporate the models’ successes or failures in capturing the seasonal cycle.

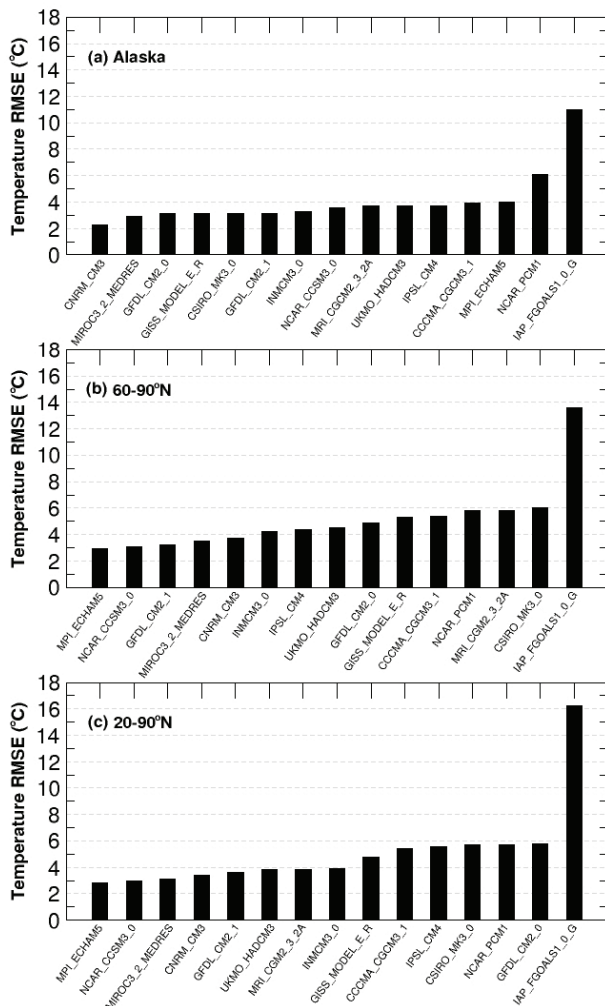


Figure 1. Area-averaged and annually-average Root Mean Square Error (RMSE) of simulated monthly mean (1981–2000) temperatures from 15 models for (a) Alaska, (b) 60–90°N, and (c) 20–90°N.

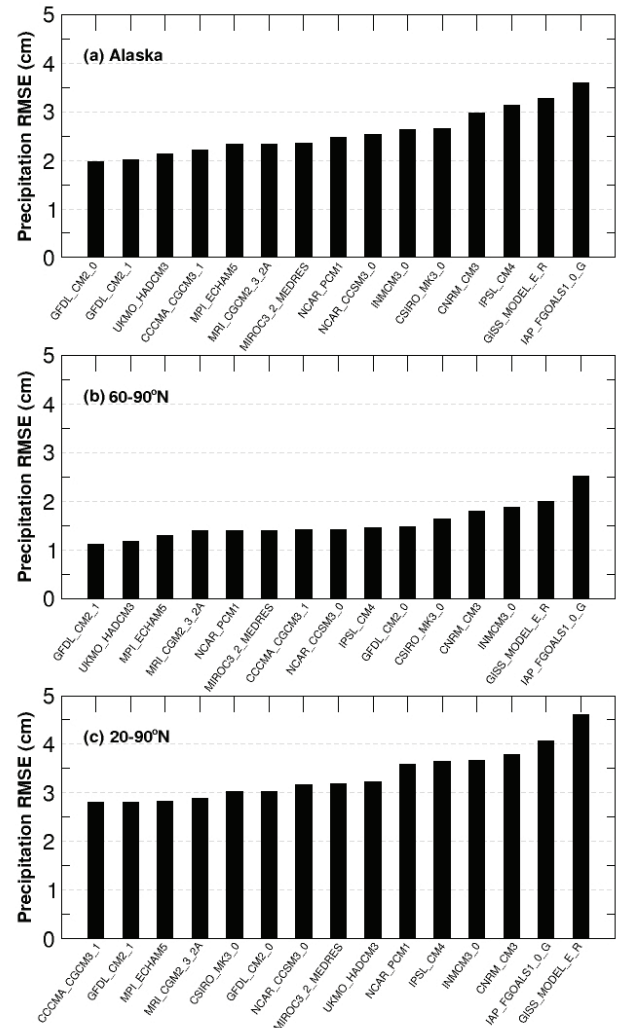


Figure 2. Area-averaged and annually-average Root Mean Square Error (RMSE) of simulated monthly mean (1981–2000) precipitation from 15 models for (a) Alaska, (b) 60–90°N, and (c) 20–90°N.

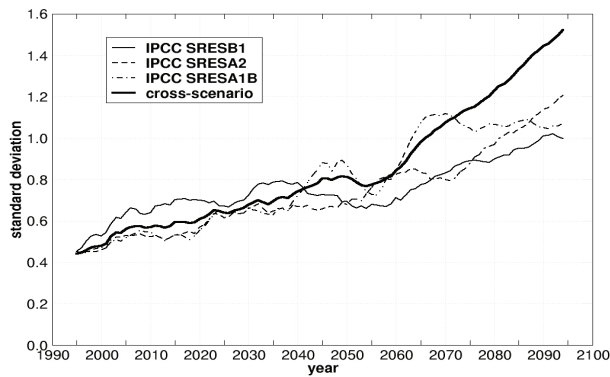


Figure 3. Across-model variability, expressed as 11-year running standard deviations of annual surface air temperature for three greenhouse gas forcing scenarios: IPCC SRES B1, A1B and A2. Also plotted is the across-scenario variability, expressed as the 11-year running standard deviation of surface air temperature across the three IPCC scenarios.

The right-most column of Table 1 is the sum of all 9 ranks (3 domains \times 3 variables) of the models. We refer to this column as our “integrated rank”. Because the domains are nested, this “integrated rank” effectively double-weights the model performance over the Arctic polar cap (60–90°N) and triple-weights the model performance over the Alaskan (i.e., Alaska is included in both larger domains).

It is apparent from Table 1 that, according to our metric and the integrated rank derived from it, two models outperform the others by a considerable margin. These two top-ranking models are MPI-ECHAM5 and GFDL-CM2.1. Both models consistently rank in the top five for all regions and variables, with the exception of temperatures over Alaska. As a cautionary note, MPI-ECHAM5 shows a large negative bias (and hence RMSE) of temperature during January–March over Alaska, illustrating that potentially important regional errors can be present in even the best-performing models. The MIROC3.2-MEDRES and UKMO-HADCM3 models are the third and fourth models in integrated rank, followed by the CCCMA-CGCM3.1 and GFDL-CM2.0 models.

The top-ranking models for Alaska are GFDL-CM2.0, GFDL-CM2.1, UKMO-HADCM3, MPI-ECHAM5, MIROC3.2-MEDRES (in a tie with CCCMA-CGCM3.1 and MRI-CGM2.3.2A). There is substantial overlap among the top performers for the larger domains (pan-Arctic and Northern Hemisphere) and the other subregional domains not discussed here (e.g., Siberia and Greenland).

Projected changes

A key issue underlying model evaluation is the possibility of a relationship between the models’ projected greenhouse changes and the relative accuracy of the simulations of present-day climate. Before addressing this question directly, we highlight uncertainties in future projections by distinguishing the effects of uncertainties in the future greenhouse forcing scenarios (A2, A1B, B1) and uncertainties inherent in the across-model variance. In order to assess the

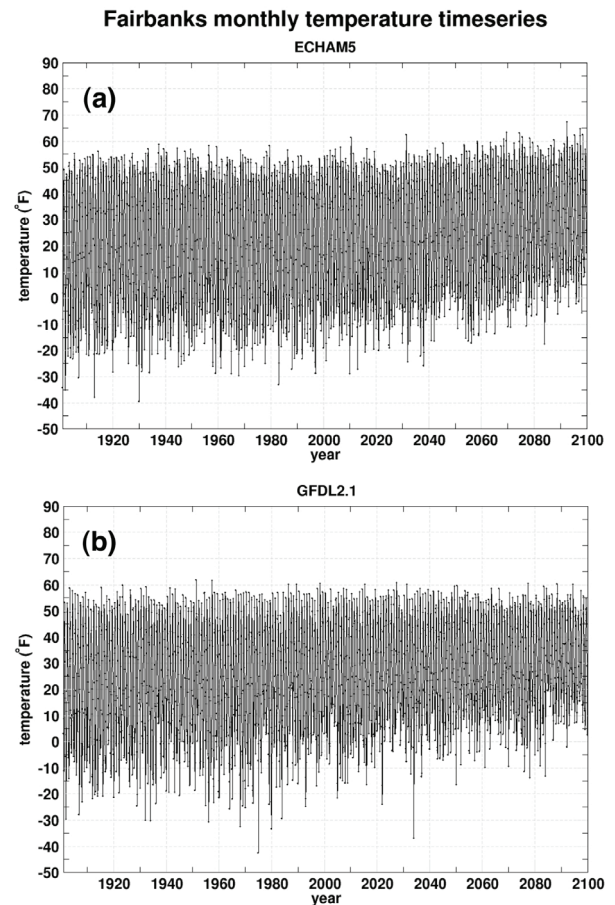


Figure 4. Monthly temperatures (°F) at the grid cell containing Fairbanks, AK in the A1B simulations by the (a) MPI ECHAM5 and (b) GFDL CM2.1 models.

relative contributions of these two sources of uncertainty, we evaluated (1) the intermodel variability for each scenario, expressed as centered 11-year running means of across-model standard deviations of annual temperature change; and (2) the across-scenario variability, expressed as standard deviations of projected temperature change across the three scenarios. The temporal evolution of these two measures of variability is plotted in Figure 3. The across-model and across-scenario variances in the projected temperatures are comparable through the first half of the 21st century, but the increases in variability associated with the choice of greenhouse gas scenario begin to outpace those of across-model variability by about year 2070. By the end of the 21st century, the across-scenario variability is about 50% greater than the across-model variability.

In order to illustrate the projected temperature changes, we show in Figure 4 the two time series of projected temperatures for a grid cell (near Fairbanks, Alaska) in which discontinuous permafrost is now present. The two models chosen for Figure 4 are MPI ECHAM5 and GFDL CM2.1, which have the highest integrated ranks in Table 1. It is apparent from Figure 4 that warming occurs in both models (as in all the other models). However, the warming

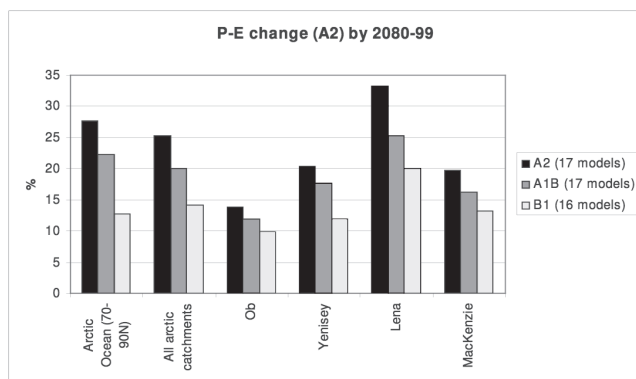


Figure 5. Percentage changes of annual mean P-E (river discharge) in A2, A1B and B1 scenarios for 2080–2099 over different regions (watersheds): the Arctic Ocean (70–90°N), all Arctic Ocean terrestrial watersheds, the Ob, the Yenisey, the Lena, and the Mackenzie.

that is readily apparent in both the minimum (winter) and maximum (summer) temperatures in the MPI ECHAM5 model is apparent primarily only in the coldest (winter) months in the GFDL model. Most of the models show this seasonal asymmetry of the warming at Arctic locations. For example, in the GFDL CM2.1 simulation, the temperature of the coldest winter month increases from about -25°C (-12°F) in the early 1900s to about -12°C ($+10^{\circ}\text{F}$) by the 2090s. There is, however, considerable interannual variability. This interannual variability is obscured by temporal (e.g., decadal) or multi-model averaging.

Figure 5 shows the percentage increase in precipitation less evapotranspiration (P-E), averaged over various Arctic terrestrial drainage basins and over the Arctic Ocean (70–90°N), for the 2080–2099 time slice relative to the 1980–1999 time slice for the A2, A1B and B1 scenarios. The strongest relative increase of P-E (a 33% increase in the A2 scenario) is projected for the Lena Basin, which is largely underlain by permafrost. The weakest relative change is shown for the Ob Basin, which is largely devoid of permafrost. P-E is also projected to increase over the Arctic Ocean, although the increased input of freshwater by P-E over the Arctic Ocean represents only about half the increase of P-E from projected river discharge (P-E over the surrounding Arctic terrestrial drainage basins). While the increase of P-E over the Arctic Ocean is largest in summer and autumn, the increases of P-E over the terrestrial drainage basins are largest in the winter, implying an increase of snowfall. Because snow insulates permafrost during winter, the effect of increased snowfall on permafrost may act to enhance the direct effects on permafrost of warming of the air temperature (Zhang 2005).

Figure 6a shows the models' projected warming for 60–90°N plotted as a function of the integrated rank of the models. The warming is defined here as the area-weighted linear change in surface air temperature from 2000 to 2099. While there is considerable scatter in the warming, there is a tendency for the highest-ranking models to simulate the greatest warming over the 60–90°N zone. The projected

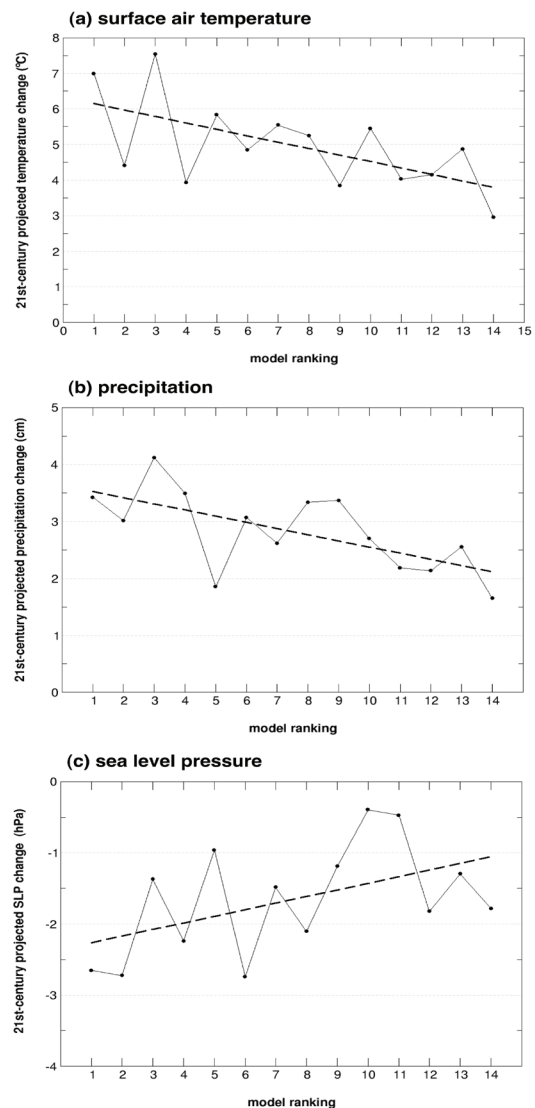


Figure 6. Projected change of (a) surface air temperature ($^{\circ}\text{C}$), (b) precipitation (cm) and (c) sea level pressure (hPa) averaged over 60–90°N for 2081–2100 relative to 1981–2000. Changes are plotted vs. model performance rank (x-axis). Linear best fit is shown as a dashed line in each plot.

changes of precipitation (Fig. 6b) show a similar dependence on the models' integrated ranks, with better performing models projecting larger increases of Arctic precipitation than the lower-ranking models. While there is more scatter in the corresponding SLP results (Fig. 6c), there is a tendency for larger 21st century decreases in Arctic sea level pressure to be projected by higher-ranking models than by lower-ranking models.

Conclusion

This study has emphasized model simulations of climate over Alaska, which we have chosen because it contains large areas of permafrost. Model performance over Alaska is generally neither better nor worse than the performance over the pan-Arctic and Northern Hemisphere domains. During

winter and autumn, the temperature errors over Alaska are somewhat smaller, but the precipitation errors are generally larger, than over the larger domains. The specific models that perform best over the larger domains tend to be the ones that perform best over Alaska. Although not shown here, model performance over other permafrost areas (e.g., Greenland) appears to be comparable to the same models' performance over Alaska.

In the context of permafrost, the most important results of the model simulations are the trends toward a warmer and wetter climate. A wetter climate implies more snowfall during winter. To the extent that snow cover insulates the soil during winter, the changes in the two main controls of permafrost temperatures will favor a warming of permafrost in areas such as Alaska. (Osterkamp 2007) However, the warming also implies a shorter snow season. A high priority for research is the determination of net effect of two competing changes of snow: larger snowfall rates during the cold season, but a shorter snow season.

There is a tendency for the models with the smaller errors to simulate a larger greenhouse warming over the Arctic. Since several models have substantially smaller systematic errors than the other models, the differences in warming imply that the choice of a subset of models may offer a viable approach to narrowing the uncertainty and obtaining more robust estimates of future climate change in regions such as Alaska and the broader Arctic. The results obtained here suggest that the uncertainty might be narrowed by eliminating models with the weaker projected warming in the Arctic, as those models tend to have the largest errors in simulations of the present-day climate. Such an approach has already been suggested by Overland & Wang (2007) and Kattsov & Sporyshev (2006), and will be pursued in future assessments of Arctic change.

A key limitation of this study is the coarse resolution of the global climate models, which are not able to resolve many of the topographic features that are crucial to permafrost distribution. The differences between north-facing and south-facing slopes within a grid cell represent one such example. In order to include finer-scale features, it will be necessary to employ either (a) statistical downscaling approaches using algorithms trained on observational data, perhaps including permafrost measurements, or (b) regional climate models, which effectively provide a "dynamical downscaling". Since regional climate models are driven at their lateral boundaries by the output from global models, and since statistically downscaling of projections requires global or regional model output, the global model assessment described here has relevance to downscaling approaches. Moreover, the permafrost community is generally ahead of the global climate modeling community in the sophistication of modules used to simulate permafrost. Given that this situation is likely to persist as permafrost models improve, the optimum strategy for projecting future changes of permafrost may be to utilize off-line permafrost simulations driven by downscaled output (including snowfall) from large-scale models.

Acknowledgments

This work was supported by the National Science Foundation, Office of Polar Programs through Grant OPP-06533 and by Grant OPP-0327664, the Cooperative Agreement between the National Science Foundation and the International Arctic Research Center.

References

- Bromwich, D.H., Fogt, R.L., Hodges, K.I. & Walsh, J.E. 2007. A tropospheric assessment of the ERA-40, NCEP and JRA-25 global reanalyses in the polar regions. *Journal of Geophysical Research* 112: D10111, doi:10.1029/JD007859.
- Chapman, W.L. & Walsh, J.E. 2007. Simulations of Arctic temperature and pressure by global climate models. *Journal of Climate* 20: 609-632.
- IPCC (Intergovernmental Panel on Climate Change). 2007. *The Physical Basis of Climate Change*. Working Group I, Fourth Assessment Report of the Intergovernmental Panel on Climate Change, Cambridge University Press, Cambridge, U.K., 1099 pp.
- Kattsov, V.M. & Sporyshev, P.V. 2006. Timing of global warming in IPCC AR4 AOGCM simulations. *Geophysical Research Letters* 33: L23707, doi:10.1029/2006GL027476.
- Kattsov, V.M., Walsh, J.E., Chapman, W.L., Govorkova, V.K., Pavlova, T.V. & Zhang, X. 2007. Simulation and projection of Arctic freshwater budget components by the IPCC AR4 global climate models. *Journal of Hydrometeorology* 8: 571-589.
- Osterkamp, T.E. 2007. Causes of warming and thawing permafrost in Alaska. *EOS, Transactions of the American Geophysical Union* 88: 522.
- Overland, J.E. & Wang, M. 2007. Future climate of the North Pacific Ocean. *EOS, Transactions of the American Geophysical Union* 88: 178-182.
- Serreze, M.C. & Francis, J. 2007. The Arctic amplification debate. *Climatic Change* 76: 241-264.
- Wang, M., Overland, J. E., Kattsov, V., Zhang, X. & Pavlova, T. 2007. Intrinsic versus forced variation in coupled climate model simulations over the Arctic during the twentieth century. *Journal of Climate* 20: 1093-1107.
- Zhang, T. 2005. Influence of the seasonal snow cover on the ground thermal regime: An overview. *Rev. Geophys.* 43: RG4002, doi10.1029/2004RG000157.

The Freezing Process Deformation of Soil Under Higher Confining Pressure

Dayan Wang, Wei Ma, Zhi Wen

State Key Laboratory of Frozen Soil Engineering, Cold and Arid Regions
Environmental and Engineering Research Institute, CAS, Lanzhou, China

Abstract

This paper describes results from a series of laboratory tests carried out after the samples subjected to the K_0 consolidation process, which could simulate the deep soil stratum-forming history. The observed results from these tests have shown that the high of the soil sample under higher confining pressure decreases with the soil temperature decreasing, and the downtrend will stop and keep a constant when the temperature reaches a desired level. The variation of the specimen size depends on the confining pressure, soil temperature, and soil type. For soil under the same temperature level, the higher the initial confining pressure, the smaller the variation of the specimen size. For a soil under the same confining pressure level, however, the high of the higher negative temperature soil specimen will reduce unceasingly. When the soil temperature is lower than -5°C , the fluctuation of the soil temperature hardly influences the final high of the soil specimen. In addition, the high variation of the loess sample is much less than the sand sample under the same other factors.

Keywords: artificial frozen soil; higher confining pressure; K_0 consolidation.

Introduction

Ground freezing has been recognized by mining and civil engineers as undoubtedly the most effective and consistently reliable method of providing temporary support and of preventing groundwater from flowing into deep excavations. Its uses does not deplete aquifer reserves by continuous pumping, nor does it pollute or alter the groundwater regime in any way, thus eliminating any adverse affect on adjacent structures, installations, and populations. Frozen wall design and construct, based on how to reasonably choose the physical-mechanical parameter of artificially frozen soils, is a key factor affecting the application of this technology. Therefore, in the last 20 years, a lot of research has been carried out in relation to the test techniques, physical parameters, mechanical characteristics, and freezing temperature of deep soils (Cui et al. 1998, Ma et al. 1993, 1995, 1999, 2000, Ma & Chang 2002, Zhou et al. 1999, Wang et al. 2002), and drawn a series of significant results. Although the obtained results could resolve some practical difficulties arising from the application of artificially frozen soil construction, we could not obtain the reasonable strength theory and the constitutive model of frozen soil forming in the deep alluvium. Generally,

the mechanical properties of the frozen soils are influenced by its physical characteristics. The study of soil deformation properties in the process of freezing under higher confining pressure is involved in the stability of the surface construction and is particularly important for establishing the constitutive model of artificially frozen soil forming under the deeper stratum. However, very few experimental data on this problem exist because of the technical difficulties; for example, how to restore the tested soil to the original state of deep alluvium and then freeze it in the laboratory, and the time-consuming nature of the above-mentioned process. Guided by the earlier studies, this paper was designed to study the features of deep soil deformation during freezing under different negative temperature, initial confining pressure, and soil type. Among these, the initial confining pressure represents the degree of the stratum depth.

Preparation of Specimens and Test Procedure

The soils used in the current study were typical Lanzhou loess and Lanzhou sand, and their engineering properties are shown in Table 1a and Table 1b. The testing scheme is found in Table 2.

Table 1a. The basic physical properties of sand specimens.

Soil type	Composition of grains (%)				Dry density	Water content
Lanzhou sands	>0.5	0.5~0.05	0.05~0.005	<0.005	g/cm^3	%
	25.6	54.23	8.04	12.13	2.0	10.5

Table 1b. The basic physical properties of loess specimens.

Soil type	Composition of grains (%)				Liquid limit	Plastic limit	Dry density	Water content
Lanzhou loess	>0.1	0.1~0.05	0.05~0.005	<0.005	(%)	(%)	(g/cm^3)	(%)
	1.7	5.4	58.6	34.3	24.6	17.7	1.78	16.5

The procedure for preparing the sample is generally performed according to the Specification of Soil Test (GB/T50123-1999) issued by the Ministry of Water Resources, PRC. All the specimens, typically 61.8 mm in diameter and 125 mm in height, were compacted in 6 layers, with a relevant density and water content according to the different soil types, shown in Table 1. The specimen was then covered with rubber sleeves to prevent evaporation of water, and put into the K_0 consolidating instrument, which was developed by our laboratory and used the working principle of oil side-limiting control with the greatest confining pressure of 15 MPa and the lowest temperature of -60°C . In this chamber, the specimen could experience drained triaxial compression before freezing. This process can simulate an increase of overburden, and restores the loading history and initial stress states of soils in the field.

To assure that the soil sample does not laterally deform,

Table 2. The controlling parameters of this experiment.

Soil type	K_0	Speed of the axial loading (MP/s)	Speed of the radial Loading (MP/s)
sands	0.32	10×10^{-5}	3.2×10^{-5}
loess	0.34	10×10^{-5}	3.4×10^{-5}

the static lateral pressure coefficient of the tested soils was obtained from preliminary experimental study (Ma & Cui 2000). The consolidating pressures were controlled at a certain rate, shown in Table 2. When the confining pressure reached the desired pressure, the loading process stopped and began to lower the temperature. The axial deformation was automatically measured by the axial pressure system monitoring the changes of axial displacement, and the data were collected continually by computer.

Results and Discussion

Influence of soil temperature on the deformation

Temperature is a key factor in the study of frozen soil formation, for frozen ground is defined as soil or rock having a temperature below 0°C . The data presented in Figure 1 show the ΔH with the time, where ΔH is defined as the variation of sample height obtained in the freezing process. From Figure 1, we can conclude that the high of the loess sample became sharply reduced with the ambient temperature decrease. When the sample temperature is consistent with the ambient temperature, the variation of the sample height is related to the frozen soil temperature status. The lower the surrounding temperature, the more steady the deformation of the sample, and the shorter the time needed to reach stabilization. With

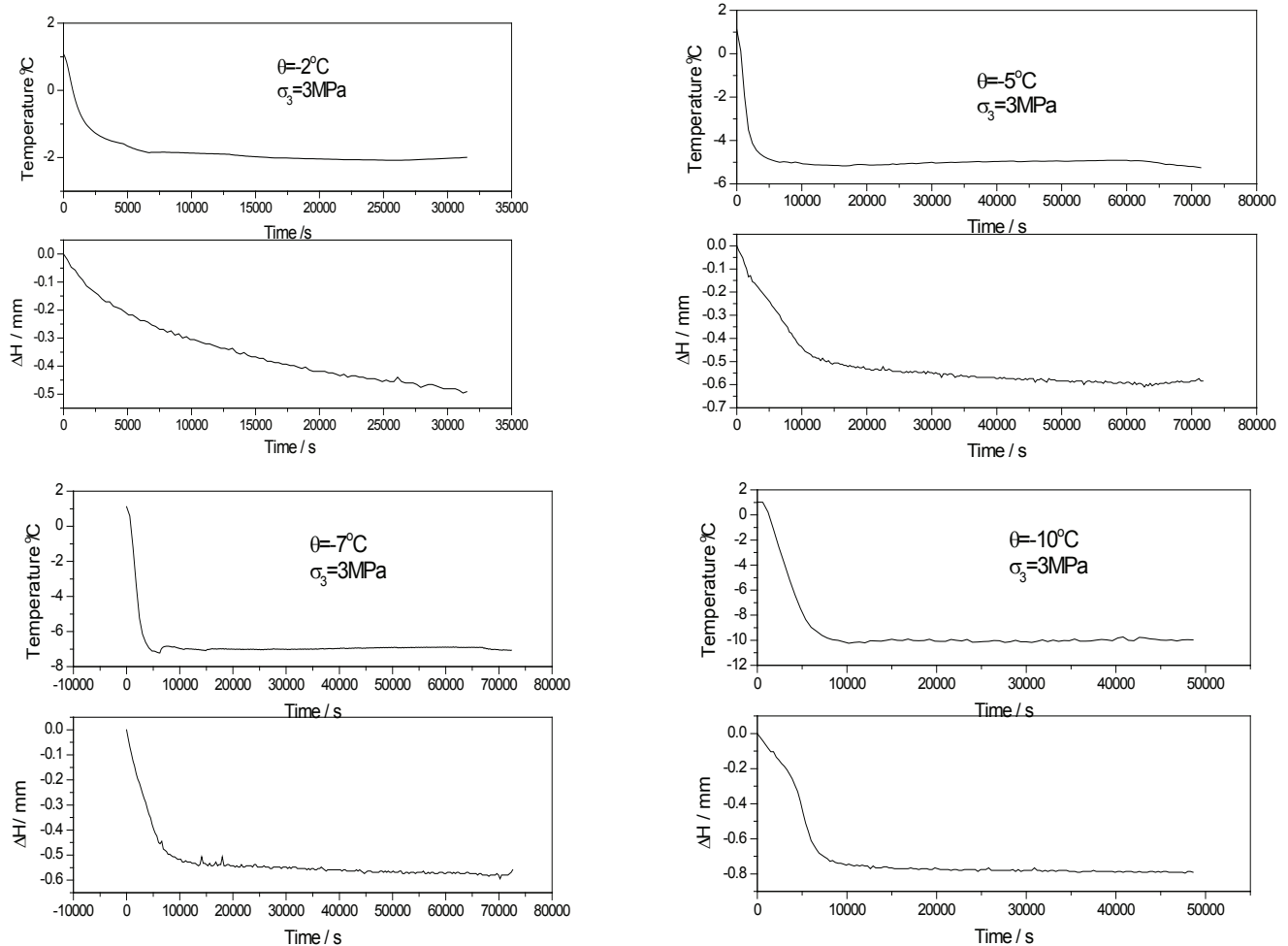


Figure 1. Effect of the frozen soil temperature on the variation of loess specimen high in the process of freezing.

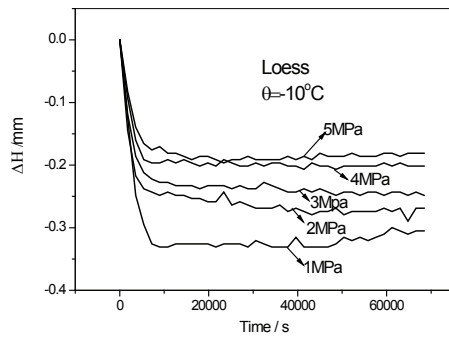


Figure 2. Effect of the initial confining pressure on the variation of loess specimen high in the process of freezing.

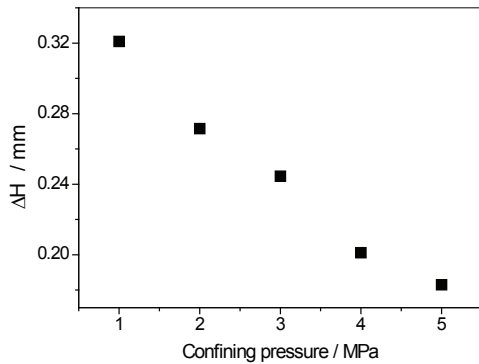


Figure 3. The variation of loess specimen high versus the initial confining pressure.

respect to soil frozen to a temperature lower than -5°C under the same initial confining pressure, the time that the sample deformation reaches stabilization almost equals the time of the surrounding temperature reaching the desired temperature. The sample high variation is about 0.6 to 0.8 mm and independent of the soil temperature. However, for frozen soil with a temperature higher than -5°C , the axial deformation progresses ceaselessly, even though the soil temperature is equal to the surrounding temperature.

Influence of the initial confining pressure on the deformation

Figure 2 shows the variation of the sample high with time from the lowering temperature to -10°C process on the loess subjected to K_0 consolidated to confining pressure σ_3 of 1~5MPa, respectively. From Figure 2, we can conclude that the sample high reduces sharply with the surrounding temperature dropping, and then stops and holds a constant when the sample temperature equals the surrounding temperature. The variation of frozen sample high was heavily influenced by the condition of the initial confining pressure. If the variation of the sample high was taken as the deformation resulted from freezing the soil, we can find from Figure 3 that the deformation of the sample after having been frozen was linearly decreased with the initial confining pressure increase.

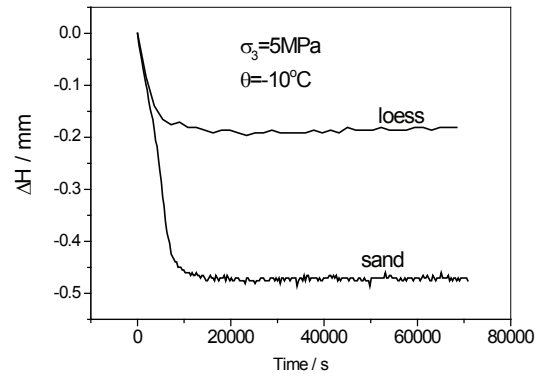
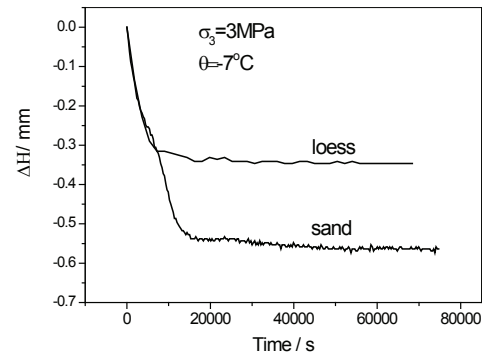


Figure 4. Comparison of the specimen high variation of the two types of soils used in this study.

Table 3. Comparison of the specimen high variation of the two types of soils used in this study.

confining stress	1MPa	2MPa	3MPa	4MPa	5MPa
sand	0.7214	0.5858	0.5364	0.6541	0.471
loess	0.3209	0.2715	0.2445	0.2012	0.183
differential value	0.4	0.314	0.2919	0.453	0.288

Influence of the soil type on deformation

The variation of deformation in the freezing process is affected by characteristics of the soil type. It can be concluded from Figure 4 that the deformation of the sample is larger than that of the loess sample under the same initial confining stress and negative temperature, despite the sample's high decrease when the temperature drops to -7°C or -10°C . After the loess sample and the sand sample experienced the K_0 consolidation process under initial confining stress varying from 1 to 5MPa and completely frozen, a comparison of the variation sample high obtained that the deformation of sand sample is larger than that of loess under the same other condition, and the difference is about 0.3 to 0.4 mm (see Table 3). This suggests that, even for the samples consolidated to the same confining pressure and frozen at the same negative temperature by the same method in the process of using artificial ground freezing to reinforce ground, the soil group would heavily influence the deformation of the freezing soil, causing differential settlement of the ground surface. The builder must consider this point in the design.

Conclusions

It is important to recognize that the deep artificial ground freezing process could cause stratum settlement. This study simulated the deep artificial ground freezing process in the laboratory by K_0 consolidation and presented the findings of a comprehensive study of the effects of the stratum depth, frozen soil temperature, and soil group on settlement expressed by the sample deformation. The following conclusions can be drawn:

1. When the surrounding temperature drops to lower than 0°C , the high of the soil sample subjected to K_0 consolidation will decrease with the temperature decreasing. Until the temperature reaches the desired temperature, the variation of soil sample high stops and keeps a constant level. Therefore, freezing the deep soil could lead to settlement of surface ground. The magnitude of settlement is decided by the soil depth, frozen soil temperature, and soil group.
2. In the process of freezing, deformation of the soil sample was linearly decreased with the initial confining stress increase; namely, with the stratum becoming deep, the sample deformation produced by freezing the soil will decrease.

Sample deformation caused by the freezing process was affected by the soil group. In the range of the studied confining pressure, the deformation of sand was always larger than that of loess. The differential value is about 0.3 to 0.4 mm.

Acknowledgments

This research was supported by the Project for Incubation of Specialists in Glaciology and Geocryology of the National Nature Science Foundation of China (J06309966), the key Program of the National Natural Science Foundation of China (No.50534040), the Talent Training Program for Young Scientists in West China of the Chinese Academy of Sciences, the Special President Scholarship of CAS for Postgraduate Students, and the PYRN Educational Stipend.

References

- Cui, G. 1998. Mechanics of frozen soil for deep alluvium: A new field of frozen soil mechanics. *Journal of Glaciology and Geocryology* 20(2): 97-100 (in Chinese).
- Ma, J. & Cui, G. 2000. Experimental study of K_0 consolidation in deep alluvium. *Annual Report of State Key Laboratory of Frozen Soil Engineering*, Vol. 9. Gansu Province: Xinhua Press, 135-142 (in Chinese).
- Ma, W., Wu, Z. & Zhang, C. 1993. Strength and yield criteria of frozen soil. *Proceedings of the Sixth International Conference on Permafrost, South China*. Beijing: University of Technology, 432-435.
- Ma, W., Wu, Z. & Chang, X. 1995. Effect of confining pressure on strength behaviour of frozen soil. *Chinese Journal of Geotechnical Engineering* 17(5): 7-11 (in Chinese).
- Ma, W., Wu, Z., Zhang, L. & Chang, X. 1999. Analyses of process on the strength decrease in frozen soils under high confining pressure. *Cold Regions Science and Technology* 29(1): 1-7.
- Ma, W., Wu, Z. & Chang, X. 2000. Effect of consolidation process on stress-strain characters of frozen soils. *Rock and Soil Mechanics* 21(3): 198-201 (in Chinese).
- Ma, W. & Chang, X. 2002. Analyses of strength and deformation of an artificially frozen soil wall in underground engineering. *Cold Regions Science and Technology* 34(1): 11-17.
- Wang, D., Ma, W. & Chang, X. 2004. Analyses of behavior of stress-strain of frozen Lanzhou loess subjected to K_0 consolidation. *Cold Regions Science and Technology* 40: 19-29.
- Zhou, G., Cui, G., Cheng, X. et al. 1999. An experimental frame for geomechanical engineering simulation and its application. *Chinese Journal of Geotechnical Engineering* 21(6): 715-718.

Tower Foundation Engineering in a Patchy Permafrost Area Along the 110-kV Power Transmission Line from Amdo to Damxung, Tibet, China

Guoshang Wang

Gansu Electric Power Design Institute, Lanzhou 730000, China

Fengxian Yu, Weidong Cao, Xiaoqi Meng, Yong Liu, Changjin Yang, Yueming Guo

Southwest Electric Power Design Institute, Chengdu 61002, China

Huijun Jin, Xiaoli Chang, Qihao Yu, Jianming Zhang

State Key Laboratory of Frozen Soils Engineering, Lanzhou 730000, China

Abstract

The 110 kV power transmission line from Amdo to Damxung, Tibet, is in the patchy permafrost zone in southcentral Tibet. Frost heave/thaw settlement of the tower foundation soil was one of the major challenges for geotechnical design and construction. Surveys on frozen ground conditions were conducted for assessing frost hazards. The thermal and strain/stress interactions of tower foundation and soils were monitored, tested in situ and in the laboratory, and analyzed. Shallow oblique and straight concrete-column foundations and thermosyphon-cooled pile foundations were proposed and adopted with proven mitigative results. Tower site selection and ground improvement were proven most cost-effective. Data-bank and engineering measures, as well as experiences from the 110 kV power line were very helpful for the design and construction of the proposed 400 and 750 kV power transmission lines and other linear foundation engineering in warm, elevational permafrost regions on the Qinghai-Tibet Plateau.

Keywords: frost-hazard mitigation; ground-improvement; 110-kV power-line; permafrost; site-selection; tower foundation.

Introduction

Towers for transmission lines are commonly either self-supporting or guyed. A tower supported on the top of frost zone will experience frost heave with the presence of frost-susceptible soil and available moisture. The seasonal vertical movement may be detrimental. If the heave is differential between footings supporting the tower, the tower will tip and/or the structure will be unevenly stressed. The guyed tower might experience an overstressing of the guys or of their anchors. Differential footing settlements may occur during thaw-weakening in spring. If the tower is on a slope, progressive downslope movement may occur with successive freeze-thaw cycles.

Granular material may be used to control or eliminate detrimental vertical movement. Due to the intense winter cold, it is usually impractical to make the mat thick enough to completely prevent frost penetration or heave in the underlying frost-susceptible mat, particularly when the mat is naturally well-drained. However, the magnitude of frost heave may be substantially reduced by a relatively modest surcharge, consisting of the weight of the gravel plus the load from the structure (U.S. Department of Defense 2004). Pile foundation with flanged sleeves to isolate the pile from frost heave forces also can be used.

However, studies closely related to the tower foundations of power transmission lines are limited. Myska & How (1978) presented a case study for installation of pile foundations for a microwave tower system, Gillam-Churchill, Manitoba, Canada. This is a route of about 250 km in the continuous and widespread permafrost zones. In this case study, grouted rod

anchors for the tower guys were installed without pre-design subsurface investigations, and the subsurface investigations for the foundations were conducted concurrently, using anchor installation drilling equipment. Precast concrete piles were installed in augered holes. To avoid on-site concreting, the pile caps were constructed of pre-fabricated structural steel.

The 110 kV transmission line from Damxung to Amdo in southcentral Tibet originally was to supply the power needed for engineering construction and operation of the Qinghai-Tibet Railway system at an average elevation of 4500 m. It was the first 110-kV transmission line in the permafrost region on the Qinghai-Tibet Plateau. The 281-km line starts from Damxung in the south and via Nagqū, ends at Amdo in the north, of which 173 km is from Damxung to Nagqū and 108 km from Nagqū to Amdo (Fig. 1). The line traverses regions of patchy permafrost, extensive taliks, and seasonally frozen ground in the vicinity of the southern lower limit of permafrost on the Qinghai-Tibet Plateau.

Large amounts of then-existing data, research papers and reports, previous engineering experiences, and lessons learned were collected and analyzed for the route selection and for the subsequent preliminary and detailed designs for construction for this unprecedented power line on the Qinghai-Tibet Plateau. These data and studies generally included, but were not limited to, published research and review papers on permafrost and cold regions engineering, frozen ground engineering geology reports for the design, construction, and operation of the Qinghai-Tibet Highway, the Golmud to Lhasa fiber-optic cables and an oil products

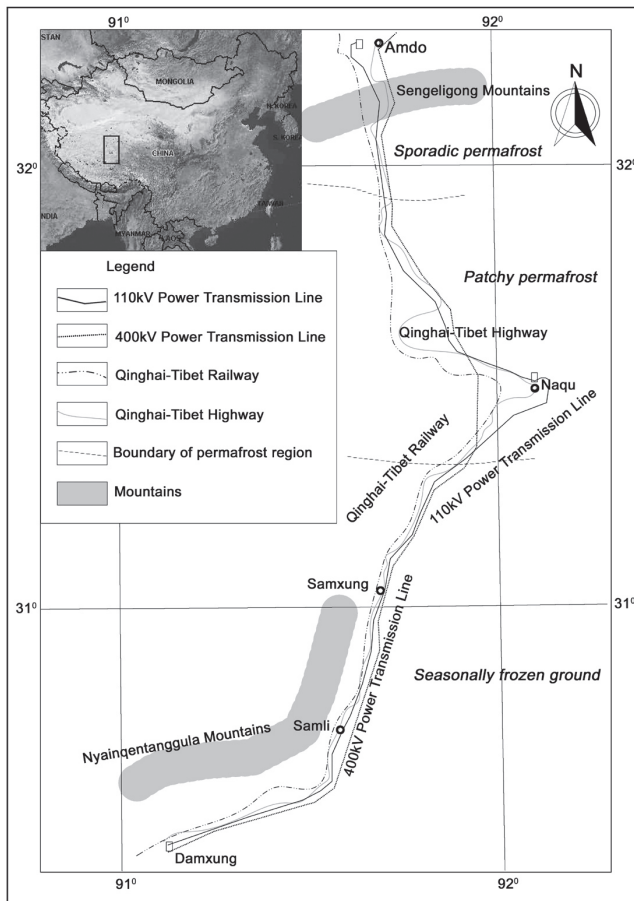


Figure 1. Sketch map of the study region from Amdo to Damxung on the Qinghai-Tibet Plateau.

pipeline. Experts on frozen ground engineering from the Cold and Arid Regions Environmental and Engineering Research Institute, Chinese Academy of Sciences were consulted and their advice sought for in situ engineering surveys, design, and construction. Data on meteorology related to the Qinghai-Tibet Railway, then under construction, also were gathered and analyzed. The planning of the power line began in September 2002. All preliminary and construction designs were completed, reported, reviewed, and delivered by December 2003.

The majority of the power line route is located in areas impacted by seasonal frost, but some sections also are affected by warm, patchy, and ice-rich permafrost. Therefore, it was highly desirable to clearly delineate the interfaces and depths of frozen ground in order to cost-effectively design and build the transmission line tower foundations. Frost heave and thaw settlement are the two most frequently occurring hazards, which can induce abnormal differential deformation strains and stresses in frozen soil foundations and subsurface infrastructures. However, studies on the impacts of frozen ground on the safety and long-term stability of tower foundations for transmission lines were very limited in China before the early 2000s.

Power transmission lines are very important for construction of key engineering projects and for the sustainable societal



Figure 2. Landscape of patchy permafrost zone north of Amdo on the Qinghai-Tibet Plateau, with the 110 kV power transmission line crossing the Amdo River in southern front of the Sengeligongshan Mountains.

and economic development in a region. However, the constraints for their engineering reliability and long-term stability are very exacting. Although the power transmission lines share some common features with other linear engineering projects, their survey, design, and construction for the frozen ground engineering geology are unique and site-specific because of the large distance between towers and the elevation/suspension nature of power lines compared to other linear engineering infrastructures such as roads and pipelines. The related surveys, selection of foundation types, design, and construction of tower foundations directly or indirectly affect the safety, integrity, long-term stability, profitability, and societal benefits. Therefore, differential frost heaving and thaw settlement are paid great attention during all phases (surveys, design, and construction) of power-line foundation engineering.

Because of its proximity to the southern lower limit of the plateau-elevation permafrost, potentials of frost heaving, sensitivity to thaw settlement of foundation soils, and depths of seasonal frost and thaw penetration in tower foundation soils vary markedly, even over short distances. Adverse cryogenic hazards resulting from freeze-thaw processes occur extensively and frequently. Their impacts on tower foundations are complicated and highly uncertain in various spatio-temporal scales due to their migratory nature. Therefore, the boundaries and depths of the permafrost table or seasonal frost penetration and frozen or unfrozen soils, as well as adverse cryogenic features, should be well understood in order to provide reliable criteria for designing cost-effective tower foundations and/or mitigative measures of hazardous foundation soils.

Frozen Ground Along the Power Line Route

The elevation along the power line route ranges from 4200 m to 4980 m. The topography is gentle and open, with relative relief generally less than 500 m. The annual mean air temperatures generally are colder than 0°C. Frozen ground, predominantly seasonally frozen ground, is found

Table 1. susceptibility classification of permafrost (revised from State Forestry Administration 2001).

coefficients	$\delta < 1$	$1 < \delta < 3$	$3 < \delta < 10$	$10 < \delta < 25$	$\delta > 25$
Thaw-sensitivity	Insensitive	Weakly sensitive	Sensitive	Very sensitive	Collapsing

extensively at all terrains from Nagqu to Damxung, and permafrost is generally found in the Amdo area.

Patchy permafrost

Patchy permafrost is generally connected with the active layer in areas north of Amdo, but it is separated from the active layer by a talik layer in the south (Wang & Wang 1982). Permafrost at elevations above 4700 m between Amdo and Damxung occurs in the Shengeligongshan Mountains, in intermontane basins in the vicinity of Highway Maintenance Squad Stations (HMSSs) 119, and 121 to 124 along the Qinghai-Tibet Highway, in the wetlands in the Liangdaohe River Basin (Figure 1). Patchy permafrost generally occurs in locations with better moisture conditions, fine-grained soils, and good vegetative cover favoring the development and protection of permafrost (Jin et al. 2007a, 2007b) (Fig. 2). Hazardous periglacial phenomena such as frost mounds and icings also are well developed.

Seasonally frozen ground

Seasonally frozen ground generally is found in intermontane basins between the Shengeligongshan Mountains and HMSSs 119, between HMSSs 121 and 122, 122 and 124, where permafrost occurs. The depths of seasonal frost penetration are 3.7–3.9 m in the Amdo area, 2.8–3.0 m in the Nagqu area, and 1.2–1.5 m in the Damxung area, as revealed by meteorological data. Ground surveys also confirm that seasonal frost penetration depths vary greatly from 1.2–4.0 m from Amdo to Damxung.

Hazardous periglacial phenomena

Pingos, seasonal frost mounds, and icing generally occur in concentrated small areas from HMSS 119 to the Liangdaohe River. Most of their occurrence is controlled by active faults (Wu et al. 2004, 2005, Jin et al. in press). Retrogressive thermal slumps also are found in very limited areas and are avoided.

Frozen Ground Engineering Geology

Classification of frozen soils for engineering purposes

On the basis of ice content, frozen soils were divided into 5 types: ice-poor, ice-medium, ice-rich, ice-saturated permafrost, and ice layers with soil inclusions. On the basis of frost heaving coefficients, the frost-heave susceptibility of soils was similarly divided into five grades: non-frost heave, weak frost heave, frost heave, strong frost heave, and very strong frost heave (State Forestry Administration 2001).

Frost heaving of seasonally frozen ground

The magnitude of vertical frost heave differs significantly with depth, even in a uniform soil layer, due to moisture

migration and subsequent ice segregation. Generally, the major frost heaving occurs at depths less than two-thirds of the maximum depth of the seasonal frost penetration (State Forestry Administration 2001).

Moisture and the content of fine-grained soil are the major factors leading to frost heave in foundation soils. Drainage conditions of excess water from the foundation soil also influence frost-heave forces. To mitigate the impact of frost heave, one needs to eliminate the effect of soil moisture by using lubricants (generally hydrophobic material such as bitumen mixed with 5% used machine oil, industrial vaseline, or heavy oil) on the walls of the tower foundation, separating foundation and soil. When foundation soils are rich in soil moisture or water supply, mixing and heating of coarse sands with used oil (1:6 in weight), placing a 20-cm-layer of this mixture around the foundation, and compacting well offered one solution. Drainage controls such as ditches and a water-retaining berm on the shaded side of the tower, especially on the slope in the permafrost regions, can be applied to prevent re-entry of ground water to tower foundation soils. The effect of fine-grained soil can be reduced by replacing it with well-compacted, clean gravel (the <0.074 mm clay less than 12%) within 0.5 m around the foundations outer surface. Refills for bedrock tower locations should be well-compacted gravels, and the outer surface of the tower foundation should be lubricated.

On the basis of coefficients (δ), which are a percentage of volumetric settlement of vertical column of tested soil, the thaw-sensitivity of permafrost, can be divided into five grades as in Table 1.

Research on Frozen Subsoil

Analysis of frost-heave forces

The normal frost-heave forces toward the bottom of foundation were mitigated by deeper (greater than maximum frost or thaw penetration depth) burial of the tower foundation. The mitigative effect was enhanced using with well-compacted gravel to a depth of 0.3–0.5 m beneath the tower foundation.

For tower foundation in areas impacted by seasonally frozen ground, a lubricant separating foundation wall from subsoil was used for tower location with weak frost-heaving subsoils. For subsoils with frost heave to very strong frost heave susceptibility, a mixture of used oil and coarse sand was placed within 0.2 m around the foundation and compacted well after lubricating the foundation walls. The impact of fine-grained soil also was mitigated by clean gravel refill within 0.5 m around the foundation outer surface. Drainage control ditches on the shady side of the tower also were used on the slopes to cut off the surface water supply to foundation soils. Deeper burial of the tower foundation, compacted

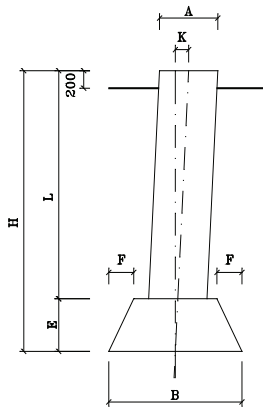


Figure 3. Sketch map of the oblique reinforced concrete column foundations for the power line tower.

gravel, reinforced structural integrity, and spatial stiffness were used to reduce deformation of foundation soils.

Soils above the permafrost table subjected to tangential seasonal frost-heave forces were mitigated using similar approaches. After the in-situ concrete-pouring during construction, permafrost temperatures beneath the bottom of the foundation rose, leading to thawing or thinning of permafrost. Therefore, the bearing capacity of unfrozen soils was used in design for safety. Deeper burial of tower foundation also was used to alleviate deformation of foundation soils.

In addition, the foundations were poured shortly after excavation, keeping the permafrost temperature as close to the original as possible. Thick ground-ice layers beneath tower foundations were removed. Local environmental and geological conditions were protected as cost-effectively as possible. Abandoned construction materials or soils were removed from around the tower foundations, and the ground surface was re-vegetated.

Design of Tower Foundations

Shallow foundation

Oblique column foundations of reinforced concrete (Fig. 3) to distribute the stresses were used extensively for the transmission line in montane areas. Frost-heave force was generally small, because the freezing of the subsoil generally lasted less than two months and resulted in very shallow (<1 m) seasonally frozen ground. Wind speed is generally less during the cold season, and frost-heave force is less than the anchorage force of the bottom of the foundation, satisfying the safety criteria for tower foundations.

Straight, reinforced concrete column foundation with constant cross-section (Fig. 4) also was used. Because the freezing time of subsoil was still short in shallow (<2 m) seasonally frozen soil regions, frost-heave forces were mainly affected by the subsoil features and moisture contents, satisfying the safety requirement of the transmission lines.

Straight reinforced concrete column foundation with variable cross-section areas (Fig. 5) was used where the subsoil freezing is long in deep (>2 m) seasonally frozen

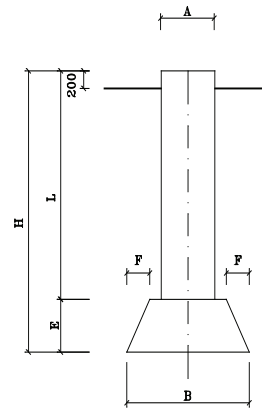


Figure 4. Straight reinforced concrete column foundation with constant cross-section.

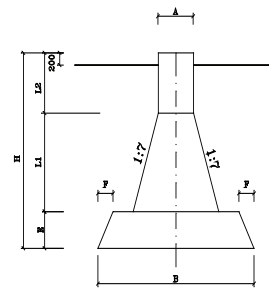


Figure 5. Straight reinforced concrete column foundation with variable cross-section.

soil regions. This form of foundation more reasonably balanced the loads, made full use of material and effectively minimized the side surface area, such as to use the cylinder column, to reduce the tangential frost-heave forces.

Pile foundation

Pile foundations were suitable for frozen subsoil under all geological conditions. When the upper structure of foundation burdens was heavy and constraints for differential settlement deformation were critical, pile foundations were usually embedded in the permafrost layer to obtain higher bearing capacity with minor changes in the ground temperature field (Heilongjiang Province Academy of Cold Area Building Research 1989). Pile foundations were divided into drilled-hole driven-in pile, inserted-in pile, and cast-in-situ pile. Pile foundations were used in deep (>4 m) seasonally frozen soil regions and in permafrost wetlands. The advantages of pile foundation include minor damage to the environs and significantly-reduced disturbance to frozen subsoil. However, the disadvantages include more precise engineering requirements and higher investment.

In critically important situations, thermal or thermosyphon-cooled pile foundations (Figs. 6, 7, 8) were adopted to supplement other techniques for maintaining the stability of the subsoil. Thermal pile foundation included pile foundations where the pile itself was the thermosyphon, and pile foundations where the thermosyphon(s) were inserted



Figure 6. Thermosyphon-cooled tower of power transmission line in alpine meadow in the vicinity of Damxung along the Qinghai-Tibet Highway. The thermosyphons were installed in each of the four feet of the tower supported by mat/pile foundation.

into or around the pile foundation. Both kinds of foundation were used in warm permafrost to maintain the ground temperatures at the predesigned conditions and subsequent long-term stability of the frozen subsoil.

Tower foundation types and improvement of subsoils

Selection of tower foundation types:

Tower foundations were placed in non-frost or weakly frost-susceptible soil zones, such as the top of mountains with bedrock, slopes and lowlands with coarse-grained soils with the least possible soil moisture content.

Subsoil improvement:

a) Replace with non-frost or weakly frost-susceptible soils, such as clean gravels and sands, with less than 12% to 15% clayey particles. Refill depth 80% of the maximum depth of frost penetration, extended about 0.3–0.5 m on side wall of the foundation.

b) Physical and chemical smearing of 2–5 mm thick hydrophobic material such as heavy oil, bitumen mixed with 5% used machine oil, or industrial vaseline on wall of the foundation to reduce cohesion between the foundation and subsoil. Wrap the outside of the foundation with bituminous felt or impervious geotextiles and thickness of about 0.2–0.3 m of sand or gravel placed around the foundation.

c) Insulating material such as EPS, furnace slag, sod, or humic soil (peat) spread on the surface.

d) Drainage control to avoid water collection established at the sides of foundation. Excessive water drained by ground gutter or basal pipe/culverts.

e) Structure methods included deep anchored foundations. Burial depth of iron tower foundation should be 0.3–0.5 m more than the maximum depth of frost penetration to increase the anchorage forces of the foundations.

Operation Status

The 440-km long Amdo-Damxung power line was the largest electric network construction project. Construction



Figure 7. Enlarged picture for details of the thermosyphon-cooled tower foundation.

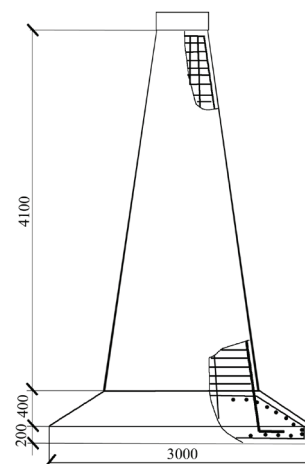


Figure 8. Sketch of reinforced concrete piling of tower foundation beneath the tower of Figures 3 and 4.

started in April 2003, and was completed and put into operation in December. As a result of the project, the Central Tibet and Nagqū Power Networks were combined, greatly benefiting the local inhabitants and providing the critical needs for building the Qinghai-Tibet Railway.

During the early operation period, frequent power outages were experienced due to bird and wind hazards. Some appreciable deformations and settlement were observed after the pouring of the concrete during construction. The deformations were later adjusted during the tower foundation installation processes. In addition, during construction in July and August 2003, the tower foundation subsoils at several sections were soaked by rain storms, resulting in differential settlement and horizontal displacement of tower foundations. It was soon rehabilitated and monitored afterwards, with satisfactory performance. Monitoring results during 2004–2007 indicated that the foundations in frozen ground were in designed condition.

Summary, Conclusions, and Prospects

a) The 110 kV power transmission line from Amdo to Damxung, Tibet Autonomous Region, China, is located in the patchy permafrost zone where frost heaving and thaw settlement were two challenging problems for design and construction of the line.

b) Surveys and assessment of frozen ground conditions for engineering geology were conducted for the evaluation of the potential of differential frost heaving and thaw settlement of tower foundation soils along the route.

c) The thermal and strain/stress of tower foundation and subsoils were analyzed for proper design and construction of the 110 kV power line.

d) Oblique and straight reinforced concrete column foundations and ordinary and thermosiphon-cooled pile foundations were proposed and adopted where appropriate. Tower site selection and ground improvement also were proven cost-effective.

e) Basic site selection principles included using bedrock foundations on mountain slopes and tops and coarse soils with least possible soil moisture on gentle slopes and lowlands.

f) Ground improvement measures generally included refilling with non- or weakly frost-susceptible soils, surface treatment to enhance water-proofing of foundation surfaces, insulation materials to decrease thaw penetration depths, drainage control to reduce frost heaving potential, and deep or bolted tower foundations exceeding the maximum depth of frost penetration.

g) The data bank and engineering measures, as well as experiences from the 110 kV power line would be very helpful for the proposed construction of 400 and 750 kV power transmission lines and other linear foundation engineering in warm, elevational permafrost.

Acknowledgments

Professor Emeritus Max C. Brewer from the U.S. Geological Survey, Alaska, provided generous assistance in English editing of the paper. The authors are very grateful for his generous assistance.

References

- Heilongjiang Province Academy of Cold Area Building Research. 1989. *Code for Design of Building Foundation in Permafrost Area* (JGJ118-89). Beijing, China: China Architecture & Building Press, 243 pp.
- Jin, H., Yu, S., Jin, R. & Sun, G. 2007a. Symbiosis of marshes and permafrost in the Xing'anling Mountains, Northeastern China. *Chinese Geographical Science* 17(4): 376-382. doi:10.1007/s11769-007-0376-3.
- Jin, H., Yu, Q., Wang, S. & Lü, L. 2007b. Changes in permafrost environments along the Qinghai-Tibet engineering corridor induced by anthropogenic activities and climate warming. *Cold Regions Science and Technology* 49(2), doi:10.1016/j.coldregions.2007.07.005
- Jin, H., Wei, Z., Ji, Y., Yu, Q., Lü, L., Wang, S. & Wu, Q. 2008. Assessment of frozen ground conditions for engineering geology along the Qinghai-Tibet Railway and Highway, China. *Engineering Geology* (in press).
- Myska, A.D. & How, G.T.S. 1978. Installation of pile foundations for a microwave tower system, Gillam-Churchill, Manitoba. In: National Research Council of Canada (sponsored), *Proceedings of the Third International Conference on Permafrost, Edmonton, Alberta, Canada, July 10-13, 1978*, Vol. 1: 827-832. State Forestry Administration, P.R. China. 2001. *Code for Engineering Geological Investigation of Frozen Ground* (GB50324-2001). Beijing, China: China Planning Press, 181 pp.
- U.S. Department of Defense. 2004. *Foundations for Structures: Arctic and Subarctic Construction. Unified Facilities Criteria (UFC), UFC 3-130-04*. Washington, DC, USA, 4-147 to 4-152.
- Wang, J. & Wang, S. 1982. *Features of Permafrost in the Southern Section of the Qinghai-Tibet Railway (South of Tanggula Mountain)*. The Geographical Society of China Conference on Glaciology and Geocryology (Cryopedology Vol.). Beijing, China: Science Press, 44-53.
- Wu, Z., Barosh, P.J., Hu, D., Wu, Z., Zhao, X., Ye, P. & Wang, J. 2004. Hazards posed by active major faults along the Golmud-Lhasa railway route, Tibetan Plateau, China. *Engineering Geology* 74: 163-182.
- Wu, Z., Barosh, P.J., Hu, D., Wu, Z., Ye, P., Liu, Q. & Zhou, C. 2005. Migrating pingos in the permafrost region of the Tibetan Plateau, China and their hazard along the Golmud-Lhasa Railway. *Engineering Geology* 79: 267-287.

Hydraulic Conductivity in Frozen Unsaturated Soil

Kunio Watanabe

Graduate school of Bioresources, Mie University, Japan

Tomomi Wake

Graduate school of Bioresources, Mie University, Japan

Abstract

Freezing experiments of silt and sand columns were carried out, and water and heat flows were observed. To estimate unsaturated hydraulic conductivity of soils, $K(h)$, at above-freezing and subzero temperatures, Darcy's law was solved under a non-isothermal condition with ice formation. $K(h)$ steeply decreased with decreasing soil water pressure, h , and more gradually decreased with soil freezing. The results show that the hydraulic model, in which water content became constant under $h < -10^5$ cm, underestimated the $K(h)$ of frozen soil, and suggest that the impedance factor, which reduced $K(h)$ for frozen soil, is not necessary when accurate soil water and soil freezing characteristics are available. The hydraulic model, which can express two types of soil water flow, such as capillary and film flows, appears to be useful for expressing the hydraulic properties of soils under the freezing process.

Keywords: soil freezing characteristic; soil water characteristic; TDR; unsaturated hydraulic conductivity; water and heat flows.

Introduction

Knowledge of water flow in frozen and thawing ground is important to investigating water and solute redistributions in soil during winter (Baker & Spaans 1997) and in studying the mechanism of frost heaving (Wettlaufer & Worster 2006). Changes in soil properties, such as hydraulic conductivity, have also received research attention. For example, changes caused by ground freezing have been examined by applying an artificial soil-freezing technique to stabilize soil and form a barrier against hazardous waste (McCauley et al. 2002). Moreover, a major concern of hydrological and climate modeling is how to express change in soil hydraulic properties.

Burt & Williams (1976) and Horiguchi & Miller (1983) measured the steep decrease in hydraulic conductivity with soil freezing, although within a small temperature range. Using oil as a fluid, McCauley et al. (2002) measured saturated hydraulic conductivity of frozen soil at various temperatures. However, few experimental studies have examined the unsaturated hydraulic conductivity of frozen soil, $K_f(h)$. The unsaturated hydraulic conductivity of unfrozen soil, $K(h)$, is usually expressed by the formula proposed by Brooks & Corey (1964), Clapp & Hornberger (1979), or van Genuchten (1980). For frozen soil, Harlan (1973) used $K(h)$ instead of $K_f(h)$, assuming the same film-water geometry between frozen and unfrozen soils. However, numerical simulations have suggested that this assumption overestimates water flow near the freezing front (Harlan 1973, Taylor & Luthin 1978, Jame & Norum 1980). Guymon & Luthin (1974) and Tao & Gray (1994) expressed $K_f(h)$ from $K(h)$ by subtracting ice content from saturated water content. When the soil is frozen, the presence of ice in some pores may block water flow. To account for this blocking, several impedance factors have been introduced (James & Norum 1980, Lundin 1990, Smirnova et al. 2000).

However, Black & Hardenberg (1991) criticized the use of an impedance factor, stating that it is a potent and wholly arbitrary correction function for determining $K_f(h)$. Newman & Wilson (1997) also concluded that an impedance factor is unnecessary when an accurate soil water characteristic curve and relationship between $K(h)$ and soil water pressure are defined.

Measuring unsaturated hydraulic conductivity for frozen soil remains difficult, and a complete expression for $K_f(h)$ is still not available. In addition, the model for $K_f(h)$ should be correlated with the soil water characteristics and soil freezing characteristics for ease of use in numerical simulations (Watanabe et al. 2007). In this experiment, we estimated $K_f(h)$ from water and heat flow measurements in a frozen soil column and discuss a model for $K_f(h)$.

Theory

Assuming that vapor and ice flows are negligible, variably saturated water flow in above-freezing and subzero soil is described using a modified Richards equation as follows (Noborio et al. 1996, Hansson et al. 2004).

$$\frac{\partial \theta(h)}{\partial t} + \frac{\rho_i}{\rho_w} \frac{\partial \theta_i(T)}{\partial t} = \frac{\partial}{\partial z} \left(K(h) \frac{\partial h}{\partial z} + K(h) + K(h) \gamma h \frac{\partial T}{\partial z} \right) \quad (1)$$

where θ is volumetric liquid water content, θ_i is volumetric ice content, t is time, z is a spatial coordinate, ρ_i is density of ice, ρ_w is density of water, h is the water pressure head, T is temperature, and γ is the surface tension of soil water. The terms in parentheses on the right-hand side of equation (1) represent the water flux, J_w , obtained from the change in the amount of liquid water and ice. Thus, if we measure the pressure and temperature gradient, $K(h)$ [or $K_f(h)$ at subzero temperature] would be derived as

Table 1. Experimental conditions and physical properties of soil.

		FSi	TDS
Bulk density	g cm ⁻³	1.18	1.45
θ when packed	m ³ m ⁻³	0.40	0.15
θ saturation	m ³ m ⁻³	0.569	0.36
Thermal conductivity*	W m ⁻¹ K ⁻¹		
at θ = 0.00 (frozen)		0.20(0.20)	0.25(0.25)
at θ = 0.17 (frozen)			0.96(1.50)
at θ = 0.24 (frozen)		0.52(0.55)	1.06(1.05)
at θ = 0.29 (frozen)			
Saturated hydraulic cond.	cm h ⁻¹	0.66(0.76)	50.6
		0.25	
van Genuchten parameter			
θ _r	m ³ m ⁻³	0.03	0.015
α	m ⁻¹	0.16	3.36
n		1.38	7
l		0.552	-0.5
Durner parameter			
θ _r	m ³ m ⁻³	0.06	0
α ₁	m ⁻¹	0.35	3.466
n ₁		3.10	6.40
l		-0.08	-0.5
α ₂	m ⁻¹	0.011	0.027
n ₂		1.70	1.40
w ₂		0.461	0.105

*The value for thermal conductivity is average of 2 to 20°C for unfrozen soil and -5 to -20°C for frozen soil.

$$K(h) = -\frac{J_w}{\left(\frac{\Delta T}{\Delta z} \gamma h + \frac{\Delta h}{\Delta z} + 1\right)} \quad (2)$$

The value of h in unfrozen soil can be obtained from the soil water characteristics (relationship between θ and h) when measuring the profile of θ , while h in frozen soil can be calculated from the temperature profile derived from the generalized form of the Clausius–Clapeyron equation by assuming a differences between ice and water. Specifically, the ice pressure is sometimes assumed to equal zero gauge pressure (Williams & Smith 1989, Hansson et al. 2004):

$$\frac{dP}{dT} = \frac{L_f}{v_i T} \quad (3)$$

where P is the pressure ($= \rho_w g h$), g is the acceleration due to gravity, L_f is the latent heat of freezing, and v_i is the specific volume of water. Thus, equation (3) gives the soil freezing characteristics (relationship between θ and T) from the soil water characteristics and vice versa.

Material and Methods

The samples used in this study were Fujinomori silt (FSi) and Tottori dune sand (TDS). Figure 1 shows the soil water characteristics measured by several physical methods (Jury & Horton 2004) for both soils as well as soil freezing characteristics measured by pulsed nuclear magnetic resonance (NMR) measurement and depicted by equation

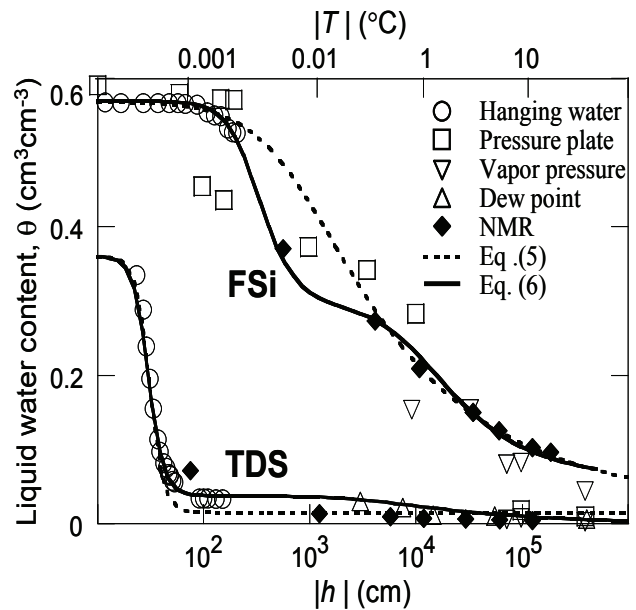


Figure 1. Soil water characteristics measured by hanging water, pressure plate, vapor pressure, and chilled mirror dew point measurement methods, and soil freezing characteristics measured by pulsed NMR measurement for FSi and TDS (in thawing process).

(3). FSi is highly susceptible to frost and retains much liquid water even when $|h| > 10^4$ cm ($T < -1^\circ\text{C}$), while for TDS, $\theta = 0.03$ when $|h| > 10^2$ cm ($T < -0.01^\circ\text{C}$).

The TDS were preliminarily washed in deionized water, and the FSi was passed through a 2 mm screen. Each sample was mixed with distilled and deionized water and packed into an acrylic column with an internal diameter of 7.8 cm and a height of 35 cm. Table 1 lists the experimental conditions and physical properties of the samples. Fifteen copper-constantan thermocouples and seven time domain reflectometry (TDR) probes were inserted into each column, and the side wall of the column was insulated. The TDR was preliminarily calibrated for measuring unfrozen water content by comparison to the pulsed NMR measurement. The column was settled at an ambient temperature of 2°C for 24 h to establish initial water and temperature profiles and then frozen from the upper end by controlling temperature at both ends of the column ($T_L = -8^\circ\text{C}$ and $T_H = 2^\circ\text{C}$). During the experiment, no water flux was allowed from either end, and profiles of temperature, water content, and solute concentration (EC_a) were monitored using thermocouples and TDRs. A series of experiments with different durations of freezing were then performed for each freezing condition (i.e., same freezing rate and temperature gradient). At the end of the experimental series, the sample was cut into 2.5 cm intervals to measure the total water content by the dry-oven method. From thermocouples and TDR readings, it was confirmed that each column had the same temperature and water profiles during the series of experiments.

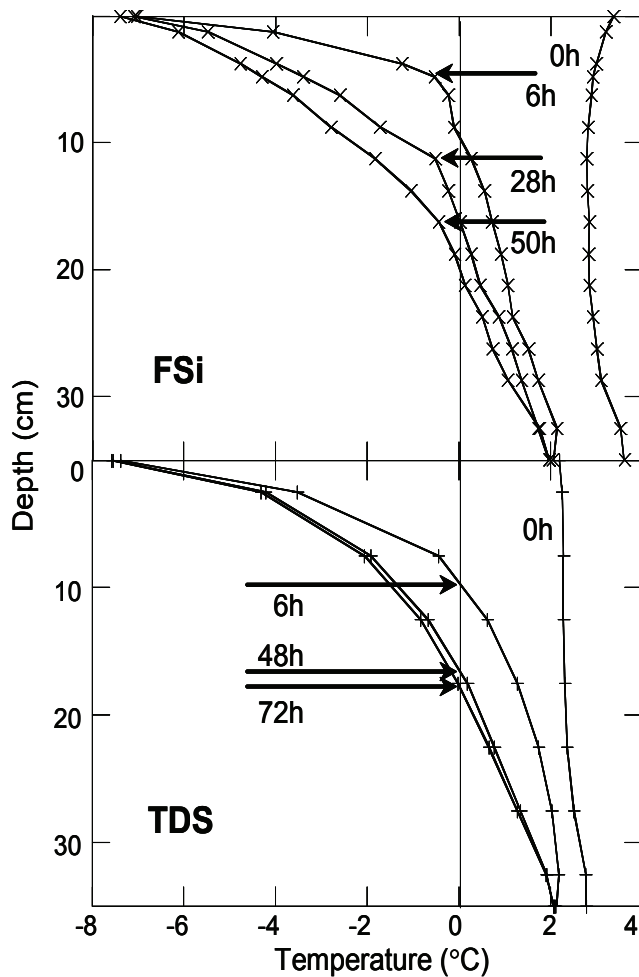


Figure 2. Temperature profiles for FSi (0, 6, 28, 50 h after freezing started) and TDS (0, 6, 48, 72 h after freezing started). Arrows represent the freezing front.

Results

Heat and water flow

Figure 2 shows temperature profiles of the freezing soils. When both ends of the column were set at different temperatures, the soil near the column ends quickly reached the required temperatures. In FSi, the advancing rate of the 0°C isotherm was 1.57, 0.34, and 0.16 cm h⁻¹ for 0–6, 6–24, and 24–48 h, respectively, and approximately 0.25°C lowering of the freezing point was observed. The freezing rate of TDS was similar to that of FSi, although TDS had larger thermal conductivity (Table 1). Even after 72 h, the temperature profile of the subzero area in TDS did not reach a linear shape as in FSi and in the unfrozen area in TDS.

Figure 3 presents water profiles in FSi and TDS at the same freezing time as shown in Figure 2. The solid line indicates total water content, θ_p , measured by the dry-oven method, and the dashed line indicates unfrozen water content measured by TDR. The ice content, θ_i , was obtained by subtracting the unfrozen water from the total water content. FSi had a relatively vertical initial θ profile, having similar θ values for $h < 100$ cm (Fig. 1). An increase of θ_p , decrease of

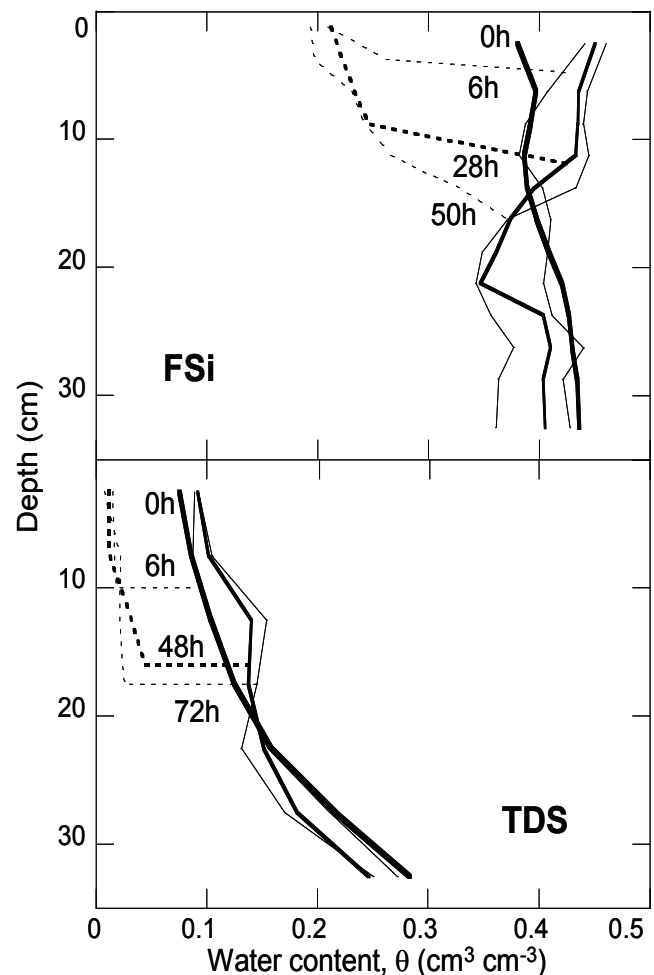


Figure 3. Moisture profiles for FSi and TDS at the same freezing time as shown in Figure 2. The solid line and dashed line represent total water and unfrozen water contents, respectively.

θ in the frozen area, and decrease of θ in the unfrozen area with the advancing freezing front were observed, implying that the soil water flowed not only through the unfrozen area, but also the frozen area. The gradient of the initial θ profile of TDS corresponded to its soil water characteristics (Fig. 1). In TDS, the soil water in the unfrozen area flowed to and accumulated near the freezing front because of suction at the freezing front caused by ice formation. Water flow in the unfrozen area continued 48 h or later after freezing began, although there was no apparent advance of the freezing front. Meanwhile, much less water flow was observed in the frozen area.

The profile of water flux, J_w , was then calculated by developing θ profiles (Fig. 3) with the boundary condition of no water flux. In early stage of freezing (0–6 h), soil water in almost the entire column moved upward at about $J_w = 0.04$ cm h⁻¹ for FSi and $J_w = 0.01$ cm h⁻¹ for TDS. The progression of the peak observed in the J_w profile coincided with the freezing front. In the frozen area, J_w in SFi was ≥ 10 times larger than that in TDS and exponentially decreased as the temperature decreased ($J_w = 0.007|T|^{-0.69}$ for FSi and $0.0012|T|^{-1.45}$ for TDS).

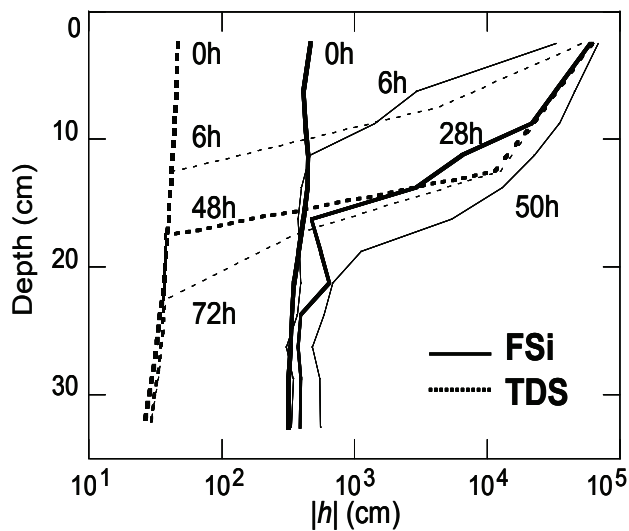


Figure 4. Profile of soil water pressure estimated from Figures 2 and 3.

Change in hydraulic conductivity

Figure 4 shows the profile of soil water pressure h estimated by the soil water characteristics (Fig. 1) with the θ profile (Fig. 3) and equation (3) with the temperature profile (Fig. 2). Solute effect was negligible during the experiments, since very low solute concentration was confirmed by TDR (EC_a) readings. Note that for equation (3) there was discontinuity in the h profiles near 0°C , especially for unsaturated soil; therefore, we used linear interpolation to connect the closest calculated h values between the unfrozen and frozen areas. With freezing, $|h|$ steeply increased ($h < -10^3$ cm). A larger difference in h between unfrozen and frozen areas was observed in TDS than in FSi.

The non-isothermal version of Darcy's law (Eq. 2) could consequently be solved with the J_w , T , and h profiles, obtaining the relationship between the unsaturated hydraulic conductivity, $K(h)$, at above-zero and subzero temperatures with the soil water pressure, as shown in Figure 5. In the range $h > -10^3$ cm (unfrozen), $K(h)$ decreased steeply with increasing $|h|$, while it decreased gradually in the range $h < -10^3$ cm (frozen). Similar $K(h)$ was observed when different freezing conditions were applied ($T_L = -5^\circ\text{C}$ and $T_H = 5^\circ\text{C}$ in Fig. 5 for TDS). These changes were clearer for $K(h)$ of TDS, which agreed well with the value obtained using the evaporation method (Sakai & Toride 2007). In the frozen area, $K(h)$ in FSi was about 10 times larger than that in TDS, which is why more water flow was observed in frozen FSi. Figure 6 shows the relationship between $K(h)$ and liquid (unfrozen) water content measured by TDR. In frozen TDS, $K(h)$ decreased steeply from 10^{-5} – 10^{-8} cm h $^{-1}$ with decreasing θ from 0.04–0.01 cm 3 cm $^{-3}$, while $K(h)$ of frozen FSi decreased more gradually.

The $K(h)$ of frozen soil also correlated with temperature T and with ice content θ_i . The decrease of $K(h)$ with lowering T and θ_i was well fitted by power law as $K(h) = 3 \times 10^{-6} |T|^{-1.49}$ and $K(h) = 2.3 \times 10^{-8} \theta_i^{-2.42}$ for FSi, and $K(h) = 0.7 \times 10^{-6}$

$|T|^{-1.75}$ and $K(h) = 8.2 \times 10^{-14} \theta^{-6.96}$ for TDS. This power law relationship was consistent with the relationship between J_w and $|T|$ mentioned above. The θ – T relationship is sometimes expressed by power law (Anderson & Tice 1972) and can be converted through equation (3) to a θ – h relationship, which may also be expressed by power law (Brooks & Corey 1964). The shape of the formula indicating $K(h)$ may arise from the soil water characteristics (θ – h) and soil freezing characteristics (θ_i – T).

Discussion

Soil freezing characteristics

Soil freezing characteristics are sometimes interpreted from the surface force, pore curvature, when solute effect is negligible (Dash et al. 1995, Watanabe & Mizoguchi, 2002). The surface force accounts for the power law shape of soil freezing characteristics and the effect of the curvature known as the Gibbs–Thomson effect, which creates a shoulder to the soil freezing characteristics by means of the freezing temperature depression, $T_m - T$ depending on the soil pore radius r :

$$T_m - T = \frac{T_m \sigma}{\rho_i L_f r} \quad (4)$$

where T_m is the freezing temperature of bulk water and σ is the ice–water interface free energy. In the soil pore size distribution, two peaks are presumed: one from pores among the soil particles ($r = 5$ – 50 μm) and the other from pores on the particle surface ($r = 3$ – 10 nm). These peaks would yield two shoulders to the soil freezing characteristics around -0.001 to -0.1°C and -2.5 to -10°C , respectively. By converting the soil freezing characteristics to soil water characteristics through equation (3), the warmer shoulder would correspond to air entry. In the range from water saturation to the other (colder) shoulder, soil water will flow predominantly as capillary flow, but will change to film flow at h lower than the colder shoulder. Soil water characteristic models proposed by Brooks & Corey (1964) and van Genuchten (1980) (Eq. 5) are intended to express unsaturated soil with moderate h and give the constant θ (defined as resident water content, θ_r) at extremely low h . These models, therefore, cannot express the area around the colder shoulder, which is an important portion for soil freezing characteristics (Fig. 1). Durner (1994) combined two van Genuchten models, which express different soil water characteristics, to describe water retention in a soil having a dual porosity distribution (Eq. 6):

$$S_e = \left(1 + |\alpha h|^n\right)^{-m} \quad (5)$$

$$S_e = w_1 \left[1 + (\alpha_1 h)^{n_1}\right]^{-m_1} + w_2 \left[1 + (\alpha_2 h)^{n_2}\right]^{-m_2} \quad (6)$$

where $S_e = (\theta - \theta_r)(\theta_s - \theta_r)^{-1}$, $m = 1 - n^{-1}$, $w_1 = 1 - w_2$, θ_s is saturated water content, α and n are empirical parameters,

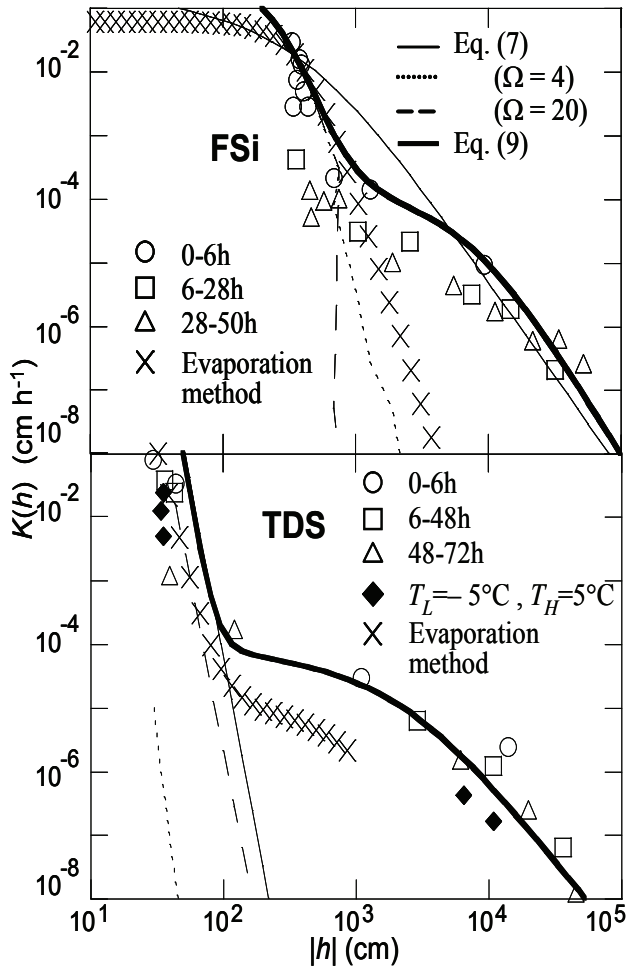


Figure 5. Relationship between unsaturated hydraulic conductivity $[K(h)]$ and soil water pressure at above-zero and subzero temperature. Table 1 lists the parameters for equations (7) and (9).

and w_2 is the weighting factor. Using the parameters listed in Table 1, equation (6) was well fitted to a wide range of soil water characteristics, including soil freezing characteristics, for FSi and TDS (Fig. 1).

Unsaturated hydraulic conductivity for frozen soils

The unsaturated hydraulic conductivity for unfrozen soil, $K(h)$, is often derived from equation (5) (van Genuchten 1980) as follows:

$$K(h) = K_s S_e^l \left[1 - (1 - S_e^{1/m})^m \right]^2 \quad (7)$$

where l is the pore-connectivity coefficient. For frozen soil, $K(h)$ is sometimes reduced by an impedance factor Ω (Lundin 1990, Hansson et al. 2004):

$$K(h)_{\text{frozen}} = 10^{-\Omega \theta / (\theta_i - \theta_e)} K(h) \quad (8)$$

Applying equations (7) and (8) to our measured $K(h)$ verified that equation (7) could not fit the gradient change of $K(h)$ around $h = 10^{-3}$ cm for FSi and underestimated $K(h)$ at

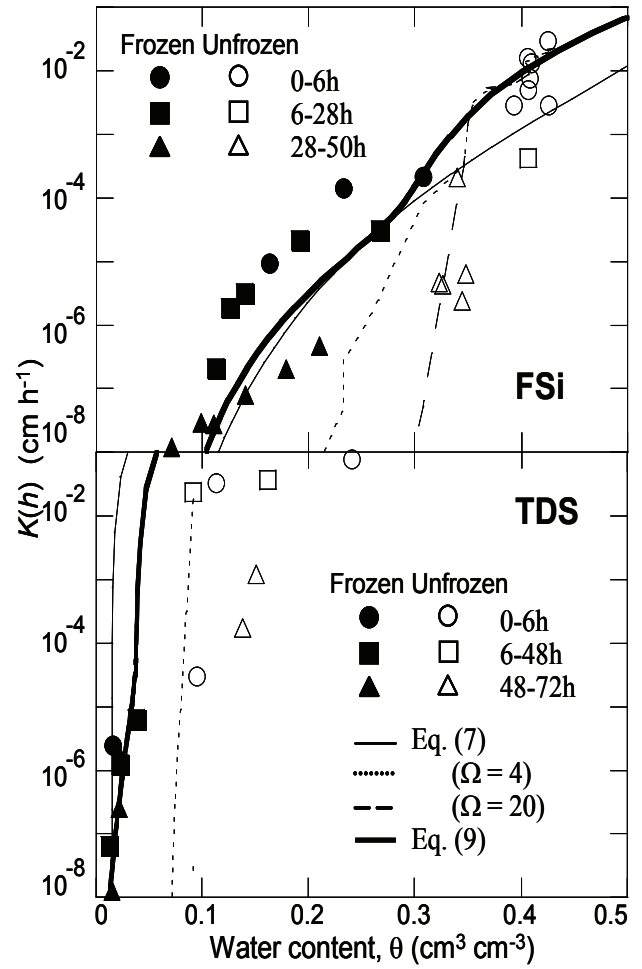


Figure 6. Relationship between unsaturated hydraulic conductivity, $K(h)$, and soil water content at above-zero and subzero temperature. Table 1 lists the parameters for equations (7) and (9).

$h < -10^2$ cm for TDS (Fig. 5). The impedance factor might be useful for expressing the steep decrease of $K(h)$ near 0°C , if equation (5) were fitted to the whole range of soil water characteristics (FSi in Figs. 5, 6). However, use of an impedance factor requires caution since it will underestimate $K(h)$ as freezing progresses.

The design of equation (7) was based on the bundle of capillary tube model in which water flow decreases with square decrease in the pore (tube) radius, as Poiseuille flow, and produces a linear reduction in $K(h)$ on a log-log scale when θ is constant. On the other hand, film water can be regarded as the flow proportional to the first or less root of film thickness. The $K(h)$ of frozen soil consequently has a lower grade than that of unfrozen soil. Thus, the Durner model was again applied to $K(h)$, taking care that θ did not become constant at $10^{-3} < h < 10^{-6}$ cm ($-0.1 < T < -100^\circ\text{C}$).

$$K(S_e) = K_s (w_1 S_{e1} + w_2 S_{e2})^l \times \frac{\left(w_1 \alpha_1 \left[1 - (1 - S_{e1}^{1/m_1})^{m_1} \right] + w_2 \alpha_2 \left[1 - (1 - S_{e2}^{1/m_2})^{m_2} \right] \right)^2}{(w_1 \alpha_1 + w_2 \alpha_2)^2} \quad (9)$$

Equation (9) showed good agreement with the $K(h)$ obtained from the column freezing experiment (Figs. 5, 6). This model was originally used for explaining water flow containing two different flow rates, such as among and within soil aggregates. Our results suggest that this model is also suitable for soils under freezing-thawing processes, in which soil water flow changes from capillary flow to film flow.

Conclusion

The sand and silt columns were frozen directionally, and the water and heat flows during soil freezing were measured. The flows depended on the soil types. Unsaturated hydraulic conductivity for frozen and unfrozen soils was estimated by solving Darcy's law under non-isothermal conditions with ice formation, although further consideration of the precision of flux measurements and limits of the Clausius-Clapeyron equation may be required. Hydraulic conductivity steeply decreased with decreasing soil water pressure and water content in unfrozen soil but more gradually decreased in frozen soil. In both unfrozen and frozen states, the silt had higher hydraulic conductivity than the sand, resulting in more water flow during silt freezing.

The shapes of soil water characteristics and soil freezing characteristics were discussed from the viewpoint of the pore size distribution. Use of an impedance factor for calibrating the hydraulic conductivity of frozen soil, which has sometimes created unstable numerical simulations, appears to be unnecessary when the hydraulic model can appropriately express both the soil water and freezing characteristics. Rather, the results suggest that the Durner model is useful for expressing the hydraulic properties affected by the change in the type of water flow during soil freezing.

References

- Anderson, D.M. & Tice, A.R. 1972. Predicting unfrozen water content in frozen soils from surface area measurements. *Highway Res. Record*, 393: 12-18.
- Baker, J.M. & Spaans, E.J.A. 1997. Mechanics of meltwater movement above and within frozen soil. *Proceedings of International Symposium on Physics, Chemistry, and Ecology of Seasonally Frozen Soils. U.S. Army CRREL Special Report 97-10*, 31-36.
- Black, P.B. & Hardenberg, M.J. 1991. Historical perspectives in frost heave research, the early works of S. Taber and G. Beskow. *CRREL Special Report*, 91-23.
- Brooks, R.H. & Corey, A.T. 1964. Hydraulic properties of porous media. *Hydrol. Paper 3*. Colorado State Univ., Fort Collins, CO, USA.
- Burt, T.P. & Williams, P.J. 1976. Hydraulic conductivity in frozen soils. *Earth Surface Processes* 1: 349-360.
- Clapp, R.B. & Hornberger, G.M. 1979. Empirical equations for some soil hydraulic properties. *Water Resour. Res.* 14: 601-604.
- Dash, J.G., Fu, H. & Wettlaufer, J.S. 1995. The premelting of ice and its environmental consequences. *Rep. Prog. Phys.* 58: 115-167.
- Durner, W. 1994. Hydraulic conductivity estimation for soils with heterogeneous pore structure. *Water Resour. Res.* 30(2): 211-223.
- Guymon, G.L., Berg, R.L. & Hromadka, T.V. 1993. Mathematical model of frost heave and thaw settlement in pavement. *CRREL Report 93-2*.
- Hansson, K., Šimůnek, J., Mizoguchi, M., Lundin, L.C. & van Genuchten, M.Th. 2004. Water flow and heat transport in frozen soil: Numerical solution and freeze-thaw applications. *Vadose Zone Journal* 3: 693-704.
- Harlan, R.L. 1973. Analysis of coupled heat-fluid transport in partially frozen soil. *Water Resour. Res.* 9: 1314-1323.
- Horiguchi, K. & Miller, R.D. 1983. Hydraulic conductivity of frozen earth materials. *Proceedings of the Fourth International Conference on Permafrost*, Fairbanks, 504-509.
- Jame, Y.W. & Norum, D.I. 1980. Heat and mass transfer in freezing unsaturated porous media. *Water Resour. Res.* 16: 811-819.
- Jury, A.W. & Horton, R. 2004. *Soil Physics*, Hoboken: John Wiley & Sons Inc., 384 pp.
- Lundin, L.-C. 1990. Hydraulic properties in an operational model of frozen soil. *J. Hydrol.* 118: 289-310
- McCaughey, C.A., White, D.M., Lilly, M.R. & Nyman, D.M. 2002. A comparison of hydraulic conductivities, permeabilities and infiltration rates in frozen and unfrozen soils. *Cold Regions Sci. Tech.* 34: 117-125.
- Newman, G.P. & Wilson, G.W. 2004. Heat and mass transfer in unsaturated soils during freezing. *Can. Geotech. J.* 34: 63-70.
- Noborio, K., McInners, K.J. & Heilman, J.L. 1996. Two-dimensional model for water, heat and solute transport in furrow-irrigated soil: I. Theory. *Soil Sci. Soc. Am. J.* 60: 1001-1009.
- Sakai, M. & Toride, N. 2007. Optimum conditions for predicting unsaturated hydraulic properties using the evaporation method. *J. Jpn. Soc. Soil Phys.* 106: 33-46.
- Smirnova, T.G., Brown, J.M., Benjamin, S.G. & Kim, D. 2000. Parameterization of cold-season processes in the MAPS land-surface scheme. *J. Geophys. Res.* 105: 4077-4086.
- Tao, Y.X. & Gray, D.M. 1994. Prediction of snowmelt infiltration into frozen soils. *Numerical Heat Transfer, Part A: Applications* 26: 643-665.
- Taylor, G.S. & Luthin, J.N. 1978. A model for coupled heat and moisture transfer during soil freezing. *Can. Geotech. J.* 15: 548-555.
- van Genuchten, M.Th. 1980. A closed-form equation for predicting the hydraulic conductivity of unsaturated soils. *Soil Soc. Am. J.* 44: 892-898.
- Watanabe, K. & Mizoguchi, M. 2002. Amount of unfrozen water in frozen porous media saturated with solution. *Cold Reg. Sci. Tech.* 34: 103-110.
- Watanabe, K., Toride, N., Sakai, M. & Šimůnek, J. 2007. Numerical modeling of water, heat and solute transport during soil freezing. *J. Jpn. Soc. Soil Phys.* 106: 21-32.
- Wettlaufer, J.S. & Worster, M.G. 2006. Premelting dynamics. *Annu. Rev. Fluid. Mech.* 38: 427-452.
- Williams, P.J. & Smith, M.W. 1989. *The Frozen Earth: Fundamentals of Geocryology*. Cambridge: Cambridge University Press, 360 pp.

Sounding Ice and Soil Wedge Structures with Ground-Penetrating Radar

Tatsuya Watanabe

Geoenvironmental Sciences, University of Tsukuba, Tsukuba, Japan

Norikazu Matsuoka

Geoenvironmental Sciences, University of Tsukuba, Tsukuba, Japan

Hanne H. Christiansen

Department of Geology, the University Centre in Svalbard, Longyearbyen, Norway

Atsushi Ikeda

Geoenvironmental Sciences, University of Tsukuba, Tsukuba, Japan

Abstract

Ground-penetrating radar (GPR) was used to sound subsurface structures below troughs delimiting non-sorted polygons in Svalbard. On marine terraces, a single hyperbolic reflection spreads downward from the ground surface, which represents an active layer soil wedge. Some large troughs are underlain by double hyperbolic reflections extending downward from the ground surface and the frost table, which correspond to a soil wedge and an underlying ice wedge, respectively. On fluvial terraces, a hyperbolic reflection extends downward from the frost table, which represents an ice wedge; the width of the hyperbola corresponds to the width of an ice wedge. The hyperbolic reflections originate from the contrast in water content between the wedge filling and the host material. These results indicate that GPR is useful for distinguishing ice and active layer soil wedges in terms of depth of the hyperbola and for estimating the width of ice wedges without excavation.

Keywords: ground-penetrating radar; ice wedge; non-sorted polygon; soil wedge; Svalbard.

Introduction

Non-sorted polygons are one of the most widespread periglacial landforms in Svalbard. Most of them occur on the bottoms and slopes of inland valleys, uplands surrounding the valleys (Sørbel et al. 2001, Tolgensbakk et al. 2001), and on strandflats (Åkerman 1980, 1987). Direct excavation and drilling revealed that ice wedges are predominant in Adventdalen (inland valley), while active layer soil wedges

are more common in Kapp Linné (strandflat) despite similar surface patterns (Matsuoka & Hirakawa 1993). Thus, surface patterns cannot indicate the presence of ice wedges. Since direct methods are time consuming, more convenient methods are required to relate surface geometry to subsurface wedge structures.

Ground-penetrating radar (GPR) is a useful tool for imaging near-surface structures. GPR has been applied to permafrost studies since the 1970s to identify areas of massive ground ice (e.g., Dallimore & Davis 1987), internal structure of rock glaciers (e.g., Berthling et al. 2000) and pingos (Ross et al. 2005, Yoshikawa et al. 2006), and to determine the depth of the permafrost table and ice wedges (Hinkel et al. 2001). A recent GPR study attempted to visualize near-surface structures in permafrost with three-dimensional images (Munroe et al. 2007). We also applied GPR to visualize subsurface wedge structures, and particularly to distinguish ice wedges from active layer soil wedges in Svalbard. Furthermore, ice wedge width was estimated from the reflection patterns of radar signal.

Study Sites

Svalbard is an archipelago situated between 74°N to 81°N and 10°E to 35°E. The largest island is Spitsbergen, which covers an area of 38,000 km² (Fig. 1).

Kapp Linné is located at the southern edge of the mouth of Isfjorden, central Spitsbergen (Fig. 1). The area is located on a wide strandflat composed of a sequence of raised marine terraces with beach ridges, small lakes, and bogs. The strandflat emerged above sea level after the Lateglacial

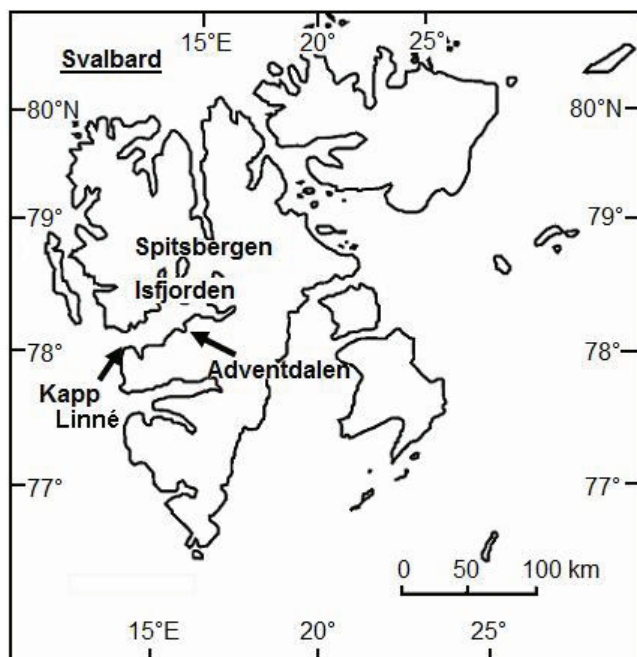


Figure 1. Locations of the study areas.

deglaciation (11–5.5 ka BP) (Landvik et al. 1987). A number of relatively small polygons (5–15 m in diameter) developed on the raised beach ridges consisting of gravely sand and lacking vegetation. The polygons are mostly high-centered and delimited by narrow and shallow troughs. The mounds and troughs are well distinguished by the presence of vegetation only in the latter. The troughs mostly lack well-defined rims at both sides except for some extraordinarily large ones. Åkerman (1980) mapped most of the troughs underlain by active layer soil wedges but extraordinary large ones having ice wedges. Similar mounds and troughs also sporadically occur on the bogs which are composed of peat and covered with vegetation. However, they rarely constitute polygonal patterns and are usually obscured by full vegetation. Åkerman (1980) classified them as ice wedge polygons. The mean annual air temperature (MAAT) is -4.9°C in Kapp Linné (Åkerman 1996). Permafrost is nearly continuous except for a karst area (Salvisen et al. 1985). The active layer thickness varies from 0.3 m in the bogs to 2 m on the raised beach ridges (Åkerman 1980).

Adventdalen is a broad, U-shaped valley joining Isfjorden at Longyearbyen (Fig. 1). The lowermost 15 km of the valley bottom is covered with fluvial sediments composed of branched river flood plain deposits (Tolgensbakk et al. 2001). Large, low-centered, hexagonal polygons are widespread on the Adventelva river terrace, where the fluvial sediments are covered with fine-grained loess about 3 m thick. The polygons are typically delineated by troughs a few centimeters to 40 cm deep and 20–100 cm wide. The variation in trough size probably represents different generations of thermal contraction cracks constituting a complex polygonal network (Christiansen 2005). MAAT is -6.5°C (1961–1990) at Svalbard Lufthavn (airport) in Longyearbyen (Hanssen-Bauer et al. 1990). Permafrost is continuous, and its thickness is estimated to be 220 m at Janssonhaugen, located in the upper Adventdalen (Isaksen et al. 2001). The thickness decreases to less than 100 m approaching the sea (e.g., Humlum et al. 2003). The active layer thickness in Adventdalen is about 1 m in the fine-grained loess (Christiansen & Humlum 2003).

Methods

Surveys were conducted in late June and late July 2007 in Kapp Linné and in early July 2006, end of July, and middle of August 2007 in Adventdalen. The numbers of survey lines in Kapp Linné and Adventdalen are 44 and 36, respectively. The GPR used in this study was a Noggin Smart Systems, produced by Sensors & Software Inc. The system consists of a cart, an antenna box (Noggin 250), an odometer wheel, a digital video logger, and a battery. The 250 MHz signal was applied to the survey of wedge structures. The resolution is enough to display the target, although the radar signal tends to attenuate in thawed fine-textured sediments.

The GPR antenna transmits electromagnetic pulses into the ground. The transmitted wave is reflected at geological boundaries that have an electromagnetic impedance

contrast. The two way travel time (TWT) for the reflected waves is recorded and plotted on a diagram. Radar records were processed with the RADPRO for Windows version 3.0 (Korea Institute of Geoscience and Mineral resources). Processing included conversion of TWT to the depth scale, removal of the direct ground wave during radar acquisition, topographic modification, and gain adjustments. Converting TWT to the depth scale requires the radar transmission velocity in the layer or layers above the reflector. The velocity was determined by direct depth measurements or a point-source reflection analysis. The latter permits estimation of the radar transmission velocity using the shape of hyperbolic patterns produced by point structures (Moorman et al. 2003). The GPR images were compared with the results of direct excavation and/or drilling at six troughs. Soil samples were taken at these troughs to determine the grain size distribution and water content to interpret GPR images, because the contrast of water content, which mainly depends on the difference in grain size distribution at a depth, results in different dielectric constants.

Results and Interpretations

Kapp Linné: Marine terraces

The GPR profiles across polygon troughs developed on beach ridges displayed strong horizontal and hyperbolic reflections (Fig. 2a). The point-source reflection analysis using the hyperbolic reflections estimated that the propagation velocity was around 0.065–0.090 m/ns. This velocity indicates that the horizontal reflections were located at about 1 m depth, which corresponded to the depth of the frost tables revealed by excavation. This coincidence demonstrates that the estimated velocity was reasonable, although the velocity was slightly small for sandy materials. Most of the polygon troughs were accompanied by a hyperbolic reflection extending downward from just below the ground surface. Ice wedges tend to show strong hyperbolic reflections (Hinkel et al. 2001), while the hyperbolas in Kapp Linné are located at depths too shallow for ice wedges. In fact, two excavated troughs on a marine terrace displayed active layer soil wedges restricted within the upper 20–40 cm depth of the active layer (Fig. 2b). The GPR profiles also displayed minor hyperbolic reflections below polygon mounds, which appear to be produced by large stones in the marine sediment.

The GPR profiles of four extraordinarily large troughs were characterized by double hyperbolic reflections extending downward from the ground surface and at about 1 m depth, respectively (Fig. 3a). The upper reflection corresponds to that of active layer soil wedges below smaller polygon troughs. In contrast, the lower reflection may indicate the presence of an ice wedge, because the top of the hyperbola approximates the permafrost table. An excavation conducted in late July exposed a soil wedge just below the trough, surrounded by marine sand partly containing gravels (Fig. 3b). The width of the wedge approximates that of the trough (ca. 80 cm). Despite consisting of similar material to the surrounding marine sediments, the

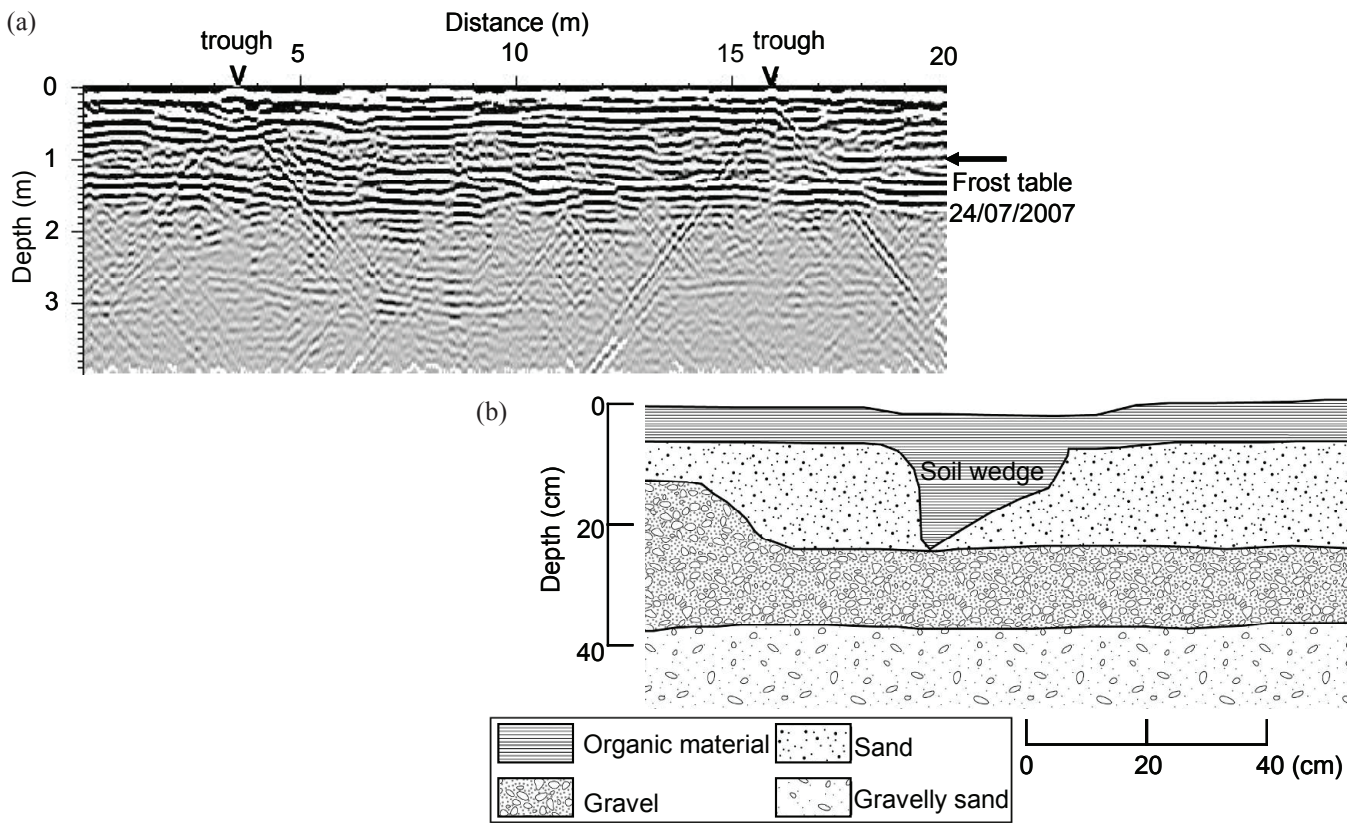


Figure 2. (a) A GPR profile across two polygon troughs on a marine terrace in Kapp Linné. (b) The cross section of the trough at the 16 m point along the above profile.

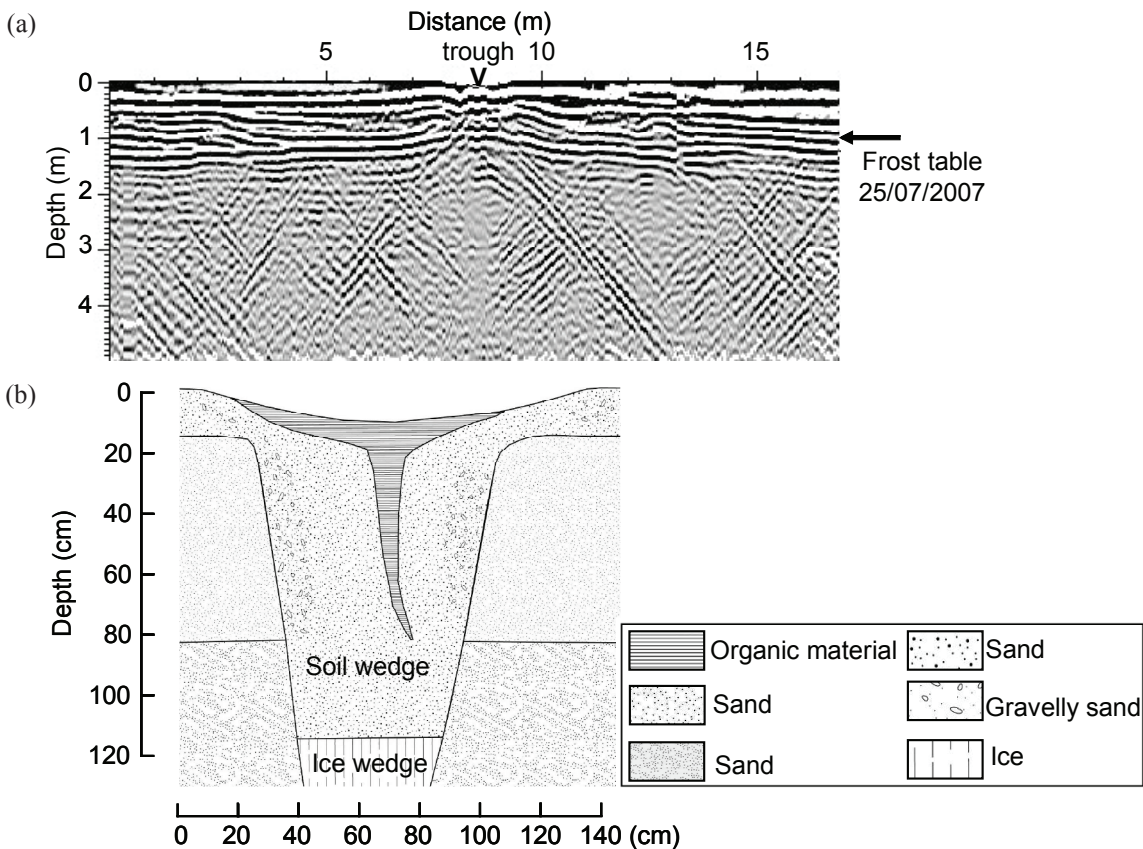


Figure 3. (a) A GPR profile across an extraordinarily large polygon trough on a beach ridge in Kapp Linné. (b) The cross section of the trough.

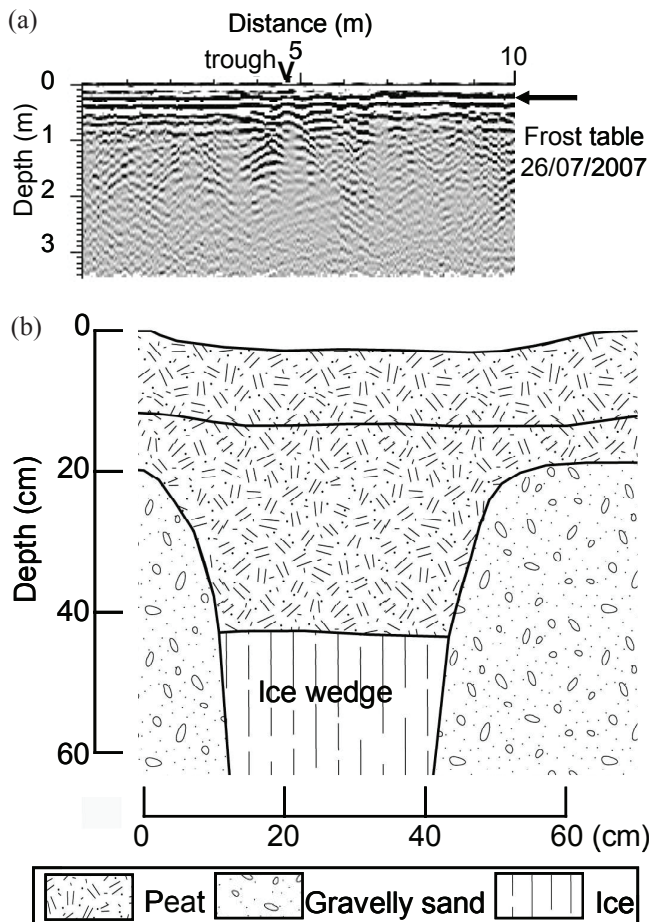


Figure 4. (a) A GPR profile across a polygon trough on a bog site in Kapp Linné. (b) The cross section of the trough.

wedge filling is distinguished by a difference in color. A thin organic layer covers the trough and intrudes into the wedge filling to about 80 cm depth. This intrusion may have originated from the latest cracking activity. The soil wedge extends below the frost table (at ca. 105 cm depth). Further drilling into the permafrost confirmed the presence of an underlying ice wedge which penetrates deeper than 270 cm. The ice wedge corresponds to the lower GPR reflection.

Kapp Linné: Bogs

GPR profiles of widely spaced polygon troughs in bogs showed a narrow hyperbolic reflection underlying a strong horizontal reflection, although the wet surface significantly attenuated the radar signals (Fig. 4a). The propagation velocity was estimated to be around 0.070 m/ns by the point-source reflection analysis using the hyperbolic reflection. This velocity suggests that the top of the hyperbola lay at about 0.3 m depth. Such a hyperbolic reflection may indicate the presence of an ice wedge. The drilling and excavation in late July actually confirmed the presence of a narrow ice wedge reaching 130 cm depth. The excavation displayed a peat layer about 20 cm thick overlying marine sediments. A peat wedge penetrates into the marine sediment below the trough. The active layer thickness was thin and varied from 25 cm in the wedge to 35 cm in the marine sediment. The

shallow frost table corresponded to the strong horizontal reflection on the GPR profile. An ice wedge with a top width of 30 cm occurred below the peat intrusion. The top of the ice wedge was located at 40 cm depth. Such a structure agrees with the narrow hyperbolic reflection. The trough lacked a double hyperbola pattern, although the peat intrusion formed an active layer soil wedge above the ice wedge. This is probably due to the difficulty in resolving two features which are so close to each other with a 250 MHz antenna.

Adventdalen: Fluvial terraces

GPR profiles displayed two kinds of reflections: (1) multiple horizontal reflections, which are slightly deformed below troughs; and (2) hyperbolic reflections, which underlie horizontal reflections below troughs (Fig. 5). The point-source reflection analysis using the hyperbolic reflections estimated that the radar velocity was about 0.050 m/ns, which was lower than the values of ice wedges in Kapp Linné. This is probably due to the low propagation rate in the poorly drained loess material. The estimated velocities suggest that the tops of the hyperbolic reflections were located at 1.2 m depth, regardless of the size of the polygon trough. A series of drilling holes across two polygon troughs reproduced the structure of the ice wedges. The drilling revealed that ice wedges were about 1.9 m wide below well-developed troughs (Fig. 5a) and about 0.5 m wide below shallow troughs (Fig. 5b). Below the shallow troughs, the centre of the ice wedge did not agree with the new crack at the ground surface. This relationship was correctly shown in the GPR profile (Fig. 5b), which indicates that the ice wedge has unevenly developed. The top of a hyperbola roughly corresponded to an edge of the ice wedge, which means that the width of hyperbola top represents the width of an ice wedge. The disturbance of the horizontal reflections below the trough may have originated from thermal contraction cracks filled with air and meltwater.

Influences of Grain Size and Water Content on GPR Profiles

Both of the ice and soil wedges showed strong hyperbolic reflections. This means that the dielectric constant is considerably different between ice and frozen soil and between a soil wedge and the host sediment. The dielectric constant varies with material of solids and air and water contents. In particular, the dielectric constant of water significantly affects the composite dielectric constant of soil, because water has an extremely high dielectric constant compared to other substances. These influences were evaluated by measurements of grain size distribution and water content of soils.

Figure 6 summarizes the grain size distribution of soils at 4 sites. The soil samples were taken from both the soil wedge and the host sediment. In Kapp Linné, the composition of the soil-wedge filling is different from that of the marine sediment. Below a marine terrace where a single hyperbola occurs by a soil wedge, the wedge filling is significantly finer than the marine sediment. Below a beach ridge where the double

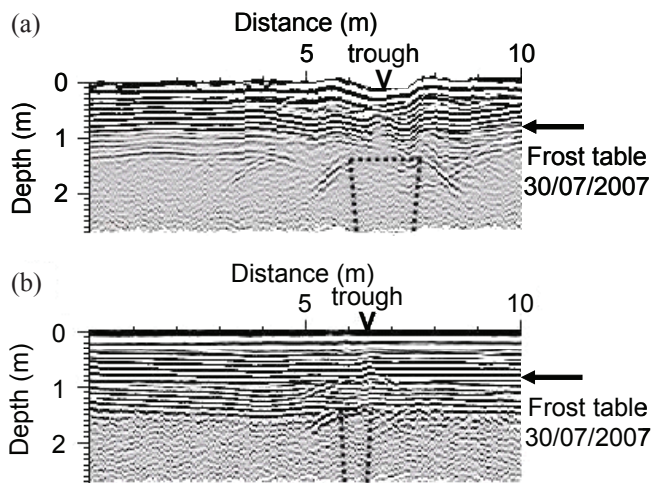


Figure 5. Subsurface structures below low-centered polygons on a fluvial terrace in Adventdalen. (a) A GPR profile across a large polygon trough. (b) A GPR profile across a small polygon trough. The broken lines illustrate ice wedges indicated by drillings.

hyperbolic reflections occur, the wedge and host sediment show similar mean grain sizes, but the wedge filling ranging from gravel to silt, shows a wider size distribution than the host sediment. The difference may result in a different porosity and influence the dielectric constant. A large difference in grain size occurs between samples derived from the bog site, although the soil wedge lacks a hyperbolic reflection. This may result from soil wedge too thin to be detected by 250 MHz signals. In contrast, the samples obtained from the Adventdalen river terrace indicate similar grain size distributions between the soil wedge and the host loess. This probably explains why double hyperbolic reflections did not occur at the Adventdalen study site, where the soil wedges are filled with similar material to the host sediments.

Table 1 shows water contents in and around the soil wedge below the marine terrace at Kapp Linné in summer. The ground surface was dry when the samples were collected. The soil wedge has significantly higher water content than the surrounding materials. This is probably because the organic materials composing the soil wedge have a high water retention capacity, while the marine sediments are highly drained. The contrast probably induces strong reflections.

Conclusions

The GPR profiles across non-sorted polygons show characteristic reflections representing ice and soil wedges. Hyperbolic reflections extending downward from the ground surface represent active layer soil wedges. Such a sharp reflection is considered to originate from the different water content between the soil wedges and the host sediments. Ice wedges show hyperbolic reflections extending downward from the frost table. The width of the hyperbola roughly coincides with the width of an ice wedge determined by drilling. Where a soil wedge in active layer is underlain by an ice wedge, troughs are underlain by double

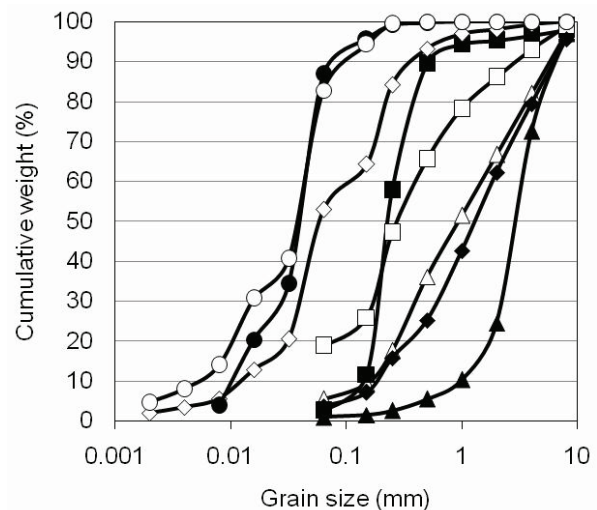


Figure 6. Grain size distribution in soil wedges and the host materials.

Table 1. Volumetric water contents in a soil wedge and the host materials at the Kapp Linné marine terrace site. Samples were taken on July 24, 2007.

Sampling point	Water content (%)
Soil wedge (organic)	40.8
Sand layer below soil wedge	15.7
Sand layer aside of soil wedge	8.8
Gravel layer below soil wedge	6.2

hyperbolic reflections extending downward from the ground surface and the frost table.

These results indicate that GPR is useful for distinguishing ice and active layer soil wedges, in terms of the depth of hyperbolic reflections, and for estimating the width of ice wedges without excavation or drilling down to permafrost.

Acknowledgments

We thank Ole Humlum and UNIS students for their cooperation in the field, UNIS technical staff for their assistance in transporting equipment and safety guidance, and H. Miura for permission to use GPR systems in the National Institute for Polar Research.

References

- Åkerman, J. 1980. *Studies on Periglacial Geomorphology in West Spitsbergen: Meddelanden från Lunds Universitets Geografiska Institution Series Avhandlingar* 89, 297 pp.
- Åkerman, J. 1987. Periglacial forms of Svalbard: a review. In: J. Boardman (ed.), *Periglacial Processes and Landforms in Britain and Ireland*. Cambridge: Cambridge University Press, 9–25.
- Åkerman, J. 1996. Slow mass movements and climate relationships, 1972–1994, Kapp Linné, West Spitsbergen. In: M. G. Anderson & S. M. Brooks (eds.), *Advances in Hillslope Processes 2*. Chichester: Wiley, 1219–1256.
- Berthling, I., Etzelmüller, B., Isaksen, K. & Sollid, J.L. 2000. Rock glaciers on Prins Karls Forland. II:—GPR soundings and the development of internal structures. *Permafrost and Periglacial Processes* 11: 357–369.
- Christiansen, H.H. 2005. Thermal regime of ice-wedge cracking in Adventdalen, Svalbard. *Permafrost and Periglacial Processes* 16: 87–98.
- Christiansen, H.H. & Humlum, O. 2003. Active layer monitoring in Ny Ålesund and in Adventdalen in the CALM Network. In: J.L. Sollid & H.H. Christiansen (eds.), *Permafrost, Periglacial Features and Glaciers in Svalbard, Excursion Guide*. Oslo: University of Oslo, 97–100.
- Dallimore, S.R. & Davis, J.L. 1987. Ground probing radar investigation of massive ground ice and near surface geology in continuous permafrost. *Geological Survey of Canada Paper* 87-1A: 913–918.
- Hanssen-Bauer, M., Soløs, M.K. & Steffensen, E.L. 1990. The climate of Spitsbergen. *Klima: Norwegian Meteorological Institute Report* 39/40. Oslo: Norwegian Meteorological Institute, 1–40.
- Hinkel, K.M., Doolittle, J.A., Bokheim, J.G., Nelson, F.E., Paetzold, R., Kimble, J.M. & Travis, R. 2001. Detection of subsurface permafrost features with ground-penetrating radar, Barrow, Alaska. *Permafrost and Periglacial Processes* 12: 179–190.
- Humlum, O., Instanes, A. & Sollid, J.L. 2003. Permafrost in Svalbard: a review of research history, climatic background and engineering challenges. *Polar Research* 22: 191–215.
- Isaksen, K., Holmund, P., Sollid, J.H. & Harris, C. 2001. Three deep alpine-permafrost boreholes in Svalbard and Scandinavia. *Permafrost and Periglacial Processes* 12: 13–25.
- Landvik, J., Mangerud, J. & Salvigsen, O. 1987. The late Weichselian and Holocene shoreline displacement on the west-central coast of Svalbard. *Polar Research* 5: 29–44.
- Matsuoka, N. & Hirakawa, K. 1993. Critical polygon size for ice-wedge formation in Svalbard and Antarctica. *Proceedings of the Sixth International Conference on Permafrost 1, Beijing, China, July 5–9, 1993*: 449–454.
- Moorman, B.J., Robinson, S.D. & Burgess, M.M. 2003. Imaging periglacial conditions with ground-penetrating radar. *Permafrost and Periglacial Processes* 14: 319–329.
- Munroe, J.S., Doolittle, J.A., Kanevskiy, M.Z., Hinkel, K.M., Nelson, F.E., Jones, B.M., Shur, Y. & Kimble, J.M. 2007. Application of ground-penetrating radar imagery for three-dimensional visualization of near-surface structures in ice-rich permafrost, Barrow, Alaska. *Permafrost and Periglacial Processes* 18: 309–321.
- Ross, N., Harris, C., Christiansen, H.H. & Brabham, P. Ground-penetrating radar investigations of open system pingos, Adventdalen, Svalbard. *Norsk Geografisk Tidsskrift* 59: 1–11.
- Salvigsen, O. & Elgersma, A. 1985. Large-scale karst features and open taliks at Vardeborgsletta, outer Isfjorden, Svalbard. *Polar Research* 3: 145–153.
- Sørbel, L., Tolgensbakk, J., Hagen, J.O. & Høgvard, K. 2001. Geomorphological and Quaternary geological map of Svalbard 1:100,000. Sheet C9Q Adventdalen. *Temakart No. 31/32*. Tromsø: Norwegian Polar Institute, 57–78.
- Tolgensbakk, J., Sørbel, L. & Høgvard, K. 2001. Geomorphological and Quaternary Geological Map of Svalbard 1:100,000. sheet C9Q Adventdalen. *Temakart No. 31/32*. Tromsø: Norwegian Polar Institute.
- Yoshikawa, K., Leuschen, C., Ikeda, A., Harada, K., Gogineni, P., Hoekstra, P., Hinzman, L., Sawada, Y. & Matsuoka, N. 2006. Comparison of geophysical investigations for detection of massive ground ice (pingo ice). *Journal of Geophysical Research* 111: E06S19, doi: 10.1029/2005JE002573.

Modeling Forecasting on Permafrost Changes in Northeastern China

Zhi Wei, Huijun Jin, Jianming Zhang, Yanjun Ji, Sizhong Yang, Ruixia He

State Key Laboratory of Frozen Soils Engineering, Cold and Arid Regions Environmental and Engineering Research Institute, Chinese Academy of Sciences, Lanzhou, China

Shaopeng Yu

Department of Geography, Harbin College, Harbin, China

Abstract

In northeastern China, mean annual air temperature (MAAT), as a main control factor, increased by 1°C between 1975 and 2000 as compared to 1951–1975 with a warming rate of 0.04°C/yr. In the absence of adequate borehole temperature data, geographic factors such as latitude, longitude, elevation, aspect, and slope were used to describe the present distribution of permafrost and to model scenarios of its potential future changes. The result showed that latitude is the primary factor that determines the distribution of MASST, enabling an equivalent latitude model (ELM) to be constructed and a GIS-based map of present-day MASST distribution to be drawn. Future permafrost changes 50 years from now were then estimated by finite-element modeling. The results indicate that permafrost thickness would not change greatly, apart from some south-oriented slopes, but that permafrost degradation would primarily be caused by increasing mean annual ground temperature.

Keywords: finite element; forecast; mean annual soils surface temperature; modeling, northeastern China.

Introduction

Permafrost in northeastern China (NE China) is warm, thin, and sensitive to atmospheric warming. Research on permafrost in northeastern China was initiated in the early 1950s. During the 1960s and 1970s numerous regional investigations, together with local studies for specific purposes such as water supply, road construction, or coal-mining, were conducted in order to meet the needs of economic development. The boundaries of continuous (>65% occupation), discontinuous (50%–60%), and sporadic permafrost (5%–30%) were empirically determined to correlate with the -5°C, -3°C, and 0°C isotherms of mean annual air temperature, respectively. This pattern has strongly changed during about 30 years of ongoing atmospheric temperature rise and heavy direct impacts from human activities. The most influencing human activities are unceasing deforestation, frequent forest fire, and some large-scale constructions. All these natural and non-natural realities affected the existing and developing conditions of permafrost in NE China. (Zhou & Wu 1965, Guo & Li 1981, Guo et al. 1981, Dai 1982, Northeastern China Permafrost Research Taskforce 1983, Guo & Huang 1989, Peng & Cheng 1990, Lu et al. 1993, Gu & Zhou 1994, Zhou et al. 1996). Degradation of permafrost in northeast China has been of considerable concern during the past decade (Gu & Zhou 1994, Chen & Yin 1996, Wang et al. 1996, Zhou et al. 1996). Many major engineering and environmental projects such as express highways and high-speed railways, the proposed China-Russia Crude Oil Pipeline from Skovorodino, Russia to Daqing, China, or a hydropower project near the Heilongjiang (Amur) River, necessitate an understanding of the status and possible future evolution of permafrost in the NE China over the next 30–50 years. This paper analyzes the effects from increasing MAAT, introduces a concept

of MASST zonality, and presents a preliminary forecast concerning the future trends of permafrost conditions in NE China.

Changes of MAAT and MASST

Climate change and permafrost condition

Long-term (1951–2000) monthly air temperature records of 117 meteorological stations (Fig. 1a) in regions with continuous or discontinuous permafrost or seasonally frozen ground within the study area of NE China showed a pronounced warming tendency comparable with warming trends observed in northward zones in Siberia (Yang et al. 2000). In the 1970s, the southern limit of permafrost (SLP) and boundaries between different types of continuous, discontinuous, and sporadic permafrost in NE China were determined by Northeastern China Permafrost Cooperation Group (NCPCG) (Guo et al. 1981). Comparison of the two time intervals 1951–1975 and 1976–2000 illustrates the notable long-term warming trend (Figs. 1a, b).

The pattern of isotherms is quite similar during both time periods but documents a shift in MAAT of about +1°C between the two considered time intervals. This change will definitely affect permafrost: its existence, distribution, thermal condition, and active layer depth. Using the MAAT range of -1°C and +1°C for southern limit of permafrost occurrence (SLP), its climate-induced northward displacement can be estimated at 40–120 km in accordance with previous studies (Jin et al. 2007). The principal cause of the observed permafrost degradation in NE China is atmospheric warming which has occurred since the end of the 19th century. Based on decadal average air temperatures (DAATs) from northeastern China, this change can be divided into three main periods: (1) persistent warming from the end of the 19th century to the 1940s; (2) quasi-stable

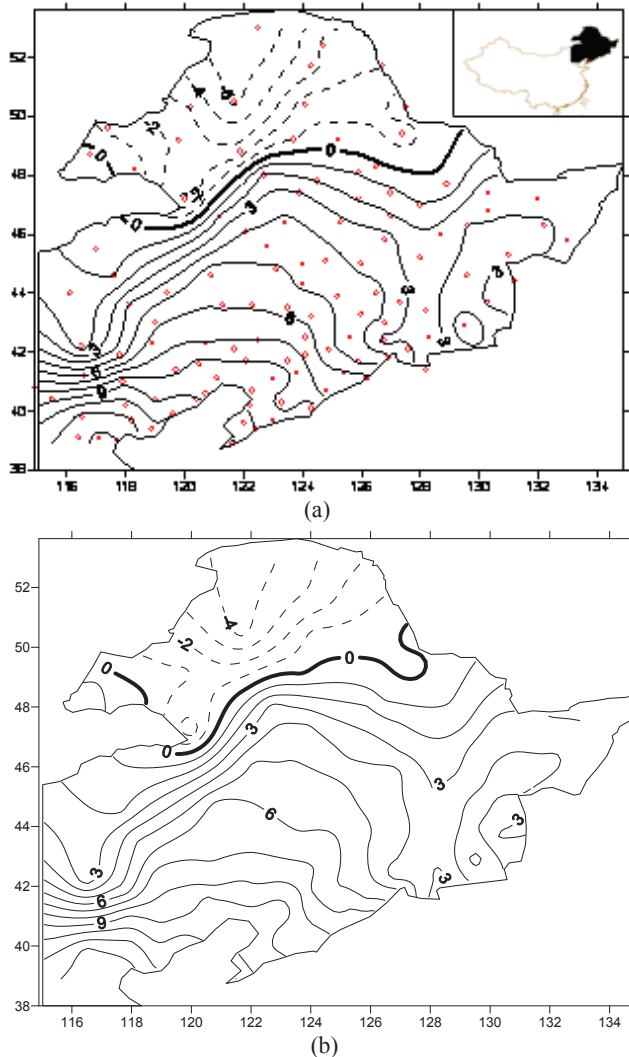


Figure 1. Mean annual air temperature isotherms during 1951–1975 (a) and 1976–2000 (b) in NE China; the embedded circles are the distribution of 117 meteorological stations in study area of NE China.

average temperatures during the 1950s to the 1970s; and (3) a second persistent warming from 1970 to 2000, particularly during 1991–2000a (Qin 2002).

Soils surface temperature and climate change

Mean annual soils surface temperatures (MASST) are primarily influenced by air temperature. In order to better understand their changes in the study area as related to conditions of atmospheric warming, data for the time period 2000–2004 from all 47 systematically observed, national meteorological stations in northeastern China and some of those in the Meng’gu and He’bei provinces in the North China district were employed to analyze the relation between MAAT and MASST. The statistical analysis identified a strong relation between the two (Fig. 2), with MASST being on average about 1.7°C higher than MAAT. Strong correlation between air and ground surface temperatures indicates that higher air temperatures induced a corresponding heat absorption and ground warming over the past decades.

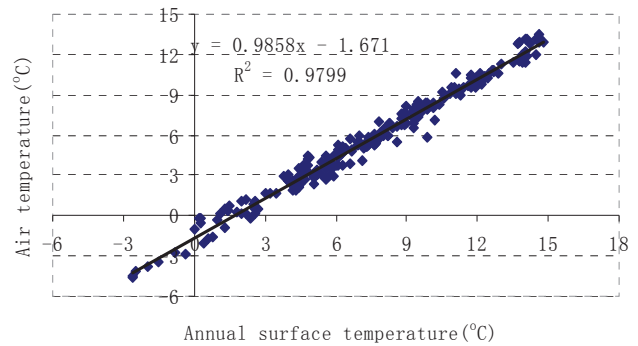


Figure 2. The correlation analysis between mean annual air temperature and soil surface temperatures.

Equivalent Latitude Model for MASST

In its spatial distribution, MASST is basically controlled by latitude (Table 1), but according to the former relative studies, permafrost condition in NE China is very different with topography such as aspect and slope at almost the same location (Brown 1973, Liu et al. 1993). These variations reflected from different mean annual ground temperature (MAGT), permafrost thicknesses, and depths of active layer (Tables 2, 3), so aspect and slope were taken into account to constitute equivalent latitude (Haugen et al 1993):

$$\varphi' = \sin^{-1}(\sin k \cosh \cos \varphi + \cos k \sin \varphi) \tag{1}$$

where k is slope of the surface ($^{\circ}$); h is surface aspect ($^{\circ}$); φ and φ' are actual latitude and equivalent latitude of the spot ($^{\circ}$).

Measured data and previous articles proved that snow has a much greater influence than vegetation on the thermal condition of permafrost, and show a un conspicuous influence if acting together (Fig. 3); but it is a complicated process how snow affects, so MASST is used in the model to remove snow influence.

When replacing the actual latitude with so-calculated “equivalent latitude,” the partial correlation between MASST and equivalent latitude increases to 0.957 compared to the previous 0.938. According to trends in altitude changes, a two-section equation was used in the model simulation. This provided more satisfactory results ($R^2=0.972>0.957$; $F=190.86>148.68$) (Fig. 4). The two-section equation (Jin et al 2007) is:

$$T_s = \begin{cases} 72.153 - 0.684\varphi' - 0.2650 - 0.007h & h \leq 250m \\ 60.369 - 1.105\varphi' - 0.0150 - 0.005h & h > 250m \end{cases} \tag{2}$$

where: T_s is mean annual soils surface temperature ($^{\circ}$); θ and h is longitude ($^{\circ}$) and altitude (m) of the spots; φ' is equivalent latitude of the spots ($^{\circ}$).

From Figure 4, the simulatn essentially reflected the MASST, F test value is 190.86, indicate that the equivalent latitude model is relatively exact and can be used to predict the MASST distribution. Based on Equation 2, a GIS-based

Table 1. Partial correlations between MASST and three elementary geographic factors.

		Latitude/°	Longitude/°	Altitude/m
Mean annual soils surface temperature/°C	Pearson correlation	0.938	-0.552	-0.805
	Sig.(2-tailed)	0.000(**)	0.000(**)	0.000(*)
	Total stations	47		

**Correlation is significant at the 0.01 level (2-tailed).

Table 2. The permafrost thickness changes to slope in NE China.

Topography (Different slope)	Lowland in river valley			Foothill			Mountain slope
Borehole No.	H ₄₋₇	H ₁₋₃	H ₅₋₂₄	H _{z-1}	H _{z-2}	H _{z-3}	H _{z-10}
Permafrost table/m	0.3-0.8	0.3-0.8	0.3-1.0	1.0-2.5	1.0-3.0	1.0-2.5	1.0-3.0
Permafrost base/m	112.65	122.6	130	31	14.9	25	16

Table 3. The affect of aspect on permafrost conditions in NE China.

items	East–West-oriented valley			South–North-oriented valley		
	S-oriented slope	lowland	N-oriented slope	W-oriented slope	lowland	E-oriented slope
MAGT/°C	0~ -1.0	-2.0~ -4.2	-1.0~ -2.0	0~ -1.0	-2.0~ -4.2	0~ -0.5
PTH/m	0~20	50~150	20~50	10~30	50~100	0~20
SMTH/m	2.0~4.0	0.5~1.0	1.0~1.5	1.0~2.0	0.5~1.0	1.0~3.0

MAGT – mean annual ground temperature; PTH – permafrost thickness; SMTH – seasonal melted thickness.

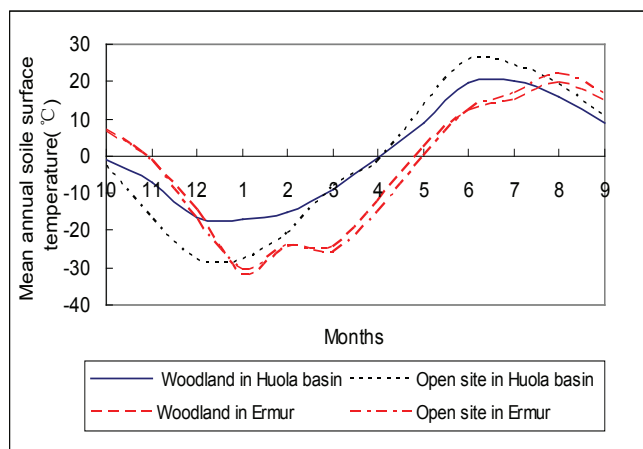


Figure 3. Influence of snow and vegetation on MASST (Huola basin cleaned snow in winter).

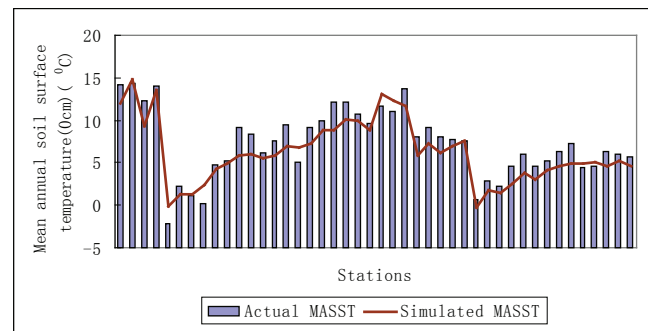


Figure 4. Simulated MASST compared to measured data.

MASST distribution map was drawn using C++ programs (Fig. 5). The DEM and other digital data were taken from GTOPO 30 with a horizontal grid spacing of 30 arc seconds (approximately 1 kilometer), Center for Earth Resources Observation and Science (EROS), U.S. Geological Survey (USGS 2007).

The w-shaped pattern of MASST-isotherms is due to elevation effects, as the Da and Xiao Xing’anling Mountains are relatively higher than their surroundings in the western and eastern parts of the study area, ranging from 1000 to 1400–1500 m a.s.l. in the middle section from A’ershan to Yi’ershi and to the source of the Zhuo’er River, but decreasing northward to 500–600 m a.s.l. in the section from Mangui to Gulian. In contrast, the Xiao Xing’anling Mountains are gentler in topography, with meandering river channels, elevations of 500–600 m a.s.l., and few peaks

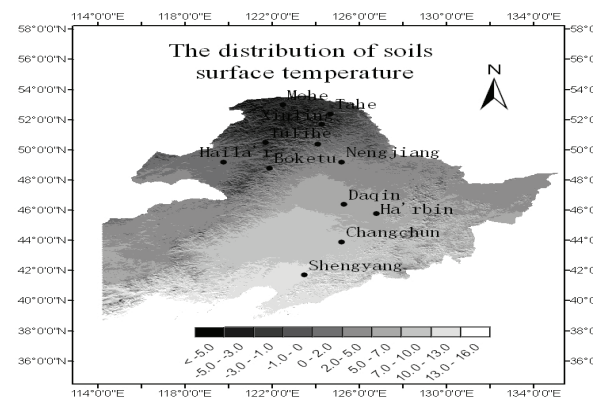


Figure 5. The distribution of MASST in NE China.

higher than 800 m a.s.l. Large quantities of eroded debris from the steeper eastern slopes have been carried by deeply incised rivers to the Nenjiang River Plain, which lies between the two mountain ranges, with the elevation ranging from several meters to 200–300 m a.s.l.

Permafrost Change with Global Warming

Mathematical model for calculation

On the basis of the MASST distribution, permafrost changes can be calculated using finite element methods of heat diffusion at depth and characteristic surface boundary conditions. The main control equation is:

$$\rho \cdot C \frac{\partial T}{\partial t} = \frac{\partial}{\partial x} \left(\lambda \frac{\partial T}{\partial x} \right) + \frac{\partial}{\partial y} \left(\lambda \frac{\partial T}{\partial y} \right) \tag{3}$$

In this equation:

$$C = \begin{cases} C_u & (T > T_p) \\ C_f + \frac{C_u - C_f}{T_p - T_b} (T - T_b) + \frac{L}{(1+W)} \frac{\partial W_i}{\partial T} & (T_b \leq T \leq T_p) \\ C_f & (T < T_b) \end{cases}$$

$$\lambda = \begin{cases} \lambda_u & (T > T_p) \\ \lambda_f + \frac{\lambda_u - \lambda_f}{T_p - T_b} (T - T_b) & (T_b \leq T \leq T_p) \\ \lambda_f & (T < T_b) \end{cases}$$

where ρ is natural density of soils (kg/m³); C is apparent specific heat of soils (J/(kg.K)); C_u , C_f are specific heats of thawed and frozen soils; λ is apparent conductivity of soils (J/(m.h.k)); λ_u , λ_f are conductivities of thawed and frozen soils; L is latent heat (K/kg); W , W_i is total water content or ice content (%); T_p and T_b are the upper and lower critical temperature related to phase changing (°C); T is temperature (°C); t is time (h); x and y are spatial variables (m).

Geometrical model for forecasting calculation

An additional geometrical model considered effects from human activities within a distance of 30 m, mainly relating to deforestation in connection with road construction, creation of fire insulation zones, or installing electrical transforming line (Fig. 6); with an additional 30 m added to each side, the total width considered is 90 m. Some borehole data in NE China approved that the gradient at depths greater than 30m is less than 0.004°C/m (Li et al. 1996). The bottom boundary was therefore chosen at this depth.

Boundary conditions

The surface boundary of calculation area presented as:

$$T = T_0 + \alpha \cdot t + A \sin \left(\frac{2\pi \cdot t}{8760} + \frac{\pi}{2} \right) \tag{4}$$

where T is SST (0 cm) (°C); T_0 is MASST (°C); α is increment of MASST, is 0.048 within 50-year period in the future (°C/a); t is time duration; A is amplitude of SST (°C, 18.5°C for the forest surface); $\pi/2$ is the initial phase (corresponding to the warmest part of the year).

In the IPCC WG2 report (Chapter 10–Asia) (IPCC 2007), the minimum future increase in surface air temperature

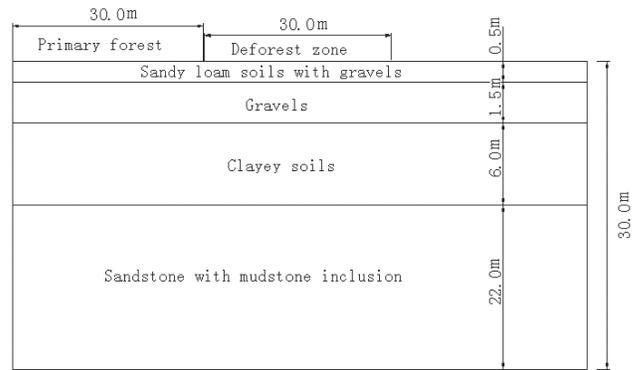


Figure 6. The geometrical model in calculation.

will be 1.4°C (2010a–2039) and 2.5°C (2040–2069), then the surface air temperature would be 2.4°C higher after 50 years in NE China, atmospheric model of A1, A1B, and A2 also examined its increment of 0.026, 0.027, and 0.05, and synthesized $\alpha = 0.048$ in connection with the actual increment. Therefore the soil surface temperature would be with an approximately same increment based on former 50-year linear relation without any large change in atmospheric circulation.

The mean annual ground temperature of present-day stable permafrost temperature regime is inferred from 200 years ahead. Calculated results (Fig. 7) indicated that present MAGT is near to MASST, future MAGT in different MASST zonal areas would increase in various extents: about 0.5°C, 0.4°C, and 0.3°C where the present MASST is -2.0°C, -1.5°C, and -1.0°C, slightly in -0.5°C and 0°C zones, because the nearer to the phase-change area, the more slowly permafrost temperature will change, but much more of that together with anthropic activities: In contrast, the permafrost table deepens most where present MASST is 0°C, the increment ranged from 1.2 m to 0.2 m in 5 different MASST zones (Table 4). Permafrost thickness would not change greatly apart from some south-oriented slopes and areas around 0°C in MAGT. The permafrost degradation would mainly take in place in the form of increasing in mean annual ground temperature.

Conclusion

Mean annual air temperature (MAAT) in NE China increased by about 1°C from 1976–2000 as compared to 1951–1975 with a yearly 0.04°C increase, i.e., higher than mean warming rate of 0.026°C/a estimated by IPCC for the Northern Hemisphere. Mean annual soil surface temperature (MASST) is linearly related to MAAT and may therefore have risen at the similar rate if there aren't any large changes in surroundings. This inevitably caused permafrost warming.

Climatic warming and increased human activity during the last century are both thought to be responsible for the degradation of permafrost in NE China. Extensive and increasing human activity for resource exploitation, agriculture, and economic development have accelerated the processes.

Table 4. Changes of MAGT (at 15 m deep location) and table of permafrost in different zones, present and within next 50 years.

MASST zonal area /°C	Mean annual ground temperature /°C (-15 m)			Permafrost table /m		
	Present	GW	GW+MA	Present	GW	GW+MA
0.0	0.06	0.07	0.10	3.00	4.20	5.85
-0.5	-0.50	-0.45	-0.40	2.80	3.40	5.20
-1.0	-0.99	-0.77	-0.64	2.65	3.10	4.70
-1.5	-1.44	-1.11	-0.86	2.50	2.80	4.00
-2.0	-2.03	-1.56	-1.12	2.40	2.60	3.20

GW – in the scenario of global warming; GW+MA – in the scenario of global warming plus human activities.

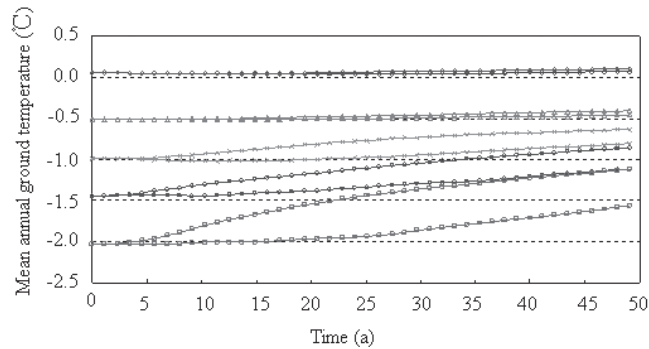


Figure 7. Calculated changing process of permafrost with various MAGT (down to 15 m) in different MASST zonal area within coming 50 years in NE China, under global warming and added anthropic activities (upper and lower line for each case).

A forward projection of atmospheric warming trends revealed that mean annual permafrost temperature would more strongly increase in zones of relatively cold MASST of around -2.0°C than in zones of warm to temperate permafrost. The permafrost table, on the other hand, is expected to deepen most strongly (about 12 m) in zones with MASST near 0°C . These effects are considerably enhanced by effects from direct human impact. Changes in permafrost thickness would be limited, and increasing mean annual ground temperatures are likely to be the predominant manifestation of permafrost degradation.

Acknowledgments

Genuine acknowledgment goes to Doctor Xujun Han for support and help in the accomplishment of the equivalent latitude model in GIS. Data supplied by 1st Team, Forest Design and Research Institute, Hei'long'jiang province.

References

- Brown, R. 1973. Influence of climatic and terrain factors on ground temperature at three locations in the permafrost region of Canada. *Proceeding of the Second International Conference on Permafrost (North American Contribution), Yakutsk, USSR, July 13–28, 1973: 27–34.*
- Chen, Y. & Yin, Y. 1996. Impacts of forest industry development in the Da Xing'anling Mountains on the seasonally thawed layer overlying permafrost. *Proceeding of the Fifth Chinese Conference on Glaciology and Geocryology (Vol. 2), Lanzhou, August 18–22, 1996: 1087–1091.*
- Dai, J. 1982. Features of permafrost temperature in northern part of the Da-Xing'anling Mountains. *Journal of Glaciology & Geocryology* 4(3): 53–63 (in Chinese).
- Gu, Z. & Zhou, Y. 1994. Changes of permafrost in the Amu'er area of the Da-Xing'anling Mountains. In Y.W. Zhou & Z.X. Yang (eds.), *Impacts and Countermeasures of Forest Fire in the Da-Xing'anling Mountains*. Beijing: Science Press, 156–161.
- Guo, D., Wang S. & Lu G. 1981. Division of permafrost regions in Da'xiao Hingganling northeast China. *Journal of Glaciology & Geocryology* 3(3): 1–9 (in Chinese).
- Guo, D. & Huang Y. 1989. The role of geological structure in the formation of permafrost in the Hola Basin, northeastern China. *Journal of Glaciology & Geocryology* 11(3): 216–222 (in Chinese).
- Guo, D. & Li Z. 1981. Geological evolution and age of formation of permafrost in northeastern China since the late Pleistocene. *Journal of Glaciology & Geocryology* 3(4): 1–6 (in Chinese).
- Haugen, K., Greeley, H. & Collins, M. 1993. Permafrost mapping using GRASS. *Proceeding of Six International conference on permafrost, (Vol. 2): Beijing, July 5–9: 1128–1131.*
- IPCC, 2007. <http://ipcc-wg2.ucar.edu>.
- Jin, H.J., Yu, Q., Lü, L., Guo, D.X., He, R.X., Yu, S.P., Sun, G.Y. & Li, Y.W. 2007. Degradation of permafrost in the Xing'anling Mountains, Northeastern China. *Permafrost & Periglacial Process* 18: 245–258.
- Jin, H.J., Zhang, J.M. & Tong, C.J. 2007. *Final Report on the Assessment and Prediction of Frozen Ground Engineering Geology Along the Mo'he to Daqing Oil Pipeline*. PetroChina DOE & CAS CAREERI (eds.): 100–120.
- Li, Y., Tong, C. & Zhang, L. 1996. Computation of the permafrost thickness in Yitulihe observations field. *Proceeding of the Fifth Chinese Conference on Glaciology and Geocryology (Vol.2), Lanzhou, August 18–22: 1143–1148.*
- Liu, Q., Sun, K. & Cui, S. 1993. Study of the law of the distribution of permafrost and vegetation in Da Higgan Ling. *Journal of Glaciology & Geocryology* 15(2): 246–251.

- Lu, G., Weng, B. & Guo, D. 1993. Geographical southern limit of permafrost in Northeastern China. *Journal of Glaciology & Geocryology* 15(2): 214-218 (in Chinese).
- Northeastern China Permafrost Research Taskforce. 1983. Major features of permafrost distribution in northeastern China. *Proceeding of the Second Chinese Conference on Geocryology, Lanzhou, October 12–15*: 36–42.
- Peng, H. & Cheng, G. 1990. Ice wedges in the Da Xing'anling Mountains, northeastern China and their implications in paleo-climatology. *Proceeding of the Fourth Chinese Conference on Glaciology & Geocryology, Lanzhou, October 6–9, 1988*: 9-16.
- Qin, D. (ed.). 2002. *Features and Evolution of Environments in Western China: Assessment of the Evolution of Environments in Western China*. Beijing: Science Press, 41–49.
- USGS. 2007. <http://edc.usgs.gov/>.
- Wang, C., Zhang, B. & Liu, F. 1996. Marks and phenomena of permafrost degradation in northern China. *Proceedings of the Fifth Chinese Conference on Glaciology and Geocryology (Vol. 2), Lanzhou, August 18–22, 1996*: 1063–1070.
- Yang, D., Kane, D.L. & Hinzman L. 2002. Siberian Lena River hydrological regime and recent change, *Journal Geophysical Research* 107 (D23): 1-10.
- Zhou, Y. & Wu, Z. 1965. Permafrost in the northern part of the Da-Xing'anling Mountains. In: *Monograph on the Geocryological Expedition Along the Qinghai-Tibet Highway*, Appendix. Beijing: Science Press, 20-25.
- Zhou, Y., Gao, X. & Wang Y. 1996. The ground temperature changes of seasonally freeze-thaw layer and climate warming in northeast permafrost in northeast China in the past 40 years. *Proceeding. of the Fifth Chinese Conference on Glacialogy and Geocryology, (Vol.1), Lanzhou, Ausust 18–22, 1996*: 3-10.

Thermokarst Lakes in Central Yakutia (Siberia) as Habitats of Freshwater Ostracods and Archives of Palaeoclimate

Sebastian Wetterich

Alfred Wegener Institute for Polar and Marine Research, Telegrafenberg A43, D-14473 Potsdam, Germany

Lutz Schirrmeister

Alfred Wegener Institute for Polar and Marine Research, Telegrafenberg A43, D-14473 Potsdam, Germany

Hanno Meyer

Alfred Wegener Institute for Polar and Marine Research, Telegrafenberg A43, D-14473 Potsdam, Germany

Christine Siegert

Alfred Wegener Institute for Polar and Marine Research, Telegrafenberg A43, D-14473 Potsdam, Germany

Abstract

Thermokarst lake deposits are useful archives of climatic and environmental changes in the past, and can contain palaeo-bioindicators such as pollen, plant macro-fossils, diatoms, chironomids, and ostracods. Nevertheless, such studies from permafrost regions including thermokarst lake deposits are still rare. We studied late Holocene ostracods from an excavation of deposits of the Alas Myuryu in Central Yakutia. In order to apply modern data to fossil records, we also studied the present-day relationships between the environmental setting and the geochemical properties of ostracods in six thermokarst lakes of the same region. The fossil ostracod record reflects lake-level fluctuations in the composition and stable isotope data ($\delta^{18}\text{O}$, $\delta^{13}\text{C}$) of both species. The modern ostracod communities of thermokarst lakes in Central Yakutia are broadly similar to those of Holocene age. Geochemical stable isotopes studies in both modern host water and ostracod calcite are a prerequisite for further interpretation of the fossil records.

Keywords: Central Yakutia; Holocene; ostracods; thermokarst lakes.

Introduction

Thermokarst is a common phenomenon of the cryolithozone generally caused by extensive melting processes of ground ice in the underlying permafrost. Widespread thermokarst processes have been climatically driven and intensified during warm periods in the Quaternary, especially since the Holocene (e.g., Katasonov 1979). They are responsible for the formation of numerous depressions in the landscape surface (alases), which are often occupied by thermokarst lakes. These landscape forms are typical for Central Yakutia (e.g., Soloviev 1973). The deposits of thermokarst lakes frequently contain fossil remains of bioindicators, e.g., freshwater ostracods, which can be used for palaeoenvironmental reconstructions. Cyclic water level changes in the lakes are related to regional climatic variations (e.g., Nemchinov 1958).

Freshwater ostracods are crustaceans, usually less than 3 mm long, with a bi-valved carapace made of low-magnesium calcite. Changes in climatic and hydrological parameters influence the diversity of freshwater ostracods as well as the geochemical composition of ostracod calcite. In general, several geochemical properties of the calcareous shells of ostracods contain environmental information about the water chemistry and stable isotope composition of the host water at the time of shell formation (e.g., Griffiths & Holmes 2000). In particular, $\delta^{18}\text{O}$ and $\delta^{13}\text{C}$ records of ostracod calcite provide a highly localized and temporally restricted reflection of the isotopic composition of water, making them useful tools in palaeolimnology (Griffiths &

Holmes 2000). The $\delta^{18}\text{O}$ of carbonates serves as proxy for temperature of the water, the isotopic composition of which is also influenced by precipitation, drainage basin hydrology, and the precipitation/evaporation ratio (P/E) (Kelts & Talbot 1990). The $\delta^{13}\text{C}$ of carbonates reflects changes in the isotopic ratio of the total dissolved inorganic carbon (TDIC) (Griffiths & Holmes 2000). Changes in $\delta^{13}\text{C}$ are attributed to changes in aquatic productivity within a lake, CO_2 exchange rates between atmosphere and water TDIC, as well as to the photosynthesis/respiration ratio within the lake (Leng & Marshall 2004).

In this respect, we present here the first combined study of modern and late Holocene ostracod assemblages from Central Yakutia. The first description of ostracods from this area was given by Pietrzeniuk (1977). Further regional studies were carried out on freshwater ostracods of the North Yakutian Lena River Delta, Laptev Sea (Wetterich 2007). In addition, Arctic freshwater ostracod associations were palaeoecologically analyzed in late Quaternary permafrost sequences from Bykovsky Peninsula, Laptev Sea (Wetterich et al. 2005).

Study Area

The studied lakes are situated on the Lena-Amga interfluvium and around Yakutsk in Central Yakutia, in East Siberia (Fig. 1). The region belongs to the southern foreland of the Verkhoyansk Mountain Range. The fieldwork on an excavation of the late Holocene deposits of the Alas Myuryu ($62^{\circ}43'\text{N}$, $131^{\circ}08'\text{E}$) was performed in summer

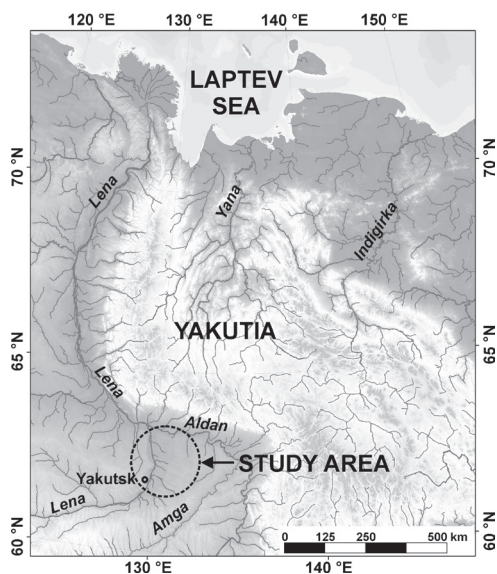


Figure 1. Schematic map of Russia showing the study site on the Lena-Amga interfluvium in Central Yakutia (East Siberia). Map compiled by G. Grosse (UAF) using data from GLOBE Task Team (1999).

1997. Six modern thermokarst lakes (between 61°32'N and 62°19'N, 129°32'E and 132°12'E) were sampled in summer 2005 under the auspices of the Russian-German expedition "Central Yakutia 2005" (Wetterich et al. 2007).

Central Yakutia is characterized by a strong continental climate with low annual precipitation (222 mm) and a high temperature gradient over the year (mean temperature in January -37.6°C and in July 19.3°C) and a mean annual air temperature of -8.7°C (Meteorological station Yakutsk; RIHMI-World Data Centre: <http://www.meteo.ru>).

Materials and Methods

The late Holocene ostracod assemblages of the Alas Myuryu were recovered from a 1.4-m-deep excavation of lake deposits at the desiccated margin of the lake. The sediment samples were freeze-dried, wet sieved through a 0.250 mm mesh size, and then air-dried. About 200 g of each sediment sample was sieved for further ostracod analysis.

Living ostracods were caught at the lake bottoms in the littoral zone of six thermokarst lakes using a plankton net and an exhaustor (Viehberg 2002) in July and August 2005. The ostracods were preserved in 70% alcohol and afterwards counted and identified under a binocular microscope by soft body and valve characteristics.

The stable isotope analyses of oxygen ($\delta^{18}\text{O}$) and carbon ($\delta^{13}\text{C}$) were performed at the isotope laboratories of the Alfred Wegener Institute (AWI, Potsdam and Bremerhaven, Germany) and the GeoForschungsZentrum (GFZ, Research Centre for Geosciences, Potsdam, Germany).

For $\delta^{18}\text{O}$ and $\delta^{13}\text{C}$ analyses on fossil and modern valves of adult ostracods we used mass spectrometers (Finnigan MAT 251 at AWI and MAT 253 at GFZ) directly coupled to automated carbonate preparation devices (Kiel II and IV, respectively). Only clean valves of adult specimens were used. Particles adhered to valves were removed with a fine

brush under microscope. To ensure enough material for isotope analysis (50–100 mg CaCO_3), multi-valve samples of single species have been created. The reproducibility as determined by standard measurements is better than $\pm 0.08\%$ (1σ) for $\delta^{18}\text{O}$ and $\pm 0.06\%$ (1σ) for $\delta^{13}\text{C}$.

The rain and lake water samples for $\delta^{18}\text{O}$ and δD were analyzed by equilibration technique (Meyer et al. 2000) using a mass spectrometer (Finnigan MAT Delta-S at AWI). The water samples for $\delta^{13}\text{C}$ analysis on TDIC were preserved by adding HgCl_2 until analysis using a mass spectrometer (Finnigan MAT 252 at AWI). The reproducibility of these data derived from standard measurements is better than $\pm 0.1\%$ (1σ).

The values are expressed in delta per mille notation (δ , ‰) relative to the Vienna Standard Mean Ocean Water (VSMOW) for water isotopes ($\delta^{18}\text{O}$, δD) and relative to the Vienna Pee Dee Belemnite standard (VPDB) for $\delta^{13}\text{C}$ on TDIC and carbonate isotopes.

The dating of organic matter and calcareous valves from seven samples (Table 1) was undertaken at the Leibniz Laboratory for Radiometric Dating and Stable Isotope Research, University of Kiel (Germany) using radiocarbon Accelerator Mass Spectrometry (AMS).

Results and Interpretation

Fossil ostracods

The late Holocene ostracod assemblage consists of 22 species (Fig. 2). The most abundant species during the periods recovered are *Candona candida*, *Fabaeformiscandona rawsoni*, *Ilyocypris lacustris*, and *Limnocythere inopinata*. According to the modern ecological requirements of these species, some facts can be concluded for the living conditions of the fossil assemblage. Most of the species show a great adaptation to changes in both temperature and salinity regime, and are mostly typical for shallow water. The tolerance to temperature ranges from cold stenotherm to warm stenotherm with a great part of thermoeuryplastic (temperature tolerant) species. Furthermore, concerning changes in salinity, most of the species have oligo- to mesohaline ranges; i.e., 0.5 to 18‰ total salt content in the host waters (Meisch 2000). In general, the habitat of the fossil ostracods was a shallow-water environment with significant changes in temperature and salinity, which are linked to lake-level changes. Three periods of different lake conditions are distinguishable (Fig. 2). However, the geochronology of the fossil record from the excavation at the lake margin of the Alas Myuryu does not yield age relations for periods B and C. Whereas period A is well-defined by three dates between about 4300 to 1500 yr BP, period B lacks direct dates, and period A was only dated in its upper part with about 300 yr BP. Furthermore, the lower part of period A is complicated by two rejected ages, which are most likely caused by re-deposition during lake-level changes after sedimentation. Therefore, geochronological interpretation of the fossil data is weak and needs further dates. Nevertheless, late Holocene variations of the lake stages are reflected in taxonomical and geochemical data of the periods A to C (Fig. 2).

Period A (about 4300 to 1500 yr BP) is characterized by moderate water level fluctuations, which are also reflected in the changes in ostracod abundance and diversity. The $\delta^{18}\text{O}$ data of *F. rawsoni* with relative ^{18}O -depleted values between about -11 to -8‰ are most likely a sign of a higher P/E due to lower evaporation that caused a generally higher lake level. The shifting $\delta^{13}\text{C}$ values of *F. rawsoni* between about -2 to 1.5‰ indicate variable aquatic productivity during period A.

The following period B (after about 1500 yr BP) shows a short-time distinct decrease (at a depth of 58–63 cm) in the abundance of all species which appeared before. That was apparently caused by drying up of the water body. The appearance of *Plesiocypridopsis newtoni* shortly before and during period B (Fig. 2) points to higher salinity, since this species tolerates and even prefers brackish conditions (Meisch 2000). The $\delta^{18}\text{O}$ data of *F. rawsoni* reflect drastic changes in the isotopic composition of the lake with shifts between about -12 and -9‰ in a very short time. Afterwards, during a gradual flooding the species composition changed again.

In period C (about 300 yr BP) the species *F. acuminata*,

F. hyaline, and *F. lepnevae* became common, and moderate lake-level fluctuations took place. In accordance with the $\delta^{18}\text{O}$ data of *F. rawsoni*, with relative ^{18}O -enriched values between about -9 to -6‰, the P/E ratio was lower (E>P) and that generally suggests higher evaporation and/or lower precipitation, resulting in a generally lower lake-level compared to period A. The $\delta^{13}\text{C}$ values of *F. rawsoni* between about -4 to -1‰ are relatively ^{13}C -depleted and can imply a general lowering in aquatic productivity compared to period A.

Modern ostracods

In six thermokarst lakes of Central Yakutia we observed 15 ostracod species (Fig. 3). In total, up to 250 adult specimens per lake were caught. The highest diversity per lake includes six species. The most abundant species from the fossil assemblages were found, but they are rare in the modern dataset. The dominant modern species are *Candona weltneri* in combination with *C. muelleri jakutica* and/or *F. rawsoni* (Fig. 3).

The studied lakes are shallow, without visible in- or outflows, and mainly fed by precipitation and meltwater from

Table 1. AMS dates of deposits of the Alas Myuryu. Rejected ages in brackets.

Lab No.	Sample No.	Depth [cm]	Material	uncal. Ages [yr BP]	cal. Ages* [yr BP] Max	cal. Ages* [yr BP] Min
KIA20827	J-97-6/161	10-15	Ostracods	275 ± 25	285	330
KIA8180	J-97-6/164	19-21	Reed leaves	285 ± 30	349	456
KIA8179	J-97-6/156	35-40	Grass and moss	(1935 ± 30)	(1820)	(1949)
KIA20828	J-97-6/156	35-40	Ostracods	(2100 ± 30)	(1995)	(2146)
KIA20829	J-97-6/147	75-80	Gastropods	1505 ± 30	1329	1417
KIA8178	J-97-6/141	105-110	Plant detritus	1945 ± 30	1823	1950
KIA20830	J-97-6/138	120-125	Gastropods	4280 ± 30	4822	4880

* Calibrated ages were calculated using the software “CALIB 5.0.” Calibration data set: intcal04.14c (Stuiver & Reimer 1993, Reimer et al. 2004).

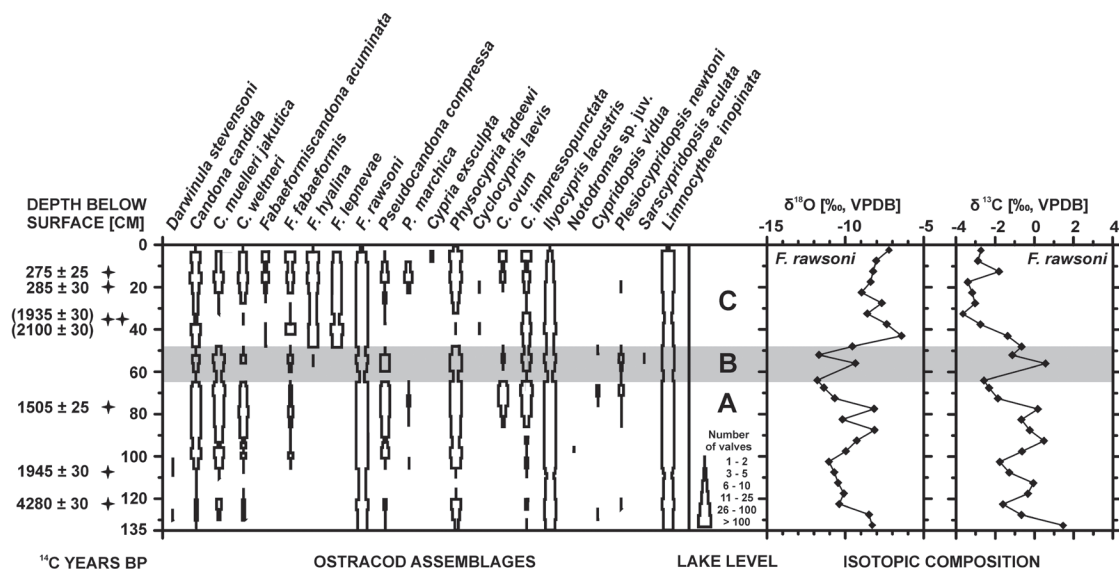


Figure 2. Ostracod assemblages and isotopic composition of ostracod valves from late Holocene lake deposits of the Alas Myuryu: A - Period of moderate lake-level fluctuations; B - Period of drastic lake-level fluctuations; C - Period of moderate lake-level fluctuations. Rejected AMS dates from deposited material are marked in brackets. Width of bars indicates ostracod number (see key).

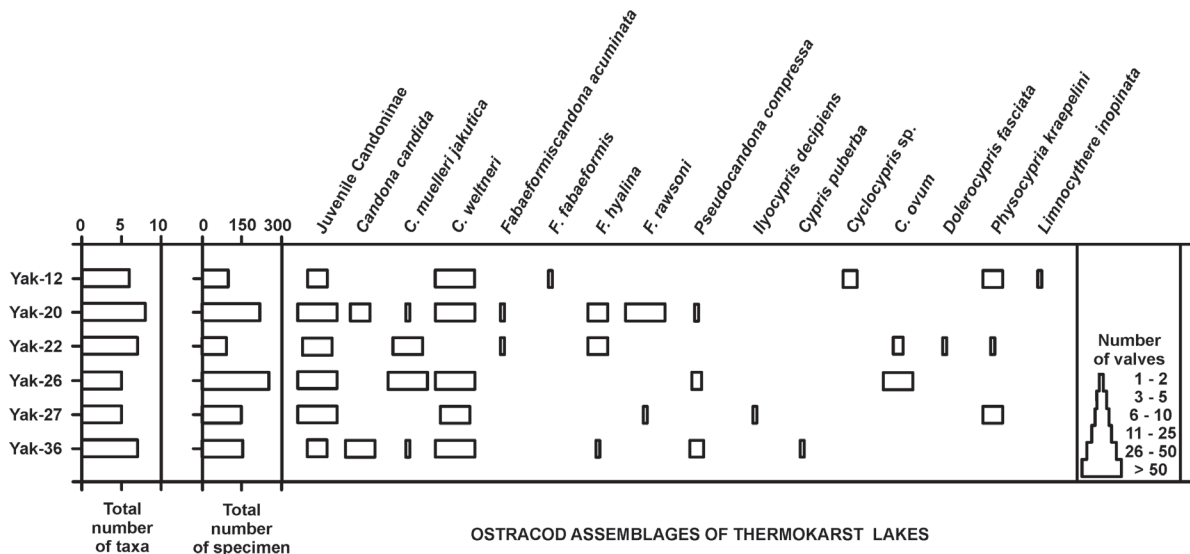


Figure 3. Modern ostracod assemblages from six thermokarst lakes on the Lena-Amga interfluvium. Width of bars indicates ostracod number (see key).

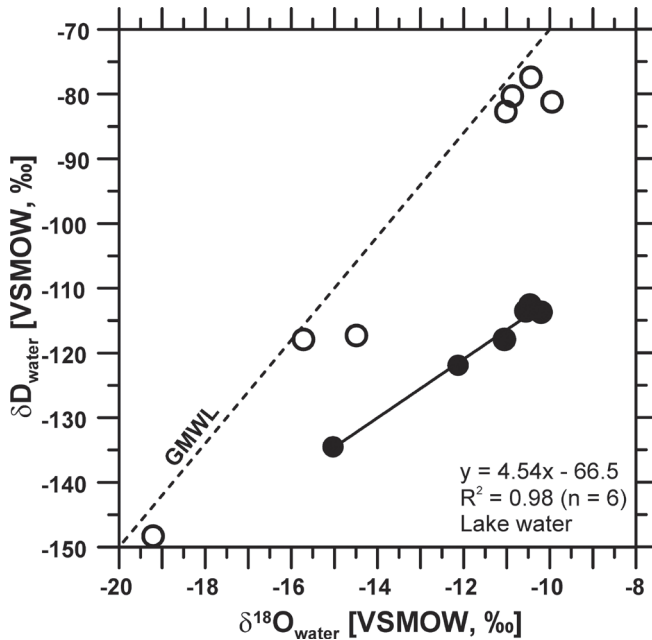


Figure 4. Isotopic composition of rain water (open circles) from Yakutsk in August 2005 and the studied lakes (filled circles) on the Lena-Amga interfluvium.

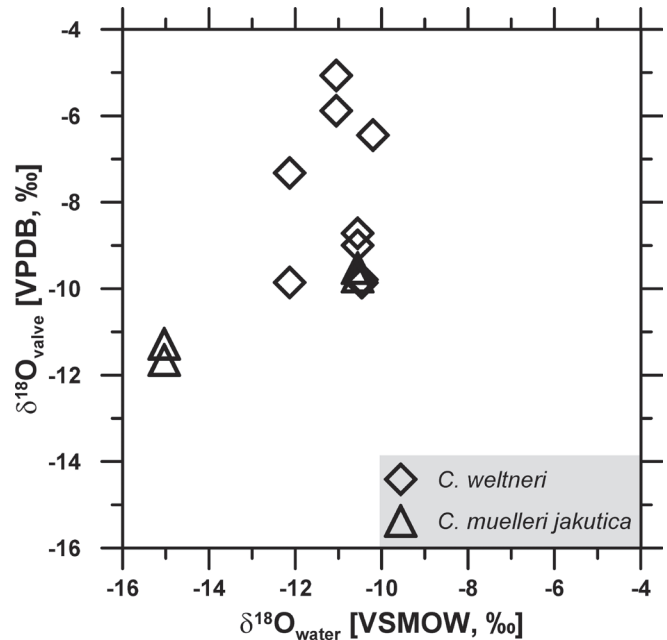


Figure 5. Stable isotope composition of $\delta^{18}\text{O}$ in ostracod calcite and host waters for female and male specimen of adult *C. weltneri* and *C. muelleri jakutica*.

the underlying permafrost. The high temperature variation in the surface lake waters during the fieldwork ranged from 12°C up to 26°C, and the ionic content expressed as electrical conductivity reached from 0.36 to 0.92 mS/cm.

The results of oxygen and hydrogen isotope analyses of the lake waters are shown in a $\delta^{18}\text{O}$ - δD plot (Fig. 4) with respect to the Global Meteoric Water Line (GMWL), which correlates fresh surface waters on a global scale (Craig 1961). Furthermore, in Figure 4 the stable isotope data of seven rainwater samples from August 2005 taken in Yakutsk are presented. Lake water samples are shifted below the GMWL, and this deviation reflects evaporation in the studied water bodies, as indicated by a slope of 4.54 ($R^2 = 0.98$; shown in Fig. 4).

The geochemical analyses of ostracod calcite ($\delta^{18}\text{O}$, $\delta^{13}\text{C}$) were performed on valves of the most common species, *C. weltneri* and *C. muelleri jakutica*. The $\delta^{18}\text{O}$ of host waters varies between about -15 to -10‰, whereas the $\delta^{18}\text{O}$ of ostracod calcite is generally shifted to ^{18}O -enriched values and ranges between about -12 to -5‰ (Fig. 5). The shift between $\delta^{18}\text{O}$ in host waters and ostracod calcite includes metabolic (vital) and temperature effects. Vital offsets on the isotopic composition of several species of Candoninae of up to 3‰ were already proposed by other studies, (Xia et al. 1997, von Grafenstein et al. 1999, Keatings et al. 2002, Wetterich et al. 2007). The temperature-dependence of $\delta^{18}\text{O}$ fractionation is reflected by the variation of the shift within a species, where increased temperatures correspond to smaller

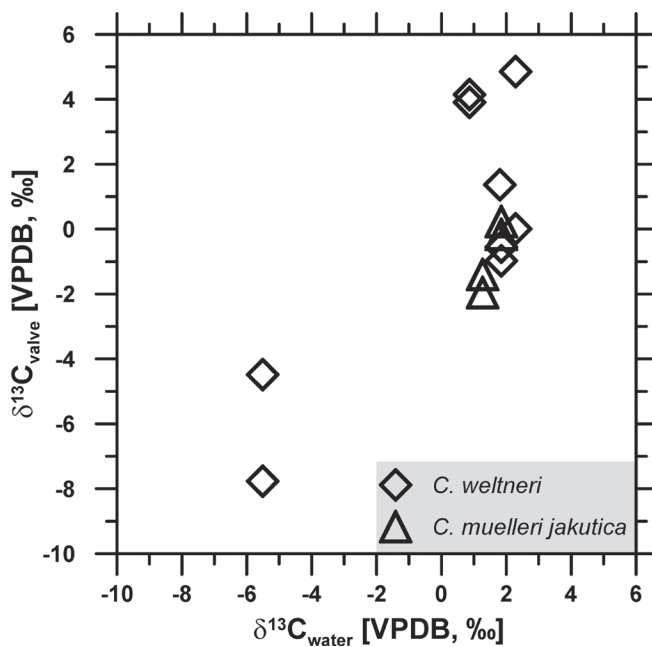


Figure 6. Stable isotope composition of $\delta^{13}\text{C}$ in ostracod calcite and ambient waters for female and male specimen of adult *C. weltneri* and *C. muelleri jakutica*.

shifts (e.g., Leng & Marshall 2004). The observed variation in the shift can be explained by different temperatures of the host water at the time of calcification.

The $\delta^{13}\text{C}$ of the studied host waters TDIC shows two different ranges at about -5.5‰ and between 1 to 2.5‰. The corresponding $\delta^{13}\text{C}$ data on ostracod calcite show considerable scatter from about -8 to -4‰ and -2 to 5‰, respectively. The scatter in $\delta^{13}\text{C}$ indicates the influence of complex abiotic and biotic effects at different times of shell secretion on $\delta^{13}\text{C}$ fractionation, as is expected in natural waters.

Discussion

For the late Holocene, Wolfe et al. (2000) detected a similar pattern of cellulose-inferred lake water $\delta^{18}\text{O}$ in a North Yakutian lake sediment record. They found most ^{18}O -depleted values between 2000 and 500 yr BP due to probably cooler conditions and less influence of evaporation. After 500 yr BP, the data change to relative ^{18}O -enriched values, as it is also recorded in the $\delta^{18}\text{O}$ record of ostracod calcite in period C, indicating a warming trend with higher evaporation.

The observed modern ostracod assemblages from Central Yakutian thermokarst lakes are characterized by species with preferences for lower water temperatures and lower salinities (e.g., *C. candida*, *C. muelleri jakutica*, *C. weltneri*, *F. hyalina*, *F. rawsoni*). The most common species, *C. weltneri*, is described as cold stenothermal to oligothermophilic and oligohalophilic (Meisch 2000). Other species are tolerant to changes in temperature and salinity. In comparison to Arctic ostracod assemblages (Wetterich et al. 2007) from North Yakutia (Lena River Delta, Laptev Sea), the Central Yakutian fauna generally lacks strictly cold-adapted species such as *F. harmsworthi*, *F. pedata*, and *Tonnacypriis glacialis*.

Nevertheless, other species, such as *C. candida*, *C. muelleri jakutica*, and *F. hyalina*, are common in both regions. The $\delta^{18}\text{O}$ record of ostracods from North and Central Yakutia shows differences. The $\delta^{18}\text{O}$ in valves of Arctic ostracods is relatively more ^{18}O -depleted and ranges between about -20 to -13‰ (Wetterich et al. 2007), whereas the $\delta^{18}\text{O}$ of the Central Yakutian ostracods ranges between about -12 to -5‰. This general tendency in the $\delta^{18}\text{O}$ records reflects the general lower temperatures and lower evaporation in the north with higher P/E ratios as compared to Central Yakutia.

Comparing the Central Yakutian $\delta^{13}\text{C}$ records of modern and late Holocene ostracods, we observe a reversed pattern, in which the fossil data are relatively more ^{13}C -depleted (mostly lighter than 0‰) than the modern ones (mostly heavier than 0‰). That may imply generally higher aquatic productivity today as compared to the late Holocene, since plants preferentially fix $^{12}\text{CO}_2$ during photosynthesis thereby leaving TDIC enriched in ^{13}C (Griffiths & Holmes 2000). The generally lower range in ostracod $\delta^{13}\text{C}$ between -2 to -11‰ from modern North Yakutian ponds (Wetterich et al. 2007) as compared to Central Yakutia may point to dominance of organic matter decay in the northern waters, since these microbiological processes release ^{13}C -depleted CO_2 and lower $^{13}\text{C}/^{12}\text{C}$ ratios in TDIC (Griffiths & Holmes 2000).

Conclusions

Periodic short- and mid-term climate variability leads to significant changes in hydrological conditions; e.g., to drastic water-level changes in thermokarst lakes of Central Yakutia, as it was first described by Nemichov (1958). A drying-up period of the thermokarst lake within Alas Myuryu in the late Holocene was observed in both taxonomical and geochemical properties of fossil freshwater ostracods. The uncertain geochronology of the record presented here renders unclear the relationship between lake changes as reflected by ostracod data and the Holocene environmental history. Nevertheless, freshwater ostracods are useful indicators for reconstruction of aquatic conditions in the past.

The modern ostracod assemblage reflects today's environmental conditions that are characterized by moderate lake-level variations due to evaporative effects during the summer season. The high variability in the modern $\delta^{18}\text{O}$ and $\delta^{13}\text{C}$ data of ostracod calcite underscores the need for further studies in this context.

Acknowledgments

We thank Hedwig Oberhansli and Birgit Plessen (GFZ, Potsdam, Germany) as well as Ulrike Herzsuh, Andreas Mackensen (AWI Potsdam and Bremerhaven, Germany), and Lyudmila Pestryakova (University of Yakutsk, Russia) for help during fieldwork and analytical work. We are very grateful to Erika Pietrzeniuk (formerly Museum of Natural History Berlin, Germany) who performed the work on the fossil ostracods. The paper benefited by critical comments from two anonymous reviewers and by English language correction from Paul Overduin (AWI Potsdam, Germany).

References

- Chivas, A.R., De Deckker, P., Cali, J.A., Chapman, A., Kiss, E. & Shelley, J.M.G. 1993. Coupled stable-isotope and trace element measurements of lacustrine carbonates as paleoclimatic indicators. In: P.K. Swart, K.C. Lohmann, J. McKenzie & S. Savin (eds.) *Climate Change in Continental Isotopic Records*. Geophysical Monograph 78: 113-121.
- Craig, H. 1961. Isotopic variations in meteoric waters. *Science* 133: 1702-1703.
- GLOBE Task Team 1999. The global land one-kilometre base elevation (GLOBE) digital elevation model, version 1.0. Boulder CO: NOAA, National Geophysical Data Center.
- Griffiths, H.I. & Holmes J.A. 2000. *Non-marine ostracods and Quaternary paleoenvironment*. Quaternary Research Association, London, 179 pp.
- Katasonov, E.M. 1979. *Structure and Absolute Geochronology of Alas Deposits in Central Yakutia*. Moscow: Nauka, 94 pp. (in Russian).
- Keatings, K.W., Heaton, T.H.E. & Holmes, J.A. 2002. Carbon and oxygen fractionation in non-marine ostracods: Results from a "natural culture" environment. *Geochimica et Cosmochimica Acta* 66: 1701-1711.
- Kelts, K. & Talbot, M.R. 1990. Lacustrine carbonates as geochemical archives of environmental change and biotic/abiotic interactions. In: M.M. Tilzer & C. Serruya (eds.). *Large Lakes: Ecological Structure and Function*. Madison: Science and Technology Publishers, 288-315.
- Leng, M. & Marshall, J.D. 2004. Palaeoclimate interpretation of stable isotope data from lake sediment archives. *Quaternary Science Reviews* 23: 811-831.
- Meisch, C. 2000. *Freshwater Ostracoda of Western and Central Europe*. Heidelberg, Berlin: Spektrum Akademischer Verlag, 522 pp.
- Meyer, H., Schönicke, L., Wand, U., Hubberten, H.-W. & Friedrichsen, H. 2000. Isotope studies of hydrogen and oxygen in ground ice-experiences with the equilibration technique. *Isotopes in Environmental and Health Studies* 36: 133-149.
- Nemchinov, A.G. 1958. About periodic lake level changes in Central Yakutia. *Scientific reports of the Yakutsk branch of the Soviet Academy of Science* 1: 30-37 (in Russian).
- Pietrzeniuk, E. 1977. Ostracoden aus Thermokarstseen und Altwässern in Zentral-Jakutien. *Mitteilungen aus dem Zoologischen Museum in Berlin* 53: 331-362 (in German).
- Reimer, P.J., Baillie, M.G.L., Bard, E., Bayliss, A., Beck, J.W., Bertrand, C.J.H., Blackwell, P.G., et al. 2004. IntCal04 Terrestrial Radiocarbon Age Calibration, 0–26 Cal Kyr BP. *Radiocarbon* 46: 1029-1058.
- Soloviev, P.A. 1973. Thermokarst phenomena and landforms due to frost heaving in Central Yakutia. *Biuletyn Peryglacjalny* 23: 135-155.
- Stuiver, M. & Reimer, P.J. 1993. Extended (super 14) C data base and revised CALIB 3.0 (super 14) C age calibration program. *Radiocarbon* 35: 215-230.
- von Grafenstein, U., Erlenkeuser, H. & Trumborn, P. 1999. Oxygen and carbon isotopes in modern freshwater ostracod valves: assessing vital offsets and autecological effects of interest for palaeoclimate studies. *Palaeogeography Palaeoclimatology Palaeoecology* 148: 133-152.
- Wetterich S., Schirrmeister, L., Meyer, H., Viehberg, F.A. & Mackensen, A. 2007. Arctic freshwater ostracods from modern periglacial environment in the Lena River Delta (Siberian Arctic, Russia): Geochemical applications for palaeoenvironmental reconstructions. *Journal of Paleolimnology* (DOI 10.1007/s10933-007-9122-1).
- Wetterich, S., Schirrmeister, L. & Pietrzeniuk, E. 2005. Freshwater ostracodes in Quaternary permafrost deposits from the Siberian Arctic. *Journal of Paleolimnology* 34: 363-376.
- Wetterich, S., Herzschuh, U., Pestyakova, L., Daibanyrova, M. & Ksenofontova, M. (2007). Limnological studies in Central and North-east Yakutia in summer 2005. In: B. Diekmann, S. Wetterich, & F. Kienast (eds.), *Russian-German Cooperation Yakutsk-Potsdam: The Expedition Central Yakutia 2005*. Reports on Polar and Marine Research 550: 259-264.
- Wolfe, B.B., Edwards, T.W.D, Aravena, R., Forman, S.L., Warner, B.G., Velichko, A.A. & MacDonald, G.M. 2000. Holocene paleohydrology and paleoclimate at treeline, North-Central Russia, inferred from oxygen isotope records in lake sediment cellulose. *Quaternary Research* 53: 319-329.
- Xia, J., Ito, E. & Engstrom, D.R. 1997. Geochemistry of ostracode calcite 1: An experimental determination of oxygen isotope fractionation. *Geochimica et Cosmochimica Acta* 61: 377-382

Hydrology, Hydrochemistry, and Vegetation of a High Arctic Wetland Complex

Ming-ko Woo

School of Geography and Earth Sciences, McMaster University, Hamilton, ON, Canada L8S 4K1

Dan K. Thompson

School of Geography and Earth Sciences, McMaster University, Hamilton, ON, Canada L8S 4K1

Xiu Juan Guan

Department of Geography, University of Saskatchewan, Saskatoon, SK, Canada S7N 5A5

Kathy L. Young

Department of Geography, York University, Toronto, ON, Canada M3J 1P3

Abstract

A wetland complex on Ellesmere Island, Canada, typical of many such complexes in the polar oases, consists of patches that include tundra pond, ice wedge trough, wet meadow, and mesic ground. In the spring, overland flow generated by snowmelt filled the topographic depressions and flooded the wetlands, flushing out the chemicals in the surface ice formed in the previous season. As floodwater receded and the surface flow connections were severed, wetland patches were largely separated. Vertical processes of evaporation and rainfall dominated. The diverse hydrological and chemical environments that emerged were possibly responsible for the different vegetation assemblages on the wetland complex. For High Arctic wetlands, permafrost significantly influences the thermal, hydrological, and chemical regimes. Frozen ground favours surface runoff, but restricts hydrological linkages among wetland patches. Shallow thaw allows prolonged active-layer saturation, and ground ice melt or thermokarst alters the concentration of various ions.

Keywords: High Arctic; hydrochemistry; hydrology; tundra pond; vegetation; wetland.

Introduction

Wetlands occur in small patches or extensively as wetland complexes in the High Arctic (Woo & Young 2003, 2006). The existence of wetlands is predicated upon frequent excess of water with gains greater than losses so as to maintain a high water table to facilitate the development of ponds or hydrophytic vegetation. The presence of permafrost enables prolonged retention of water in the wetlands, as the frozen soil limits percolation and has only a shallow thawed layer that does not require a large amount of water to saturate.

Cowell et al. (1978) noted that the formation of wetland in permafrost areas is favoured by shading and insulation provided by vegetation, peat which insulates the frozen substrate, and the lack of water movement largely due to low gradients. While the factor of vegetation cover is less important in the tundra and polar desert than in the forested areas, the presence of peat is a major consideration in retarding ground thaw (Yi et al. 2007). Poor drainage allows frequent saturation that is requisite for wetland occurrence. While the hydrology and the vegetation of Arctic wetlands have been studied (e.g., Bliss 1977, Bowling et al. 2003, Rovaneck et al. 1996) and hydrochemical sampling of wetland and pond waters (e.g., Keatley et al. 2007) has been made across the Arctic, there has not been an integrative investigation on the hydrology, hydrochemistry, and vegetation of a wetland complex. It is proposed that these wetland characteristics are interrelated, and the present study examines these several aspects at a High Arctic wetland in Canada. Results of this study are applicable to other wetlands in the continuous permafrost region.

Study Area and Methods

The study area is located near Eastwind Lake on Fosheim Peninsula, Ellesmere Island, Nunavut, Canada (80°08'N, 85°25'W) (Fig. 1). This High Arctic site has a polar oasis climate that is generally warmer than the polar desert (Edlund & Alt 1989, Woo & Young 1997). The weather station at Eureka, 20 km away, measured 76 mm annual precipitation, though this value may be an underestimation due to poor gauge catch (Woo et al. 1983).

The wetland complex where the study was undertaken in 2005 occupies a shallow depression at the foot of a long slope. This topographic setting favours the collection and storage of surface and subsurface runoff. The wetland complex drains northwestward via a small channel. Within the wetland complex are six tundra ponds and wet grounds criss-crossed by ice-wedge polygons (Fig. 2). Two lines of palsa-like features follow the rims of the polygons to deflect the paths of the surface runoff from the hill slope to the ponds. The entire area is underlain by fine-grained diamict to a depth of at least 2 m. The diamict has a high carbonate content, while the wetland complex lies below the Holocene marine limit (Bell 1996) so that the soils have a high salt content. In the wet meadow and mesic ground, a 0.1 m layer of organic litter and peat lies atop silt and clay. Part of the mesic ground and the pond rims have also a thin peat layer below mineral soil, likely buried during the last glaciation.

Hydrological methods are given in detail in Woo & Guan (2006). A vegetation survey (presence/absence) was conducted in July 2005 for the main terrain types following



Figure 1. Location of the study site on Fosheim Peninsula, Ellesmere Island, Nunavut, Canada.

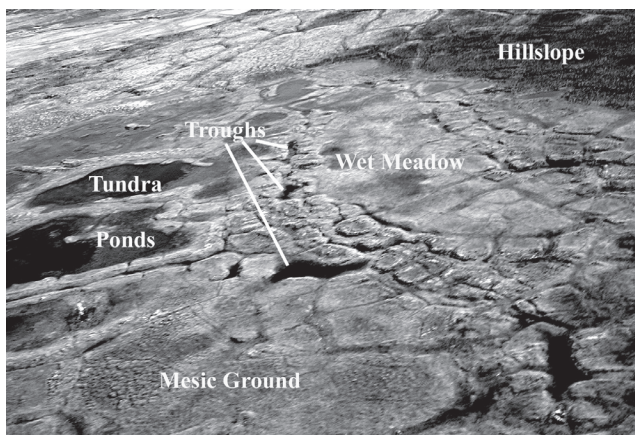


Figure 2. Photograph of the wetland complex showing hill slope, tundra ponds, ice-wedge troughs, mesic, and wet meadow sites.

the approach of Edlund et al. (1990) to determine the floristic diversity of the wetland-complex.

Water samples were collected once every six days from the start of overland flow on June 2 until mid-August. Samples were taken from the water in the northern ice wedge trough and from one of the six tundra ponds. Water was also sampled from a pool in the wet meadow and from a 15-cm diameter pit dug down to the frost table in the mesic area. In the pond, daily electrical conductivity measurements were combined with pond volume estimates to yield total solute load values in units of $\text{mS m}^{-3} \text{cm}^{-1}$. All water samples were kept cool ($\sim 4^\circ\text{C}$) and in the dark prior to field analyses. Immediately after collection, samples were analyzed for total Fe. Hach FerroVer pre-measured reagents were used for total Fe measurements. The FerroVer reagent acidifies and extracts colloidal iron and iron sorbed to organic matter otherwise not detected in analyses for “dissolved” iron. Samples were acidified to pH 2.5 using concentrated nitric acid before filtration through a $0.45 \mu\text{m}$ glass microfibre filter, prior to cation (Ca^{2+} , Mg^{2+} , Na^+ , K^+) analysis at York University in Toronto, Ontario, using a Spectra-10 Atomic Absorption

Spectrometer. This technique yields concentrations as a sum of the dissolved, colloidal, and acid-soluble suspended constituents.

Hydrological Processes

Throughout the long and cold winter, the dominant hydrological processes were the accumulation and redistribution of snow. By early June, just prior to the onset of snowmelt, the snow was unevenly distributed, as governed largely by terrain. The uplands and slopes had 163 ± 65 mm, the wet meadows accumulated 95 ± 4 mm, the mesic site had 80 ± 8 mm, while the tundra ponds collected 68 ± 18 mm of snow (all in snow water equivalent unit). From the melt period until the onset of freezeback, the magnitude of various hydrological processes varied, giving rise to strong seasonality in the wetland hydrological behaviour. The melt period occurred when the winter snow cover melted within about 10 days, generating substantial overland flow on most hill slopes and across the wetland. This was the major event that flooded large parts of the study area, infilling depressions and ponds and saturating the thinly thawed soils. Lateral surface flow enhanced hydrological connectivity across the landscape and evaporation was effective at this time around the summer solstice. Evaporation rate from the ponds averaged 2.7 mm d^{-1} and was 2.5 mm d^{-1} for the saturated areas. Ground thaw accelerated soon after the snowmelt season and the thawed active layer was able to accommodate more infiltration. A deepening of the frost table together with high evaporation loss led to a drop in the water table. Surface flow ceased, first on the hill slopes, then the mesic ground, and finally the wet meadows and between the tundra ponds.

Subsurface flow in the active layer was meager due to the shallow thaw, the low gradient (an elevation drop of 10 m over a distance of 1625 m) and the low hydraulic conductivity once the water level fell into the mineral soil layer (pumping tests and falling head tests yielded hydraulic conductivity values of 10^{-2} to 10^{-4} m s^{-1} in the organic layer and 10^{-6} to 10^{-7} m s^{-1} in the mineral substrate). The curtailment of hydrological connectivity is a major consideration in the wetland complex, as individual wetland patches became largely separated from their surroundings. Only vertical processes of rainfall, evaporation, and to a limited extent, ground ice melt controlled the water balance of the wetland patches. In summer, different types of wetland exhibited divergent hydrological behaviour. The wet meadows were no longer flooded, and the pools of water shrank as the water table dropped (Fig. 3). The ponds not only had lower water levels, but drying along their edges allowed wet meadows to emerge. Only the ice-wedge troughs with a steady supply of water from ground ice melt and confined by high rims retained water throughout the summer. The mesic ground often had dry patches between the wet areas that had a water table below the surface, partly maintained by meager subsurface flow from hill slopes. Summer rain was seldom sufficient (total of 27 mm in 2005) to rejuvenate surface flow, though a rainfall event in the following year raised the pond levels to the point of overflow (Woo & Guan 2006).

Table 1. Average pH, electrical conductivity ($\mu\text{S cm}^{-1}$) and concentration of selected major ions ($\mu\text{mol L}^{-1}$) for four types of wetland waters in the 2005 summer. Standard deviations are shown in brackets.

	Tundra pond	Wet meadow	Mesic ground	Ice wedge
pH	6.8 (0.2)	7.0 (0.1)	6.2 (0.2)	6.8 (0.2)
EC	151 (62)	116 (30)	194 (26)	170 (42)
Ca ²⁺	257 (162)	185 (91)	170 (60)	368 (200)
Mg ²⁺	203 (96)	181 (59)	232 (47)	230 (61)
K ⁺	92 (23)	25 (8)	107 (36)	143 (25)
Na ⁺	184 (84)	136 (17)	219 (17)	148 (15)
no. of samples	15	13	13	15

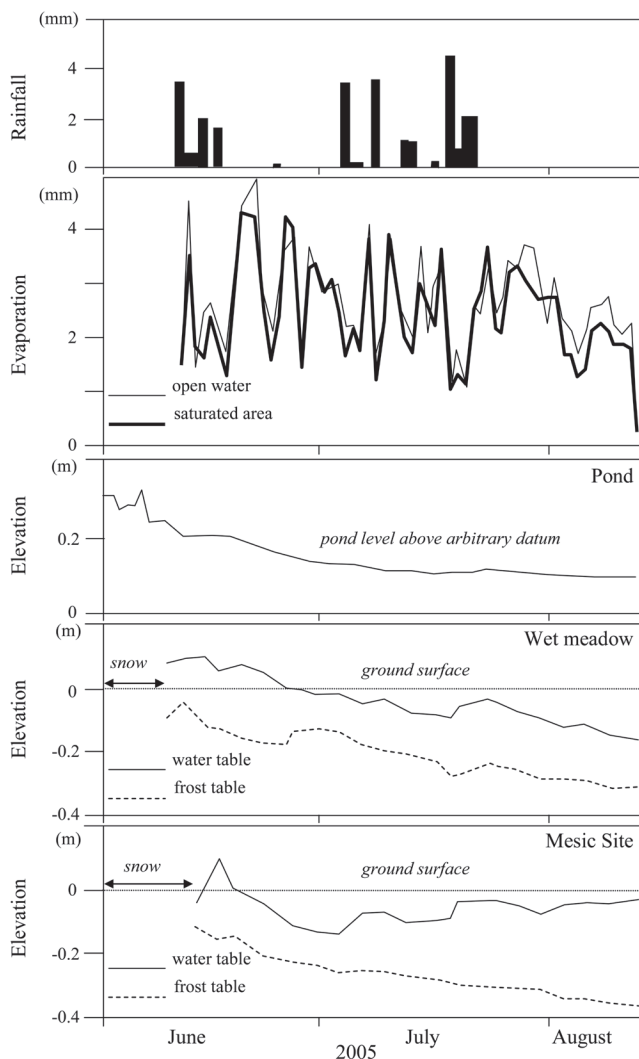


Figure 3. Daily rainfall, pond evaporation, pond water level, frost and water tables of wet meadow and mesic ground.

Hydrochemical Processes

The mean values and seasonal changes in the concentration of selected ions (Ca²⁺, Na⁺, K⁺) and pH for four types of wetlands are shown in Table 1 and Figure 4. In the spring season, extensive inundation by snow meltwater runoff of low ionic concentration (electrical conductivity-

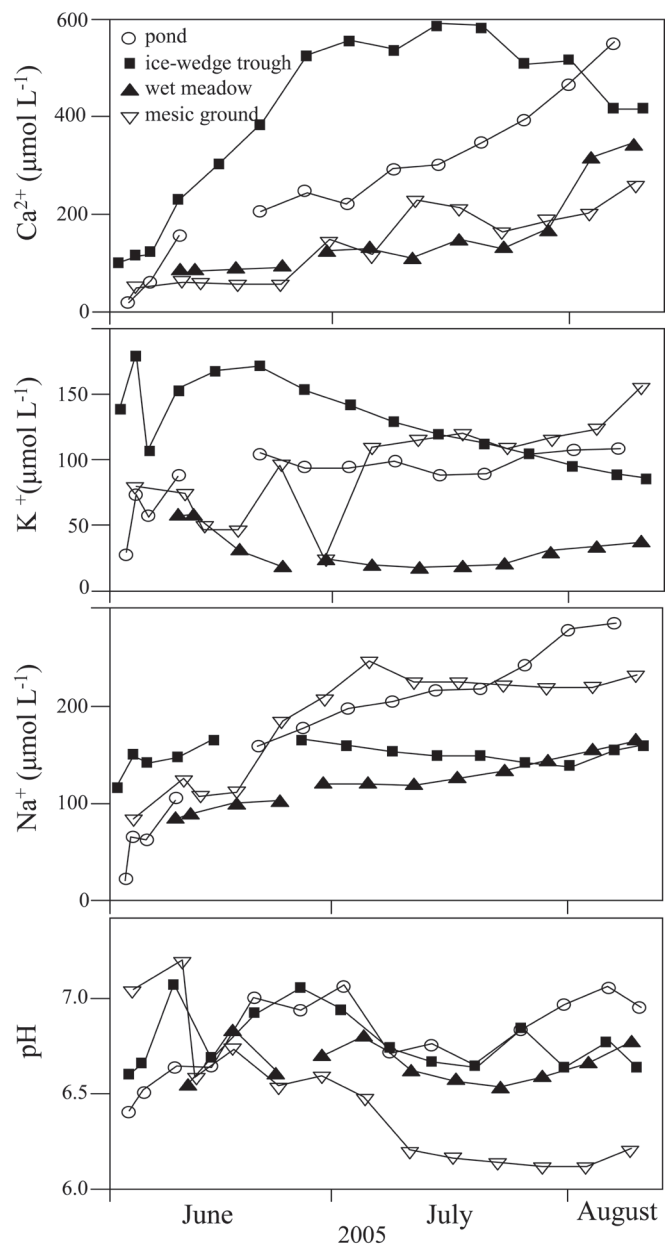


Figure 4. Seasonal change in concentration of selected major ions (Ca²⁺, Na⁺, K⁺) and pH in the water of four types of wetlands (pond, ice wedge trough, wet meadow, and mesic ground).

EC = $13 \pm 7 \mu\text{S cm}^{-1}$, pH = 6.0 ± 0.6) homogenized the hydrochemical environment of the entire wetland complex. The hydrochemistry of different wetland types was similarly low in ionic concentrations, except for potassium in the ice-wedge troughs. Its initial high value may be attributed to the trough water being in contact with the organic soil exposed on the trough walls. Later in the thaw season, however, the concentration declined as plant growth took up more K⁺ from the trough water. With the cessation of snowmelt runoff, a weakening of hydrological connectivity between the wetland patches and their surroundings became a major consideration in the evolution of wetland hydrochemistry. Rainfall was low (27 mm) and the rainwater has low chemical concentrations (Ca²⁺ = $20 \pm 16 \mu\text{mol L}^{-1}$, equivalent to $10 \mu\text{S}$

cm⁻¹) so that rainfall dilution of the wetland waters was not a major consideration.

Evaporation was effective in reducing the amount of water stored in the wetland. Thus, while the solute load remained relatively unchanged during the summer, a continuous loss of water to evaporation caused a distillation of solute cations, responsible largely for their increasing concentrations after the snowmelt season. This effect is typically evident in the tundra ponds which showed a steady increase in all cations concentrations but not in the total load (Fig. 5). Without surface runoff, both the input of chemicals and the export of soluble ions were limited by the low subsurface flow. By late summer, the in situ suprapermafrost groundwater which is a mixture of meteoric and soil water, and meltwater from seasonal ground ice and from wedge-ice (samples of ground ice showed an electrical conductivity of 233 $\mu\text{S cm}^{-1}$) had enhanced chemical concentrations compared with the spring conditions. A decrease in pH from late July onwards was possibly related to senescence of the pond vegetation that started around the same time, leading to leaching of organic acids from the plants.

Of particular interest was a thermokarst collapse event along an ice-wedge trough. Prior to the collapse, Ca²⁺ alone increased while K⁺ declined steadily, a pattern seen only in the trough (Fig. 4). Afterwards, the concentration of Fe increased from 47 to 276 $\mu\text{mol L}^{-1}$, and of Na⁺ from 149 to 160 $\mu\text{mol L}^{-1}$, but the concentrations of the other cations measured were reduced. The iron is likely to be colloidal Fe, but our analyses cannot differentiate between its soluble and colloidal forms. The thermokarsting episode showed an abrupt addition of constituents from the soil and ground ice, and an influx of ice meltwater that quickly altered the chemical content of the water in the trough.

In summary, hydrochemical behaviour of the wetlands is strongly influenced by the hydrological processes. Surface and subsurface runoff bring in or remove chemicals; vertical processes of snowmelt and direct rainfall on the wetland add atmospheric fallout (both dry and wet) while ground ice melt (including thermokarst) contributes chemicals from the soil and the ground ice to the water. The addition of water from horizontal and vertical fluxes may dilute or increase the chemical concentration, but evaporation reduces the water volume, thus increasing the concentration but not the chemical load. Vegetation growth further modifies the water chemistry.

Vegetation

Climate, geology, and topography control the hydrological and hydrochemical behaviour which, together with the soil factor, govern the wetland ecology. Different ecological settings give rise to distinct vegetation niches (Table 2). The non-wetland hill slopes have good drainage and are covered by a large diversity of vascular plants ranging from grasses to a variety of saxifrages. The mesic areas experience more frequent saturation than the hill slopes, and the vegetation typically reflects these conditions with the presence of cotton-grass (*Eriophorum scheuchzeri*), mosses and a range of graminoid species. The wet meadows lack the diversity

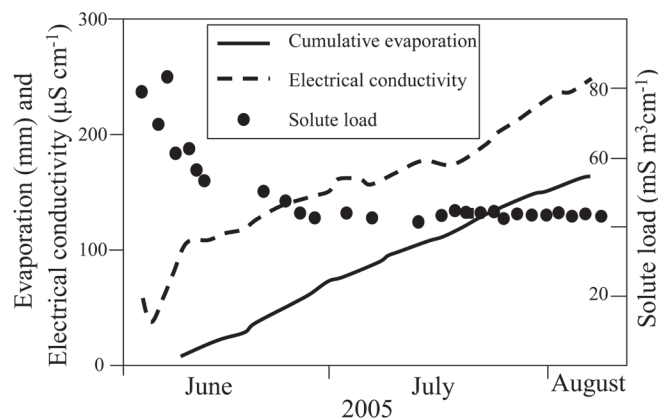


Figure 5. Cumulative evaporation, electrical conductivity, and solute load in tundra pond.

in vascular plants when compared to the mesic sites, but contain various algae species, some graminoids, and cotton-grass (e.g., *Eriophorum scheuchzeri* and *Eriophorum angustifolium*) which reflect their saturated substrate, as was typically noted by other ecologists (Bliss & Matveyeva 1992, Edlund & Garneau 2000). Rims of the ponds experience drying in the summer, and vascular diversity here is comparable to the drier hill slopes. These small strips also appear to represent a transition zone from flooded pond sites with the presence of cotton-grass and algae. As the ponds shrink, the emergent plants include grasses and sedges such as *Alopecurus alpinus*, *Agrostis mertensi*, *Calamagrostis neglecta*, *Carex misandra*, and cotton-grasses such as *Eriophorum scheuchzeri* and *Eriophorum angustifolium*. Only a few vascular plants exist in these flooded zones (e.g. *Lycopodium alpinum*, *Pedicularis hirsuta*). The water-filled troughs of the ice-wedge polygons have low vascular diversity (e.g. *Salix arctica*, *Saxifraga cernua*) and are more typical of flooded sites dominated by mosses and graminoids.

Roles of Permafrost

Permafrost plays an important role in affecting the hydrology and hydrochemical evolution of arctic wetlands, thus also exerting an indirect influence on the development of wetland vegetation.

(1) Ground saturation and water storage: Frozen soil prevents or limits deep percolation, and most hydrological and hydrochemical activities in the High Arctic are restricted to the shallow thawed zone. A thin active layer does not accommodate much water so that where drainage is poor, as in low gradient terrain, the ground is frequently saturated to form wetlands. Annually, rapid release of ample snow meltwater to the thinly thawed soil enables replenishment of surface water storage and homogenization of the chemical conditions of the wetland complex.

(2) Runoff and hydrological connectivity: The extremely poor hydraulic conductivity of permafrost restricts hydrological linkages while low gradient further limits lateral subsurface flow, so that the hydrochemistry of the wetland patches evolves differentially in the thaw season. In the long run, divergent hydrological regimes and

Table 2. Plant species found in the study area.

Species	Hill slope	Mesic Ground	Wet meadow	Pond rim	Pond	Polygon trough
<i>Alopecurus alpinus</i>	x	x	x	x	x	
<i>Agrostis mertensi</i>				x	x	
<i>Algae sp.</i>			x	x	x	
<i>Calamagrostis neglecta</i>	x	x	x	x	x	
<i>Carex saxatilis</i>				x		
<i>Carex supine</i>						x
<i>Carex bigelowii</i>		x				
<i>Carex misandra</i>	x	x	x	x	x	
<i>Carex sp.</i>	x	x	x	x	x	x
<i>Cassiope tetragona</i>	x					
<i>Draba sp.</i>		x		x	x	x
<i>Dryas integrifolia</i>	x	x		x		x
<i>Eriophorum scheuchzeri</i>		x	x	x	x	x
<i>Eriophorum angustifolium</i>			x	x	x	x
<i>Fungii sp.</i>				x		
<i>Graminoid sp.</i>	x	x	x	x	x	x
<i>Juncus biglumis</i>				x		
<i>Lichen sp.</i>	x			x		
<i>Lycopodium alpinum</i>					x	
<i>Melandrium apetalum</i>	x	x	x	x		
<i>Moss sp.</i>	x	x	x	x	x	x
<i>Papaver radicum</i>	x	x		x		
<i>Pedicularis flammea</i>	x			x		
<i>Pedicularis hirsute</i>	x	x	x	x	x	
<i>Polygonum viviparum</i>		x	x	x		
<i>Potentilla nivea</i>	x	x		x		
<i>Oxyria digyna</i>	x	x		x		
<i>Salix arctica</i>	x	x	x	x		x
<i>Saxifraga cernua</i>	x		x	x		x
<i>Saxifraga oppositifolia</i>	x			x		
<i>Saxifraga tricuspidata</i>	x					
<i>Stellaria longipes</i>	x	x		x		

hydrochemical environments lead to the development of different vegetation assemblages. The vegetation itself has feedback on the chemistry as previously discussed.

(3) Ground ice melt: Although the amount of water provided by the melting of ground ice is small relative to other water sources, it nonetheless is important in affecting the water chemistry due to the ionic constituents of the thawing soil and of the ice-water. Ground ice contribution may come steadily through the seasonal thaw of the active layer or arrive rapidly through occasional thermokast events that inject new chemicals and add ice melt water to the wetland environment in relatively short periods.

Conclusion

The wetland complex in the polar oasis of Ellesmere Island shows strong interactions among the hydrology, hydrochemistry, vegetation, and permafrost. A large influx of snow meltwater in the spring leads to general flooding and replenishment of wetland storage. The floodwater also homogenizes the hydrochemistry across the wetland complex. Shallow ground thaw maintains saturated conditions and prevents drainage of the tundra ponds but limits subsurface flow, hence restricting hydrological

connectivity among the wetland patches. Vertical processes of rainfall, evaporation, and ground ice melt dominate in the post-snowmelt period. These processes concentrate or dilute the chemical concentration of the wetland waters, leading to divergent chemical evolution paths of the hydrologically isolated wetland patches. Vegetation development represents a long-term response to the divergent physical and chemical environments within the complex. Vegetation growth and the formation of peat significantly reduce the ground thermal conductivity while the abundance of seasonal ground ice in the wetland soils requires much latent heat for ground thaw (Woo et al. 2006a). These conditions give rise to a thinner active layer than in the mineral soils. Such feedback mechanisms among wetland soil saturation, vegetation growth and peat formation, and shallow seasonal thaw, sustain the presence of the arctic wetlands (Woo et al. 2006b).

Acknowledgments

This study was supported by the Natural Sciences and Engineering Research Council of Canada. Logistical support was provided by the Polar Continental Shelf Project of Natural Resource Canada. We thank the reviewer for helpful comments that improved this article.

References

- Bell, T. 1996. The last glaciation and sea level history of Fosheim Peninsula, Ellesmere Island, Canadian High Arctic. *Canadian Journal of Earth Sciences* 33: 1075-1086.
- Bliss, L.C. 1977. *Truelove Lowland, Devon Island, Canada: A High Arctic Ecosystem*. Edmonton, Alberta: University of Alberta Press, 714 p.
- Bliss, L.C. & Matveyeva, N.V. 1992. Circumpolar arctic vegetation. In: Chapin, S.F. III, Jeffries, R.L., Reynolds, J.F., Shaver, G.R., Svoboda, J. and Chu, E.W. (eds.), *Arctic Ecosystems in a Changing Climate*. San Diego: Academic Press, 59-89.
- Bowling, L.C., Kane, D.L., Giech, R.E. & Hinzman, L.D. 2003. The role of surface storage in a low-gradient Arctic watershed. *Water Resources Research* 39 (4): 1087, DOI: 10.1029/2002WR001466.
- Cowell, D.W., Jeglum, J.K. & Merriman, J.C. 1978. Preservation of seasonal frost in peatlands, Kinoje Lakes, southern Hudson Bay Lowland. *Proceedings, Third International Conference on Permafrost, Edmonton, Alberta*, Vol. 1: 453-459.
- Edlund, S.A. & Alt, B.T. 1989. Regional congruence of vegetation and summer climate patterns in the Queen Elizabeth Islands, Northwest Territories, Canada. *Arctic* 42: 3-23.
- Edlund, S.A. & Garneau, M. 2000. Overview of vegetation zonation in the Arctic. In: M. Garneau & B.T. Alt (eds.), *Environmental Response to Climate Change in the Canadian High Arctic*. Geological Survey of Canada Bulletin 529, 113-127.
- Edlund, S.A., Woo, M.K. & Young, K.L. 1990. Climate, hydrology and vegetation patterns, HWC, Ellesmere Island, Arctic Canada. *Nordic Hydrology* 21: 273-286.
- Keatley, B.E., Douglas, M.S.V. & Smol, J. 2007. Limnological characteristics of a High Arctic oasis and comparisons across Northern Ellesmere Island. *Arctic* 60: 294-308.
- Rovaneck, R.J., Hinzman, L.D. & Kane, D.L. 1996. Hydrology of a tundra wetland complex on the Alaskan Arctic Coastal Plain. *Arctic and Alpine Research* 28: 311-317.
- Woo, M.K. & Guan, X.J. 2006. Hydrological connectivity and seasonal storage change of tundra ponds in a polar oasis environment, Canadian High Arctic. *Permafrost and Periglacial Processes* 17: 309-323.
- Woo, M.K. & Marsh, P. 1977. Effect of vegetation on limestone solution in a small High Arctic basin. *Canadian Journal of Earth Sciences* 14: 571-581.
- Woo, M.K., Mollinga, M. & Smith, S.L. 2006a. Simulating active layer thaw in a boreal environment. *Geographie Physique et Quaternaire* 60: 9-17.
- Woo, M.K. & Young, K.L. 1997. Hydrology of a small drainage basin with polar oasis environment, Fosheim Peninsula, Ellesmere Island, Canada. *Permafrost and Periglacial Processes* 8: 257-277.
- Woo, M.K. & Young, K.L. 2003. Hydrogeomorphology of patchy wetlands in the High Arctic, polar desert environment. *Wetlands* 23: 291-309.
- Woo, M.K. & Young, K.L. 2006. High Arctic wetlands: their occurrence, hydrological characteristics and sustainability. *Journal of Hydrology* 320: 432-450.
- Woo, M.K., Young, K.L. & Brown, L. 2006b. High Arctic patchy wetlands: hydrologic variability and their sustainability. *Physical Geography* 27: 297-307.
- Yi, S., Woo, M.K. & Arain, A. 2007. Impacts of peat and vegetation on permafrost degradation under climate warming. *Geophysical Research Letters* 34: L16504, DOI: 10.1029/2007GL030550.

Soil and Permafrost Temperature Data Obtained During the First International Polar Year, 1882–1883

Kevin R. Wood

Joint Institute for the Study of the Atmosphere and Ocean, University of Washington, Seattle, USA

Dmitry A. Streletskiy

Dept. of Geography, Center for Climatic Research, University of Delaware, Newark, USA

Abstract

Synoptic meteorological data from Arctic stations established during the first International Polar Year (IPY-1) have recently been collected and digitized. The research program at seven of fourteen stations included ground temperature observations at regular depth intervals. We have analyzed data obtained at the IPY-1 stations at Jan Mayen, Sodankylä, Finland, and at Malye Karmakuly and Sagastyr, Russia. Descriptive records and more fragmentary data are available for most stations. Initial comparisons indicate that ground temperatures are consistent with surface air temperature (SAT) observations obtained using well-calibrated standard instruments. Using these data, we compare ground-temperature observations with contemporary measurements made at nearby locations.

Keywords: climate change; ground temperature; historical data; permafrost; Polar Year.

Introduction

Ground temperature measurements were recorded at seven of fourteen research stations established in the Polar Regions during the first International Polar Year (IPY-1) (Fig. 1) (Heathcote & Armitage 1959). Time series data were collected in soil at four or more levels down to 1.6 or 2.0 m depth where possible. Measurements were made with calibrated instruments and recorded values tracked variations in surface air temperature (SAT) as expected. The two U.S. stations were not equipped for systematic observation of ground temperature, but at Point Barrow a shaft was sunk to a depth of 37.5 feet for the purpose of obtaining the temperature of the earth, which at the bottom was reported to be a near-constant 12°F (-11.1°C) (Ray 1885). Descriptive observations covering a wide range of cryosphere-related features are commonly found in expedition reports, including notes on ice and ice-processes that were features of the regional landscape. All data obtained during IPY-1 were published *en extenso* by each of

the national expeditions. There has been renewed interest in historical data of this type in recent years due to the potential value they hold for improving our understanding of climate change and its impact on the environment.

We present an analysis of the four most complete ground temperature data sets recorded during IPY-1 in the Northern Hemisphere. These were obtained by the Austro-Hungarian expedition at Jan Mayen (von Wohlgemuth 1886); the Finnish expedition at Sodankylä (Lemström & Biese 1886); and by the Russian expeditions at Malye Karmakuly, on Novaya Zemlya, and Sagastyr, in the Lena River delta (Lenz 1886a, 1886b). Descriptive records obtained at these locations are discussed. Data and an extensive image collection are available at: www.arctic.noaa.gov/aro/ipy-1.

Inspired by Carl Weyprecht (1838–81), the aim of IPY-1 was to investigate those fundamental problems in geophysics which could only be studied effectively through a program of coordinated observation at a widely distributed network of stations anchored in Polar Regions (Weyprecht 1875).

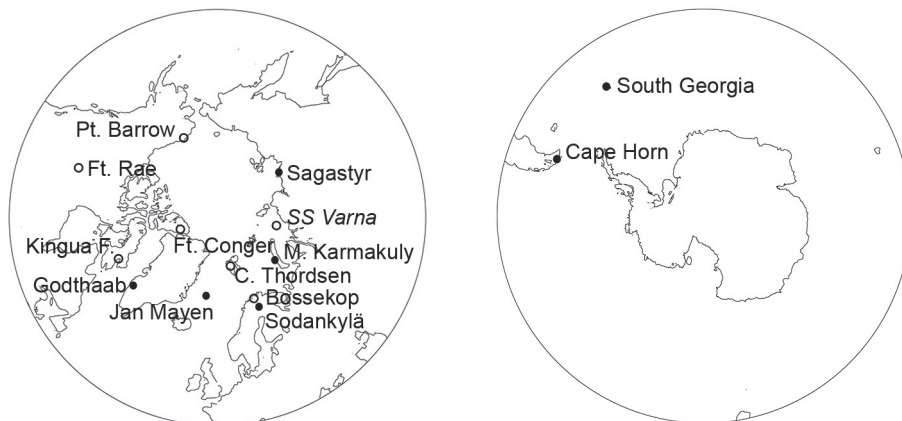


Figure 1. IPY-1 stations in the Northern and Southern Hemispheres. Filled circles indicate stations where ground temperature measurements were obtained. Open circles indicate stations where fragmentary data or descriptive observations only were obtained. The Dutch expedition (SS *Varna*) was trapped in the Kara Sea and did not reach land.

The three main fields of inquiry were meteorology, terrestrial magnetism, and the aurora. The science plan of IPY-1 also encompassed a wide range of additional subjects under the heading of optional observations. In addition to the ground temperature data discussed here, research was undertaken in a variety of subject areas including ethnology, natural history, and oceanography.

It is not surprising that ground temperature and related geocryological studies were undertaken during IPY-1 given the interest in the subject over the previous 40 or more years and the personal involvement of H. Wild, the president of the International Polar Commission (IPC) in this research area (Wild 1878), and G. Wild, president of the Russian Polar Commission and noted permafrost scientist (Baker 1982, Shiklomanov 2005).

Direct comparisons between IPY-1 and modern ground temperature regimes proved to be impossible, primarily due to a lack of modern data at these stations. Landscape transformation was also a factor, especially at Sodankylä, where a reservoir now covers the station site. Since the data were collected simultaneously, we are able to discuss the spatial variability between stations. Given the connection between upper level ground temperatures and synoptic meteorology, we also draw some tentative conclusions about where IPY-1 observations fall within the spectrum of recent monthly mean SAT variability.

Data and Methods

The most complete time series of ground temperature observations in soil obtained during IPY-1 were recorded at Jan Mayen (71.00°N, 008.47°W), Sodankylä (67.41°N, 026.6°E), Malye Karmakuly (72.38°N, 052.7°E), and Sagastyr (73.38°N, 124.08°E). Two years of observations were recorded at Sodankylä and Sagastyr. A temperature time series in rock was obtained at Godthaab, and fragmentary data of various types were obtained at Cap Thorsen, Fort Rae, and Point Barrow. We have concentrated our analysis on the first four data sets. Data collected at the two Southern Hemisphere stations have not been addressed.

Details on the methods adopted at each station and descriptions of the ground cover and soil type are provided in the expedition reports cited above. An idea of the different environments around each station can also be gleaned from Figure 2 and other graphical information in the reports.

The most detailed metadata available for the four stations relates to the Russian station at Sagastyr. Given that procedures at this station and the stations at Malye Karmakuly, and Sodankylä were all initiated by H. Wild, IPC president and director of the Central Physical Observatory in St. Petersburg, we can expect that many particulars are common to these three stations. In general, separate holes were excavated to 40, 80, and 160 cm and either glass or wooden tubes inserted. The earth thermometers themselves were enclosed in brass cylinders with their bulbs embedded in a mixture of brass filings and tallow. The cylinders were then attached to wooden sticks that were placed in each tube.



Figure 2. IPY-1 stations and surrounding terrain (from top): Jan Mayen, Sodankylä, Malye Karmakuly, and Sagastyr.

The tubes were then closed with brass caps. Thermometers at the ground surface were installed horizontally, usually on two small brackets. Surface instruments were often buried in snow and were susceptible to breakage when the snow was removed each time they were read. Instruments on the surface and at 40 cm were read hourly, while the deeper ones were read less frequently (either 3x or daily). Thermometers were calibrated at a range of temperatures against standard instruments at the Central Physical Observatory and verified more frequently at the station at the 0°C calibration point.

The Sagastyr station was established on a small island on the northern edge of Lena River delta. A. Bunge, one of the expedition scientists, noted the dynamic effects of the river upon the terrain in the delta (Lenz 1886a). Old islands were continually being eroded and new ones created. The ground was generally composed of sandy soils overlaid with peat, the thickness of which Bunge suggested was proportional to the length of time the place was undisturbed. The vegetation around the station was dominated by mosses and lichens, with sparse dwarf-shrubs (mostly *Salix polaris*). The data record was interrupted in the summer of 1883 due to meltwater infiltrating from the surface and refreezing in the tubes at deeper levels which prevented the extraction of the thermometers. The location was also moved at this time to an area less susceptible to the building-induced snow drift that was problematic during the first year. Several reported changes of equipment produced small inhomogeneities in the record, but these had minimal influence on the interpolated mean annual ground temperature (MAGT) at particular depths.

The expedition to Malye Karmakuly was dispatched hurriedly and was not prepared for as thoroughly as the others (Barr 1985). Here, soil temperatures were measured at the standard depths in gravelly soil characteristic of the island.

Wooden tubes rather than glass were used. Continuous snow cover at the measurement site was registered from 6 October 1882 to 25 May 1883. The measurements at 160 cm were interrupted on 30 May, again due to the infiltration and freezing of meltwater, as was the case in Sagastyr.

The metadata for Sodankylä is sparse. The earth thermometers were located about 20 m south of the buildings shown in Figure 2, on flat grassy terrain about 300 m from the Kitala River. Instruments at the surface and 40 cm were read hourly; others were read at least daily but the interval was not clear in the report. In the second year, observations were taken three times daily (0600, 1400, and 2200). Training

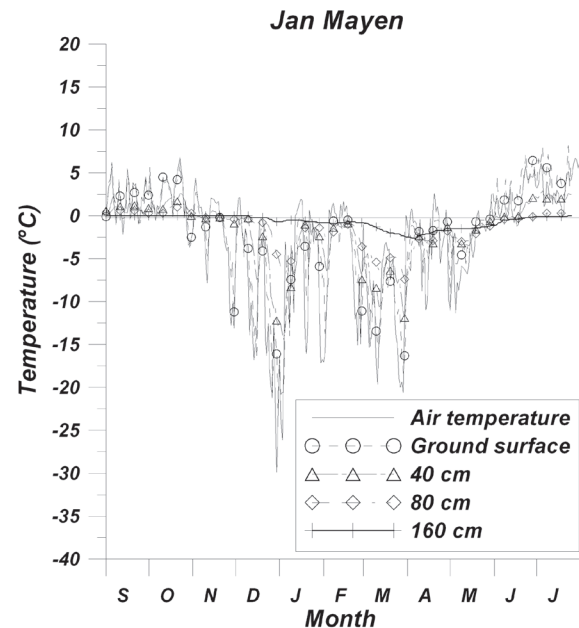


Figure 3. Air and ground temperatures observed at Jan Mayen, 1882–1883. Markers are placed at 10-day intervals throughout.

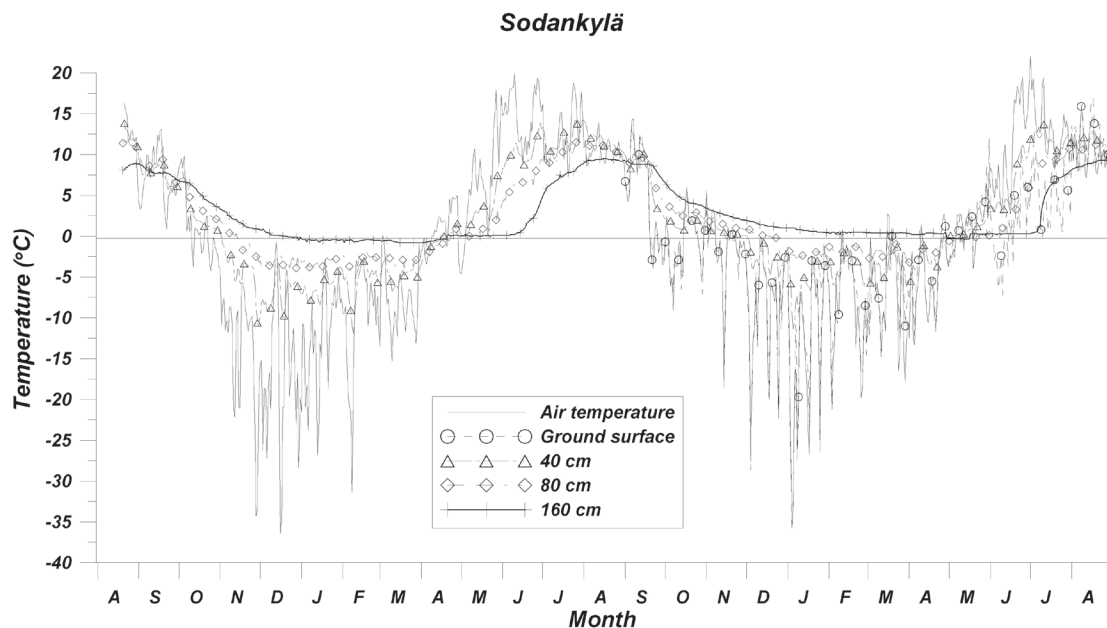


Figure 4. Air and ground temperature measurements at Sodankylä, 1882–1884. Note the difference between the years, which is especially clear in the 160 cm temperature curve. During the second year, the temperature at this level remained above freezing, but then did not warm appreciably until 7 July, nearly four weeks later than in 1883. This is a hallmark of a warmer, snowier winter followed by a cold spring.

and equipment, including glass tubes and thermometers, were provided by the Central Physical Observatory in St. Petersburg. The methods followed at Sodankylä most likely resembled those used at Sagastyr.

At Jan Mayen, rather different procedures were used. Temperatures were recorded at 6 levels down to 1.56 m depth, but the thermometers were graduated in whole degrees and read once per day at 1130. The thermometers were constructed such that they could be buried vertically in the ground while their scales remained above the surface where they could be read. Frozen ground was encountered at 80 cm depth. The expedition's standard thermometers were verified at the Kew Observatory in Great Britain, and they were, in turn, used to calibrate the earth thermometers at the station. We have interpolated the Jan Mayen data to match the standard depth intervals used at the other three stations.

The four stations were located where distinct types of climate and permafrost occur in the Arctic, from seasonal freezing to low temperature permafrost. At Jan Mayen and Sodankylä, the climate can be generally characterized as maritime type, with relatively warm winters and cool summers, even though both are geographically within the Arctic. The milder climate at these stations is due primarily to the dynamics of the atmospheric circulation over the North Atlantic and the influence of the warm ocean currents of the Atlantic Drift. The climate of Fennoscandia is more sensitive to fluctuations in large-scale circulation of the sort indicated by the North Atlantic Oscillation (NAO) (e.g., Thompson & Wallace 2001). The climate at Malyye Karmakuly, and especially Sagastyr, tends toward the more severe arctic-continental type with low temperatures and high amplitude variability. At the latter station, the Siberian high-pressure area is an important factor in winter, which tends to limit the influence of warm advection from the West.

Analysis

Four time series plots of ground temperature data were produced and these are briefly interpreted with respect to mean SAT and other key factors. Differences between subsequent years are pointed out. Gaps in the data were interpolated between other depth levels with data using standard polynomial interpolation.

Jan Mayen

The mean annual air temperature (MAAT) below -2.0°C that was registered at Jan Mayen was enough to form a thin layer of frozen ground (Fig. 3). Despite this there is a sharp attenuation of climatic signal with depth which implies that this layer is unstable to climatic fluctuations. It is possible that the ground at 150 to 200 cm depth was frozen for more than two years, meaning that permafrost was present. This would be consistent with the fact that frozen ground was encountered below 80 cm during the placement of the earth thermometers, but it is also possible that this layer could thaw completely during a warmer year. An interesting feature is the prolonged presence of a zero-degree curtain at 160 cm.

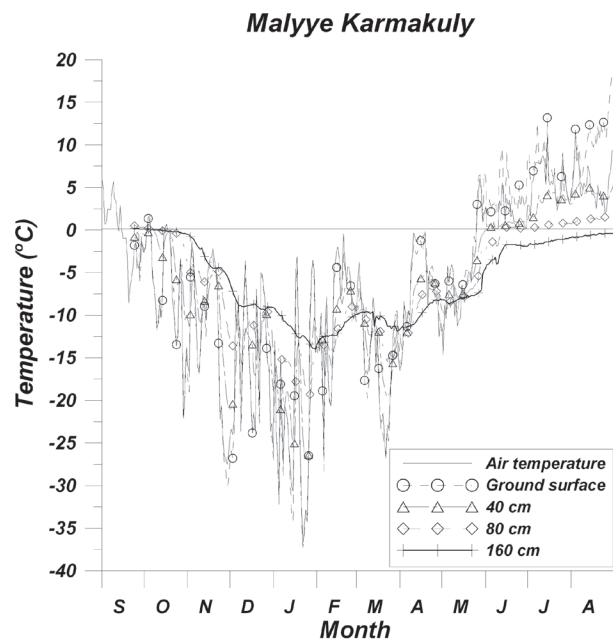


Figure 5. Air and ground temperature observations at Malyye Karmakuly, 1882–1883.

Assuming that there was no instrumental error involved, one possible explanation is that there was a massive body of ground ice present below the study site.

Sodankylä

Despite its position above the Arctic Circle, the climate at Sodankylä is relatively mild, with MAAT just below 0°C . Even though MAAT during IPY-1 was slightly above the value of the reference climatology (1968–1997) the winter cold signal was enough to create seasonal freezing during the two years of observation. The depth of freezing was down to 165 cm during the first winter and 190 cm during the second (Fig. 4). The difference can be attributed to the fact that the cold climatic signal expressed as Degree-Days of Freezing (DDF) of the second winter was less than 80% of the first winter. This resulted in less penetration of cold into the ground.

A marked difference in meteorology between 1882–83 and 1883–84 was noticed by both scientists and the local inhabitants, who considered 1882–83 much more representative of the typical climate than the following year. The second winter was warmer than the first, but the spring and early summer were much colder. There were also 201 days of rain or snow precipitation during the second year compared to 134 days during the first, which could also have affected the ground temperature regime (GTR).

Malyye Karmakuly

Malyye Karmakuly is located on the west coast of Novaya Zemlya, where North Atlantic circulation patterns also influence the climate, but to a somewhat lesser extent than in Fennoscandia. The MAAT observed in 1882–83 was -6.6°C , which is 1.4° below the reference climatology value of

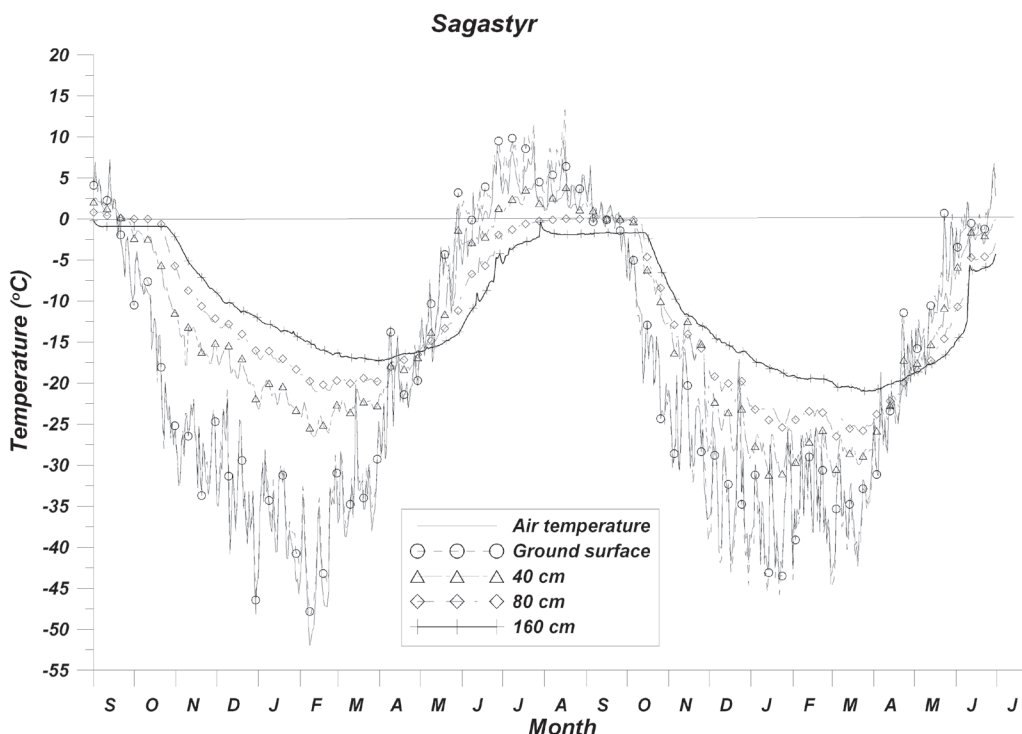


Figure 6. Air and ground temperature measurements at Sagastyr, 1882–1884. While there were differences in the meteorology of the two years, the difference in GTR is primarily due to the reduction in snow cover resulting from the relocation of the instruments away from an area of building-induced snow drift.

-5.1°C. The GTR at this location was more favorable for the formation of permafrost than either Jan Mayen or Sodankylä. This is because of the lower MAAT and greater range of air temperature expressed as Mean Annual Amplitude (MAAA) here. The mean annual ground temperature (MAGT) at 160 cm was -6.0°C at this location, but daily values were still highly sensitive to synoptic meteorology. There was no zero-curtain feature like in the locations discussed previously. Based on the ground temperature gradient, the interpolated permafrost depth was about 12 m in 1883.

Sagastyr

The overall pattern of variability in SAT anomalies at Sagastyr over the two year period was similar to the pattern observed at Sodankylä. The second winter was warmer than the first, especially February, while the spring was cooler. Notwithstanding the warmer winter, MAGT was lower during the second year. This is most likely the result of the drastic change in snow cover that resulted from the shift in location. During the first year, the depth of the snow drift next to the thermometers reached nearly 2 m compared to an accumulation of ~25 cm in the open tundra. The GTR at the second location was quite different due to much less snow cover. MAGT the second year was more than 3.0°C colder even though MAAT was 0.6°C warmer. This clearly demonstrates the critical role snow cover plays with respect to the GTR.

It is also quite interesting to note that SAT in all seasons at Sagastyr was apparently much colder than the mean of the recent climatology (1968–1997). There were no

positive anomalies in the entire 22 months of record, and 18 months were more than one standard deviation below the reference means. SAT records at every other IPY-1 station in the Northern Hemisphere showed fluctuations about the mean of the reference climatology that were generally consistent with month-to-month variations in the large-scale atmospheric circulation patterns, particularly the NAO. The nearest modern station with data comparable to Sagastyr was Tiksi, about 200 km south, but an average displacement of more than ~2.5°C in the reference anomaly values would be required to bring Sagastyr observations into line with the rest of the IPY-1 monthly anomalies.

Discussion

There were distinct differences in GTR evident between the IPY-1 stations studied. Both SAT and ground temperatures decreased toward the north and east, consistent with regional climatology. The GTR at Jan Mayen and Sodankylä was much warmer than either Malye Karmakuly or Sagastyr where MAGT ranged between -5°C and -10°C. Expected exponential attenuation of the temperature signal with depth and delayed phase shifts proportional to depth below the surface can be seen in the data.

If the GTR data from IPY-1 are broadly representative, then we can see that permafrost landscapes situated in the Atlantic-maritime climate zone would have been more sensitive to climate fluctuations even at that time than those toward the East with a more polar-continental type climate. This speculation is supported to some extent in that marked

changes in permafrost landscapes were reported during the climate warming that occurred in this region early in the 20th century (Jensen 1939, Wood & Overland, in prep.). This region has certainly experienced changes in vegetation, hydrological regime, and geomorphologic processes during the recent period, and this process would likely expand in the case of increased warming as the boundary of the less-sensitive region to the eastward shifted in response.

We also note that the month-to-month fluctuations in SAT and GTR during the winter were often consistent with large-scale variability in atmospheric circulation. In February 1883, for example, the NAO index was 2.4 and the SAT anomaly distribution over the Atlantic and northern Europe closely resembled the canonical pattern (e.g., Hurrell 1995). Positive SAT anomalies occurred at Jan Mayen, Sodankylä, and Malye Karmakuly; the effect on GTR is particularly evident at the latter station. However, the effects of increased westerly advection did not extend as far as Sagastyr, where SAT was especially low during this month. It would be reasonable to expect that GTR in Fennoscandia and northern Russia would be sensitive to those fluctuations in atmospheric circulation that produce well-known SAT anomaly patterns in winter.

Historical data such as these we have been discussing are particularly interesting now in light of the large environmental impacts that have been observed in the Arctic and elsewhere associated with a warming climate. The practical use of this type of data, however, is encumbered by a number of well-known issues, not least of which is the lack of comparable site-specific modern data. Even without the ability to make direct comparisons, we can certainly use historical information to study questions suited to the material and also to discover where new investigations might be leveraged by historical resources.

Acknowledgments

This publication was supported in part by the NOAA Arctic Research Office and JISAO under cooperative agreement NA17RJ1232, Contribution #1478.

References

- Baker, F. 1982. The first International Polar Year. *Polar Record* 21(132): 275-285.
- Barr, W. 1985. The expeditions of the first International Polar Year, 1882-83. In *Technical Paper No. 29*, 223. Calgary: Arctic Institute of North America.
- Heathcote, N.H.d.V. & Armitage, A. 1959. The First International Polar Year (1882-1883). In *Annals of the International Geophysical Year*, ed. ICSU. London; New York: Pergamon Press.
- Hurrell, J.W. 1995. Decadal trends in the North Atlantic Oscillation: Regional temperatures and precipitation. *Science* 269: 676-679.
- Jensen, A.S. 1939. Concerning a change of climate during recent decades in the Arctic and Subarctic regions. *Kgi. Dansk. Vid. Selsk. Biol. Medd.* 14.
- Lemström, S. & Biese, E. (eds.) 1886. *Observations Fait aux Stations de Sodankylä et Kultala*. Helsingfors: L'Imprimerie des Héritiers de Simelius.
- Lenz, R. (ed.) 1886a. *Beobachtungen der Russischen Polarstation an der Lenamündung*: Russischen Geographischen Gesellschaft.
- Lenz, R. (ed.) 1886b. *Beobachtungen der Russischen Polarstation auf Nowaya Semlja*: Russischen Geographischen Gesellschaft.
- Ray, P.H. 1885. *Report of the International Polar Expedition to Point Barrow, Alaska*. Washington, D.C.: Government Printing Office.
- Shiklomanov, N.I. 2005. From exploration to systematic investigation: development of geocryology in 19th- and early 20th-century Russia. *Physical Geography* 26(4):249-263.
- Thompson, D.W.J. & Wallace, J.M. 2001. Regional Climate Impacts of the Northern Hemisphere Annular Mode. *Science* 293: 85-89.
- von Wohlgemuth, E.E. (ed.) 1886. *Österreichische Polarexpedition nach Jan Mayen. Beobachtungsergebnisse*. Wien: Der Kaiserliche-Königliche Hof- und Staatsdruckerei.
- Weyprecht, C. 1875. Fundamental principles of scientific Arctic investigation. An address delivered before the 48th meeting of German naturalists and physicians at Graz, on the 18th of September 1875.
- Wild, H. 1878. Über die Bodentemperaturen in St. Petersburg und Nukuss. *Repertorium für Meteorologie* VI(4): 1-88.
- Wood, K.R. & Overland, J.M. In Prep. Early 20th century Arctic warming in retrospect.

The Monitoring Network of Permafrost Conditions and Embankment Performance Along the Qinghai-Tibet Railway

Qingbai Wu

State Key Laboratory of Frozen soil Engineering, Cold and Arid Regions Environmental and Engineering Research Institute, Chinese Academy of Science, Lanzhou

Yongzhi Liu

State Key Laboratory of Frozen soil Engineering, Cold and Arid Regions Environmental and Engineering Research Institute, Chinese Academy of Science, Lanzhou

Hui Yu

State Key Laboratory of Frozen soil Engineering, Cold and Arid Regions Environmental and Engineering Research Institute, Chinese Academy of Science, Lanzhou

Abstract

Some effective engineering measures (crushed-rock-based embankment, crushed-rock cover, U-type crushed-rock embankment, and thermal pile in the embankment) have been used to mitigate the impact of engineering disturbance on the thermal regime of permafrost and to avoid permafrost thawing and surface subsidence affecting railway performance. A network of 43 automated sections was installed in 2004 along the Qinghai-Tibet Railway to monitor at regular intervals the ground temperature at different locations (in the embankment shoulders and slope foot and in the permafrost underneath the embankment and away from the embankment) for studying the thermal regime of permafrost. The thawing front location in the embankment and ground underneath the embankment also can be monitored based on temperature data. In addition to this network, 12 subsidence benchmarks and one 20 m deep pile as a reference benchmark in each section were also installed for monitoring the surface subsidence of the railway embankment. Recent monitoring results of two years showed that the roadbed was stable during observed periods. Under the crushed-rock-based embankment and the embankment with thermal piles, the permafrost temperatures decreased and permafrost tables were raised noticeably; but the temperature of permafrost under the embankment with a crushed-rock revetment was slightly decreased, and the permafrost table was basically unchanged.

Keywords: embankment performance; monitoring network; permafrost conditions; Qinghai-Tibet Railway; subsidence; temperature.

Introduction

Surface disturbance from engineering construction and other human activities can cause significant permafrost warming and thawing by altering the surface energy balance. Permafrost thawing can result in ground surface subsidence, which can disrupt infrastructure stability and operations in cold regions (Smith & Burgess 1999, Nelson et al. 2001). As a consequence, understanding, evaluation, and anticipation of changes in permafrost under engineering construction are of great scientific interest.

Of the 1142 km of the Qinghai-Tibet Railway (QTR) from Golmud to Lhasa, about 542 km go through continuous permafrost regions. In the 542 km of continuous permafrost regions, there are 275 km in warm permafrost (mean annual ground temperature is higher than -1.0°C), with 134 km of high ice content (including ice-rich frozen soil, saturated-ice frozen soil, and ice with soil), and 171 km in cold permafrost (mean annual ground temperature is lower than -1.0°C), with 97 km of high ice content (Wu et al. 2004). Widespread, warm, ice-rich permafrost along the QTR is easily subject to thaw settlement caused by climate warming and engineering construction, which can affect the stability of highways or railways in permafrost regions (Wu et al. 2004, 2005a, Cheng & Wu 2007). To prevent ground ice near the

permafrost table from thawing caused by climate warming and engineering effects, some effective measures, such as crushed-rock-based embankments, crushed-rock cover, and substituting a bridge for embankments, were applied to cool the permafrost under embankments (Ma et al. 2002, Cheng 2005, Wu et al. 2006). The results of permafrost variation during the QTR construction indicated that these measures could effectively reduce the thermal impact of climate warming and engineering disturbance (Wu et al. 2005b, Ma et al. 2006, Cheng et al. 2007). However, under the long-term effect of climate warming and thermal disturbance of engineering, whether these measures can maintain the long-term effect of cooling the permafrost is an important issue for roadbed stability in permafrost regions along the QTR.

The main objective of this article is to introduce the long-term monitoring system of permafrost condition and embankment performance along the Qinghai-Tibet Railway. We first discuss the principles of the long-term monitoring system setup, then the systematic composition and monitoring methods. We focus on roadbed deformation and variation of the permafrost table under embankments with various engineering measures. The relationship between roadbed stability and permafrost variation under embankments caused by the thermal disturbance of engineering were investigated.

Principles of Monitoring Network Setup

The goal of the long-term monitoring network for the Qinghai-Tibet Railway in permafrost regions is mainly to monitor permafrost changes, including artificial permafrost table, permafrost temperature, freezing and thawing process under embankments with and without engineering measures and under the natural surface, roadbed deformation and the variation of seasonal freezing depth under the embankment in seasonally frozen soil areas and thawed areas of permafrost regions. The principles of the long-term monitoring network setup mainly included the following factors:

Permafrost thermal stability

Permafrost thermal stability is one of the most important factors in roadbed stability, including the mean annual ground temperature (MAGT) of permafrost and the frozen soil types (ice content). The permafrost regions along the Qinghai-Tibet Railway are divided into four areas by the MAGT: (1) extremely unstable areas of warm permafrost where the MAGT is higher than -0.5°C , (2) unstable areas of warm permafrost where the MAGT ranges from -0.5°C to -1.0°C , (3) basically stable areas of cold permafrost where the MAGT ranges from -1.0°C to -2.0°C , and (4) stable areas of cold permafrost where the MAGT is lower than -2.0°C . Each area defined by the MAGT could be further divided into two sub-areas by ice content near the permafrost table: (1) ice-rich permafrost areas including ice-rich permafrost, saturated ice permafrost, and ice layer with soil; and (2) ice-poor permafrost areas. We focused on establishing some monitoring sections in warm, ice-rich permafrost areas, where many measures were applied to decrease the permafrost temperatures under embankments.

Engineering measures

The application of engineering measures for the Qinghai-Tibet Railway was to effectively cool the permafrost temperature under embankments. Under the effect of climate warming and engineering construction, the long-term impact of engineering measures on permafrost under embankments is closely related to roadbed stability.

Some measures that were focused on included (1) crushed-rock-based embankment with length up to 142 km, (2) embankment with crushed-rock cover with length up to 156 km, (3) U-type crushed-rock embankment; (4) embankment with thermal piles, and (5) general embankment.

The goals of the permafrost monitoring network on the QTR were to investigate permafrost variations (under the natural surface and the embankments) and surface deformation of the embankment. So, the monitoring network is divided into two parts: one is to investigate the variation of active layer thickness—the soil temperatures at the ground surface as well as near the permafrost table and the MAGT under climate warming; the other is to investigate the variation of the permafrost table—the temperature under the embankments and the total deformation on railway surface under the effect of the railway.

Monitoring Sites Description

According to the principles of the monitoring network setup, 43 monitoring sections were established in 2004, including the monitoring of road surface deformation and permafrost temperatures under the embankment and natural surface. In each section, the permafrost temperatures under both the right and left shoulders of the embankment, under the embankment slope foot, and under the natural surface away from the railway were monitored. Additionally, 12 deformation benchmarks were installed on the road surface for each section. All of these instruments comprised the deformation monitoring system in each site. Meanwhile, two weather stations will be established at the Kaixinling and Tanggula Mountains in 2008. Together with a weather station at Beiluhe basin, they will consist of a weather system in the whole monitoring network along the Qinghai-Tibet Railway.

These 43 monitoring sites along the 542 km of the QTR, from Xidatan to Anduo, span about 3.4 latitudinal degrees and about 2.6 longitudinal degrees on the eastern Qinghai-Tibet Plateau (Fig. 1). The elevation of these sites vary from 4423 m a.s.l. at Xidatan site to 5080 m a.s.l. at the Tanggula Mountain site, with an average elevation of about 4713 m a.s.l. All monitoring sites are located in the permafrost region except the XD1 site, located in seasonal frozen soil areas near the northern limit of permafrost. Among the sites located in permafrost regions, the QH1 and ZH1 sites are in thaw areas of the permafrost region, and the ZR1, XQ1, and WT1 sites are in degraded areas of the permafrost region, where the MAGT is higher than 0°C . These observed sites are distributed in various terrains, including high altitude mountains, high plains, and basins from north to south of the plateau. In the high altitude mountains along the QTR, that is, the Kunlun Mountains, Kekexili Mountains, Fenghuo Mountains, Tanggula Mountains, and Touerjiu Mountains, the MAGTs are lower than -1.5°C or -2.0°C , the active layer thickness ranges from 1.2 m to 2.0 m, the permafrost thickness is larger than 60 m, and ice-rich permafrost exists from the permafrost table to 10 m deep below the ground surface. In the high plain along the QTR, that is, the high plain of the Chumaer River, the MAGTs range from -0.5°C to -1.5°C , the active layer thickness ranges from 2.0 m to 3.0 m, the permafrost thickness is lower than 50 m, and ice-rich permafrost is widespread from the permafrost table to 10 m deep below the ground surface. In the basins along the QTR, that is, the Beilu River, Wuli, Tuotuo River, Buqu River, Zajiazangbu River and Anduo, the MAGTs are higher than -0.5°C , exceptionally lower than -0.5°C , most of the active layer thickness is larger than 3 m, but some is exceptionally lower than 2.5 m, permafrost thickness ranges from 10 m to 25 m, and thaw area is widespread.

The areas in the high plain and in the basin are key sections for monitoring permafrost variation under the embankment and the total deformation of road surface due to warm, ice-rich permafrost.

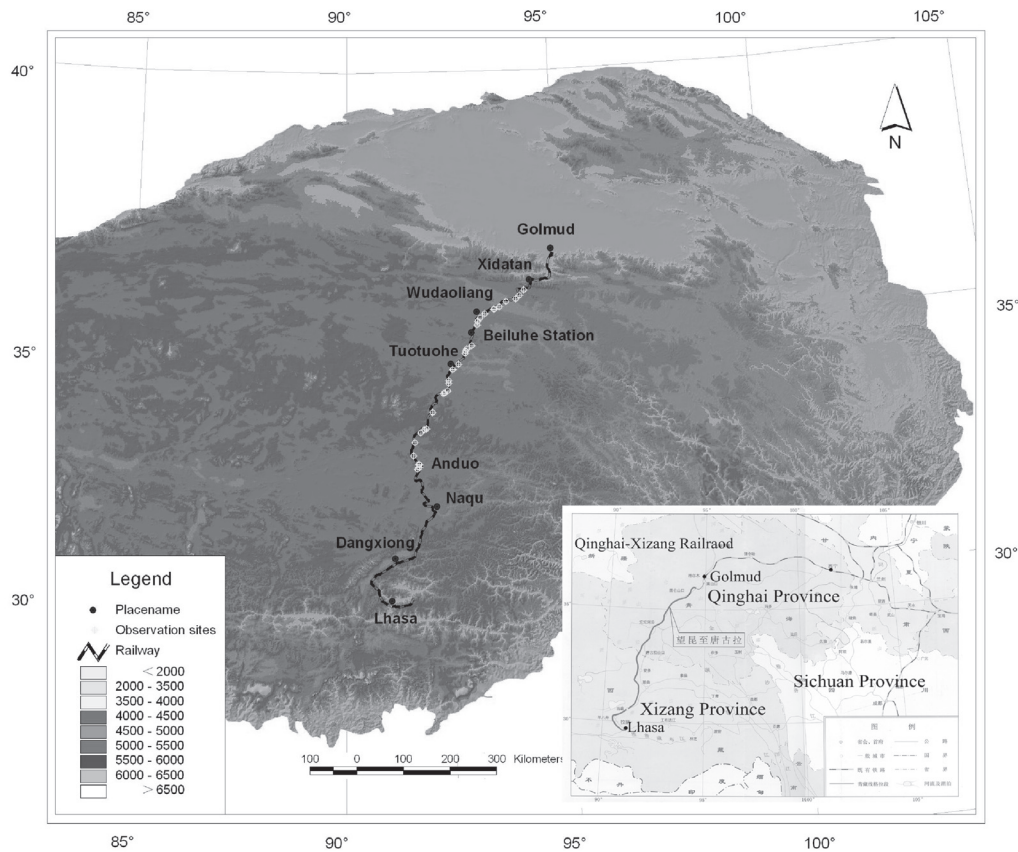


Figure 1. Monitoring network of the permafrost along the Qinghai-Tibet Railway.

Measuring Methods

Soil temperature measuring method

Soil temperatures were measured in three embankment locations: from the road surface to 20 m deep through the borehole at the right and left shoulders, from the natural surface to 8 m deep through the borehole at the embankment slope foot, and from the natural surface to 18 m deep through the borehole at a place away from the railway (Fig. 2). All measurements were obtained by a string of thermistors installed with the interval of 0.5 m from each other along the borehole, except at the places away from the railway. There the thermistors were installed at depths of 10, 20, 40, 80, 120, 160, and 200 cm from the surface to 2 m deep, and with the interval of 0.5 m from 2 m to 18 m deep. These thermistors, with sensitivities of $\pm 0.05^\circ\text{C}$, were made by the State Key Laboratory of Frozen Soil Engineering (SKLFSE). The in situ measurement data acquisitions were automatically conducted by the Datataker of DT500 series (made in Australia). Well-trained technicians and professionals manually download the data from the Datataker every two months, and they check the operational condition of the equipment, including power, communication, etc., every month.

Deformation measuring method

Total deformation of embankment surface monitoring consists of two parts in each site. One part is constructed

of 12 thin-steel benchmarks inserted 20 cm deep from the embankment surface. The other part is constructed of standard piles, as a reference benchmark, buried 20 m deep under the embankment near the deformation benchmarks (Fig. 3). Relative elevations of the deformation benchmarks and the reference benchmark are measured by electronic theodolite. The absolute heights are calculated by comparison of the elevation differences between deformation benchmarks and the reference benchmark. The deformation measurements of the embankment surface are conducted on day 20 of every month by well-train technicians and professionals, strictly following the standard guideline.

Estimation method of active layer thickness and permafrost table

Active layer thickness (ALT) under the natural surface or the artificial permafrost table under the embankment can be estimated by soil temperature data measured by the methods mentioned above. The ALT can be estimated by various methods: mechanical probing, temperature measurements, visual measurements, etc. (Brown et al. 2000). The soil temperature measurement method is available in our study. The maximum thawing depth can be shown by the profile of the soil temperature versus the depth-mapped base on the data of the daily soil temperature during any time extent, commonly several months from August to November. The

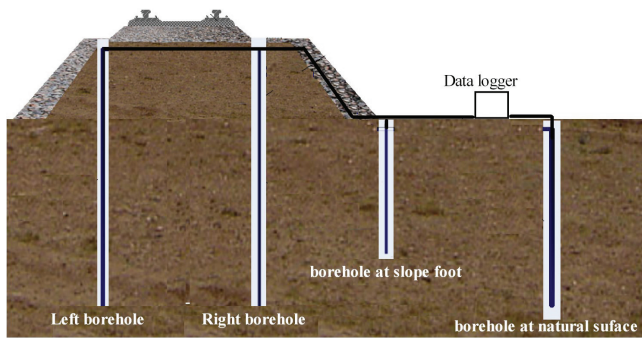


Figure 2. Section of the permafrost temperature observed site; depth of borehole at both left and right shoulders is 20 m, at the slope foot is 8 m, and at the natural surface is 18 m. Generally, the borehole at the natural surface is away from the railway.

deepest intersection between the profile mentioned above and the 0°C axes is the deepest depth of soil thawing in summer, which is the active layer thickness from the ground surface. The artificial permafrost table under the embankment is estimated by the same method.

Results

Permafrost variation and deformation for general embankment

Table 1 shows the variation of the artificial permafrost table under the general embankment and deformation of the embankment surface. During the period of observation, the artificial permafrost table rose, ranging from 0.55 m to 0.9 m under the right shoulder of the embankment and from 1.1 m to 2.9 m under the left shoulder of the embankment for KM1, CR2, CR5, LD1, WL3, and WQ1 sites; the artificial permafrost table dropped, ranging from -0.35 m to -4.1 m for CR1, YH1, YH2, DB1, RR1, and AD3 sites. However, the sections where the artificial permafrost table dropped are located in extremely warm permafrost regions where mean annual ground temperature is high, up to -0.5°C, except at the CR2 site. This indicates that extremely warm permafrost could gradually thaw if special design methods are not used.

However, deformation of the embankment surface seems to be unrelated to the variation of the artificial permafrost table (Table 1). The amount of average deformation at the sections of CR1, CR5, WQ1, and AD3 is larger than 20 mm, and only CR1 and AD3 sites found that the artificial permafrost table dropped during observed periods. Drilling data show that the deformation of embankment surface obviously depends on ice content of permafrost. The ice content of permafrost is more than 30% for these sites.

Permafrost variation under crushed-rock-based embankment

Table 2 shows the variation of the artificial permafrost table under a crushed-rock-based embankment. During observed periods, the artificial permafrost table under the embankment rose except at the left shoulder of the WL1 and TG1 sites, ranging from 0.05 m to 3.35 m. The artificial permafrost table under the left shoulder of the embankment was still deeper than the permafrost table

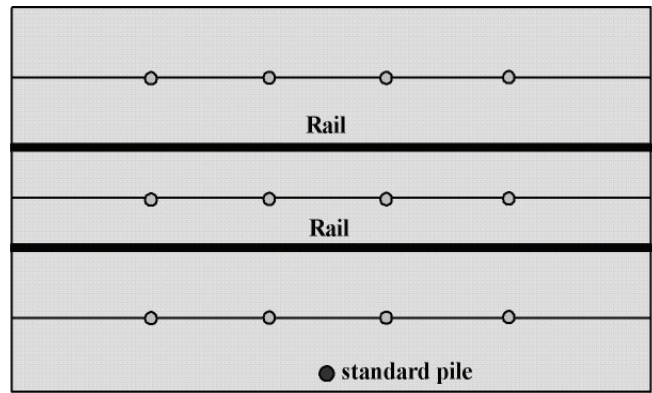


Figure 3. Planform of thin-steel benchmarks setup of the deformation in embankment surface in each section. Grey solid circles are thin-steel benchmarks of deformation, and black solid circles are standard piles as a reference benchmark of deformation.

under the natural surface. These results indicate that using a crushed-rock-based embankment is effective in raising the artificial permafrost table under the embankment. The cause of the artificial permafrost table under the left shoulder of the embankment for WL1 and TG1 sites is unclear, and probably is related to the crushed-rock-based embankment construction.

Permafrost thawing under embankments resulted in subsidence of the embankment. For WL1 and TG1 sites, the average deformation at the left shoulder of the embankment surface was more than 10 mm—up to 15 mm and 32 mm, respectively, during observed periods. For other sites, the average deformation is lower to 2 mm, indicating that the roadbed is stable.

The monitoring results before 2006 testified that the artificial permafrost table was not only raised, but also the temperatures had a trend of decreased permafrost temperatures under the crushed-rock-based embankment (Wu et al. 2005b, Ma et al. 2007), indicating that it is a good engineering measurement to avoid permafrost thaw.

Discussion and Summary

The network that monitors permafrost conditions and embankment performance along the QTR began to run in 2005, and some very useful data have been obtained successfully, including variation of the permafrost temperature, active layer under the natural surface, artificial permafrost table, temperature under the embankment, and total deformation of railway surface. These helpful data can be used to investigate and analyze the relationship between roadbed stability and permafrost variation under the embankment. The data about active layer can be used to investigate spatial features of active layer thickness along the QTR. These data are useful also for understanding the response of permafrost and active layer to climate warming and engineering construction.

To check permafrost variation in the early stage of the QTR operation, we first analyzed the obtained data of these 43 sites. The results of two recent years showed that

Table 1. Rising of permafrost table under embankment and deformation on embankment surface.

Site	Location	MAGT (°C)	PT(m)	H(m)	APT(m)		ΔH(m)		Aver. Def. (mm)
					Right	Left	Right	Left	
KM1	Kunlun Mts.	-3.17	1.9	1.0	2.35	1.75	0.55	1.15	-2
CR1		-0.75	1.1	5.5	7.5	5.5	-0.90	0.90	34
CR2	Chumaerhe	-0.90	5.1**	4.0	7.3	5.0	0.90	2.90	0
CR5	high plain	-0.50	4.7	2.8	7	5.0	0.50	2.50	20
LD1		-0.65	4.0	0.9	4.9	4.5	0.00	0.40	3
YH1	Yamaerhe	-0.50	2.95	4.2	7.5	7.75	-0.35	-0.60	1
YH2		-0.24	5.22	2.4	11.7	9.0	-4.10	-1.38	2
WL3	Wuli Basin	-0.54	2.8	3.6	6.2	5.6	0.20	0.80*	12
DB1	100daoban	-0.12	4.5	4.0		9.0		-0.50	0
WQ1	Wenquan	-0.40	3.1	3.0	5.5	5.0	0.60	1.10	31
RR1	Riazangbuqu	-0.27	5.3	5.0	11.5	11.3	-1.20	-1.00	0
AD3	Anduo	-0.20	2.3	3.5	5.8	6.2	0.00	-0.40	88

MAGT means mean annual ground temperature, PT means permafrost table, APT means artificial permafrost table in 2006, H means height of embankment, and ΔH means the rising value of artificial permafrost table during observed periods. Aver. Def. means average deformation of embankment surface. All data used in this table is before Oct. 2007. ** The temperatures at the slope foot of embankment are a reference due to no temperature data under natural surface.

Table 2. Variation of artificial permafrost table after the CRBE construction.

Site	MAGT (°C)	PT(m)	H(m)	APT(m)		ΔH (m)	
				Right	Left	Right	Left
CR3	-1.5	2.7	3.10	3.6	<0*	2.1	>2.7*
WD1	-1.48	1.85	3.2	2.65*	2.1	2.4*	2.95
KK1	-2.4	1.8	4.0	2.45	3.1	3.35	2.4
HL3	-1.28	2.3	3.5	3.2	3.72	2.6	2.08
WL1	-0.5	3.2	3.70	5.8*	7.1	1.1*	-0.2
KL1	-0.67	2.35	3.40	4.4	4.85	1.35	0.9
BB1	-0.33	2.4	5.7	4.5	6.5	3.6	1.6
TG1	-1.24	2.85	4.4	7.2	7.8	0.05	-0.55

All signs are the same as that in Table 2. * means the value under roadbed centerline. <0 means artificial permafrost table entered into embankment.

the total roadbed deformation was smaller than 10 mm, which indicates roadbed stability. Under the crushed-rock-based embankment and the embankment with thermal piles, permafrost temperatures were noticeably decreased, and the permafrost table was noticeably raised. Under the embankment with crushed-rock revetment, permafrost temperatures were slightly decreased, and the permafrost table was basically stable. However, the following problems deserve more attention:

- For all observed sites, the permafrost temperatures were uneven due to the radiation difference of the two embankment slopes. The permafrost table depth under the sun-side slope of the embankment is greater than that under the shade-side slope, and the permafrost table slope inclining to the sun-side slope of the embankment could be deformed possibly, resulting in roadbed crack.
- The thaw layer between the upper permafrost and the seasonal freezing layer occurred under the embankment in

the warm permafrost areas where the MAGT is higher than -0.5°C. The thickness of the thaw layer ranged from 50 cm to 150 cm with an average of 85 cm, which could potentially result in larger deformation of the roadbed.

- The frozen layer which would not thaw within a year formed under the left shoulder (shade-side) of the embankment in both of the seasonal frozen soil areas and the thaw areas of permafrost regions. This frozen layer formation beneath the left side of the embankment could be an inducement to roadbed damage.

- The permafrost temperatures under the slope foot of the embankment were higher than those under the natural surface. Under the thermal effect of the railway, the active layer thickness under the slope foot of the embankment was larger than that under the natural surface. Rainfall could accumulate here possibly because of the lateral thermal influence.

Acknowledgments

Many technicians contributed greatly during construction of the permafrost monitoring network along the QTR, and the authors are very thankful. This research was funded by the Outstanding Youth Foundation Project, the National Natural Science Foundation of China (Grant No. 40625004).

References

- Brown, J., Hinkel, K.M. & Nelson, F.E. 2000. The Circumpolar Active Layer Monitoring (CALM) program: research designs and initial results. *Polar Geography* 24(3): 165-258.
- Cheng, G. 2005. A roadbed cooling approach for the construction of Qinghai-Tibet Railway. *Cold Regions Science and Technology* 42: 169-176.
- Cheng, G.D. & Wu, T. 2007. Responses of permafrost to climate change and their environmental significant, Qinghai-Tibet Plateau. *J. Geophys. Res.* 112: F02S03, doi:10.1029/2006/JF000631.
- Cheng, G.D., Sun, Z.Z. & Niu, F.J. 2007. Application of the roadbed cooling approach in Qinghai-Tibet railway engineering. *Cold Regions Science and Technology*: doi:10.1016/j.coldregions.2007.02.006.
- Ma, W., Cheng, G.D. & Wu, Q.B. 2002. Preliminary study on technology of cooling foundation in permafrost regions. *Journal of Glaciology and Geocryology* 24(5): 579-587.
- Ma, W., Shi, C.H., Wu, Q.B., Zhang, L.X. & Wu, Z.J. 2006. Monitoring study on technology of the cooling roadbed in permafrost region of Qinghai-Tibet Plateau. *Cold Regions Science and Technology* 44(1): 1-11.
- Ma, W., Feng, G.L., Wu, Q.B. & Wu, J.J. 2007. Analyses of temperature fields under the embankment with crushed-rock structures along the Qinghai-Tibet Railway. *Cold Regions Science and Technology*: doi:10.1016/j.coldregions.2007.08.001.
- Nelson, F.E., Anisimov, O.A. & Shiklomanov, N.I. 2001. Subsidence risk from thawing permafrost. *Nature* 410: 889-890.
- Smith, S.L. & Burgess, M.M. 1999. Mapping the sensitivity of Canadian permafrost to climate warming, in Interaction between Cryosphere, Climate and Greenhouse Gases. *Proceeding of the IUGG-99 Symposium HS2, Birmingham*, IAHS Publ. 256: 71-80.
- Wu, Q.B., Cheng, G.D. & Ma, W. 2004. The impact of climate warming on Qinghai-Tibetan Railroad. *Science in China, Series D* 47(Supp. I): 122-130.
- Wu, Q.B., Dong, X.F. & Liu, Y.Z. 2005a. Responses of permafrost on the Qinghai-Tibet Plateau to climate change and engineering action. *Journal of Glaciology and Geocryology* 27(1):50-54. (In Chinese with English abstract).
- Wu, Q.B., Zhao, S.Y., Ma, W., Liu, Y.Z. & Zhang, L.X. 2005b. Monitoring and analysis of cooling effect of block-stone embankment for Qinghai-Tibet Railway. *Chinese Journal of Geotechnical Engineering* 27(12): 1386-1390.
- Wu, Q.B., Cheng, G.D., Ma, W., Niu, F.J. & Sun, Z.Z. 2006. Technical approaches on ensuring permafrost thermal stability for Qinghai-Xizang Railroad construction. *Geomechanics and Geoengineering*, 1(2): 119-128.

Freezing/Thawing Index Variations During the Last 40 Years Over the Tibet Plateau

Tonghua Wu, Lin Zhao, Shuxun Li, Changwei Xie, Qiangqiang Pang, Wengang Zhang
Cryosphere Research Station on the Qinghai-Tibet Plateau, Cold and Arid Regions Environmental and Engineering Research Institute, Chinese Academy of Sciences

Abstract

This paper presents the freezing/thawing index variation over the Tibet Plateau based on the analysis of the mean monthly air temperature and ground surface temperature data from 101 meteorological stations during the period of 1961 to 2000. The statistical results showed that the mean annual air and ground surface freezing indices equal 959 and 780 degree-days, respectively, and that the mean annual air and ground surface thawing indices equal 2494 and 3532 degree-days, respectively. The multivariate regression analysis results indicated there is a high correlation between the freezing/thawing index and the latitude and elevation on the plateau. On a decadal scale, the annual air freezing indices indicated a decrease of 146 degree-days during the last four decades. As to the annual ground surface freezing indices, the values indicated a decrease of 95 degree-days. Moreover, the annual air thawing index displayed an increase of 209 degree-days, and the annual ground surface thawing index also displayed an increase of 150 degree-days since 1961. The decrease of freezing index and the increase of thawing index may be responsible for the permafrost degradation in recent years on the plateau.

Keywords: freezing index; permafrost; thawing index; Tibet Plateau.

Introduction

In permafrost regions, the annual air and ground freezing and thawing indices are of great significance in predicting and mapping permafrost distribution (Nelson & Outcalt 1987) and active layer thickness (Nelson et al. 1997, Shiklomanov & Nelson 2002, Zhang et al. 2005). Both of the indices are also important parameters for engineering design in cold regions (Steurer 1996). Generally, the annual freezing and thawing indices are defined as the cumulative number of degree-days below and above 0°C for a year (Permafrost Subcommittee 1988). Among the four main types of freezing and thawing indices which have been used, the annual freezing and thawing indices may be representative of the freezing and thawing climatology (Legates & Willmott 1990). A recent study also demonstrated the validity of approaching the

freezing/thawing index by means of calculations of mean monthly air temperature data, which is originally defined based on daily observations (Frauenfeld et al. 2007).

This paper aims to provide the variations of annual air and ground surface freezing/thawing indices from 1961 to 2000 on the Tibet Plateau. The estimation of the annual freezing/thawing index would contribute to an understanding of climate change and variations in ground thermal regime on the plateau.

Data and Methods

We collected the mean monthly air and ground surface temperature data at 101 meteorological stations from 1961 to 2000 on the Tibet Plateau (Fig. 1). The air temperature is based on the observations at 1.5 m above the ground, and the

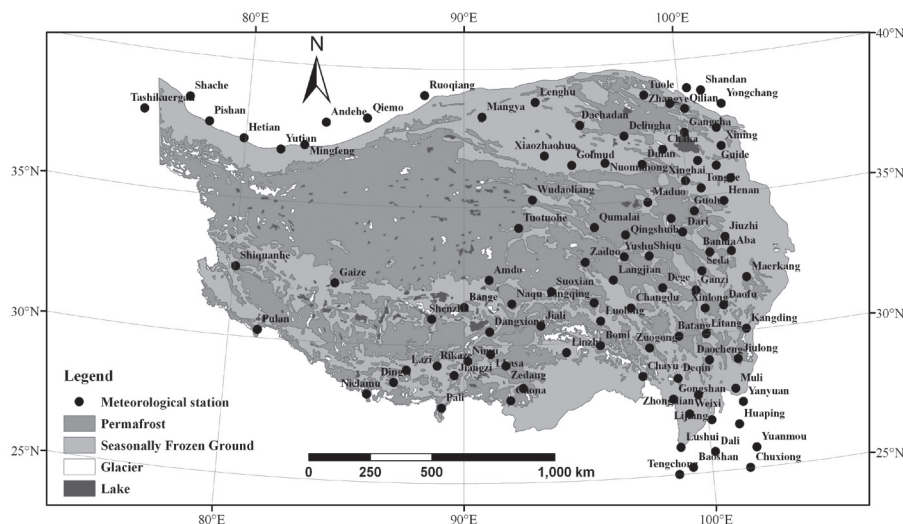


Figure 1. Permafrost distribution and the locations of meteorological stations on the Qinghai-Tibet Plateau.

ground surface temperature is based on the measurements at 0 cm of earth surface.

The annual air and ground surface freezing indices are calculated as the following equations (Frauenfeld et al. 2007). The duration in estimating the freezing index includes those months when temperatures were below 0°C degree:

$$FI_a = \sum_{i=1}^{M_F} |\bar{T}_{ai}| \cdot D_i, \bar{T}_{ai} < 0^\circ C \quad (1)$$

$$FI_s = \sum_{i=1}^{M_F} |\bar{T}_{si}| \cdot D_i, \bar{T}_{si} < 0^\circ C \quad (2)$$

where FI_a and FI_s are the annual air and ground surface freezing indices; M_F are those months when the mean monthly temperature is below 0°C; D is the number of days in the month of M_F .

Similarly, the annual air and ground surface thawing indices are calculated as the following equations. The duration in estimating the thawing index includes those months when temperatures were above 0°C degree:

$$TI_a = \sum_{i=1}^{M_T} \bar{T}_{ai} \cdot D_i, \bar{T}_{ai} > 0^\circ C \quad (3)$$

$$TI_s = \sum_{i=1}^{M_T} \bar{T}_{si} \cdot D_i, \bar{T}_{si} > 0^\circ C \quad (4)$$

where TI_a and TI_s are the annual air and ground surface freezing indices; M_T are those months when the mean monthly temperature is above 0°C; D is the number of days in the month of M_T .

The FI_a , FI_s , TI_a , and TI_s are calculated for each year from 1961 to 2000. Then the decadal values of those indices are obtained for avoiding great interannual fluctuations (Thompson 1963, Shur & Slavin-Borovski 1993).

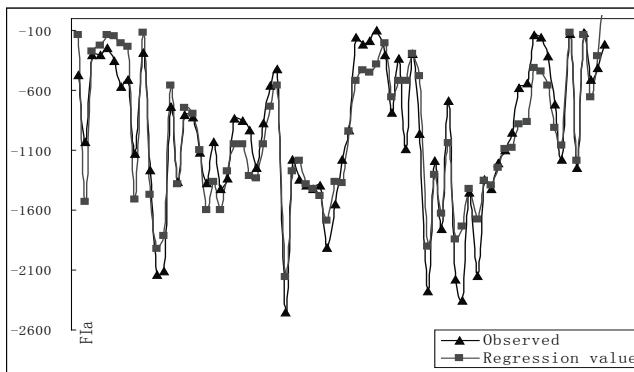


Figure 2. Regression analyses for the air freezing indices.

Table 1. Analysis of variance for the regression model of air freezing indices.

Source	Sum of squares	df	Mean square	F	Sig.
Regression	23443987.090	2	11721993.545	187.842	0.000(a)
Residual	4493051.921	72	62403.499		
Total	27937039.012	74			

Results

Variations of air and ground surface freezing indices

Among the 101 meteorological stations, there are 26 stations where monthly mean air temperature and monthly mean ground surface temperature are above 0°C. Therefore, the remaining 75 stations are selected for the calculation of freezing index on the plateau. The statistical results indicated that the mean annual air freezing index during the 40 years was 959 degree-days and that the mean annual ground surface freezing index was 780 degree-days. The maximum value of air freezing index occurred at Wudaoliang station, which is located at the hinterland of the plateau, equaling 2450 degree-days. The maximum value of ground surface freezing index also occurred at Wudaoliang station, which equals 1792 degree-days. The minimum value of air freezing index occurred at Lhasa station, which is located in the south of the plateau, equaling 97 degree-days. The minimum value of ground surface freezing index occurred at Zhongdian station, which is located in the southeast of the plateau, equaling 42 degree-days.

The calculated annual air and ground surface freezing indices showed a close correlation with the altitude (h) and the latitude (φ). As shown in Figures 2 and 3, validation with FI_a and FI_s from field data shows good correlation ($R_{af}=0.916$ and $R_{sf}=0.943$). We used the multivariate regression method to determine the function between air and ground surface freezing indices and the latitude and elevation. The analyses of variance indicated a high significance level (Tables 1 and 2).

$$FI_a = 8029.077 - 192.541\varphi - 0.738h \quad (5)$$

$$FI_s = 6513.638 - 162.230\varphi - 0.537h \quad (6)$$

Table 3 showed the interdecadal variations of air and ground surface freezing indices (degree-days) at nine stations

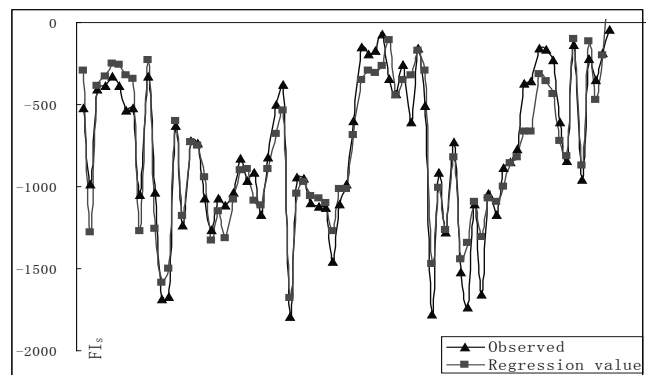


Figure 3. Regression analyses for the ground surface freezing indices.

Table 2. Analysis of variance for the regression model of ground surface freezing indices.

Source	Sum of squares	df	Mean square	F	Sig.
Regression	14206138.964	2	7103069.482	287.283	0.000(a)
Residual	1780197.600	72	24724.967		
Total	15986336.564	74			

Table 3. Interdecadal variations of air and ground surface freezing indices (degree-day) at nine selected stations.

Station name	F _{af} 60	F _{af} 70	F _{af} 80	F _{af} 90	F _{af} mean	F _{sf} 60	F _{sf} 70	F _{sf} 80	F _{sf} 90	F _{sf} mean
Golmud	1120	809	709	707	836	999	809	742	763	829
Wudaoliang	2562	2406	2443	2389	2450	1912	1732	1853	1670	1792
Amdo	2069	1851	1831	1896	1912	1712	1388	1328	1389	1454
Naqu	1779	1514	1517	1382	1548	1265	1063	1115	997	1110
Tuotuohe	2316	2179	2374	2238	2277	1841	1702	1882	1695	1780
Zaduo	1228	1198	1151	1156	1183	987	922	877	882	917
Qumalai	1842	1729	1781	1689	1760	1335	1298	1302	1175	1277
Maduo	2274	2252	2155	2050	2183	1657	1619	1330	1470	1519
Qingshuihe	2383	2369	2333	2331	2354	1737	1788	1674	1740	1735

located in permafrost regions where there is seasonally frozen ground. The data showed an obvious decrease in the air and ground surface freezing indices since the 1960s.

On a decadal scale, the average values of air freezing index in the 1960s, 1970s, 1980s, and 1990s are 1047, 960, 928, and 901 degree-days, respectively. As a signal of climatic warming on the plateau, the air freezing index on the plateau indicated a decrease of 146 degree-days during the past 40 years. While the average values of ground surface freezing index in the 1960s, 1970s, 1980s, and 1990s are 838, 785, 753, and 743 degree-days, respectively. The ground surface freezing index on the plateau also showed a decrease of 95 degree-days since 1961. This conclusion coincides with the general opinion of greater warming in winter than in summer on the plateau during the last 40 years.

Variations of air and ground surface thawing indices

We also excluded 9 stations where air temperature and ground surface temperature showed great difference with the other stations. Most of them are located in the southeast of the plateau with a low elevation and high monthly temperature. The remaining 92 stations were selected to calculate the thawing indexes on the plateau. The averaged air thawing index on the plateau is estimated at 2494 degree-days, and the averaged ground surface thawing index is estimated at 3532 degree-days. The minimum value of air and ground surface thawing indices also occurred at the hinterland of the plateau, while the maximum value occurred in the northwest of the plateau, where the West Kunlun Mountain range is situated.

Similar to the freezing index, the calculated annual air and ground surface thawing indices also showed close correlation with the altitude (h) and the latitude (ϕ). As shown in Figures 4 and 5, Validation with TI_a and TI_s from observed data also shows good correlation ($R_{at}=0.961$ and $R_{st}=0.937$). We also used the multivariate regression method to determine the function between air and ground surface thawing indices and latitude and elevation. The analyses of variance indicated a high significance level (Tables 4 and 5).

$$TI_a = 11971.781 - 157.441\phi - 1.370h \tag{7}$$

$$TI_s = 13130.046 - 161.442\phi - 1.366h \tag{8}$$

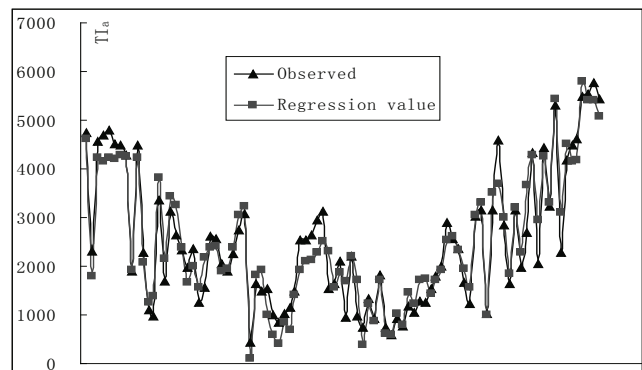


Figure 4. Regression analyses for the air thawing indices.

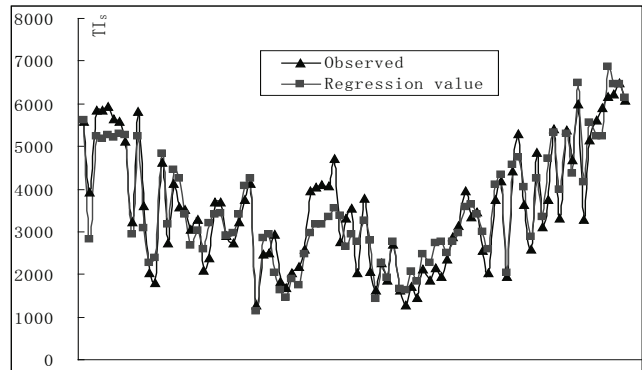


Figure 5. Regression analyses for the ground surface thawing indices.

Table 4. Analysis of variance for the regression model of air thawing indices.

Source	Sum of squares	df	Mean square	F	Sig.
Regression	160157223.662	2	80078611.831	538.553	0.000(a)
Residual	13233611.063	89	148692.259		
Total	173390834.725	91			

Table 5. Analysis of variance for the regression model of ground surface thawing indices.

Source	Sum of squares	df	Mean square	F	Sig.
Regression	160228386.337	2	80114193.168	320.168	0.000(a)
Residual	22270071.547	89	250225.523		
Total	182498457.884	91			

Table 6. Interdecadal variations of air and ground surface thawing indices (degree-day) at nine selected stations.

Station name	F _{at} 60	F _{at} 70	F _{at} 80	F _{at} 90	F _{at} mean	F _{st} 60	F _{st} 70	F _{st} 80	F _{st} 90	F _{st} mean
Golmud	4417	4500	4503	4609	4507	5563	5666	5594	5784	5652
Wudaoliang	934	940	944	1041	965	1764	1790	1748	1951	1813
Amdo	1883	1950	1953	2082	1967	2866	2949	3085	3304	3051
Naqu	2319	2345	2321	2500	2371	3277	3219	3188	3428	3278
Tuotuohe	1476	1464	1512	1666	1530	2942	2777	2852	3196	2942
Zaduo	1018	905	1002	1063	997	1796	1771	1800	2001	1842
Qumalai	821	803	832	888	836	1578	1663	1649	1862	1688
Maduo	1082	1106	1171	1217	1144	2093	2184	2176	2286	2185
Qingshuihe	1423	1473	1507	1566	1492	2439	2443	2701	2793	2594

Table 6 implies the interdecadal variations of air and ground surface thawing indices (degree-days) at nine stations. The data show an obvious increase in the air and ground surface thawing indices since the 1960s.

On a decadal scale, the average values of air thawing index in the 1960s, 1970s, 1980s, and 1990s are 2433, 2472, 2488, 2584 degree-days, respectively, which indicate an increase of 209 degree-days in the last 40 years. Similarly, the average values of ground surface thawing index are much higher than the air thawing index. The ground surface thawing indices in the 1960s, 1970s, 1980s, and 1990s are 3448, 3485, 3539, 3657 degree-days, respectively, which show an increase of 150 degree-days. Compared with the variations of air and ground surface freezing indices, the amplitude of changes in thawing index on the plateau was much less than that of freezing index.

Changes of permafrost and active-layer thickness

The observation results of borehole temperature data from sporadic permafrost regions and discontinuous permafrost regions both indicated that permafrost on the Tibet Plateau has undergone significant degradation during the past 40 years (Cheng & Wu 2007). From the 1970s to the 1990s, the ground temperature in sporadic permafrost regions and seasonally frozen ground regions has risen by 0.3–0.5°C, while the permafrost temperature in discontinuous permafrost regions has risen by 0.1–0.3°C. The permafrost where mean annual ground temperature was 0––0.5°C has been accelerating in warming and thinning (Jin et al. 2000, Wang et al. 2000).

In the recent 10 years, the thickness of the active-layer on the Tibet Plateau showed an increasing tendency, with increasing velocity approximating 3.1 cm/yr in discontinuous permafrost regions and 8.4 cm/yr in sporadic permafrost regions (Wu et al. 2005).

To a great extent, the recent changes of permafrost and active-layer thickness could attribute to the significant decrease in the air and ground surface freezing indices and great increase in the air and ground surface thawing indices.

Conclusions and Discussion

We calculated the freezing and thawing indices based on monthly air temperature and ground surface temperature data on the Tibet Plateau, provided that the freezing and thawing indices can be reliably calculated based on monthly data. The calculation results showed that the 1961–2000 air and ground surface freezing indices which represent the cold-season temperature climatology displayed a drastic decrease, while the thawing indices which are reminiscent of the warm-season temperature climatology showed a significant increase on a decadal scale. Meanwhile, the freezing and thawing indices on the plateau both illustrated close correlation with latitude and altitude. The analysis provided a basis for estimating the temporal and spatial variations of permafrost distribution and active-layer thickness on the plateau.

All of the calculations conducted above are based on the validity of using monthly air temperature data and ground surface temperature data to obtain freezing and thawing indices. Although the idea of utilizing monthly rather than daily temperature values to calculate the freezing and thawing indices is already an acceptable method in estimating degree-days variations (Nelson & Outcalt 1987, Zhang et al. 1996, Brown et al. 2000), the precision of using monthly data is still not assessed on the plateau until now. This would be the focus of our following work.

Acknowledgments

We are grateful to the Cryosphere Research Station on the Qinghai-Tibet Plateau, Chinese Academy of Sciences for obtaining the monthly data. This study was supported by the 973 Key Projects for Basic Research (No. 2007CB411506 and No. 2007CB411505) and the Chinese National Science Foundation (No. 40471026 and No. 40701029).

References

- Brown, J., Hinkel, K.M. & Nelson, F.E. 2000. The Circumpolar Active Layer Monitoring (CALM) program: Research designs and initial results. *Polar Geography* 24(3): 163–258.

- Cheng, G. & Wu, T. 2007. Responses of permafrost to climate change and their environmental significance, Qinghai-Tibet Plateau. *Journal of Geophysical Research-Earth Surface* 112: F02S03, doi:10.1029/2006JF000631.
- Frauenfeld, O.W., Zhang T. & McCreight, J.L. 2007. Northern Hemisphere freezing/thawing index variations over the twentieth century. *International Journal of Climatology* 27: 47-63.
- Jin, H., Cheng, G. & Zhu, Y. 2000. Chinese geocryology at the turn of the twentieth century. *Permafrost Periglacial Processes* 11(1): 23-33.
- Nelson, F.E. & Outcalt, S.I. 1987. A computational method for prediction and regionalization of permafrost. *Arctic and Alpine Research* 19(3): 279-288.
- Nelson, F.E., Shiklomanov, N.I., Mueller, G.R., Hinkel, K.M., Walker, D.A. & Bockheim, J.G. 1997. Estimating active-layer thickness over a large region: Kuparuk River basin, Alaska, U.S.A. *Arctic and Alpine Research* 29(4): 367-378.
- Legates, D.R. & Willmott, C.J., 1990. Mean seasonal and spatial variability in global surface air temperature. *Theoretical and Applied Climatology* 41: 11-21.
- Permafrost Subcommittee 1988. *Glossary of Permafrost and Related Ground-Ice Terms*. Associate Committee on Geotechnical Research, National Research Council of Canada.
- Shiklomanov, N.I. & Nelson, F.E. 2002. Active-layer mapping at regional scales: a 13-year spatial time series for the Kuparuk Region, North-Central Alaska. *Permafrost and Periglacial Processes* 13: 219-230.
- Shur, Y.L. & Slavin-Borovski, V.B. 1993. N-factor maps of Russian permafrost region. *Proceedings of the Sixth International Conference on Permafrost, Vol. 2, Beijing, China, July 5-9, 1993: 564-568*. Wushan, Guangzhou, China: South China University of Technology Press.
- Steurer, P.M. 1996. Comparison of probability distributions used in estimating the 100-year return period of the air-freezing index. *Journal of Cold Regions Engineering* 10: 23-35.
- Thompson, H.A. 1963. Freezing and thawing indices in Northern Canada. *Proceedings of the First Canadian Conference on Permafrost*. NRC of Canada, Ottawa: 18-36.
- Wang, S., Jin, H. & Li, S. 2000. Permafrost degradation on the Qinghai-Tibet Plateau and its environmental impacts. *Permafrost and Periglacial Processes* 11(1): 43- 53.
- Wu, Q., Lu, Z. & Liu, Y. 2005. Permafrost monitoring and its recent changes in Qinghai-Tibet Plateau. *Advances in Climate Change Research* 1(1): 26-28.
- Zhang, T., Osterkamp, T.E. & Stamnes, K. 1996. Some characteristics of the climate in northern Alaska, U.S.A. *Arctic and Alpine Research* 28(4): 509-518.
- Zhang, T., Frauenfeld, O.W., Serreze, M.C., Etringer, A.J., Oelke, C., McCreight, J.L., Barry, R.G., Gilichinsky, D., Yang, D., Ye, H., Feng, L. & Chudinova, S. 2005. Spatial and temporal variability in active layer thickness over the Russian arctic drainage basin. *Journal of Geophysical Research-Atmospheres* 110: D16101, doi:10.1029/2004JD005642.

Hydrological Dynamics of the Active Layer in the Permafrost Region, Qinghai-Tibetan Plateau

Changwei Xie, Lin Zhao, Yongjian Ding, Tonghua Wu

Cold and Arid Regions Environmental and Engineering Research Institute, Cryosphere Research Station on the Qinghai-Tibet plateau, Chinese Academy of Sciences

Abstract

Due to recent climate warming, the heat energy absorbed by the ground surface of the permafrost in the Qinghai-Tibetan plateau region has increased, thereby, leading to a continuous rise in ground temperature and the persistent increase in the thickness of the active layer. In recent years, with an increase in the thickness of the active layer, a large amount of shallow water diffused downward and thus resulted in the migration of water, enriching deeper horizons. Water infiltration carried much heat and increased heat storage in the deep subsoil; hence the freezing time was delayed. The positive feedback relation between the increase in active layer thickness and the water-heat transfer toward the deep soil exerted a profound influence on surface water resources.

Keywords: active layer; changes; hydrological effects; permafrost; Qinghai-Tibet Plateau; water-heat coupling.

Introduction

Traditionally, the active layer has been defined as the surficial layer above permafrost which thaws during summer (Burn 1998). The active layer serves as an energy-water exchange passage between the permafrost and the outer atmosphere. It is also a most sensitive zone for the response of permafrost to climate change. The Qinghai-Tibetan plateau (QTP) is a concentrated, distributed region of continuous permafrost at the world's highest altitude. Under the background of recent global warming, the active layer of permafrost has been affected by a series of changes, such as increase in thickness, vegetation degradation, and swamp drainage. These changes exert a profound influence on the regional ecosystems, hydrological environment, and even engineering construction (Ding et al. 2000). The increase in the thickness of the active layer of permafrost on the QTP has been verified by the data observed in the past few decades, and an increasing trend in active-layer thickness has been even more obvious in recent years. Such a trend is roughly consistent with the changes of the permafrost in other arctic regions (Osterkamp & Romanovsky 1997, Tarnocai et al. 2004). Studies show that in a 20-year period from the 1970s to the 1990s the active layer thickness has increased by 80–100 cm in the Chumar River valley (Tong et al. 1996). It has also been demonstrated that the increase in active-layer thickness was significantly larger in the high-temperature permafrost region than in the low-temperature permafrost region; the mean thickening rate of active layer in the $<-1.5^{\circ}\text{C}$ low temperature region was 3.1 cm/yr, while that in the $>-1.5^{\circ}\text{C}$ high-temperature region was 8.3 cm/yr, and the largest thickening rate was 12.6 cm/yr (Wu et al. 2005). Existing studies and observation data show that the rise in the ground temperature of permafrost and the increase in the thickness of the active layer are a basic trend explaining the variations in permafrost in the QTP at present. Permafrost as an impermeable stratum adjusts the regional hydrological

processes mainly through the dynamic changes of the active layer. The increase trend of active-layer thickness will inevitably lead to the lowering of the freeze-thaw surface and water drawdown in the active layer, which enhances precipitation infiltration into deep subsoil, reduces surface runoff, and increases subsurface flow (Yang, et al. 2000).

Several questions need to be answered about this deepening. For example, what is the internal mechanism for the hydrological process variations caused by the thickness changes of the active layer under the present global warming background? What are the influences of the increase in active layer thickness and the rise in ground temperature on water-heat transfer processes? What is the feedback mechanism for the water-heat coupling process to the dynamic changes of the active layer? In response to the water-heat changes in the active layer of permafrost in QTP region, since the 1970s the cryosphere research station on the Qinghai-Tibetan plateau, Chinese Academy of Sciences, has selected more than ten observation sites. They are distributed within a 5 km section on both sides of the Qinghai-Tibetan Highway, from the northern limit of the permafrost-Xidatan to the southern limit of permafrost-Liangdaohe (Table 1). Of these, six sites have a continuous record of 8 years and 4 sites have an observation history of two years.

Temperature of the active layer was measured by a Pt resistance probe with an observation error of $\pm 0.1^{\circ}\text{C}$. Soil moisture content was measured by TDR probe, with an observation error of $\pm 0.5\%$. The buried depths of the probes were different at different sites, and the maximum buried depth of the probes exceeds by 20 cm the largest active layer depth at the observation site. The data were recorded automatically at one hour intervals by a data logger. This paper attempts to analyze the influences of the increase in active layer thickness, the rise in ground temperature on the water-heat transfer processes, and the impact on the regional hydrological environment.

Table 1. The locations of study sites on the Qinghai-Tibet Plateau.

Serial number	Latitude (N °)	Longitude (E °)	Altitude (m)	Amount of Observation layers	Thickness of active layer in 2006(cm)	Place name	Observation begin time
QT01	35.1449	93.0426	4740	12	155	Kekexili	2005.8
QT02	34.8229	92.9218	4620	10	72	Beiluhe 1	2005.8
QT03	34.8231	92.9219	4620	10	221	Beiluhe 2	2005.8
QT04	33.070	91.9400	5100	10	>300	Tanggula	2005.8
QT05	33.9560	92.3381	4660	10	303	Kaixinlin	2005.8
QT06	33.7717	92.2387	4670	10	250	Tongtianhe	2005.8
QT07	32.5766	91.8593	5133	10	-*	Taoerjiu	2005.8
QT08	35.1226	93.0673	4619	10	-*	Wudaoliang	2005.8
Ch01	34.7290	92.8946	4820	12	165	Fenhuoshan	1998.5
Ch02	35.4332	93.5988	4488	12	260	Suolandajie	1998.5
Ch03	34.4706	92.7270	4620	12	280	Wuli	1998.5
Ch04	31.8180	91.7368	4850	12	115	Liandaohel	1998.5
Ch05	31.8180	91.7368	4808	12	240	Liandaohel2	1998.5
Ch06	35.6212	94.0625	4750	12	145	Konlongshan	1998.5

* apparatus had been destroyed

Water-Heat Changes in Active Layer During the Freeze-Thaw Processes

Ground temperature changes

According to the annual freeze-thaw processes, the annual variations in the active layer can be divided into four stages: summer thawing stage, autumn freezing stage, winter temperature-falling stage, and spring temperature-rising stage (Zhao et al. 2000). In this environment, during the summer thawing stage the interior of the active layer had a positive ground temperature gradient, the ground temperature was significantly higher in the shallow layer than in the deep layer, the active layer and the underlying permafrost were in a heat-absorbing state, and the internal temperature exhibited a rising trend. Generally, several days after the atmospheric temperature reached the annual maximum value, the ground temperature below the depth of 10 cm also reached the annual maximum value. With an increase in active layer depth, the time at which the annual ground temperature in different horizons reached the maximum value was delayed. As the climate turned cold and the ground surface temperature fell below 0°C, the active layer entered the autumn freezing period and the ground temperature gradient became negative. The ground temperature was higher in the deeper layer than in the shallower layer, the active layer started to release heat to the atmosphere, and the ground temperature started to drop. Other studies have shown that both the positive and negative ground temperature gradients in the active layer could be maintained for more than 100 days, while the period of no ground temperature gradient lasts only 10–30 days or so in the autumn freezing process and spring temperature thawing period (Ding et al. 2000). Figure 1 is the pattern of annual ground temperature variations at different depths in the active layer of permafrost at the CN1 observation point on the QTP in 2003. The thickness of the active layer in 2003 was 147 cm.

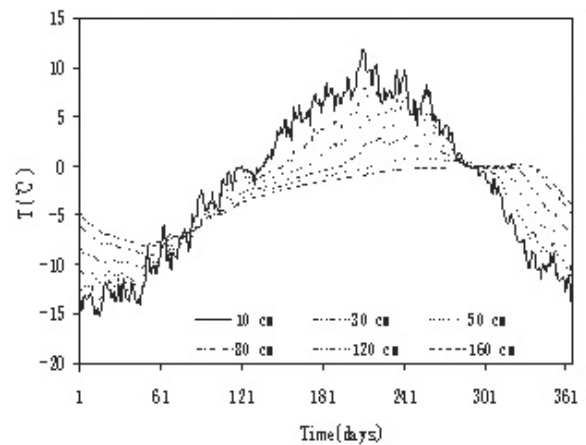


Figure 1. Pattern of annual ground temperature variations at different depths in the active layer of permafrost at CN1 point on the QTP in 2003 (the temperatures at 12 levels were measured and the graph showed the data of 6 levels).

Figure 2 shows the ground temperature isoline in the active layer of permafrost at the CN1 observation point in 1999 and 2006. The observation point is located at the north slope of Mt. Fenghuoshan on the QTP, where continuous permafrost exists. It can be seen that the curves are wide near the 0°C isoline, suggesting that the transformation of the two phases of ice and water during the thawing and freezing course is a slow process, and during the process the soil temperature is prolonged at 0°C. But as the soil is entirely thawed or frozen, the isoline density obviously increases, and the ground temperature variation with time significantly speeds up. It can be seen from the annual variation of the 0°C isoline that about 100 days or more were required for the active layer to thaw entirely, but to freeze-back to the surface only required 10 days or so. The statistical results at different observation sites on the QTP show that the thawing time was far larger

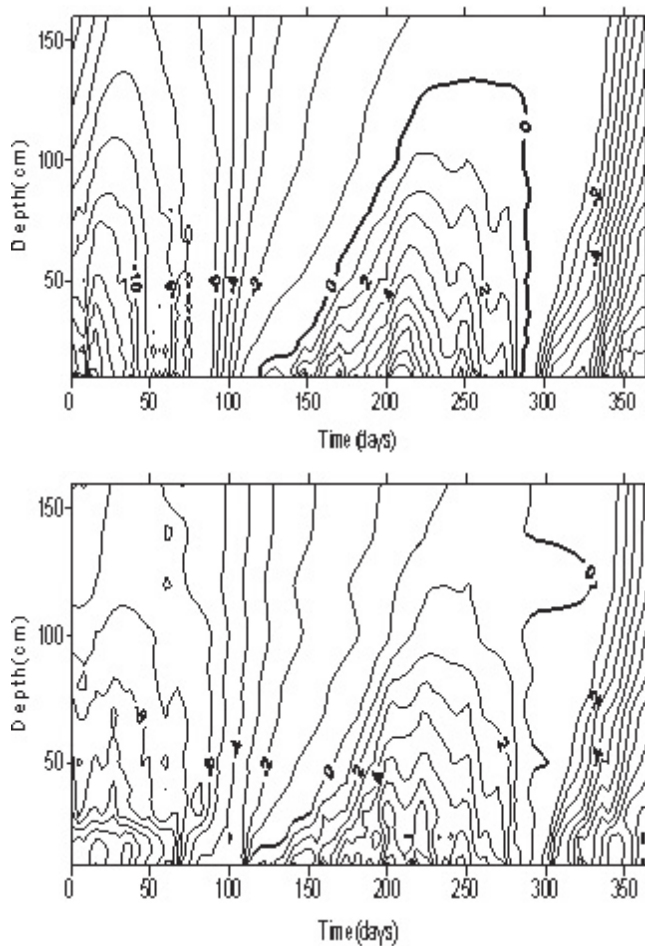


Figure 2. Ground temperature isoline at the different depth in the active layer of permafrost at CN1 observation point on the QTP in 1999 (upper) and 2006 (lower).

than the freezing time, but in some other places, such as in northeastern China, the freezing time of the active layer is approximately as long as the thawing time (Zhou et al. 2000).

Water change during the thawing process

As the frozen soils started to thaw, the solid water changed into liquid water and was redistributed in the active layer. In the meantime, activities of precipitation and evaporation, etc., in the active layer took place. Due to the limitations of the equipment, the soil water study in this paper was confined to the changes in liquid water; solid water cannot be discussed. Figure 3 shows the soil water isoline at CN2 in 2000 and 2006. It can be seen that the density of isolines during the soil freezing or thawing periods is very high. Water content changes rapidly near the thawing or freezing front. During the thawing period the soil water content increases rapidly, while in the freezing period it decreases quickly. The correlation statistics of soil temperature and water data at different depths and different observation points show that as the ground temperature drops below 0°C, soil water gradually increases, with increasing ground temperature, and reaches a maximum value at a ground temperature of 0°C.

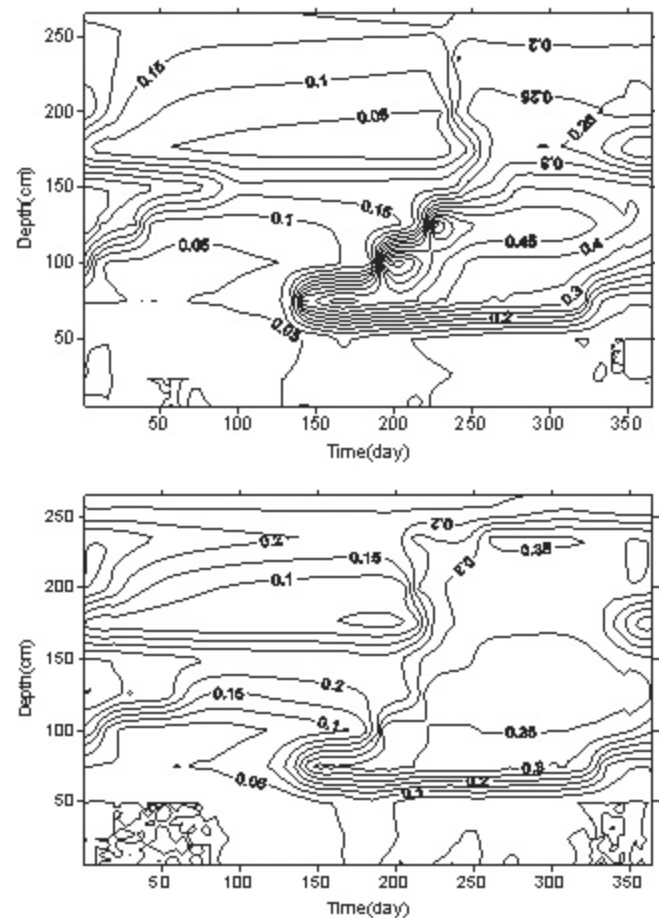


Figure 3. Soil water isoline at different depth in the active layer of permafrost at CN2 observation point on QTP in 2000 (upper) and 2006 (lower).

As the ground temperature exceeded 0°C, soil water tended to decrease with increasing ground temperatures (Fig. 4). It can be seen from Figure 4 that the water contents at different horizons in the active layer all reached a maximum value at a ground temperature of 0°C; as the soil temperature exceeded 0°C, soil water tended to decrease, and such a trend was quite obvious in the shallow soil layer.

This phenomenon can be explained as follows: first, instrumentation can only measure liquid water as the frozen solid water gradually melts and the ground temperature gradually approaches 0°C, the percentage of liquid water continuously increases until it is entirely changed into liquid water. The changes in water content in 0°C soil are mainly caused by this process. Second, it results from the water-heat coupling action during the thaw-freeze period of the active layer. The simultaneous transfer process of water and heat in the active layer is called the water-heat coupling process. In this process, material (water) and energy are transferring simultaneously (Zhao et al. 2000). The temperature gradient is an important factor controlling the soil water transfer.

As soil is entirely thawed, gravity promotes water infiltration; when the ground temperature gradually rises to form a ground temperature gradient, water will migrate

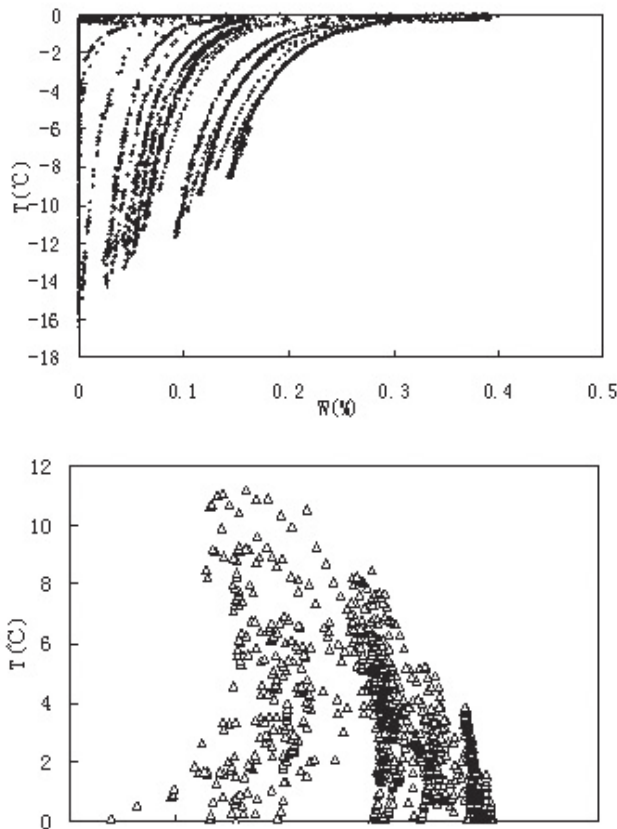


Figure 4. The scatter diagram showing the change trend of water content when soil temperature is below 0°C (upper) and above 0°C (lower) in the active layer of permafrost on QTP (CN1 observation point in 1999).

to the ground surface; this results in water concentration at the freezing front. Soil water migration in any form is accompanied by heat transfer. This can be clearly seen from the isoline changes in Figures 2 and 3.

Water-Heat Changes and Their Hydrological Effects in Recent Years

As the thickness of the active layer increased, the temperature in it also continuously rose. Taking the CN1 site as an example, the temperature in the active layer at this area has been recorded since May 1998. The statistics of annual mean temperature at different horizons show that the temperature at various horizons rose at different rates over the last 10 years (Fig. 5). The ground temperature at the bottom of the active layer exhibited a steady temperature-rising trend, while that of the shallow layer was more variable.

As viewed from the fluctuated variations of ground temperature at different horizons, in September the rising trend of ground temperature close to the permafrost table could not be affected by the annual fluctuation changes of air temperature, while the variations in the upper active layer apparently coincided with the fluctuation changes of annual mean air temperature. Of course, viewed from the annual mean value of ground temperature, the ground temperature

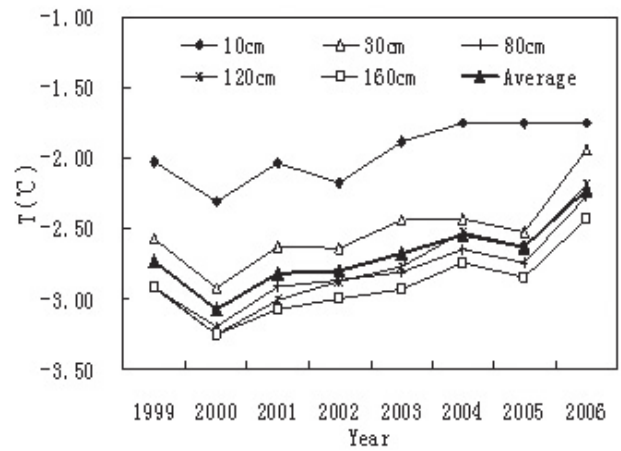


Figure 5. Change of the ground temperatures at different levels during 1999–2006 in CN1 observation site (the temperatures at 12 levels were measured and the graph showed the data of 5 levels and the average value of 12 levels).

at the bottom of the active layer could be affected by annual air temperature fluctuations.

In December, the general trend of the ground temperature fluctuation changes in the deep layer was consistent with that in the shallow layer. The main reason for this is that the downward transfer of surface heat is a slow process. When the thawing reaches a maximum value in September, the temperature at the lowest part of the active layer still changes. Statistical data reveal that the mean ground temperature in the active layer at the CN1 observation point increased by 0.4°C since 1998, the rising amplitude of ground temperature was significantly higher in the deep layer than in the shallow layer (Fig. 5). The largest rise in temperature occurred at a depth of 120 cm. The freezing time at this depth also significantly changed. It can be seen from Figure 2 that soil at a 120 cm depth froze in the middle of September 1999, and the duration of ground temperature higher than 0°C was 71 days. In 2006, this duration increased to 124 days, while the freezing period was delayed to the end of November, and the thickness of the active layer exceeded the initial observed depth.

Measured data indicate that the 120 cm depth was the horizon with the highest moisture content, and it also had the highest heat storage. Climate warming leads to an increase in energy input in the active layer, but energy storage delays the freezing time of the region with the highest water content. If the annually received energy is persistently greater than the released energy during the freezing period, the winter freezing front cannot reach the bottom of the active layer and therefore a discontinuous layer can be formed in the active layer. The presence of the discontinuous layer will further promote the downward migration of water and thus change the spatial distribution pattern of water in a permafrost region. This is one of the most striking feedbacks of the water-heat coupling process.

Analysis on the vertical profile in the active layer in recent years shows that the water distribution in the active layer has changed and is triggered by a rise in ground temperature.

The downward transfer of originally stored water in the dry and shallow soil layer caused the downward migration of the water-enriching zone. A comparison of water isolines of 2000 and 2006 at CN2 point is shown in Figure 3. It can be seen that in 2000 the soil water-enriching zone was located at a depth of 100–150 cm, and the maximum water content was 60% or so (volumetric ratio). As the depth of the active layer increased from 235 cm in 2000 to 270 cm in 2006, the soil water content in the 100–150 cm layer decreased below 40%, while the water content in the 200–250 cm soil layer, which originally had a lower water content, greatly increased, thereby forming two soil water-enriched zones. As a rule, the increase in active-layer thickness led to soil water migration from the shallower layer to the deeper layer, and the downward migration of water carried more heat to the bottom of the active layer. Therefore the freezing time of the bottom of the active layer was delayed and the thickness of the active layer further increased.

Conclusion

It can be seen from the above analysis that under the background of climate warming the increase in active-layer thickness and the rise in ground temperature are favorable to downward migration of soil water. In turn, the water heat coupling action causes a positive feedback to active-layer changes. The intensification of the downward migration trend of soil water will inevitably lead to a decrease in surface runoff yield and an increase in regional groundwater storage. The decrease in surface soil water content strengthens the infiltration of precipitation; on the other hand it promotes soil water loss to evaporation. In one word, the rise in ground temperature in the active layer and the increase in active-layer thickness are unfavorable to the storage of surface water resources in the permafrost, and they likely have a negative effect on regional runoff yield. Of course, this final point needs further study.

Acknowledgments

We would like to express our gratitude to the Cryosphere Research Station on the Qinghai-Tibet Plateau, Chinese Academy of Sciences, for the observation data collection and logistic support. This work was supported by a grant from the Major State Basic Research Development Program of China (973 Program, No.2007CB411506) and the Chinese National Fundamental Research Program (No. 40701029).

References

- Burn, C.R. 1998. The Active Layer: Two contrasting definitions. *Permafrost Periglac. Process.* Vol 9: 411-416.
- Charles T., Nixon, F.M. & Kutny, L. 2004 Circumpolar-Active-Layer-Monitoring (CALM) sites in the Mackenzie Valley, Northwestern Canada. *Permafrost and Periglac. Process.* 15: 141–153.
- Ding, Y.J., Ye, B.S., Liu, S.Y. et al. 2000. Macro-scale monitoring study of permafrost hydrology in Tibetan Plateau. *Bulletin of Science* Vol. 45(2): 208-214.
- Osterkamp, T.E. & Romanovsky, V.E. 1997. Freezing of the active layer on the coastal plain of the Alaskan Arctic. *Permafrost Periglac. Process* Vol. 8: 23-44.
- Perfect, E. & Williams, P.J. 1980. Thermally induced water migration in frozen soils. *Cold Region Science and Technology* Vol. 9(3): 101-109.
- Tong, C.J. & Wu, Q.B. 1996. The effect of climate warming on the Qinghai-Tibet Highway. *Cold Regions Science and Technology* Vol. 24: 101~10.
- Wu, Q.B., Lu, Z.J. & Liu, Y.Z. 2005. Permafrost monitoring and its recent changes in Qinghai-Tibet Plateau. *Advances in Climate Change Research* Vol. 1(1): 26-28.
- Yang, Z.N., Liu, X.R., Zeng, Q.Z. et al. 2000. *Frozen Soil Hydrology in China*. Beijing: Science Press, 90-12.
- Zhao, L, Cheng, G.D., Li, S.X. et al. 2000. Thawing and freezing processes of active layer in Wudaoliang Region of Tibetan Plateau. *Chinese Science Bulletin* Vol. 45(23): 2181-218
- Zhou, Y.W., Guo, D.X., Qiu, G.Q. et al. 2000. *Geocryology in China*. Beijing: Science Press: 37-41.

Variation of Atmospheric Methane Over the Permafrost Regions from Satellite Observation During 2003 to 2007

Xiaozhen Xiong

Perot Systems Government Services, Fairfax, Virginia; and Satellite Meteorology & Climatology Division, Center for Satellite Applications and Research, National Environmental Satellite, Data, and Information Service, NOAA, USA

Chris Barnet

Satellite Meteorology & Climatology Division, Center for Satellite Applications and Research, National Environmental Satellite, Data, and Information Service, NOAA, USA

Eric Maddy, Xingpin Liu

Perot Systems Government Services, Fairfax, Virginia; and Satellite Meteorology & Climatology Division, Center for Satellite Applications and Research, National Environmental Satellite, Data, and Information Service, NOAA, USA

Mitch Goldberg

Satellite Meteorology & Climatology Division, Center for Satellite Applications and Research, National Environmental Satellite, Data, and Information Service, NOAA, USA

Abstract

Thawing permafrost as a major source of climate feedback could accelerate climate change by releasing methane (CH₄) into the atmosphere. However, current estimation of CH₄ emissions from thawing permafrost or northern wetlands has large uncertainty. The Atmospheric Infrared Sounder (AIRS) on EOS/Aqua platform provides a measurement of global CH₄ in the mid-upper troposphere. Based on more than four years' AIRS data in high northern hemisphere, it is found (1) a significant CH₄ increase when the surface temperature becomes above the freezing point; (2) a decreasing trend of -1.3 ppbv/year in Canada-Alaska and -3.9 ppbv/year in Siberia from August 2003 to 2007; (3) a lower CH₄ in 2005; and (4) a possibly large unknown source in Siberia between Jan to March. This study demonstrates that a long-term monitoring of CH₄ using AIRS and other satellites will enable us to better study the CH₄ trend and its relation with thawing permafrost.

Keywords: AIRS; High Northern Hemisphere; methane; northern wetlands; thawing permafrost.

Introduction

As one of the most important greenhouse gas next to carbon dioxide (CO₂), CH₄ is about 20 times more powerful at warming the atmosphere than CO₂ by weight, and plays an important role in atmospheric chemistry. CH₄ is highly variable in the northern hemisphere, and its concentration over the globe has been observed to rise dramatically since the preindustrial era (Dlugokencky et al. 1995). However, the increase rate of CH₄ varies significantly, for example, an anomalous increase of the growth rate of CH₄ was observed in 1998, and the anomalous increase of the growth rate of CH₄ was partially attributed to wetland emission (Dlugokencky et al. 2001). As the largest single source wetlands emission contributes CH₄ around 100–230 Tg/yr (IPCC, 2001), which represents ~20–45% of total methane emissions (~500 Tg/yr). However, the emission of CH₄ from wetlands is dominated by climate, and as demonstrated from model simulations, ±1°C changes in temperature could lead to ±20% changes in the CH₄ emission from wetlands, and ±20% changes in the precipitation alter CH₄ emission by about ±8% (Walter et al. 2001).

The permafrost thaw beneath wetlands and lakes may enhance methane production and emission by biological decomposition of organic matter previously sequestered in permafrost. i.e., permafrost degradation may lead to

environments that produce methane. Since the Arctic is vulnerable to climate changes, the accelerated thawing of subarctic peatland permafrost, as observed in the discontinuous permafrost zone of northern Canada (53–58°N) over the last 50 years (Payette et al. 2004), may lead to the increase of CH₄ emission to the atmosphere. Field measurements showed that CH₄ emission from mires increased by about 22–66% over the period of 1970 to 2000 and this increase was associated with the permafrost and vegetation changes (Christensen et al. 2004). The world's northern wetlands as a much larger source of CH₄ were observed to release more CH₄ into the atmosphere than previously believed. For instance, Walter et al. (2006) observed a large emission through ebullition from Siberia thaw lakes, which increases present estimates of CH₄ emissions from northern wetlands by 10 to 63%. The thawing permafrost along the margins of the thaw lakes is the primary source of CH₄ released from the lake. Since the impacts to CH₄ emissions from northern wetlands and thawing permafrost are hard to isolate, later in this paper we just refer to emissions from these regions in the High Northern Hemisphere (HNH) as emissions from wetlands/thawing permafrost.

Current ground-based measurements of CH₄ emissions and CH₄ concentration in the atmosphere are sparse and not representative at large scales, particularly in the subarctic wetlands and permafrost regions. Sampling of the vertical

variation of CH₄ in the atmosphere is much more sparse than current ground-based measurement. Therefore, space-borne measurements are crucial, as they provide the large spatial and temporal coverage needed to help us better understand the variation of CH₄ and its relation with surface emission in hemispheric scale. CH₄ in the middle atmosphere to near the tropopause region was observed from Halogen Occultation Experiment (HALOE) measurement on Upper Atmosphere Research Satellite (UARS), and its most sensitive region is in the stratosphere to near tropopause (Schoeberl et al. 1995, Park et al. 1996). CH₄ total columns were recently observed by the SCanning Imaging Absorption spectromETER for Atmospheric CHartographY (SCIAMACHY) instrument on board the European Space Agency's environmental research satellite (ENVISAT) (Frankenberg et al. 2005). Compared with SCIAMACHY which uses the absorption spectra of solar radiation in the near-infrared, AIRS is a nadir cross-track scanning infrared spectrometer on EOS/AQUA with 2378 channels at high spectral resolution (Aumann et al. 2003), and is most sensitive to CH₄ in the middle to upper troposphere. Moreover, the sensitivity of SCIAMACHY in the HNH is worse than that in lower latitudes due to large solar zenith angles at high latitudes. A combination of both AIRS and SCIAMACHY may provide more information on the CH₄ than either of them separately, but to combine these two data sets to derive CH₄ requires taking into account their difference in spatial resolution and many other aspects and is outside the scope of this paper.

This paper attempted to utilize AIRS observation of CH₄ from August 2003 to 2007 to investigate its seasonal variations and trend in the HNH, particularly in Canada, Alaska, and Siberia which are mostly underlain by wetlands and permafrost. The relation between AIRS CH₄ with surface temperature is also investigated. Through a combination of AIRS data with model simulation, a trend in the past four years was derived. This study demonstrates the value of satellite observations of CH₄ to the study of the effect of permafrost on climate change. However, it is still preliminary considering some uncertainties and caveats in current retrieval, the limited validation in the HNH and only a few years' data available.

Data and Method

AIRS on EOS/AQUA is a nadir cross-track scanning infrared spectrometer with about 200 channels near the absorption band of CH₄ around 7.6 μm at high spectral resolution ($\lambda/\Delta\lambda = 1200$, $\sim 0.5 \text{ cm}^{-1}$), and the noise equivalent change in temperature ($\text{Ne}\Delta T$), referred to 250K target temperature, ranges from 0.14K in the critical 4.2 μm lower tropospheric sounding wavelengths to 0.35K in the 15 μm upper tropospheric sounding region (Aumann et al. 2003). The spatial resolution of AIRS is 13.5 km at nadir, and in a 24-hour period AIRS nominally observes the complete globe once per day and once per night. In order to retrieve CH₄ in both clear and partial cloudy scenes, 9 AIRS pixels in the footprint of an Advanced Microwave Sounding Unit (AMSU) pixel are used to derive the cloud cleared radiance

in this field of regard (FOR), from which the retrieval is made with the spatial resolution of about 45 km. The atmospheric temperature profile, water profile, surface temperature and surface emissivity required as inputs in CH₄ retrieval are derived from other AIRS channels.

A detailed description of CH₄ retrieval from AIRS can be obtained from Xiong et al. (2007), in which over 70 AIRS channels sensitive to CH₄ but less sensitive to water vapor and HNO₃ are selected for CH₄ retrieval. The most sensitive region is in the middle to upper troposphere at about 300–400 hPa in the HNH. Validation using *in situ* aircraft observations of NOAA Earth System Research Laboratory, Global Monitoring Division (ESRL/GMD) shows the bias of the retrieved CH₄ profiles is $-1.4\% \sim +0.1\%$ and its rms difference is about 0.5–1.6% (Xiong et al. 2007). In this paper, the AIRS data in the retrieval are in 3 x 3 degrees in latitude and longitude.

Data of *in situ* observation of CH₄ mixing ratio at the Marine Boundary Layer (MBL) at Barrow, Alaska are obtained from <ftp://ftp.cmdl.noaa.gov/ccg/ch4/in-situ/brw> (GLOBALVIEW-CH₄, 2005). The global CH₄ concentration data from transport model simulations, as reported by Houweling et al. (2006), were obtained using a source scenario (S3) as input to the atmospheric transport model TM3 (Heimann & Körner 2003). Model simulations have been performed on 3.75° x 5° for the period 2001–2004 with meteorological fields derived from the NCEP reanalysis (Kalnay et al. 1996).

Due to the change of information content inherent in the infrared observation, which is related to the atmospheric temperature-moisture profiles, the averaging kernels have to be used to convolve the model data as below (Rodgers 2000, Xiong et al. 2007):

$$\hat{x} \approx Ax + (I - A)x_a \quad (1)$$

where \hat{x} is the convolved CH₄ mixing ratio profile, x is the profile from model simulations, and x_a is the first-guess profile (“*a priori*”), which is a function of latitude and pressure but does not vary with time and longitude (Xiong et al. 2007). I is the identity matrix, and A is the averaging kernels (Maddy & Barnett 2007). Difference between AIRS observation with the model convolved data will reflect the biases between satellite observation and the model simulation (as a “truth”) but taking into account the retrieval scale associated with the variation of information content in satellite observation. To analyze the seasonal variation of CH₄ from August 2003 to 2007, the average needs to be removed for both AIRS and model data. Thus, the difference between AIRS observation and model convolved data after removing their mean values individually will remove the systematic bias between AIRS and the model. By using the model data in 2004 only and the averaging kernels from every satellite observation from August 2003 to 2007, we obtained convolved data using Equation (1). Such data can be used as a “baseline,” which considers the retrieval scales but no annual variation in the “truth,” to drive the trend of CH₄ from its difference with AIRS observation.

Results and Discussion

Spatial and vertical distribution of CH₄ in the HNH

In the HNH, the ground surface is usually frozen and covered by the snow in the winter and early spring, so emissions of CH₄ from the wetlands/permafrost are very low, if not zero, during this period. As snow starts to melt in the late spring, soil temperature increases above the freezing point, and vegetation grows quickly into the summer; hence, CH₄ emission starts to increase in the late spring or early summer. The maxima of CH₄ emission occurs around July (Zhuang et al. 2004), and the most CH₄ emissions from wetlands/thawing permafrost occur in June, July and August (JJA). For example, Figure 1 shows the averaged distribution of AIRS CH₄ at 200–300 hPa from June to August 2004 in North America and Eurasia, respectively. It is evident that CH₄ is enhanced in Siberia and Canada-Alaska, which are mostly underlain by wetlands and permafrost. For further analysis, we chose two regions in Canada-Alaska (60–70°N, 165–90°W) and Siberia (50–70°N, 75–170°E).

The seasonal variation of mean CH₄ profiles averaged in Canada-Alaska and Siberia from 2004 to 2007 is shown in Figures 2a and 2b, respectively. Since the sensitivity of AIRS is low in the lower troposphere and stratosphere, the profiles shown are from 150 to 500 hPa only. Here, only the daytime profile (from the ascending node at 1:30pm LST) of each day is used, as the information content of AIRS in daytime is relatively larger than that in the nighttime (Xiong et al. 2007). Evidently, CH₄ starts to increase from June to August in both Canada-Alaska and Siberia. However, the maxima of CH₄ occurs in early spring in Siberia, which is possibly due to the leakage of natural gases, and worthy of further study. In late spring, CH₄ observed from AIRS is low, which is consistent with ground-based measurement of CH₄ in Barrow, Alaska. As indicated by Dlugokencky et al. (1995), the reason for the low CH₄ in late spring can be attributed to the break-down

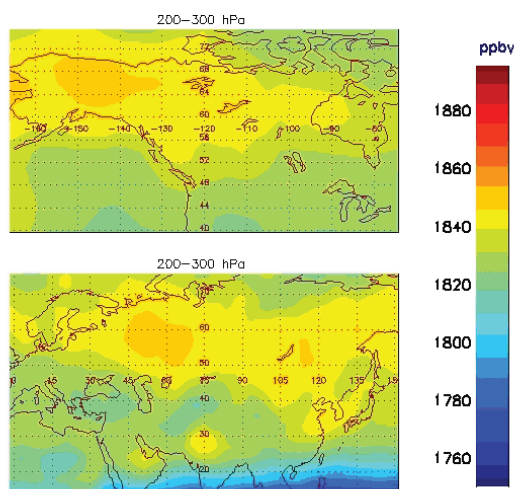


Figure 1. Seasonal averaged distribution of AIRS CH₄ in layer 200–300 hPa in June, July and August 2004 over North America (upper) and Eurasia (right). Enhancement of CH₄ CH₄ is evident over Canada-Alaska and Siberia which are underlain by wetlands and permafrost.

of atmospheric inversion in the HNH, allowing dilution of northern air with the air from the upper level.

Seasonal variation of CH₄ in the HNH from August 2003–2007 and its relation with surface temperature

Figure 3 shows the seasonal variation of CH₄ at 300 hPa (after removing the average) from AIRS observation and models from August 2003 to 2007. Here the model data are fixed in 2004, and then convolved using the averaging kernels corresponding to each AIRS observation. One common feature at both regions is the increase of CH₄ in June every year. The period for the increase of CH₄ has a good correlation with the increase of surface temperature (*T_{surf}*). The decrease of CH₄ in the summer also follows the decrease of surface temperature, but with a delay of about 2–3 weeks.

Compared to the model convolved data in 2004, CH₄ from AIRS in Canada-Alaska is much higher than that from the model, which may be associated with the large forest fires in 2004. In Siberia, the maxima of CH₄ from AIRS occur mostly from January–March each year, and they are much higher than those from model convolved data. This large difference between AIRS and the model indicates a possible unknown, strong source occurring in the winter to early spring in Siberia. One possibility is the gas leakage in Siberia, and this gas leakage or other sources are not well characterized in the model, if they are included at all.

Trend of CH₄ in the HNH and its relation with surface temperature

Figure 4 shows the difference of the seasonal variation (after removing the mean) of AIRS CH₄ minus the model convolved data and the trend. Since most emissions occur from May to October, the data in this period (red) are fitted

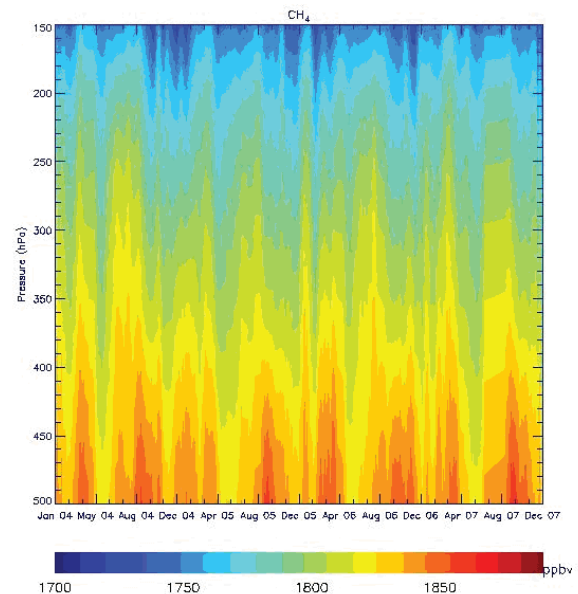


Figure 2a. Seasonal variation of CH₄ profiles (using daytime data from ascending node only) from 2004 to 2007 at Canada-Alaska.

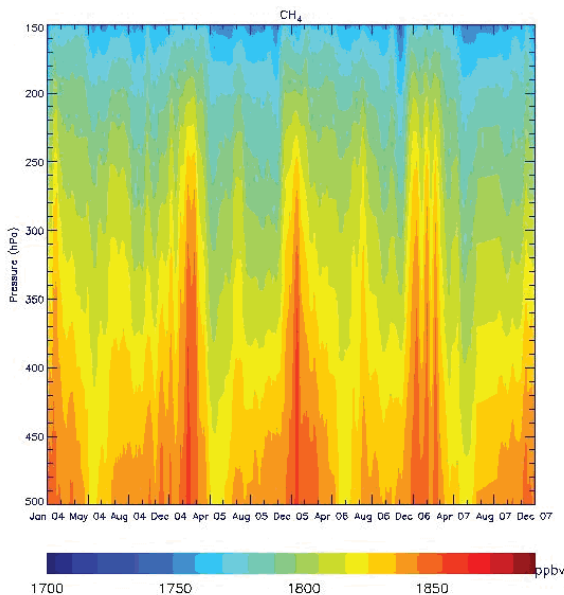


Figure 2b. Same as Figure 2a, but in Siberia.

using a second order polynomial of date (starting from Aug. 6, 2003), as shown in the solid line. The equations are given in the legends of Figure 4. The CH₄ trend is about -1.3 ppbv/year in Canada-Alaska and -3.9 ppbv/year in Siberia.

We note that in Figure 4, in the summer of 2005, CH₄ is biased lower than the fitting in both regions. This indicates that CH₄ emission in 2005 is smaller than that in 2004 and 2006. If this argument, based on satellite observation, is reasonable, lower CH₄ in 2005 may exist in the ground-based observation since its variation has a closer link with surface emission than CH₄ in the mid-upper troposphere observed by satellite. Therefore, we analyzed the seasonal variation of CH₄ measured by NOAA/ESRL/GMD in Barrow, Alaska and the surface temperature retrieved from AIRS. The hourly CH₄ observed at MBL were used to compute the daily average in Figure 5 (upper panel). In agreement with AIRS observation, CH₄ at the MBL in the summer of 2005 is lower than that of 2004 and 2006. Analysis of surface temperature provides more evidence to lower emission of CH₄ from high northern wetlands/thawing permafrost in 2005 as the surface temperature from June to September in 2005 is lower than that at 2004 and 2006 (Fig. 5). Further study of the trend of CH₄ emission from high northern wetlands/permafrost from model simulations may help to validate whether this observed trend from AIRS is reasonable.

Uncertainty analysis

It is important to keep in mind some uncertainties and caveats in current AIRS retrievals and limited validation made in the HNH. As addressed in Xiong et al. (2007), the uncertainty of CH₄ retrieval corresponding to a noise equivalent bias in AIRS radiances can be evaluated by putting a noise equivalent bias to the observed radiance in CH₄ channels, and then comparing the differences in their retrieved profiles. As an example, Figure 6 (upper left panel) shows the mean retrieved bias resulted from a

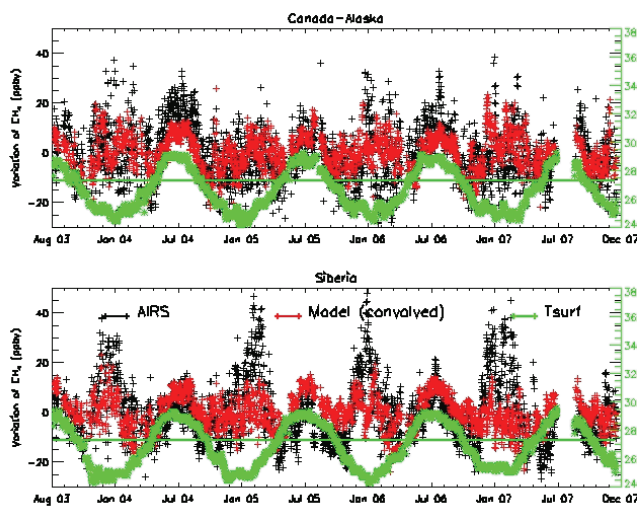


Figure 3. Seasonal variation of CH₄ (300 hPa) from AIRS (black), model convolved (red), and surface temperature (Tsurf, green) at Canada-Alaska and Siberia. There is a good correlation between CH₄ and Tsurf in the summer.

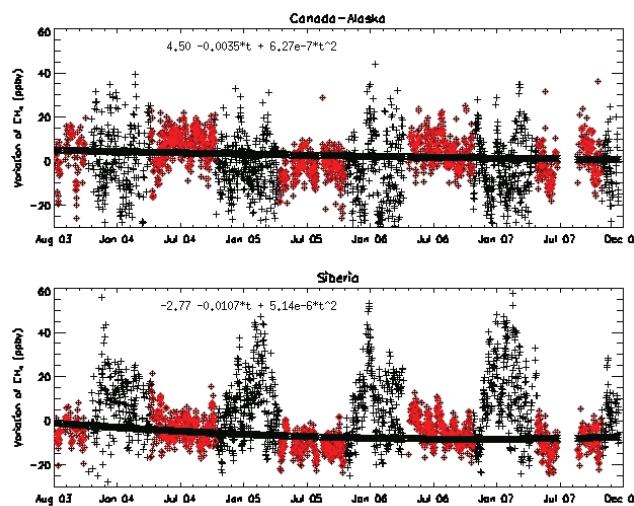


Figure 4. Trend of CH₄ (300 hPa) derived as the difference of AIRS observation minus the model convolved data (model data are fixed to 2004) at Canada-Alaska and Siberia. Black solid lines are the second-order polynomial fitting to their differences from May to October (red), and the legends are the equations.

noise equivalent bias based on two days' AIRS data (in 3 x 3 degree) in the HNH above 50°N. These two days are chosen randomly, and one is Aug. 10, 2004 (summer) and another one is Feb. 15, 2005 (winter). The largest bias is 24.9±6.0 ppbv at 350–400 hPa, and below 600hPa the bias is less than 10 ppbv. The standard deviation for all cases, represented by the error bar in the figure, is mostly less than 10 ppbv. A similar methodology is used to estimate the uncertainties of retrieval due to errors in temperature-moisture profiles and surface temperature. The mean CH₄ biases resulted from the AIRS temperature and moisture profile biases are mostly less than 10 ppbv. The errors in cloud clearing could be the largest source of uncertainty, however an examination to the variation of AIRS retrieved CH₄ within 200 km in the same granule and its relation with cloud amount, and

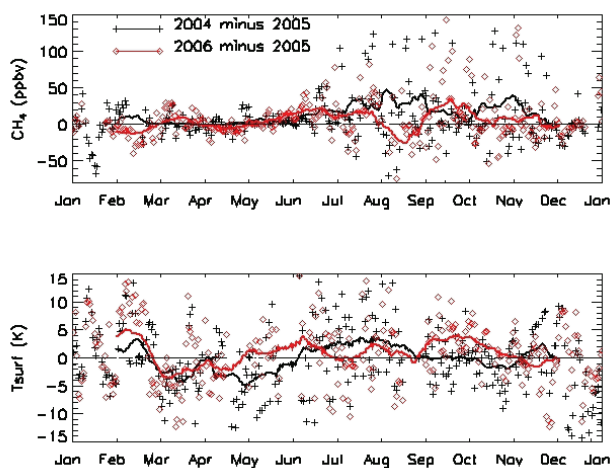


Figure 5. Difference of CH_4 at the MBL in 2004 and 2006 minus that in 2005 in Barrow, Alaska (upper). Lower CH_4 in the summer of 2005 is consistent with the lower CH_4 in the middle to upper troposphere observed from AIRS. Lower panel is surface temperature (T_{surf}) in 2004 and 2006 minus that in 2005 at Canada-Alaska. Lower T_{surf} from June to September in 2005 may indicate the lower emission of CH_4 from high northern wetlands/thawing permafrost in 2005.

found the difference of CH_4 between clear cases (with the cloud fraction less than 0.1) and cloudy cases (with the cloud fraction over 0.8) is usually less than 1.0%. Since the magnitude of the seasonal variation of CH_4 (see Fig. 3) is significantly larger than the uncertainties of the retrieval, these uncertainties should not undermine the conclusions.

We noted that there are some correlations between the retrieved CH_4 with the surface temperature and water vapor amount. Therefore, variation of water vapor and temperature profiles make the interpretation of the retrieval results complicated, and the averaging kernels have to be taken into account in the interpretation of the variation of CH_4 from AIRS, and in the comparison of AIRS with model simulation and/or other observations. A better retrieval of CH_4 also depends on a more accurate computation of radiance from the radiative transfer model, and further improvement to current model is required (Xiong et al. 2007).

It is almost impossible to isolate the impact of wetland emissions and emissions from thawing permafrost on the seasonal variation and trend illustrated above; therefore, it is hard to say whether the observed trend is related to the thawing permafrost. This will require long-term monitoring of CH_4 from satellite and more model studies.

Conclusion

Satellite observations using AIRS, show that the CH_4 in middle to upper troposphere increases in the summer in regions that are mostly underlain by the northern wetlands and permafrost, and that this increase has a good relation with the surface temperature. Preliminary analysis using AIRS observation from August 2003 to 2007, in conjunction with model simulation, shows a small but negative trend of CH_4 of -1.3 ppbv/year in Canada-Alaska and -3.9 ppbv/

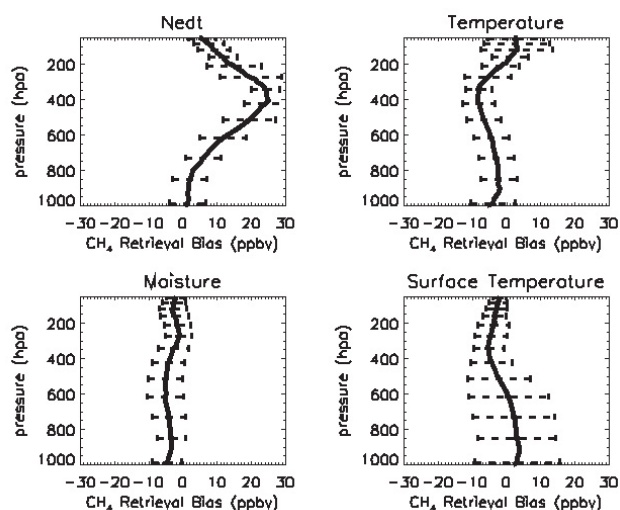


Figure 6. The mean bias of the retrieved CH_4 profiles in the HNH assuming a radiance bias equivalent to the noise of the AIRS $N_e\Delta T$ for CH_4 channels (upper left), AIRS biases in temperature (upper right) and moisture profile, and a bias in surface temperature of 2 K. Two days' AIRS data in Aug. 20, 2004, and Feb. 15, 2005 are used. Solid lines are the mean bias, and dashed lines represent the standard deviation.

year in Siberia. Moreover, lower trend of CH_4 in 2005 is observed from AIRS which is in good agreement with the lower CH_4 from ground-based observation and lower surface temperature in 2005. These results have demonstrated that AIRS can provide valuable information of CH_4 in the middle to upper troposphere. Further use of AIRS CH_4 appropriately in conjunction with model simulation will provide a way to better estimate source emissions from wetlands and/or permafrost in the HNH. NOAA plans to utilize the Infrared Atmospheric Sounding Interferometer (*IASI*) (2006–2021) and the Cross-track Infrared Sounder (*CrIS*) (2009–2023) to derive atmospheric CH_4 in the same method as used for AIRS for the next 20 years. These long-term observations will be useful to monitor the trend of CH_4 associated with the thawing of permafrost and climate warming.

Acknowledgments

This research was supported by funding from NOAA Office of Application and Research Climate Program. The views, opinions, and findings contained in this paper are those of the authors and should not be construed as an official National Oceanic and Atmospheric Administration or U.S. Government position, policy, or decision. The model data were provided by Dr. Sander Houweling at the Netherlands Institute for Space Research.

References

- Aumann, H.H., Chahine, M.T., Gautier, C., Goldberg, M.D., Kalnay, E., McMillin, L.M., Revercomb, H., Rosenkranz, P.W., Smith, W.L., Staelin, D.H., Strow, L.L. & Susskind, J. 2003. AIRS/AMSU/HSB on the Aqua mission: Design, science objectives, data products, and processing systems. *IEEE Trans. Geosci. Remote Sens.* 41:253-264.
- Christensen, T.R., Johanson, T., Akerman, H.J. & Mastepanov, M. 2004. Thawing sub-arctic permafrost: Effects on vegetation and methane emissions. *Geophys. Res. Lett.* 31:L04501, doi: 10.1029/2003GL018680.
- Divakarla, M., Barnet, C., Goldberg, M.D., McMillin, L., Maddy, E.S., Wolf, W.W., Zhou, L. & Liu, X. 2006. Validation of Atmospheric Infrared Sounder temperature and water vapor retrievals with matched radiosonde measurements and forecasts. *J. Geophys. Res.* 111: doi:10.1029/2005JD006116.
- Dlugokencky, E.J., Steele, L.P., Lang, P.M. & Masaire, K.A. 1995. Atmospheric methane at Mauna Loa and Barrow observatories: Presentation and analysis of in situ measurements. *J. Geophys. Res.* 100: 23, 103-23, 113.
- Dlugokencky, E.J., Walter, B.P., Masaire, K.A., Lang, P.M. & Kasischke, E.S. 2001. Measurement of an anomalous global methane increase during 1998. *Geophys. Res. Lett.* 28: 499-502.
- Frankenberg, C., Meirink, J.F., van Weele, M., Platt, U. & Wagner, T. 2005. Assessing methane emissions from global space-borne observations. *Science* 308: 1010-1014, doi:10.1126/science.1106644.
- Heimann, M. & Körner, S. 2003. The global atmospheric tracer model TM3, Max Planck Institute of Biogeochemistry, Model description and user's manual. Release 3.8a.
- Intergovernmental Panel on Climate Change. 2001. Climate Change 2001: The Scientific Basis. New York: Cambridge University Press, 881 pp.
- Kalnay, E. et al. 1996. The NCEP/NCAR 40-year Reanalysis Project. *Bull. Amer. Meteor. Soc.* 77: 437-471.
- Maddy, E.S. & Barnet, C. D. 2008. Vertical resolution estimates in Version 5 of AIRS operational retrievals. IEEE TGRS, Accepted.
- Park, J.H., Russell, J.M. III, Gordley L.L., Drayson, S.R., Benner, D.C., McInerney J.M., Gunson, M.R., Toon, G.C., Sen, B., Blavier, J.F., Webster, C.R., Zipf, E.C., Erdman, P., Schmidt, U. & Schiller, C. 1996. Validation of Halogen Occultation Experiment CH₄ measurements from the UARS. *J. Geophys. Res.* 101(D6): 10,183-10,204.
- Payette S., Delwaide, A., Caccianiga, M. & Beauchemin, M. 2004. Accelerated thawing of subarctic peatland permafrost over the last 50 years. *Geophys. Res. Lett.* 31:L18028, doi: 10.1029/2004GL020358.
- Rodgers, C.D. 2000. Inverse Methods for Atmospheric Sounding. *World Sci.*, Hackensack, N. J.
- Schoeberl, M.R., Luo, M. & Rosenfield, J.E. 1995. An analysis of the Antarctic Halogen Occultation Experiment trace gas observations. *J. Geophys. Res.* 100: 5159-5172.
- Walter, B.P., Heimann, M. & Matthews, E. 2001. Modeling modern methane emissions from natural wetlands. 1. Model description and results. *J. Geophys. Res.* 106: 34,189-34,206.
- Walter, K.M., Zimov, S.A., Chanton, J.P., Verbyla, D. & Chapin, F.S. III. 2006. Methane bubbling from Siberian thaw lakes as a positive feedback to climate warming. *Nature* 443: 71-75.
- Xiong, X., Barnet, C.D., Maddy, E., Sweeney, C., Liu, X., Zhou, L. & Goldberg, M. 2007. Characterization and Validation of Methane Products from the Atmospheric Infrared Sounder (AIRS). *J. Geophys. Res.* doi:10.1029/2007JG000500, in press.
- Zhuang, Q., Melillo, J.M., Kicklighter, D.W., Prinn, R.G., McGuire, A.D., Steudler, P.A., Felzer, B.S. & Hu, S. 2004. Methane fluxes between terrestrial ecosystems and the atmosphere at northern high latitudes during the past century: A retrospective analysis with a process-based biogeochemistry model. *J. Geophys. Res.* doi:10.1029/2004GB002239.

Numerical Analysis of a Thermosyphon Foundation of High-Voltage Transmission Towers in a Permafrost Region

Xue-yan Xu , Lin-lin Yu, Li-yue Wang

School of Civil Engineering, Harbin Institute of Technology, Harbin 150090, China

Abstract

A new-model thermosyphon foundation (the portion of thermosyphon under ground is wrapped with concrete) is applied in the project, because this special foundation can bear the loads from superstructure, preserving permafrost soil from thawing. Research contents: According to the conditions of permafrost regions and considering global warming, the thermal and mechanical finite element model of thermal pipe foundation is made with the function of thermal and nonlinear mechanical analysis of ANSYS. Temperature distributions are compared between a thermosyphon foundation and a traditional pole foundation. The thermal calculation results indicate that the natural permafrost table rises by 0.5 m, and the inner temperature lowers by 2°C, in comparison to those with a traditional foundation. This proves the distinct permafrost-preserving effect of thermal pipes. In response to the distributions of the temperature fields of ten years in permafrost regions, it is concluded that the permafrost-preserved effect of thermal pipes is in direct ratio to working years. With the increase of areas ratio, pile space, and pile length, a better cooling effect is obtained; when the spacing between thermal pipes is 4 m, the cooling effective is optimum. On the basis of the above thermal analysis, the appropriate design parameters of a thermosyphon foundation are presented.

Keywords: design parameters; global warming; permafrost-preserved effect; temperature fields; thermosyphon foundation.

Introduction

The permafrost area of the Northern Hemisphere is about 25% of the land surface. In China, permafrost is about 22.4% of the country (Zhou et al. 2000). The Direct-Current (± 500 kV) Transmission Project will be built from Hu Lun Bei Er to Liao Ning Province, and it will pass across the permafrost region (Daxing'an Mountain Range, A Er Mountainous Region, and the northwest of SongNen Plain). When the project is constructed, disturbed frozen soil and the seasonally thawed layer will have great influence on the thermal regime of the permafrost region. Often permafrost in these regions is ice-rich and makes large deformation for consolidation if thawing occurs. Global warming tends to warm the permafrost in these regions and makes it susceptible to thaw. (Mingyi Zhang et al. 2005). So it is very significant and practical to study the design method to ensure the construction security and the regular service of the project.

So far, in China, systemic test research and numerical calculations have not been conducted on the combination of

the bearing capacity of the foundation of the transmission tower with the permafrost-preserving effect.

In this paper, we consider the effect of global warming on a thermosyphon foundation (one thermosyphon pile under each tower foot, total of four) shown in Figure 1. In order to research the cooling effects of different pile spacing distances with or without a thermosyphon, we have used numerical modeling by ANSYS. Some numerical simulations are carried out during the course of this study. Namely, the temperature fields of a traditional pile foundation and a thermosyphon foundation have been analyzed under the assumption that the average atmosphere temperature will be warmed by 1°C in 10 years.

Governing Equations, Numerical Model, and Boundary Conditions

The thermal convection of foundations is the process of heat transfer. In the analysis, circular cylindrical coordinates are introduced and then the corresponding governing equations as follows (Yuanming Lai et al. 2004).

$$\text{Energy: } \rho c \frac{\partial T}{\partial t} + \rho_w c \left(u_z \frac{\partial T}{\partial z} + u_r \frac{\partial T}{\partial r} \right) = \lambda \left(\frac{\partial^2 T}{\partial z^2} + \frac{\partial^2 T}{\partial r^2} \right) + s_3 \quad (1)$$

where c and λ are specific heat and coefficient of heat conductivity separately, T is temperature, t is time, and s_3 is heat source of the whole system.

Continuity and energy:

$$\lambda_r \frac{\partial T_f}{\partial n} - \lambda_n \frac{\partial T_u}{\partial n} = L \rho \frac{\partial \xi}{\partial t} \quad (2)$$

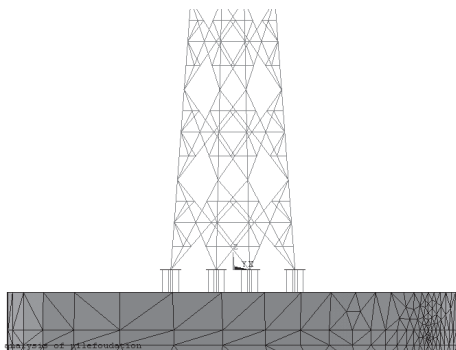


Figure 1. Sketch of the connection of tower and thermosyphon foundation.

Table 1. Thermal-physical parameters of soil used in numerical simulation.

		Temp. (°C)						
		-10	-5	-2	-1	-0.5	0	15
Fine sand	$\rho(\text{kg/m}^3)$	1680	1680	1680	1680	1680	1680	1680
	$W_u(\%)$	0.44	1.1	1.76	3.3	4.84	22	22
	$\lambda(\text{J/m} \cdot ^\circ\text{C} \cdot \text{h})$	5760	5760	5760	5760	5760	4680	4680
Marl soil	$\rho(\text{kg/m}^3)$	1600	1600	1600	1600	1600	1600	1600
	$W_u(\%)$	2.2	5.4	6.3	7.4	8.1	30	30
	$\lambda(\text{J/m} \cdot ^\circ\text{C} \cdot \text{h})$	5004	5004	5004	5004	5004	2304	2304
Mud stone	$\rho(\text{kg/m}^3)$	1890	1890	1890	1890	1890	1891	1890
	$W_u(\%)$	4.4	5.5	6.6	7.7	8.8	35	35
	$\lambda(\text{J/m}^\circ\text{C} \cdot \text{h})$	8640	8640	8640	8640	8640	5544	5544

$$T_f(\xi(t), t) = T_u(\xi(t), t) = T_m \tag{3}$$

where f and u indicate frozen state and thaw state separately. t is time; L is critical heat; ξ is interface between freeze and thaw; T_m is the temperature of freezing front; n is normal vector of frozen-thaw interface.

In this study, numerical solutions are obtained using a two-dimensional finite ANSYS model through the function of the thermal and nonlinear mechanical analysis.

According to the engineering geological exploration and requirements of The Direct-Current (± 500 kV) Transmission Project, the simplified computational domain including thermosyphon foundation is shown in Figure 2, 18 m depth, 30 m width, the distance between two thermosyphon foundations is 6 m. And there are no thermal flows on boundaries E-F and D-G; that is, $q = 0$.

The thermal-physical parameters of the three kinds of soils (A, B, and C) used in numerical simulation are shown in Table 1.

The temperature at the native surface E-D is changed according to the follow expression:

$$T_a = -1.0 + \frac{1}{50 \times 365 \times 24} t + 10 \sin\left(\frac{2\pi}{8760} t + \frac{\pi}{2}\right) \tag{4}$$

where, t is working time of the thermosyphon foundation, and is given in hours for ten years.

The temperature on the sub-permafrost boundary (18 m depth) F-G is -2.5°C .

In this study model, the thermosyphon $\phi 89$ (7.5 m long totally) is simplified to a 7.5 m long line, and divided into three parts, and the finite width in computation area is concrete in the results Figures 6a-h. The first one is aboveground (1.5 m length), that is, the condensation part; the second one is 3.0 m underground, which is heat-insulating; the third one, the bottom part, namely the evaporation part, is 3.0 m, and when air temperature is higher than the temperature of the thermosyphon foundation, its density of heat flow is 0; on the contrary, it starts to work, and then the density of heat flow changes as the air temperature does, and the refrigerating output per second is changed according to the following expression:

$$q = \frac{T_s - T_a}{R_s + R_f} \tag{5}$$

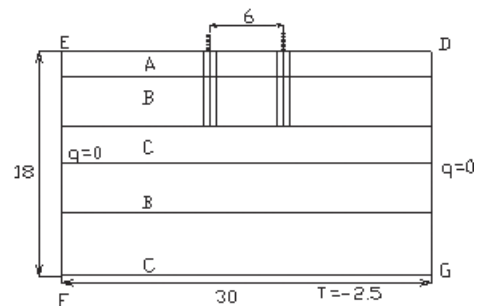


Figure 2. The simplified computational domain. A is fine sand; B is marl soil; C is mud stone (unit: m).

where, q is refrigerating output per second, T_s is average ground temperature, T_a is air temperature, R_s is thermal resistance on the soil-syphon interface, R_f is thermal resistance of the radiator on the air-syphon interface (cooling portion).

$$R_f = 1/A\alpha \tag{6}$$

where, A is the effective area of the cooling portion of the thermosyphon; α is the heat-release coefficient of the cooling portion of the thermosyphon.

$$R_s = \frac{\ln\left(\frac{2r}{D}\right)}{2\pi\lambda L_e} \tag{7}$$

where, D is the outside diameter of the thermosyphon; L_e is length of cooling portion of the thermosyphon; λ is the coefficient of heat conductivity of the soil; r is the maximum radiator of area influenced by the thermosyphon.

The heat transfer quantity of the thermosyphon bar is expressed as follows:

$$Q = M\Delta T(t) \tag{8}$$

where, Q is heat transfer quantity, M is heat transfer quantity, and it is altered as follows:

$$M = \begin{cases} \frac{1}{R_s + R_f} & T_a - T_s \geq 1 \\ 0 & T_a - T_s \leq 1 \end{cases} \tag{9}$$

$\Delta T(t)$ is the difference in temperature between soil around the thermosyphon foundation and the inner thermosyphon.

In this analysis, the 10-year simulation starts on July 15, 2007, when the high-voltage transmission tower is applied

according to the requirements of the project. We choose the representative calculation results on autumnal equinox and spring equinox. On autumnal equinox, the seasonal thaw layer is the deepest, and the thermosyphon works because of the temperature difference; on spring equinox, the active layer is frozen totally, and the thermosyphon stops working.

Numerical Results and Comparisons

Characteristics of the temperature fields of thermosyphon foundation

The temperature field of (traditional) foundation is shown in Figure 3. It can be seen that the initial temperature distribution is even in the same soil layer. The temperature field in Figure 3 also shows the temperature field of traditional foundation.

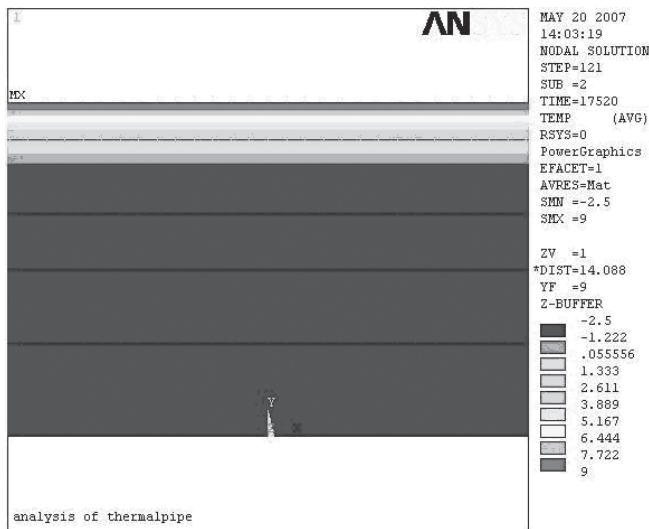
Figures 4 and 5 are the temperature distributions of soil next to a traditional foundation and a thermosyphon foundation on autumnal equinox and spring equinox along depth. It is evident that the natural permafrost table rises by 0.5 m and the

average temperature decreases by 2°C due to the permafrost-preserving effect of the thermosyphon foundation.

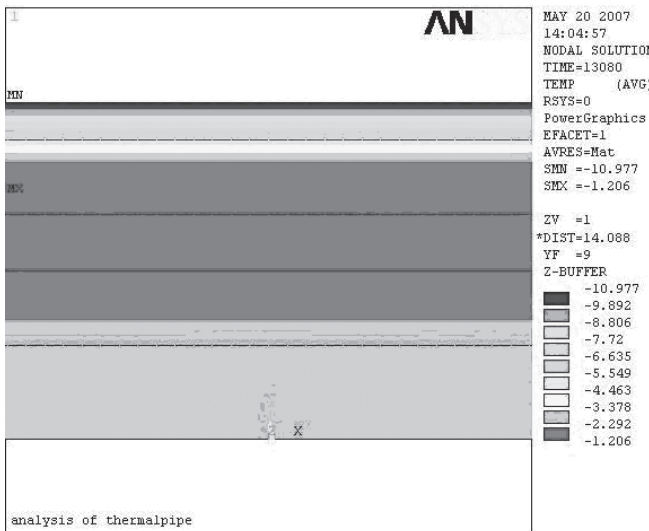
Figures 6a–6f separately display isotherms of the thermosyphon foundation on autumnal equinox and spring equinox in the second, fifth, and tenth working year. From Figure 6b, it can be seen that the isotherms of the thermosyphon foundation change in evidence, which reveals that the thermosyphon has worked; however the affected region is only as big as twice the diameter of the thermosyphon foundation on the first spring equinox after the first cold season.

As shown in Figures 6a, 6d, and 6f, with the working years going, the influenced region surrounding the thermosyphon foundation has become wider and deeper and relative temperatures descend obviously, especially for the soil layers around the bottom of the thermosyphon foundation; so it is demonstrated that the cooling effect becomes more powerful.

From Figures 6a, 6c, and 6e, because of the heat-absorbing effect of the evaporation part of the thermosyphon, there is an approximate elliptic low-temperature (isotherm of -4.2°C to -4.9°C) region, and we can state that cold power stored in the soil near the thermosyphon foundation increases greatly; therefore, the stability of the foundation can be protected effectively from rising air temperatures in permafrost regions.



a) Isotherm of autumnal equinox.



b) Isotherm of spring equinox.

Figure 3. Temperature field of (traditional) foundation.

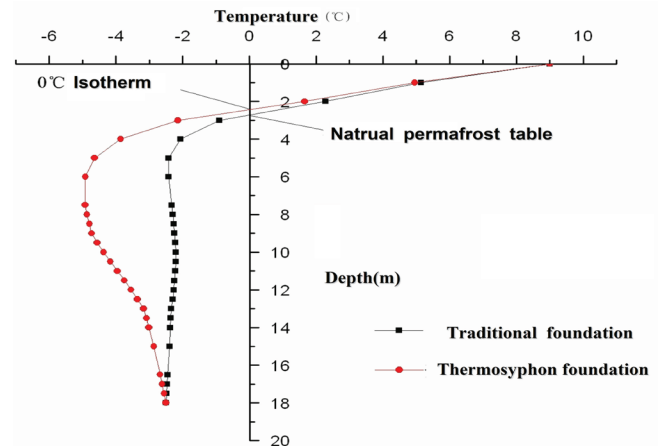


Figure 4. Temperature distributions of the two kinds of pile foundations on autumnal equinox.

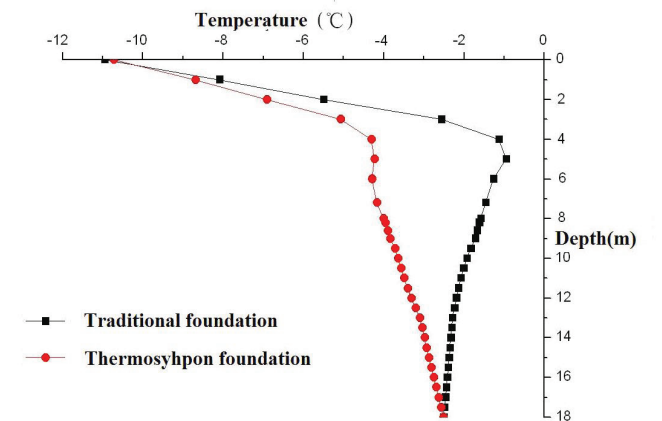
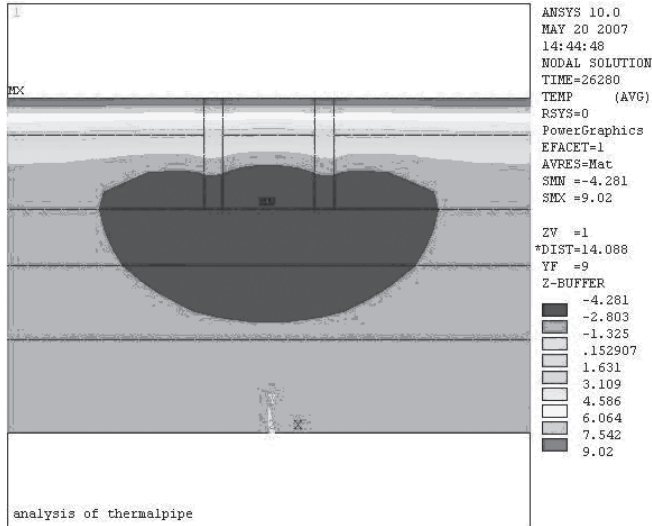


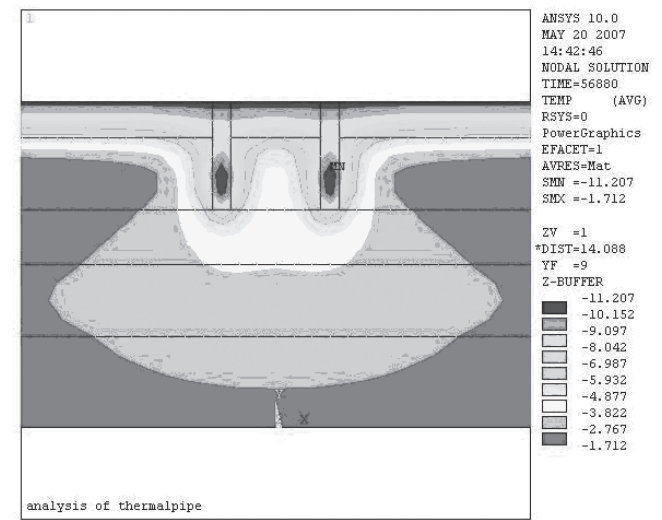
Figure 5. Temperature distribution of the two kinds of pile foundations on spring equinox.

Figures 6a–6f show that it is obvious that the cooling effect of the thermosyphon foundation gets stronger and better as working time goes, per annum. Through each cold season’s cooling effect and each warm season’s heat-absorbing effect,

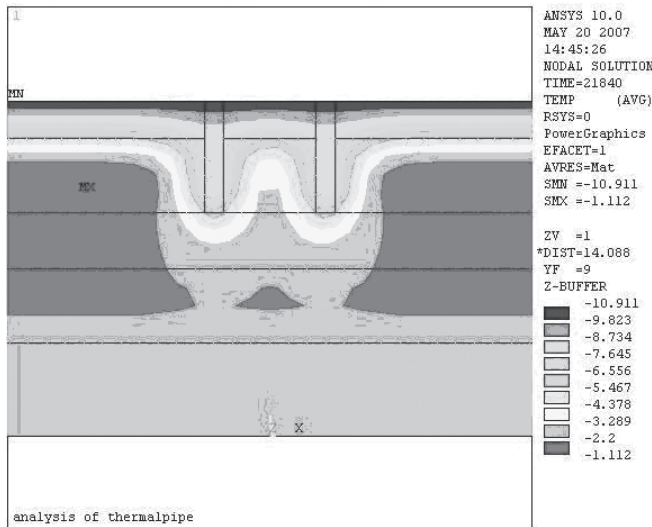
cooling power gradually increases in the thermosyphon foundation each year, which illuminates that the longer the working time of a thermosyphon foundation, the better the permafrost-preserving effect will be in the application life.



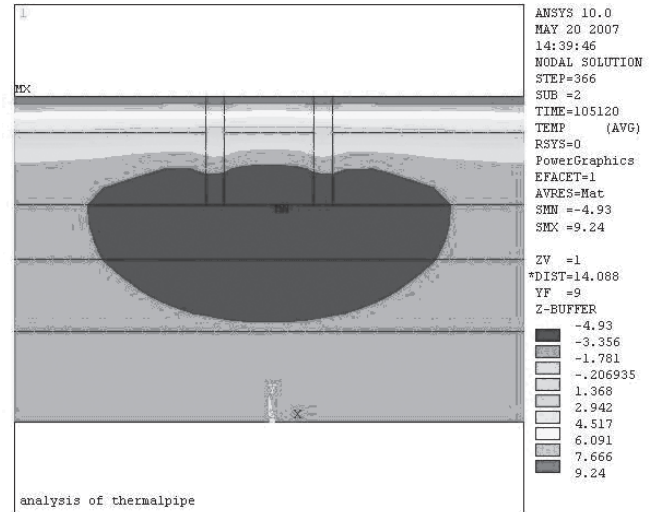
a) Isotherm on the second autumnal equinox.



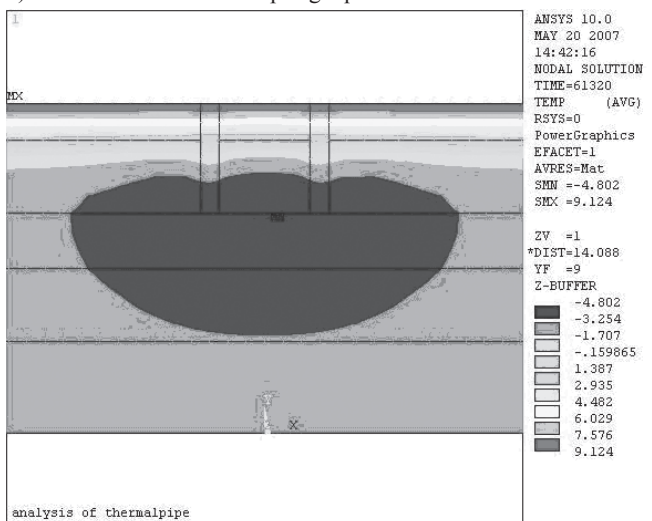
d) Isotherm on the fifth spring equinox.



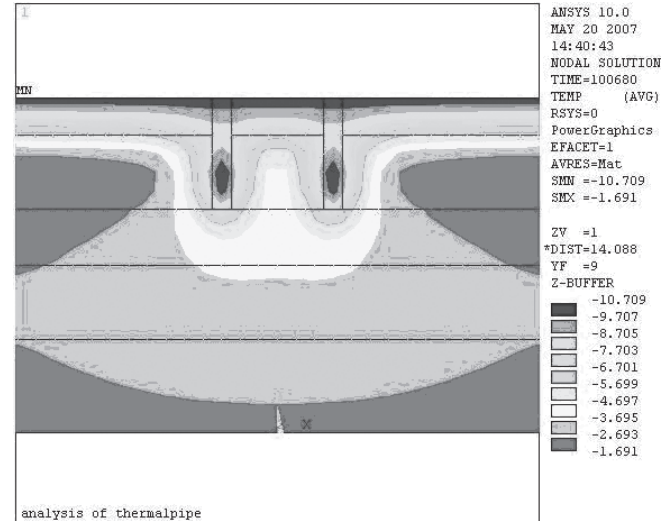
b) Isotherm on the second spring equinox.



e) Isotherm on the tenth autumnal equinox.

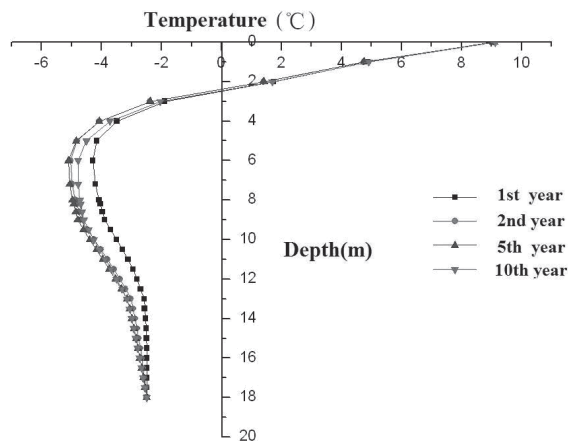


c) Isotherm on the fifth autumnal equinox.

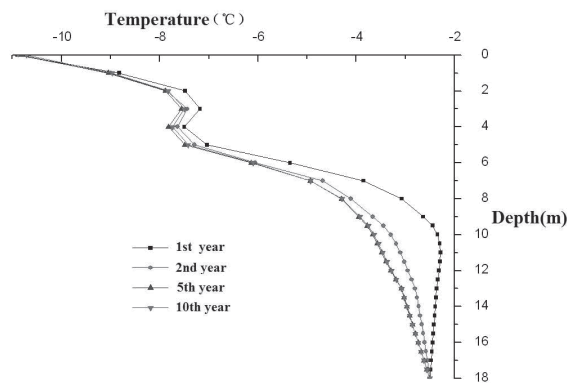


f) Isotherm on the tenth spring equinox.

Figure 6. Isotherms of the thermosyphon foundation in different years (the second, the fifth, and the tenth year taken, for instance).



a) Temperature distribution on autumnal equinox.



b) Temperature distribution on spring equinox.

Figure 7. Temperature distributions in different years.

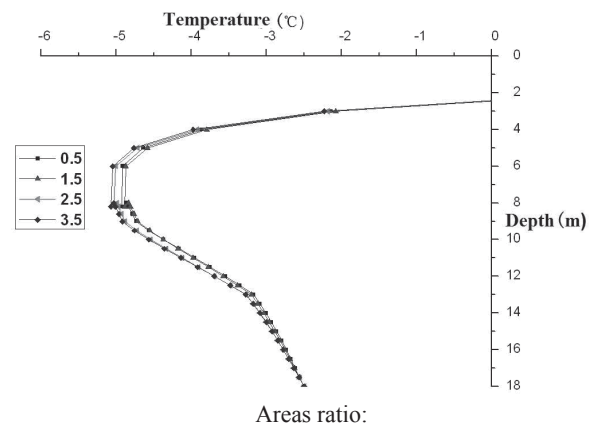
Figure 7 is temperature distribution in which is as far as the diameter of thermosyphon foundation away from the foundation, along depth in different years. The average temperature in year 1 is apparently higher than those in other years, and as working time goes, it continuously drops but the falling range becomes smaller and smaller. At the same time, there is a rising trend for the temperature of permafrost due to the influence of global warming. For the cooling effect of thermosyphon foundation, the natural permafrost table keeps in a certain level, so the foundation is safe and steady enough to sustain structures.

The influence of parameters of thermosyphon foundation on temperature field

The article investigates the influence of parameters (areas ratio, length, pile space) of thermosyphon foundation on temperature fields to gain reasonable design parameters. The total calculation time is ten years. Areas ratio is defined with the surface area of the condensation part divided by that of the evaporation part.

Influence of areas ratio on temperature field

Figures 8 and 9 separately show temperature fields that are one diameter away from the thermosyphon foundation with different ratios of areas, such as 0.5, 1.5, 2.5, and 3.5 along depth on the tenth autumnal equinox and spring equinox. It is clear that the temperature of soil layers near to the foundation



Areas ratio:

Figure 8. Temperature distribution with different ratios of areas (0.5, 1.5, 2.5, 3.5) on the tenth autumnal equinox.

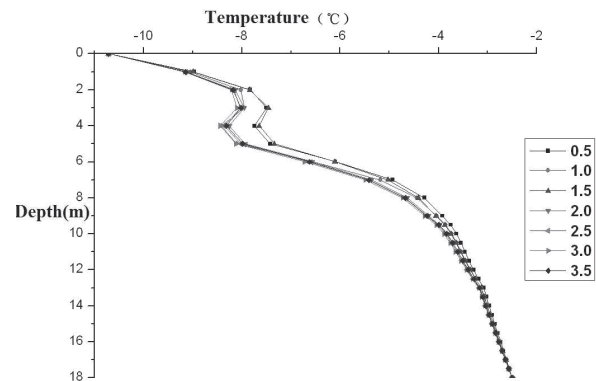


Figure 9. Temperature distribution with different ratios of areas (0.5, 1.0, 1.5, 2.0, 2.5, 3.0, 3.5) on the tenth spring equinox.

changes slightly with areas ratio 0.5–1.5, distinctly with 1.5–2.0, less with 2.0–3.5. From Figure 7, we can state that from -3 m to the bottom, namely the evaporation part, the temperature of soil layers near to this part is greatly affected by the variation of areas ratio, and the temperature falling range rises with areas ratio increasing, especially from 1.5 to 2.0, so that we choose 2.0 as the reasonable ratio of areas in the study.

Due to the limitation of the transmission tower structure, the length of condensation part is not appropriate to be changed, so the length of evaporation part varies with 3.0 m, 3.5 m, 4.0 m, 4.5 m, 5.0 m for calculation. Figure 10 represents temperature distributions with different lengths of thermosyphon ϕ 89 pile along depth on the tenth autumnal equinox, from which we can see that the temperature falling range of soil increases, as well as the cooling efficiency, with the evaporation part becoming longer. Meanwhile, the influencing region is getting wider and deeper. In view of facts such as project cost, design requirements and so on, the article suggests that the reasonable length of evaporation part is 3 m.

The pile spaces for numerical analysis between thermosyphon ϕ 89 piles are 3.0 m, 4.0 m, 5.0 m, and 6.0 m with areas ratio 2.0, and all these chosen spaces (3.0 m, 4.0 m, 5.0 m, and 6.0 m) are limited by the structural sizes. All these data points are node points in the analysis. Figure 11 shows temperature distributions (below 0°C) of the foundation with different pile spaces along depth. It reveals that when pile space is 3.0 m the cooling effect of thermosyphon founda-

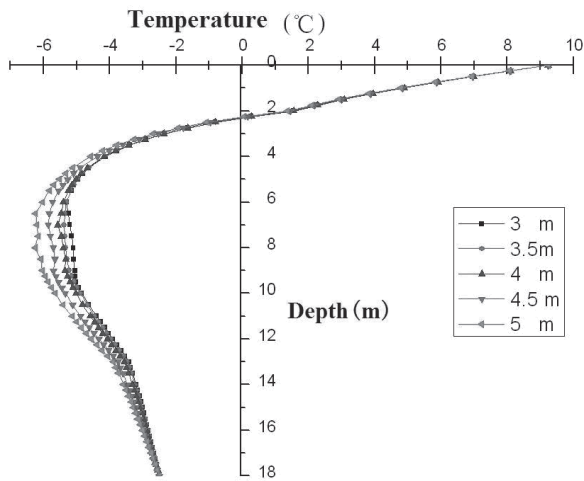


Figure 10. Temperature distributions with different lengths of thermosyphon.

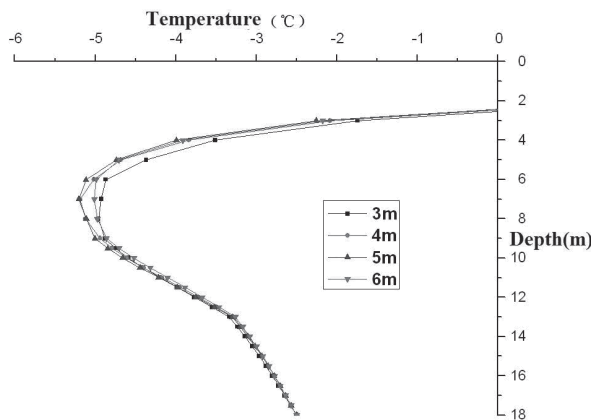


Figure 11. Temperature distributions of different spaces of the thermosyphon.

tion decreases, but increases with pile space getting large; the cooling effect with pile space 6.0 m is not as good as that with 4.0 m or 5.0 m, and 4 m is optimum, because the mutual influence (i.e. group action of piles) between thermosyphon $\phi 89$ piles turns strong with small pile space, but if the pile space is too large, there will be a weak region (with relatively high temperature) between two thermosyphon piles. According to the calculation result and the type of transmission tower applied in this project, 6.0 m is the best pile space, and in order to reinforce the cooling effect, it can be considered to add a thermosyphon pile in the central zone of the four ones with the pile space among them about 4.0 m.

To sum up, as a result of the cooling effect, the average temperature of permafrost with the thermosyphon foundation is lower than that with a traditional foundation.

After ten years, the natural permafrost table moves up 0.5 m owing to the thermosyphon foundation. Although ten years of global warming makes permafrost near the ground surface degenerate, from the above analysis and figures, it can be stated that permafrost surrounding the bottom part of the thermosyphon foundation can be refrozen completely in cold seasons; a big central frozen zone is formed with -5.2°C ; after the tenth whole warm season the temperature of this zone is even -3.7°C . Therefore, the permafrost-preserving effect of a

thermosyphon is strong enough to keep the whole structure stable and resistant to the influence of global warming.

Conclusions

Based on the continuity equation, momentum equation, and energy equation, the temperature characteristics of a thermosyphon foundation of a high-voltage transmission tower in permafrost regions are calculated and analyzed using FEM with the aid of ANSYS, and reasonable design parameters are obtained considering global climatic warming. The results provided a theoretical basis for the design of a thermosyphon foundation. It can be concluded that: (1) Under the stated climatic conditions and the project requirements, the temperature fields of a thermosyphon foundation and traditional foundation compared on autumnal equinox and spring equinox reveal that the natural permafrost table rises by 0.5 m due to the cooling effect of the thermosyphon pile, and the average temperature of soil near to the foundation drops by 2°C , which proves that the thermosyphon foundation has a distinct permafrost-preserving effect. (2) The temperature fields of a thermosyphon foundation in the first year and the tenth year are also compared, and the average temperature in the tenth year is 2.0°C lower than in the first year, which indicates that the cooling effect increases as working years pass. (3) The influence of the design parameters of a thermosyphon—for instance, areas ratio, pile length, and pile space on temperature fields—is analyzed in ten years. The computation results suggest that the temperature of soil layers near the foundation changes slightly with areas ratio 0.5–1.5, distinctly with 1.5–2.0, less with 2.0–3.5, so this paper chose 2.0 as the reasonable areas ratio. In order to satisfy the project requirements and economy, the appropriate length of the evaporation part is taken as 3.0 m. According to the analysis stated above, 4 m is the optimum pile space, and considering the type of transmission tower applied in this project, 6.0 m is the best pile space. In order to reinforce the cooling effect, a thermosyphon pile can be added in the central zone of the four ones with the pile space among them about 4.0 m.

Acknowledgments

This research was supported by the National Science Fund (No. 40571032), the Research Fund for The Direct-Current (± 500 kV) Transmission Project from Hu Lun Bei Er to Liao Ning Province.

References

- Lai, Y., Wang, Q. & Niu, F. 2004. Three-dimensional nonlinear analysis for temperature characteristic of ventilated embankment in permafrost regions. *Cold Regions Science and Technology* 38: 165-184.
- Zhang, M., Lai, Y., Liu, Z. & Gao, Z. 2005. Nonlinear analysis for the cooling effect of Qinghai-Tibetan Railway embankment with different structures in permafrost regions. *Cold Regions and Technology* 42: 237-249.
- Zhou, Y.W., Guo D.X., Qiu, G.X. et al. 2000. *Geocryology in China*. Beijing: Science Press, p. 37(in Chinese).

“Permafrost Is No Excuse”: Geoarchaeology and Zooarchaeology of the Little John Paleoindian Site, Alaska/Yukon Borderlands

David R. Yesner
University of Alaska Anchorage

Kristine J. Crossen
University of Alaska Anchorage

Norman A. Easton
Yukon College

Abstract

Permafrost deposits have affected archaeological excavations in interior and northern Alaska in numerous ways. Here we consider a new geoarchaeological context for Paleoindian sites in eastern Beringia: permafrost-shattered bedrock colluvium which has sealed deep loess deposits within swales between bedrock knobs. These loess deposits contain paleosols with early archaeological materials, including Nenana complex artifacts and Late Pleistocene megafauna. They are often underlain by additional permafrost. In order to discover such deeply buried deposits, it may be necessary to excavate through bedrock colluvium. Under such situations, “permafrost is no excuse.” These principles are illustrated by recent excavations at the Little John Paleoindian site in the Alaska/Yukon Borderlands.

Keywords: Beringia; Little John site; Nenana complex; Paleoindian archaeology; permafrost; Pleistocene megafauna.

Introduction

Numerous archaeological excavations in interior and northern Alaska have encountered permafrost conditions either prior to or during excavation, and have been forced to develop methodologies to confront that situation. Permafrost interacts with archaeology in two ways: by creating unique preservation conditions for organic materials, and by creating difficult conditions for excavation to retrieve those materials. In northern Alaska, conditions which allowed for the development of permafrost “freezers” for storing meat and other organic materials by Inupiaq people have also created conditions for organic preservation over periods of hundreds to thousands of years. Excavation in northern Alaskan coastal sites in areas of permafrost (e.g., St. Lawrence Island) often yields not only bone, ivory, and wood, but also food remains and rendered seal, whale, or fish oil, some of which still emits odors when newly exposed. Long-term preservation of such organic residues allows an additional source of materials for radiocarbon dating, although calibrated date corrections to account for the marine reservoir effect frequently add several hundred years to dates, whether produced by standard or AMS methods. Preservation of categories of material culture such as clothing is generally only possible under permafrost conditions, as was the case in the Utqiagvik project in the Barrow region. Human bodies have also preserved in ice, again in the Utqiagvik site, and on St. Lawrence Island. In the former case, soft tissue pathologies (e.g., pneumoconiosis due to soot inhalation) and even evidence of late-life pregnancy could be determined. In the latter case, tattooed symbols were visible, similar to those of the Pazyryk bodies, encased in ice within kurgans (traditional burial mounds) in the Altai and upper Yenisei River regions of westernmost Beringia.

All of these unique discoveries come at a methodological expense. Excavation through permafrost is difficult, and

requires the use of specialized archaeological techniques. Traditionally, until 30 years ago, sites were only excavated a few centimeters at a time as the surface was exposed and allowed to thaw. The use of such techniques meant that even some well-known Paleoindian site excavations in interior Alaska were abandoned because of difficulties or slowness of these procedures. The Utqiagvik project experimented with warm water thawing of the surface, and the gradual extraction of organic materials such as clothing from the ice. This technique was extremely successful, and has become the standard in recent years.

The results of ice on archaeological materials embedded in soft sediments such as loess (fine-grained glacial silt) are somewhat an issue of debate. While it is recognized that ice may preserve organic remains, it is also possible that higher permafrost tables result in a greater degree of cryoturbation, frost jacking, and displacement if not destruction of materials. For example, at the Broken Mammoth site near Big Delta in interior Alaska (Fig. 1), there is excellent preservation of organic material (bone, ivory, eggshell) in paleosols at the base of a 2 m loess deposit, dated from 9500 to 12,000 ¹⁴C yr BP (Fig. 2); this has been suggested by some to have been at least partly the result of a higher permafrost table in the Late Pleistocene and/or Early-to-Mid Holocene. However, in our view, this preservation is more likely attributable primarily to the calcareous nature of the loess and the depth of the loess, with the latter retarding the downward mobilization of acidic ions in the soil column as a result of rainfall percolating through the coniferous needle mat associated with the contemporary (2–3,000 year old?) closed spruce forest (Holmes 2001, Yesner & Pearson 2002). Today, there is no permafrost present at the Broken Mammoth site, although it is found both to the north of the site (in the vicinity of Richardson) and to the south (in Shaw

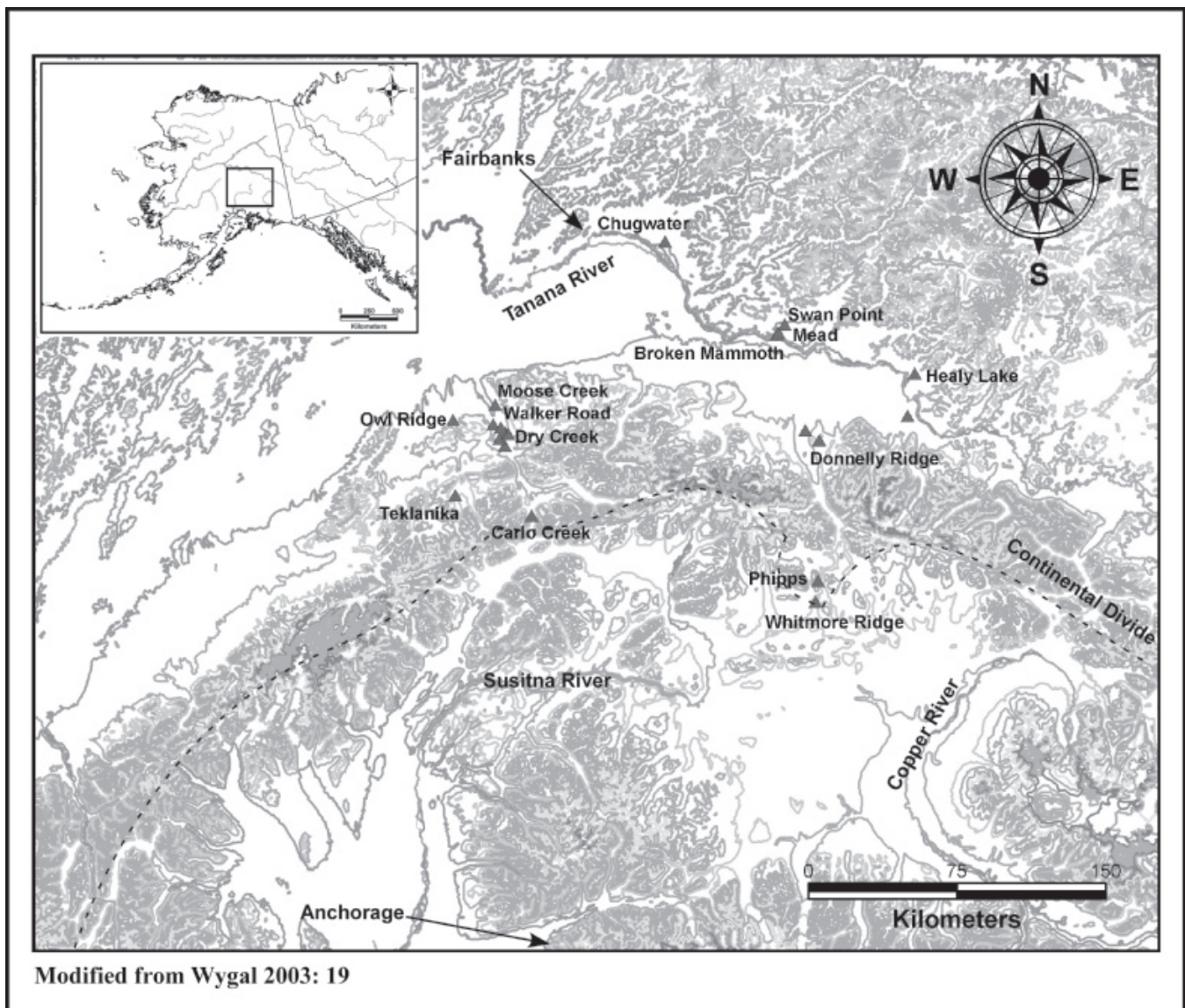


Figure 1. Early sites in Interior Alaska.

Creek Flats). This may be related to the fact that the site is on a south-facing slope, which has produced a microhabitat of relict Beringian flora in the site vicinity, including sage (*Artemisia* sp.). The result is that stratigraphic layers at the site are extremely flat lying, with even relatively thin (<5 cm thick) paleosols traceable horizontally over 30 meters or more. This suggests no previous experience with a higher permafrost table, a condition which differs strongly from Late Pleistocene/Early Holocene archaeological sites found elsewhere in interior Alaska (e.g., the Dry Creek, Walker Road, Moose Creek, Panguingue Creek, Owl Ridge, and Teklanika West sites in the Nenana Valley/Denali Park region; and the Chugwater and Gerstle River Quarry sites in the Tanana Valley region), all of which display evidence of cryoturbation, including distortion of archaeological stratigraphy (Powers & Hoffecker 1989, Hoffecker et al. 1993). Some of these sites also contain gleyed soils which are linked to reduced ions resulting from permafrost table saturation of the soil column.

The Little John Site, KdVo-6

Located just off the Alaska Highway, approximately 2 km due east of the International Boundary, the Little John Site occupies a knoll overlooking Mirror Creek, the easternmost tributary of the Tanana River basin. Unglaciated during the Wisconsin (Rampton 1971), this site contains evidence of human occupation from the Late Pleistocene to the recent past.

The western area of the site exhibits a geoarchaeological context similar to that of northern Alaskan sites or sites in the Tangle Lakes region of interior Alaska, with shallow, gravelly deposits entraining a basal loess layer at no more than 30–40 cm depth, directly overlying frost-shattered bedrock (West 1967, 1996). An archaeological component associated with this thin, shallow loess contains abundant microblades, burins on microblades, several core tablets, and irregular core fragments (although as yet no complete microcores). It also contains numerous scrapers and a limited bifacial industry, which may suggest that it be assigned

to the Northern Archaic or the “Late Denali complex.” Unfortunately, this area of the site is so far undated, due to a lack of datable organic material.

The eastern portion of the Little John site presents a completely different geoarchaeological context. In terms of paleogeomorphology, this portion of the site represents a swale between two bedrock knobs which has served as a sediment trap throughout the Late Quaternary. Here, a combination of frost jacking and gravitational processes has produced a series of colluvial episodes in which blocks of bedrock have become dislodged and transported into the swale. The last of these episodes, about 10–30 cm below surface, has produced a frost-shattered bedrock “pavement” in some areas which is extremely difficult to excavate through, but which may have helped preserve some of the underlying package of sediments. Underlying this colluvium is at least 30 cm to 40 cm of brunisol strata overlying 40 cm to 60 cm of (probably colluvially reworked) loess containing thick (10–30 cm), darkly stained paleosols. These paleosols also exhibit evidence of B horizon eluviation, indicative of gleyed conditions associated with a formerly higher permafrost table; a similar phenomenon can be seen at the Gerstle River Quarry site in the central Tanana valley to the NW. There are additional lenses of colluvial frost-jacked bedrock found within the loess, including some materials near the base of the loess that are Late Pleistocene or Early Holocene in age. There is also permafrost in some units at the base of the loess. The paleosols within the loess contain a diverse assemblage of culturally modified fauna, with AMS assays to date on three samples dating to 8890 \pm 50 RCYBP (Beta 182798), 9530 \pm 40 RCYBP (Beta 217279), and 9550 \pm 50 RCYBP (Beta 218235). None of these bone samples, however, was from the lowest paleosol stringer within the loess, from which will have dates available shortly from new, stratigraphically-lower bone samples.

Nenana complex materials

The artifact assemblage from the eastern area of the site is assignable to the Nenana Complex or Early Beringian Tradition, previously established for the lower Tanana Valley and Nenana Valley areas (Bever 2006, Easton & MacKay 2007). It contains four teardrop-shaped Chindadn points, two biconvex bifacial knives, other large bifaces, macroblades, a variety of scraper forms, waste flakes, and two chisel-like bone tools; some of these are directly associated with dated fauna (see below). These materials are all characteristic of Denali assemblages in interior Alaska, including both the Nenana and central Tanana valleys.

Zooarchaeological and paleoecological data

Fauna identified to date from the palesol complex (cf. Hutchinson et al. 2007) include the following taxa: bison (cf. *Bison priscus*), elk or wapiti (*Cervus elaphus*), caribou (*Rangifer tarandus*), moose (*Alces alces*), hare (*Lepus sp.*), swan (*Cygnus sp.*) and other as yet unidentified birds, rodents, and canids. This diverse faunal assemblage indicates a broad-spectrum subsistence strategy, similar to that

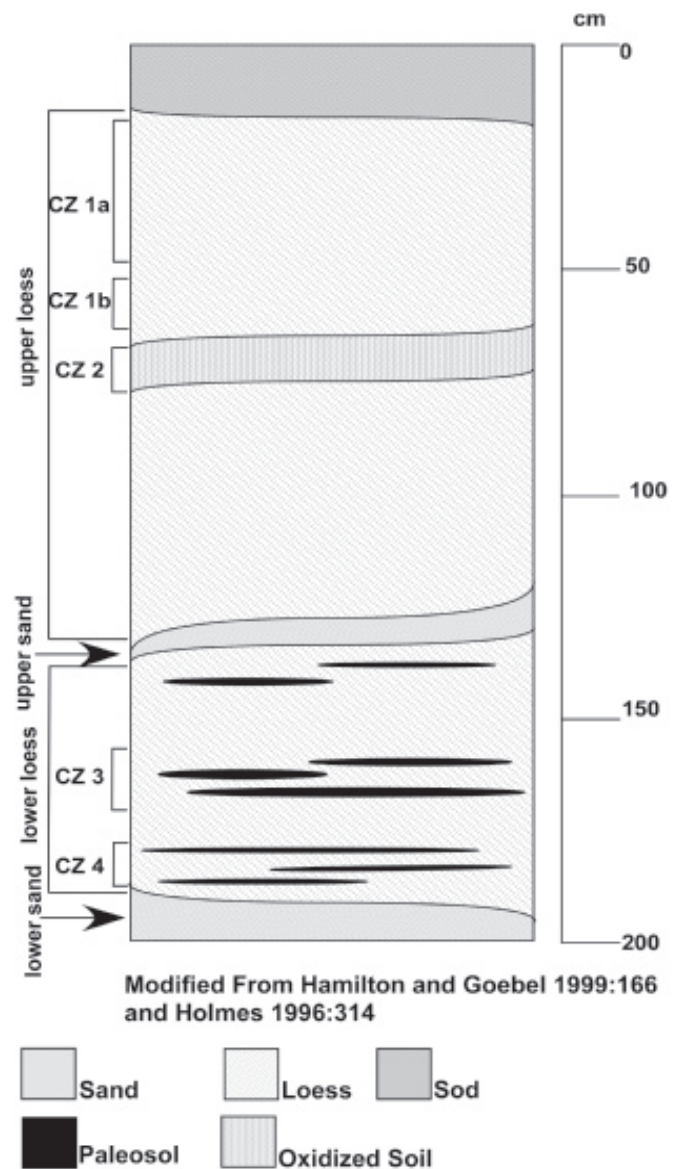


Figure 2. Broken mammoth profile.

displayed at a few other Late Pleistocene/Early Holocene sites in the central Tanana valley and Nenana valley with good bone preservation (Broken Mammoth, Mead, Swan Point, Dry Creek).

A core sample from a lake called *Yihkah Männ'* (~5 km from the Little John site) indicates that a transition from herb tundra (“tundra-steppe”) to shrub tundra occurred ~11,000 ^{14}C yr BP, perhaps some 500–1000 years later than in the Tanana Valley (MacIntosh 1997). Occupation of the Little John site may correspond with this transition (cf. Bigelow & Powers 2001, Hoffeecker & Elias 2007). The importance of this transition was to provide not only a more mesic, ameliorated environment for human occupation of the region, but also wood resources (especially with the appearance of *Populus* at ~11,000 ^{14}C yr BP) for hunting technology, dwellings, and other purposes. Simultaneously, these mesic conditions allowed soil formation and the entrainment of archaeological materials which might otherwise not have been preserved.

A successive eastward movement of Nenana and Denali culture bearers adapted to the subsistence opportunities offered by the shrub tundra environment of the Tanana Valley may explain the appearance of these complexes in the southwest Yukon. The Little John site extends the range of the Nenana complex to the far southeast edge of Beringia during the terminal Pleistocene.

Summary and Conclusions

Archaeological excavation in interior Alaska has provided data for Early Eastern Beringian archaeological assemblages (~12,000 to 9000 C¹⁴ yr BP) typically entrained in paleosols within deep loess units deposited on bedrock or river gravel terraces above river floodplains. In the middle Tanana Valley, deep, calcareous loess deposits have resulted in excellent faunal preservation at some of sites (e.g., the Broken Mammoth and Mead sites). New work at the Little John site in the upper Tanana Valley, Yukon Territory, extends the eastern Beringian record another 250 km eastward, and simultaneously provides a new geoarchaeological context within which early (Nenana Complex or Early Beringian Tradition) sites with excellent faunal preservation are found: fine-grained sediments deeply buried in swales between bedrock knobs above the valley floor. Discovery of additional such early sites may, however, be difficult, because such deeply buried deposits may be similarly covered by extensive sheets of colluvially-transported bedrock fragments, a fact of life in a region dominated by permafrost activity.

Acknowledgments

The authors would like to thank Daniel Stone and Rita Eagle for supervising the 2007 field season at the Little John Paleoindian site. The University of Alaska Anchorage and Yukon College provided joint funding for the 2007 excavations, with partial support for graduate students from IPY and EPSCOR initiatives. We also thank the White River First Nation, based in Beaver Creek, Yukon Territory, for permission to undertake excavations on their ancestral lands. The slogan of the Little John project is "Permafrost is no Excuse."

References

- Bever, M.R. 2006. Too little, too late? The radiocarbon chronology of Alaska and the peopling of the New World. *American Antiquity* 71: 595-620.
- Bigelow, N.H. & Powers, W.R. 2001. Climate, vegetation, and archaeology 14,000–9000 cal yr BP in central Alaska. *Arctic Anthropology* 38: 171-195.
- Easton, N.A. & MacKay, G. 2007. Early bifaces from the Little John Site (KdVo-6), Yukon Territory, Canada. In: R. Carlson (ed.), *Projectile Point Sequences in Northwestern North America*. Burnaby: Simon Fraser University Press (in press).
- Hoffecker, J.F., Powers, W.R. & Goebel, F.E. 1993. The colonization of Beringia and the peopling of the New World. *Science* 259: 46-53
- Hoffecker, J.F. & Elias, S.A. 2007. *Human Ecology of Beringia*. New York: Columbia University Press, 290 pp.
- Holmes, C.E. 2001. Tanana Valley archaeology circa 14,000 to 9,000 BP. *Arctic Anthropology* 38: 154-170.
- Hutchinson, V., Easton, N.A. & MacKay, G. 2007. *Faunal remains from the Little John Site (KdVo-6): An Early Holocene Assemblage from the Yukon–Alaska Borderlands*. Paper presented at the Annual Meeting of the Alaska Anthropological Association, Fairbanks.
- MacIntosh, G.D. 1997. *Paleoecology of the Scottie Creek District*, Beaver Creek, Yukon. M.A. Thesis. Department of Geology, University of Alaska Fairbanks.
- Powers, W.R. & Hoffecker, J.F. 1989. Late Pleistocene settlement in the Nenana Valley, central Alaska. *American Antiquity* 54: 263-287.
- Rampton, V. 1971. Late Pleistocene glaciations of the Snag Klutlan area, Yukon Territory. *Arctic* 24: 277-300.
- West, F.H. 1967. The Donnelly Ridge site and the definition of an early core and blade complex in central Alaska. *American Antiquity* 32: 360-382.
- West, F.H. (ed.) 1996. *American Beginnings: The Prehistory and Paleoecology of Beringia*. Chicago: University of Chicago Press, 576 pp.
- Yesner, D.R. & Pearson, G.A. 2001. Microblades and migrations: Ethnic and economic models in the peopling of the Americas. In: R.G. Elston & S.L. Kuhn (eds.), *Thinking Small: Global Perspectives on Microlithization*. Arlington, VA: Archaeological Papers of the American Anthropological Association 12: 133-161.

Stable Isotope Composition of Ice in Seasonally and Perennially Frozen Mounds

Kenji Yoshikawa

Water and Environmental Research Center, Institute of Northern Engineering, University of Alaska Fairbanks

Abstract

Ice-cored mounds develop in regions of continuous and discontinuous permafrost. Isotopic composition not only clarifies the growth process of the ice, but also indicates groundwater environments, such as open or closed environments and residual water fraction. Isotope stratigraphy of ice cores from the various types of frozen mounds (open- and closed-system pingos, palsas, icing blisters, frost blisters) can be applied to reconstruct the growth mechanism of each mound. An ice-cored mound in an open hydrological environment (such as an open-system pingo or a frost blister) froze relatively fast (enrichment of isotope ratio) at the top of the ice layer and remained an open environment during the main growth period. However, a major part of the ice (60% or more) was formed in a closed environment by continuous downward freezing. At the end of the growth period, a discontinued groundwater supply and slow freeze-up was followed by Rayleigh distillation. Palsas and closed-system pingos were in a semi-closed environment during the entire period.

Keywords: frost blister; icing blister; ice core; pingo; palsa; stable isotope.

Introduction

Ice-cored mounds are known for their unusual growth process and ice structure. However, a detailed physical mechanism for the formation of such mounds is still poorly understood. This study discusses the isotopic characteristics of ice from ice-cored mounds around Alaska, Canada, and Svalbard. Isotopic composition can indicate the groundwater source and physical environment of the ice development. The stable isotopic composition of ice formation is relatively well-studied for lake ice (Gibson & Prowse 2002), river ice (Gibson & Prowse 1999), and frost blister ice (Michel 1986), especially by Canadian scientists. Clark & Fritz (1997) reviewed well-documented surface and groundwater isotope studies. These well-documented isotopic works are useful in the study of ground ice processes. Isotope stratigraphy can be applied in reconstructing growth mechanisms with a variety of ice-cored-mound signals to understand differences between and the developmental process for these mounds. Definitions for each type of permafrost mound follow the terminology used by the Associate Committee on Geotechnical Research (1988).

Isotope study for permafrost mounds

The term *pingo* is an Eskimo word for a conical, more or less asymmetrical mound or hill, with a circular or oval base and commonly fissured summit. Pingos occur in areas of continuous and discontinuous permafrost, have a core of massive ground ice covered with soil and vegetation, and exist for at least two winters. A pingo has two general types of origin based on hydrological environments: open system (hydraulic) and closed system (hydrostatic). Mackay (1990) reported stable isotope results from one of the closed-system pingos at the Tuktoyaktuk Peninsula area. The isotope value slowly trends lighter, with a $\delta D/\delta^{18}O$ ratio of about 6. Yoshikawa (1993) reported oxygen isotope results from one of the Svalbard open-system pingos. The $\delta^{18}O$ values remain at -13‰ from top to bottom of the ice core except

where there is dilation crack ice.

Two basic differences between pingos and seasonal frost mounds are (1) the time necessary for development and (2) the stability of ice conditions. Seasonal frost mounds are less than a decade old because their ice is situated over (or near) the thawing zones. Therefore, ice conditions are unstable in frost mounds.

Icing mounds and icing blisters are formed by hydraulic pressure during winter. These ice formations are usually continuous during the winter. In High Arctic regions, some icing mounds have been reported to exist longer than a decade (Sharp 1942). Excellent stable isotope studies for seasonal frost mounds were reported by Michel (1986) and Clark & Lauriol (1997). Michel (1986) successfully collected frost blister isotope signals as an entire fractionation process at North Fork Pass, Canada. The present study examines several ice cores from the same site at North Fork Pass.

The purpose of this study is to identify and characterize groundwater discharge and freezing processes of the different types of ice-cored mounds in permafrost regions. The source of water, freezing rate, and groundwater pressure are fundamental parameters. Stable isotopes were applied to reveal these parameters in understanding the formation process of the mounds.

Methods

During 2001 and 2006, ice samples from locations in Alaska, Canada, and Svalbard were taken to examine three open-system pingos, one closed-system pingo, two palsas, four icing blisters, and four frost blisters. Table 1 and Figures 1 and 2 show the sample sites and their profiles. In Table 1, the numbers in column $\epsilon^{18}O_{i-w}$ are the values for fractionation relationships for ^{18}O in water-ice reactions. Ground ice was obtained using a portable drill core sampler (5-cm diameter stainless steel hollow Stein auger with hand or 1 kW electric drill). Obtained samples were analyzed

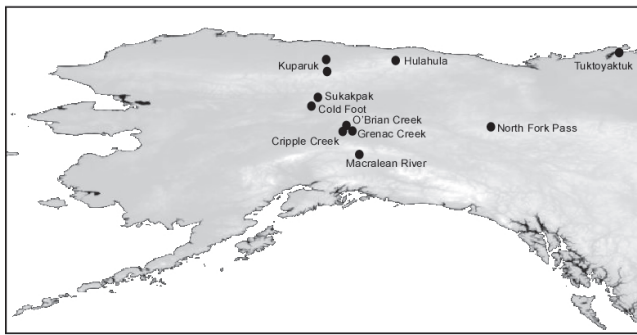


Figure 1. Sample sites in Alaska and Yukon, Canada.

for stable isotopes at the Alaska Stable Isotope Facility at the Water and Environmental Research Center (WERC), University of Alaska Fairbanks (UAF), using Pyrolysis Elemental Analysis-Isotope Ratio Mass Spectrometry (pyrolysis-EA-IRMS) DeltaV system. This method utilizes a ThermoFinnigan MAT high-temperature elemental analyzer (TC/EA) and ConFlo III interface with a DeltaV Mass Spectrometer. The pyrolysis reactor consists of a reaction tube packed with glassy carbon/graphite and silver wool. Other TC/EA conditions are as follows: Pyrolysis tube temperature 1450°C, He flow rate 120 mL/min, GC column 3 m 5Å mol sieve and GC oven temperature 75°C to 100°C. Water from ice samples in the amount of 0.2 µL are injected into the TC/EA with a CTC Analytics A200SE liquid autosampler. The sample is pyrolyzed into H₂ and CO gases, then separated chromatographically. These gases are then transferred to the IRMS, where the isotopes are measured.

The values $\delta^2\text{H}_{\text{V-SMOW}}$ and $\delta^{18}\text{O}_{\text{V-SMOW}}$ are reported in reference to international isotope standards. The typical quality control scheme involves analyzing laboratory working standards every seven replicate samples. Each sequence batch is calibrated to NIST standards to confirm quality assurance. NIST standards are analyzed in replicate throughout the sequence.

The freezing of water in a closed system is a good example of Rayleigh distillation (Fig. 3, closed circles). During the closed-system freezing process, ice is progressively enriched; however, such enrichment does not occur in an open-system environment.

Results

The series of the ice-core signature contain a unique isotope value that reveals freezing processes. Figure 4 shows perennial ice-cored-mound results. Closed-system pingos (Mackay 1990) and palsas show a similar gradually decreasing trend of oxygen isotopes. Thus, frozen ice at an early stage is heavier than that at a later stage. The isotopic structure of the palsa is considered a semi-closed hydrological environment, similar to a closed-system pingo. However, an open-system pingo does not have this trend. The values of $\delta^{18}\text{O}$ are nearly constant for all sampling points deeper than 2 m at different horizons except for the sample of the upper 2 m of ice. As the water of the open-system pingo continuously comes from sub-permafrost and/

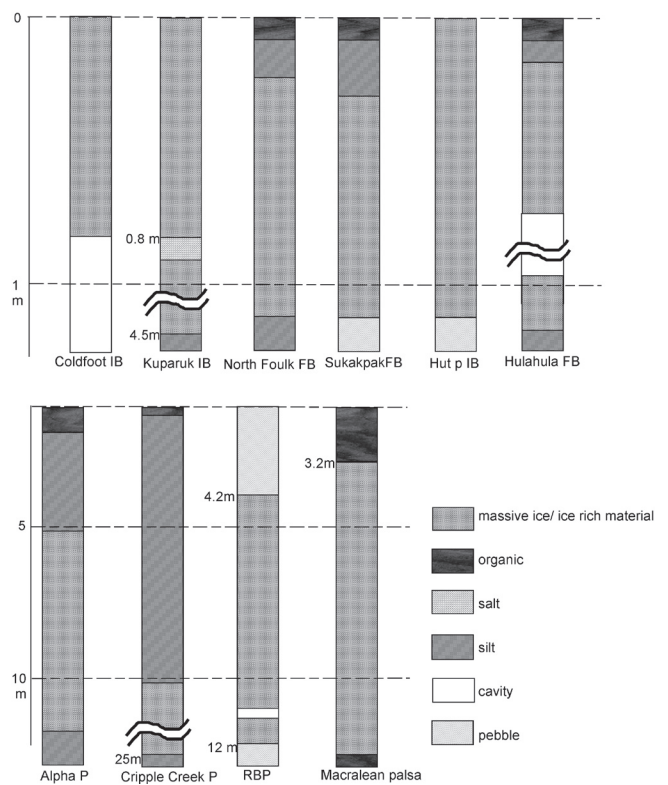


Figure 2. Drill logs for sampling frost mounds (FB: frost blister; IB: icing blister; P: pingo). Palsa samples taken include the organic layer up to 3.2 m, and focus on the ice layer below 3.2 m.

or a talik, the value of $\delta^{18}\text{O}$ does not change (ca. -16‰) when the water source is constant. However, the early stage of the open-system pingo has complicated signals. This upper layer indicates rapid freezing similar to the frost blister. Figure 5 shows the relationship between δD and $\delta^{18}\text{O}$ from various ice-cored mounds and spring water adjacent to the mounds. The local water sources are at the local meteoric water line (LMWL). The freezing process of the mounds follows Rayleigh-type evolution.

Figure 6 shows seasonal ice-cored mound results. All of the signals have similar trends. At the top of the ice, the isotope value is quickly enriched 2–3‰, which is the equilibrium fractionation factor to the ice. When freezing continues, ice formed from the depleted water preserves this trend of increasingly lighter oxygen isotope values. These mounds are produced through doming of groundwater due to hydraulic pressure. Once the dome shape is established, the downward freezing continues forming ice in a water-filled cavity under closed-system conditions. Some frost blisters are observed in a over several winters. Sukakpak frost blister (Fig. 6) is a good example. This ice core (2 m) indicated two times of enrichment.

During the winter of 2005–2006, one icing blister near Cold Foot (in the south-facing foothills of the Brooks Range) developed 2 m in height and about 30 m in diameter (Fig. 7). The details of ice grain size and C-axis measurements were observed. The upper 20 cm of the icing blister had overflow of white ice with very fine random crystals (<

Table 1. A list of the sampled frost mounds (FB: frost blister; IB: icing blister; OP: open-system pingo; CP: closed-system pingo).

site	type	ice sample thickness (m)	$\epsilon^{18}\text{O}_{i-w}$	$\delta\text{D}/\delta^{18}\text{O}$ slope	location	permafrost	MAGST	size (D/H)	reference
Hulahula	FB	1.4	-2.17	4.06	69° 9'50.86"N/144°35'19.46"W	cold	-7.79	20/4.5	
Sukakpak Mountain	FB	1.5	1.68	5.74	67°36'20.21"N/149°46'42.08"W	warm	-1.11	10/0.8	
Sukakpak Mountain	FB	1.5	3.3	6.13	67°36'20.21"N/149°46'42.08"W	warm	-1.11	12/1.1	
North Fork Pass	FB	1.5	-3.09	4.68	64°28'31.87"N/138°11'48.30"W	moderate	ND	15/1.5	Michel 1986
Coldfoot	IB	1.5	2.37	6.5	67°30'3.76"N/149°51'29.07"W	warm	ND	30/1.5	
Kuparuk	IB	0.6	-1.11	5.64	68°58'42.14"N/149°42'49.42"W	moderate	ND	5/0.5	
Svalbard	IB	1.2	0.08	na	78°10'34.55"N/16°16'50.57"E	cold	-5.7	8/1.2	
Cripple Creek	OP	4	1.7	5.46	64°48'33.66"N/148°2'48.60"W	warm	-1.00	55/10	
O'Brian Creek	OP	8	1.4	5.63	64°54'4.85"N/147°54'25.19"W	warm	ND	100/6.5	
Grenac Creek	OP	6.5	na	5.33	64°53'52.47"N/147°45'25.25"W	warm	ND	80/6	
Tuktoyakhuk	CP	na	na	7.34	69°40'24.32"N/130°46'16.84"W	cold	ND	50/12	Mackay 1990
Svalbard	OP	5	na	na	78°10'34.55"N/16°16'50.57"E	cold	-5.7	60/9.6	Yoshikawa 1993
Kuparuk	Palsa	1	na	6.78	68°47'21.72"N/149°56'12.61"W	moderate	ND	10/0.5	
Macralean	Palsa	6	0.32	na	63° 7'27.22"N/146°29'55.72"W	warm	ND	80/4.5	

The numbers for $\epsilon^{18}\text{O}_{i-w}$ are the values for the difference in ^{18}O between water (spring) and uppermost (oldest) ice. Permafrost conditions are classified by zero annual amplitude permafrost temperature: warm ($0^\circ \sim -2^\circ\text{C}$), moderate ($-2^\circ \sim -4^\circ\text{C}$), and cold ($< -4^\circ\text{C}$). Size is indicated by diameter (D) and height (H) ratio.

mm). The stratification extended from below the overflow ice to the base of the cavity, with three layers of different ice crystal size. The icing blister ice had two major joint thresholds by the iron extraction (Fig. 7b). This chemical extraction indicated discontinuity of the freezing process. Ice crystals have a candle-like, slender, elongated shape. There were several air bubbles inside the crystals (Fig. 7a). The long-axis orientation demonstrates the direction in which the crystals grew, which was vertically toward the freezing front. Once the dome shape was established, downward freezing stopped at least two times; however, the water-filled cavity froze under the closed system conditions (Fig. 6: IB Cold Foot).

Frost blisters from both the south- and north-facing foothills of the Brooks Range were sampled to the bottom of the ice. Drilling was performed June 2, 2004, at the Hulahula River frost blister to obtain an ice core. Below the 188 cm of ice and overburden was a large water-filled cavity 262 cm in height. This pressured cavity was developed by groundwater artesian water which continues to flow and discharge as a spring (Fig. 8). The isotope signals from this core did not reveal a Rayleigh distillation curve for ice that indicates open-system conditions during freezing in the water-filled cavity.

Sukakpak Mountain (in the south-facing foothills of the Brooks Range) and North Fork Pass, Yukon Territory, Canada, are two of the most well-studied areas for frost blisters (Brown et al. 1983, Michel 1986). For this study, six frost blisters were drilled at these two sites. The frost blisters at Sukakpak Mountain are considered to be at least 5–10 years old, but no more than 20 years old. The locations of previously studied frost blisters from the 1980s (Brown et al. 1983) were confirmed, but the frost blisters have completely disappear.

The grain size and shape of ice crystals in perennial and seasonal ice-cored mounds were different. Seasonal mound ice usually has small, elongated ice crystals, the average crystal size being 1–5 mm. Perennial mound ice has big crystals (30–200 mm), and there are fewer bubbles observed

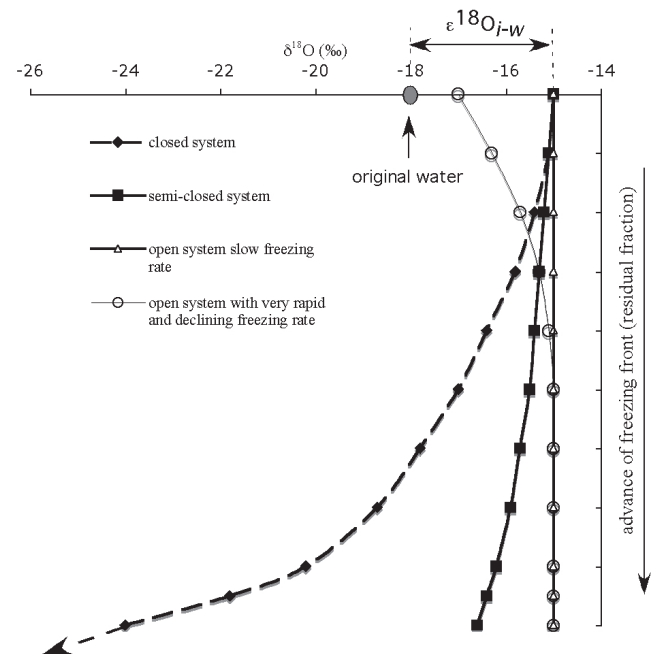


Figure 3. $\delta^{18}\text{O}$ versus freezing condition and water source effects (after Gibson & Prowse 1999).

in each crystal. Open-system pingos can be separated into two sections based upon grain size and isotope signals. The upper part of pingo ice is similar to that of a frost blister; the lower part consists of massive ice with bigger crystals.

The petrofabric analyses of icing mounds show that the c -axis orientations are normal for crystal elongations, with crystal growth along the basal plane in an a -axis direction (Pollard & French 1985). Mackay & Stager (1966) reported that in closed-system pingo ice beneath 5.5 m of overburden, the c -axis tended to point toward the pingo center. The isotope results also support development of ice formation similar to the petrofabric analyses results. The isotope analysis indicated the last residual water body in the ice core was located at the lower center of the mound. Ice-fabric analysis of the three samples taken from the basal pingo ice shows a changing c -axis pattern from the edge of the pingo

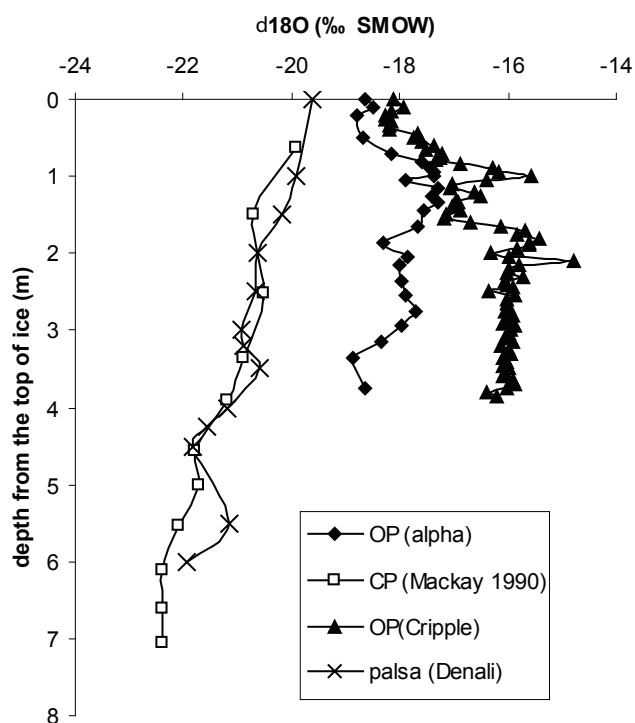


Figure 4. Oxygen isotope results versus ice thickness for perennial ice-cored mounds. Signals from an open-system pingo (OP) are quite different from those of a closed-system pingo (CP) and palsa.

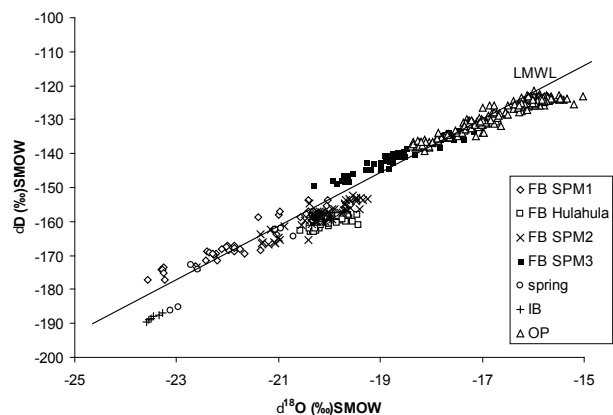


Figure 5. δD and $\delta^{18}O$ relationship from various ice-cored mounds in Interior Alaska. LMWL is from Fairbanks.

to its center. The lattice orientation apparently coincides with vertically oriented columnar ice crystals. However, usually there is a maximum of four *c*-axis concentrations at the center of the pingo, which indicates that the ice received a strong force after crystallization due to residual water. As a result, pingo ice has significant pressure at the center. The edge of the ice has only a small amount of this force (Yoshikawa 1993).

Discussion

One of the important processes of closed-system freezing is chemical extraction or enrichment. Mackay (1990) reported

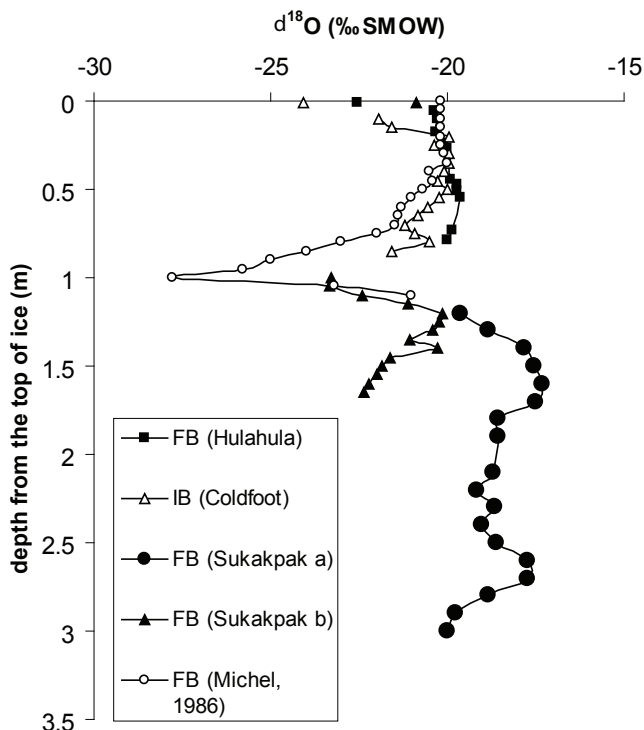


Figure 6. Oxygen isotope results against fraction (ice thickness) of the remaining ice on seasonal ice-cored mounds.

several layers of high ion concentrate in the closed-system pingo ice body. The isotope fraction analysis can detect this layer associated with delayed freezing (residual water) by the descending freezing point. Chemical extraction or salt precipitation during the freezing process is commonly observed in icing formation during the winter period. An icing blister from the Kuparuk River area, which was examined for this study, had developed only a week before the drilling sample was taken. The blister is 50 cm in height and 20 m in diameter. A highly concentrated and pressurized mineral layer was found 80 cm below the surface. This mineral layer is relatively easy to see from the air (Fig. 9). During core sampling 80 cm below the surface, about 5 cm of the cavity was found to have minerals with yellow fine form (bubbles) throughout, rising to the ground surface (Fig. 9, lower right). The majority of the minerals consists of carbon and calcium. Calcium and alkalinity concentrations indicate 14 times enrichment, and total carbon indicated 10 times. Isotope results follow chemical enrichments and indicated closed conditions for freezing both from the top down (Fig. 10, between 25–80 cm) and from the bottom up (Fig. 10, between 80–180 cm). The isotope fractionation demonstrates this freezing process. These enrichments are examined in terms of the Rayleigh distillation model (Fig. 11). The equilibrium-type curve of the fractionation factor (α) is 1.0028 for oxygen and 1.0206 for hydrogen (O'Neil 1968). However, the models show both oxygen and hydrogen, indicating the existence of non-equilibrium conditions ($\alpha = 1.006$ for oxygen, $\alpha = 1.030$ for hydrogen) (Fig. 11). The reason for the higher number in the fractionation factor (α)

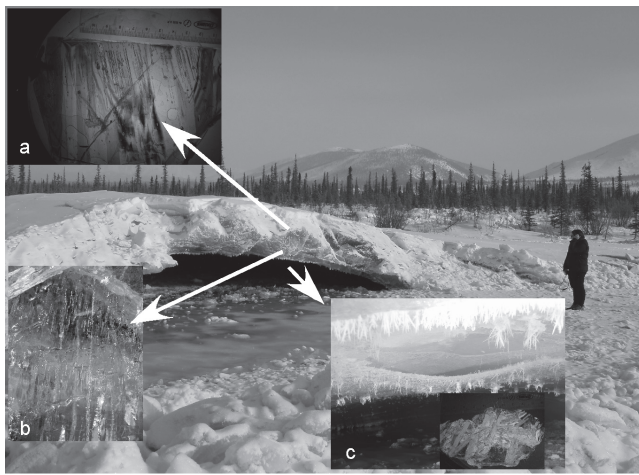


Figure 7. Icing blister transect profile near Coldfoot. Three layers of elongated ice crystals (a) with bubbles contained in a majority of the ice body. Iron-extracted layer (b) was observed in the lower 20 cm. Needle-shaped crystals develop at the bottom.

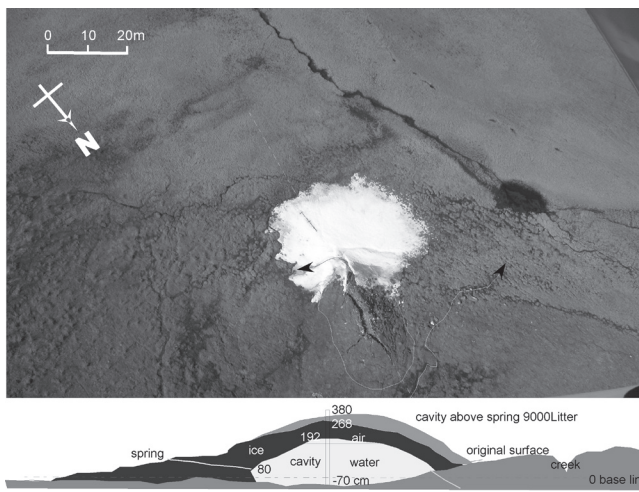


Figure 8. Diagram (lower) and aerial view (upper) of frost/icing blister at Hulahula River.

is unknown. It may be caused by the continual addition of water while freezing, resulting in a partially open system which will affect the fractionation.

The source water for this icing blister has high alkalinity (200–300mg/L) and was observed precipitating during the freezing process. This icing blister is not associated with hydraulic pressure from the groundwater; rather it is formed by hydrostatic pressure caused by freezing of the residual ion-rich water. There are a number of days that reach the freezing (thawing) point during spring months in this area. The unfrozen mineral-rich layer can associate with and move to an unfrozen layer.

Conclusions

Stable isotope signals from different types of ice-cored mounds (open- and closed-system pingos, palsas, icing blisters, frost blisters) were studied in relation to mound formation. An open-system ice-cored mound, such as an

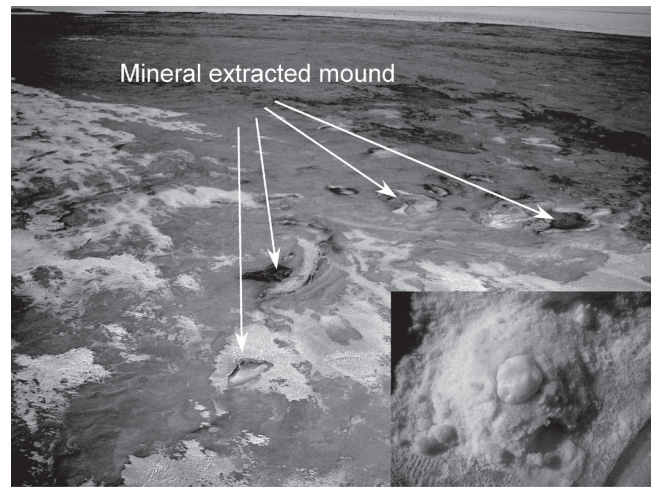


Figure 9. Salt extraction mounds (dark spots) are found at the Kuparuk River icing site during the spring period (April). After the drilling operation, highly concentrated minerals with yellow fine form rose to the ground surface (bottom right).

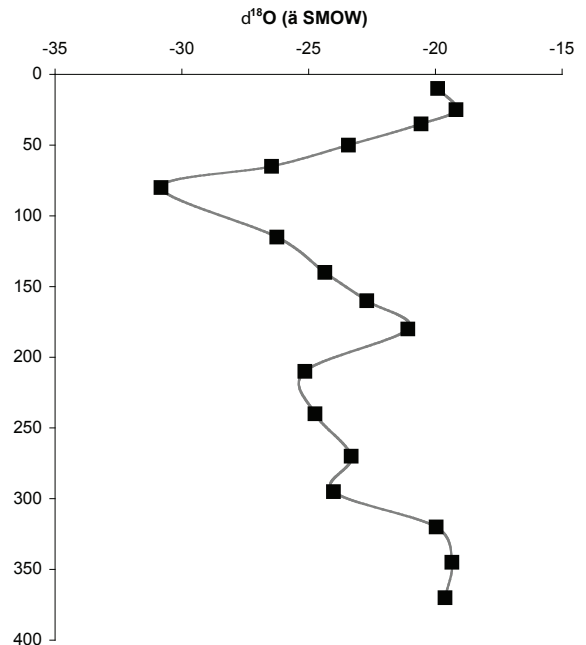


Figure 10. Strong (top down and bottom up) freezing process is observed between 30 cm and 180 cm depth. This is closed-system fractionation, where ice is progressively enriched under Rayleigh distillation of isotope signals and high concentrated ion layer at 80–110 cm.

open-system pingo or frost blister, freezes relatively fast with delayed enrichment of the isotope ratio at the uppermost ice layer. Once the stable freezing point is reached, the isotope value remains the same as that of an open environment.

The ice cores from palsas and closed-system pingos have signals of a semi-closed environment. The reservoir seems much bigger than the other closed-system mounds, but still follows Rayleigh distillation during freezing of the water. Icing blisters and frost blisters have very similar isotopic

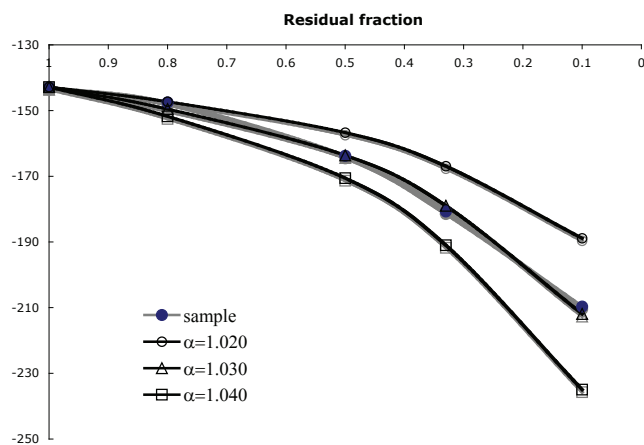


Figure 11. Sample value and calculated δD value for estimation of the fraction.

signals and ice structures. They develop (uplift) relatively quickly with a pressurized water source. The mound consists mainly of ice and water (cavity filling water). The water freezes downward following Rayleigh distillation. However, during the freezing process, especially with an icing blister, the chemical extraction involves dropping freezing point.

This study classifies the perennial and seasonal ice-cored mounds of four different stable isotope types by ice formation: 1) superimposed/crack ice, typically observed open-system condition; 2) upper part of frost blister, open system-pingo ice, rapid freezing with delaying enrichment; 3) open-system freezing ice, constant values of the isotope signals, and 4) semi-closed (or closed) freezing, following the Rayleigh distillation curve. Each of these isotope signals plays a critical role in revealing the growth mechanism of ice formation.

Acknowledgments

This project was funded by the National Science Foundation, Office of Polar Programs, Arctic System Science Program (ARC-0229705). We would like to thank Mr. Tohru Saito (University of Alaska Fairbanks), Dr. Atsushi Ikeda (University of Tsukuba), VECO Polar Resources for logistical support, and Tim Howe and other Water and Environmental Research Center staff members and students at the University of Alaska Fairbanks for help with laboratory analyses and field support.

References

Brown J., Nelson, F., Brockett, B., Outcalt, S.I. & Everett, R. 1983. Observations on ice-cored mounds at Sukakpak Mountain, southcentral Brooks Range, Alaska. *Proceedings of the Fourth International Conference on Permafrost, Fairbanks, Alaska, July 17–22*: 1983.

Clark, I.D. & Fritz, P. 1997. *Environmental Isotopes in Hydrogeology*. New York: Lewis Publishers, 328 pp.

Clark, I.D. & Lauriol, B. 1997. Aufeis of the Firth River Basin, Northern Yukon, Canada: Insights into permafrost hydrogeology and karst. *Arctic and Alpine Research* 29(2): 240-252. doi:10.2307/1552053.

Gibson, J.J. & Prowse, T.D. 1999. Isotopic characteristics of ice cover in a large northern river basin. *Hydrological Processes* 13: 2537-2548.

Gibson, J.J. & Prowse, T.D. 2002. Stable isotopes in river ice: Identifying primary over-winter streamflow signals and their hydrological significance. *Hydrological Processes* 16: 873–890. doi:10.1002/hyp.366.

Mackay, J.R. 1979. Pingos of the Tuktoyaktuk Peninsula, Northwest Territories. *Geographie physique et Quaternaire* 33: 3-61.

Mackay, J.R. 1990: Seasonal growth bands in pingo ice. *Canadian Journal of Earth Sciences* 27: 1115-1125.

Mackay, J.R. & Stager, J.K. 1966. The structure of some pingos in the Mackenzie Delta area, N.W.T., Ottawa. *Geogr. Bull.* 8: 360-368.

Michel, F.A. 1986. Isotope geochemistry of frost-blister ice, North Fork Pass, Yukon, Canada. *Canadian Journal of Earth Sci.* 23: 543-549.

Müller, F. 1959. Beobachtungen ber Pingos. *Meddelelser om Grønland*. 153: 1-127.

O’Niel, J.R. 1968. Hydrogen and oxygen isotope fractionation between ice and water. *Journal of Physical Chemistry* 72: 3683-3684.

Pollard W.H. 1988. Seasonal frost mounds. In: M.J. Clark (ed.), *Advances in periglacial geomorphology*. Chichester: John Wiley & Sons Ltd., 201-229.

Pollard, W.H. & French, H.M. 1985. The internal structure and ice crystallography of seasonal frost mounds. *Journal of Glaciology* 31: 157-162.

Seppälä, M. 1972. The term “palsa.” *Zeitschrift für geomorphologie* 16: 463.

Washburn, A.L. 1983. What is a palsa? In: H. Poser & E. Schunke (eds.), *Mesoförmern des reliefs im Heutigen periglazialraum. Gottingen, Mathematisch, physikalische Klasse, Drilte folge*, nr. 35, 34-47.

Yoshikawa, K., 1993. Notes on open-system pingo ice, Adventdalen, Spitsbergen. *Permafrost and Periglacial Processes* 4: 327-334.

Hydrologic Status of High Arctic Ponds in a Continuous Permafrost Environment, Somerset Island, Nunavut, Canada

Kathy L. Young

Geography Department, York University, Toronto, Ontario, Canada, M3J 1P3

Anna Abnizova

Geography Department, York University, Toronto, Ontario, Canada, M3J 1P3

Abstract

In 2004, a suite of ponds, 71 in total, situated in moraine, coastal, and bedrock-wetland terrains were surveyed, in order to assess their sustainability in a continuous permafrost, polar desert environment. Snow cover, ground thaw, water table, and water quality were measured. In 2005 and 2006, detailed hydrological studies were undertaken on a selection of these ponds. The 2004 results indicate that snow depth, melt, frost table, and water table variations exist between the ponds located in the different geomorphic settings. Electrical conductivity of water varied due to differences in Na^+ , Mg^{2+} and Ca^{2+} . The 2005 and 2006 results signaled the importance of pond substrate (e.g., texture, colour) in modifying ground thaw, vertical seepage, and evaporation rates. Terrestrial linkages of ponds to late-lying snowbeds, wet meadows, and streams sustain pond levels during dry, warm episodes, but not frost cracks which can divert water from ponds. Ponds in this extensive wetland might show a range of responses to future climate change.

Keywords: climate change; continuous permafrost; extensive wetland; High Arctic; ponds; wetland hydrology.

Introduction

Wetlands are important ecological sites in the High Arctic. They are often the only zones where sufficient grasses and sedges exist to supply northern ungulates, such as muskox and caribou, with sufficient grazing grounds. They also provide food and water for migratory birds and help to cleanse and store water. Permafrost is critical to their existence; it serves to maintain water tables near the ground surface and allows for the growth of hydric vegetation. Despite the ecological importance of wetlands, a limited understanding of their hydrology and chemical status still exists. Progress has been made in understanding small patchy wetlands lying in continuous permafrost terrain (e.g., Woo & Young 2003, Young & Woo 2003a, b), but less information exists about extensive wetlands. Woo & Young (2006) recognize three groups: periglacial polygonal areas (low-centered polygons, ice-wedge cracks), glacial terrain, and coastal zones. A recent study by Woo & Guan (2006) focused on the first type: tundra thaw ponds, lying within a polar oasis environment (warm/dry; see Woo & Young 1997). They found that linkages between ponds and the surrounding landscape were good at the time of snowmelt (shallow thaw), but connectivity dropped off with deep ground thaw and prolonged evaporation.

Here, an extensive wetland-complex, underlain by continuous permafrost and possessing a polar desert climate (cool/wet; see Woo & Young 1997) is examined. It is characterized by numerous ponds, lakes, wet meadows, streams, and dry ground, and encompasses a range of surfaces: glacial terrain, bedrock, and coastal zones. The region is considered ecologically significant to migratory birds (Latour et al. 2005), but a clear understanding of the area's present and future sustainability has not yet been achieved.

Here we report on the characteristics of the typical ponds situated in three broad geomorphic zones (moraine, bedrock, and coastal) in relation to several environmental factors (e.g., snow, sediment, frost, water tables, and water quality). Detailed hydrological studies conducted on a selection of these ponds (small to large in area) during 2005 and 2006 are useful in confirming and understanding these spatial patterns. Finally, our study provides an indication of how these ponds might respond to future climate change.

Study Area

The study area is located in an extensive low-gradient wetland complex situated on the southern shore of Creswell Bay, Somerset Island, Nunavut (72°43'N, 94°15'W). Continuous permafrost exists here, and active layers approach 0.40 m in boggy areas and about 1.0 m in sandy and gravelly zones. There are no continuous climate records from Somerset Island, but the area is considered to have a polar desert climate similar to Resolute, Bay, Cornwallis Island (200 km to the north) with its long, cold, dry winters and brief, cool, damp summers (Dyke 1983).

The study encompasses about 23 km², and the site contains two contrasting landscapes, the northern part being modified by beach and coastal processes and the southern section showing evidence of glacial and periglacial influence (Brown & Young 2006). Figure 1 provides an aerial photograph, depicting the general area. Letters indicate ponds in the main geomorphological zones (moraine, bedrock, and coastal). Ponds in the moraine area exist both in an upper plateau area (>40 m a.s.l) and at a lower elevation (c.a. 25 m) with the latter fed by a stream draining the upland. Lingering snowbeds are typical of the west bedrock ponds, while major and minor frost cracks running generally east-west across the landscape are typical in the coastal wetland zone (see Fig. 2).

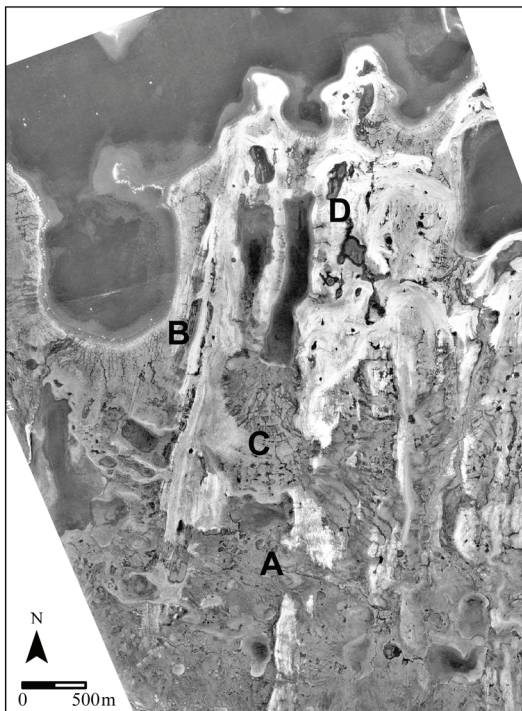


Figure 1. Aerial photograph of the study area: A-moraine zone; B-west bedrock zone; C-coastal area; and D-east bedrock zone. Creswell Bay is at the top of the diagram, and an Automatic Weather Station (AWS) is located near A.

In 2005 and 2006, at least three ponds (small, medium, and large) were selected from each zone for detailed study (late May to early August).

Methodology

Fieldwork 2004

Ponds dominate the landscape, so an earlier map of this region (Brown & Young 2006) was used as a guide to select the study ponds. In total 71 ponds ranging in size (small-median 510 m², medium-median 1,710m², and large-median 11,624 m²) were examined. Due to logistical constraints (traveling by foot), we selected eight of these ponds to conduct detailed snow surveys in early June 2004. These ponds represented the three main geomorphic areas: in total, four moraine ponds with one situated on the upper plateau; two coastal ponds; one west bedrock pond and one small east bedrock pond. Snow surveys (i.e., snow depths, density) were conducted at each pond site. A physically-based snowmelt model described by Woo & Young (2004) was used to model melt for the ponds in 2004. Meteorological information (net radiation, incoming and outgoing solar radiation, air temperature, relative humidity, precipitation, and wind speed and direction) obtained at the AWS was used to drive the model.

During the post-snowmelt period, a comprehensive survey of the 71 ponds was conducted from July 18–July 25. The ponds occurring in the main geomorphic regions: moraine,

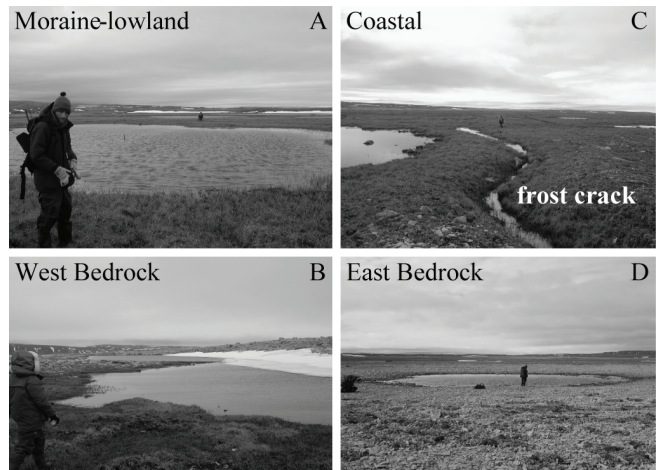


Figure 2. Photographs of typical ponds in the study area: A-Moraine; B-West Bedrock; C-Coastal and D-East Bedrock pond. Note frost crack adjacent to Coastal pond and late-lying snowbed beside the West Bedrock pond.

west and east bedrock, and coastal are examined here. Position and area of ponds was determined using a Garmin 12 XL GPS (± 3 m). The frost table divides the zones between thawed and frozen ground and provides an indication of water storage and seepage potential. Development of the thaw zone usually develops rapidly after the snow cover is depleted, but is also influenced by temperature gradients, surficial materials, and ice content. At each pond site, frost table position was measured by probing with a frost rod (± 5 mm) until frozen ground was encountered. Three measurements at each pond site were made: 1 m from shore, 1 in the center of the pond, and then 1 between the center of the pond and the shore. Water table, the height of the water level above or below the ground surface, was determined adjacent to frost table measurements with a metric ruler (± 5 mm). Estimates of water and frost tables for each pond at the time of sampling were averaged prior to analysis (see Fig. 4). Presence of plants (i.e., type and amount) was recorded, and a soil core of the near-shore sediment was obtained (250 cm³). This soil sample allowed volumetric soil moisture to be determined, and was used to assess organic content (loss on ignition), soil color, and grain size (Sheldrick & Wang 1993).

Water quality information is helpful in determining relative water sources and periods of dilution and drying. The pH and water temperature were measured with a Hanna #18424 ± 0.01 type meter. The electrical conductivity was measured with an YSI 30 ± 0.1 $\mu\text{S}/\text{cm}$ meter. A water sample was obtained from each pond, kept cool and returned to the York University Biogeochemistry Laboratory. Here the samples were analyzed for major cations (Ca²⁺, Mg²⁺, Na⁺, and K⁺) using a Spectra-10 Atomic Absorption Spectrometer, and laboratory standards and blanks were run to ensure quality control. The means and standard deviation of samples are reported. A Student t-test with unequal variance ($\alpha = 0.05$) was used to assess differences between ponds and aid in the discussion.

Fieldwork 2005, 2006

A detailed water balance framework was employed to investigate the hydrology of typical ponds (small to large) lying within the three broad geomorphic zones. Similar to 2004, snow surveys were conducted to determine initial pond and catchment's snow amount (in snow water equivalent units). Snowmelt was modeled and confirmed in the field with ablation measurements. In August 2004, perforated and screened water wells were placed along transects at each study site, dissecting both the pond and its catchment. Water tables were measured routinely in these wells at least every other day in 2005, 2006. Frost table was measured adjacent to these wells twice a week. Groundwater movement was estimated using the Darcy's approach. Soil moisture was measured both indirectly (Theta Probe) and directly (gravimetrically). Evaporation loss was determined using the Priestley-Taylor approach, with meteorological data supplied from the main AWS, and a portable AWS station which roved between the pond sites. Pond shrinkage was accounted for in the evaporation estimates. Streamflow both into and out of the moraine zone was estimated using the velocity-area approach. Retreat of a late-lying snowbed, which continued to supply moraine ponds with meltwater after the main melt period, was quantified on a daily basis. All ponds and their catchments were surveyed with a Total Survey Station in July 2005. In 2005 and 2006, no measurements were made of west bedrock ponds. Here, logistical and time constraints prevented these types of detailed measurements.

Results and Discussion

July 2004 was colder than 2005 and 2006, and much rain fell towards the end of July. In 2005, rain events were more frequent but of shorter duration than in 2006. Poor conditions during the early part of the season in 2006 resulted in greater rain and snow.

Environmental factors

Snowfall in the High Arctic usually occurs from September until May. Spatial variation in snow coverage and variations in the timing and duration of melt is important in the initiation of water for runoff, in defining the pattern and timing of ground thaw, and for providing waters for evaporation and/or infiltration.

Table 2 indicates the range of snow water equivalent (SWE, mm) for the study ponds in 2004. Initiation and duration of melt is also shown. For comparison, snow data from medium-sized ponds (2005, 2006) are also presented. Snow amount varies amongst the different pond types and within the same zones due to subtle differences in topography. However, snow amounts are still higher than that observed for a polar oasis environment (Woo & Guan 2006), but timing of melt and duration is generally later and longer. Hence, these ponds experience a polar desert climatic regime.

Ponds in the lee of slopes (e.g., a moraine pond-258 mm w.e.) can accumulate much snow, being sheltered from high winds. Other ponds on exposed ridges (e.g., west bedrock

Table 1. Summary of climatic conditions.

Year/Month	Ta (°C)	PPT (mm)	Thaw Days
2004			
July	3.8	37.7	117
2005			
June	1.2	8.1	36
July	4.8	31.8	145 (121*)
Aug.	5.0	6.7	15
2006			
June	0.6	47.0	15
July	5.6	21.2	138 (till JD 207)

*Thaw days up until JD 207 (July 26).

Table 2. Range of snow conditions for study ponds: SWE (mm), initiation and duration of melt; 2005 and 2006 data are for medium-sized ponds.

Year/Ponds	S W E (mm)	Initiation of Melt	Melt Duration (days)
2004			
Moraine	77-258	June 22 (JD 174)	6-9
Coastal	101-108	June 21 (JD 173)	8
East Bedrock	124	June 21 (JD 173)	9
West Bedrock	58	June 10 (JD 162)	11
2005			
Moraine	148	June 7 (JD 163)	10
Coastal	163	June 4 (JD 155)	9
East Bedrock	258	June 8 (JD 159)	14
2006			
Moraine	115	June 12 (JD 163)	10
Coastal	122	June 11 (JD 162)	9
East Bedrock	163	June 12 (JD 163)	11

pond-58 mm w.e) have less snow due to steady winds redistributing snow. Topographic depressions (east bedrock-124 mm w.e.) provide shelter from wind and are effective in capturing much snow. Table 2 indicates that snow accumulation patterns are typical from one year to the next, though variations in amount can exist. Melt duration also varies amongst the sites. Some pond sites with shallow snow become isothermal and melt out earlier (e.g. west bedrock, 2004) than other sites with much snow (e.g. moraine, east bedrock, 2004).

Soil texture and organic content are important factors in the evolution of ground thaw and storage capacity. Fine soils (e.g., silts/clays) with high organic contents can hold considerable ground ice and can store much water, delaying thaw as ice melts and energy is consumed in evaporation. Once vegetation and organic materials start to dry out, they can serve as an effective insulator delaying the thaw of ice further and even encouraging permafrost growth. While coarse soils can contain ground ice, these soils and areas with little vegetation or organic cover will generally experience enhanced thaw (e.g., Woo & Xia 1996; Young & Woo 2003a). Figure 3 provides an assessment of grain-size distribution and organic content of surveyed ponds (small to large).

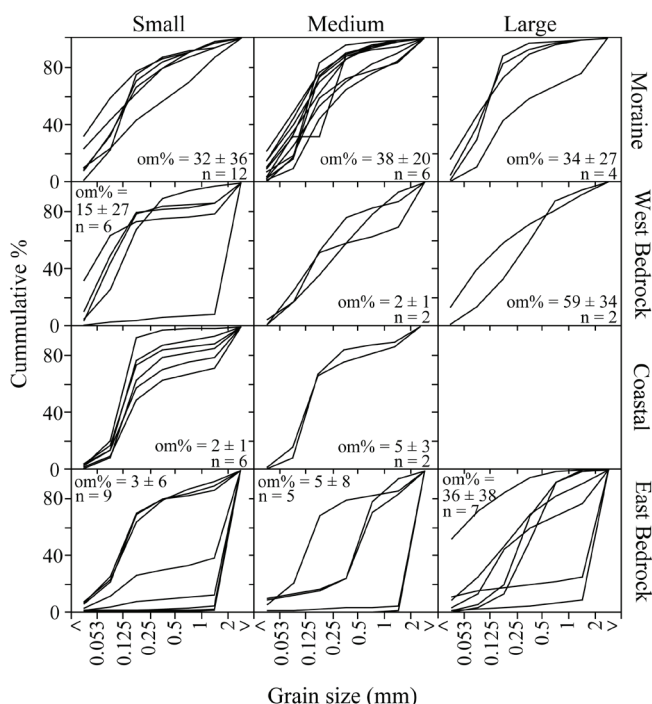


Figure 3. Grain size analysis and % organics (\pm standard deviation, and sample size [n]) of soil samples obtained at surveyed ponds (small to large).

Moraine ponds have a high amount of fines, while coastal ponds comprise fine sands and have the most uniform soil texture. West bedrock pond substrates are generally coarse, and soil texture is most variable in the east bedrock ponds. This reflects a longer period for these ponds to accumulate fine sediments through the dissolution of rocky material.

Moraine pond soils contain high organic contents, arising from extensive wet meadows with grasses and sedges surrounding most ponds in this area. In small and medium ponds (both bedrock types and coastal), organic percentages are low, reflecting the sparse vegetation coverage around these pond-types. However, as pond size increases, organic content also rises. The slow accumulation of fines in these areas eventually gives rise to a prolific wet-meadow community.

Environmental response

Figure 4 indicates a range of environmental factors which were measured over a short time span (mid-July to early August 2004). All ponds surveyed (small to large) are grouped here for analysis. A similar diagram for “small” ponds emerged, but these results are not reported here. The data indicate that we sampled more “large” east bedrock ponds, with some much larger than the other ponds.

The position of the frost table defines the position of the water table and can influence the presence of both surface and subsurface flow. Moraine ponds had the shallowest thaw (0.2 m) at the time of sampling, an observation which is supported by process studies in 2005 and 2006 (see Fig. 5). The frost table is deepest in the coastal ponds and is indicative of the coarser soils here and the lack of vegetation. Frost tables in the west and east bedrock ponds are all deeper than moraine

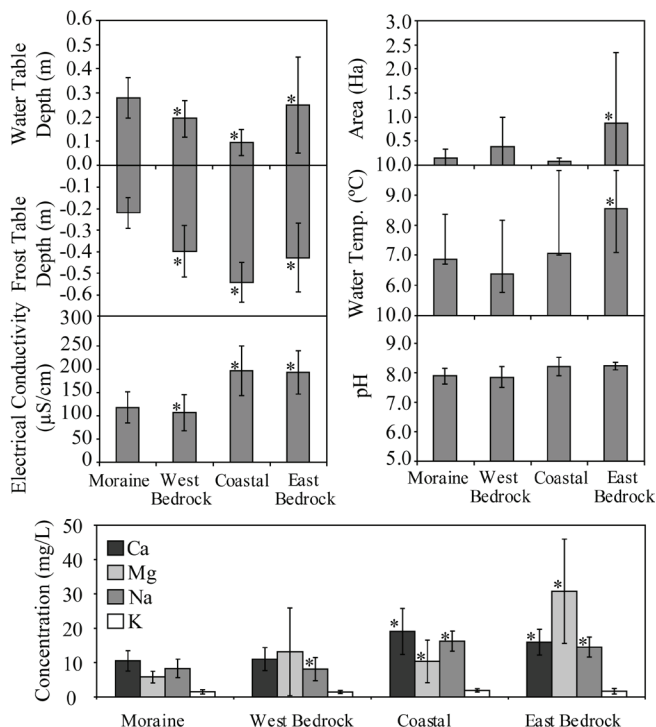


Figure 4. Selected environmental factors of all surveyed ponds. Significant differences of coastal and bedrock ponds to moraine ponds are indicated by an asterisk (*). Analysis is based on Student T-tests ($\alpha=0.05$). Standard deviation bars are plotted.

ponds, arising from their coarser substrate, which enhances deeper thaw and vertical seepage. Some east bedrock ponds also possess black (blue-green algae) substrates (e.g. 5YR 2.5/1). This dark surface triggers two processes. Radiation penetration through clear pond water can be absorbed by this dark surface ($\alpha = 0.10$, 2005), and the heat generated can then be used to warm the water and enhance evaporation, leading to lower water levels. It can also accelerate ground thaw and vertical seepage by elevating the thermal gradient at the water/substrate interface (see Oke 1987).

Water table is an important indication of the balance between water inputs and losses in a pond. High water tables may encourage runoff and sustain evaporation, and its persistence throughout a dry summer is indicative of lateral water inputs (i.e., surface and/or groundwater). Low water tables in the absence of rain can suggest an isolated system where vertical processes dominate; evaporation and/or seepage to the subsurface. Landscape alterations, such as erosion of a pond rim or an enlarged drainage outlet, may also encourage pond drainage and desiccation (e.g., Woo & Guan 2006).

Figure 4 indicates that water tables in the moraine ponds are greater than the other ponds. This is a reflection of the materials (greater % of fines and organics) which give rise to shallow frost tables, ensuring elevated water tables (Young & Woo 2003a). This area, especially the low-lying area, also received much water from a stream which drained the upland area. Several ponds in this area were also adjacent to late-lying snowbeds which continued to supply this area with meltwater long after the seasonal snowpack had disappeared (Fig. 5).

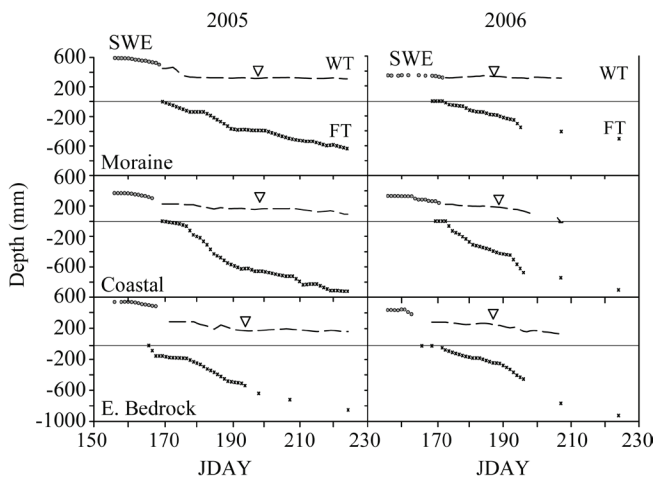


Figure 5. Seasonal patterns of frost and water table at the medium-sized ponds in 2005 and 2006.

Coastal ponds have the lowest water tables, owing to the higher proportion of coarser materials here and less vegetation, two factors which promotes deeper thaw and vertical water seepage. Frost cracks which dissect this zone serve as “sinks” during dry episodes, channeling water out of the ponds by setting up a hydraulic gradient (i.e., reversal of flow). Groundwater outflow from these ponds was estimated to be $1.3 \times 10^{-2} \text{ m}^3/\text{d}$ per unit m in 2005 and $2.8 \times 10^{-2} \text{ m}^3/\text{d}$ per unit m in 2006.

Water tables are higher in the east bedrock ponds. Many ponds occur in slight topographic depressions which are effective in trapping and sheltering much snow. Deeper snow prolongs melt, and delays ground thaw and evaporation losses. In warm years, ground-ice melt from the surrounding rocky catchment helps to maintain water levels (e.g., 2006).

All ponds are slightly alkaline owing to the underlying bedrock materials: limestone and dolostone. Water temperatures are the highest in the east bedrock ponds due to the dark substrate of most ponds here, which readily absorbs radiation and warms the waters. This pattern was similarly repeated in 2005 and 2006. Cooler water prevails at the other sites, which suggests frequent additions of cool water; i.e., stream water recharging ponds (e.g., moraine), and/or meltwater from late-lying snowbeds (e.g., west bedrock).

Electrical conductivity of the bedrock ponds and the coastal ponds are significantly different than the moraine ponds. Deeper thaw and shallower water tables ensure that waters have prolonged contact with the substrate, allowing additional solutes to be absorbed. Nearness to the sea allows salts and aerosols to be easily carried by sea breezes, fog, and rain, helping to elevate levels. Electrical conductivities are dampened in moraine ponds owing to high water tables, which are maintained by shallow ground thaw and the continual recharge by stream water and melting of late-lying snowbeds. West bedrock ponds have slightly lower electrical conductivities than the moraine ponds. Steady meltwater inputs from snowbeds, which lie in the breaks-of-slopes above many of these ponds, is effective in diluting pond waters.

Higher electrical conductivity values at the east bedrock

and coastal pond sites can be attributed to higher values of Ca^{2+} , Mg^{2+} , and Na^{+} at these sites. Elevated values of Ca^{2+} and Mg^{2+} reflect the bedrock type and greater ground thaw. Na^{+} is much higher at the bedrock ponds owing to its nearness to the ocean and occurrence of sea breezes. The west bedrock ponds are on the west side of a NE-SW bedrock ridge lying adjacent to an inlet of Creswell Bay (see Figs. 1, 2). Winds blew from the NW in 2004, about 40% of the time and likely were effective in transferring sodium into these ponds.

All sites had low values of K^{+} , less than 5 mg/L. This is a common occurrence, given that any available K^{+} is readily taken up by plants.

Response to climate change

The recently published ACIA (2005) suggests that arctic regions will be significantly affected by climate warming, with increases in precipitation (likely rainfall) and warmer temperatures. It is postulated that these ponds, despite occurring within a small landscape, will likely respond differently to these anticipated changes. For example, warmer and drier summers might mean the disappearance of many of the late-lying snowbeds which now feed several ponds both in the moraine and bedrock zones. These late-lying snowbeds are vulnerable to short-term changes in climate (Woo & Young 2003) and can disappear from the landscape, depriving downslope areas and ponds of water (Brown & Young 2006). Given the likelihood that these snowbeds will be vulnerable to shifting and changing climatic conditions, then it is probable that the electrical conductivity levels and solutes will also shift. The electrical conductivity levels of west bedrock ponds are now similar to moraine ponds largely due to the diluting effect of the late-lying snowbeds. However, with no additional meltwater inputs in the summer period, these waters will become more comparable to east bedrock ponds where electrical conductivity values are twice as high.

The ponds able to sustain themselves the best will be the low-lying moraine ponds. The occurrence of fine soils with much organics is able to promote ground ice and shallow thaw. Continual discharge of stream water into this zone, along with melting late-lying snowbeds, ensures elevated water tables, and buffers most of these ponds against warmer and drier summers.

Coarse and darkened substrates encourage ground thaw and vertical seepage. If water supplies are not sufficient to overcome losses, then many of these types of ponds might disappear. One other possibility is that emergent grasses may start to encroach and transform ponds into wet meadows. This process was observed for a small pond near Eastwind Lake, Ellesmere Island, in 2005. Others have noticed similar trends (e.g., Smith et al. 2005).

It is postulated that large ponds in all areas will likely sustain themselves in a warmer climate. They often have more fine material than smaller ponds and are linked to both wet meadow areas and smaller ponds which can funnel water into their watersheds during melt and rainfall events.

Summary and Conclusions

This pond survey undertaken in 2004 reveals the following:

(1) Within a polar desert wetland-complex, there can be significant differences in the types of ponds existing. Response of the ponds in terms of water table position, ground thaw, and water quality is strongly controlled by the substrate type, topography (level versus depression), and linkages with other water sources (streams, frost cracks). Ponds found in moraine areas tend to have fine substrates, higher water tables and shallower ground thaw than ponds occurring in coarse textured areas (e.g. coastal, east bedrock), unless additional sources of water are available (e.g., west bedrock ponds-meltwater from late-lying snowbeds). Higher conductivities and solute levels are common in the coastal and east bedrock ponds where water inputs are limited.

(2) It is likely in a warmer/drier climate that the ponds which possess a greater percentage of fine materials and organics and receive additional contributions of water aside from snowmelt and rainfall (e.g., stream water recharge, meltwater from late-lying snowbeds, groundwater inflow) will be able to sustain themselves in the future. It is the "isolated" ponds, shallow and poorly defined ponds (wind-swept), and/or ones with coarse and/or dark substrates which will be the most susceptible to demise.

(3) It is expected that the low-lying moraine zone of this wetland-complex will remain little changed; ponds receive multiple sources of water and have much fine sediments and organics to minimize thaw and maintain relatively high water tables. The coastal and east bedrock ponds, especially small ones, will be the most vulnerable. Years with low snowfall, little rain, and warm summers may see many of these ponds dry up and/or be overtaken by emergent grasses.

(4) The west bedrock ponds can be considered to be in "transition." Presently, they behave much like moraine ponds. Water tables are elevated despite coarse bedrock, with water being supplied by melting late-lying snowbeds. However, these snowbeds are vulnerable to warm/dry years and can be severely reduced in size or disappear completely from the landscape (Brown & Young 2006, Woo & Young 2006). In the long-term, climate warming will likely result in the disappearance of these snowbeds, and when this occurs, west bedrock ponds will begin to behave like the east bedrock ponds.

Acknowledgments

Funding for this project was provided by NSERC and NSTP. Logistical support from PCSP is gratefully acknowledged. Excellent field assistance was provided by Dan Thompson and Markus Anastasiades. Laboratory assistance by Jackson Langat is also appreciated. The authors are grateful to an anonymous reviewer whose suggestions have improved the paper.

References

- ACIA (Arctic Climate Impact Assessment). 2005. Impacts of a warming Arctic: Arctic climate impact assessment. Cambridge: Cambridge University Press, 1042 pp.
- Brown, L. & Young, K.L. 2006. Assessment of three mapping techniques to delineate lakes and ponds in a Canadian High Arctic wetland complex. *Arctic* 59: 283-293.
- Dyke, A. 1983. Quaternary geology of Somerset Island, District of Franklin. Geological Survey of Canada, Memoir 404.
- Latour, P.B., Machtans, C.S. & Beyersbergen, G.W. 2005. Shorebird and passerine abundance and habitat use at a High Arctic breeding site: Creswell Bay, Nunavut. *Arctic* 58: 55-65.
- Oke, T. 1987. *Boundary Layer Climatology* (3rd edition). London: Meuthen and Co., 435pp.
- Sheldrick, B.H. & Wang, C. 1993. Particle size distribution: Soil sampling and methods of analysis. In: M.R. Carter (ed.), *Canadian Society of Soil Science*. Boca Raton: Lewis Publishers, 499-511.
- Smith, L.C., Sheng, Y., MacDonald, G.M. & Hinzman, L.D. 2005a. Disappearing Arctic lakes. *Science* 308: 1429.
- Woo, M.K. and Xia, Z.J. 1996. Effects of hydrology on the thermal conditions of the active layer. *Nordic Hydrology* 27: 129-142.
- Woo, M.K. & Young, K.L. 1997. Hydrology of a small drainage basin with polar oasis environment, Fosheim Peninsula, Ellesmere Island, Canada. *Permafrost and Periglacial Processes* 8: 257-277.
- Woo, M.K. & Guan, X.J. 2006. Hydrological connectivity and seasonal storage change of tundra ponds in a polar oasis environment, Canadian High Arctic. *Permafrost, Periglacial Processes* 17: 309-323.
- Woo, M.K. & Young, K.L. 2006. High Arctic wetlands: Their occurrence, hydrological characteristics and sustainability. *Journal of Hydrology* 320: 432-450.
- Woo, M.K. & Young, K.L. 2004. Modelling arctic snow distribution and melt at the 1-km grid scale. *Nordic Hydrology* 35: 295-307.
- Woo, M.K. & Young, K.L. 2003. Hydrogeomorphology of patchy wetlands in the High Arctic, polar desert environment. *Wetlands* 23: 291-309.
- Young, K.L. & Woo, M.K. 2003a. Frost table development beneath patchy wetlands in a continuous permafrost, High Arctic setting. *Proceedings, Eighth International Conference on Permafrost, Zurich, Switzerland July, 2003*: 1265-1270.
- Young, K.L. & Woo, M.K. 2003b. Thermo-hydrological responses to an exceptionally warm, dry summer in a High Arctic environment. *Nordic Hydrology* 34: 51-70.

Recent Comparative Investigations and Monitoring of Permafrost of the Eastern and Western Qinghai-Tibet Plateau, China

Qihao Yu

State Key Laboratory of Frozen Soil Engineering, Cold and Arid Regions Environmental and Engineering Research Institute, Chinese Academy of Sciences, Lanzhou 730000, China

Kurt Roth

Institute of Environmental Physics, University of Heidelberg, Heidelberg D-69120, Germany

Huijun Jin

State Key Laboratory of Frozen Soil Engineering, Cold and Arid Regions Environmental and Engineering Research Institute, Chinese Academy of Sciences, Lanzhou 730000, China

Abstract

To further understand the degradation process of permafrost on the Qinghai-Tibet Plateau (QTP) and its environmental impacts, a Sino-German joint team conducted a pilot research project in the interior and on the eastern and western parts of the QTP. Preliminary results show that characteristics of surface landscapes have important influences on heat and mass transfer in soils. Major differences between cold ($<-4^{\circ}\text{C}$) permafrost in the Tianshuihai Lake region and warm ($>-1^{\circ}\text{C}$) permafrost in the interior and eastern QTP lie in their features of lithology, ice content, and ground temperature. The ecological environments in the Tianshuihai region have changed greatly in the past 30 years: large areas of vegetation have degenerated or vanished with considerable surface soil salinization. Extensive occurrences of small pingos, unsorted circles, sand wedges, and polygonal ground, and other periglacial phenomena were identified in the Tianshuihai area. Geophysical surveys indicate that topography, vegetation, and surface moisture conditions have substantial impact on the permafrost table and ground ice.

Keywords: environments; permafrost; Three Rivers Sources; Tianshuihai area; vegetation.

Introduction

The Qinghai-Tibet Plateau (QTP) is considered the third largest cold region on earth and is the source region of most major rivers in Asia (Zhou 2000). The source region of the Three Rivers (Yangtze, Yellow, and Lancang-Mekong) is in the interior and on the eastern part and feeds about 6×10^{10} m³ of water per year into the three rivers. The water flow volume in the source of each of the Three Rivers respectively accounts for 49%, 15% and 1% in the total volume of each river (Li et al. 2006). The cold-region hydrological processes, especially the modification of hydrologic cycling by climate warming, have attracted increasingly more public attention in recent years. To understand the degradation of permafrost and its environmental impact in the source regions of the Three Rivers in the interior and eastern QTP, as well as in the Tianshuihai region in the Western Kunlun Mountains on western QTP, a series of preliminary research and field investigations have been conducted.

The source region of the Three Rivers is in the continuous and discontinuous plateau permafrost zones, where cold climate and permafrost produce a special hydrologic cycle, cryogenic phenomena, and fragile ecological environments (as shown in Fig. 1). The changes in cold-region ecological environments have directly impacted the water storage. Major ecosystems, such as the paludified alpine meadows, grasslands, and steppes degraded markedly between the 1970s and 1990s (Cao et al. 2006). Degradation of permafrost and ecological environments represented by aeolian desertification has been accelerated since the 1990s because

of persistent regional droughts and overgrazing (Cheng & Wang 1998, Wang et al. 2000, Yang et al. 2004, Jin et al. 2007). In recent years, the aggravated ecological environment in the source region of the Yellow River has been seriously impacting its regional sustainable development, and could be one of the primary reasons for the decreasing runoff of the Yellow River from Qinghai Province, and for the increasing soil and water erosion (Kang 1996, Cheng et al. 1998). Thus, permafrost degradation modes and processes, and their ecological impacts are subjects of major research (Jin et al. 2006).

The distribution and degradation of permafrost in regions along the the Qinghai-Tibet Highway and Railway have been studied in more detail using meteorological measurements and the established long-term monitoring systems (Li et al. 2005, Wu et al. 2005, Jin et al. 2006, Cheng & Wu 2007). However, these observation systems are close to regions frequently and significantly impacted by human activities, and vast regions in the west and east remain unknown due to difficult access to and subsequent paucity of data.

The active layer is the crucial link between the climate and permafrost during the permafrost degradation process and can buffer climatic impact on permafrost. However, other than along the Qinghai-Tibet Highway, the heat, moisture, and mass transfer processes in permafrost soils had not been studied in detail (Li & He 1990, He 1991, Li et al. 1998). There also are remarkable differences between cold ($<-4^{\circ}\text{C}$) permafrost in the Tianshuihai Lake region in the western Kunlun Mountains and warm ($>-1^{\circ}\text{C}$) permafrost in the interior and eastern parts of the QTP.

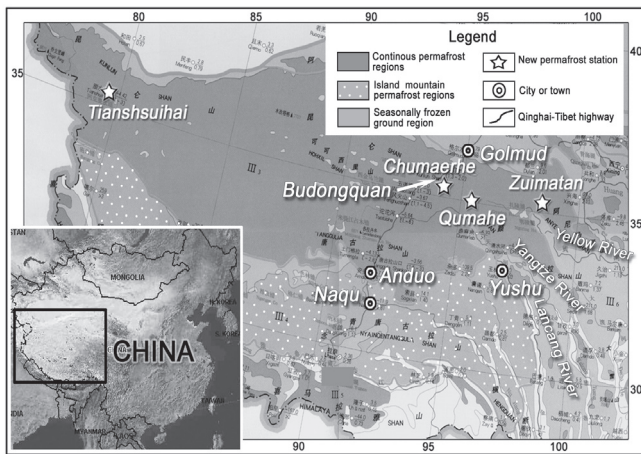


Figure 1. The extent of permafrost on Qinhai-Tibet Plateau in China and the positions of new permafrost stations established on QTP in the Sino-German joint research project.

Two joint teams from the Institute of Environmental Physics, University of Heidelberg, Germany, and the Cold and Arid Regions Environmental and Engineering Research Institute, Chinese Academy of Sciences conducted field investigations on the degradation of permafrost on the QTP and its environmental impacts in the source regions of the Three Rivers, in the east from August to October in 2006, and in the Tianshuihai Lake region in the Western Kunlun Mountains in August to September 2007. Three long-term monitoring stations were established in Zuimatan, Qumahe, and Chumaerhe along the access road from Yushu, along National Highway 214 (Xi'ning to Yushu section) to Budongquan along National Highway 109 (Golmud to Lhasa section) in 2006; a long-term monitoring station was established in Tianshuihai (Fig. 1). These stations are the very first in these regions.

Methods

Conventional exploratory methods such as hand-dug pits, water and soil sampling, in situ measurements of soil moistures and temperatures, and surface surveys were augmented with new geophysical investigation methods (Fig. 2), such as electrical resistivity tomography (ERT), new multi-channel ground penetrating radar (GPR), electromagnetic survey (EMS), and DC-resistivity (Arcone et al. 1998, Jared et al. 2003, Pettersson & Nobes 2003, Sass 2000, Schwaborn et al. 2000, Yu & Cheng 2003). They were applied for investigating the structures of the active layer, permafrost, cryogenic phenomena and vegetative differentiations, distribution of ground water tables and soil moistures, migration of salts, the physical properties of permafrost in the vicinity of the permafrost table, and the thickness of permafrost.

Results and Discussion

1) Based on investigations in the source regions of Three Rivers, three sites with representative landscapes were in-

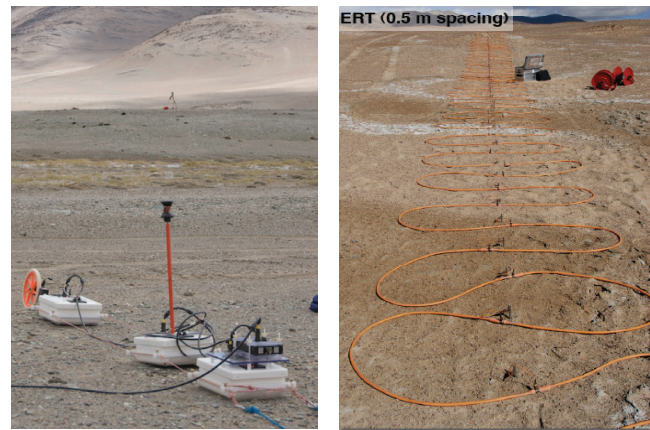


Figure 2. Some of the geophysical methods used in permafrost investigation in this project. The left is ground penetrating radar, and the right is electrical resistivity tomography.

strumented for soil and weather data as shown in Figure 1.

The landscape at the Chumaerhe Station is characteristic of barren land with sparse vegetation, but rich in ground water. The Qumahe Observation Plot is more densely vegetated and is covered by about 20 cm of peat layer. The Zuimatan Observation Site is sparsely vegetated, with saline soils and groundwater. The three sites were chosen along a gradient of the permafrost; with Chumaerhe in the continuous permafrost region, Qumahe in the patchy permafrost region and Zuimatan at the edge of the patchy permafrost region. In addition to measurements of wind direction and speed, air temperature, precipitation, and net radiation, there are profiles of temperature sensors and of CS616 and TDR100 soil moisture sensors down to the ice table at depths between 1.3 m and 2.8 m. The interval of the temperature sensors is 10 cm to 20 cm, and that of the moisture sensors is 20 cm to 40 cm. Furthermore, there are borehole temperature sensors from 3 m to 15 m with intervals between 0.5 m and 1.0 m (Table 1).

2) In Three Rivers source region and Tianshuihai Lake area, water and soil samples at different depths were collected in the active layer of various surface landscapes for studying the cryogenic phenomena and migration of salts.

Early data on ground temperatures at three stations in the east from early September to mid-October 2006 were read (Fig. 3). As indicated from the change in ground temperature, geomorphic units and surface landscapes have important influences on ground temperatures. The highest ground temperature is at the Chumaerhe Station, and the lowest is at the Qumahe Station. The temperature was always positive in this period, while the other two started freezing from the bottom. This shows that more vegetation in Qumahe tends to shade solar radiation onto the ground surface in summer, which helps in protection of permafrost by reducing surface heating (Fig. 3b). However, the freeze-up of ground is significantly later at the Zuimatan Station (Fig. 3a).

The Tianshuihai Lake region is the center of low air temperatures in China, and it could be the last region of permafrost degradation on the QTP in future (e.g. Li & Chang 1999). Continued research in this region is important

Table 1. The positions and observations of the comprehensive observation stations.

Stations	Chumaerhe (No.1)	Qumahe (No.2)	Zuimatan (No.3)	Tianshuihai
Characters	Discontinuous vegetation, shallow organic soil	Continuous vegetation, thick organic soil	Slight saline soil at surface, salty ground water	Slight saline soil at surface, no vegetation
Permafrost table	2.45	1.25	2.65	1.6
Ground water table	1.51	—	2.05	1.4
Latitude	93°57'E	94°47'E	99°08'E	79°32' E
Altitude	35°11'N	34°54'N	35°22'N	35°24'N
Elevation	4443m	4447m	4187m	4840m
Observations	Net radiation, precipitation, air temperature at depth 2 m, atmospheric pressure wind speed, wind direction ground temperature, soil moisture.			

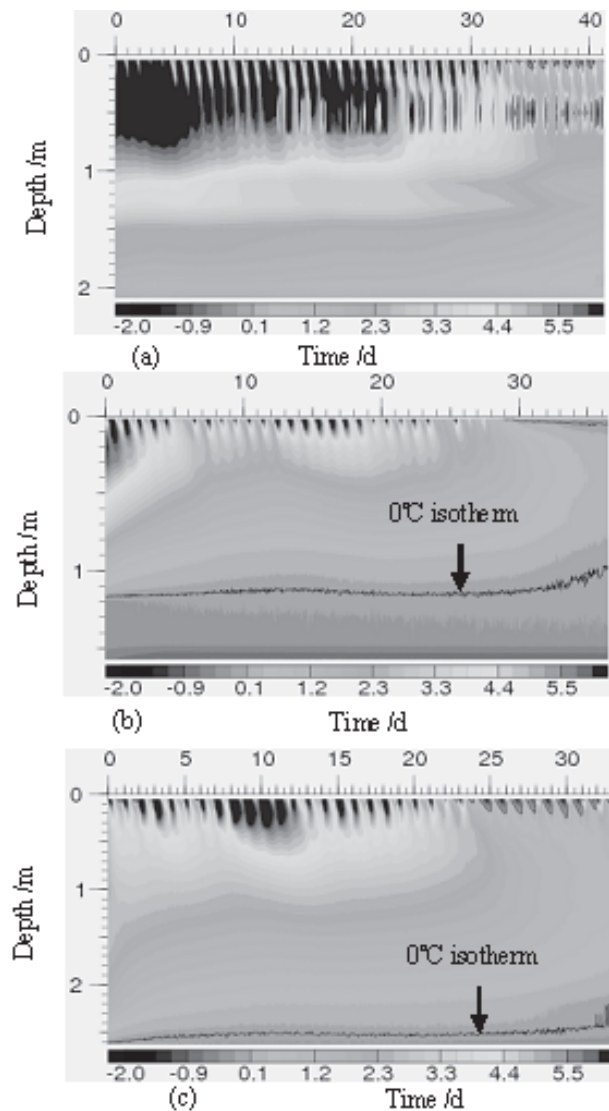


Figure 3. The ground temperature for the three weather stations are from Sept-Oct 2006. a. Chumaerhe station; b. Qumahe station; c. Zuimatan station.

for better understanding of existing permafrost conditions on the QTP as a whole and of its developing trends.

3) In the continuous permafrost region of Tianshuihai Lake area (79°26'E, 35°45'N, 4952 m to 79°59'E, 34°53'N, 5055 m) in Xinjiang Uygur Autonomous Region, although there is little precipitation, plenty of suprapermafrost water exists

at the opened areas in alluvial-fluvial plains, and the ground water table is only about 1.0 to 1.2 m. Most of the surface is sparsely vegetated or completely barren; the coverage is generally less than 5% even on the gentle slopes. The ground ice was probably formed in the relict permafrost during the Late Quaternary, and the drainage patterns and mass and salt migration control the distribution of vegetation and permafrost. During the last 40 years, vegetation has changed significantly. For example, there was thick vegetation, and wild animals (like bronco) were at Tielongtan (79°40'E, 35°03'N, 4958 m) in the 1960s and 1970s, but it is barren land now (Li et al. 1998).

4) The geology and permafrost along the Xinjiang-Tibet Highway (K513~K650) significantly differ from those in the interior and on the eastern QTP.

Along the 80-km-long segment of the highway on the Tielongtan fluvial plain, the active layer is gravelly and with high ice content, sometimes even consisting of ice layers with soil inclusions on the gentle mountain slopes. Along the 30-km-long Gytija section in the Tianshuihai Lake area, the soil consists of clayey sands with gravels or sandy clay. Dirty ice layers with volumetric ice content greater than 90% at depths of 1.0–1.4 m, are common.

5) At the Tianshuihai Lake region, permafrost is saline. The salinity of soils is low at the alluvial-proluvial fans; it is high on the gently sloped mountains, and even water at the low ground is salty. However, cryopegs were not detected during the investigation in the Tianshuihai area, whereas they are common on the northern QTP.

6) Extensive and various relict cryostructures, such as sand wedges and involutions, formed by soil movement during the freeze-thaw cycles were found in both research regions, and they have important influences on vegetation (Fig. 4) (Jin et al. 2007). There are many other periglacial phenomena, such as pingos and unsorted circles, and others, on the Tianshuihai Lake terraces and recently dried lakebeds (Fig. 5).

7) GPR exploration results show that landscape, vegetation distribution, and soil moisture content can significantly influence the permafrost table and ground -ice content. The coverage of small sand dunes, vegetation, and soil moisture conditions in or near ground surface are favorable for permafrost development and protection, while roads and tracks, as well as other human activities can lead to permafrost degradation (Fig. 6).

8) Geophysical methods, such as electromagnetic survey

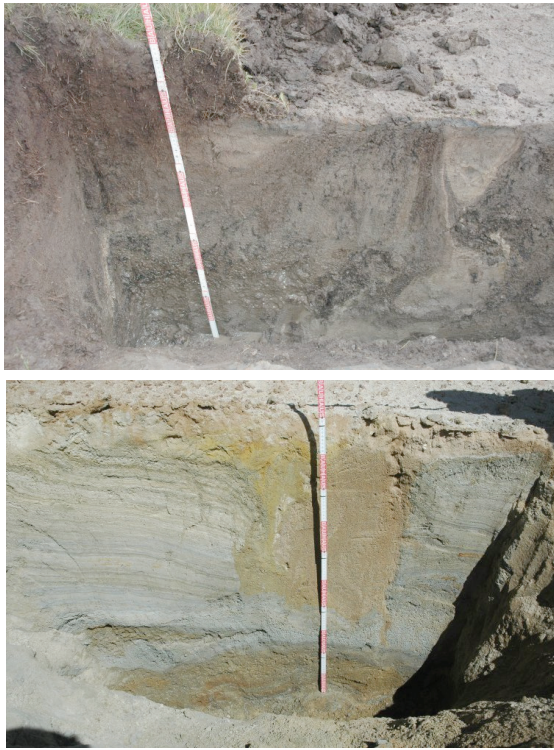


Figure 4. The upper picture is the involution found in river sources region, and the lower picture is the sand wedges found on the second Tianshuihai Lake terrace.

(EMS), can better reveal the thickness of permafrost, especially for permafrost thicker than 50 m.

The EMS investigation results show that the thickness of permafrost is about 100 m in the Tianshuihai Lake area. Mean annual ground temperatures measured at depths from 15 m to 20 m in boreholes are about -2°C to -4°C . Considering the ground temperature gradient, the survey data with EMS should have good consistency with the average ground temperature.

9) The latest geophysical techniques have proven indispensable and effective tools for field permafrost research, particularly for revealing subsurface soil structures, moisture conditions, and other properties of permafrost, using various geophysical methods or their combinations.

Detailed information on the processes in the active layer and on the spatio-temporal changes of the permafrost table, such as soil strata and moisture contents, depth of the permafrost or ground water table, and distribution of ground ice can be obtained using GPR (better with multi-channel GPR) and ERT. To reveal the permafrost table and base, ERT is better for shallow permafrost, but EMS is better for thick permafrost. Soil moisture and salinity have strong influences on applicability and results of geophysical methods. In general, the quality of GPR survey data from areas with high soil moisture and salinity are usually poor and difficult (if not impossible) to interpret; ERT, EMS and DC-resistivity can provide viable alternatives under this circumstance. In dry areas, the situation is reversed.

The data and samples from field investigation and



Figure 5. The landscape of cryogenic phenomena in Tianshuihai regions, the upper photo is pingo, the lower photo is unsorted circles.

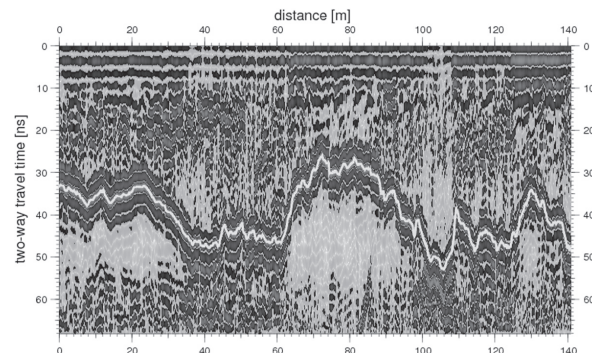


Figure 6. The investigation result of GPR in Tianshuihai.

monitoring are being studied. In the future, plans with emphasis on study of the western Kunlun Mountains will be executed. Further plans call for a north to south transect study through the permafrost province of the Tanggula Mountains and for construction of a third biodiversity transect in China, for the very important study of permafrost and cold-region ecology and biodiversity.

Acknowledgments

This research was supported by the Deutsche Forschungsgemeinschaft (DFG, Grant No. RO 1080/10-2), Chinese Academy of Sciences 100 Talents Project (Grant No. 0481811), National Science Foundation of China Outstanding Youth Foundation Project (Grant No. 40625004). Professor Yu Sheng, Dr. Ute W., Mr. Philip S., Mr. Tobias P. with

University of Heidelberg, and Mr. Xichai Pan, Mr. Zhi Wei, Miss Xiaoli Chang, Miss Ruixia He and Miss Yang Bai with State Key Laboratory of Frozen Soils Engineering, Cold and Arid Regions Environmental and Engineering Research Institute, Chinese Academy of Sciences also participated in fieldwork and some data analyses. Their assistance is thus acknowledged.

References

- Arcone, S.A., Lawson, D.E., Delaney, A.J., Strasser, J.C. & Strasser, J.D. 1998. Ground-penetrating radar reflection profiling of groundwater and bedrock in an area of discontinuous permafrost. *Geophysics* 63(5): 1573-1584.
- Cao, W.B., Wan, L. & Zeng, Y.J. 2006. Impacts of global warming on the eco-environments in the headwater region of the Yellow River. *Earth Science Frontiers* 13(1): 40-47 (in Chinese).
- Cheng, G.D. & Wang, G.X. 1998. Eco-environmental changes and causal analysis in the source regions of Yangtze, Yellow and Lancang-Mekong Rivers. *Advance in Earth Science* 13 (Suppl.): 24-31 (in Chinese).
- Cheng, G.D. & Wu, T.H. 2007. Response of permafrost to climate change on the Qinghai-Tibetan Plateau and its environmental impacts. *Journal of Geophysical Research* 112: F02S03.
- He, Y.X. 1991. The permafrost investigation with electronic sound method along Xingjian-Tibetan Highway. *Journal of Glaciology and Geocryology* 13(3): 255-259 (in Chinese).
- Jin, H.J., Zhao, L., Wang, S.L. & Jin, R. 2006. Modes of degradation and thermal regimes of permafrost along the Qinghai-Tibet Highway. *Science in China* 49 (D11): 1170-1183.
- Jin, J.H., Chang, X.L. & Wang, S.L. 2007. Evolution of permafrost on the Qinghai-Tibet Plateau since the end of the Pleistocene. *Journal of Geophysical Research* 112: F02S09 DOI: 10.1029/2006JF000521.
- Kang, X.C. 1996. Analysis on the climate change characteristics in the Tibetan Plateau regions. *Journal of Glaciology and Geocryology* 18(Suppl.): 281-288 (in Chinese).
- Li, L., Zhao X., Wang, Q.C. & Wang, Z.Y., 2005. Mapping and analyses of permafrost change in the Qinghai Plateau using GIS. *Journal of Glaciology and Geocryology* 27(3): 320-328 (in Chinese).
- Li, S.D. & He, Y.X. 1990. Features of permafrost in the West Kunlun Mountains. *Proceedings of Fourth National Conference on Glaciology and Geocryology*, Beijing: Science Press, 1-8 (in Chinese).
- Li, S.D., He, Y.X. & Wang, Y.X. 1998. Permafrost and periglacial environments in the Karakorum and Kunlun Mountains. *Glaciers and Environments in the Karakorum and Kunlun Mountains*. Beijing: Science Press, 181-215 (in Chinese).
- Li, X. & Cheng, G.D. 1999. A GIS-aided response model of high-altitude permafrost to global change. *Science in China* 42(D 1): 72-79.
- Li, Y.B., Yang, G.H. & Wang, D.X. 2006. Dryness (aridity) and wetness changes in climate during the recent decades in the source regions of Yangtze, Yellow and Lancang-Mekong Rivers. *Journal of Northwest Sci-Tech University of Agriculture and Forestry* (Natural Sciences) 34(3): 3-77 (in Chinese).
- Pettersson, J.K. & Nobes, D.C. 2003. Environmental geophysics at Scott Base: ground penetrating radar and electromagnetic induction as tools for mapping contaminated ground at Antarctic research bases. *Cold Regions Science and Technology* 37: 187-195.
- Sass, O. 2006. Determination of the internal structure of alpine talus deposits using different geophysical methods (Lechtaler Alps, Austria). *Geomorphology* 80: 45-58
- Schwamborn, G., Rachold, V. & Schneider, W. 2000. Ground penetrating radar and shallow seismic-stratigraphy and permafrost investigations of Lake Nikolay, Lena Delta, Arctic Siberia. In: *Proceedings, 8th International Conference on Ground Penetrating Radar*. Washington DC, USA: SPIE-The International Society for Optical Engineering, Vol. 4084: 783-789.
- Wang, G.X., Sheng, Y.P. & Cheng, G.D. 2000. Eco-environmental changes and causal analysis in the source regions of the Yellow River. *Journal of Glaciology and Geocryology* 22(3): 200-205 (in Chinese).
- Wu, Q.B., Lu, Z.J. & Liu, Y.Z. 2005. Permafrost monitoring and its recent changes on the Qinghai-Tibet Plateau. *Advances in Climate Change Research* 1(1): 26-28 (in Chinese).
- Yang, J.P., Ding, Y.J., Chen, R.S. & Sheng, Y. 2004. Permafrost change and its effect on eco-environment in the source regions of the Yangtze and Yellow Rivers. *Journal of Mountain Science* 22(3): 278-285 (in Chinese).
- Yu Q.H. & Cheng G.D. 2003. The progress of permafrost investigation with geophysical methods in China. In: M. Phillips, S.M. Springman & L.U. Arenson (eds.), *Proceedings, 8th International Conference on Permafrost, 21-25 July 2003, Zurich, Switzerland*. Lise, Abingdon, Exton, PA, Tokyo: A. A. Balkema Publishers, 1271-1276.
- Zhou Y.W., Guo D.X., Qiu G.Q. & Cheng G.D. 2000. *Geocryology in China*. Beijing: Science Press, 37-45 (in Chinese).

Severity of Climate Conditions in the Russian Federation

S. I. Zabolotnik

Melnikov Permafrost Institute, SB RAS, Yakutsk, Russia

Abstract

This paper evaluates the severity of permafrost and climate conditions and the distribution of permafrost in the Russian Federation. It presents a permafrost and climate severity map of the Russian Federation, drawn on the basis of long-term air temperature records from over 3000 weather stations. The map delineates 6 environmental-climatic zones at a 1250°C·day interval. The mapping shows that the most extreme conditions occur north of 60°N latitude in Yakutia, where the so-called Cold Pole of the Northern Hemisphere is located, and in the adjacent parts of Krasnoyarsk Krai and Magadan Oblast. The permafrost of these regions has the lowest temperatures and largest measured thicknesses. Harsh conditions exist in the remainder of these provinces, in Chukotka, northern West Siberia, and the adjacent Arctic islands. The least cold areas are located in the southwestern part of European Russia where only seasonal freezing of soils is observed and no permafrost exists.

Keywords: air freezing index; climatic conditions; permafrost.

Introduction

The Russian Federation extends across the whole of northern Asia and much of north-eastern Europe. Because of its northern location, Russia has a cold climate and widespread permafrost which underlies about 65% of the country (Shepelev & Shatz 2005). Permafrost is a natural integral indicator of environmental and climatic conditions. The frozen ground greatly influences human life and activities. For example, the existence of ground ice poses many engineering problems for the construction and maintenance of buildings and facilities; the great thicknesses of permafrost, reaching 1000–1500 m in Yakutia, make water supplies difficult to obtain; the development of cryogenic processes require additional measures and costs for agricultural developments. In view of these harsh conditions, there is a continuing need for comprehensive appraisal of the natural environment in which humans live and work. Such assessment requires an aggregate indicator that would be able to measure both the permafrost conditions and the extremity of the environment.

At the first stage, the indicator selected was the degree of climate severity since permafrost is a product of climate, and its formation, distribution, temperature, and thickness largely depend on the intensity and duration of winter cold. It is defined as the sum of negative (below 0°C) air temperatures during the year (air freezing index), which was used as a basic mapping criteria. Then, the climate severity index was correlated with the distribution and type of frozen ground within the identified zones.

The climate severity zonation of Russia has been an issue for a long time. The problem remains unsolved and is still much debated.

The first subdivision of Russia into the regions of the Far North and territories equated to it was undertaken in 1932 in order to stimulate industrial development of the northern and remote eastern regions by providing incentive payments. The list of Far North areas included the Kola Peninsula, Murmansk Okrug, Yakut Autonomous Republic, Kamchatka

Oblast, as well as the Okhotsk, Koryak, and Chukotka Okrugs of the Far East Krai.

This list has been continuously revised by adding more areas. At present, 28 federal units are categorized as the regions of the Far North and equivalent areas and 41 units use regional coefficients. In 2002, the additional burden on federal and local budgets for the cost of “non-northern” territories reached 65 billion rubles (Zhukov 2005). The regions where employees are entitled to northern allowances (0% to 80% increase to wages depending on the length of employment) or regional coefficients (fixed regional rates of extra wage payment) now comprise more than 88% of the total area of the Russian Federation.

Huge financial expenditures for extra wage payments in the federal units, which do not incorporate areas with the far northern and equivalent regions status, generated a need to improve the labour compensation system and to introduce changes into the current legislation. The State Duma Committee for North and Far East Affairs resolved to revise existing criteria and to develop a science-based system for assessing living conditions. For this purpose, an interdepartmental working group was established including representatives from regional governments and parliaments, as well as those from relevant research institutions, including the Melnikov Permafrost Institute at Yakutsk.

State of the Problem

Some work on this topic was done in 1998, when the Federal Ministry of Economy and Trade together with the Institute of Geography Russian Academy of Sciences (RAS), and the Institute of Economic Problems, RAS Kola Scientific Centre devised a methodology for environmental and climatic zonation of Russia. Much consideration in this document was given to zonation criteria.

Earlier, the Institute of Geography proposed “a new version of the method that takes into account both zonal and azonal factors affecting the selection of indicators and criteria of extremity of environmental and social conditions



Figure 1. Zonation of environmental and climatic conditions affecting human life with consideration of azonal factors, Northern and Eastern Russia (after Zolotokrylin et al. 1992). I – absolutely unfavorable; II – extremely unfavorable; III – unfavorable; IV – relatively unfavorable; V – favorable.

of life” (Zolotokrylin et al. 1992). The new scheme was applied for zoning and mapping the Russian North and East (Fig. 1). Four unfavorable zones were distinguished in this map, based on a large number of indicators. However, analysis of the final product gives rise to many questions. For example, why are the populated centers with very different environmental conditions which show a range of 11°C in mean annual air temperature, t (*USSR Climate References 1964–1967*) placed into the same extremely unfavorable zone (zone II)? This zone includes Murmansk ($t = +0.3^{\circ}\text{C}$), Salekhard ($t = -6.4^{\circ}\text{C}$), Turukhansk ($t = -7.0^{\circ}\text{C}$), Yakutsk ($t = -10.3^{\circ}\text{C}$), Magadan ($t = -4.7^{\circ}\text{C}$) and Palana in Kamchatka ($t = -2.8^{\circ}\text{C}$). Similar examples can be found for other zones. The difference in living conditions among these populated centers is obvious and needs no comment.

The understanding that “the map was inadequate in reflecting the azonal factors that affect human life, such as strong winds, high humidity, frequent fogs in coastal areas, paludification, and others” (Krenke et al. 2001) caused a need for further work. The author analyzed seven bioclimatic indices, applied clothing insulation and seasonal freeze and thaw depths as azonal factors, and adjusted the zone boundaries in relation to geobotanical and permafrost physiographical boundaries. As a result, a new map of unfavorable zones was produced (Krenke et al. 2001). This map also has shortcomings. For one, the northernmost absolutely unfavorable zone (I) was significantly extended

to the south to include the Okhotsk coastal areas with Ayan ($t = -2.7^{\circ}\text{C}$ to -3.3°C) and all the localities listed above except the coldest one, Yakutsk. All these localities were within the extremely unfavorable zone (II) of the earlier map (see Fig. 1).

The usefulness and necessity of the multiple-factor taking into account different environmental parameters is beyond question. However, these two maps seem to have over-estimated the role of secondary parameters, leading to such results. In order to avoid misjudgments in future, it is necessary to re-examine and re-define the significance of each comparison factor.

A few such attempts were made by Gavrilova et al. (2003, 2004). Building on the earlier works, they proposed “the number of days below 5°C ” as “an additional criteria of nordicity.” The results obtained were reflected in two maps: “Climate and Economic Subdivision of the North” (Gavrilova et al. 2003) and “Zonation of the Russian North” (Gavrilova et al. 2004). These maps, however, take no account of such important factors as the length of a period of extreme cold temperature (e.g., below -40°C). As a result, the later map (Gavrilova et al. 2004) places the northern part of the Kola Peninsula with the ice-free port of Murmansk where winters are as mild as in Moscow (long-term mean winter temperature, t_{win} is -6.8°C to -7.0°C at both localities (*USSR Vol. 2 1965*, *USSR Vol. 8 1964*) into the absolute unfavorable (Arctic) zone (1). Palana in Kamchatka,

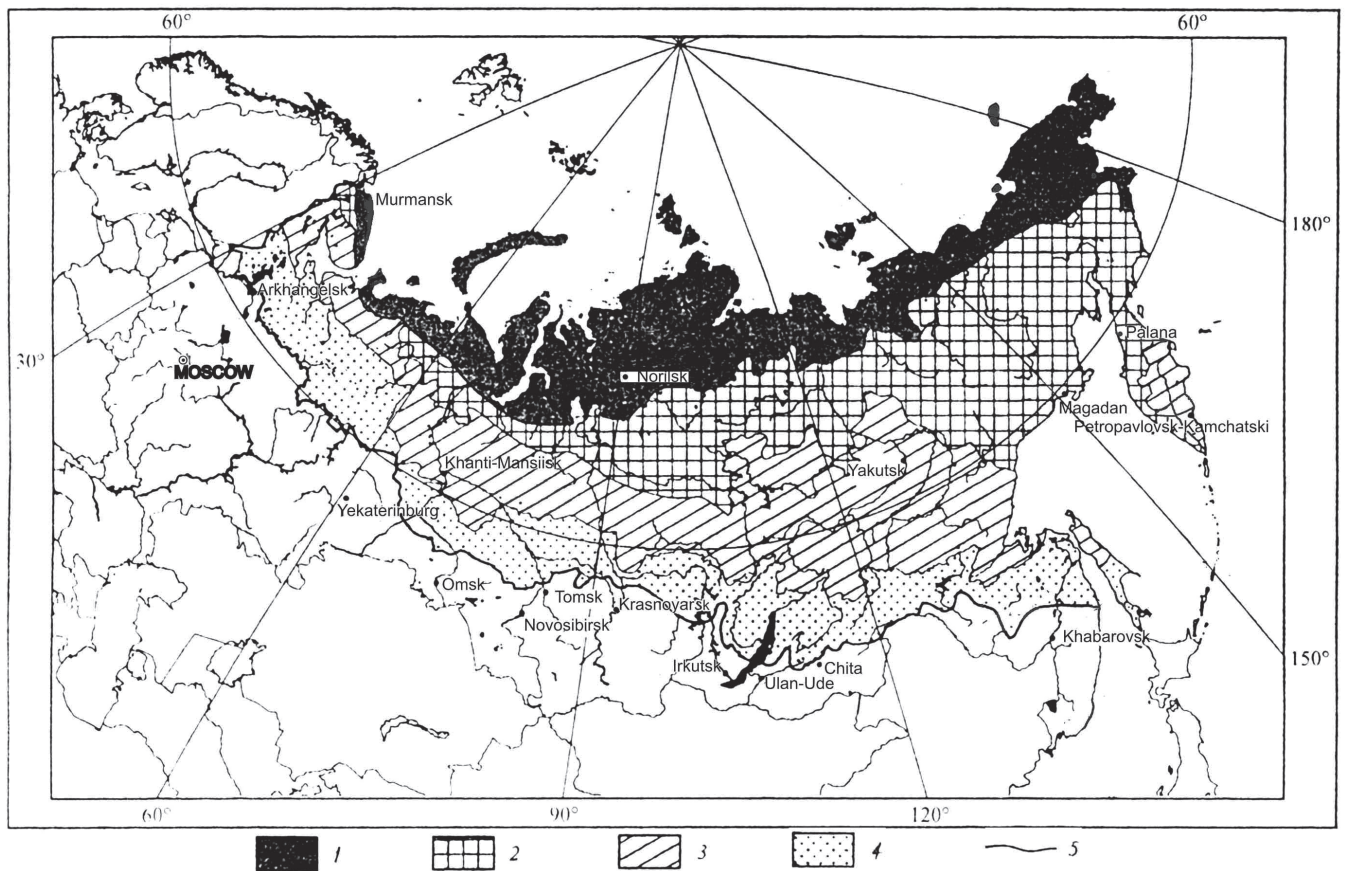


Figure 2. Zonation of the Russian North (after Gavrilova et al. 2004). 1 – Far North– absolutely unfavorable (arctic) zone, 2 – Far North equivalent – extremely unfavorable (subarctic) zone, 3 – North – unfavorable zone, 4 - North equivalent - relatively unfavorable zone, 5 – limit of the North.

and Magadan, where t_{win} is -10.4°C (*USSR Vol. 27 1966*) and -14.2°C (*USSR Vol. 33 1966*) respectively, are in the extreme unfavorable (Subarctic) zone (2), while northerner and much colder Yakutsk where $t_{win} = -26.5^{\circ}\text{C}$ (*USSR Vol. 24 1966*) is in the most southern of the three enumerated zones – unfavorable zone 3 (Fig. 2).

It is obvious that shortcomings in the zonation schemes result from the fact that all investigators try to incorporate a large number of different (often incomparable) environmental parameters into a single scheme, and such attempts are not always successful. Besides, it is time to abandon efforts to regionalize the North only, because, conditions for life in the Altai and Sayan Mountains in southern Russia, for example, are much worse than in Chukotka. The present author shares M.A. Zhukov's view that "zonation should be made not for the North ..., but for the whole country based on the main significant unfavorable factors ... And unfavorable conditions should be taken into account where conditions are unfavorable, not where it is the North, South, West, or East" (Zhukov 2005).

Attempts to regionalize the entire territory of Russia have been made before, based, among others, on the air freezing index. The Working Group's report contains a map (author not given), which delineates the areas with the air freezing indices ($\Sigma\tau$) of $0^{\circ}\text{C}\cdot\text{days}$ to $-4000^{\circ}\text{C}\cdot\text{days}$ (five zones) and

below $-4000^{\circ}\text{C}\cdot\text{days}$ (one zone). The latter zone includes all regions where the freezing index varies from -4000°C to $-7700^{\circ}\text{C}\cdot\text{days}$; i.e., the range of variation is nearly the same as in the first five zones combined. Resultantly, the same climatic zone includes Oymyakon (the air freezing index is -7300°C days to $-7670^{\circ}\text{C}\cdot\text{days}$), Yakutsk ($\Sigma\tau = -5550^{\circ}\text{C}$ days to $-5575^{\circ}\text{C}\cdot\text{days}$), and Anadyr ($\Sigma\tau = -3570^{\circ}\text{C}$ days to $-4200^{\circ}\text{C}\cdot\text{days}$) (*USSR Vol. 24 1966*, *USSR Vol. 33 1966*), which is totally incorrect.

Results

The particular climatic qualities of a territory are the most important factors affecting human activities and quality of life. Their effects are not at all uniform. In relatively favorable regions, including much of European Russia and the southern parts of West Siberia and the Far East, the climate variation is not so great as to exert a strong effect on the human organism. But in the continental areas of East Siberia, Yakutia, and the adjacent northwestern part of Magadan Oblast, the climate harshness increases so greatly, that all indicators showing the possibility of long outdoor activity and residence change radically.

To demonstrate this, published air temperature data from all Russian weather stations were analyzed (*USSR Climate*



Figure 3. The permafrost and climate severity map of the Russian Federation. Dot-and-dash line – boundary of the Republic of Sakha (Yakutia).

References 1964–1967). For each weather station the average air freezing index for the whole period of record (τ), which in many cases exceeded 100 years, was calculated. The air freezing indices ($\Sigma\tau$) for more than 3000 stations were drawn on a base map, and interpolated and extrapolated accounting for topography. This work resulted in “The Permafrost and Climate Severity Map of the Russian Federation” at a scale of 1:5,000,000. This map is presented, in a reduced form, in Figure 3. The map provides a climatic severity rating and identifies six zones, as in the earlier mapping schemes, but with equal air index intervals.

It is shown that absolutely extreme conditions (score 6) occur in the northeastern mountainous part of Yakutia and in the adjacent part of Magadan Oblast where $\Sigma\tau$ varies from $-6251^{\circ}\text{C}\cdot\text{days}$ to $-7669^{\circ}\text{C}\cdot\text{days}$ (Fig. 3). This zone is smallest in size and occupies only 3% of the country. At the same time, it is the coldest zone where the coldest places of the Northern Hemisphere, Verkhoysk and Oymyakon, are located. The mean annual air temperature at these populated centers is -15.7°C to -17.0°C , and the minimum temperatures are -68°C to -70°C (USSR Vol. 24 1966). The mean winter air temperatures (for the persistent period of freezing temperatures) vary from -24.5°C to -32.5°C in the zone.

Extreme conditions (score 5, $\Sigma\tau = -5001^{\circ}\text{C}\cdot\text{days}$ to $-6250^{\circ}\text{C}\cdot\text{days}$) are characteristic of the arctic archipelagos of Severnaya Zemlya and the New Siberian Islands, the vast areas of East Siberia, Yakutia, Magadan Oblast, and Chukotka Autonomous Okrug, as well as the high mountainous areas of northern Buryatia, Chita Oblast, Amur

Oblast, and Khabarovsk Krai. Winters are very cold in these regions, with average temperatures varying from -17.0°C to -27.5°C . This zone covers extensive areas in northeastern Russia, comprising 22.4% of the area of the country.

The regions with severe conditions (score 4, $\Sigma\tau = -3751^{\circ}\text{C}\cdot\text{days}$ to $-5000^{\circ}\text{C}\cdot\text{days}$) are Franz Josef Land, islands in the Kara Sea, northern West Siberia, central East Siberia, southern Yakutia, the mountainous parts of Tuva and Altai, the northern parts of Buryatia, Irkutsk, Chita and Amur Oblasts, and Khabarovsk Krai, as well as parts of Magadan and Kamchatka Oblasts, Chukotka Autonomous Okrug, and Wrangel Island. This zone fringes the previous zone semi-circularly, intruding to the mountains of Trans-Baikal and Pre-Amur, and comprises about 18.2% of the area of Russia. Winters are still cold in this zone, with mean temperatures ranging from -13.5°C to -24.0°C .

The zone of unfavorable conditions (score 3, $\Sigma\tau = -2501^{\circ}\text{C}\cdot\text{days}$ to $-3750^{\circ}\text{C}\cdot\text{days}$) borders all the above zones in the west, south, and east (Fig. 3). It covers about 22.5% of the area of the country and includes the Novaya Zemlya and Vaigach Islands, the eastern part of Nenets Autonomous Okrug, the northern Urals, northwestern and southern areas of West Siberia, and parts of Krasnoyarsk, Khabarovsk and Primorsky Krai, Magadan and Kamchatka Oblasts, and Chukotka. Winters are still long, especially in the Arctic islands, but now not so cold. The mean winter temperatures vary from -10.5°C to -20.5°C .

Temperate conditions (score 2, $\Sigma\tau = -1251^{\circ}\text{C}\cdot\text{days}$ to $-2500^{\circ}\text{C}\cdot\text{days}$) are characteristic of much of the North-western and Privolzhsky Federal Districts, the southern part

of the Urals Federal District and southwestern part of the Siberian Federal District. To the east, such conditions are found along the southern edge of Lake Baikal and in a small part of southern Chita Oblast. In the Far East, the temperate zone includes Khabarovsk Krai, most of Primorsky Krai, Sakhalin, and Kamchatka, and narrow coastal areas of Magadan Oblast and Anadyr Bay in Chukotka. This zone is largest in size (approximately 25% of the area of the country), and winters are relatively mild. The mean winter air temperatures vary from -6.5°C to -16.5°C .

The zone of relatively favorable living conditions (score 1, Σt above $-1250^{\circ}\text{C}\cdot\text{days}$) in the proposed map includes only those areas where the mean air temperatures for the cold season ($t < 0^{\circ}\text{C}$) are above -8.5°C . This zone occupies the Kola Peninsula coast in the Barents Sea, the northern part of the Onega Peninsula, the southwestern coasts of Onega Bay in the White Sea, Kaliningrad Oblast, the Central Federal District, southwestern Privolzhsky District, and Southern Federal District in the European part of Russia. Virtually all of Siberia, the Far East, and Chukotka have more severe conditions. Relatively favorable conditions are found here only along the sea coasts in Primorsky Krai, in southern parts of Sakhalin, along southeastern coasts and the southernmost part of Kamchatka, and on the Kuril and Komandorskie Islands. The relatively favorable zone lies mostly in the west of the country (Fig. 3), and its total area comprises about 9% of the Russian Federation.

In addition to climate severity analysis, the character of permafrost distribution within the identified zones was evaluated by the present author together with V.V. Kunitsky, M.M. Shatz and V.V. Shepelev (Shepelev et al. 2007).

The evaluation shows continuous permafrost in the areas with absolutely extreme or extreme conditions where Σt is $-5001^{\circ}\text{C}\cdot\text{days}$ to $-7669^{\circ}\text{C}\cdot\text{days}$ (zones 5 and 6 on Fig. 3).

In zone 4 with severe conditions (Σt of $-3751^{\circ}\text{C}\cdot\text{days}$ to $-5000^{\circ}\text{C}\cdot\text{days}$), either continuous (mainly in the northern parts) or discontinuous permafrost and permafrost islands occurs. It should be noted that, except the Barents Sea islands, "the continuous permafrost zone lies entirely within the Asian part of Russia" (Shepelev & Shatz 2005).

In the areas with unfavorable conditions (see Figure 3, zone 3) where Σt ranges from $-2501^{\circ}\text{C}\cdot\text{days}$ to $-3750^{\circ}\text{C}\cdot\text{days}$, permafrost islands mostly occur.

In zone 2 with temperate conditions (Σt of $-1251^{\circ}\text{C}\cdot\text{days}$ to $-2500^{\circ}\text{C}\cdot\text{days}$), permafrost is of limited occurrence and exists as islands or isolated patches in the European North and in the Sayan foothills in the southeast of the country. The zone is generally free of permafrost, as is zone 1 with relatively favorable conditions ($\Sigma t > -1250^{\circ}\text{C}\cdot\text{days}$) where only seasonal freezing of soils is observed, and permafrost never exists (Fig. 3).

For the purpose of illustration, permafrost zone boundaries from Baranov's (1977) Geocryological Map of the USSR were overlain on the present map. Although Baranov's map was published 30 years ago, it remains one of the best frozen-ground maps for Russia and former Soviet Union republics. More recent maps only add details for individual

areas or refinements to the limits of seasonal and perennial frost which can not be reflected on this small-scale map.

Comparison shows that the presented map radically differs from all the earlier maps. The major distinction is that this map shows, for the identified zones, both the real extreme conditions with the coldest and thickest permafrost and the areas with milder and relatively favorable conditions where permafrost occurs as isolated patches or is absent. For example, Yakutia has always, now and 100 years ago, been the coldest region in Russia with the largest measured depth of permafrost (up to 1500 m). But the earlier classifications placed only the northern part of Yakutia in the absolutely and extremely unfavorable zones. Moreover, these zones included the Kola Peninsula coasts washed by the warm Gulf Stream (Figs. 1, 2) with the open sea near Murmansk where permafrost never forms, and the continental areas of the peninsula where only patches of frozen ground less than 50 m in thickness are encountered (*Geocryology of USSR* 1988).

As for the problem of defining the Far North and equivalent areas and the territories with regional coefficients, their total area is within a reasonable range. The geographic location of the Russian Federation is such that most of the country has difficult climatic conditions. The regionalization presented in this paper shows that the regions with extreme, severe, and unfavorable conditions, where the air freezing index ranges from $-2500^{\circ}\text{C}\cdot\text{days}$ to $-7700^{\circ}\text{C}\cdot\text{days}$, occupy little more than 66% of the country. If the zone of temperate living conditions is added, the total area will reach 91%.

Conclusions

The present work is not yet sufficient to provide a basis for establishing regional coefficients in the entire Russian Federation. For this purpose, it is necessary to investigate in greater detail the effect of many other natural factors. In particular, more detailed consideration should be given to the geocryological situation in the regions and to their impact on human life and activities. Nevertheless, the proposed map can help compare temperature conditions with permafrost and other environmental factors, as well as value at the validity of previous elaborations.

References

- Baranov, I.Y. 1977. *The Geocryological Map of the USSR*. Scale 1:5,000,000. Moscow: USSR Agency for Geodesy and Cartography, 4 sheets, 62×92 cm.
- Gavrilova, M.K., Fedorova, E.N. & Lazebnik, O.A. 2003. Zoning the Russian North by discomfort for living. *Nauka i Obrazovanie* 2(30): 16-24.
- Gavrilova, M.K., Fedorova, E.N. & Lazebnik, O.A. 2004. On the problem of delineating boundaries and zoning the Russian North. *Bulletin of Russian Geographical Society* 136(1): 63-69.
- Geocryology of USSR*. 1988. European Part of the USSR. In: E.D. Ershov (ed.), Moscow: Nedra, 358 pp.

- Krenke, A.N., Zolotokrylin, A.N. & Vinogradova, V.V. 2001. Zonation of the Russian North and East based on environmental and climatic conditions for living. In: V.M. Kotlyakov (ed.), *Regional Aspects in the Development of Russia under Global Environmental and Climatic Changes*. Moscow: NTs ENAS, 65-74.
- Shepelev, V.V. & Shatz, M.M. 2005. Zonation of Russia based on living conditions and geocryological environment. *Nauka i Obrazovanie* 4(40): 72-79.
- Shepelev, V.V., Zabolotnik, S.I., Kunitsky, V.V. & Shatz, M.M. 2007. Permafrost-related factors in zonation of the Russian North. In: V.V. Philippov (ed.), *Zonation of the North of the Russian Federation*. Yakutsk: Permafrost Institute SB RAS Press, 14-26.
- USSR Climate References*. 1964–1967. Part II. Air and Soil Temperatures. Leningrad: Gidrometeoizdat.
- , Volume 1. 1965. Archangel and Vologodsk Oblasts, Karelian and Komi ASSR: 358 pp.
- , Volume 2. 1965. Murmansk Oblast: 144 pp.
- , Volume 3. 1965. Karelian ASSR. Leningrad, Pskov and Novgorod Oblasts: 343 pp.
- , Volume 6. 1965. Lithuanian SSR and Kaliningrad Oblast RSFSR.
- , Volume 8. 1964. Yaroslavl, Kalinin, Moscow, Tula, Vladimir, Smolensk, Kaluga and Ryazan Oblasts: 355 pp.
- , Volume 9. 1965. Perm, Sverdlovsk, Chelyabinsk, Kurgan Oblasts and Bashkir ASSR: 362 pp.
- , Volume 12. 1965. Tatar ASSR, and Ulyanovsk, Kuibyshev, Penza, Orenburg and Saratov Oblasts.
- , Volume 13. 1966. Volgograd, Rostov and Astrakhan Oblasts; Krasnodar and Stavropol Krai; and Kalmyk, Kabardino-Balkaria, Chechen-Ingush and North Ossetia ASSR.
- , Volume 15. 1966. Dagestan ASSR, Azerbaijan SSR and Nakhichevan ASSR.
- , Volume 17. 1965. Tyumen and Omsk Oblasts: 276 pp.
- , Volume 20. 1965. Kemerovo, Novosibirsk and Tomsk Oblasts and Altai Krai: 396 pp.
- , Volume 21. 1967. Krasnoyarsk Krai and Tuva ASSR: 504 pp.
- , Volume 22. 1966. Irkutsk Oblast and Western Buryat ASSR: 360 pp.
- , Volume 23. 1966. Buryat ASSR and Chita Oblast: 320 pp.
- , Volume 24. 1966. Yakut ASSR: 398 pp.
- , Volume 25. 1966. Khabarovsk Krai and Amur Oblast: 312 pp.
- , Volume 26. 1966. Primorsky Krai: 220 pp.
- , Volume 27. 1966. Kamchatka Oblast: 184 pp.
- , Volume 28. 1965. Tambov, Bryansk, Lipetsk, Orel, Kursk, Voronezh and Belgorod Oblasts.
- , Volume 29. 1964. Ivanovo, Kostroma, Kirov, Gorky Oblasts; Mari, Udmurt, Chuvash and Mordovian ASSR: 208 pp.
- , Volume 33. 1966. Chukotka National Okrug and Magadan Oblast: 288 pp.
- , Volume 34. 1966. Sakhalin Oblast: 205 pp.
- Zhukov, M.A. 2005. Struggle for the “norths,” or a Long road to common sense. *Nauka i Obrazovanie* 4(40): 141-145.
- Zolotokrylin, A.N., Kantsebovskaya, I.V. & Krenke, A.N. 1992. Zonation of Russia territory based on environmental extremity for life. *Tidings of the Academy of Sciences, Geographical Series* 6: 16-30.

Recent Climate and Active Layer Changes in Northeast Russia: Regional Output of Circumpolar Active Layer Monitoring (CALM)

Dmitry Zamolodchikov

Center for Ecology and Productivity of Forests, Russian Academy of Sciences, Moscow, Russia

Anatoly Kotov

Scientific Center, Chukotka, Anadyr, Russia

Dmitry Karelin

Center for Ecology and Productivity of Forests, Russian Academy of Sciences, Moscow, Russia

Vladimir Razzhivin

Komarov Botanical Institute, Russian Academy of Sciences, St. Petersburg, Russia

Abstract

This paper presents recent observations of active layer changes at three CALM (Circumpolar Active Layer Monitoring) tundra sites in northeastern Russia (Chukotka region). Results show that regional changes of climate became evident after 2000. In the Anadyr area (CALM sites R9 and R11) air temperatures in June–September significantly increased from 7.4°C (1901–2000) to 9.3°C (2001–2007), with corresponding increase in accumulated thawing degree days (DDT). At the Lavrentiya site (R27), DDT in 2001–2007 rose by 217°C as compared to 1929–2000. After 2000, all sites demonstrate significantly greater end-of-season grid-averaged thaw depths in response to the increase of incoming warmth. Annual values of edaphic factors display significant positive trend (0.03 y⁻¹) at R9 ($P = .026$) and no trends at R11 and R27. This demonstrates a different response of the active layer in local ecosystems to warming. Analysis shown that microhabitats with shallower thaw depths are more sensitive to warming.

Keywords: active layer; monitoring; Northeast Russia; permafrost; tundra.

Introduction

The CALM (Circumpolar Active Layer Monitoring) network includes three sites in the northeastern part of the Russian Federation (Chukotka peninsula). All sites are located near the Russian coast of the Bering Strait in the continuous permafrost zone (Fig. 1). The Cape Rogozhny site (R9) was established in 1994 on the northern coast of Onemen Bay (64°49'N 176°50'E) off the Bering Sea, and is the closest to the coast of the Chukotka CALM sites. Site R11 (Mount Dionisiya, 64°34'N 177°12'E), operating since 1996, is 25 km to the south of Anadyr city and about 11 km from the nearest seacoast. The direct distance between these two sites is 33 km. Both sites are dominated by cotton grass tussocks on Gleyi-Histic Cryosols. Site R27 was initiated in 2000 in the vicinity of Lavrentiya settlement (65°36'N 171°03'W), 3 km from the coast of the Bering Strait. The direct distance between the Lavrentiya site and the above-mentioned sites in the Anadyr area is 560 km. Within the landscape of the Lavrentiya site, wet sedge-*Salix* mosses tundra on Gleyi-Histic Cryosols are dominant. More detailed site descriptions are available in our earlier papers (Zamolodchikov et al. 2004).

Methods

The standard sampling design recommended under the CALM program (Brown et al. 2000) was applied, with minor modifications, at all northeastern CALM sites. Permanent 100x100 m grids were established, with 10 m

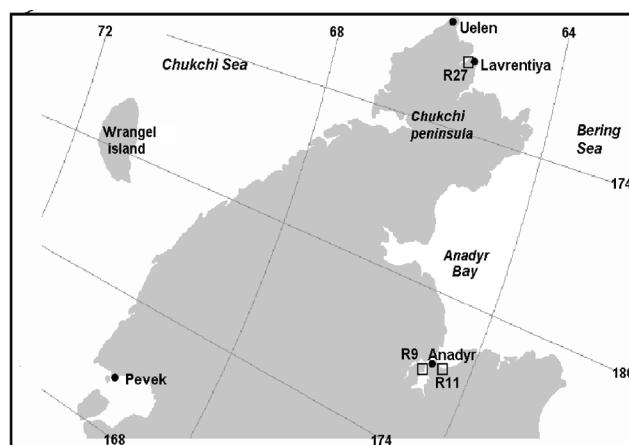


Figure 1. CALM sites in Northeast Russia: R9–Cape Rogozhny; R11–Mount Dionisiya; R27–Lavrentiya.

intervals between grid nodes marked with stakes (121 per grid). Thaw depth was measured at each grid node using a steel rod. Grids at the Cape Rogozhny and Mt. Dionisiya sites had one measurement replication per node, with four replications per node at the Lavrentiya grid. The active-layer was measured once each year at the end of the warm season at the Cape Rogozhny and Mt. Dionisiya sites, whereas the Lavrentiya grid was monitored throughout thaw season, with a maximum of four complete replications over the season.

An additional set of parameters was monitored at the three sites in order to estimate the influence of different natural controls over the temporal and spatial variability of the active

layer. At the Cape Rogozhny site, we inventoried the surface characteristics of microhabitats such as tundra, vehicle tracks, and frost boils. At Mt. Dionisiya, the relative areas occupied by tundra vegetation, water tracks, and frost boils was determined accompanied by grid leveling. The most comprehensive set of additional parameters was collected on the Lavrentiya grid including a topographic survey, qualitative characteristics of microhabitats, measurements of volumetric soil moisture, projective cover of vegetation, moss cover, and organic layer thickness.

The Cape Rogozhny and Mt. Dionisiya grids are presently equipped with temperature data loggers measuring air and soil temperatures to a depth of 1 m. The Lavrentiya grid is equipped with a 21X Campbell data logger, recording a wide spectrum of meteorological characteristics. Unfortunately, these data loggers were not initiated at the very beginning of site occupation. It is therefore not surprising that in further analyses we used climate data from the nearest long-term government weather stations. The nearest to sites R9 and R11 is the weather station at Anadyr city (the direct distance from this weather station to the sites is 25 and 30 km, respectively), and for the Lavrentiya site (R27) it is the weather station in the native settlement of Uelen (direct distance of 85 km). Previously it was shown that air temperatures at the sites are well correlated with the temperature data from the nearest weather stations (Zamolodchikov et al. 2004).

In addition to observations made according to the CALM protocol (Nelson et al. 1996), several other geocryological and ecological surveys were conducted at the sites. Detailed descriptions of cryolithological structure and cryogenic processes were compiled for Cape Rogozhny site (Kotov et al. 1998, Kotov 2001). Mt. Dionisiya was one of the official sites of the International Tundra Experiment (ITEX; Arft et al. 1999), a program designed to examine variability in arctic and alpine plant species response to increased temperatures. The Lavrentiya site is the location of intensive year-round investigations of CO₂, water vapor fluxes, and energy balance using the eddy-covariance technique (Zamolodchikov et al. 2003).

Results

Regional climate changes become evident after the year 2000 (Fig. 2). Near the sites R9 and R11, the Anadyr weather station recorded a mean annual air temperature of -7.6°C in the 1901–2000 period and -6.3°C in 2001–2006, which is significantly warmer ($P < .05$). Warm season (June–September) mean air temperature increased from 7.4°C in 1901–2000 to 9.3°C in 2001–2007. The corresponding increase in accumulated thawing degree days (DDT) was 214°C at Anadyr region (R9, R11). The same tendencies could be found in data taken from other long-term weather stations in the region. For example, in the Lavrentiya area (R27), mean DDT values in 2001–2007 increased by 217°C compared to the 1929–2000 period.

After the year 2000, all three sites demonstrate a clear trend of increased of end-of-season grid-averaged thaw

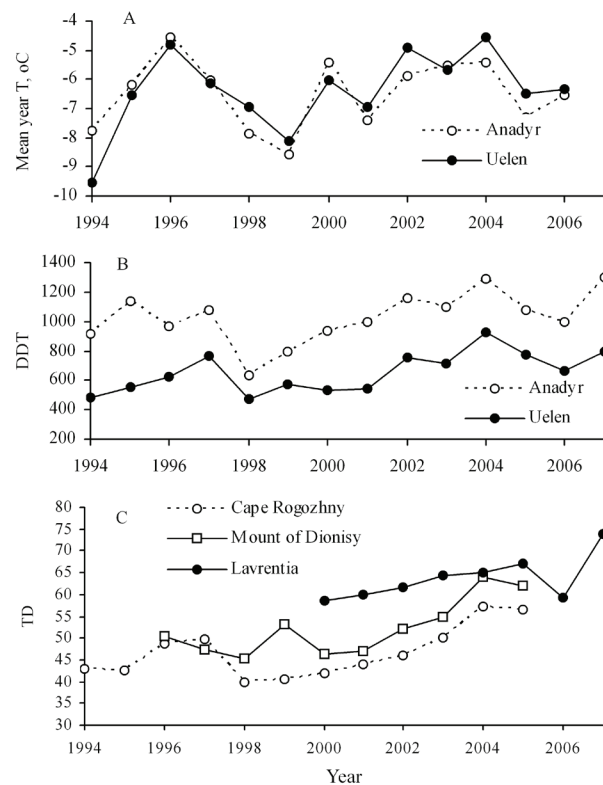


Figure 2. Mean air temperature dynamics (A) and accumulated thawing degree-days (B) at Anadyr and Uelen weather stations, and mean end-of-season depth of thaw (C) at the CALM sites in East Chukotka (Russia). Missing thaw depth data points in Anadyr sites in 2006–2007 (C) are due to logistical problems.

depths. Thus, in 2000, thaw depths were 42 cm at R9, 46 cm at R11 and 59 cm at R27. Five years later, thaw depth increased by 15 cm (35%) and 16 cm (34%) at Anadyr sites R9 and R11, respectively. Thaw depth increased by 15 cm (21%) at Lavrentiya site R27 by 2007.

The specificity of thawing processes at different sites can be characterized by the so-called edaphic factor (E), estimated as a rate, or coefficient of proportionality, between thaw depth and the square root of DDT (Nelson & Outcalt 1987). This approach was very effective in application to different sites at circumpolar Arctic sites (Hinkel & Nelson 2003; Mazhitova et al. 2004; Zamolodchikov et al. 2004, and many others). For the period of observation, mean edaphic factors were estimated as 1.49 at the R9 site, 1.70 at R11, and 2.43 at R23. It was found that the values of E display positive interannual trends (0.02 – 0.03 y^{-1}) at tussock tundra sites R9 ($P = 0.026$) and R11 ($P = 0.25$), though not significant in the latter case, and have no significant trend ($P = 0.56$) at site R27 (sedge-Salix moss tundra).

The R9 grid exhibits rather low spatial variability in active-layer thickness. The average annual coefficient of spatial variation (CV) is only 0.11. The R11 and R27 sites demonstrate more expressed spatial variability within the grid, with CV coefficients of 0.20 and 0.21, respectively. This is about twice the value observed on the R9 grid.

The interannual node variability (INV, %) reflects the level of interannual changes of spatial thaw depth distributions (Hinkel & Nelson 2003). R11 and R27 grids have similar INV estimates (21 and 19%, respectively). The R9 site demonstrates the greatest interannual node variability (29%). We note that CALM grids in East Chukotka have significantly

greater INV values, as compared to East European tundra sites (Mazhitova et al. 2004).

Nonuniform rates of thawing in different habitats is one possible factor of interannual spatial variability. Spatial distributions of interannual thaw depth increments (Figs. 3C, 4C) are essentially different from those of thaw depth (Figs 3A, 3B, 4A, 4B). To put it another way, maximum thaw depth at a given location within the plot does not necessarily result in the maximum incremental increase in thaw under warming conditions.

The question arises as to whether different grid nodes demonstrate different rates of thawing. To answer this question, grid nodes were grouped and ranked by thaw depths measured in the first year of observation for each grid. The first group included the 40 nodes (33%) with the shallowest thaw depth, the second group had 41 nodes with intermediate thaw depths, and the third group incorporated the 40 nodes with the deepest thaw. Table 1 shows the average thaw depths by groups at the beginning and the end of the observation periods on different grids.

The results show that at all CALM grids, the maximum incremental increase were observed at nodes with the shallowest initial thaw depth. Hence, microhabitats with shallow thaw depths are more sensitive to warming. This is also evident from the negative coefficients of correlation between incremental thaw increase and initial thaw depths values. The correlations were highly significant for grids R9 ($R = -0.47, P < 0.01$) and R27 ($R = -0.30, P < 0.01$), but not significant for R11 ($R = -0.11, P = 0.21$).

Discussion

We have shown a well-defined general tendency for increasing thaw depth at all East Chukotka tundra CALM sites within the last 10–15 years of observations. This is due to a significant rise in mean annual temperature and accumulated thawing degree days. The recent tendency of increased summer temperatures are observed in most regions of the Russian Arctic (Pavlov & Malkova 2005).

The anomalous year of 2006 demonstrates a

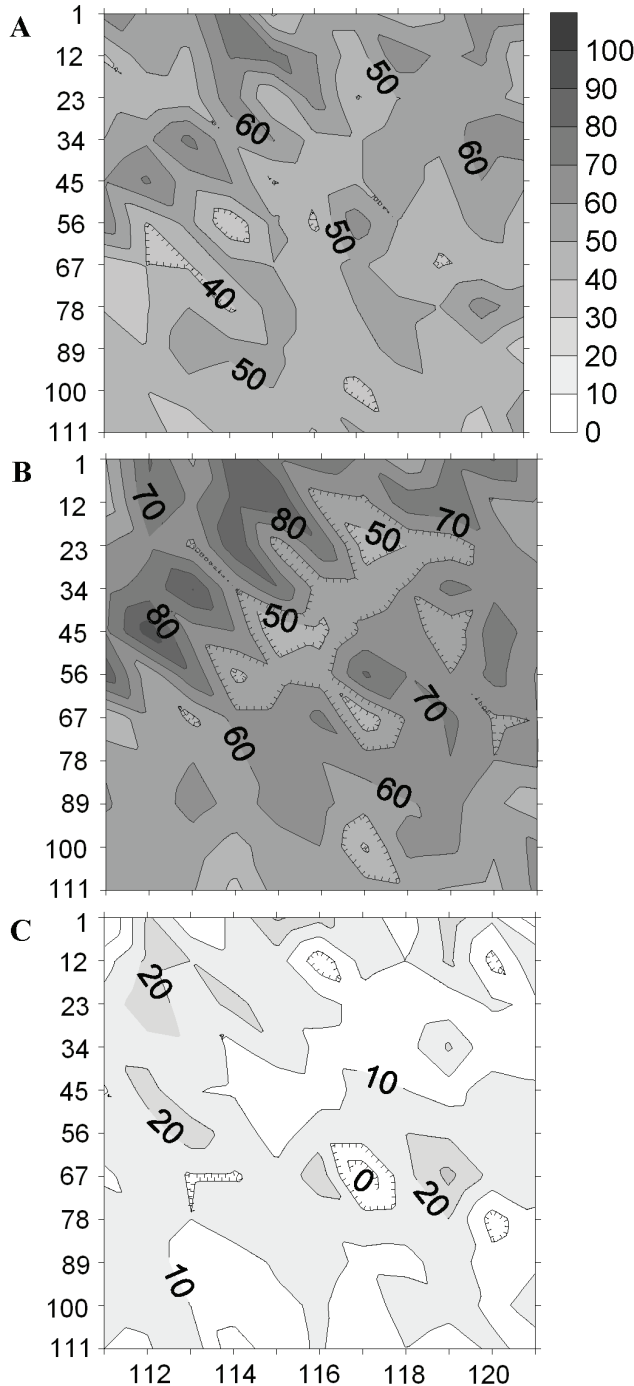


Figure 3. Thaw depth patterns and increments (cm) at the Mt. Dionisiya grid (R11). Parameters are mapped over the grid area using triangulation with linear interpolation algorithm; grid node numbers are shown on left and bottom margin. A: thaw depth, August 21, 1996; B: thaw depth, September 14, 2005; C: increments of thaw depth between 1996 and 2005.

Table 1. Incremental change in thaw depth by node groups at CALM grids in northeastern Russia.; see text for explanation.

Grid, periods of observations	Grid nodes grouped by thaw depth at first year	Average thaw depth, cm		Thaw depth increment, cm
		first year	last year	
R9, 1994–2005	low	38	54	16
	medium	43	56	13
	high	48	59	11
R11, 1996–2005	low	40	53	13
	medium	49	61	11
	high	62	72	11
R27, 2000–2007	low	46	64	19
	medium	58	73	15
	high	72	86	14

disproportionately low thaw depth at the Lavrentiya site (Fig. 2C) if compared to the Uelen weather station temperature data only (Fig. 2A, B). The explanation is due to the influence of local weather conditions. The Gulf of Lavrentiya, adjacent to the experimental site, is part of the Bering Strait. Throughout most of the summer season of 2006, the Gulf was completely blocked with ice due to

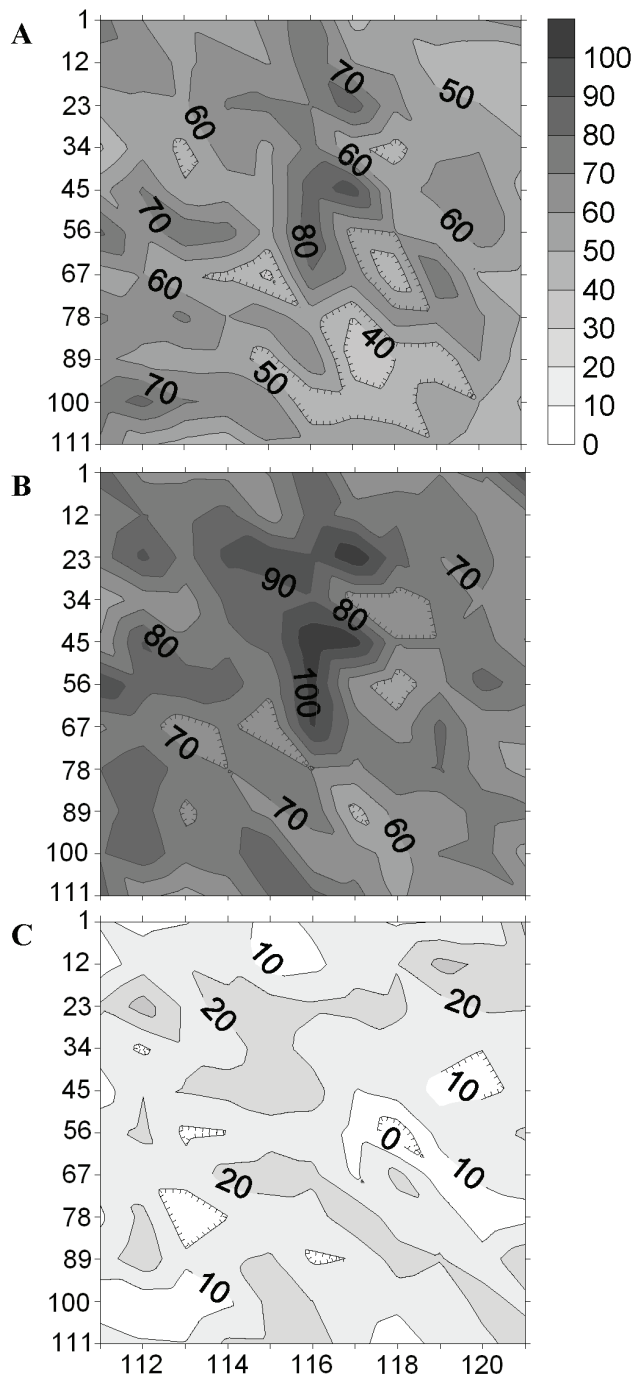


Figure 4. Thaw depth spatial patterns and increments (cm) at the Lavrentiya grid (R27). Parameters are mapped over the grid area using triangulation with linear interpolation algorithm; grid node numbers shown at left and bottom margins. A: thaw depth, September 29, 2000; B: thaw depth, September 25, 2007; C: increments of thaw depth between 2000 and 2007.

prevailing winds from the Arctic Ocean. This resulted in a well-expressed local cooling effect. This was not the case in other regions of the Chukotka peninsula, as is apparent from the corresponding values of mean annual temperatures at the Uelen and Anadyr weather stations (Fig. 2A).

In the following year (2007), the average thaw depth at the Lavrentiya site returned to the overall general tendency. In doing so, the deepest active layer measurement for all years of observation and at all sites was recorded (Fig. 2C). In 2007, the Anadyr weather station recorded the greatest annual sum of thawing degree days for the entire period of 108 years of observation since 1899, which exceeded 1300°C. This DDT sum matches the normal range characteristic of the northern geographical zone of boreal forest (north taiga).

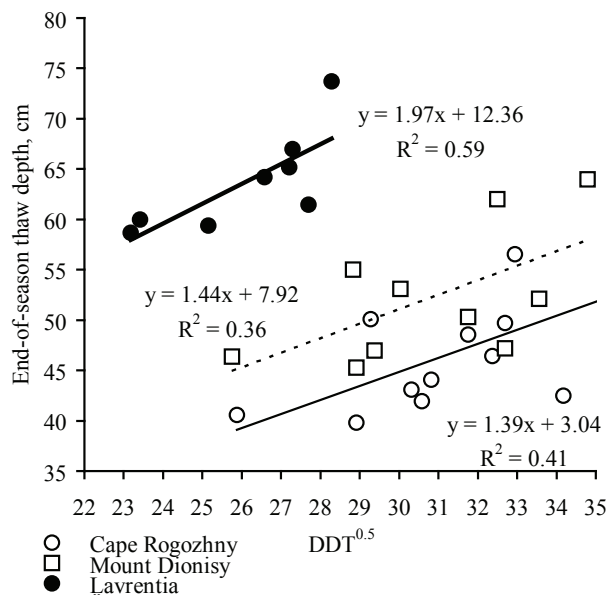


Figure 5. End-of-season thaw depth (cm) vs. accumulated thawing degree days (DDT^{0.5}) at East Chukotka CALM sites (Russia).

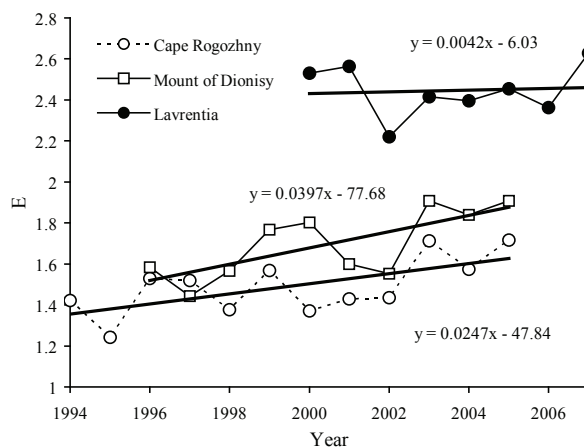


Figure 6. Interannual changes of calculated edaphic factors (*E*) at East Chukotka sites (Russia). Missing data points in curves for the Anadyr sites (trend lines below) are due to logistical problems in 2006–2007.

The average thawing-degree-days sums during the periods of observations at both Anadyr experimental sites are almost 1.5 times greater than at the Lavrentiya site (Fig. 5). The latter site is located much further north and is a substantially colder climate (Fig. 2B). Despite this fact, the average interannual thaw depth at the Lavrentiya site is significantly greater than at the two sites in the Anadyr region. According to our data, we believe that the difference is mostly due to the greater storage of aboveground phytomass, including more developed moss and lichen mats, bodies of *Eriophorum* tussocks, dwarf-shrub and shrub layers, and litter reserves in tussock tundras. All these factors result in better insulation.

Nevertheless, in spite of overall long-term trend of thaw depth increase, different local ecosystems could demonstrate site-specific reactions. The so-called edaphic factor *E* (the rate of active layer thickness to incoming warmth) is supposed to be an estimate of the response rate of a permafrost layer in a given ecosystem to external warming. Factor *E*, as a general property of a given soil and vegetation complex, defines a slope of a direct proportion between the rate of soil thawing and the accumulated sum of incoming warmth depending on soil structure and its other important characteristics (Brown et al. 2000). Hence, this factor is bound to demonstrate a relatively constant value in a given ecosystem. However, as is shown in Figure 6, it is not true in all cases.

In the wet sedge-Salix mosses coastal ecosystem of the Lavrentiya site, the rate of soil thawing during the entire period of observations remains constant (Fig. 6). At least one of two tussock tundra sites in the Anadyr area (Cape Rogozhny, R9) demonstrates a highly significant linear trend for this rate to increase ($P = .026$). The positive nature of this tendency suggests that, in contrast to other two ecosystems, continuous warming more affects the latter ecosystem, which possibly fails this growing pressure and degrades, or begins to change adaptively.

The spatially more heterogeneous Lavrentiya and Mount Dionisiya sites possibly remain more stable and relatively tolerant to recent warming. Such a well-expressed reaction of the Cape Rogozhny ecosystems may be also due to more intense local anthropogenic stress (pressure of all-terrain vehicles in the past), as compared to the other sites.

As was shown, the greater the depth of seasonal thaw at a given microhabitat, the less the anticipated impact of warming. This means that a given micro- and meso-habitat structure of ecosystem (i.e., the degree of its spatial heterogeneity) can seriously impact the average rate of thawing within the landscape. Under extended rise of temperature, this could offset the warming effect in permafrost ecosystems.

To estimate the stability and significance of the trends and patterns found, it is highly desirable to continue monitoring using the CALM design.

Acknowledgments

We devote this paper to the memory of Dr. Anatoly Kotov, our friend and colleague. The study was supported by NSF

grants OPP-9732051 and OPP-0352958. Thanks are also due to O.D. Tregubov, Yu.A. Verbebsky (Anadyr), G.M. Zelensky (Lavrentiya), and A.I. Ivaschenko (Moscow State University) for logistical support and assistance in the field.

References

- Arft, A.M., Walker, M.D., Gurevitch, J., Alatalo, J.M., Bret-Harte, M.S., Dale, M., Diemer, M., Gugerli, F., Henry, G.H.R., Jones, M.H., Hollister, R.D., Jonsdottir, I.S., Laine, K., Levesque, E., Marion, G.M., Molau, U., Molgaard, P., Nordenhall, U., Raszhivin, V., Robinson, C.H., Starr, G., Stenstrom, A., Stenstrom, M., Totland, O., Turner, P.L., Walker, L.J., Webber, P.J., Welker, J.M. & Wookey, P.A. 1999. Responses of tundra plants to experimental warming: meta-analysis of the International Tundra Experiment. *Ecological Monographs* 69(4): 491-511.
- Brown, J., Hinkel, K.M. & Nelson, F.E. 2000. The Circumpolar Active Layer Monitoring (CALM) program: research design and initial results. *Polar Geography* 24(3): 165-258.
- Hinkel, K.M. & Nelson, F.E. 2003. Spatial and temporal patterns of active layer thickness at circumpolar active layer monitoring (CALM) sites in northern Alaska, 1995-2000. *Journal of Geophysical Research* 102(D2): 8168, doi: 10.1029/2001JD000927.
- Kotov, A.N., Brazhnik, S.N., Galanin A.V., Maslov, V.Ya. & Samokhvalov V.D. 1998. Organization of ecological monitoring at "Onemen" research station. In: *Chukotka: Nature and Human*. Chukotka North-East Scientific Center, Far-East Branch, Magadan: Russian Academy of Sciences, 93-111. (in Russian).
- Kotov, A.N. 2001. Stratigraphy, composition and constitution of massive ground ice bodies of tabular type on northern coast of Onemen Bay (Chukotka). In: *Materials of the Second Conference of Russian Geocryologists, June 6-9, 2001*. Moscow: Lomonosov State University, 218-225. (in Russian).
- Mazhitova, G., Malkova (Ananjeva), G., Chestnykh, O. & Zamolodchikov D. 2004. Active layer spatial and temporal variability at European Russian Circumpolar Active Layer Monitoring (CALM) sites. *Permafrost and Periglacial Processes*. 15: 123-139.
- Nelson, F.E. & Outcalt, S.I. 1987. A computational method for prediction and regionalization of permafrost. *Arctic and Alpine Research* 19(3): 279-288.
- Nelson, F., Brown, J., Lewkowicz, T. & Taylor, A. 1996. Active layer protocol. In: U. Molau & P. Molgaard, (eds.), *ITEX Manual, Second Edition*. Copenhagen: International Tundra Experiment, 14-16.
- Pavlov, A.V. & Ananjeva, G.V. 2004. Assessment of recent air temperature changes in the territory of the cryolithozone of Russia. *Kriosfera Zemli* VIII(2): 3-9. (in Russian).

- Zamolodchikov, D.G., Karelin, D.V., Ivaschenko, A.I., Oechel, W.C. & Hastings, S.J. 2003. CO₂ flux measurements in Russian Far East tundra using eddy covariance and closed chamber techniques. *Tellus* 55B(4): 879-892.
- Zamolodchikov, D.G., Karelin, D.V., Ivaschenko, A.I. & Lopes de Gerenyu, V.O. 2005. Micrometeorological assessment of biogenic fluxes of carbon dioxide in typical tundra ecosystems of Eastern Chukotka. *Eurasian Soil Science* 38(7): 759-763.
- Zamolodchikov, D.G., Kotov, A.N., Karelin, D.V. & Razzhivin, V.Yu. 2004. Active layer monitoring in Northeast Russia: spatial, seasonal, and interannual variability. *Polar Geography* 28(4): 286-307.

N-Factors and Soil Temperatures Adjacent to the Vertical Support Members on the Trans Alaska Pipeline System

John P. Zarling

Zarling Aero and Engineering and University of Alaska Fairbanks, Fairbanks, Alaska, USA

Steve Sorensen

BP Exploration, Prudhoe Bay, Alaska, USA

Melody Shangin

Alyeska Pipeline Service Company, Fairbanks, Alaska, USA

Abstract

This paper describes the results from several data logger systems that were installed along the above-ground portion of the Trans Alaska Pipeline System (TAPS) which transverses Interior Alaska and discontinuous permafrost terrain. These data logger systems record air, ground surface, and subsurface ground temperatures using thermistor strings. From these freezing and thawing data, n-factors are calculated and are presented for a few sites. Several of the instrumentation sites also included installing a pressure transducer in the heat pipe within the thermal vertical support members (VSM). These heat pipes are used to cool the ground around VSM during winter and can be used as thermometers to sense the temperature at the base of thermal VSM. The heat pipe pressure-derived temperature measurements correlate well with subsurface thermistor data. Reading heat pipe pressures has been adopted as a strategy for determining permafrost temperatures along the TAPS in the discontinuous permafrost region.

Keywords: data loggers; heat pipes; *n*-factors; permafrost; pipeline; temperatures.

Introduction

Design of the Trans Alaska Pipeline System (TAPS) began in 1970, and construction of the access road, pipeline, marine terminal, and pump stations started in 1974. The pipeline went into operation in 1977. The 800 mile (1270 km) pipeline has its origin at Prudhoe Bay on the North Slope of Alaska and its terminus at the ice-free port of Valdez. About one half on the pipeline is built above ground where it crosses non-thaw stable permafrost. North of the Brooks Range, where the climate is the coldest, the permafrost is continuous. South of the Brooks Range, where the climate is warmer, the permafrost is discontinuous across most of Alaska's Interior. Along the southern portion of Interior Alaska, in the Copper River Basin, discontinuous permafrost transitions to sporadic permafrost and to seasonal frost before reaching Valdez. Thermal issues relating to permafrost design of the TAPS were presented by Jahns (1983).

The above-ground pipeline is supported by bents formed by two to four piles, a cross-beam with a sliding shoe riding on the cross beam and attached to the pipe. The piles on each end of the crossbeam are called vertical support members or VSM. Bents are generally spaced approximately 60 ft (18.3 m) apart.

In the non-thaw stable discontinuous permafrost zone, each VSM has two heat pipes installed which are called thermal VSM. These heat pipes are one-way heat transfer devices that extract thermal energy from the ground during the winter when the air temperatures are less than the ground temperatures. During the summer, the heat pipes become inactive.

Much of the field testing of thermal VSM that occurred

during the design phase of the pipeline was conducted in the early 1970s when the climate conditions were somewhat colder than present, with a large portion of this testing occurring near Fairbanks, Alaska. Figure 1 shows freezing and thawing indices for the last 55 years for Fairbanks. Based on a linear least squares best fit trend line through these data, the average freezing index has decreased about 11%, and the average thawing index has increased about 8% over the last 35 years. Because a safety factor of two was applied to conservative thermal design criteria, the constructed above-ground pipeline system continues to perform well, despite warming trends. This is evidenced by the very small number of VSM which have undergone measurable settlement or heave.

Throughout the operating life of the pipeline, more than 80 sites along the TAPS rout have monitored subsurface soil temperatures. However, air temperatures at these sites were not monitored. As a proactive measure to evaluate the above-ground pipeline support system under current climate conditions, Alyeska Pipeline Service Company (APSC) initiated an additional ground and air temperature monitoring program in 2003. This program consists of the installation of data loggers and temperature measuring sensors at over 40 sites along the pipeline, from fairly continuous permafrost regions just south of the Brooks Range to sporadic permafrost regions near the Little Tonsina River north of Big Thompson Pass. Each data logger site monitors air temperature, ground surface temperature, and sub-surface ground temperatures. Several of the data loggers also monitor the pressure inside the heat pipes (thermosyphons) installed in the thermal VSM.

Data from these sites have been analyzed in terms of air

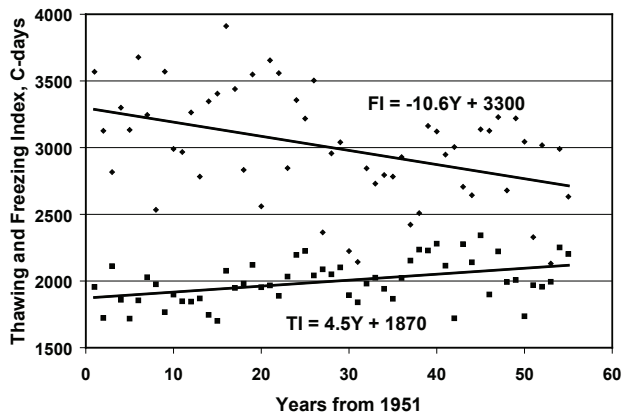


Figure 1. Freezing and thawing index data and trends for Fairbanks, Alaska beginning in 1951.

and surface freezing and thawing degree days and indices. From these data, freezing and thawing n -factors have been calculated and are presented for three of the data logger sites near Fairbanks. These n -factors are commonly used by engineers to predict depths of freeze or thaw. Many of these sites are undisturbed during the winter months, i.e., there is no snow removal. Surfaces are typically graveled, with either sparse grasses and/or brush growing, but growth is controlled by mowing from time to time (see Fig. 2).

Because the working fluid inside the heat pipes is in the two phase region, the heat pipes can be used as thermometers. The measured pressure inside a heat pipe can be converted to temperature of the liquid pool at its base. Thermistor strings have also been installed adjacent to several vertical support members that have pressure transducers installed. During the summer season when the heat pipes are non-operational and soil temperatures surrounding the VSM have come to equilibrium, the temperatures measured by these two methods are almost equal. During the winter months, the base of heat pipe temperatures are colder than the soil temperatures adjacent to the vertical support member, as expected when the heat pipes are operational. Graphs are presented showing air temperature, base of heat pipe temperature, and soil temperature surrounding the VSM.

Instrumentation System

Power for each of the instrumentation systems consists of a nominal 20 watt solar voltaic panel connected through a charge controller to a sealed 12-volt, 100 amp-hour lead acid battery. The data logger system is a Campbell Scientific CR10X data logger coupled to an AM/16/32 multiplexer housed in a fiberglass all weather enclosure. Air temperatures are measured with a thermistor housed in a Campbell Scientific six gill radiation shield. Ground surface temperatures and ground temperatures at depth are measured using thermistors. Ground surface temperature thermistor strings use two-pair direct burial telephone cable which has a polyethylene jacket providing mechanical protection over the range of temperatures experienced under arctic conditions.



Figure 2. Installation of photovoltaic panel, battery box, data logger enclosure on VSM and thermistor string enclosure.

Air and vertical ground thermistor strings are single pair or multi-pair, respectively, Halar coated conductors, with a Halar outer jacket. The thermistors are 16,320 ohms at 0°C, +/- 0.1°C, YSI P/N 44034. KPSI pressure transducers with a range of 0 to 600 psia (0 to 4.1 MPa), or programmable Honeywell PPT pressure transducers with a range of 0 to 1,000 psia (0 to 6.9 MPa) were used to measure heat pipe pressures. Because the nominal output-range of the pressure transducers are 0 to 5 volts, a Campbell Scientific VDIV2.1 voltage divider is used to reduce the input voltage to match the CR10X's 0 to 2.5 volt input range. The photovoltaic panel, polyethylene battery box, and all-weather enclosure are mounted to Unistrut. The Unistrut supporting the photovoltaic panel and enclosure are banded to the VSM, and the battery box is banded to the cross-beam as shown in Figure 2.

Data were retrieved from the data logger by swapping SM4 storage modules, or downloaded using Campbell Scientific's PConnect software with a Palm handheld or by directly connecting to a laptop computer through the data logger's serial port.

N -Factor Results

N -factors are empirically determined and used to estimate ground surface temperatures based on air temperatures. These factors are used in the modified Berggren method for depth of freeze and thaw calculations. Geotechnical finite element thermal modeling programs typically use n -factors to arrive at an annual surface temperature variation. To determine an n -factor, the air and surface temperatures are measured at a chosen site. The freezing and thawing degree days are calculated based on the following relationships:

$$TDD = T_{AVE} - 0^{\circ}C \text{ if } T_{AVE} < 0^{\circ}C \text{ and}$$

$$FDD = 0^{\circ}C - T_{AVE} \text{ if } T_{AVE} > 0^{\circ}C$$

From these data, air and surface freezing and thawing indices are calculated on a seasonal basis, using the cumulative method. Then the ratio of the surface and air freezing indices and surface and air thawing indices are calculated from measured and recorded temperatures to arrive at the site-specific *n*-factor. The equations stating these relationships are:

$$n_F = \frac{\text{Surface} \cdot \text{Freezing} \cdot \text{Index}}{\text{Air} \cdot \text{Freezing} \cdot \text{Index}} \text{ and}$$

$$n_T = \frac{\text{Surface} \cdot \text{Thawing} \cdot \text{Index}}{\text{Air} \cdot \text{Thawing} \cdot \text{Index}}$$

A compilation of measured *n*-factors has been published by (Lunardini 1978). However, there have been very few *n*-factors published for surfaces other than paved and gravel roads, and airport runways and taxiways.

Air and surface temperature data have been collected at most of the sites for the last four years. Three of the instrumented sites are along a section of above-ground pipeline between Chena Hot Springs Road and Nordale Road, northeast of Fairbanks. This section of above-ground pipeline is usually referred to as the Love Road site.

The Love Road site is typical for a low-lying, non-thaw stable permafrost area in Interior Alaska. It is a marshy lowland flood plain area, underlain by ice-rich silt with more than 95% typically passing a no. 200 sieve (Pearson 1977). The natural vegetation around the gravel pad area consists of tussocks, mosses, tamarack, black spruce, and willows and other brushy plants, as well as various varieties of grasses. This area represented a “worst case scenario” in terms of thermal stability design in a warmer permafrost horizon. During construction, the natural ground was covered with a gravel work pad to allow installation of VSM supports and the pipeline. The work pads have been maintained over the years by application of additional gravel surfacing. The northern end of this section of pipeline was the first above-ground pipeline constructed, with the work pad placed in March of 1974 and 14 VSM in early October of 1974 (Pearson 1977). It is also the area where initial field testing of several pre-construction heat pipes was performed. Twelve of the VSM became part of the pipeline, with production heat pipes installed in these VSM in March of 1975 (Pearson 1977). Table 1 identifies the three instrumented sites as A, B, and D, with their corresponding pipeline mileposts. Soil temperature data for the VSM at Site A, at elevations below the surface of the gravel pad, were recorded from 1974 through 1976 (Pearson 1977).

Air temperature and ground surface temperature curves are shown in Figure 3 for Site A. The *n*-factors for the three sites A, B, and D, along this section of pipeline are presented in Table 2, beginning with winter 2003–4 through summer 2007.

Thermistor strings at the Love Road Sites A and C were installed to a depth of 18 m and within 0.8 m of the VSM on

Table 1. Site location in miles from Prudhoe Bay and comments about location.

Site	Mile Post	Comments
A	456.130	VSM/Bent Station at preconstruction test site
B	456.183	Thermistor string 18 m north of Site C
C	456.189	VSM/Bent Station adjacent to preconstruction test site
D	458.178	VSM/Bent Station at transition to below ground

Table 2. Year and *n*-factors for Sites A, C, and D.

Year and N-Factor	Site A	Site C	Site D
2003–4 N _F	.22	.17	N.A.
2004 N _T	1.08	1.07	1.12
2004–5 N _F	.21	.18	.25
2005 N _T	1.04	1.08	1.09
2005–6 N _F	N.A.	0.35	0.48
2006 N _T	1.02	1.10	1.09
2006–7 N _F	.034	0.32	0.49
2007 N _T	1.04	1.07	1.09

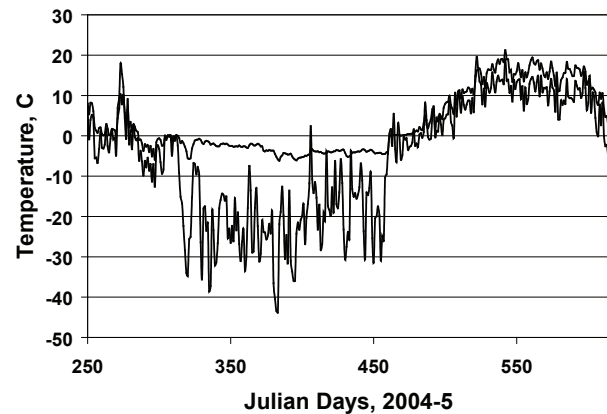


Figure 3. Air (highly variable curve) and ground surface temperatures for instrumentation Site A near Fairbanks. The soil surface temperature measured 6 m from VSM.

the drive lane side of the work pad. An additional thermistor string, Site B, was installed to a depth of 18 m at the mid-point between bent C and the bent station immediately north (upstream). Whiplash curves are shown in Figures 4 and 5 for the thermistor strings installed at Sites B and C.

Comparing Figures 4 and 5 shows the ground cooling effect provided by the heat pipes in the thermal VSM. It is also noted, that the top of the permafrost next to the thermal VSM is about 2 m below the ground surface after 30 years of pipeline operation. Midway between bents, the top of the permafrost has receded to about 4 m below the ground surface nearly 30 years after pile placement. Design phase calculations predicted 3.3 m of seasonal thaw after 20 years of operation (Jahns et al. 1978) and from 4 m to 6 m of thaw after 20 to 30 years of operation, (Jahns 1983).

The top of the permafrost was at a depth of about 2 m

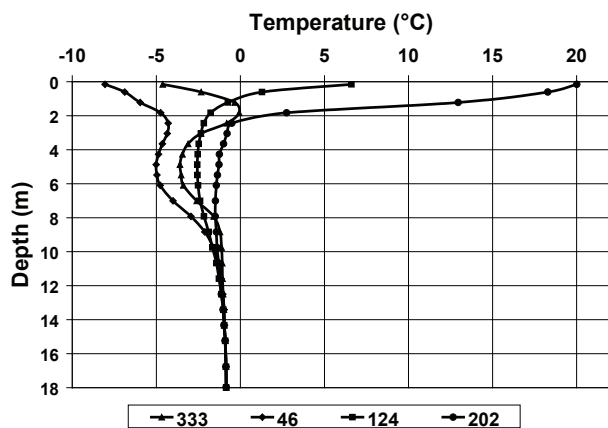


Figure 4. Site C whiplash curves for Julian days 46, 124, 202, and 333 within 1 m of thermal VSM in 2004.

in October of 1976 (Pearson 1977). In 2004, the top of the permafrost had receded to about 4 m midway between bents as shown by the whiplash curves in Figure 5. The temperature at a depth of 8 m beneath the work pad was about -0.5°C in October of 1976. Figure 5 indicates about the same temperature at a depth of 8 m in 2004.

End of summer temperatures at 8 m depth in October 1976 adjacent to the VSM at Site A were about -2.2°C . The warm side trumpet curve shown in Figure 6 in 2003–2004 shows similar recorded temperatures at the 8 m depth.

Figure 6 shows the cold side and warm side trumpet curves for Site A. It is observed the ground temperatures at depth are about 1°C colder at this site than Site B referenced in Figure 4 which is about 92 m away. There is a remote gate valve close to Site A, which is supported by four thermal VSM which provide greater combined ground cooling in the immediate area. It is worth noting, that installing free-standing heat pipes next to existing thermal VSM is a way to mitigate potential climate warming effects and have been successfully employed at a few locations on the TAPS.

Heat Pipes as Thermometers

The 124,300 heat pipes installed in the VSMs of TAPS were manufactured by the McDonnell Douglas Corporation. The heat pipes are 2-inch (51 mm) OD steel pipe below the top of the VSM and 3-inch OD pipe above the top of the VSM. Inside diameter is a uniform 1.5-inches (38 mm). Heat pipes with a 4-foot (1.22 m) long extruded aluminum fin were made in lengths of 28 ft (8.5 m) to 37 ft (11.3 m) in 3-foot (0.9 m) increments. Heat pipes with a 6-foot (1.83 m) long extruded aluminum fin were manufactured in lengths from 42 ft (12.8 m) to 75 ft (22.9 m) in 3-foot (0.9 m) increments. These heat pipes were originally charged with anhydrous ammonia.

In 1983, (Johnson 1983), six years following completion of TAPS, it was reported that many of the heat pipes were experiencing an accumulation of non condensable gas inside the units. The gas was determined to be hydrogen. During operation, the hydrogen is swept by the ammonia vapor

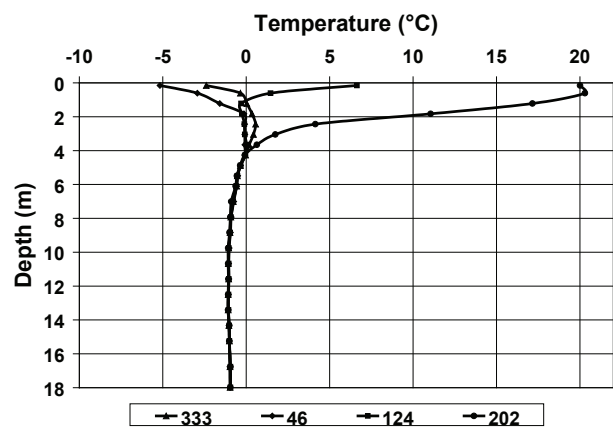


Figure 5. Site B whiplash curves for Julian days 46, 124, 202, and 333 midway between bent stations in 2004.

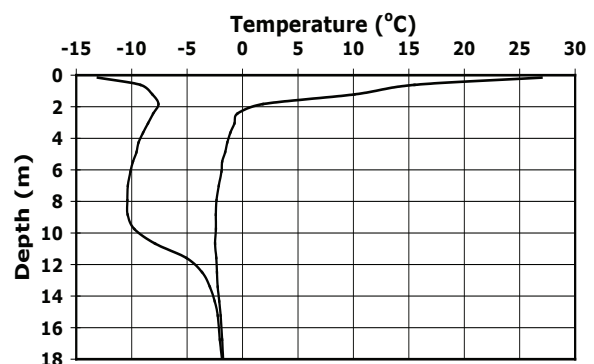


Figure 6. Site A cold and warm side trumpet curves for the period of 2003 to 2005 at 1 m from the thermal VSM.

to the top of the heat pipe. The ammonia then condenses, leaving the hydrogen behind, partially blocking the top finned section from condensing additional ammonia. Using infrared camera technology, the amount of blockage or “cold topping” is determined. In the 1980s through the 1990s, getter pins were installed in the top of the heat pipes to absorb the hydrogen. The getter pins contained a metal halide, zirconium dimanganese. When the getter pins became saturated with hydrogen, non-condensable gas blockage would return. In 2001, Sorensen et al. (2003), developed a program of bleeding-off the ammonia and non-condensable gas and recharging with carbon dioxide. This process required the installation of a valve at the top of the heat pipe.

The pressure transducers were attached to valves installed above the finned section of the heat pipes. A thread-o-let was welded on the side of the steel pipe above the fins, and a hole drilled through the heat pipe wall to within 1/8 inch of breaking through. A hot tapping tool was then attached to the thread-o-let, and the final drilling was completed through the wall of the heat pipe. The ammonia was bled off, and the heat pipe was evacuated and purged with nitrogen before the final charge of carbon dioxide was performed.

Because the working fluid in the heat pipe is in the two phase region, pressure and temperature are not independent

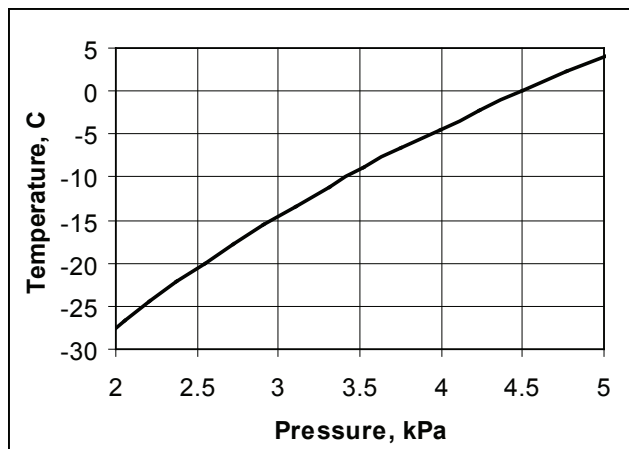


Figure 7. Saturation temperature–pressure relationship for carbon dioxide.

properties for a single component fluid. Therefore, by measuring the pressure inside the heat pipe, the temperature is readily determined by referencing the thermodynamic tables of the specific working fluid. At those instrumented sites where the temperature at the base of the VSM was desired, a hot taping operation was performed to bleed-off the ammonia, and then the heat pipe was recharged with carbon dioxide. The saturation temperature–saturation pressure relationship for carbon dioxide is shown in Figure 7. The pressure indicated by the pressure transducer was corrected for the hydrostatic head of vapor in the heat pipe to arrive at the pressure at the liquid pool vapor interface at the base of the heat pipe. Then, using a chart as shown in Figure 7, the temperature at the base of the heat pipe was established.

When the air temperature is colder than the ground temperature surrounding the VSM, the heat pipe operates and removes heat from the ground. When the air temperature is warmer than the ground temperature surrounding the VSM, the heat pipe ceases to reject heat.

Figure 8 shows air temperature, base of heat pipe temperature, and the ground temperature as measured by a thermistor at the same elevation as the base of the heat pipe. This thermal VSM is at the northern end of the Love Road site. Temperatures of air, base of heat pipe, and ground at the 10 m depth are plotted in the Figure for Julian days 65 through 195. During the winter, it is seen that when the air temperature is coldest, the base of heat pipe temperature is warmer, and the temperature of the surrounding ground the warmest. It is noted that there are a few days during the winter period that the outdoor air temperature exceeded the ground temperature and the heat pipe would become inoperative. When the heat pipe ceases to function in the spring of the year, the base of heat pipe temperature and the surrounding ground temperature trend to equilibrium. It is observed that the temperature measured by the thermistor and the temperature calculated from measuring the heat pipe pressure (refer to Fig. 7) are almost exactly the same.

By measuring the pressure in the heat pipe during or after maintenance is performed, the temperature of the permafrost

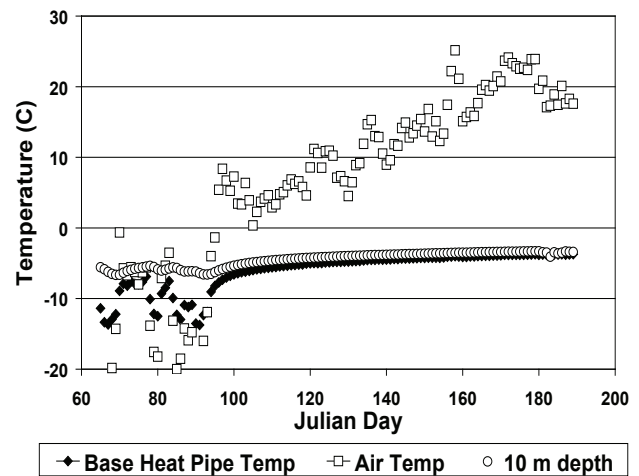


Figure 8. Comparison of air, base of heat pipe, and ground temperature near base of VSM.

at the bottom of the VSM can be determined. Measurements in late summer using this method have revealed that most VSM base temperatures remain below freezing, even in cases of severe cold topping. In many cases, where temperatures are initially near or slightly above freezing during maintenance, re-freezing tends to occur within one to two years, even in sporadic permafrost areas. In addition, the method assists in providing a relatively dense map of late summer subsurface temperatures along the TAPS right-of-way that would be difficult to achieve by any other method.

Conclusions and Discussion

The Campbell Scientific data loggers and multiplexers have proven to be very reliable. A few intermittent problems that occurred initially with respect to data logging among the 40 sites included flooding of one data logger due to stream icing/overflow, broken thermistor lead wires at two sites due to frost heave and settlement, and low battery voltage in valleys where the sun does not shine on the photovoltaic panels for several months during mid-winter at two locations. Because batteries are mounted on the crossbeams of the bents, they are exposed to ambient temperatures. Their capacities are decreased with decreasing temperature, and their charging efficiency is also decreased at low temperatures. Many researchers bury batteries beneath the snow to avoid exposure to low ambient temperatures. However, in this case, mounting the batteries on the crossbeams provided greater security and allowed better access for periodic maintenance. All of these challenges were addressed early in the project to ensure effective monitoring.

The thawing n -factors are lower than typical thawing n -factors for gravel surfaces (Lunardini 1978). Early morning and late evening shading by trees and brush along the sides of the right-of way, daily shading of the ground from the shadow cast by the pipeline, and ground shading by vegetation are all causes for the lower thawing n -factors.

The freezing n -factors show more variation from year to

year. The amount and timing of the snow cover has the major effect on the freezing n -factors. Early and deep snow covers yield lower freezing n -factors.

The trumpet and whiplash curves presented for sites A, B, and C show no significant changes in temperature from the data presented by Pearson (1977). The heat pipes installed in the VSM have been effective in maintaining reduced permafrost temperatures around the VSM. The drive lane for this section of pipeline serves as a summer and winter recreational trail. Wintertime activities include dog mushing, Nordic skiing, and snowmobiling, which tend to compact the snow. Additionally, APSC plows this section of drive lane from time to time in the winter for access to the two remote gate valves along this section. The effects of compacting and/or removing snow enhance cooling of the ground as the thermal resistance of the snow is reduced.

Using the heat pipes as thermometers is a very effective method of determining the late summer base of heat pipe temperatures. This tends to be a more cost effective method of obtaining these temperatures in comparison to the installation of thermistor strings.

The dynamics of heat pipe cooling in thermal VSM as a function of time and air temperature is better understood. Thanks to the early work by others at the Fairbanks sites during design of the pipeline, a good comparison of long-term thermal data is possible. By evaluating thermal conditions at several sites in a region, n -values have been determined for use in trending and predictive maintenance of thermal VSM.

Acknowledgments

The authors would like to acknowledge Christopher Swaim, Commissioning Engineer, Pipeline Maintenance Engineering, and Wiley Splain, Engineer II, Integrity Management Engineering, both with the Alyeska Pipeline Service Company, for the installations of the data logger systems, and Tracy Shields for downloading and analyzing some of the data. The authors would also like to thank the Alyeska Pipeline Service Company for permission to publish this paper.

References

- Jahns, H.O. 1983. Pipeline Thermal Considerations. *Proceeding of the Fourth International Conference on Permafrost. Vol. 2. Fairbanks, Alaska, USA.*: 101-111.
- Jahns, H.O., Miller, T.W., Power, L.D., Rickey, W.P., Taylor, T.P. & Wheeler, J.A., 1978. Permafrost protection for pipelines. *Proceeding of the Second International Conference on Permafrost. Yakutsk, Russia.* North America Contribution. National Academy of Science. Washington DC: 673-683.
- Lunardini, V.J. 1978 Theory of n -factors and correlation of data. *Proceeding of the Third International Conference on Permafrost, Vol. 1. Edmonton, Alberta, Canada.* 40-46.
- Johnson, E.R. 1983. Performance of the Trans-Alaska Oil Pipeline *Proceeding of the Fourth International Conference on Permafrost. Vol. 2. Fairbanks, Alaska, USA.*:109-111.
- Pearson, S.W. 1977. Thermal Performance Verification of Thermal Vertical Support Members for the Trans-Alaska Pipeline. ASME Winter Annual Meeting, Atlanta, Georgia. Paper 77-WA/HT-34. 1-9.
- Riseborough, D.W. 2003. Thawing and freezing indices in the active layer. *Proceeding of the Eighth International Conference on Permafrost. Vol. 1. Zurich, Switzerland.*: 953-958.
- Sorensen, S., Smith, J. & Zarling, J. 2003. Thermal performance of TAPS heat pipes with non-condensable gas blockage. *Proceeding of the Eighth International Conference on Permafrost. Vol. 1. Zurich, Switzerland.*: 1097-1102.

Study of Western Taymyr Permafrost in the Framework of the IPY Education Program

Alexandra M. Zemskova

Lomonosov Moscow State University, Faculty of Geography, Dept. of Cryolithology and Glaciology, Moscow, Russia

Abstract

A 10-day course on Permafrost and Periglacial Geomorphology of Western Siberia and Western Taymyr (PPG), as part of the framework of the IPY education program, was jointly developed by faculty of the Geography Department of Moscow State University and researchers from the Earth Cryosphere Institute. The course was held at the end of July and beginning of August 2007 aboard the *Fedor Naianov* vessel, which sailed on Yenisey River from the town of Dudinka to the port of Dikson on the Arctic coast. The course attracted six Russian upper-level undergraduate and graduate students from Moscow State and St. Petersburg State Universities. The main topics of the course were (1) landscape-specific permafrost conditions and characteristics of the lower Yenisey River region, (2) ground ice and cryolithology, (3) Quaternary history of Western Taymyr, and (4) field methods of geomorphologic investigations. The course consisted of extensive field excursions at nine stops along the Yenisey and a lecture series and laboratory work aboard the ship.

Keywords: ground ice; IPY education program; landscapes; permafrost; Quaternary deposits; Western Taymyr.

Introduction

The expedition was organized under the supervision of two doctors of science: Irina D. Streletskaia (Lomonosov Moscow State University, Faculty of Geography, Dept. of Cryolithology and Glaciology, Moscow, Russia) and Aleksander A. Vasiliev (The Earth Cryosphere Institute SB RAS, Tyumen, Russia).

The young participants of the expedition were Alexandra M. Zemskova, Mikhail N. Ivanov, Ivan V. Kopytov, Sergey A. Simonov (Lomonosov Moscow State University, Faculty of Geography, Dept. of Cryolithology and Glaciology, Moscow, Russia), Maria A. Medvedeva, and Alexandra G. Cherkasheva (St Petersburg State University, Faculty of Geography, St. Petersburg, Russia) (Fig. 1).

Students participated in applied geocryology,



Figure 1. Our research group: Maria A. Medvedeva, Aleksander A. Vasiliev, Alexandra M. Zemskova, Alexandra G. Cherkasheva, Ivan V. Kopytov, Irina D. Streletskaia, Sergey A. Simonov, Mikhail N. Ivanov.

geomorphology, biology, and Quaternary research. This included the study of the spatial distribution of major landscapes, vegetation, and soil along the prime climatic gradient from Dudinka to Dikson; the study of geological cryogenic structures of Pleistocene sediments; collection of characteristic vegetation, soil, and sediment samples; and collection of ground ice samples for isotopic analysis. Contemporary cryogenic processes of the Western Taymyr coastal zone were studied, including coastal dynamics, ice wedges, thermokarst, etc.

Study Area

The study area was along the Yenisey River from Dudinka to Dikson Island. The eastern coast of the Yenisey Gulf from Sopochnaya Karga Cape to Dikson Island is the northwest periphery of the Taymyr Peninsula. Geographical characteristics of the region are influenced by the high latitude and the cold Kara Sea currents (Fig. 2).

Despite a general increasing trend of summer precipitation from north to south, the difference is not large: Ust'-Port, 137 mm; Igarka, 213 mm. The radiation balance in the warm period varies by latitude: Dikson Island, 891.7 MW; Turuhansk, 1218.3 MW.

The radiation balance during the cold period at Dikson Island is equal to 380.9 MW and in Turuhansk, 255.3 MW. The difference in the degree-hour sum for the cold period in the north and in the south is not more than 25%. The precipitation variance from north to south is large: Gol'chiha, 107 mm, and Igarka, 294 mm. The reason for this contrast is in the barrier for the western air masses, such as Putorana Plato. The Yenisey River valley is the territory of increased snow accumulation. Changes in topography effect the development of cryogenic processes.

The northern portion of the described region has relief with stepped construction. We can observe continuity of



Figure 2. The map with the route of research: 1 - Dudinka, 2 – Sopkarga, 3 – Vorontsovo, 4 – Budenovsk, 5 – Dixon, 6 – Krest'yanka, 7 – Narzoi, 8 – Zverevsk, 9 – Innokentevskoe.

relief levels from interfluvial to river valley. Formation of these levels is connected with the presence of Pleistocene sea basins, lake reservoirs, and rivers. According to the main exogenic processes, which form contemporary relief, it is possible to abstract three types of relief in this area: Pleistocene marine terraces; Pleistocene-Holocene, lake-limnetic accumulative depressions; and alluvial terraces.

The continuity of landscape zones with its own complex of cryogenic processes goes from the south to the north. The southern zone of low-bush tundra stretches from the latitude of Dudinka to Karaul. The northern zone of moss-lichen tundra extends close to 72°N latitude. Finally the arctic zone extends northward to the town of Dikson. (Tumel' 1988, Popov & Tumel' 1989).

Our research was in the northern part of this region. This polar region of the permafrost distribution consists of a tundra zone that stretches for 450 km from Dudinka latitude to the coast of the Kara Sea. Permafrost is continuous here. The permafrost thickness is greatest at the mouth of the Yenisey River: from 10 m to 600 m. Minimal thickness is observed at the low inundable levels where contemporary permafrost is forming. The annual average air temperature spectrum is wide: from 0°C to -9°C or -10°C. To the north from Ust'-Port the average air temperature is -7°C to -9°C.

Quaternary history of Western Taymyr

Mesozoic aqueous rocks crop out only to the north from Kuznetsovskiy Cape. To the south Pleistocene sediments have practically solid sedimentary cover above the bedrock. The intensive erosion of bedrock came before the Quaternary period, therefore the overdeepening of the Yenisey valley was 380 m lower than contemporary sea level. The thickness of Pleistocene sediments increases regularly from 100 to 200–400 m from south to the north. Quaternary deposits are as follows: alluvial, marine, glacial-marine, fluvio-glacial, glaciolacustrine, and deluvial- soliflual Pleistocene-Holocene sands, loams, and clays (Troickiy 1966).

Methods

Seven scientific-educational field trips have been undertaken by the participants of the expedition. We were doing observations, collecting samples of frozen ground and ice for different analyses, and making some field measurements (e.g., evaluation of the moisture content of frozen samples). For study of the contemporary permafrost state, ground ice specifics, and paleogeographical reconstructions a complex of field and laboratory methods has been used: geomorphological, cryolithological, geobotanical, landscape, geological, paleontological, radiocarbon, isotopic,



Figure 3. Packing samples of ice from the ice wedges.

optically stimulated luminescence (OSL), geochemical, pellet-mineralogical analysis by the Surkov method, and spore-pollen analysis. For these purposes, samples of frozen ground, snow, and ice were collected from coastal exposures (Fig. 3).

Geothermal survey methods were used in two wells equipped with loggers to monitor the temperature regime of the Western Taymyr accumulative land forms (alluvial spits). The boreholes are situated at the flat coast of the Sopochnaya Karga lagoon.

During the expedition students acquired fieldwork skills (describing boreholes and transverse sections, defining ice fraction, and collecting and registering of samples) and field and cameral treatment of collected materials (evaluation of solid natural moisture content, herborization, and sorting of samples).

Field Observations

During the expedition, Pleistocene-Holocene deposits in the coastal exposure of the east bank of the Yenisey River and Yenisey Bay were studied. The two types of frozen rocks showed epigenic type (freezing after the rock forming) and syngenetic type (freezing synchronously with sediment formation). The Samarovskaya (MIS (marine isotopic stage) 10) moraine deposits of middle Pleistocene, Sanchugovskie (MIS 8-6) marine and Kazancevskie (MIS 5) (Late Pleistocene) glacial-marine, marine and coastal-



Figure 4. Ice complex (coastal area of Sopochnaya Karga polar station).



Figure 5. Collecting the samples of ice from the “ice complex.”

marine deposits of Late Pleistocene refer to the epicryogenic type. As usual, the Middle-Pleistocene deposits are characterized by comparatively low ice content: up to 20% in volume and massive or nonregular cryogenic structure. The Late Pleistocene Kazancevskie deposits have greater ice content—up to 50%—and tabular massive ground ice with visible thickness more than 10 m were found (Figs. 4, 5).

Late Pleistocene-Holocene deposits of ice complex and Holocene deposits of contemporary deluvium and accumulative marine and fluvial formations refer to the syncryogenic type of permafrost. Ice complex deposits are characterized by high ice content—up to 80% in volume—and lenticular-stratified cryostructure (Karpov 1986). They contain polygonal ice wedges 4 m wide in the upper part of the section and up to 12 m high (Fig. 6).

Contemporary cryogenic processes of the Western Taymyr coastal zone were also studied. They are the following: coastal dynamics, ice wedges, thermokarst, etc. It is possible to see that for the last several decades the permafrost gas degraded in the explored region. Two wells were equipped with loggers for temperature regime monitoring of Western



Figure 6. Ice wedges near the Dikson.

Taymyr accumulative land forms (alluvial spits). The boreholes are situated at the flat coast of the Sopochnaya Karga lagoon.

Conclusions

Natural conditions at the Yenisei delta and at the Yeniseyskiy Bay coastal area from Sopochnaya Karga polar station to Dikson were studied.

Research methods in arctic landscapes, plant formation and soil covering, transverse sections of permafrost thicknesses have been taught in real, natural settings. Areal differentiation and variability of dominant landscapes, plant formations, soil cover in relation to the nature climatic zone at the Dudinka–Dixon transect have been studied. Geology aspects and cryolithological specifics of Middle-Late Pleistocene and Holocene deposits of Western Taymyr were studied too.

The samples of snow and ice from ice wedges and ice complex for study of isotopic composition of ground ice have been selected. Samples for optically stimulated luminescence (OSL) analysis of sand deposits have been selected with the purpose to determine absolute age of Middle-Late Pleistocene deposits.

Solids and ice samples were collected for laboratory study of their properties. We get new data for different parameters such as grain texture, mineralization of soils, spore-pollen compound and OSL, and radiocarbon age. Isotopic sampling was done almost for the first time ever at this part of Taymyr Peninsula.

Detailed data about flora specifics and their ratios in the different natural and climatic zonality—from forest tundra to arctic tundra—were collected.

Unique deposits of ice complex, inclosing repeated-wedge ice of great thickness, have been defined. It is established that the ice complex of Western Taymyr is represented by Late Pleistocene-Holocene sabulous deposits, the youngest deposits in the transverse section.

We plan to continue our observations on loggers. This will help to get new data about offshore permafrost on the lowland accumulative forms of relief (beach, bay bar); the speed and dynamic of permafrost formation; and how permafrost follows annual air temperature; that is, its reaction on climate changes.

Our research helps to improve the methods of field investigation and the use of new technologies and methods in the field. Results of these analyses would apply as a foundation for master and Ph.D. student work.

This expedition is a first step in international research group organization to do research work in this region.

But of course, some things need to be improved. If our group were able to use more portable technical equipment (e.g., modern GPS, salinity meter – to compare water in the Yenisey River and Yenisey Bay and ground, different soil and meteorological portable equipment, etc.) it could have made information, that we got more accurate and our trip would have been even more informative and productive. This would be useful because the region of our investigations is unique and poorly studied.

Acknowledgments

Research has been sponsored by ConocoPhillips Russia, Inc., and by the Oceanology Institute in Saint Petersburg. Special thanks to Elena Zemskova, to the management of the Great Arctic Reserve, to Mrs. A. F. Lubnina and Mr. G. I. Lubnin for lectures and for historical and ecological tour arrangements in the town of Dikson. I also express thanks to the reviewers of this paper for their comments and editorial changes.

References

- Karpov, E.G. 1986. *Ground Ice of Yeniseyskiy North*. Novosibirsk: Nauka, 133 pp.
- Saks, V.N. & Antonov, K.V. 1945. Quaternary deposits and geomorphology of Ust'-Yeniseyskiy port region. *Proceedings of the Glavsevmorput' Mining-and-Geological Administration*. Issue 16, N: Nauka, 56-117.
- Troickiy, S.L. 1966. *Quaternary Deposits and Relief of Yeniseyskiy Bay Flat Coastal Areas and Neighboring Part of Byrranga Mountains*. Moscow: Nauka, 207 pp.
- Tumel', N.V. 1988. *Cryolithological Research at the Educational Field Practice*. Moscow: Moscow State University, 97 pp.

Active Layer Monitoring at a New CALM Site, Taimyr Peninsula, Russia

F.N. Zepalov, V.I. Grebenets
Moscow State University, Moscow, Russia

D.A. Streletskiy, N.I. Shiklomanov
University of Delaware, Newark, USA

Abstract

The Circumpolar Active Layer Monitoring (CALM) site was established in the Taymir Peninsula to compensate for some deficiencies in the CALM observational network in Russia. The regular active layer measurements were initiated in 2005 followed by detailed characterization of landscapes and surface conditions. Periodic frost heave and thaw subsidence measurements by optical leveling were initiated in 2007. A short three-year period of observations allowed for only preliminary conclusions. The grid-average ALT for the study period is 87 cm. The thickness of the active layer varies from 45-50 cm to 125-150 cm, depending on landscape-specific conditions. The maximum thickness of the active layer is observed at landscapes represented by sparsely-vegetated patterned ground and dry hillocks. The minimum ALT was found in the polygonized peatlands. In the near future we intend to extend the observational program to include air and ground temperature monitoring. The establishment of complementary sites in underrepresented landscapes is currently under consideration.

Keywords: active layer thickness; CALM; Taimyr Peninsula.

Introduction

The active layer is the most dynamic and sensitive part of the climate-permafrost system. Knowledge of spatial and temporal characteristics of the active layer and factors affecting its long-term behavior and spatial pattern is required for assessing and predicting environmental conditions and socio-economic development of permafrost regions. Active layer investigations have a long history in Russia (Shiklomanov 2005) and include both empirical (Garagulya 1985, Kudryavstsev 1979) and modeling studies (Feldman 1977, Anisimov et al. 2002, Malevsky-Malevich et al. 2006).

Beginning in the 1990s systematic, standardized active layer and shallow permafrost observations were initiated under the international Circumpolar Active Layer Monitoring (CALM) program (Brown et al. 2000, Nelson et al. 2004). The series of 41 CALM sites that constitute the Russian portion of the network extends from the European tundra of the Pechora and Vorkuta regions to Chukotka and Kamchatka (Shiklomanov et al. 2008). However, the area adjacent to the Taimyr Peninsula, which constitutes a vast portion of Russian permafrost regions, is largely underrepresented by CALM. Two sites established in the Taymur region in the early 1990s were discontinued due to logistical circumstances (Fig. 1). To compensate for this CALM network deficiency, in 2005 a new Talnah site was established on the Taimyr Peninsula, in the Norilsk Industrial Region. This report provides a detailed description of the Talnah CALM site, observational methodology, and initial results obtained over the 2005-2007 period.

Study Area

The Talnah grid (R32 according to CALM classification) is located (69°26'01"N, 88°28'03"E) in the northern part of

Eastern Siberia on the Taimyr Peninsula (Fig. 1) at the Noril-Rybnin interfluvium, about 2.5 km southeast of the settlement of Talnakh (Norilsk Industrial Region). Kharaelakh Ridge of the Putorana Mountains lies 1.5 km north of the site. The site is situated on a fluvial terrace, characterized by loamy soils and underlain by low-temperature, continuous permafrost (Sheveleva & Khomichvskaya 1967, Ershov 1991). The climate of the region is temperate continental with prolonged, snowy winters and short, cool summers (Tushinskiy & Davydova 1976). On average, the period with negative mean daily air temperatures extends 245 days. Mean annual air temperature is -9.8°C . Mean air temperature of the coldest month (January) is -27.6°C , of the warmest month (July), $+13.4^{\circ}\text{C}$. Average annual wind speed is 6.3 m/s and the annual sum of precipitation is 340 mm/yr. The climatologically average maximum snow-cover thickness is 80 cm.

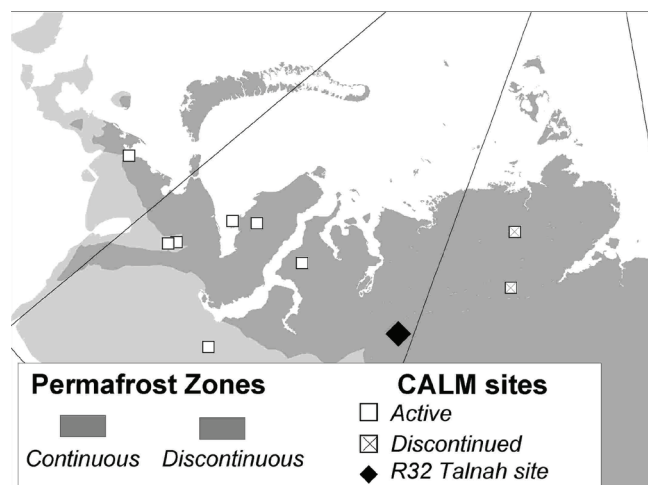


Figure 1. Distribution of permafrost zones (Brown et al. 1997) and location of CALM sites in Russian European North, West Siberia and Taimyr Region.

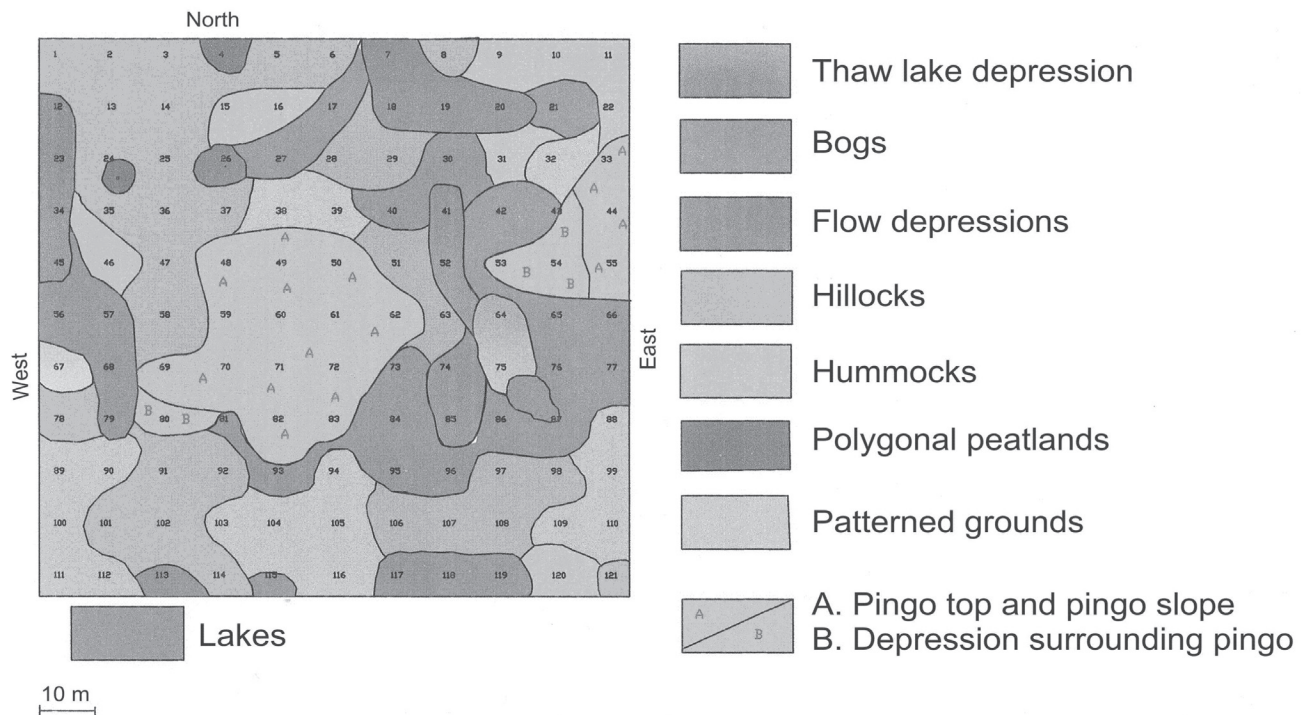


Figure 2. Results of landscape classification within the R32 Talnakh 1-ha CALM site.

Sediments primarily consist of loam with small intrusions of pebbles and overlain by a thin peat layer. The grid is situated on subhorizontal surface with elevation decreasing in a southeast direction. A small frost mound (pingo) 30 m in diameter and 1.5 m high occupies a portion of the site. The frost mound is surrounded by flow depressions and polygonized peatlands. The size of the polygons varies from 6 to 8 m across. Hummocks up to 20 cm in height and hillocks up to 60-70 cm in height are widely present. Typical tundra vegetation occupies the site and consists of shrubs, dwarf-shrub and sedges. Mosses and lichens are largely absent from the site. The environmental and geocryologic conditions of the site closely correspond to those of the southwestern part of the Taimyr Peninsula.

Methodology

A regular 100 x 100 m (1 ha) grid was established at the site in the summer of 2005 according to recommendations provided by CALM protocol (Brown 2000).

The establishment of the grid was followed by detailed characterization of landscapes and surface conditions. Nine main landscape categories, characteristic of the southwestern part of the Taimyr Peninsula are contained within the grid (Fig. 2).

Periodic annual active layer measurements were initiated in 2005 at grid nodes separated by 10 m, yielding an array of 11 x 11 nodes across the grid (Fig. 2). The measurements are performed by mechanical probing using a graduated metal rod. As a rule, each point is probed twice. However, if the difference between two measurements is significant, additional observations are taken at close proximity to the

sampling point. An average value is calculated for each sampling point, yielding a total of 121 data values for the grid per probing date.

During the 2007 field season the optical leveling of grid nodes was initiated following CALM-approved procedure described in detail at the CALM website (<http://www.udel.edu/Geography/calm/research/MazhitovaMethod.pdf>).

Records of major climatic parameters are available from the Russian meteorological station, Alykel Airport, located 50 km west of the grid. In the near future we intend to instrument the Talnah site for continuous air and ground temperature monitoring.

Results and Discussion

The Digital Elevation Model (DEM) of the site for the year 2007 is shown in Figure 3. DEM indicates a slight increase in elevation in the northwest direction. The optical leveling will be continued annually and will be used to evaluate changes in the position of the ground surface associated with frost heave and thaw subsidence.

To analyze the spatial distribution of the active layer thickness, grid-node values of ALT were interpolated using krigging technique to produce annual maps of ALT. Annual ALT maps for the 2005-2007 period and map of three-year averages are shown in Figure 4. The summary statistics for three years of available ALT measurements are presented in Table 1.

The maximum three-year grid average ALT is 87.3 cm, with the minimum 50 cm and the maximum 126.5 cm; standard deviation is relatively small and does not exceed 15 cm (Fig. 4).

Constructed annual maps of ALT show high spatial variability of this parameter, despite the fact that the variation of the summer climatic signal expressed as Degree-Days of Thawing on a moment of measurements did not exceed 10% and on average was around 980°C days.

To evaluate landscape-specific contributions to overall active layer pattern, the ALT values, as measured at each particular landscape presented in Figure 2, were analyzed. The landscape-specific statistical distributions of ALT values, obtained over a three-year period and representing both temporal and spatial ALT variability, are shown in Figure 5.

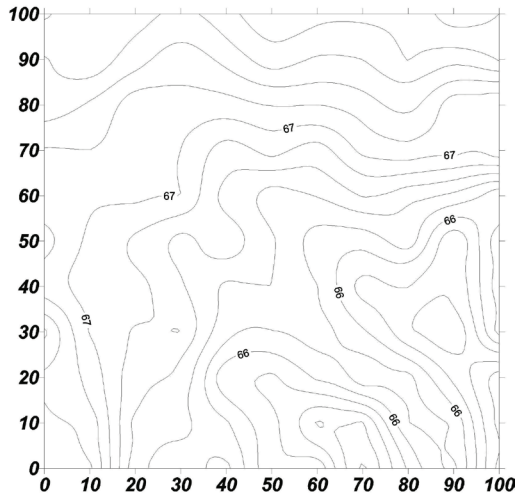


Figure 3. Digital elevation model developed by optical leveling. Isolines are given at 0.2 m interval. In-between grid interpolation performed by krigging.

Table 1. Annual ALT statistics for the R32 Talnakh site.

Year	2005	2006	2007
Mean	81.3	90.8	89.5
Minimum	49.0	42.5	49.0
Maximum	150.0	164.0	150.0
St.Deviation	19.0	22.4	19.9

The highest degree of variability was encountered at patterned ground features represented by frost mounds. It

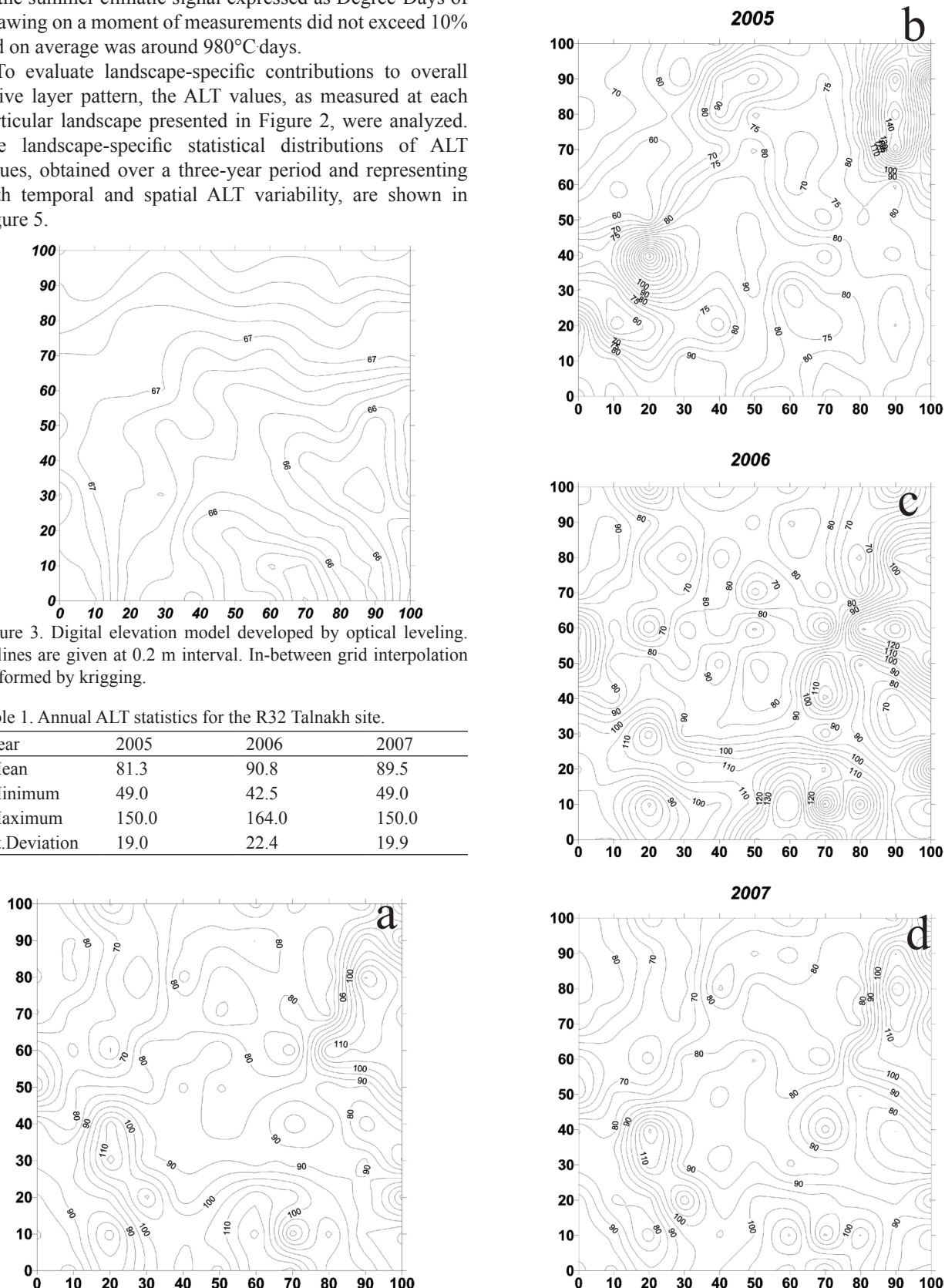


Figure 4. Results of annual ALT surveys at R32 Talnakh grid for 2005 (b), 2006 (c), 2007 (d) and average values of ALT for 2005-2007 period (a). Isolines are given at 5 cm intervals.

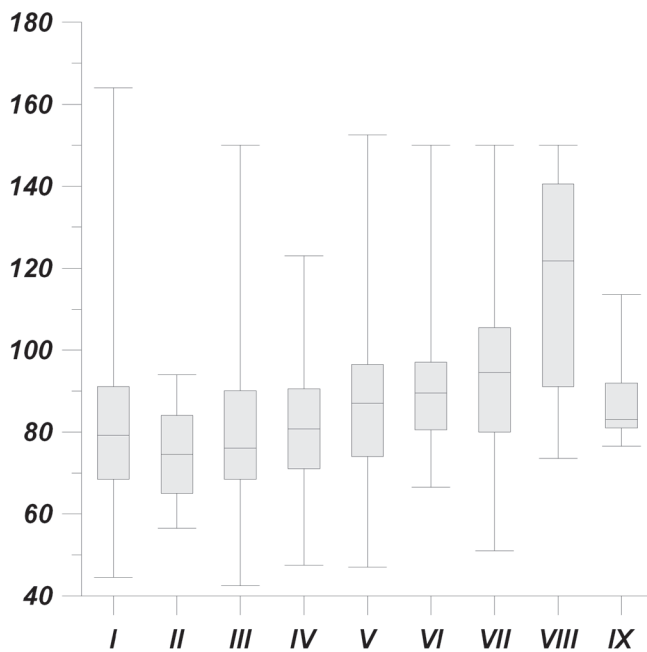


Figure 5. Box-whisker plots of ALT in characteristic landscape units. I – Hillocks, II – Polygonal peatland, III – Hummocks, IV – Flow depressions, V – Bogs, VI – Pingo, VII – Patterned ground, VIII – Depression surrounding pingo, IX – Thaw lake depression.

Table 2. Average (2005–2007) values of ALT for characteristic landscape units. Landscapes are identified in captions for Figure 5.

Unit	I	II	III	IV	V	VI	VII	VIII	IX
ALT	82	74	80	81	90	92	95	114	87

can be attributed to sparse vegetation cover and thin organic layer characteristic of these landscapes. Dense vegetation and thick organic layer significantly mitigate the influence of variability in climatic forcing resulting in less temporally and spatially heterogeneous active layer. This effect is illustrated by small ALT variations, observed at densely-vegetated, polygonized peatlands and thaw lake depressions. These landforms are also characterized by thick accumulations of peat. The high degree of active layer variability observed at hillocks and hummocks can be largely attributed to significant differences in ALT values obtained from the tops of hummocks and from interhummock depressions. The high spatial heterogeneity of the active layer in a tussocky and hummocky landscape was observed in Alaska and reported by Nelson et al. (1999). Flow depressions, surrounding frost mounds, are characterized by a high degree of variability around mean, but a relatively small range of values. This can be explained by the relatively small sample of points representing this landscape unit.

The landscape-specific three-year means of ALT are presented in Table 2. The highest value of 114 cm was observed at flow depressions, which are subject to convectional heat transfer by running water. The thinnest ALT (74 cm) is characteristic of polygonized peatlands with dense vegetation cover and thick organic layer.

Conclusions

The Talnah CALM site was established in the Taymir Peninsula to compensate for some deficiencies in the CALM observational network in Russia. Regular active layer measurements were initiated in 2005. A short, three-year period of observations allowed for only preliminary conclusions. The grid-average ALT for the study period is 87 cm. The thickness of the active layer varies from 45–50 cm to 125–150 cm, depending on landscape-specific conditions. The maximum thickness of the active layer is observed at landscapes represented by sparsely-vegetated patterned ground and dry hillocks. The minimum ALT was found in the polygonized peatlands. Periodic heave and subsidence measurements by optical leveling were initiated in 2007. In the near future we intend to extend the observational program at the Talnah site to include air and ground temperature monitoring. The establishment of complementary sites, characteristic of regional landscapes underrepresented by the Talnah site, is currently under consideration.

Acknowledgments

This study was conducted as part of the research and educational plan of the Department of Geography at Moscow State University. We are also grateful to the U.S. National Science Foundation for their partial financial support through an OPP-0352957 grant, administered by the University of Delaware.

References

- Anisimov, O.A., Shiklomanov, N.I. & Nelson, F.E. 2002. Variability of seasonal thaw depth in permafrost regions: a stochastic modeling approach. *Ecological Modeling* 153(3): 217-227.
- Brown, J., Hinkel, K.M. & Nelson, F.E. 2000. The circumolar active layer monitoring (CALM) program: Research designs and initial results. *Polar Geography* 24(3): 165–258.
- Brown, J., Ferrans, O.J., Heginbottom, J.A. & Melnikov, E.S. 1997. *Circum-Arctic Map of Permafrost and Ground-ice Conditions*. Circum-Pacific Map Series, Report: CP- @0045, 1 sheet.
- Ershov, E.D. & Kondrateva, K.A. 1991. *The Geocryological Map of the USSR*. Scale 1:2,500,000. Moscow: GUGK, 1 p.
- Feldman, G.M. 1977. Forecast of ground temperature regime and development of cryogenic processes. Nauka: Novosibirsk, 192 pp. (in Russian).
- Garagulya, L.S. 1985. Metodika prognoznoy otsenki antropogennih izmeneniy merzlotnih usloviy. Izd. Moskovskogo Universiteta. 224 pp. (in Russian).
- Kudryavtsev, V.A., Garagulya, L.S., Kondrat'yeva, K.A. & Melamed, V.G. 1974. Osnovy merzlotnogo prognoza. Moscow State University Press, 431 pp. (in Russian).

- Malevsky-Malevich, S.P., Molkentin, E.K., Nadyozhina, E.D., Pavlova, T.P. & Semioshina, A.A. 2006. Validation problems of permafrost evolution modeling. *Proceedings of International Conference: Earth Cryosphere Assessment: Theory, Applications and Prognosis of Alterations, Tumen'* Vol. 1, 78-82.
- Nelson, F.E., Shiklomanov, N.I., Christiansen, H.H. & Hinkel, K.M. 2004. The circumpolar-active-layer-monitoring (CALM) Workshop: Introduction. *Permafrost and Periglacial Processes* 15: 99-101.
- Nelson, F.E., Shiklomanov, N.I. & Mueller, G.R. 1999. Variability of Active-Layer Thickness at Multiple Spatial Scales, North-Central Alaska, U.S.A. *Arctic, Antarctic, and Alpine Research* 31 (2): 179-186.
- Sheveleva, N.S. & Khomichevskaya, L.S. 1967. *Geocryological Conditions of Enisey North*. Moscow, Nauka, 126 pp.
- Shiklomanov, N.I., Nelson, F.E., Streletskiy, D.A., Hinkel, K.M. & Brown, J. 2008. The Circumpolar Active Layer Monitoring (CALM) program: data collection, management, and dissemination strategies. *Proceedings of the Ninth International Conference on Permafrost, Fairbanks, Alaska, June 29-July 3, 2008* (this proceedings).
- Shiklomanov, N.I. 2005. From exploration to systematic investigation: Development of geocryology in 19th- and early-20th-century Russia. *Physical Geography* 26(4): 249-263.
- Tushinskiy, G.K. & Davydova, M.I. 1976. *Physical Geography of the USSR*. Moscow: Prosvetschenie, 543 pp.

Experimental Study on Mechanisms of Subgrade Deformation in Permafrost Regions Along the Qinghai-Tibetan Railway

Jianming Zhang

State Key Laboratory of Frozen Soil Engineering, Cold and Arid Regions Environmental and Engineering Research Institute, Chinese Academy of Sciences, Lanzhou, China

Xiaojie Ma

Zhejiang College of Construction, Hangzhou, China

Bo Zheng

China Academy of Railway Science, Beijing, China

Abstract

Field observations at the Beiluhe test site along the Qinghai-Tibetan Railway indicate that, even though the permafrost table under the embankment has moved up since the railway was built, the embankment still has suffered quite a lot of settlement, and the settlement has been mainly due to deformation of the warm and ice-rich frozen soils under the original permafrost table. In order to understand the mechanism of the subgrade deformation in permafrost regions, pressure meter tests were conducted under the embankment, and compression tests were carried out in the laboratory. Based on the test results, the settlement in the embankment at the Beiluhe test site was estimated taking into consideration the compression of the warm and ice-rich permafrost. Over the next 50 years, the estimated settlement in the embankment is about 40 cm, even though the permafrost under the embankment will not thaw at all.

Keywords: embankment settlement; permafrost regions; Qinghai-Tibetan Railway; warm and ice-rich frozen soils.

Introduction

In permafrost regions, the construction of a roadway embankment changes not only the thermal regime of the permafrost under the embankment but the stress state in the subsoil as well. With the adjustment of both temperature and stress in the subsoil, the stability of the embankment will inevitably be modified, and settlement of the embankment takes place. According to experience gained from the Qinghai-Tibetan Highway, the settlement of a roadway embankment in permafrost regions is generally composed of three parts: (1) compression of the fill, which depends on the material of the embankment and the density of the fill; (2) consolidation of the active layer, which is controlled by the soil type and its water content; (3) thaw settlement of the permafrost, which is related to the thickness of the embankment and the ice content in the permafrost. Of the three kinds of deformations, the thaw settlement of permafrost under the embankment is the most significant for the stability of the roadway embankment (Wu et al. 1988, Wu & Liu 1989, Yu & Yan 1986).

During the construction of the Qinghai-Tibetan Railway in 2001, many measures were taken to protect the permafrost in the subsoil. Among them the most common practice was to build an embankment thick enough to prevent the permafrost from thawing. However, field observations from 2002 to 2005 at Beiluhe test site along the railway indicated that, even though the permafrost table under the embankment has moved up since the railway was built, the embankment has still suffered quite a lot of settlement, and the settlement has been mainly due to deformation of the ice-rich frozen soils under the original permafrost table. In order to understand the mechanism of this kind of deformation and to estimate

the settlement of the railway embankment in the future, pressure meter tests were conducted under the embankment in the summer of 2005, and compression tests on ice-rich frozen soils under a stepped temperature rise were carried out in the laboratory in 2006. In this paper, we present the field observation data, the test results, and then an estimate of the settlement of the railway embankment in the coming 50 years.

Field Observation

Test section

Since 2002, after the embankment was built, six test sections have been set up at Beiluhe test site along the railway to monitor the ground temperature under the embankment and the layered settlement of the subgrade. The layout of the test sections is shown in Figure 1, and the permafrost conditions at each section are given in Table 1.

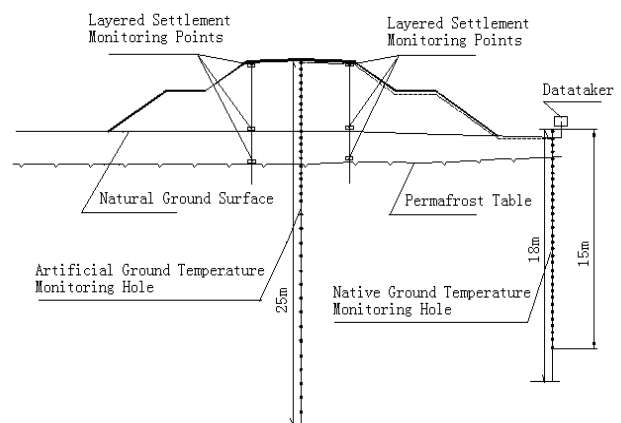


Figure 1. Component layout at the test section.

Table 1. Permafrost conditions at each test section.

Test section (km+m)	Embankment thickness (m)	Permafrost table in natural ground (m)	Mean annual ground temperature (°C)	Thickness of ice-rich frozen soils (m)
DK1136+520	2.9	2.2	-0.74	4.4
DK1136+540	4.5	2.0	-0.78	3.5
DK1136+580	5.0	1.9	-1.01	5.6
DK1136+755	3.0	2.0	-0.46	2.0
DK1136+775	4.2	2.0	-0.45	3.0
DK1136+800	5.4	2.3	-0.46	4.5

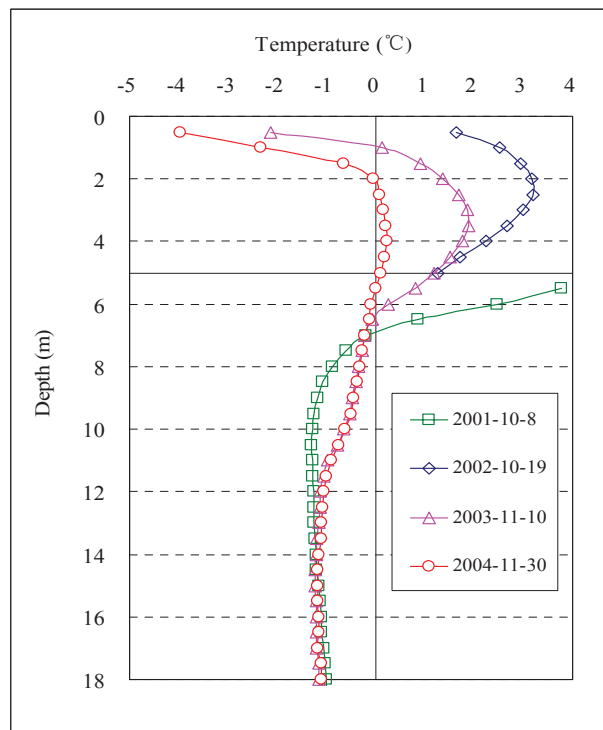


Figure 2. Ground temperature profiles in the embankment.

Ground temperature

Figure 2 shows the typical ground temperature profiles at the centerline of the embankment at DK1136+580 during 2001 to 2004 in the seasons of max. thawing depth. It can be seen that, though the permafrost table under the embankment has moved up gradually since the embankment was built, the ground temperature under the original permafrost table also rose remarkably at the same time. The ground temperature rise will certainly cause changes in mechanical properties of the permafrost, resulting in settlement of the embankment.

Embankment settlement

Figure 3 presents layered settlement processes of the embankment at DK1136+580 from 2002 to 2005. Taking a close look at the processes, we can see that the difference in settlement between the roadway surface and the natural ground surface, which is the compression of the fill, is rather small. The difference between the ground surface and the original permafrost table, which is the consolidation of the active layer, is also small. However, the settlement at the

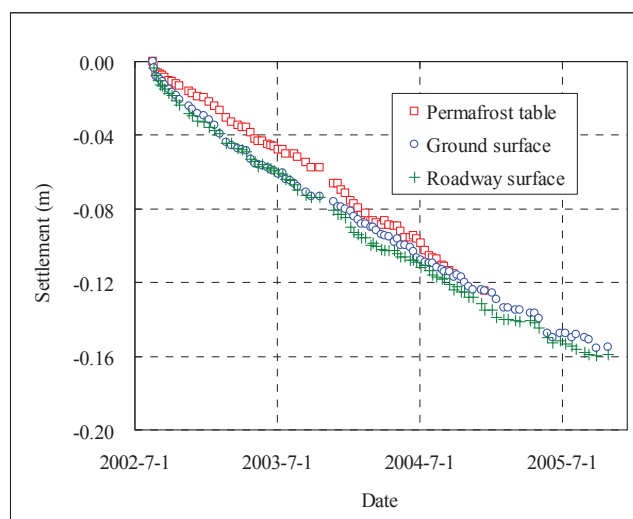


Figure 3. Layered settlement processes of the embankment.

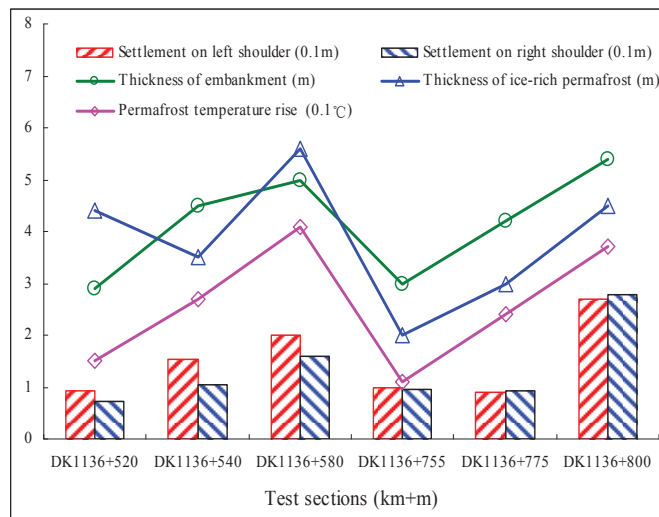


Figure 4. Embankment settlement and permafrost conditions in the subgrade.

original permafrost table is much larger. It is clear that the total settlement of the roadway embankment is largely due to the deformation of the warm and ice-rich frozen soils under the original permafrost table.

Discussion

Figure 4 shows the total settlement values at each of the six test sections and the possible factors which have an effect on the settlement, such as the thickness of embankment and

Table 2. Soil conditions of the pressure meter tests.

Test position	Under embankment				Natural ground	
	1.4	2.1	3.6	4.0	3.6	4.7
Depth (m)	1.4	2.1	3.6	4.0	3.6	4.7
Soil type	Silty clay					
Temp. (°C)	-0.25	-0.31	-0.50	-0.69	-0.85	-0.89
Moisture (%)	20.8	101	36	63.9	37.3	24.5
Density (g/cm ³)	2.27	1.39	2.09	1.66	2.07	2.12

the thickness of ice-rich permafrost in the subgrade, as well as the temperature rise of the ice-rich permafrost due to the construction of the embankment. In this figure, it can be seen that the settlement values relate well with the factors at most of the test sections. At the sections with thicker embankment, thicker ice-rich permafrost, and more temperature rise, the settlement of embankment is greater.

Pressure Meter Test

Test condition

In order to investigate the variation of mechanical properties of the permafrost in the subgrade, pressure meter tests were carried out under the railway embankment as well as in the adjacent natural ground in September 2005. The device used in the tests was a TEXAM pressure meter made by ROCTEST with a metallic probe of 58mm in diameter. The tests were performed in the strain controlled mode, and the test conditions are given in Table 2. In the table, it is obvious that, at the same depth below the original ground surface, the soil temperatures under the embankment are always higher than those in the natural ground.

Test result

Figure 5 and Figure 6 show the pressure meter test results of shear modulus and max. pressure, respectively, at different depths under the embankment and in the natural ground. It is evident that both the shear modulus and the max. pressure in the subgrade are lower than those in the natural ground. This means the mechanical properties of the permafrost in the subgrade have been changed considerably since the railway embankment was constructed. It also confirms that the settlement of the embankment was mainly due to the deformation of the ice-rich frozen soils under the original permafrost table caused by temperature rise in the subgrade.

Compression Test

Test condition

In order to determine the compressibility of the ice-rich frozen soils caused by temperature rise, compression tests were carried out in the laboratory. The soil samples of silty clay from the test sections were prepared with water contents

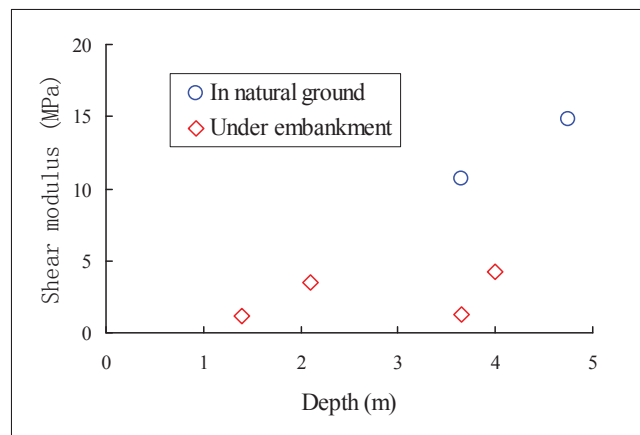


Figure 5. Comparison of shear modulus between under embankment and in natural ground

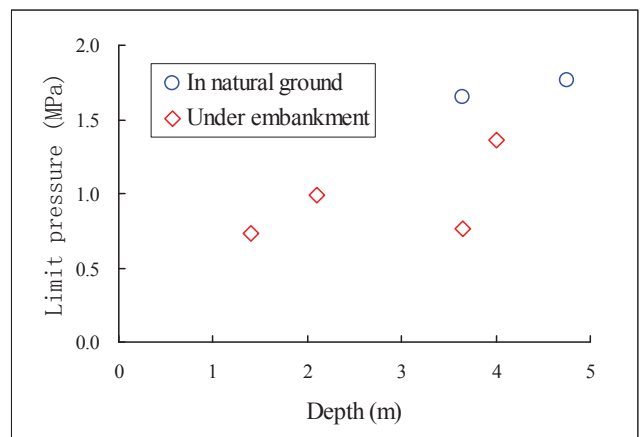


Figure 6. Comparison of max. pressure between under embankment and in natural ground

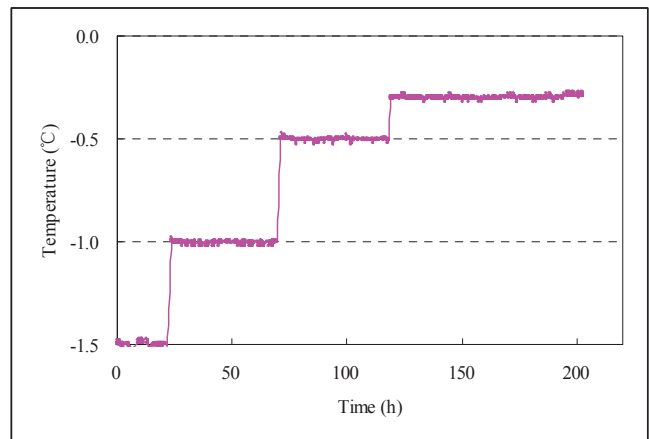


Figure 7. Temperature process in the compression test.

of 40% and 80%, respectively, and the water contents were kept constant during the tests. The tests were performed in an oedometer with a diameter of 61.8mm and a height of 40mm. In order to understand the influence of temperature on the compressibility of frozen soil, the load was kept constant in each test, and the temperature was controlled in a stepped rise mode as shown in Figure 7.

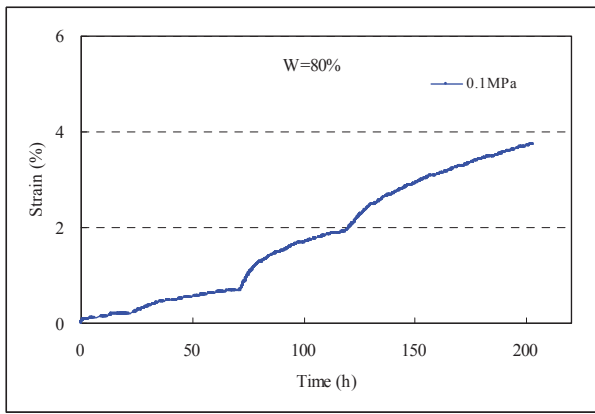


Figure 8. Deformation process in the compression test.

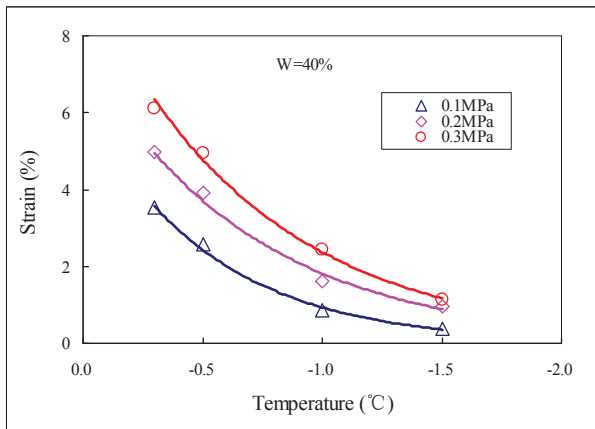


Figure 9. Total compressibility vs. temperature step.

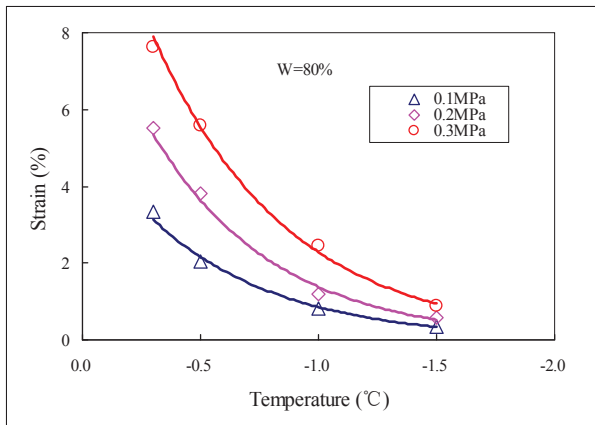


Figure 10. Total compressibility vs. temperature step.

Test result

Figure 8 shows the deformation process of the frozen soil with water content of 80% and under pressure of 0.1MPa, corresponding to the temperature steps shown in Figure 7. It is apparent that, even under such low stresses, the frozen ice-rich, silty clay can produce quite a lot of deformation during the temperature rise process, especially when close to 0°C. Figure 9 and Figure 10 present the test results of compressibility under different temperature steps and different pressures. It should be noted that the compressibility is more sensitive to pressure when temperature approaches 0°C.

Settlement Estimation

Calculation model

Based on the test results and concepts mentioned above, we can estimate the settlement of the railway subgrade in permafrost regions. According to experience obtained from both the Qinghai-Tibetan Highway and the Qinghai-Tibetan Railway, the settlement of the subgrade must include both the thaw settlement and the compression of the permafrost under the embankment, and it should be calculated as:

$$S = S_1 + S_2 + S_3 = \sum_{i=1}^n A_i \cdot h_i + \sum_{i=1}^n \alpha_i \cdot P_i \cdot h_i + \sum_{j=1}^m \Delta\alpha_j^z \cdot P_j \cdot h_j$$

where S is the total settlement of the subgrade, S_1 is the thaw settlement of the permafrost, S_2 is the consolidation of the permafrost after thawing, and S_3 is the compression of the warm and ice-rich permafrost. In detail, A is the thaw-strain parameter of permafrost, h is the thickness of soil strata assumed in the calculation, α is the compression coefficient of thawed soil, P is the pressure applied on the soil strata, and $\Delta\alpha^z$ is the variation of the compression coefficient of frozen soil caused by temperature change.

According to the geological conditions at Beiluhe test site, the permafrost profile adopted in the calculation is shown in Figure 11. The compressible layer is the ice-rich frozen soil under the embankment from 2 to 8 m below the natural ground surface. The mechanical parameters of the ice-rich frozen soil in the subgrade are: $A=0.084$, $\alpha=0.45$ MPa. The variation of a^s with temperature is shown in Figure 12, and h is taken as 0.25 m referring to the calculation of the ground temperature profiles over the next 50 years.

Ground temperature prediction

Before the settlement of the subgrade is estimated, it is necessary to predict the ground temperature profiles under the embankment. According to the numerical model to calculate heat transfer in frozen ground (Zhang et al. 2006), the ground temperature profiles in the centerline of the embankment over the next 50 years in the seasons of max. thawing depth are shown in Figure 13. In this figure, it is clear that the ground temperature in the subgrade will increase with the service life of the railway embankment.

Calculation result

Based on the subgrade deformation model and the ground temperature profiles, the settlement of the subgrade in future can be calculated. Figure 14 presents the estimate of the subgrade settlement processes for different embankment thickness. It can be seen that the settlement increases with increase in embankment thickness, and it will be about 40 cm by the end of the next 50 years even though the permafrost under the embankment does not thaw at all.

Conclusions

The results of both pressure meter tests and compression tests confirm that the warm and ice-rich permafrost in the railway subgrade can produce quite a lot of deformation

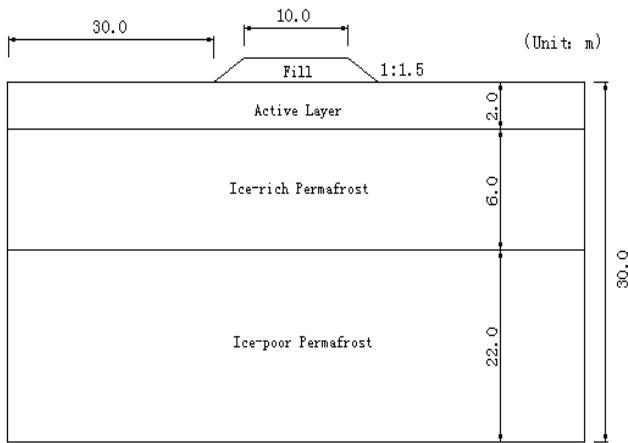


Figure 11. Permafrost profile under the embankment.

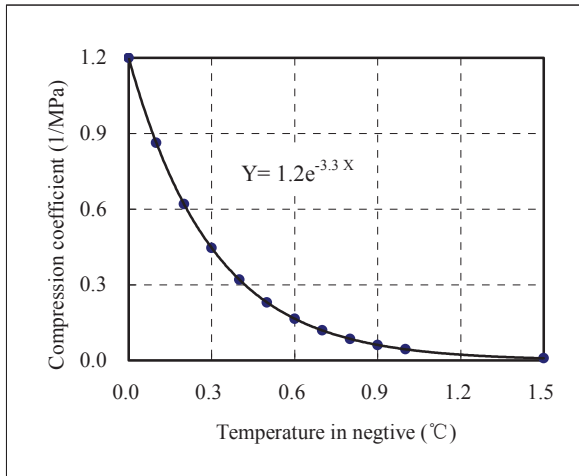


Figure 12. Relationship between compression coefficient of frozen soil and temperature.

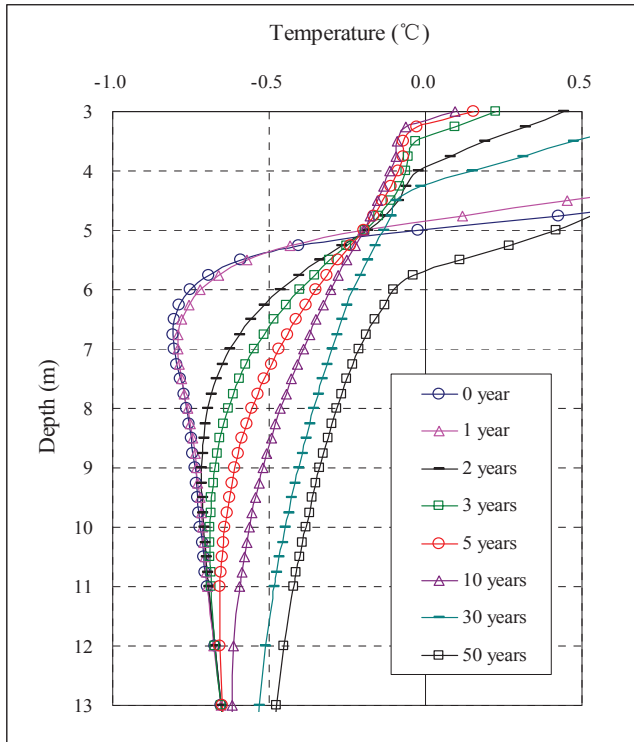


Figure 13. Prediction of the ground temperature under embankment (embankment thickness: 3 m, MAGT: -0.5°C).

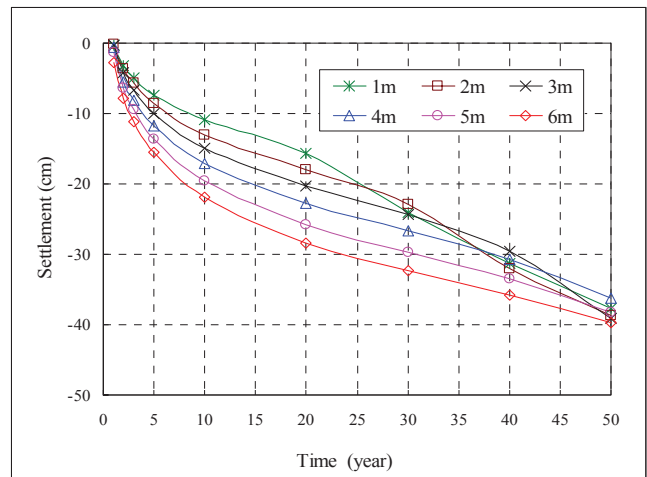


Figure 14. Estimate of the subgrade settlement process (embankment thickness: 1~6m, MAGT: -0.5°C).

due to the temperature rise in the subgrade, even though the permafrost table under the embankment moves up after the railway is built. The estimate of the subgrade settlement indicates that the settlement increases with the increase in embankment thickness and ground temperature. Therefore, if this kind of deformation is to be controlled, active cooling measures must be taken to lower the ground temperature in the subgrade. The traditional method of increasing the embankment thickness is ineffective and even worse for the stability of the railway subgrade in the warm and ice-rich permafrost regions.

Acknowledgments

This work was supported by the Knowledge Innovation Program of Cold and Arid Regions Environmental and Engineering Research Institute, Chinese Academy of Sciences (2004104), the Knowledge Innovation Important Program of the Chinese Academy of Sciences (KZCX3-SW-351), and the National Natural Science Foundation of China (40730736).

References

- Wu, Z.W., Cheng, G.D., Zhu, L.N. & Liu, Y.Z. 1988. *Roadbed Engineering in Permafrost Regions*. Lanzhou: Lanzhou University Press, 61-84.
- Wu, Z.W. & Liu, Y.Z. 1989. Forecasting of deformation of asphalt paved frozen roadbed of the Qinghai-Xizang Highway. *Proceedings of the 3rd Chinese Conference on Permafrost*. Beijing: Science Press, 333-338.
- Yu, W.X. & Yan, Q.P. 1986. Primary analysis of the subgrade deformation along the Qinghai-Xizang Highway in permafrost regions. *Journal of Xi'an Highway University* 1986 (1): 49-70.
- Zhang, J.M., Zhang, J.Z. & Liu, Y.Z. 2006. Study on the reasonable embankment height of the Qinghai-Tibetan Railway in permafrost regions. *China Railway Science* 27(5): 28-34.

Designing the Height of the Qinghai-Tibet Highway in Permafrost Regions

Jinzhao Zhang

Laboratory of Cold Regions Road Engineering, The First Highway Survey and Design Institute of China, Xi'an, 710068

Fujun Niu

State Key Laboratory of Frozen Soil Engineering, Cold and Arid Regions Environmental and Engineering Research Institute, CAS, Lanzhou, China 730000

Shuangjie Wang

Laboratory of Cold Regions Road Engineering, The First Highway Survey and Design Institute of China, Xi'an, 710068

Yongguo Zhao

Laboratory of Cold Regions Road Engineering, The First Highway Survey and Design Institute of China, Xi'an, 710068

Abstract

The Qinghai-Tibet Highway is a significant engineering structure built in the permafrost regions of China. When the highway was initially constructed in the 1950s and permafrost was encountered, the road embankment was just paved with the nearby materials. Since the 1970s, the highway has been rebuilt or repaired on a large scale three times, mainly to treat problems caused by the permafrost. Along with continuous repairing activities, research work was carried out three times, focusing on embankment stability and permafrost status. In the first research work before 1979, the main factor considered in the embankment height designing was the buried depth of the local permafrost table. In the second research work during 1979–1985, when it was paved with asphalt, the embankment height was increased and a permafrost-protecting principle was adopted. In the third research work after 1985, roadbed problems along the whole length were investigated. The investigation showed that 152 km of the highway were damaged by settlement. To avoid future thaw settlement, comprehensive remedy methods were applied to actively protect the permafrost and, subsequently, the roadway.

Keywords: designing principle; embankment height; permafrost; roadbed; Qinghai-Tibet Highway.

Introduction

The total length of the Qinghai-Tibet Highway (QTH) is 1937 km from Xi'ning of the Qinghai province to Lhasa of the Tibet Autonomous Region. The length of the section from Golmud to Lhasa, which is a second-class highway, is 1150 km. The highway is very important, as more than 85% of materials and more than 95% of passengers to Tibet were transported this way since 1954. The highway crosses a permafrost area with a length of more than 630 km from

Xidatan Valley to Andou County (Fig. 1), where the average elevation is over 4500 m a.s.l.

The QTH was initially constructed in the 1950s, and then about 20 years later, an asphalt layer was paved on the surface. Since the 1990s, the highway has been rebuilt or repaired greatly three times, and research work has been carried out which focuses on the embankment design principle and height. Though some problems of the QTH have not been thoroughly solved so far, the average driving speed can be 60 to 100 km/h now. Such a speed is the highest value in the servicing history of the highway.

Embankment Height Designing of the QTH Before 1979

The QTH research group drafted an Asphalt Layer Construction Manual of the QTH in Permafrost Regions in October 1978. In the report, it was pointed out that there were more than 100 km of ice-saturated and massive-ice permafrost along the highway. As the underlying permafrost was not effectively treated during roadbed construction, some problems, including thaw slumping, roadbed deformation, and frost boiling, occurred when the road was opened to service. The problems were eliminated after repair and remedy over 20 years. However, it was pointed out that the heat balance would be destroyed again if the asphalt layer were paved. Also, new diseases would occur if the permafrost were not protected effectively. It was also

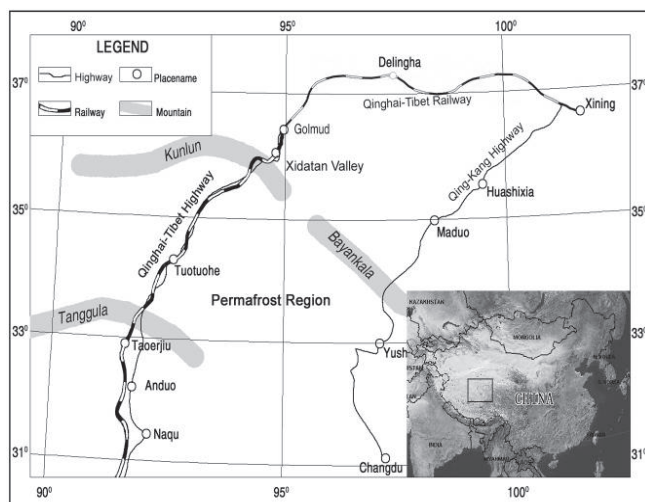


Figure 1. The location of the QTH and permafrost distribution in the Qinghai-Tibet Plateau.

pointed out that a filling-but-not-cutting principle should be followed in roadbed construction in permafrost regions, except in icy soil, ice-poor soil, and seasonally frozen ground sections. Embankments in ice-poor and icy soil regions may be designed without any special structure. The frozen ground should be properly protected in sections of ice-rich permafrost. Necessary measures were suggested to protect the underlying frozen ground in ice-saturated permafrost regions, and to strictly protect massive-ice permafrost regions. These prescripts indicated that the design principle during this period was to protect the permafrost in roadbed construction.

The results of the field experiments along the highway showed that the sandy surface lowered the permafrost table with a value of 15–25cm. The relation between embankment height (H) and the depth of permafrost table (h) was

$$h = 0.95H - 0.15 \tag{1}$$

However, the permafrost table lowered 25–30 cm under the black asphalt surface. Considering the different thermodynamic conditions of asphalt and gravel surface, suggestions on the embankment height were given as listed in Table 1, based on monitored results (QTH Research Group 1978).

According to Table 1, the maximum embankment height of QTH was less than 1.5 m. Based on the principle of protecting permafrost and suggestions on the embankment height, an embankment design scheme between Wudaoliang (mileage of K3007) and the Tanggula Mountain (mileage of K3350) was recommended. At the same time, it was confirmed that a black asphalt surface can be paved on the embankment in permafrost regions.

Embankment Height Designing of the QTH from 1979 to 1985

Since 1979, black road surface was mainly paved in permafrost regions where geological conditions were poor and frozen damage easily occurred. In order to ensure the quality of the project, the embankment height was suggested to be increased to protect the underlying frozen ground, based on engineering practice and observation. Some methods were proposed such as: (1) a principle of protecting frozen ground should be followed in permafrost regions; (2) embankment height should be increased to counteract

Table 1. Suggested embankment height in different permafrost regions (unit: m).

Permafrost	Embankment soil		
	Silty clay and clay	Sand and sandy soil	Gravel soil
Ice-rich soil	0.5 - 0.8	0.5 - 0.8	0.5 - 0.8
Ice-saturated soil	0.8 - 1.0	0.8 - 1.1	0.8 - 1.2
Massive ground-ice	1.0 - 1.2	1.1 - 1.3	1.2 - 1.4

the influence of black road surface, and two lateral sides should be protected too; (3) necessary embankment height should be determined, keeping the permafrost table stable or a little lowered in regions where the frozen ground has low ice-content (lower than the ice-content in ice-rich soil), instead of keeping the roadbed totally frozen. To practice these methods, the permafrost along the way was classified into 4 classes. Two sets of embankment height value were suggested in 1980 and 1981 (QTH Research Group 1978, 1981). The values were listed in Tables 2 and 3.

Comparing the values listed in Tables 2 and 3, the embankment height was higher in 1980 and 1981 than that in 1978 and 1980. At same time, the embankment height values suggested in 1981 were higher up to 1.0 m than those in 1980. The embankment height values suggested in 1980 were based on considerations of frozen soil types and embankment soils. The values suggested in 1981 were based on considerations of frozen soil types, permafrost table, and topography. Therefore, the values of 1981 were increased in accord with protecting frozen soil and status of the QTH.

The repair design in this period was changed according to the suggested height values in 1980. Then part of the embankment was repaired considering investment capacity and building time.

Along with progress of research work on the QTH, some other suggestions were proposed, such as the filling soils could be cut from the nearby ground as it was lack of sand and stone materials along the highway, but it was strictly

Table 2. The suggested minimum embankment height for protecting the underlying permafrost in 1980 (unit: m)

Permafrost	Embankment soil		
	Silty clay and clay	Sand and sandy soil	Gravel soil
Ice-rich soil	0.8 - 1.0	0.9 - 1.1	1.0 - 1.2
Ice-saturated soil	0.9 - 1.2	1.0 - 1.3	1.2 - 1.5
Massive ground-ice	1.1 - 1.4	1.2 - 1.5	1.3 - 1.7

Table 3. The suggested minimum embankment height for protecting the underlying permafrost in 1981 (unit: m).

Permafrost	Depth of the natural permafrost table /m	Critical height H_0 /m	Design height /m	Topography
Icy soil	>2.5	1.0	(0.6~0.7) H_0	Valley zone
Ice-rich soil	2.0 - 2.5	1.0 - 1.3	H_0	High plateau regions
Ice-saturated soil	1.6 - 2.0	1.3 - 1.6	(1.1 - 1.2) H_0	High plateau and river terrace
Massive ground-ice	>1.2~≤1.8	1.4 - 1.8	(1.2 - 1.3) H_0	Mountain regions
Massive ground-ice	≤1.2	>1.8 - 2.0	(1.2 - 1.3) H_0	Frozen peat soil island

restricted to excavating filling materials within 10 m away from the road slope toe. According to different engineering geological conditions, permafrost along the highway was classified into five types: ice-poor soil, icy soil, ice-rich soil, ice-saturated soil, and massive ground-ice. In determining an embankment height designing formula suggested in this period, deformation compressed by seasonal thawing layer and traffic loads were also considered. The calculating method was given as the formula below, and the relevant parameters were listed in Table 4, 5, and 6 (Yu & Wu 1986).

$$H_d = mH_c + S \tag{2}$$

where H_d is the designed embankment height and H_c is the critical minimal height; m is corrected comprehensive coefficient. It is determined by frozen soil type, the permafrost table, and water-containing status of seasonal thawing layers, and its values are suggested in Table 4. The value is suggested to adopt the higher one when the buried depth of the permafrost table is shallow and the ground-ice is rich; contrarily, it is suggested to adopt the lower one.

S is the compressed deformation value of the seasonal thawing layers and is determined with the formula below.

In the maximum thawing season:

$$s = \sum_1^n a_{0i} \delta_{0i} \tag{3}$$

During the freezing period:

$$s = \sum_1^N A_{0i} h_i + \sum_1^N a_{0i} \delta_{0i} h_i \tag{4}$$

where N is the number of seasonal thawing layers above the embankment bottom; h_i is the thickness of the i layer; δ_{0i} is the average total stress of i layer, which equals to average appending stress and weight stress; A_{0i} and a_{0i} is thawing subsidence coefficient and frost-heave coefficient of i layer correspondingly. The values of A_{0i} and a_{0i} were listed in Table 5 and 6.

The embankment design principle and embankment height suggested in 1985 were reasonable at that time; however, it was not widely applied as asphalt-paving work was finished in 1985. It was only used in the embankment repair in a section from the Kulun Mountains (mileage of K2898) to Wudaoliang (mileage of K3007) in 1986.

Embankment Height Designing of the QTH after the 1990s

The QTH crosses 630 km of permafrost region, of which 83.6% is continuous permafrost and 16.4% is island permafrost. Engineering geology conditions of frozen soil along the highway are complex and variable, as they are controlled by many factors. On one hand, the air temperature in the Qinghai-Tibet Plateau gradually increased from 1962 to 1999 with a value of 0.02–0.03°C/a during wintertime. The value changed to 0.01–0.02°C/a during summertime

Table 4. Corrected comprehensive coefficient m of formula (2).

Frozen soil type	Icy soil	Ice-rich soil	Ice-saturated soil	Massive ground-ice
m	0.6 - 0.7	0.9 - 1.0	1.1 - 1.2	1.15 - 1.25

Table 5. Thawing subsidence coefficient.

Frozen soil type	Icy soil	Ice-rich soil	Ice-saturated soil	Massive ground-ice
Thawing index A / %	<5	5 ≤ - <10	10 ≤ - <40	≥40

Table 6. Frost-heave coefficient of seasonally thawing layer.

Frost-heaving type of seasonally thawing layer	Sections with permafrost table buried deep, coarser soil with low moist content	Seasonally thawing layer above ice-rich soil	Seasonally thawing layer above ice-saturated soil	Seasonally thawing layer above massive ground-ice
Frost-heaving coefficient a_{0i} / %	1.0 - 1.5	1.5 - 2.0	2.0 - 3.0	3.0 - 5.0

(Wei et al. 2003). On the other hand, the permafrost was in degradation, influenced by global warming (Wu et al. 2000, 2003). Especially as the black road surface absorbed radiation energy, the situation of the underlying frozen ground was worsening and resulted in new problems. According to statistical data in 1990, the total length of damaged section caused by thawing deformation was 152 km, which was 24% of the total length in the permafrost region. Aiming at solving the problems, the Ministry of Communication approved the First Repair Project Plan to repair the 339 km section of the QTH with serious problems. The designed embankment height in the project still followed the principle of protecting permafrost. It was designed following the principle that the settlement caused by lowering of the permafrost table should be less than the maximum displacement of the road surface in servicing life of the asphalt pavement. The embankment height was increased 30 cm based on formula (2), considering global warming influences on permafrost, so to avoid new damages. During the repair, the neighboring environment was required to be recovered. The suggested embankment height values were listed in Table 7 during the time.

In the first repair project, a longitudinal crack with a width of 15–20 cm and a length of 300 m appeared in the embankment of a section from mileage K3403 to K3409, north to Anduo in winter, 1993. Longitudinal cracks with a width of 15–25 cm and a length of 500 m also appeared in sections of K2932–K2935 and K2947–K2951 in winter, 1995. The total length of the highway damaged by longitudinal cracking was up to 14 km according to an investigation in April 1997. It was found that more than 80% of longitudinal

Table 7. The minimum embankment height of roadbed suggested in 1991 (unit: m).

Frozen soil type	Icy soil	Ice-rich soil	Ice-saturated soil	Massive ground-ice
Embankment height	1.5	1.8	2.2	2.6



Figure 2. Longitudinal cracks and settlement developed in the embankment of the QTH.



Figure 3. Crack damage of the concrete surface layer.

cracks along with settlement appeared in the sun-facing side of the embankment (Fig. 2). The embankments once seriously damaged on Kunlun Mountains Pass, Kekexili Mountains, Fenghuoshan and Tanggulashan Mountains Pass had less damage this time, while the embankments in Chuma'erhe Plateau, Beiluhe Basin, Wuli, Kaixinling to Tongtianhe and north of Anduo regions suffered more longitudinal cracking and subsidence deformation. Sections of these regions possessed more than 95% of the total length damaged by longitudinal crack. Based on analysis of ground temperature data of the QTH for many years, it was found that when the mean annual ground temperature (MAGT) was lower than -1.5°C , the longitudinal cracking and embankment deformation were minor, while when the MAGT was higher than -1.5°C , such problems were serious. This indicated that MAGT has a close relationship to the embankment problems. As the longitudinal crack problems were very serious, paving with a concrete surface layer was tested to see if it was able

Table 8. Height values of embankment with asphalt surface suggested in 1995 (unit: m).

Designing principle	Protecting frozen ground (low temperature district)			Controlling thawing rate (high temperature district)		
	Frozen soil type	Icy soil	Ice-rich soil	Ice-saturated soil	Icy soil	Ice-rich soil
Embankment height	1.6 - 2.0	1.8 - 2.6	2.4 - 3.2	1.8 - 2.4	2.2 - 3.2	2.6 - 3.4

to resist crack damage. The tested results showed that such a surface could not solve the problem when the roadbed was not stable enough. The concrete layer was damaged seriously, too (Fig. 3). Therefore, the surface damages were mainly caused by deformation of the embankment.

The first repair project of the QTH was finished in 1995, and survey and design work for the second repair project was soon followed. In order to use index of ground temperature to evaluate the roadbed stability, researchers suggested -1.5°C as the dividing value for classifying high-temperature permafrost (warm permafrost) and low-temperature permafrost (cold permafrost), considering the ground thermal regime along the highway. As the different temperature districts were divided, a new principle was proposed, as (Zhang 1996) protecting the frozen ground, controlling the thawing rate, and comprehensive treatment. In low-temperature permafrost regions, embankment designing should follow the principle of protecting the frozen ground. In high-temperature regions, it should follow the principle of controlling thawing rate. Comprehensive treatments can be used to avoid roadbed problems in poor geological condition sections. According to the principle, the minimal embankment height is given in Table 8. It was also suggested that on the basis of considering frozen soil type, geomorphology, and water conditions along the two sides, an additional embankment on the slopes be constructed 0.8–1.5 m in height and 2–3 m in width.

Maintaining and Repairing Project from 2002 to 2004

Construction of the Qinghai-Tibet Railway (QTR) started in 2001. This project was regarded as one of the four major projects in West China. The railway construction depended very much on the QTH to transport workers, materials, prefabricated concrete structures, machines, etc. This greatly increased traffic load on the highway. Though the highway was a second-class way, it was hard to support too much, as its main part was in permafrost regions. To ensure the railway construction, 12.2 billion Yuan were invested to carry out a large-scale repair project of the QTH from 2002 to 2004. According to research and statistics in 2001, embankments of the QTH with serious subsiding deformations and longitudinal cracks were mainly in warm and ice-rich permafrost regions. The total length of such sections was 60 km. The sections had never been reconstructed or repaired, and the embankment



Figure 4. Thermosyphone installed along the QTH to treat thawing settlement.



Figure 5. Insulation layer installed along the QTH to keep the underlying permafrost.

was somewhat high. High embankment might cause new problems, which mainly resulted from disturbance of the surrounding environment. The designing principles in this period included: (1) recovering the damaged permafrost environment of both sides of the road; (2) using artificial ground-freezing methods (such as thermosyphone, Fig. 4) and increasing heat resistance (such as using EPS, XPS material, Fig. 5) to treat the subsiding and cracking problems; (3) properly adjusting the roadbed according to actuality of embankment and bearing capacity of surface layer; (4) strengthening drainage structure. The route-change section was designed according to the recommended values for asphalt surface roads in 1995. Focusing on treating roadbed problems in warm and ice-rich permafrost regions, some field experimental research work was carried out at same time. The work included study on the genesis and mechanism of roadbed settlement and longitudinal cracks, and new construction methods for highways in permafrost regions and their engineering effects. The new methods included thermosyphone embankments, crushed-stone embankments, duct-ventilated embankments, and also thermal-insulated embankments. Some testing sites were constructed along the highway during the time. Among the testing sites, some of them were installed to study the reasonable embankment height along both the QTH and the Qinghai-Tibet Railway (QTR). In the Beiluhe region, several testing embankments with different height were studied (Cheng et al. 2004). The tested results showed that the minimum embankment height has a close relationship to the surface conditions of the roadway and the local mean annual air temperatures. The minimum embankment height needed to be increased when the mean annual air temperature was higher. There was no minimum embankment height effective unless the local

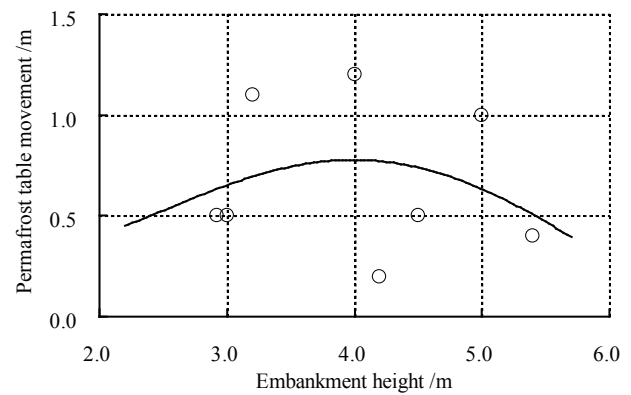


Figure 6. Relation of permafrost table movement with embankment height (Cheng et al. 2004).

mean annual air temperature was lower than a critical value (-3.8°C). That means no matter how high the embankment was, the permafrost table under the roadway would fall.

The tested results of relationship between the permafrost table movement and embankment height is drawn in Figure 6. The figure indicates that when the embankment rose to a certain range the permafrost table would drop but not rise. Therefore, the range of the applied height was a function of properties of the fill materials, the surface conditions, and the mean annual air temperatures.

Now after years of study, a comprehensive design principle for determining embankment height and protecting roadbed stability in permafrost regions is proposed. It suggests that in low-temperature regions, the permafrost is recommended to be protected. Some methods such as increasing the height, installing an insulation layer, or installing the side berm, can be applied. The height values may be referred to the data listed in Table 8. In high-temperature regions, the critical height values are not the controlling index of embankment design. Some methods, including crushed stone embankment, thermosyphone associatex with insulation layer embankment, duct-ventilated embankment, and land bridge, can be adopted. Certainly a minimal height of embankment to install the structures mentioned above is necessary.

Conclusions

(1) The Qinghai-Tibet Highway was constructed in the 1950s. Permafrost was not considered at that time, and roadbed problems were rooted thereby. After that, large-scale repair was carried out three times to maintain the roadbed stability. The embankment height was an important research content during the past, and it was suggested differently during different time.

(2) The suggested embankment height before 1979 was mainly based on considering the depth of the permafrost table, along with kinds of frozen ground and soil fill materials.

(3) The suggested embankment height value was increased from 1979 to 1985, as a permafrost-protecting principle, and the critical minimal height was proposed.

(4) The influences of global warming and ground temperature on roadbed stability were considered after the 1990s. District division of permafrost according to the ground temperature was applied, and different designing principles were proposed after that.

(5) In the last maintenance and repair projects of the highway from 2002 to 2004, the permafrost environment, new construction methods, and drainage systems were considered. The permafrost-protecting principle was confirmed. To realize the principle, some of the new methods were tested, and their effectiveness was evaluated. Now the Qinghai-Tibet Highway is in its best servicing status in history.

Acknowledgments

This work was supported in part by the Chinese Natural Science Fund (No. 40471023), the National Science Supporting Project of the Ministry of Science and Technology of China (2006BAC07B02), and the grant of the Knowledge Innovation Programs of the CAS (No. KZCX1-SW-04, KZCX-XB-10).

References

- Cheng, G.D. Zhang, J.M. & Sheng, Y. 2004. Principle of thermal insulation for permafrost protection. *Cold Regions Science and Technology* 40: 71-79.
- Research group of QTH. 1978. Construction of black road surface of QTH on permafrost regions. *Research Report of the First Highway Survey and Design Institute of China*, Xi'an.
- Research group of QTH. 1980. Embankment height of asphalt roadbed surface of the QTH. *Research Report of the First Highway Survey and Design Institute of China*, Xi'an.
- Research group of the QTH. 1981. Embankment height of asphalt roadbed surface of QTH. *Research Report of the First Highway Survey and Design Institute of China*, Xi'an.
- Wei, Z.G., Huang, R.H. & Dong, W.J. 2003. Inter-annual and inter-decadal variations of air temperature precipitation over the Tibetan Plateau. *Chinese Journal of Atmospheric Sciences* 27(2):157-170.
- Wu, Q.B., Li, X. & Liu, W.J. 2000. The Prediction of Permafrost Change along the Qinghai-Tibet Highway, China. *Permafrost and Periglacial Processes* 11(4): 371-376.
- Wu, Q.B., Shi, B. & Fang, H.Y. 2003. Engineering geological characteristics and processes of permafrost along the Qinghai-Xizang (Tibet) Highway. *Engineering Geology* 68: 387-396.
- Yu, W.X. & Wu, J.M. 1986. Embankment height of asphalt roadbed surface of the QTH. *Journal of Xi'an Highway Institute*: 1986 (1): 25-42
- Zhang, J.Z. 1996. Discussion on embankment height designing principles of QTH with asphalt road surface in permafrost regions. *Proceeding of the Fifth Symposium on Glaciology and Geocryology of China*. Lanzhou: Gansu Culture Press, 383-387.

Modeling Long-Term Dynamics of Snow and Their Impacts on Permafrost in Canada

Yu Zhang and Wenjun Chen

Canada Center for Remote Sensing, Natural Resources Canada, Ottawa, Canada

Daniel W. Riseborough

Geological Survey of Canada, Natural Resources Canada, Ottawa, Canada

Abstract

Seasonal snow, controlled mainly by temperature and precipitation, has a significant impact on ground temperature; therefore, it is essential to integrate snow dynamics for assessing the impacts of climate change on permafrost. In this study, we simulated snow dynamics in a permafrost model over the years 1850–2100 in Canada at a spatial resolution of 0.5° latitude/longitude. We validated the results by comparing them with snow measurements at climate stations. This long-term spatial modeling shows that snow depth would be thinner in eastern and northern Canada, and the duration of snow cover would be shorter almost everywhere in Canada by the end of the 21st century, causing a 1°C–2°C warming of annual mean ground temperature compared to changes in the annual mean air temperature. That means the concurrent change in snow condition would reduce the amount of permafrost degradation in response to climate warming.

Keywords: climate change; ground temperature; model; permafrost; snow dynamics.

Introduction

Annual mean ground temperature near the surface at high latitudes is usually several degrees warmer than the annual mean air temperature due to the insulating effects of snow (Zhang 2005, Zhang et al. 2005, Goodrich 1982). Changes in air temperature and precipitation would directly alter snow dynamics through changes in snowfall, snow density, and snowmelt. Therefore, it is essential to integrate snow dynamics in assessing the impacts of climate change on ground temperature and permafrost.

Some of the permafrost modeling studies used measured snow-depth or snow-water equivalent (SWE) as input. However, field, satellite, and climate station data are usually limited in temporal and spatial coverage, especially for observations of snow density, which is critical for quantifying the insulating properties of snow. Therefore, modeling the dynamics of snow is essential for assessing the impacts of climate change on permafrost and for other applications, such as estimating the feedbacks of snow on climate system, assessing avalanche risks, quantifying flooding and other hydrological processes, and modeling ecosystems and soil biogeochemistry.

Snow models can be categorized based on the purpose for which the models are developed. Models for snow avalanche risks consider the details of the mechanical features of snowpack and their changes (e.g., Bartelt & Lehning 2002); models for the impacts of snow on hydrology and flooding pay more attention to the spatial distribution of the total SWE and the rate of snowmelt; models for the impacts of snow on ground temperature and permafrost are concerned primarily with the thermal effects of the snow, while snow models for climate systems consider the thermal and hydrological effects of snow and the effects on surface energy processes, especially albedo. Tempo-spatial scales

also vary significantly depending on the models' purposes.

Although it is recognized that snow cover has significant effects on ground temperature and permafrost, few permafrost models integrate snow dynamics. The major challenges include the following: (1) The model should have the capacity to simulate the dynamics of snow depth and snow density, since both are important for the thermal effects of snow on the ground. (2) The response of permafrost to climate change could take centuries; therefore, long-term climate data are needed to drive the models. (3) Detailed climate station data usually have limited spatial coverage. Monthly data are usually the only available historical climate datasets with long-term and spatial coverage.

Recently, we developed a process-based model—NEST, a model for northern ecosystem soil temperature—to quantify the impacts of climate change on permafrost, including the concurrent changes of snow (Zhang et al. 2003). Monthly climate data were down-scaled to run the model over the years 1850–2100 in Canada at a spatial resolution of 0.5° latitude/ longitude (Chen et al. 2003, Zhang et al. 2006). In this paper, we describe the procedures and validation of the snow sub-model, and then analyze the simulated long-term patterns of snow dynamics in Canada and the effects on ground temperature and permafrost. The simulated distribution and changes in soil temperature and permafrost conditions have been presented in other papers (Chen et al. 2003, Zhang et al. 2005, 2006, 2008a, b).

Methods and Data

The NEST model

The NEST model was developed to simulate the transient response of ground thermal regime to climate change. It explicitly considered the effects of different ground

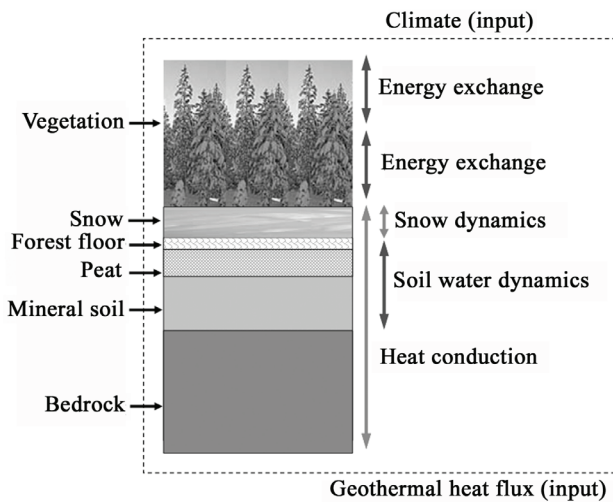


Figure 1. The components and processes considered in the NEST model (Zhang et al. 2003, 2008a)

conditions, including vegetation, snow, forest floor or moss layers, peat layers, mineral soils, and bedrock (Fig. 1). The dynamics of the ground temperature were simulated by solving the one-dimensional heat conduction equation. The upper boundary conditions (the ground surface or snow surface when snow is present) were determined based on the energy balance, and the lower boundary conditions (at a depth of 120 m) were defined based on the geothermal heat flux. The ground profile was divided into 63 layers with the thickness of the layers increased gradually from 0.1 m for top layers to 4.8 m close to the lower boundary. Soil water dynamics, including phase change, were simulated, and their effects on energy balance and on soil thermal properties were considered as well. A detailed description of the model and its validation were provided by Zhang et al. (2003).

The snow sub-model

The dynamics of snow were integrated in the NEST model. The thickness of the snow was determined based on snow density and the amount of snow (in SWE) on the ground, calculated as the cumulative difference between snowfall and snowmelt. Daily snowfall was determined by precipitation and air temperature (discussed below), and the density of fresh snow was estimated using air temperature. Snowmelt was determined based on the available energy calculated from the energy balance on the surface. The snowpack was divided into layers of about 0.1 m in thickness. The profile of snow density and its change with time were simulated considering compaction and destructive metamorphism, following Kongoli & Bland (2000). The equations and the calculation procedures were described by Zhang et al. (2003). Since the spatial resolution of this study (0.5° latitude/longitude) was much coarser than the fetch scale of blowing snow, wind effects on snow redistribution were not considered in this study.

Precipitation was designated as rainfall or snowfall based on air temperature. Measurements from climate stations in Canada show that snowfall occurs over a range of air

temperatures around 0°C , and the range differs from place to place. Rather than defining a constant critical air temperature, we used a probability distribution function, similar to the approach of Riseborough and Smith (1993), to designate precipitation as rainfall or snowfall

$$P_s = 1 - 1/\{1 + \exp[-k(T_a - T_0)]\} \quad (1)$$

where P_s is the probability of precipitation as snowfall in a day. T_a is daily mean air temperature ($^\circ\text{C}$), k is a parameter determining the slope of the frequency changing with air temperature around 0°C , and T_0 is the temperature at which rainfall and snowfall are equally likely. We selected 37 climate stations across the whole Canada landmass and determined the parameters k and T_0 for each station using historical daily measurements of temperature and the fractions of rainfall and snowfalls. Except for one station on the west coast, k was closely correlated with mean annual vapor pressure (V in mb), and T_0 was correlated with the total precipitation from October to December (P in mm)

$$k = -0.0517V + 0.7605 \quad (r=0.78, n=36) \quad (2)$$

$$T_0 = -0.0135P + 2.2928 \quad (r=0.74, n=36) \quad (3)$$

V and P were calculated as long-term averages. The above statistical relationships are probably related to the regional climate conditions and weather systems (e.g., wet and mild southeast Canada frequently has rainfalls when air temperature is below 0°C , while the Prairies, Yukon, and high Arctic frequently have snowfalls when air temperature is above 0°C . T_0 is also related to annual total precipitation ($r=0.66, n=36$) but not as significant as for the precipitation from October to December). Equations 2 and 3 were used for each grid except for the west coast region, where k and T_0 were assigned according to the station data ($k=0.8, T_0=0.7$). For each day with precipitation, a random number from 0 to 1 was generated. If this number was smaller than P_s calculated based on the daily air temperature, the precipitation was assigned as snowfall, otherwise the precipitation was assigned as rainfall (We did not consider the cases with mixed rainfall or snowfall in a day, since such cases are relatively few).

Data

Inputs to the model include information about vegetation (land cover types, leaf area index), ground conditions (thickness of organic layers, texture of the mineral soils, soil organic carbon content in mineral soils, ground ice content, and the geothermal heat flux) and atmospheric climate (air temperature, precipitation, solar radiation, vapor pressure, and wind speed). Climate data from 1901 to 2002 were from Mitchell and Jones (2005). Six climate scenarios were selected for the 21st century, generated by six general circulation models (GCMs): NCAR, CGCM, CSIRO, GFDL, HadCM, and ECHAM. These six scenarios covered most of the possible range of GCM projected scenarios for Canada (Zhang et al. 2008b). A

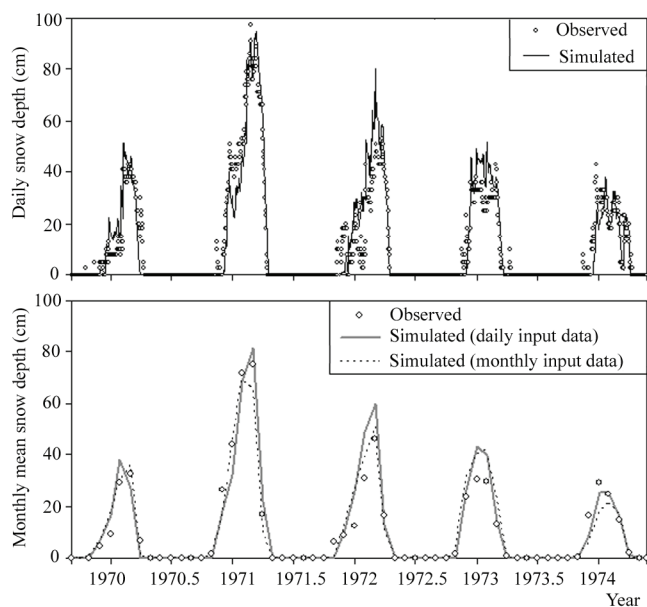


Figure 2. Comparisons between the measured and simulated snow depth at Ottawa climate station. a) comparing daily snow depth between the measured (circles) and the simulated (curves) using daily climate data as input. b) comparing monthly mean snow depth between the measured (circles) and the simulated using daily climate data as input (gray curves) and using month climate data as input (dash curves).

detailed description of the vegetation and ground input data were provided by Zhang et al. (2006, 2008b). Several studies indicate that the current climate warming in Canada began largely from the end of the Little Ice Age (circa 1850) (Overpeck et al. 1997). Therefore, we initialized the model in 1850 assuming the ground thermal regime was in equilibrium with the atmospheric climate. We then simulated continuously from 1850 to 2002, and then from 2002 to 2100 under six climate change scenarios. Climate for 1850–1900 was extrapolated linearly from the data during 1901–1990. During the simulation, the monthly climate data were down-scaled to half-hourly to accommodate the short time-step requirement of the NEST model (Chen et al. 2003).

We validated the model using measured snow depth at climate stations. First, we validated the model by comparing measured daily snow depth with the simulated using daily climate data as input. We then ran the model using monthly climate data as input (derived from the daily observations and then down-scaled to half hourly in the model) and compared the simulated monthly snow depth with the observations. We selected the Ottawa climate station (45.4°N, 75.7°W) since this station has a long and continuous record of snow depth and other climate variables. Finally, we compared the nationwide simulation results with observations at 1670 climate stations which have at least 20 years of measurements. The daily and monthly climate station data were from Environment Canada (1999, 2000).

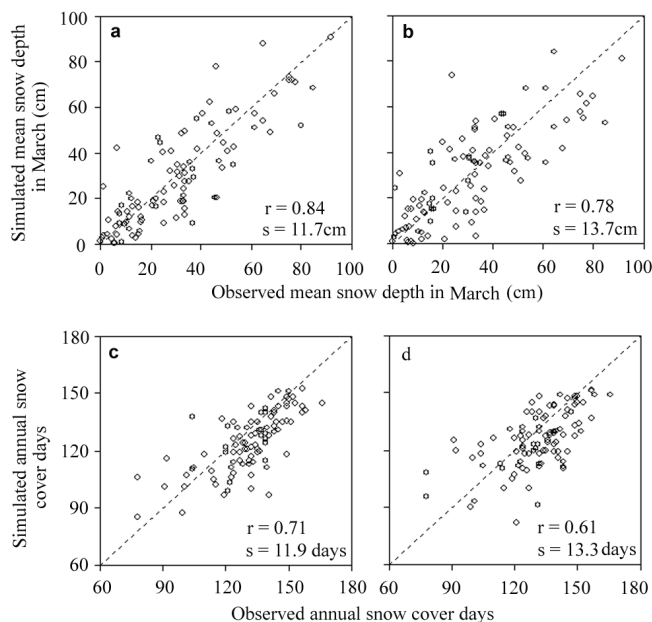


Figure 3. Comparisons between the simulated and the measured mean snow depth in March (a and b) and snow-cover days in a year (c and d) for Ottawa climate station from 1901 to 1999. The left panels (a and c) were simulated using daily climate data as input, and the right panels (b and d) were simulated using monthly climate data as input. r is correlation coefficient, and s is standard deviation.

Result and Analysis

Comparing with measurements

Using daily climate data as input, the model was able to capture the observed patterns of snow-depth variation (Fig. 2a). The major difference was usually caused by the errors in defining precipitation as rainfall or snowfall. For dates on which daily measurements of snow depth were available from the snow database (Jan. 1, 1961, to Dec. 31, 1999; only monthly data were available in the database before 1961), the correlation coefficient between measured and simulated daily snow depth was 0.88 ($n = 14149$, standard deviation was 5.7 cm). A similar positive validation was presented for the Whitehorse climate station (60.9°N, 135.7°W) and for two boreal forest sites in Canada (Zhang et al. 2003).

Snow usually reaches the maximum depth in March in most of Canada. Figure 3a shows a comparison between measured and simulated mean snow depth in March using daily climate data as input (data from 1901 to 1999). It shows that the model can well capture the long-term variation patterns. Figure 3c shows a comparison between observed and simulated snow-cover days (days with snow depth >0 cm) in a year using daily climate data as input.

Using monthly climate data as input, the model could still capture seasonal patterns of snow dynamics (Fig. 2b). Monthly mean snow depths simulated using monthly and daily climate data as inputs were similar, and both are comparable to the observed monthly mean snow depth. The model could also capture the long-term (from 1901 to 1999) pattern of the snow depth in March using monthly data as

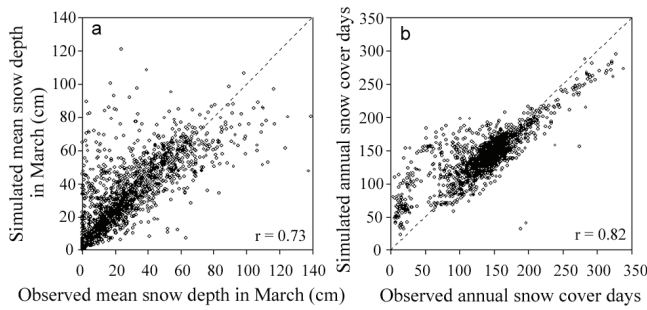


Figure 4. Comparisons between the simulated and observed mean snow depth in March (a) and mean annual snow-cover days (b) for 1670 climate stations in Canada. Each dot represents a climate station comparing between the observed and the simulated using the grid climate covering this station. The data for each station were averaged for all the observational years.

input (Fig. 3b), although the modeling skill was less than using daily climate data as input. Similarly, the simulated annual snow-cover duration and its long-term change using monthly climate data as input were also comparable with the measurements, although the relationship was not as good as when using daily climate data as input (Fig. 3d).

Figure 4 compares simulated and measured mean snow depth in March and the annual snow-cover days (averaged for all years with measurements) at about 1670 climate stations across Canada. The simulation was conducted using gridded monthly climate data as input. These results show that the simulated spatial distributions of snow-depth and snow-cover days were generally comparable with station measurements, although there were differences for some stations, especially in the province of British Columbia, where the terrain is complex and mountainous. This is mainly due to the differences between station and grid climate data. Local conditions could have significant effects on precipitation and snow conditions, while the model results were for average conditions in grid cells.

Changes in snow conditions in Canada over 1850–2100

Figure 5 shows the spatial distributions of changes in mean snow depth in March and annual snow-cover days from the 1850s to the 1990s and from the 1850s to the 2090s simulated using the HadCM and CSIRO scenarios, in which the simulated difference between changes in soil and air temperatures were smallest and biggest, respectively (and the simulated snow conditions are near the extremes of the six GCMs). Snow depth in northern and eastern Canada would be thinner by the end of the 21st century, while becoming thicker in some regions in the western and southwestern regions. The annual snow-cover duration would be shorter almost everywhere in Canada by the end of the 21st century. On average for the major permafrost regions of Canada (latitude higher than 55°N), the mean snow depth in March shows a general decline over 1850–2100. The annual snow-cover duration shows a more consistent decline, with a more significant reduction during the 21st century (Fig. 6). These changes in thickness and duration of snow cover would affect the soil thermal conditions and permafrost.

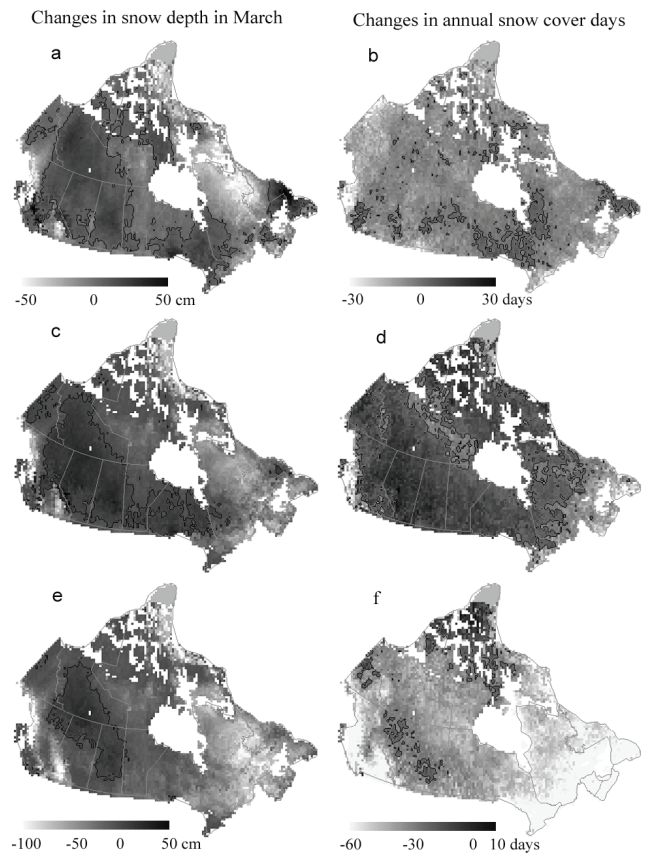


Figure 5. Simulated spatial distributions of changes in mean snow depth in March (the left panels) and annual snow-cover days (the right panels) from the 1850s to the 1990s (a, b), and from the 1850s to the 2090s (c–f) simulated using the scenarios of HadCM (c, d) and CSIRO (e, f). The uniform grey area at the top is glacier, which was not simulated.

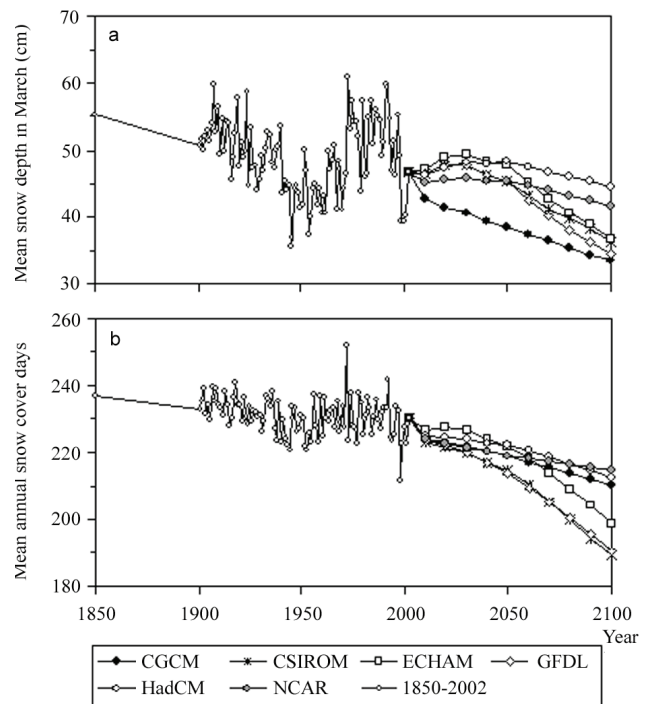


Figure 6. Simulated changes in mean snow depth in March and mean snow-cover days in a year in Canada with latitude higher than 55°N.

Effects of snow change on soil temperature and permafrost

Annual mean soil temperature near the ground surface generally responded strongly to the changes in air temperature, but they were not exactly in parallel. From 1850 to 2100, the rate of the increase in soil temperature near the ground surface was 1°C – 2°C smaller than that of the air temperature, and the difference mainly occurred during the 21st century when warming was more significant (Figs. 7a, 7b).

Rates of change in air and soil temperatures were not significantly different in the summer months (Figs. 7c, 7d). The difference mainly occurred in winter months, with a much smaller increase in soil temperature than in air temperature (Figs. 7e, 7f), due mainly to the changes in snow conditions (snow depth and annual snow-cover days). As a result, the amount and the rate of permafrost degradation would be smaller than the estimates based on air temperature alone, although the influence of this seasonal differentiation would have little effect on the summer thaw depth. As for the possible effects on the southern boundary of permafrost under equilibrium conditions, a difference of 1°C – 2°C in annual mean temperature is equivalent to about 100–200 km distance in latitudinal direction (the typical latitudinal air temperature gradient in Canada is about $0.01^{\circ}\text{C}/\text{km}$).

Discussion

Climate station measurements in Canada from 1946 to 1995 show that snow cover and snow depth in spring are decreasing, especially in March (Brown & Braaten 1998). Earlier ablation of snow in spring would mean shorter annual snow-cover duration, which is in agreement with the simulated trend of this study. A shorter snow season was also simulated by GCMs for the 21st century (Räisänen 2007). The simulated decrease pattern of snow depth during the 21st century is generally consistent with GCM projections reported by Christensen et al. (2007). Räisänen (2007) found that SWE generally increases in coldest areas but decreases in other places during the 21st century, with the -20°C isotherm broadly defining the borderline. Our results show a more complex pattern in Canada, with a reduction in northern and eastern regions. The simulated changes in snow-cover days were stronger and more consistent than the simulated changes in snow depth during the 21st century, probably because the former is more dependent on temperature, while the latter is more directly affected by precipitation, which was projected to increase in most high latitudes during the 21st century. Statistical analysis also shows that temperature variations and trends play a significant role in variability and trends of snow-cover area in the Northern Hemisphere in the 20th century (Lemke et al. 2007). Our simulation shows that average snow-cover days in a year could be reduced by 13 to 37 days during the 21st century, which is comparable to the projected increase of 20–50 days in growing season length in the high latitudes (Wrona et al. 2005).

Field measurements and modeling studies have shown that the mean annual soil temperature near the ground surface can be several degrees warmer than the mean annual air temperature in permafrost regions, mainly due to snow-

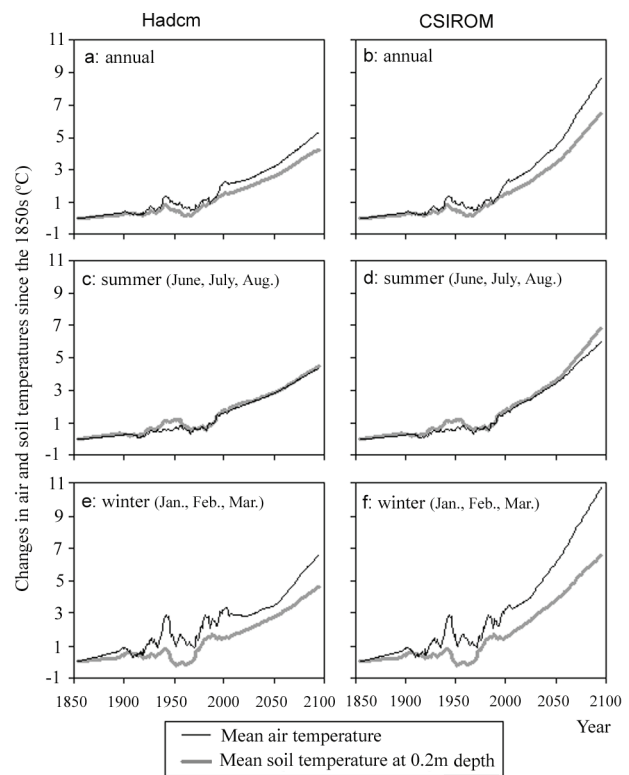


Figure 7. Changes in mean air and soil temperatures since the 1850s in Canada with latitude higher than 55°N . The values are calculated as 10-year running averages minus the averages in the 1850s.

cover, which could last for about half of a year in these cold regions (Goodrich 1982, Zhang, 2005, Zhang et al. 2005). Reduction in the depth and duration of snow cover would reduce the insulating effects of snow, thereby reducing the difference between the annual means of soil and air temperatures. In other words, the increase in annual mean soil temperature in these cold regions would be smaller than that of the air temperature with climate warming (Zhang et al. 2005). On average for all the landmass of Canada with latitudes higher than 55°N , the mean annual soil temperature in the 1850s was about 3°C warmer than the annual mean air temperature. With a 1°C – 2°C smaller increase in annual mean ground temperature than the air temperature over 1850–2100, the annual mean ground temperature on average for Canada would be only 1°C – 2°C warmer than the annual mean air temperature by the end of the 21st century.

We used the general patterns of climate scenarios without considering the interannual variations for the 21st century. The large fluctuation during 1901–2002, when observations were available, shows that the actual variation pattern of snow depth in the 21st century could be different from the simulated general patterns because of the year by year fluctuations of climate. In addition, climate stations are sparser and the years of observations shorter in higher latitudes. This would induce errors in input data and the simulation results. In the current model, we did not consider snow drift by wind and the changes in vegetation conditions from year to year. For a more realistic

simulation, especially at fine spatial resolutions, these features will need to be considered.

Conclusions

This study shows that it is necessary and possible to integrate the dynamics of snow when simulating the long-term impacts of climate warming on ground thermal regimes and permafrost. Comparisons with climate station measurements showed that the model not only could simulate snow dynamics using daily climate data as input, but also captured the seasonal patterns and long-term changes of snow using monthly climate data. Driven by monthly grid climate data, the simulated spatial distribution of snow in Canada was comparable with the measurements at climate stations.

This long-term simulation shows that snow depth would be thinner in northern and eastern Canada and annual snow-cover duration would be shorter almost everywhere in Canada by the end of the 21st century. These decreasing trends in snow-cover days and in snow depth were mainly due to the increase in air temperature. The simulated increase in annual mean ground temperature was 1°C–2°C less than that of the annual mean air temperature, due mainly to the concurrent change in snow conditions. This study shows that the interaction between air temperature and snow conditions would reduce permafrost degradation by a noticeable amount in response to climate warming.

Acknowledgments

The authors thank Richard Fernandes and Fuqun Zhou for the internal critical review of the paper. This study is supported by the climate change program in Natural Resources Canada and Canada's IPY funding (CiCAT).

References

- Bartelt, P.B. & Lehning, M., 2002. A physical SNOWPACK model for the Swiss avalanche warning: part I. Numerical model. *Cold Reg. Sci. Technol.* 35, doi:10.1016/S0165-232x(02)99974-5.
- Brown, R.D. & Braaten, R.O. 1998. Spatial and temporal variability of Canadian monthly snow depths, 1946–1995. *Atmosphere-Ocean* 36: 37-45.
- Chen, W., Zhang, Y., Cihlar, J., Smith, S.L. & Riseborough, D.W. 2003. Changes in soil temperature and active-layer thickness during the twentieth century in a region in western Canada. *J. Geophys. Res.* 108 (D22): 4696, doi:10.1029/2002JD003355.
- Christensen, J.H. et al. 2007. Regional climate projections. In: Solomon, S. et al. (eds.), *Climate Change 2007: The Physical Science Basis. Contribution of Working Group I to the Fourth Assessment Report of the Intergovernmental Panel on Climate Change*. Cambridge, UK, and New York, USA: Cambridge University Press.
- Environment Canada. 1999. Canadian daily climate data (CD-ROM).
- Environment Canada. 2000. Canadian snow data CD-ROM. CRYSYS Project, Meteorological Service of Canada, Downsview, ON, Canada.
- Goodrich, L.E. 1982. The influence of snow cover on the ground thermal regime. *Can. Geotech. J.* 19: 421-432.
- Kongoli, C.E. & Bland, W.L. 2000. Long-term snow depth simulation using a modified atmosphere-land model. *Agric. For. Meteorol.* 104: 273-287.
- Lemke, P. et al. 2007. Observations: Changes in snow, ice and frozen ground. In: Solomon S. et al. (eds.), *Climate Change 2007: The Physical Science Basis. Contribution of Working Group I to the Fourth Assessment Report of the Intergovernmental Panel on Climate Change*. Cambridge, UK, and New York, USA: Cambridge University Press.
- Mitchell, T.D. & Jones, P.D. 2005. An improved method of constructing a database of monthly climate observations and associated high-resolution grids, *Int. J. Climatol.* 25: 693-712. doi:10.1002/joc.1181.
- Overpeck, J. et al. 1997. Arctic environmental changes of the last four centuries. *Science* 278: 1251-1256.
- Räisänen, J. 2007. Warmer climate: less or more snow? *Clim. Dyn.* doi:10.1007/s00382-007-0289-y (in press).
- Riseborough, D.W. & Smith, M.W. 1993. Modelling permafrost response to climate change and climate variability. *Proceedings, Fourth International Symposium on Thermal Engineering and Science for Cold Regions*. Hanover, New Hampshire, U.S.A.: 179-187.
- Wrona, F.J., Prowse, T.D. & Reist, J.D. 2005. Freshwater ecosystems and fisheries. In: *Arctic Climate Impact Assessment*. Cambridge University Press.
- Zhang, T. 2005. Influence of the seasonal snow cover on the ground thermal regime: An overview. *Rev. Geophys.* 43, RG4002. doi:10.1029/2004RG000157.
- Zhang, Y., Chen, W. & Riseborough, D.W. 2008a. Disequilibrium response of permafrost thaw to climate warming in Canada over 1850–2100. *Geophys. Res. Lett.* 35, L02502, doi:10.1029/2007GL032117.
- Zhang, Y., Chen, W. & Riseborough, D.W. 2008b. Transient projections of permafrost distribution in Canada during the 21st century under scenarios of climate change. *Global and Planetary Change* 60: 443-456, doi:10.1016/j.gloplacha.2007.05.003.
- Zhang, Y., Chen, W. & Riseborough, D.W. 2006. Temporal and spatial changes of permafrost in Canada since the end of the Little Ice Age. *J. Geophys. Res.* 111, D22103, doi:10.1029/2006JD007284.
- Zhang, Y., Chen, W., Smith, S.L., Riseborough, D.W. & Cihlar, J. 2005. Soil temperature in Canada during the twentieth century: complex responses to atmospheric climate change, *J. Geophys. Res.* 110, D03112, doi:10.1029/2004JD004910.
- Zhang, Y., Chen, W. & Cihlar, J. 2003. A process-based model for quantifying the impact of climate change on permafrost thermal regimes. *J. Geophys. Res.* 108(D22), 4695, doi:10.1029/2002JD003354.

—Plenary Paper—

Regional Changes of Permafrost in Central Asia

Lin Zhao

Cryosphere Research Station on the Qinghai-Tibet Plateau and State Key Laboratory of Cryospheric Sciences, Cold and Arid Regions Environmental and Engineering Research Institute, Chinese Academy of Sciences

S.S. Marchenko

Geophysical Institute, University of Alaska Fairbanks, AK 99775-7320, USA

N. Sharkhuu

Geo-Ecology Institute, Mongolian Academy of Sciences

Tonghua Wu

Cryosphere Research Station on the Qinghai-Tibet Plateau and State Key Laboratory of Cryospheric Sciences, Cold and Arid Regions Environmental and Engineering Research Institute, Chinese Academy of Sciences

Abstract

Recent progress in research about permafrost changes induced by climatic warming in Central Asia is summarized in this paper. Most permafrost in Central Asia is located on the Qinghai-Tibet Plateau in China, the Tien Shan Mountain regions in China, Kazakhstan, and Kyrgyzstan, Pamir and mountain regions in Tajikistan and Mongolia. Monitoring of the permafrost thermal regime has been carried out in all these regions in the past several decades. Accompanying climate warming, the thermal regime of permafrost changed greatly in all the permafrost regions in central Asia. Permafrost in the Tibetan Plateau is widespread, and occupies about 1.5 million square kilometers. In the continuous permafrost regions on the plateau, the annual mean temperature has risen by 0.1–0.2°C, while in the discontinuous permafrost regions the annual mean temperature has risen by 0.2–0.5°C from 1995 to 2002. The thickness of the active layer has increased by 0.15 to 0.50 m between 1996 and 2001 and residual thaw layers recently. The average rate of increase in mean annual permafrost temperatures is from 0.2°C to 0.4°C per decade in Hovsgol Mountains of Mongolia. Permafrost has been degrading more intensively during the last 15 years (since 1990s) than during the previous 15–20 years (1970s and 1980s). Permafrost occupies about 0.16 million square kilometers in the Tien Shan Mountain regions. Geothermal observations during the last 30 yr indicate an increase in permafrost temperatures from 0.3°C up to 0.6°C. During the same period, average active-layer thickness increased by 23% in comparison to the early 1970s.

Keywords: Central Asia; climate changes; Mongolia; permafrost changes; Qinghai-Tibet Plateau; Tien Shan Mountains

Introduction

The most recent report of the Intergovernmental Panel on Climate Change (IPCC) provided a comprehensive assessment of the climatic changes that have occurred during the last 100 years. The report indicated that the global average surface temperature has increased dramatically, especially since about 1950 (IPCC 2007). Permafrost was identified as one of the key indicators of climate change (WMO 1997). Permafrost measurements are particularly important for determining the long-term terrestrial responses to surface climate change. Climate warming during the 20th century has a great influence on the contemporary thermal state of permafrost. Recent changes in permafrost conditions related to climate warming have been documented in Alaska, Canada, Europe, Siberia, and the high mountains of Central Asia (Jorgenson et al. 2001, Walker 2007, Osterkamp 2007, Camill 2005, Isaksen et al. 2007, Oberman & Mazhitova 2001, Cheng & Wu 2007, Marchenko et al. 2007, Sharkhuu et al. 2007).

Changes in the permafrost thermal regime can have significant impacts on local hydrology, land surface energy and moisture balances, carbon exchange between the land and the atmosphere, and ecosystems, as well as engineering

infrastructure in cold regions (Cheng & Zhao 2000, Nelson et al. 2001, Zhang et al. 2005, Zimov et al. 2006a, b). It is, therefore, of great importance to study the permafrost dynamics of past decades. This paper summarizes recent response of permafrost to climatic changes in Central Asian regions, primarily on the Qinghai-Tibet Plateau, the mountain permafrost regions of Mongolia, and in the Tien Shan Mountains.

Study Region and Methods

The Central Asian region is the largest area underlain by alpine permafrost in the world, and includes the territories of southern Siberia, Mongolia, China, Kazakhstan, and adjacent countries (Fig. 1) (Brown et al. 2001). The mountain permafrost area of Central Asia is estimated to be 3.5×10^6 km², about 15% of the total areal extent of permafrost in the Northern Hemisphere (UNEP/GRID-Arendal 2007). Under climatic warming and increasing human activities in this region, the permafrost has been undergoing great changes. Here, we present a historical overview of recent permafrost investigations on the Qinghai-Tibet Plateau, Tien Shan Mountains, and Mongolia.

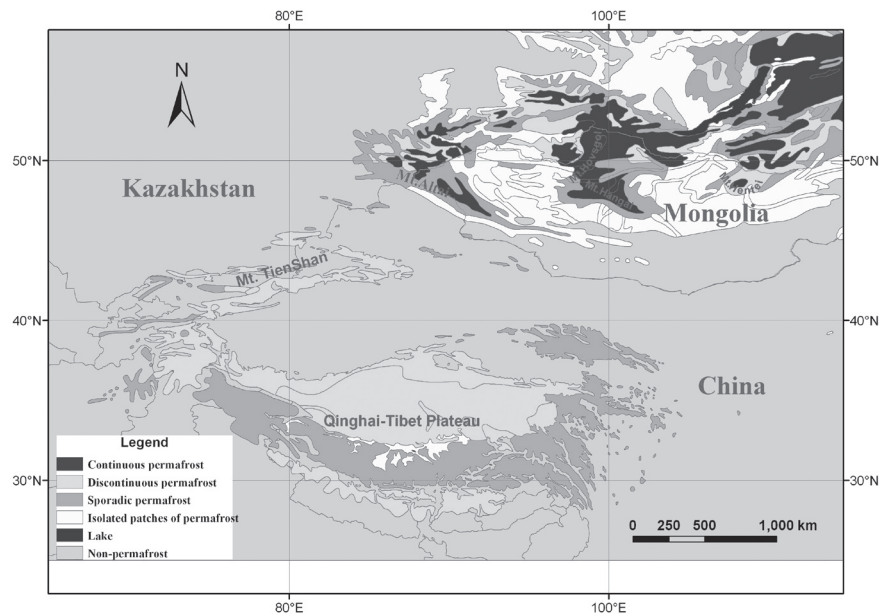


Figure 1. Permafrost distribution in the Central Asian regions (Brown et al. 2001).

Qinghai-Tibet Plateau in China

Systematic permafrost investigations on the Qinghai-Tibet Plateau began in 1954 when the Qinghai-Tibet Highway from Golmud to Lhasa was paved. In the early 1960s, intensive field investigations were conducted along the Qinghai-Tibet Highway to assess geological engineering conditions related to permafrost. Zhou and Du (1963) described permafrost characteristics, distribution, temperature, ground ice distribution, and related periglacial phenomena in detail along the highway. In 1974, a more systematic survey of permafrost was conducted by several research institutions and universities to solve the challenging problems involved in constructing a gas pipeline and the Qinghai-Tibet Railway in permafrost regions. After this survey, the work team summarized knowledge about permafrost distribution and characteristics, thermal and physical properties of frozen ground on the plateau, the thermal regime of permafrost and calculations related to permafrost, and the application of geophysical methods in permafrost studies (Tong & Li 1983). Permafrost on the Qinghai-Tibet Plateau was classified as predominantly continuous permafrost (continuity from 70% to 90%), widespread island permafrost (continuity from 30% to 70%), and sparse island permafrost (continuity less than 30%) (Zhou et al. 2000). During the 1980s, geocryologists and engineers made great progress involving the regularity of permafrost distribution, mechanisms of ground-ice formation, moisture and salt migration during the freezing and thawing process of frozen ground, and application of remote sensing techniques in periglacial geomorphic studies (Cheng 1982). After many field surveys and much analysis, the regularities of altitudinal, latitudinal, and continental mountain permafrost zonation based on the mean annual ground temperature (MAGT) of permafrost and mean annual air temperature (MAAT) were summarized and subsequently applied by the international permafrost community (Cheng

and Wang 1982, Cheng and Dramis, 1992, King et al. 1992). In 1989, the Cryosphere Research Station on the Qinghai-Tibet Plateau was established in Golmud, Qinghai Province to perform long-term and continuous observations on permafrost temperatures and related climatic factors. To satisfy the needs for solving engineering problems in cold regions, further understanding the regularities of permafrost formation and evolution, and assessing the environmental significance of permafrost regions, the State Key Laboratory of Frozen Soil Engineering affiliated to Chinese Academy of Sciences was established in 1991. In the 1990s, permafrost studies on the plateau were improved to create a more detailed and comprehensive science that includes mapping of permafrost and seasonally frozen ground, conducting long-term programs of monitoring the thermal regime of permafrost and the active layer, exploring the thermal, physical and mechanical properties of frozen ground, investigating cold region hydrology and engineering, and especially assessing the impacts and feedbacks of permafrost degradation on engineering infrastructures, the climate system, and related aspects of the environment. Zhang (2005) summarized the historical development of permafrost studies from the 1950s to the present on the Qinghai-Tibet Plateau. A permafrost monitoring network along the Qinghai-Tibet Highway (Fig. 2) has been established, and includes 18 boreholes with depths from 20 to 127 m, 13 sets of active layer measurements systems, 4 automatic weather stations, and 2 eddy covariance systems to collect related data (Cheng & Wu 2007).

Mongolia

Permafrost regions occupy about two-thirds of the territory of Mongolia, predominantly in Altai, Hovsgol, Khangai, and Khentei mountainous regions, which are located in the southern reaches of the Siberian permafrost regions (Fig.

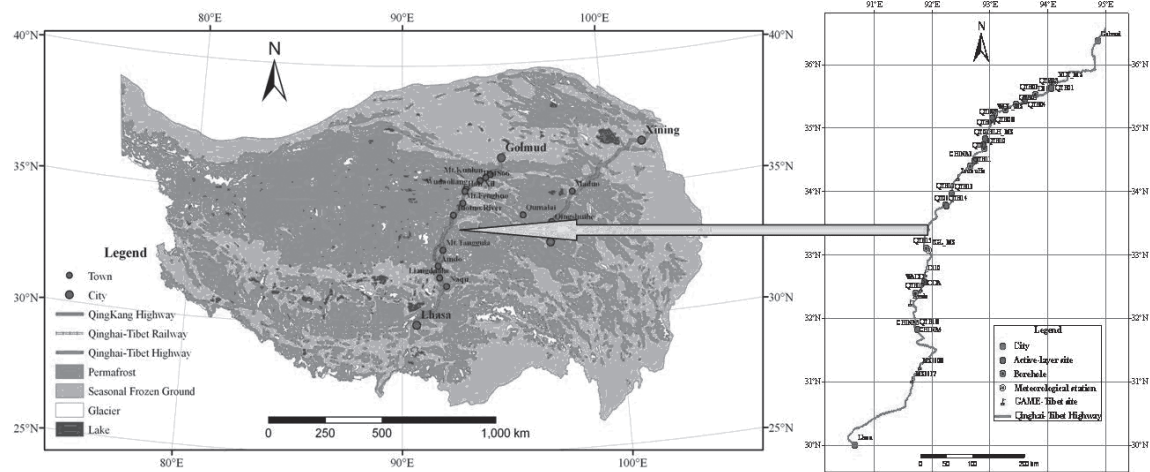


Figure 2. Permafrost monitoring network along the Qinghai-Tibet Highway.

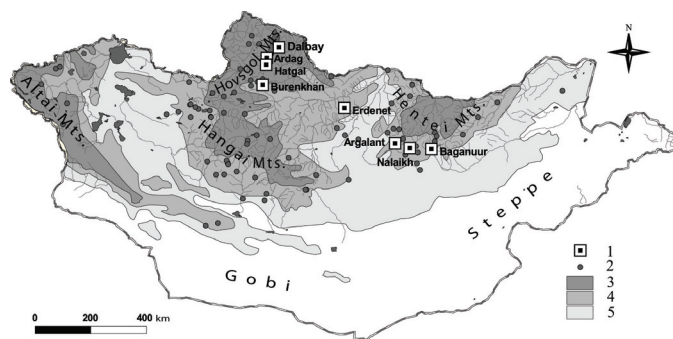


Figure 3. Permafrost distribution and the monitoring network in Mongolia (Sharkhuu et al. 2007).

3). Generally, permafrost temperatures in most regions of Mongolia are close to 0°C , and are thus very sensitive to climatic changes (Sharkhuu et al. 2006). In order to assess the responses of permafrost to recent climatic warming and human activities, Mongolian scientists began systematic observations of permafrost in 1996. The observation sites belong to the Circumpolar Active Layer Monitoring (CALM) and Global Terrestrial Network for Permafrost (GTN-P) programs. Furthermore, some cryogenic processes and phenomena are observed at different sites. Active layer depth and mean annual soil temperature at different levels are measured on the same dates of each year. Temperature data loggers and thaw tubes have been installed in some of the boreholes.

At present, there are fourteen sites for permafrost observations in Mongolia. Five of the sites are in Khentei (Baganuur, Nalaikh, Argalant, Terelj, and Gurvanturuu), two in Khangai (Terkh and Chuluut), six in Hovsgol (Sharga, Burenkhan, Hatgal, Ardag, Hovsgol Project, and Darhad), another site (Tsengel) is in the Altai mountains (Fig. 3). The depth of six boreholes ranges from 50 m to 80 m. So far, there are 37 boreholes belonging to the CALM network and the GTN-P program in Mongolia. Observations on periglacial processes, including thermokarst lakes, frost heaving, and icings, have been carried out seven sites in Hovsgol, Khangai, and Khentei mountains.

Tien Shan Mountains in Kazakhstan

The alpine permafrost region in the Tien Shan Mountains belongs to the Asian high-mountain permafrost area (Marchenko et al. 2007). It is estimated that permafrost in the Tien Shan Mountains formed about 1.6 million years ago due to its high elevation (Aubekerev and Gorbunov 1999). The permafrost in the Tien Shan Mountains has undergone repeated aggradation and degradation since the Holocene. Relict permafrost is found in many places in this region (Gorbunov 1996). Furthermore, mountain permafrost and associated periglacial landforms contain a large amount of ground ice. Moraines, rock glaciers, and other coarse blocky material have especially high ice content (40% to 90% by volume). Preliminary evaluation indicates that the total volume of ground ice is about 320 km^3 (Gorbunov and Ermolin 1981). Water derived from thawing permafrost could, therefore, become an important source of water for vegetation in this region.

The earliest reference to the occurrence of permafrost in the Tien Shan Mountains was in a Russian report in 1914 (Bezsonov 1914). Systematic investigations of mountain permafrost in the Tien Shan Mountains began in the mid-1950s (Gurbonov 1967, Gurbonov 1970). Traditionally, the alpine permafrost area of the Tien Shan Mountains is divided into altitudinal sub-zones of continuous, discontinuous, and sporadic permafrost (Gurbonov 1978, Gurbonov 1988). The earliest permafrost temperature measurements in the Northern Tien Shan began in 1973. Many methods have been used to observe permafrost temperatures, including measuring the active layer's thermal regime and thickness and spring water temperatures and DC resistivity soundings (Gurbonov & Nemov 1978, Zeng et al. 1993, Gorbunov et al. 1996). Permafrost investigations in the Inner Tien Shan were conducted from 1985 to 1992. Ground temperature measurements were conducted in 20 boreholes in the Ak-Shiyrak massif, and in more than 25 boreholes in the Kumtor valley. Thermistor sensors MMT-4 with a sensitivity 0.02°C and an accuracy less than 0.05°C were used during the observations (Ermolin et al. 1989, Marchenko et al. 2007).

Recent Climatic Changes in Central Asia

In Central Asia, including the Qinghai-Tibet Plateau, the air temperature is strongly affected by changes in the winter and spring snow cover. It is predicted that the area-averaged annual mean warming would be about 3°C in the decade of the 2050s over the land regions of Asia as a result of future increases in atmospheric concentration of greenhouse gases (IPCC 2007). Recent atmospheric warming particularly affects terrestrial systems where surface and sub-surface ice are involved. The retreat of glaciers and changes in permafrost in the central Asia in recent years is unprecedented as a consequence of climate warming. Kharlamova and Revyakin (2006) considered the oldest weather station in Asia, the Barnaul station as a benchmark for central Asia with 166 years measurement of air temperature. The statistical analysis showed that the MAAT has increased by 2.8°C over the 166-year period (1.8°C/100yr). The climatic warming in Central Asia is rather noticeable. The trend of MAAT from 1838 to 1958 amounts to 0.015°C/yr and 0.034 °C/yr from 1959 to 2003. During the last 166 years, the MAAT of the warm season (from April to October) has increased by 2.3°C (1.4°C/100yr) and of 3.4°C (2.2°C/100yr) warming found in the cold season (November to March). The most pronounced warming occurred in January (4.8°C), March (4.4°C), and April (4.5°C). The fourth IPCC assessment report (IPCC 2007) also documented that all of Asia is very likely to warm during this century and that the warming is likely to be well above the global mean in Central Asia. The long-term observation results in precipitation amount showed a significant increase in Central Asia from 1900 to 2005 (IPCC 2007).

Many previous studies have demonstrated that dramatic climatic warming has occurred on the Qinghai-Tibet Plateau (Liu and Hou 1998, Yao et al. 2000, Liu and Chen 2000, Duan et al. 2006, Wang et al. 2007). Liu & Chen (2000) collected monthly surface air temperature data from 97 meteorological stations above 2000 m a.s.l. on the plateau. Analysis of the temperature series indicated that most of the territory of the Qinghai-Tibet Plateau has undergone significant warming since the mid-1950s. The statistically significant warming trends in MAAT ranging from 0.016°C/yr to 0.032 °C/yr were found between 1955 and 1996. There is also a tendency for the warming trend to increase more in the high-elevation regions than in the surrounding low-elevation regions. It is evident that the Qinghai-Tibet Plateau region is among the most sensitive to global climatic changes. Wu (2005) analyzed inter-decadal changes of MAAT from 101 meteorological stations on the Qinghai-Tibet Plateau over the 1961–2000 period. Their statistical results indicate that there are 94 stations where the NAAT has increased. The MAAT has increased by about 0.70°C with a trend of 0.017°C/yr over the entire plateau during the last 40 years, which is much greater than the mean value in China (0.005°C/yr).

Based on systematic observations at 25 meteorological stations established beginning in 1936 in Mongolia, Batima and Dagvadorj (2000) it appears that the annual air

temperature in Mongolia has increased by 1.56°C (0.026°C/yr) during the last 60 years. Winter temperature has increased by 3.61°C and the spring-autumn temperature by 1.4°C to 1.5°C. Furthermore, winter warming is more pronounced in high mountains and in open valleys (Batima et al. 2005). In the Altai Mountains, the MAAT has increased with a trend of 0.03°C/yr during the last 50 years. Summer precipitation has increased by 11% while spring precipitation has decreased by 17% from 1940 to 1998. The mean annual precipitation in Mongolia has displayed little increasing trend during the past 50 years.

Aizen et al. (1997) analyzed climatic data from 110 sites in the Tien Shan Mountains from 1940 to 1991. Their results show that the MAAT increased by an average rate of 0.01°C/yr over the entire Tien Shan Mountains and by 0.006°C/yr in the northern Tien Shan Mountains below 2000 m. The rise in air temperature was greater, especially in the central Tien Shan Mountains (0.012°C/yr) and in the high altitudes of the peripheral northern and western regions. Mean annual precipitation has increased 100 mm, or about 12-14%, during the past 52 years. Research also indicates that the average trend of MAAT ranges from 0.006°C/yr to 0.032°C/yr in different parts of the Tien Shan Mountains during the last 70 years (Dikih 1997, Marchenko et al. 2007).

Permafrost Changes

Qinghai-Tibet Plateau

The results outlined above indicate that extensive permafrost degradation has occurred during the past several decades on the Qinghai-Tibet Plateau. Evidence includes the thickened active layer, thinned permafrost, increased permafrost temperatures, talik formation, and disappearance of permafrost islands (Cheng & Wu 2007). In areas of discontinuous permafrost, the MAGT has increased by 0.1°C to 0.3°C (Wang et al. 2000, Cheng & Wu 2007) and active-layer thickness has increased during the 1980s and 1990s by several centimeters to 1 m, even 2 m at some sites (Wang & Zhao 1997). Observations of ground temperature at the Kunlun Pass site and Mt. Fenghuo site showed a warming trend in permafrost from 1996 to 2002 (Fig. 4). In undisturbed permafrost regions, the permafrost surface temperature has increased by about 0.1°C to 0.7°C from 1996 to 2001 and the thickness of the active layer has increased by 10–40 cm (Wu & Liu 2004, Yang et al. 2004). Temperature at the permafrost surface and at the depth of 6 m rose at different rates from 1996 to 2001 (Table 1) (Wu et al. 2005). The change in cold (<-1.5°C) permafrost is greater than that in warm (>-1.5°C) permafrost under the effect of climate warming. However, warm permafrost is very susceptible to climatic warming and the thermal regime of warm permafrost will be impacted more directly and immediately by surrounding warming (Wu et al. 2007).

In the sporadic permafrost regions, ground temperature measurements at Xidatan, located in the vicinity of the northern altitudinal lower limit of permafrost (i.e., the zone above which permafrost occurs), indicate that the MAGT at 20 m depth increased by 0.2–0.3°C in the same period and

Table 1 Permafrost observation from 7 sites on the plateau (Wu et al. 2005).

Site	ALT* (m)		TTOP (°C)		TP ₆ * (°C)	
	1996	2001	1996	2001	1996	2001
Kunlun Pass No.1	1.09	1.50	-3.05	-2.68	-3.19	-2.90
Kunlun Pass No.2	1.22	1.40	-3.08	-2.78	-3.06	-2.77
Mt. Fenghuo	1.26	1.60	-3.73	-3.36	-3.67	-3.48
Wudaoliang	2.53	2.75	-1.82	-1.75	-1.63	-1.50
HohXil	1.64	2.00	-2.14	-1.63	-2.01	-1.69
HMS 66	1.94	2.40	-0.82	-0.63	-0.91	-0.83
Cumar Riverside	3.24	3.50	-0.43	-0.30	-0.56	-0.40

TP₆* denotes permafrost temperature taken at 6 m depth. ALT is the abbreviation of Active Layer Thickness.

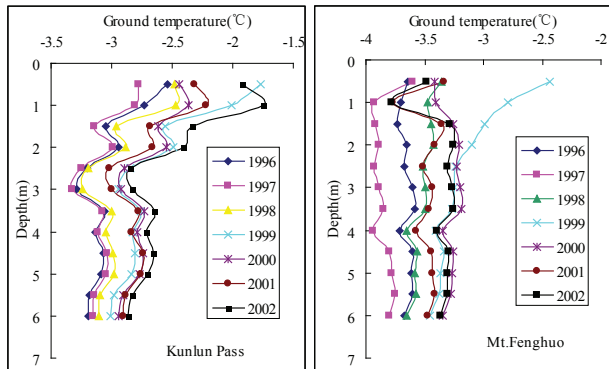


Figure 4. Variations of permafrost temperatures in the Kunlun Pass and the Mt. Fenghuo from 1996 to 2002.

permafrost has disappeared at some locations. The base of permafrost rose by about 4 m from 1983 to the end of the 1990s. A borehole was drilled in 1983 to a depth of 30 m at the Cryosphere Research Station on the Qinghai-Tibet Plateau (CRSQTP) site (35°43'N, 94°05'E) to monitor changes in permafrost temperature. The measurements indicate that ground temperatures at depths of 12–20 m have risen by 0.15–0.36°C and soil temperatures at depths from 5 to 10 m increased by about 0.2°C between 2001 and 2003. The permafrost base monitored from a borehole profile at the Jingxiangu Valley (10 km south of the CRSQTP site) has risen by 10–15 m and the MAGT has increased by 0.5–0.8°C over the last 20 years.

The Amdo-Liangdaohe section of the Qinghai-Tibet Highway is located in the vicinity of the southern lower altitudinal limit of permafrost and is underlain by sporadic permafrost. Permafrost has decreased in area by 35.6% and the lower altitudinal limit of permafrost has risen by 50–80 m. The southern boundary of permafrost has been displaced northward by 1.0–2.0 km over the past 30 years (Wang and Zhao 1997). A 19.53 m borehole was drilled near Amdo in July 1975 to monitor permafrost change. Drilling records indicate that the permafrost table was at a depth of 3.5 m and that the thickness of permafrost was 6.5 m. However, temperature measurements made in July 1989 demonstrate that the MAGT had increased by 0.1–0.2°C and no frozen layer was detected. Another borehole was drilled in June of 1975 to the south of the Highway Maintenance Squad (HMS) 124. Records show that the permafrost table was at a depth

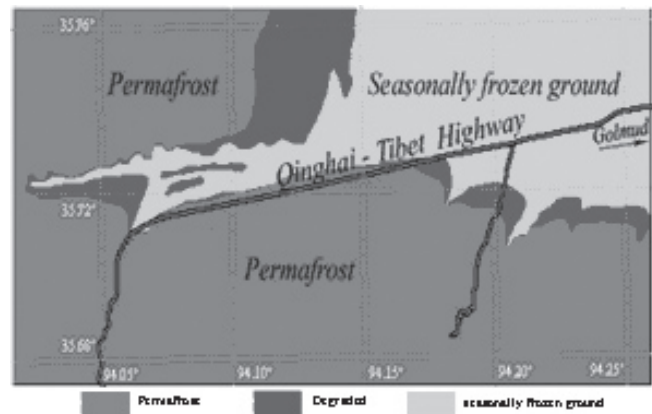


Figure 5. Permafrost change in Xidatan during the last 30 years.

of 3 m and the thickness of permafrost was 5.5 m. However, ground temperature records taken in 1989 indicate that the MAGT had increased by 0.2–0.3°C and permafrost had completely disappeared (Cheng & Wu 2007). The Qinghai-Kang (West Sichuan) Highway travels through the hilly terrain of eastern Qinghai-Tibet Plateau, which is underlain by sporadic and discontinuous permafrost. Approximately 300 km of the Qinghai-Kang Highway is over permafrost. Recent studies reveal that permafrost along the highway in the eastern part of the plateau is undergoing degradation. Taliks have developed at Madoi, Qingshuihe, and the Huashixia Permafrost Station. To the east of Huashixia, a 2.2 m test pit was dug in a marsh at an elevation of 4230 m in June 1992. At that time, soil was thawed to a depth of 0.60 m; ice was found from 0.60 to 1.20 m. A thawed layer was located between 1.20 and 1.60 m; soil was frozen below. A 7 m borehole was drilled near Qingshuihe in May 1995. The borehole records indicate that the ground was frozen to a depth of 1.5 m and a talik was located between 1.5 and 3.0 m. The layer below was frozen from 3 to 7 m. Another borehole, 154.88 m deep, was drilled in 1990 at Qingshuihe. The drilling records indicate that a talik was located between 1.50 and 15.34 m and the layer below was frozen from 15.34 to 37.32 m. A number of boreholes and test pits were drilled or dug to map the distribution of permafrost along the Qinghai-Kang Highway in the 1960s and 1990s. It appears that the lower altitudinal limit of permafrost along the highway rose by approximately 50–100 m over a 30-year period. Ground Penetrating Radar investigations in the northern plateau indicated that the lower altitudinal limit of permafrost has risen by 25 m and permafrost shrank in area considerably over the last 30 years (Fig. 5) (Wu et al. 2005).

Based upon field observations of permafrost temperatures, Wu (2005) discovered that the annual rate of increase in MAGT is 0.042 to 0.065°C/yr for stable permafrost (MAGT < -3°C), 0.016 to 0.098°C/yr for quasi-stable permafrost (MAGT between -0.5 and -3°C), and 0.011 to 0.041°C/yr for unstable permafrost (MAGT > -0.5°C), respectively. It is estimated that the base of permafrost rose at a rate of 0.1 to 0.2 m per decade on average during the last four decades throughout the plateau (Zhao et al. 2003). This trend is expected to continue under the current climate conditions.

Mongolia

The preliminary results of observation indicated that permafrost is degrading to a different extent depending on the regional and local changes in climate and human activities. The change of permafrost condition in bedrock is greater than that in unconsolidated sediments, in ice-poor substrates greater than that in ice-rich ones, on south-facing slopes greater than that on north-facing slopes, and at sites influenced by human activities greater than those undisturbed ones. In generally, permafrost degradation during the last 15-20 years (from 1990s to 2000s) was more intensive than that during the 1970s to 1990s. Spatially, permafrost in the Hovsgol Mountains changed more intensively than that in the Khentei, Khangai Mountains (Sharkhuu et al. 2006).

The Hovsgol Mountain region of northern Mongolia is located at the southern fringe of the Siberian continuous permafrost zone. Monitoring results obtained through measuring ground temperatures and active layer thickness in boreholes indicate that the average rate of increase in mean annual permafrost temperatures is from 0.02°C/yr to 0.04°C/yr. The observation results from selected Sharga, Hatgal, Tsagaan-nuur, and Burenkhan long-term monitoring sites (Fig. 3) showed an apparent trend of increase in mean annual permafrost temperatures at a depth of 10–15 m during the measurement period, ranging between 0.026 and 0.045°C/yr (Fig. 6). The highest rate, 0.042°C/yr with an increasing trend ($r^2=0.91$, $P<0.0001$) in permafrost temperatures during the last 11 years, is observed in the Burenkhan 1 borehole on a mountain slope composed of high thermal conductivity bedrock. Moreover, MAGTs in the Burenkhan mountain area

have increased by 0.027°C/yr on south-facing slope, while 0.019°C/yr on north-facing slope, 0.023°C/yr in the upper watershed and 0.011°C/yr in the valley bottom (Sharkhuu et al. 2007).

Increasing temperature gradients in the Dahard and Burenkhan 2 deep boreholes (Fig. 7) support the hypothesis that the observed change in thermal gradient with depth in addition to lithological factors might be associated with a warming temperature pulse. The Darhad site would be considered as a benchmark of warming trend in the early 1980s, while the Burenkhan site would be considered as a benchmark of warming trend in the early 1960s. Estimated trends of the increase in mean annual permafrost temperatures over 20–30 years in Mongolia are 0.01–0.02°C/yr in the Hangai and Hentei region, and 0.02–0.04°C/yr in the Hovsgol region (Sharkhuu et al. 2006).

Observation of thermokarst processes at Chuluut (in Khangai Mountain region) and Nalaikh (in Khentei Mountain region) during the last 30 years showed that subsidence of 3–10 cm/yr has taken place in the land surface. The maximum subsidence of land surface amounts to 20 to 40 cm/yr during the formation of a thermokarst pond at the Chuluut site. Until late August of 2004, active layer thickness on 5-meter-high pingo in Nalaikh has deepened to 1.50 m from 1.35 m in 1998, and the southeastern side of the pingo has subsided. The subsiding trend of the ice-rich lacustrine clays by the Chuluut River bank is estimated to be 15-30 cm/yr (Sharkhuu et al. 2006).

Tien Shan Mountains

There is some evidence indicating that climatic changes in the 20th century have exerted a significant impact on the thermal condition of mountain permafrost in the Tien Shan Mountains. The geothermal observations during 1974–1977 and 1990–2004 indicate that permafrost has been warming during the last 30 years (Fig. 8). Ground temperatures increased by 0.2–0.3°C at undisturbed sites, and up to 0.6°C at those influenced by human activities. In the northern Tien Shan Mountains, average active layer thickness has increased from 3.2 to 3.4 m in the 1970s to a maximum of 5.2 m in 1992 and to 5.0 m in 2001 and 2004 (Fig. 8),

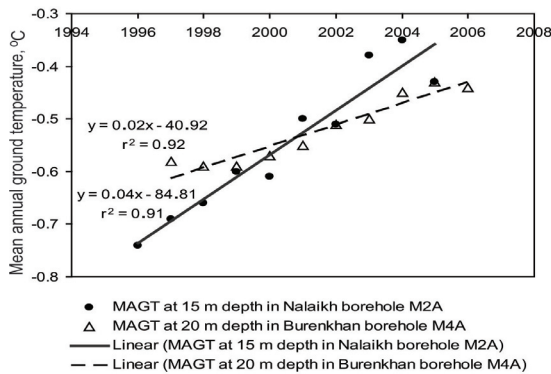


Figure 6. Trend of mean annual permafrost temperatures.

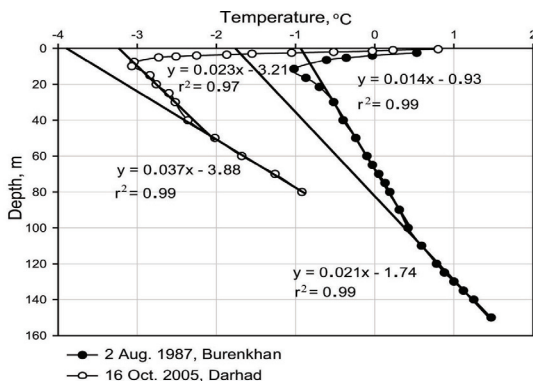


Figure 7. Change in permafrost temperature gradients with depth.

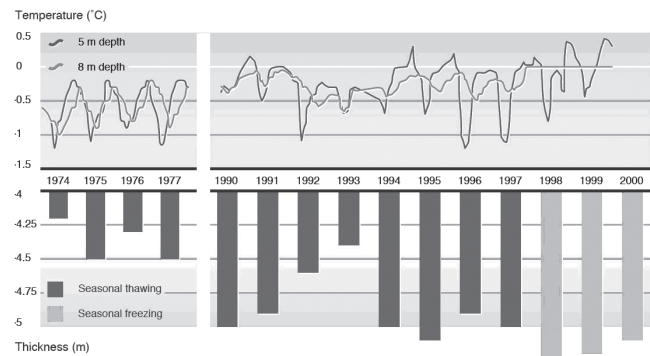


Figure 8. Permafrost temperatures and active layer thickness variations during 1974-1977 and 1990-2000 measured in Borehole K1, 3328 a.s.l., northern Tien Shan Mountain (Marchenko et al., 2007).

a major increase from the early 1970s (Marchenko et al. 2004). As a result of a deep ground thawing, a talik between 5 and 8 m in depth at different sites has formed. Permafrost temperatures in the Inner Tien Shan Mountains have also increased by 0.1°C over 1986-1993 both in the valley and on the mountain slopes (Marchenko et al. 2007).

Summary

Extensive climatic warming has taken place in Central Asia. MAAT has increased with a trend of 0.017°C/yr on the Qinghai-Tibet Plateau during the last 40 years, 0.026°C/yr in Mongolia in the past 60 years, and 0.01°C/yr over the entire Tien Shan Mountains over the 1940–1991 period. The climatic changes occurring in Central Asia have had a pronounced influence on the thermal condition of permafrost. In the different permafrost regions in Central Asia, permafrost degradation has occurred as shown by increasing ground temperatures, thickening of the active layer disappearance of permafrost patches, formation of taliks and development of thermokarst terrain. Permafrost degradation will impact engineering infrastructure, surface and subsurface hydrology, ecosystems, and will even feedback to climatic changes by means of emission of stored carbon from permafrost. In the high-mountains regions of Central Asia, the further near-surface permafrost degradation will probably accompany a transformation in environmental conditions and may lead to slope instability and permafrost-related hazards such as landslides, thermokarst, and glacial lake outburst causing mudflows.

Acknowledgments

We express our gratitude to Dr. Jerry Brown, the president of the International Permafrost Association, for all his help. This paper would not have been possible without his kindly help. Thanks for all the suggestions from Dr. Frederick E. Nelson, Dr. Douglas Kane, and other anonymous reviewers. Thanks for the support from the Chinese Key Basic Research development Project (973 Project: No. 2005CB422003), the Chinese National Science Foundation (No. 40471026), and the Innovation Project of the Chinese Academy of Science (KZCX3-SW-345, KZCX3-SW-351).

References

- Aizen, V.B., Aizen, E.M., Melack, J. & Dozier, J. 1997. Climatic and hydrologic changes in the Tien Shan, Central Asia. *Journal of Climate* 10(6): 1393-1404.
- Aubekerov, B. & Gorbunov, A.P. 1999. Quaternary permafrost and mountain glaciation in Kazakhstan. *Permafrost and Periglacial Processes* 10: 65-80.
- Batima, P. & Dagvadorj, D. (eds.). 2000. *Climate Change and Its Impacts in Mongolia*. Mongolia: JEMR Publishing, 1-227.
- Batima, P., Natsagdorj, L., Gombluudev, P. & Erdenetsetseg, B. 2005. Observed climate change in Mongolia. AIACC Working Paper. No. 12: 1-25.
- Bezsonov, A.I. 1914. Preliminary report on organizing and performance of the soil investigation in the Asian Russia in 1913. St. Petersburg, 245-260.
- Brown, J., Ferrians, O.J., Heginbottom, J.A. & Melnikov, E.S. 1998 (revised February 2001). Circum-arctic map of permafrost and ground ice conditions. Boulder, CO: National Snow and Ice Data Center/World Data Center for Glaciology. Digital media.
- Camill, P. 2005. Permafrost thaw accelerates in boreal peatlands during late-20th century climate warming. *Climatic Change* 68: 135-152.
- Cheng, G. 1982. Formation of massive ground ice near the permafrost surface. *Science in China (Series B)* 3: 281-287.
- Cheng, G. & Dramis, F. 1992. Distribution of mountain permafrost and climate. *Permafrost and Periglacial Processes* 3: 83-92.
- Cheng, G. & Wang, S. 1982. On zonation of mountain permafrost in China. *Journal of Glaciology and Geocryology* 4: 1-17.
- Cheng, G. & Wu, T. 2007. Responses of permafrost to climate change and their environmental significance, Qinghai-Tibet Plateau. *Journal of Geophysical Research-Earth Surface* 112, F02S03, doi: 10.1029/2006JF000631.
- Cheng, G. & Zhao, L. 2000. The problems associated with permafrost in the development of the Qinghai-Xizang Plateau. *Quaternary Science* 20(6): 521-531 (in Chinese with English abstract).
- Dikih, A.N. 1997. Globalnoe poteplenie klimata, ego proyavlenie na Tyan-Shane i reaktsia lednikov. (Global climate warming event in the Tien Shan and glaciers reaction). Data of Glac. Studies. Moscow, vol. 83, pp. 135-139 (in Russian).
- Duan, A., Wu, G., Zhang, Q. & Liu, Y. 2006. New proofs of the recent climate warming over the Tibetan Plateau as a result of the increasing greenhouse gases emissions. *Chinese Science Bulletin* 51 (11): 1396-1400.
- Ermolin, E.D., Nemov, A.E. & Popov, M.V. 1989. Geotermicheskiye harakteristika mestorojdeniya Kumtore. (Geothermal characteristic of the Kumtor gold mine). Geocryological Investigations in the Mountains of USSR, Yakutsk, pp. 31-40 (in Russian).
- Gravis, G.F., Melnikov, E.S., Guo, D.X., Li, S.X., Li, S.D., Zhao, L., Nan, Z.T., Sharkhuu, N., Gorbunov, A.P., Marchenko, S.S. & Seversky, E.V. 2003. Principles of classification and mapping of permafrost in Central Asia. *Proceedings of the 8th International Conference on Permafrost*, Zurich, Switzerland. Balkema, Lisse, 297-302.
- Gorbunov, A.P. 1967. Vechnaya Merzlota Tyan-Shanya (Permafrost of the Tien Shan). Ilim, Frunze (in Russian).
- Gorbunov, A.P. 1970. Kriogennyye yavleniya Tyan-Shanya (Cryogenic phenomena of the Tien Shan). Gidrometeoizdat, Moscow (in Russian).
- Gorbunov, A.P. 1978. Permafrost investigations in high-mountain regions. *Arctic and Alpine Research* 10: 283-294.

- Gorbunov, A.P. 1988. The alpine permafrost of the USSR. *Proc. Of Fifth Int. Conf. on Permafrost*, Vol. 1. Tapir, Trondheim, Norway, 154-157.
- Gorbunov, A.P. 1996. Monitoring the evolution of permafrost in the Tien Shan. *Permafrost and Periglacial Processes* 7(3): 297-298.
- Gorbunov, A. & Ermolin, E. 1981. Ground ice of Central Asian Mountains. *Glaciers Studies*, Moscow 41: 59-62 (in Russian).
- Gorbunov, A.P. & Nemov, A.E. 1978. K issledovaniyu temperatury rykhlooblochnykh tolsesh vysokogornogo Tyan-Shanya (On **temperature research of loose deposits** in the Tien Shan high mountains). Cryogenic Phenomena of High Mountains. Nauka, Novosibirsk, 92-99 (in Russian).
- Gorbunov, A.P., Seversky, E.V. & Titkov, S.N. 1996. Geocriologicheskie Usloviya Tyan-Shanya i Pamira (Geocryological Conditions of the Tien Shan and Pamir). Permafrost Institute publishers, Yakutsk (in Russian).
- IPCC, 2007: *Climate Change 2007: The Physical Science Basis*. Contribution of Working Group I to the Fourth Assessment Report of the Intergovernmental Panel on Climate Change. Edited by S. Solomon, D. Qin, M. Manning, Z. Chen, M. Marquis, K.B. Averyt, M. Tignor & H.L. Miller. Cambridge, U.K., and New York: Cambridge University Press, 996 pp.
- Isaksen, K., Sollid, J.L., Holmlund, P. & Harris, C. 2007. Recent warming of mountain permafrost in Svalbard and Scandinavia. *Journal of Geophysical Research* 112, F02S04, doi:10.1029/2006JF000522.
- Jin, H., Yu, Q., Lu, L., Guo, D., He, R., Yu, S., Sun, G. & Li, Y. 2007. Degradation of permafrost in the Xing'anling Mountains, Northeastern of China. *Permafrost and Periglacial Processes* 18: 245-258.
- Jorgenson, M.T., Racine, C.H., Walters, J.C. & Osterkamp, T.E. 2001. Permafrost degradation and ecological changes associated with a warming climate in central Alaska. *Climatic Change* 48: 551-579.
- Kharlamova, N.F. & Revyakin, V.S. 2006. Regional climate and environmental change in Central Asia. Vogtmann H. & Dobretsov N. (eds.), Environmental Security and Sustainable Land Use, with special reference to Central Asia. Netherland: Springer, 19-26.
- King, L., Gorbunov, A.P. & Evin, M. 1992. Prospecting and mapping of mountain permafrost and associated phenomena. *Permafrost and Periglacial Processes* 3: 73-82.
- Liu, X. & Chen, B. 2000. Climatic warming in the Tibetan Plateau during recent decades. *International Journal of Climatology* 20: 1729-1742.
- Liu, X. & Hou, P. 1998. Relationship between the climatic warming over the Qinghai-Tibet Plateau and its surrounding areas in recent 30 years and the elevation. *Plateau Meteorology* 17: 245-249 (in Chinese with English abstract).
- Marchenko, S.S., Gorbunov, A.P. & Romanovsky, V.E. 2007. Permafrost warming in the Tien Shan Mountains, Central Asia. *Global and Planetary Change* 56: 311-327.
- Marchenko, S.S., Gurbunov, A.P. & Romanovsky, V.E. 2004. Permafrost degradation in the Tien Shan Mountains, Central Asia. American Geophysical Union, Fall Meeting 2004, abstract #A13B-0109.
- Nelson, F.E., Anisimov, O. & Shiklomanov, N. 2001. Subsidence risk from thawing permafrost. *Nature* 410: 889-890.
- Oberman, N.G. & Mazhitova, G.G. 2001. Permafrost dynamics in the north-east of European Russia at the end of the 20th century. *Norwegian Journal of Geography* (55): 241-244.
- Osterkamp, T.E. 2007. Characteristics of the recent warming of permafrost in Alaska. *Journal of Geophysical Research* 112, F02S02, doi:10.1029/2006JF000578.
- Sharkhuu, N. 2003. Recent changes in the permafrost of Mongolia. *Proceedings of the 8th International Conference on Permafrost*, Zurich, Switzerland. Balkema, Lisse, pp 1029-1034.
- Sharkhuu, N. & Sharkhuu, A. 2006. Monitoring of Permafrost in Mongolia. *Proceedings of Asian Conference on Permafrost*, Abstracts, Lanzhou, China, 184-186.
- Sharkhuu, A., Sharkhuu, N., Etmuller, B., Heggem, E.S.F., Nelson, F.E., Shiklomanov, N.I., Goulden, C.E. & Brown, J. 2007. Permafrost monitoring in the Hovsgol mountain region, Mongolia. *Journal of Geophysical Research* 112, F02S06, doi: 10.1029/2006JF000543.
- Sodnom, N. & Yanshin, A.L. 1990. Geocryology and geocryological zonation of Mongolia. Digitized 2005 by Parsons, M.A. Boulder, Colorado, USA, National Snow and Ice Data Center/World Data Center for Glaciology, Digital Media.
- Tong, B. & Li, S. 1983. Characteristics and controlling factors of permafrost distribution on the Qinghai-Tibet Plateau. Special Issue of Professional Papers on Permafrost Research on the Qinghai-Tibet Plateau. Beijing, China, Science Press, 1-11.
- UNEP, 2007. Global Outlook for Ice and Snow. In: J. Eamer (ed). Norway: UNEP/GRID-Arendal, 235 pp. Also available at: http://www.unep.org/geo/geo_ice/.
- Walker, G. 2007. A world melting from the top down. *Nature* 446: 718-721.
- Wang, S., Jin, H., Li, S. & Zhao, L. 2000. Permafrost degradation on the Qinghai-Tibet Plateau and its environmental impacts. *Permafrost and Periglacial Processes* 11: 43-53.
- Wang, S., Yin, Y., Zheng, D. & Yang, Q. 2007. Climatic trends over the Tibetan Plateau during 1971-2000. *Journal of Geographical Sciences* 17(2): 141-151.
- Wang, S. & Zhao, X. 1997. Environmental change in patchy permafrost zone in the south section of Qinghai-Tibet Highway. *Journal of Glaciology & Geocryology* 19: 231-239 (in Chinese with English abstract).

- World Meteorological Organization (WMO). 1997. Global Climate Observing System: GCOS/GTOS Plan for terrestrial climate-related observations, Version 2.0. GCOS-32, WMO/TD-No. 796, UNEP/DEIA/TR97-7, WMO, Geneva, Switzerland, 130.
- Wu, Q. & Liu, Y. 2004. Ground temperature monitoring and its recent change in Qinghai-Tibet Plateau. *Cold Regions Science and Technology* 38: 85-92.
- Wu, Q., Dong, X. & Liu, Y. 2005. Response of permafrost to climate change and engineering activity along the Qinghai-Tibet Highway. *Journal of Glaciology and Geocryology* 27(1): 50-54 (in Chinese with English abstract).
- Wu, Q., Dong, X., Liu, Y. & Jin, H. 2007. Responses of permafrost on the Qinghai-Tibet Plateau, China, to climate change and engineering construction. *Arctic, Antarctic, and Alpine Research* 39 (4): 682-687.
- Wu, T. 2005. A study on responses of permafrost to global climate change in Qinghai-Tibetan Plateau. Ph.D. Thesis, 117 pp., Graduate University of Chinese Academy of Sciences, Beijing, China (in Chinese with English abstract).
- Yang, J., Ding, Y., Chen, R. & Shen, Y. 2004. Permafrost change and its effect on eco-environment in the source regions of the Yangtze and Yellow Rivers. *Journal of Mountain Science* 22(3): 278-285.
- Yao, T., Liu, X. & Wang, N. 2000. Amplitude of climatic changes in Qinghai-Tibetan Plateau. *Chinese Science Bulletin* 45(13): 1236-1243.
- Zeng, Z., Wang, S. & Nemov, A.E. 1993. Some new data of DC electrical soundings of permafrost in the Northern Tien Shan. *Studies of alpine permafrost in central Asia, Northern Tien Shan* Vol. 1. Yakutsk Institute, Yakutsk, 37-41.
- Zhang, T. 2005. Historical overview of permafrost studies in China. *Physical Geography* 26(4): 279-298.
- Zhang, T., Frauenfeld, O.W., Serreze, M.C., Etringer, A.J., Oelke, C., McCreight, J.L., Barry, R.G., Gilichinsky, D., Yang, D., Ye, H., Feng, L. & Chudinova, S. 2005. Spatial and temporal variability in active layer thickness over the Russian arctic drainage basin. *Journal of Geophysical Research-Atmospheres* 110: D16101, DOI:10.1029/2004JD005642.
- Zhao, L., Cheng, G. & Li, S. 2003. Changes of frozen-ground and its environmental engineering effects on the Qinghai-Tibet Plateau. In: Zheng Du (ed.), *The Formation Environment and Development of Qinghai-Tibet Plateau*. Shijiazhuang: Hebei Science and Technology Press, 143-150 (in Chinese).
- Zhou, Y. & Du, R. 1963. Preliminary investigation of permafrost on the Qinghai-Tibet Plateau. *Science in China* 2: 23-34.
- Zhou, Y., Guo, D., Qiu, G., Cheng, G. & Li, S. 2000. *Geocryology in China*. Beijing, China: Science Press.
- Zimov, S.A., Davydov, S.P., Zimova, G.M., Davydova, A.I., Schuur, E.A.G., Dutta, K. & Chapin, F.S. 2006a. Permafrost carbon: Stock and decomposability of a globally significant carbon pool. *Geophysical Research Letter* 33: L20502, doi: 10.1029/2006GL027484.
- Zimov, S.A., Schuur, E.A.G. & Chapin, F.S. 2006b. Permafrost and the global carbon budget. *Science* 312: 1612-1613.

Monitoring Permafrost Changes on the Qinghai-Tibet Plateau

Lin Zhao, Tonghua Wu, Yongjian Ding, Changwei Xie

Cryosphere Research Station on the Qinghai-Tibet Plateau, Cold and Arid Regions Environmental and Engineering Research Institute, Chinese Academy of Sciences

Abstract

This paper summarizes recent research conducted on permafrost changes on the Qinghai-Tibet Plateau. Long-term temperature data were collected and analyzed for assessing the variations of permafrost thermal regimes. The field investigations indicated that the lower altitudinal limit of permafrost has moved up by 50 to 100 m over the plateau during the last 20 years. Research also indicated that the thinning and disappearance of permafrost has taken place in the southern and northern limit of the plateau. The mean annual temperature of permafrost has risen in the continuous permafrost regions, as well as in the discontinuous permafrost regions with different annual rate of increase in mean annual soil temperatures. Permafrost degradation has significant influence on greenhouse gas emission, local hydrology, and ecology on the plateau. The extensively occurring climatic warming on the plateau could be responsible for the permafrost degradation during the past decades.

Keywords: climatic warming; environmental significance; permafrost degradation; Qinghai-Tibet Plateau.

Introduction

Recently more and more attention has been paid to permafrost degradation all around the world under scenarios of climatic warming. A large amount of research based on long-term continuous temperature observations indicates that the permafrost on the Earth is undergoing extensive warming (Osterkamp 2007, Isaksen et al. 2007, Cheng & Wu 2007, Walker 2007). Variations in the permafrost thermal regime in cold regions have exerted profound impacts on the local hydrology, the surface energy and moisture balance, carbon emission, engineering constructions, as well as on the whole

ecosystem (Cheng & Zhao 2000, Nelson et al. 2001, Zhang et al. 2005, Zimov et al. 2006).

The permafrost area in the Qinghai-Tibet Plateau covers about $1.50 \times 10^6 \text{ km}^2$ and is the largest mid-latitude permafrost zone in the world. This permafrost was formed during the late Pleistocene (Fig. 1). Research has shown that the permafrost has been degrading and shrinking in areal extent with a general tendency of warming during the Holocene (Jin et al. 2007). In this paper, we have summarized some recent observation results about the evolution of permafrost on the plateau.

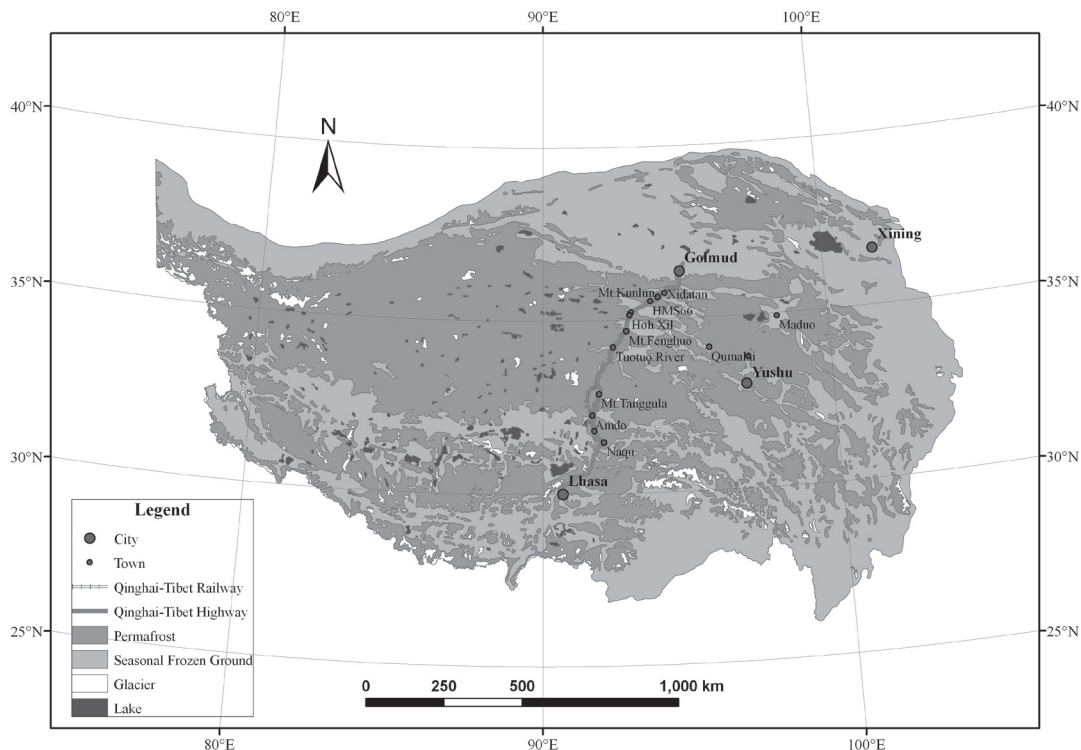


Figure 1. Permafrost distribution and the locations of study sites on the Qinghai-Tibet Plateau.

Site Conditions and Methods

Over the last 40 years Chinese researchers and engineers have established a permafrost monitoring network along the Qinghai-Tibet Highway (Fig 2). Eighteen boreholes, whose depths range from 20 to 127 m, have been drilled along the Qinghai-Tibet Highway to monitor the thermal regime of permafrost. Calibrated thermistor thermometer sensors were installed on cables at certain depth intervals and were put into these boreholes. Initially, soil temperatures at different levels were measured manually three times per month and then averaged over a year. The precision of the temperature data was estimated to be within 0.01°C. In 1998 automatic temperature data loggers were installed to collect temperature data at different depths. Since then the temperature readings have been automatically recorded 12 times per day at 2-hour intervals. We selected those sites whose measurements are continuous to be analyzed and discussed in this paper.

Furthermore, thirteen integrated monitoring sites were installed to collect soil temperature, moisture content, and heat flux data within the active layer. Some of these sites are close to the above-mentioned boreholes. Four automated weather stations and two eddy covariance systems were set up to measure parameters including air temperature, soil temperature and moisture content, precipitation, wind speed and direction, surface evaporation, radiation and CO₂ fluxes. All sites are in undisturbed natural conditions and represent the predominant types of landscape on the plateau. This paper focuses on the recent research carried out on the Qinghai-Tibet Plateau on permafrost warming and its environmental implications.

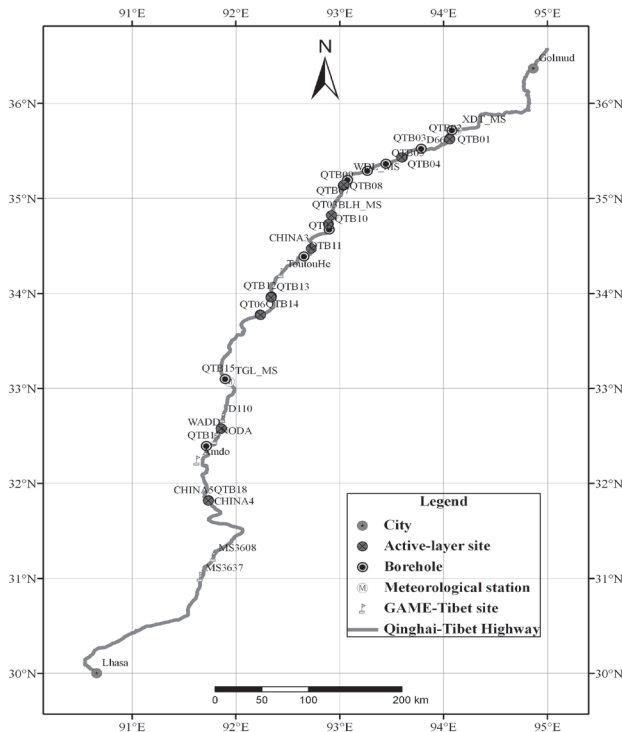


Figure 2. Permafrost monitoring network along the Qinghai-Tibet Highway.

Results and Analysis

It is apparent that permafrost on the Qinghai-Tibet Plateau has undergone severe degradation during the past decades. Various observation data indicates that the mean annual ground temperature has increased and that the active-layer has thickened; talik and thermokarst development and disappearance of sporadic permafrost has occurred in some regions.

Borehole drillings and testpit excavations on the plateau in the 1970s and 1990s indicated that the lower altitudinal limit of permafrost has uplifted by 50 to 100 m (Wang et al. 1997) (Table 1). Ground-penetrating radar investigations at the northern limit of the continuous permafrost zone on the plateau also showed an uplift of 25 m for the lower altitudinal limit in the past 20 years (Wu et al. 2005). In the 1960s ground temperature data taken from a borehole drilled in Xidatan, which is the northern lower limit of permafrost on the plateau, suggested the existence of permafrost at depths between 11.4 m and 16.0 m; but no frozen layer was observed at the same site in 1975 (Wang et al. 1996). The Amdo-Liangdaohe section of the Qinghai-Tibet Highway is located in the vicinity of the southern lower limit of the continuous permafrost zone on the plateau. The temperature observations from a 19.53 m deep borehole drilled in 1975 indicated that the permafrost table was at a depth of 3.5 m and that the permafrost thickness was about 6.5 m. However, temperature measurements in 1989 showed that the permafrost has disappeared (Zhao et al. 2004).

Observed ground temperature changes in the discontinuous permafrost regions on the plateau

The Xidatan site is located in the transitional area from the discontinuous permafrost zone to the continuous permafrost zone. Another 30 m deep borehole was drilled in 1998 as a long-term observation site. The borehole site is situated at a down-faulted basin in the west section of the Kunlun Mountains. The surficial geology consists of fluvial sands and gravel. The available meteorological data in 1976 showed that the mean annual air temperature was -2.9°C. We installed the thermistor thermometers (precision was

Table 1. Changes in the lower altitudinal limit of permafrost on the Qinghai-Tibet Plateau.

Site	Latitude	Lower altitudinal limit (m)		Uplift of altitude (m)
		1960s	1990s	
North slope of southern Mt. Qinghai	36°25'N	3650-3700	3700-3800	50-100
North slope of Mt. Heka'nanshan	35°49'N	3800-3840	3860-3900	60
North slope of Mt. Ngola	35°25'N	3850	3900	50
Southwest slope of Mt. Animaqing	34°35'N	4180	4250	70

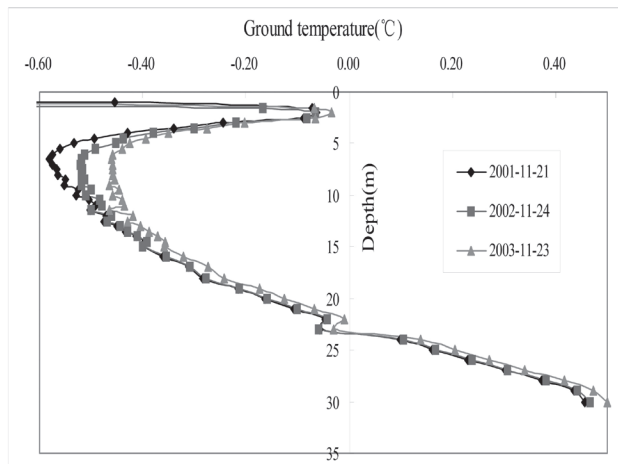


Figure 3. The changes of soil temperature at the Xidatan site.

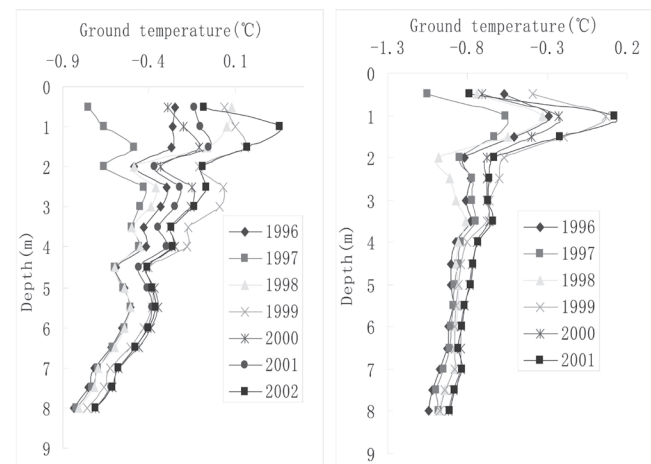


Figure 5. The changes of MAST at the HMS 66 sites.

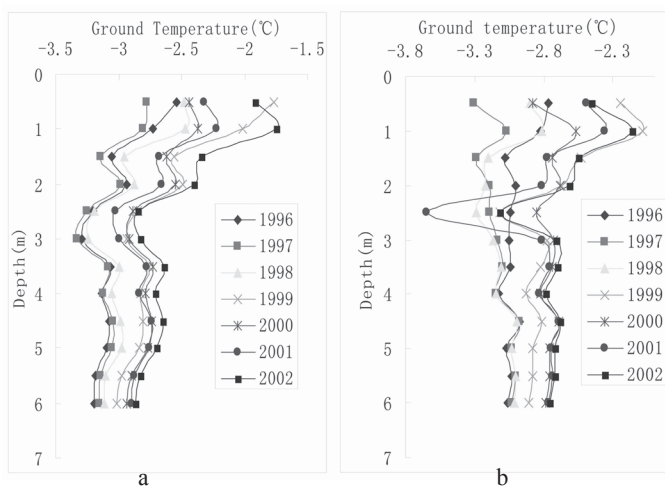


Figure 4. The changes of MAST at the Mt. Kunlun sites.

0.01°C) in the borehole. The available observation results in November of 2001 to 2003 indicated that the permafrost temperature had increased by 0.04~0.10°C on average (Fig. 3). The change in ground temperatures at a depth of 5 m to 8 m was estimated to be more than 0.10°C during the 3 years.

Observed ground temperature changes in the continuous permafrost regions on the plateau Mt. Kunlun sites

In 1995 two boreholes were drilled to a depth of 6 m in 1995 in an undisturbed plain. The observation results indicated that the upper ground temperatures of permafrost were between -3.5°C and -2.0°C. The mean annual soil temperatures (MAST) in one borehole had increased by 0.50°C in the 7 years, which annual rate of increase in mean annual soil temperatures amounts to 0.086°C/yr. The MAST at a depth of 1 m had risen by 0.98°C. The ground temperatures at different levels showed a clear warming trend although there was some fluctuation (Fig. 4a). The MAST in the other borehole had increased by 0.34°C on average at an annual increase rate of 0.072°C/yr from 1996 to 2002 (Fig. 4b). The MAST at a depth of 1 m had risen by 0.66°C. We think the sudden decrease in the value of soil temperature at a depth of

2.5 m results from the un-recalibration or malfunction of the sensor. And the soil temperatures at both sites had increased greatly at depths of 0.5 m to 2.0 m.

HMS 66 sites

The HMS (Highway Maintenance Squad) 66 site is located in a plain near the Xieshui stream, a branch of the Chumaer River. The ground surface is covered by sand and gravel, and sand dunes can be found in this region. The observation records showed that the mean annual ground temperature in the borehole was approximately -0.6°C to -0.7°C. The mean annual soil temperatures in this site also displayed a warming tendency from 1996 to 2001. The collected observation data from two 8 m deep boreholes also showed that the soil temperatures in 7 years had increased by 0.11°C with an annual increasing rate of 0.030°C/yr at one borehole, and by 0.22°C with an annual increasing rate of 0.041°C/yr at the other borehole (Fig. 5). The mean annual soil temperatures were mostly higher than -1.0°C, which was delimited as high-temperature permafrost. From Figure 5 we can conclude that permafrost warming has taken place from 1996 to 2001.

Hoh Xil site

An 8 m deep borehole was drilled in 1995 to measure the ground temperatures at this site. The results showed that the MAST is between -1.3°C and -2.2°C. The ground temperatures had increased by 0.26°C ~ 0.89°C in the 7 years; the annual increase rate amounted to 0.098°C/yr. The MAST above 5 m depth had increased by 0.67°C, while the MAST between the 5 m to 8 m levels by 0.34°C during the 7 years. Soil temperatures at different levels showed a clear warming trend (Fig. 6).

Wudaoliang site and Mt. Fenghuo site

The Wudaoliang site is located in hilly land with an elevation of about 4735 m a.s.l. The soil profiles are composed of eolian and solifluction deposits. The permafrost table is located between 1.5 m to 1.8 m in this site, and the vegetation is alpine meadow with the coverage of about 50%

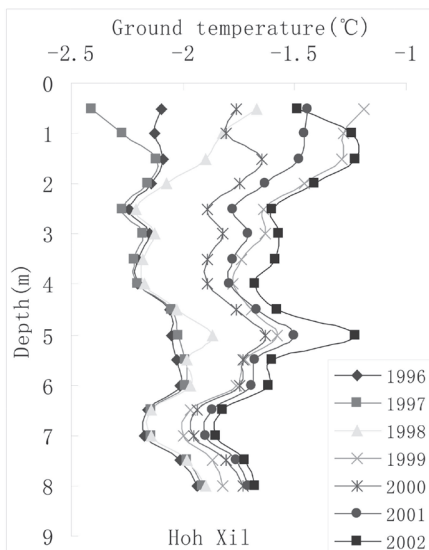


Figure 6. The changes of MAST at the HMS 66 sites.

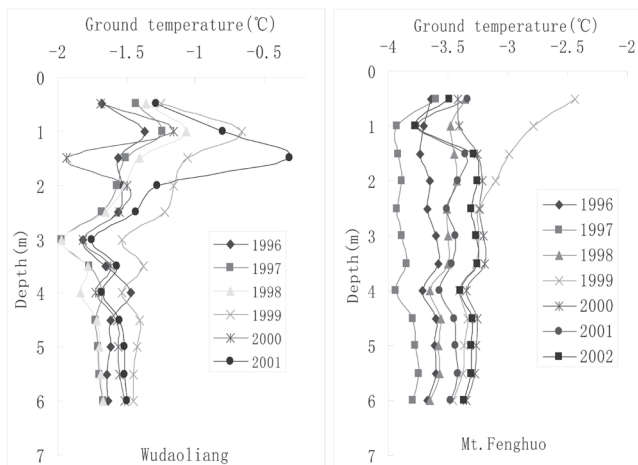


Figure 7. The changes of MAST at the Wudaoliang site and the Mt. Fenghuo site.

(Zhao et al. 2000). Observation results from the 6 m deep borehole at the Wudaoliang site indicated that the MAST has increased by 0.07~0.57°C, from 1996 to 2001 with an annual increasing rate of 0.047°C/yr (Fig. 7). The drastic fluctuation in the value of soil temperature at a depth of 1.5 m in 2000 and 2001 results from the malfunction or the unrecalibration of the sensor.

The Mt. Fenghuo site is located in the hinterland of the Qinghai-Tibet Plateau. The permafrost temperatures at the Mt. Fenghuo site were lower than -3.5°C, which were delimited as low-temperature permafrost. The MAST at the Mt. Fenghuo site has increased by 0.32°C on average with an annual increasing rate of 0.065°C/yr (Fig. 7).

Mt. Tanggula sites

There are two boreholes whose ground temperatures were very close to 0°C drilled to the south of Tanggula Mountain. The observation results from a 10.8 m deep borehole indicated that the MAST had increased by 0.01°C~0.07°C from 1999

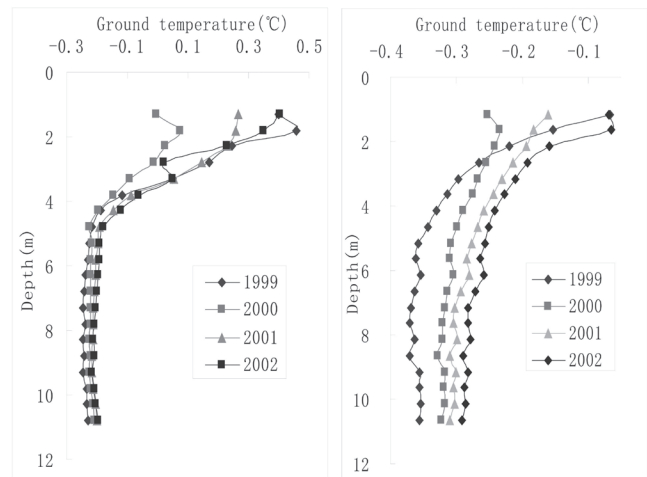


Figure 8. The changes of MAST at the Mt. Tanggula sites.

to 2002. The observation results from another 10.65 m deep borehole indicated that the MAST had increased by 0.06~0.10°C over the 4 years. The annual increasing rates of MAST were 0.011°C/yr and 0.027°C/yr respectively (Fig. 8). At both boreholes, mean annual temperatures of the lower layer of permafrost have changed steadily, and permafrost will disappear if the warming continues.

The environmental implications of permafrost degradation on the plateau

The experiments to measure the emission of CH₄ and CO₂ from the permafrost regions of the plateau indicated that the CO₂ exchange between the ground and atmosphere is characterized by emission, while the CH₄ exchange is characterized by absorption (Lin et al. 1996). Jin et al. (1999) estimate that methane emission from the wetland on the plateau amounts to 0.7–1.0 Tg per year.

Permafrost degradation closely interacts with hydrological and thermal processes near the ground surface, as well as with other components of the ecosystem. Permafrost degradation also results in the lowering of local water tables and lake water levels and the shrinking of wetlands and grazing grasslands (Cheng & Zhao 2000). Cao et al. (2006) concluded that the deterioration of marshy meadows at the source area of the Yellow River results from the lowering supra-permafrost water table.

Climatic Change on the Qinghai-Tibet Plateau

Using mean monthly air temperature data for 1961–2000 at 101 weather stations located all over the plateau and adjacent regions (Fig. 9), we analyzed the decadal changes of mean annual air temperature in the study regions during these 40 years. The results indicated that there are 19 stations where the mean annual air temperature has increased by more than 1.0°C, 50 stations where it increased by 0.5°C–1.0°C, and 25 stations where the mean annual air temperature had increased by 0.0°C–0.5°C (Fig. 9).

Among the above-mentioned 101 weather stations, we analyzed the data of 4 stations located in permafrost regions

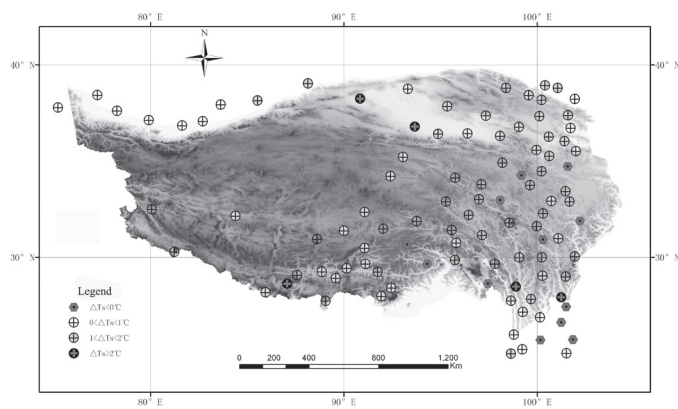


Figure 9. Location of the 101 weather stations with mean monthly air temperature observations on the Qinghai-Tibet Plateau and adjacent regions.

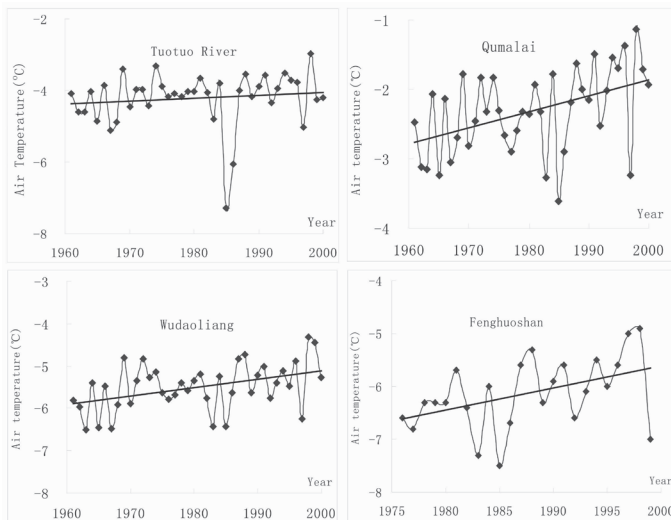


Figure 10. The changes of mean annual air temperature during the last several decades at the stations located in permafrost regions.

to reveal the climate changes occurring in permafrost zones. The results showed the mean annual air temperature in Tuotuo River increased by 0.46°C , 0.79°C in Qumalai, 0.68°C in Wudaoliang from 1961 to 2000, and 0.65°C in Mt. Fenghuo from 1975 to 2000 (Fig. 10). The climatic warming has occurred predominantly in winter. The mean annual increasing rates of air temperature at those 4 stations amounted to $0.022^{\circ}\text{C}/\text{yr}$. The dramatic increase of air temperature in winter decreased the seasonally frozen depth and deepened the active layer, which finally led to the permafrost degradation. With no doubt the extensively occurring climatic warming during the last decades is one of the principal factors leading to permafrost degradation on the plateau.

Conclusions

Observation results from most sites on the Qinghai-Tibet Plateau indicate that extensive permafrost degradation has taken place during the last years. In the northern and southern lower limits of the discontinuous permafrost

regions, permafrost has thinned and disappeared in some areas, and the lower limit of permafrost has risen in altitude. In the hinterland of the plateau where continuous permafrost regions predominate, the ground temperatures have displayed an obvious warming tendency in recent years. In general, the annual rate of increase in MAST is 0.042°C to $0.065^{\circ}\text{C}/\text{yr}$ for low-temperature permafrost (mean annual ground temperature is lower than -3.0°C), 0.016°C to $0.098^{\circ}\text{C}/\text{yr}$ for the permafrost whose mean annual ground temperature is between -0.5°C and -3.0°C , and 0.041°C to $0.041^{\circ}\text{C}/\text{yr}$ for high-temperature permafrost (mean annual ground temperature is higher than -0.5°C). Previous studies indicated that freezing and thawing processes have great impacts on carbon absorption and emission on the plateau. In the mean time, the regional lowering of ground water tables triggered by degrading permafrost is likely mainly responsible for the deteriorating environment on the plateau, as evidenced by dropping lake water levels, shrinking wetlands, and degenerating grasslands.

Based on the analysis of the decadal changes of mean annual air temperature, we revealed that extensive climatic warming has occurred on the plateau during the last decades. Records from weather stations in permafrost regions also indicated that mean annual air temperature has increased especially in winter. The observed climatic warming could be responsible for permafrost degradation.

Acknowledgments

We would like to express our gratitude to the Cryosphere Research Station on the Qinghai-Tibet Plateau, Chinese Academy of Sciences for the observation data collection and logistic support. Especially we thank Dr. Stephen Robinson and another anonymous reviewer for their constructive comments and suggestions to improve this manuscript. This work was supported by a grant from the Major State Basic Research Development Program of China (973 Program, No.2007CB411506) and the Knowledge Innovation Project of the Chinese Academy of Sciences (No. KZCX3-SW-345 and KZCX3-SW-351).

References

- Cao, W., Wan, L., Zeng, Y., Hu, F. & Chen, J. 2006. Impacts of global warming on the eco-environment in the headwater region of the Yellow River. *Earth Science Frontiers* 13(1): 40-47.
- Cheng, G. & Wu, T. 2007. Responses of permafrost to climate change and their environmental significance, Qinghai-Tibet Plateau. *Journal of Geophysical Research* 112: F02S03, doi: 10.1029/2006JF000631.
- Cheng, G. & Zhao, L. 2000. The problems associated with permafrost in the development of the Qinghai-Xizang Plateau. *Quaternary Science* 20(6): 521-531.
- Isaksen, K., Sollid, J.L., Holmlund, P. & Harris, C. 2007. Recent warming of mountain permafrost in Svalbard and Scandinavia. *Journal of Geophysical Research*, 112: F02S04, doi:10.1029/2006JF000522.

- Jin, H., Chang, X. & Wang S. 2007. Evolution of permafrost on the Qinghai-Xizang (Tibet) Plateau since the end of the late Pleistocene. *Journal of Geophysical Research* 112: F02S09, doi:10.1029/2006JF000521.
- Jin, H. & Cheng, G. 1997. Methane emissions in permafrost regions. *Journal of Glaciology & Geocryology* 12(3): 276-283.
- Lin, Q., Jin, H., Cheng, G. & Li, N. 1996. CH₄ and CO₂ emission from permafrost surface in Wudaoliang in the Tibetan Plateau. *Journal of Glaciology & Geocryology* 18(4): 325-330.
- Nelson, F., Anisimov, O. & Shiklomanov, N. 2001. Subsidence risk from thawing permafrost. *Nature* 410: 889-890.
- Osterkamp, T.E. 2007. Characteristics of the recent warming of permafrost in Alaska. *Journal of Geophysical Research* 112: F02S02, doi:10.1029/2006JF000578.
- Walker, G. 2007. A world melting from the top down. *Nature* 446: 718-721.
- Wang, S. 1997. Study of permafrost degradation in the Qinghai-Xizang plateau. *Advance in Earth Science* 12(2): 164-167.
- Wang, S., Zhao, X. & Guo D. 1996. Response of permafrost to climate change in the Qinghai-Tibet Plateau. *Journal of Glaciology & Geocryology* 18(Supplement): 157-165.
- Wu, T., Li, S., Cheng, G. & Nan Z. 2005. Using ground-penetrating radar to detect permafrost degradation in the northern limit of permafrost area on the Tibetan Plateau. *Cold Regions Science and Technology* 41: 211-219.
- Zhang, T., Frauenfeld, O.W., Serreze, M.C., Etringer, A.J., Oelke, C., McCreight, J.L., Barry, R.G., Gilichinsky, D., Yang, D., Ye, H., Feng, L. & Chudinova, S. 2005. Spatial and temporal variability in active layer thickness over the Russian arctic drainage basin. *Journal of Geophysical Research-Atmospheres* 110: D16101, DOI:10.1029/2004JD005642.
- Zhao, L., Cheng, G. & Ding Y. 2004. Studies on frozen ground of China. *Journal of Geographical Sciences* 14(4): 411-416.
- Zhao, L., Cheng, G., Li, S., Zhao, X. & Wang, S. 2000. Thawing and freezing processes of active layer in Wudaoliang region of Tibetan Plateau. *Chinese Science Bulletin* 45(23): 2181-2186.
- Zimov, S., Schuur, E. & Chapin, F. 2006. Permafrost and the global carbon budget. *Nature* 312: 1612-1613.

Impact of Freezing on Water Migration in Silty Clay Samples

Shu-ping Zhao

State Key Laboratory of Frozen Soil Engineering, CAREERI, CAS, Lanzhou, Gansu 730000, China

Jian-feng Zheng

State Key Laboratory of Frozen Soil Engineering, CAREERI, CAS, Lanzhou, Gansu 730000, China

Wei Ma

State Key Laboratory of Frozen Soil Engineering, CAREERI, CAS, Lanzhou, Gansu 730000, China

Yi-bin Pu

State Key Laboratory of Frozen Soil Engineering, CAREERI, CAS, Lanzhou, Gansu 730000, China

Abstract

A group of tests were conducted to study the impact of freezing on the re-distribution of water and on dry density in silty clay soil samples. Tests determined that freezing has nearly no influence on dry density. Tests also show that, in those standard samples with evenly distributed water content initially, the water content will be re-distributed following freezing. The extent of water re-distribution in a sample is determined by the soil type, the state of saturation, and the freezing method. For water-unsaturated Lanzhou Loess samples, a great amount of water appears to have migrated during radial freezing or axial freezing, and the maximum range of water content in one specimen reaches 4.46%. For water-saturated Lanzhou Loess and water-unsaturated Beiluhe Soil frozen by the axial method or the radial method, and for water-saturated Beiluhe Soil specimens frozen by the axial freezing method, water migration is minor and the range of water content in each specimen is less than 2%.

Keywords: axial freezing; radial freezing; silty clay; water migration; water-saturated; water-unsaturated.

Introduction

Laboratory mechanical experiments are usually performed to evaluate mechanical properties of frozen soil for geotechnical engineering as well, as to obtain a variety of parameters for the modeling of constitutive relationship. Standard cylindrical soil samples with a diameter and a length being twice the diameter are usually used in laboratory mechanical experiments. The soil samples include two types: undisturbed samples which are drilled in-situ directly, and remoulded samples which are made and frozen under artificial cryogenic environment indoors. A large number of studies show that water migration toward freezing front will occur during the soil freezing process (Solomatin & Xu 1994, Butler et al. 1996, Spaans & Baker 1996, Newman & Wilson 1997, Zhao et al. 1997, Stahli et al. 1999, Dawson et al. 1999, Brouchkov 2000, Brouchkov 2002, Iwata & Hirota 2005, Qi et al. 2006). Even if rapidly freezing method and close system are applied to making remoulded frozen soil samples, there still exists slight moisture migration. The effect caused by this migration might be possibly ignored if the results of mechanical tests on remoulded frozen soil samples are used in engineering. However, in theoretic modeling which assumes an ideally evenly moisture distribution throughout soil sample, a more precise measurement is required. In this context moisture migration should be taken into account. This paper will be dedicated

to the study of moisture redistribution in remoulded frozen silty clay samples in association with a specific specimen-preparing method and varying freezing approaches.

Test Preparation

Materials

The materials used in this investigation are remoulded silty clay from the Donggang town of Lanzhou City, termed “Lanzhou Loess” in this paper, and from the Beiluhe area of the Qinghai-Tibet plateau, referred to here as “Beiluhe Soil.” Their physical properties and particle distribution curves are shown in Table 1 and Figure 1, respectively. Both of them are classified as CL based on the Unified Soil Classification System.

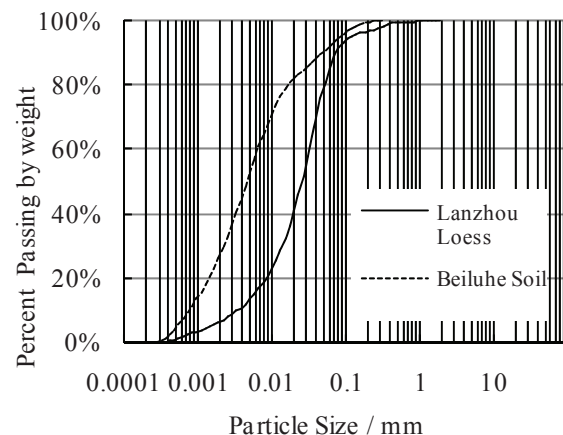


Figure 1. The particle distribution curves of test soils.

Table 1. The physical properties of test soils.

	Liquid limit	Plastic limit	Plastic index
Lanzhou Loess	29.36	14.92	14.44
Beiluhe Soil	32.88	17.50	15.38

Testing apparatus

All samples were prepared using the Standard Specimen Instrument (Fig. 2a) designed by Zhao (1998) consisting of mainframe, control system, mould, and drain system. Press-poles and press-caps of various sizes are assembled with high precision load sensors. The maximum loading capacity is up to 180 kN. In this test, a press-pole with a loading capacity of 30 kN was used. The nominal size of the soil specimen is 61.8 mm in diameter by 125 mm long.

Moulding

Our earlier tests (Zheng et al. in press) found that the dry-density distribution in samples prepared by the pressure method was better than that in samples prepared by the layered-bumping method which has been widely adopted in literature (Zhu & David 1987, Zhao et al. 1998, Yang et al. 2000). In this paper the pressure method is used to make soil samples.

First, raw soil samples were air-dried, ground and sifted with a 2 mm sieve. Second, distilled water was added to dry soil to form a moist soil with the required water content. After storage overnight to allow for moisture equilibration, the moist soil was carefully put into the mould. Third, the press-pole was descended to compact the moist soil, with the descending velocity adjusted through the control system. A higher velocity was used at the very beginning, and then at a constant but lower velocity after the press cap touches soil sample. The pressing lasted a certain time, after which the sample was turned over and pressed with the same lower speed. The overall pressing time periods are 8 h and 4 h, respectively, for Lanzhou Loess and Beiluhe Soil. In this way, water-unsaturated specimens can be obtained.

After compaction, partial specimens were deaerated under a vacuum of 73 mm Hg and then water saturated with distilled water for more than 12 h. The set-up for Water-saturation is shown in Figure 2b.

Both water-unsaturated and water-saturated specimens were put into special moulds. The moulds were then placed into a freezing cabinet and quickly frozen in a close system (without water supply) with an upper boundary temperature of lower than -30°C. Two freezing approaches were used: axial freezing and radial freezing. The axial freezing approach is to use a heat-insulated sponge to pack peripheral and bottom parts of the moulds so that specimens are frozen downwards. The radial freezing approach places plastic

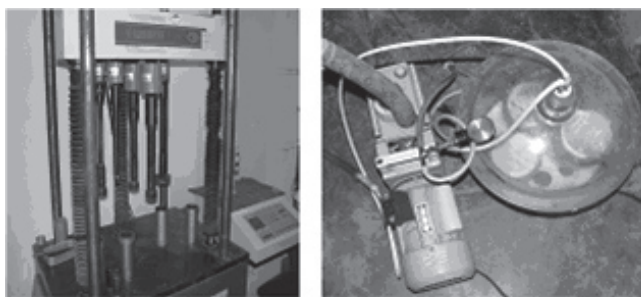


Figure 2. Standard specimen instrument and set-up for water-saturation.

caps to both ends of a specimen, causing the specimen to be frozen from the exterior to the center. After freezing more than 24 h, the specimens were removed from the moulds.

Testing procedure

Each specimen was partitioned vertically into four layers to test the dry density. The inner part (symbolized as part A in Fig. 3) and outer part (symbolized as part B in Fig. 3) of each layer were detached to test water content. For each specimen, four dry density values and eight water content values can be obtained.

Test Results

The dry density distribution in specimens

To study the dry density distribution, the mean value (ME), standard deviation (SD) and range (R) for each specimen were calculated and shown in Tables 2 and 3.

Tables 2 and 3 show a similar change trend of dry density in Lanzhou Loess and Beiluhe Soil from the unfrozen to frozen states. The standard deviations observed in all specimens are small. Moreover, there are minor variations in standard deviation for each group of specimens (unfreezing, axial and radial freezing), which proves that the freezing process has nearly no influence on dry density distribution.

The water content distribution in specimens

To analyze the water content distribution, the mean value (ME), standard deviation (SD) and range (R) were calculated and are shown in Tables 4 and 5.

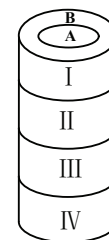


Figure 3. The sampling scheme for testing dry density and water content.

Table 2. The dry density (g/cm³) distribution in Lanzhou Loess.

Specimen no.	Water unsaturated				Water saturated				
	1#	2#	3#	4#	1#	2#	3#	4#	
Un-freezing	ME	1.725	1.705	1.705	1.698	1.690	1.693	1.700	
	SD	0.015	0.022	0.015	0.015	0.014	0.019	0.019	
	R	0.03	0.06	0.04	0.04	0.04	0.05	0.05	
Radial freezing	ME	1.761	1.761			1.734	1.715	1.691	1.687
	SD	0.018	0.006			0.016	0.008	0.009	0.006
	R	0.044	0.015			0.04	0.021	0.025	0.015
Axial freezing	ME	1.763	1.757	1.753	1.744	1.721	1.723		
	SD	0.009	0.003	0.009	0.001	0.003	0.017		
	R	0.024	0.007	0.025	0.027	0.008	0.042		

Table 3. The dry density (g/cm³) distribution in Beiluhe Soil.

Specimen no.	Water unsaturated				Water saturated				
	1	2	3	4	1	2	3	4	
Un-freezing	ME	1.863	1.850	1.803	1.863	1.813	1.805	1.747	1.761
	SD	0.008	0	0.029	0.004	0.011	0.005	0.006	0.008
	R	0.02	0	0.07	0.01	0.03	0.01	0.017	0.02
Radial freezing	ME	1.768	1.769		1.802	1.793	1.742	1.762	
	SD	0.016	0.019		0.013	0.017	0.013	0.011	
	R	0.037	0.045		0.031	0.044	0.031	0.028	
Axial freezing	ME	1.775	1.768		1.792	1.805	1.801	1.792	
	SD	0.011	0.018		0.008	0.005	0.017	0.009	
	R	0.03	0.03		0.021	0.013	0.04	0.023	

Table 4. The water content (%) distribution in Lanzhou Loess.

Specimen no.	Water unsaturated				Water saturated				
	1	2	3	4	1	2	3	4	
Un-freezing	ME	16.29	14.30	14.15	14.49	21.79	21.75	21.68	
	SD	0.35	0.15	0.17	0.05	0.54	0.66	0.72	
	R	0.95	0.47	0.54	0.19	1.57	2.11	2.40	
Radial freezing	ME	15.56	15.68		20.34	20.87	21.65	21.37	
	SD	1.31	1.56		0.45	0.43	0.39	0.42	
	R	3.20	3.48		1.4	1.49	1.19	1.44	
Axial freezing	ME	15.34	15.65	15.33	14.98	20.67	20.52		
	SD	1.54	1.73	1.28	1.52	0.27	0.49		
	R	3.91	4.46	3.33	3.61	0.77	1.41		

Table 4 shows that in the water-unsaturated Lanzhou Loess samples, the initial water content distributes evenly, and R of water content for each sample is less than 1%. In the process of freezing, a significant amount of water migration was observed with both the radial and axial freezing approaches. The maximum difference of water content between different positions of a specimen can reach up to 4.46%. This difference will make sense, especially when we study the impact of water content on frozen soil mechanical or thermal characteristics through indoor experiments. Therefore, in such a case, we should take into account water content variations inside a specimen rather than using simple mean water content.

Table 4 also suggests that the amounts of SD and R in the water-saturated state are larger than those in water-unsaturated for Lanzhou Loess. However, after axial or radial freezing, SD and R of water content will decrease. Each R for samples of frozen water-saturated Lanzhou Loess is less than 1.5%, indicating to some degree that moisture in frozen water-saturated Lanzhou Loess is evenly distributed. These results are in accordance with the conclusion of Liu et al. (2002).

Table 5 shows the initially even water content distribution in water-unsaturated Beiluhe Soil, with R of water content for each sample being less than 1%. Only minimal water migration was observed during the axial or radial freezing process. The R of water content for each sample is still under

Table 5. The water content (%) distribution in Beiluhe Soil.

Specimen no.	Water unsaturated				Water saturated				
	1	2	3	4	1	2	3	4	
Un-freezing	ME	16.00	16.28	16.33	16.12	18.54	18.63	19.96	19.51
	SD	0.23	0.13	0.13	0.23	0.75	0.21	0.63	0.37
	R	0.71	0.45	0.46	0.73	2.29	0.70	1.67	1.15
Radial freezing	ME	15.30	15.50		18.69	19.02	19.61	19.18	
	SD	0.24	0.23		0.68	0.68	1.05	0.86	
	R	0.59	0.57		1.95	1.71	2.81	2.44	
Axial freezing	ME	15.82	15.82		18.90	18.55	18.44	18.68	
	SD	0.32	0.28		0.64	0.56	0.52	0.41	
	R	0.97	0.71		1.93	1.53	1.63	1.43	

Table 6. The mean value and range of water content (%) for the inner and outer parts of Lanzhou Loess.

	Specimen no.		Unfreezing		Radial freezing		Axial freezing		
			ME	R	ME	R	ME	R	
			Water unsaturated	1	Inner	16.47	0.88	14.31	0.60
		Outer	16.10	0.48	16.81	1.33	16.65	0.93	
	2	Inner	14.33	0.35	14.13	0.24	14.21	3.18	
		Outer	14.27	0.41	17.23	0.59	17.10	1.31	
	3	Inner	15.22	0.47			14.22	2.07	
		Outer	15.06	0.29			16.45	0.99	
	4	Inner	14.51	0.13			13.75	2.84	
		Outer	14.47	0.12			16.22	0.78	
Water saturated	1	Inner	21.93	1.37	20.29	0.95	20.70	0.74	
		Outer	21.65	1.44	20.39	1.40	20.68	0.59	
		2	Inner	21.94	1.30	20.80	0.57	20.54	1.18
			Outer	21.55	1.97	20.95	1.49	20.50	1.34
		3	Inner	21.95	1.32	21.68	0.99		
			Outer	21.40	2.19	21.62	1.15		
		4	Inner			21.08	0.69		
			Outer			21.65	0.95		

1% after freezing.

Table 5 also shows that SD and R for water-saturated Beiluhe Soil samples are larger than those for water-unsaturated samples. The SD and R of water content will increase after radial freezing, but decrease after axial freezing. The R for water-saturated Beiluhe Soil samples frozen by the axial freezing approach is less than 2%.

The water migration in specimens

To study the direction of water migration, the water content of the inner part and outer parts were collected. The mean value (ME) and range (R) were then calculated, and results are shown in Tables 6 and 7.

A number of similar change trends in water content can be found for these two types of soils in Tables 6 and 7. First, for unfrozen water-unsaturated samples, there is small variation of the mean water content between inner and outer positions of a specimen. Meanwhile, the R of water content in both inner and outer parts is rather small. After water-saturating, a similarly small variation of mean value of water content

Table 7. The mean value and range of water content (%) for the inner and outer parts of Beiluhe Soil.

	Specimen no.	Unfreezing		Radial freezing		Axial freezing		
		ME	R	ME	R	ME	R	
Water unsaturated	1	Inner	16.05	0.51	15.07	0.16	15.57	0.7
		Outer	15.95	0.71	15.53	0.13	16.07	0.39
	2	Inner	16.37	0.30	15.28	0.14	15.59	0.53
		Outer	16.19	0.22	15.73	0.12	16.05	0.23
	3	Inner	16.42	0.19				
		Outer	16.25	0.32				
	4	Inner	16.28	0.46				
		Outer	15.95	0.38				
Water saturated	1	Inner	18.74	1.84	18.06	0.43	18.33	0.84
		Outer	18.35	1.97	19.32	0.93	19.46	0.69
	2	Inner	18.81	0.31	18.37	0.22	18.02	0.34
		Outer	18.45	0.26	19.66	0.68	19.07	0.61
	3	Inner	20.41	1.4	18.70	0.52	18.02	0.74
		Outer	19.52	0.13	20.52	1.81	18.87	0.64
	4	Inner	19.58	1.13	18.44	0.83	18.34	0.31
		Outer	19.44	0.79	19.93	1.38	19.02	0.77

between inner and outer parts was preserved. But a larger R of water content at either the inner or outer parts appears, proving that the degree of water supply at different position along the axial direction differs. Secondly, for all unfrozen samples, the mean value for the central inner part is slightly larger than that for the outer part, while for all frozen samples, the mean value for the outer part is larger than that for the inner part, implying that water moves outwards during the freezing process.

Table 6 shows that when the water-unsaturated Lanzhou Loess samples were radial frozen, there is a distinguishing difference between mean water content in the inner and outer parts of a same specimen, along with invariant R statistics in those parts. This observation indicates water has migrated outwards along the radial direction. When the water-unsaturated samples were axially frozen, not only was there is great difference between ME at inner and outer parts, but also R at both parts are large, proving water has migrated along radial and axial direction at the same time.

Table 6 also shows that, when water-saturated Lanzhou Loess samples were frozen by the radial or axial freezing approach, there is still little difference between the ME of the inner and outer parts; moreover, R in both parts decreases. These results prove that water moves mainly along the axial direction and makes the water content distribution more uniform.

Table 7 shows that, when the water-unsaturated Beiluhe Soil samples were frozen by radial or axial freezing, there is still little variation between the ME in the inner and outer parts, and that R in both parts is still small. This proves that there is nearly no water migration during the freezing process.

Table 7 also shows that when the water-saturated Beiluhe Soil samples were frozen by radial freezing, the difference

between the mean value of water content of the inner and outer parts clearly increase, while R in both parts is still as much as that for unfrozen water-saturated samples. This proves that the water moves mainly along the radial direction.

Furthermore, the following result can also be observed in Table 7. When water-saturated Beiluhe Soil samples were frozen by axial freezing, the variation between the mean value of the water content in the inner and outer parts increases slightly, and R in both parts decrease.

The influence of soil type on water migration

If specimens are prepared by the pressure method, the longer the pressing time, the more uniform the samples will be. The pressing time is 8h and 4h for Lanzhou Loess and Beiluhe Soil, respectively, which proves that it is easier to obtain uniform specimens with Beiluhe Soil.

For water-unsaturated samples, there is obvious water migration in Lanzhou Loess, and there is nearly no water migration in Beiluhe Soil. The main reason can be expressed as follow. The particle-size analysis results show that silty particles and clay particles account for 77.73% and 13.55% by weight in Lanzhou Loess, while accounting for 40.79% and 52.78% in Beiluhe Soil. Lanzhou Loess mainly consists of silty particle, which can form better channel for water migration. In Beiluhe Soil, the percentage of silty grain and clay grain both occupy higher proportions. The grain gradation is good; it is therefore difficult to form channels for water migration.

For water-saturated samples, water migration in Beiluhe Soil is more obvious than that in Lanzhou Loess. Beiluhe Soil contains more fine grains with lower thermal conductivity, so the freezing front penetrates more slowly during freezing and there is enough time for water migration.

If those samples with water content R of less than 2% can be considered as feasible, then, both water-saturated Lanzhou Loess and water-unsaturated Beiluhe Soil--frozen by the axial or radial freezing approach--can meet this requirement. The water-saturated Beiluhe Soil specimens frozen by the axial freezing approach also meets this requirement. However, for the water-unsaturated Lanzhou Loess, the internal unevenness of water content must be considered.

Conclusions

To summarize the test results, the following conclusion can be drawn.

The water content distribution in specimens prepared by the pressure method is uniform. The degree of water supply at different position along the axial direction differs during the water- saturating process.

For all unfrozen samples, the mean value of water content for the inner part is slightly larger than that for the outer part, while for all frozen samples, the mean value for the outer part is larger than that for the inner part, implying that water moves outward during the freezing process.

The freezing process has nearly no influence on dry

density distribution.

For water-unsaturated Lanzhou Loess samples, in the process of freezing a significant amount of water migration was observed with both the radial and axial freezing approaches. The maximum difference in water content between different positions of a specimen can be up to 4.46%. This difference will make sense, especially when we study the impact of water content on frozen soil mechanical or thermal characteristics, through indoor experiments. Therefore, in such cases, we should take into account internal water content variation rather than simple average water content of a specimen.

For water-saturated Lanzhou Loess and water-unsaturated Beiluhe Soil, proper specimens can be obtained by the axial or radial freezing approaches. The water-saturated Beiluhe Soil specimens frozen by the axial freezing method also meets the requirement.

Acknowledgments

The project is supported by the National Natural Science Foundation of China (No. 40501016), the National Natural Science Fund for Talent Training in Basic Research (No. J0630966), and the Western Project Program of the Chinese Academy of Sciences (No. KZCX2-XB2-10).

References

- Brouchkov, A. 2000. Salt and water transfer in frozen soils induced by gradients of temperature and salt content. *Permafrost and Periglacial Processes* 11(2): 153-160.
- Brouchkov, A. 2002. Nature and distribution of frozen saline sediments on the Russian Arctic coast. *Permafrost and Periglacial Processes* 13(2): 83-90.
- Butler, A.P., Burne, S. & Wheeler, H.S. 1996. Observations of 'freezing-induced redistribution' in soil lysimeters. *Hydrological Processes* 10(3): 471-474.
- Dawson, R. Sego, D. & Pollock, G. 1999. Freeze-thaw dewatering of oil sands fine tails. *Canadian Geotechnical Journal* 36(4): 587-598.
- Iwata, Y. & Hirota, T. 2005. Monitoring over-winter soil water dynamics in a freezing and snow-covered environment using a thermally insulated tensiometer. *Hydrological Processes* 19(15): 3013-3019.
- Liu, Z.L., Li, H.S. & Zhu, Y.L. 2002. A distinguish model for initial and additional micro-damages on frozen soil. *Journal of glaciology and geocryology* 24(5): 676-680.
- Newman, G.P. & Wilson G.W. 1997. Heat and mass transfer in unsaturated soils during freezing. *Canadian Geotechnical Journal* 34(1): 63-70.
- Qi, J.L., Vermeer, P.A. & Cheng, G.D. 2006. A review of the influence of freeze-thaw cycles on soil geotechnical properties. *Permafrost and Periglacial Processes* 17(3): 245-252.
- Solomatin, V.I. & Xu, X.Z. 1994. Water migration and ice segregation in the transition zone between thawed and frozen soil. *Permafrost and Periglacial Processes* 5(3): 185-190.
- Spaans E.J.A. & Baker, J.M. 1996. The soil freezing characteristic: Its measurement and similarity to the soil moisture characteristic. *Soil Science Society of America Journal* 60(1): 13-19.
- Stahli, M., Jansson, P.E. & Lundin, L.C. 1999. Soil moisture redistribution and infiltration in frozen sandy soils. *Water Resource Research* 35(1): 95-103.
- Yang, S.L., Sandven, R. & Lin, L. 2000. Improved preparing technique of silt sample. *Chinese Journal of Geotechnical Engineering* 22(3): 379-380.
- Zhao, J.J. 1998. *Development of standard specimen instrument and frost heave model* (Article for the Degree of Master). Lanzhou: Lanzhou Glacier and Frozen Soil Research Institute, Chinese Academy of Science.
- Zhao, L.T., Gray, D.M. & Male, D.H. 1997. Numerical analysis of simultaneous heat and mass transfer. *Journal of Hydrology* 200(1-4): 345-363.
- Zhao, Z.Y., Zhou, C.E. & Cao, X.R. The simple sample-preparing method and its application in engineering. *GuangDong GongLu JiaoTong* 93(1): 57-60.
- Zheng, J.F., Zhao, S.P & Ma, W. Study on the specimen-preparing method for remoulded silty clay samples. *Journal of Glaciology and Geocryology* (in press).
- Zhu, Y.L. & David, L.C. 1987. *Creep and strength behavior of frozen silt in uniaxial compression*. U.S. Army Cold Regions Research and Engineering Laboratory, CRREL Report 87-10: 3-6.

Variation of CO₂ Concentrations in the Active Layer in Alpine Grasslands Soil on the Qinghai-Tibet Plateau

Yong-hua Zhao

Cold and Arid Regions Environment and Engineering Research Institute, CAS; Observation and Research Station of Qinghai-Tibet Plateau, CAREERI, CAS, Lanzhou Gansu730000, China

Lin Zhao

Cold and Arid Regions Environment and Engineering Research Institute, CAS; Observation and Research Station of Qinghai-Tibet Plateau, CAREERI, CAS, Lanzhou Gansu730000, China

Tian-yun Wu

Cold and Arid Regions Environment and Engineering Research Institute, CAS; Observation and Research Station of Qinghai-Tibet Plateau, CAREERI, CAS, Lanzhou Gansu730000, China

Abstract

CO₂ concentrations from 0 to 180 cm in active layer soil were measured by static dark enclosed chamber technique from January in 2006 to January in 2007 in alpine grassland located on the Qinghai-Tibet Plateau. Results revealed: (1) CO₂ concentrations increasing gradually from 0 cm to 140 cm depth, and feebly decreasing from 140 cm to 180 cm. The ranges of CO₂ concentrations changed successively from 1138 to 3162 ppm. (2) Seasonal variations from 0 to 100 cm depth showed the highest concentrations occurring in the active layer thawing period and lowest occurring in the frozen period. The CO₂ concentration's seasonal changing ranges at deeper layers were all significantly higher than those at surface layers, but the deeper (100–180 cm) layers did not show clear trends. The variations of CO₂ concentrations in the soil were hardly explained by soil temperature at any depth. A significant correlation was found between CO₂ concentrations and active layer unfrozen-water content.

Keywords: active layer; alpine grasslands soil; CO₂ concentrations; Qinghai-Tibet Plateau; variation.

Introduction

Global warming has been of great concern, and the accumulation of greenhouse gases in soils is assumed to be responsible for the rise in mean global temperatures (Crowley 2000). As one of the most effective greenhouse gases, carbon dioxide (CO₂) is a maximum atmospheric trace gas and responsible for almost 63.7% (Rodhe 1990) of anticipated annual global warming undergoing an atmospheric concentration exceeding 367 ppm (IPCC 2001). Some evidence from the literature indicated that the elevated atmospheric CO₂ could affect many belowground processes of grassland such as grassland types, root respiration, and soil microbes (Pietikainen et al. 1999).

There are many sources of CO₂, but the most important natural source of atmospheric CO₂ is assumed to be microbial activities in environments like soil and water (Andersen et al. 2001). The partial pressure of CO₂ in the soil may differ greatly from that in the atmosphere. Due to the respiratory activity of plant roots and soil biota, the higher CO₂ concentration can be measured compared to that in the atmosphere. Several studies have shown that a high spatial variation of the CO₂ efflux from the soil can be efficiently explained by fine root and microbial biomass distribution, and by physical and chemical soil properties (Pangle & Seiler 2002, Maestre & Cortina 2003). Much of that heterogeneity occurs within short distances (Stoyan et al. 2000) and is especially high in areas where the distribution of ecological factors and organisms is markedly patchy (Maestre & Cortina 2003).

In comparison to data on atmospheric CO₂ enrichment, surprisingly, less is known about soil CO₂. To our knowledge, however, there is no study on temporal and spatial variation in permafrost soil on Qinghai-Tibet Plateau.

The mean altitude of the plateau is more than 4000 m above sea level with an area about 2,500,000 km². Great uplift of the plateau since the Late Cenozoic has been strongly affecting the physical environment of the plateau itself and its neighboring regions. Meanwhile, the plateau is also a sensitive trigger of climate change in Asian monsoon region, which is closely related to the global change (Zheng and Zhu 2000). Due to the topographic features and the characteristics of the atmospheric circulation, typical alpine zones of forests, meadows, grasslands, and deserts appear in succession from southeast to northwest in the plateau. Alpine grassland is one of the most important ecosystems on the Qinghai-Tibet Plateau because of its large area. Besides, the area is special for its lack of human activity. It provides an ideal scientific field for understanding on CO₂ exchanges in a soil-plant-atmosphere profile.

Freeze–thawing fluctuations are common characters in cold areas. Their effects on soil biogeochemical processes are a subject of major ecological interest, because it is often suggested that freeze–thawing events may be a major factor contributing to the microbial release of C in plant available form (Lipson et al. 1999, Grogan & Jonasson 2003). Furthermore, since plant productivity is often strongly limited by nutrient availability (Vitousek et al. 1991), freeze–thawing effects on soil nutrient transformations may

substantially influence the C balance of cold ecosystems. Freezing and subsequent thawing of soils often results in an initial flush of microbial respiration and CO₂ effluxes (Muller et al. 2002). Laboratory incubation studies indicate that freeze–thawing cycles can lyse a substantial proportion of microbial cells, resulting in C releases into the surrounding soil, that may be immobilized by surviving microbes as they consume the enhanced supply of C substrate (Skogland et al. 1988). Thus, the extent and biogeochemical significance of freeze–thawing processes to overall ecosystem C cycling remains unclear, and may vary substantially depending on the character of the plants and temperature the freeze–thawing process is largely uninvestigated. Most of the above conclusions have been based on studies of soils without freeze–thawing process on the Qinghai-Tibet Plateau. CO₂ fluxes responses to freeze–thawing are clearly important, since soils in cold ecosystems generally contain large CO₂ concentrations (Zhao et al. 2005). Therefore, studies on the variations of CO₂ concentrations in active layer are necessary to fully evaluate freeze–thawing processes effects on whole ecosystem C cycles.

Materials and Methods

Site description

The experimental site is at Beiluhe Experimental Station, Cold and Arid Regions Environmental and Engineering Research Institute, Chinese Academy of Sciences (34°51.24'N, 92°56.39'E, 4628 m a.s.l.). The station is located in continuous permafrost area with cold and dry climate condition, and top soil is frozen from September to April of the next year. The annual average temperature is -5.2°C with the lowest temperature of -37.7°C and the highest of 23.2°C.

The sampling site is located in an area near the station. The soil, under typical vegetation type (alpine grassland) was collected, and its basic chemical and physical properties were analyzed.

The sampling site is at a river bank where the vegetation type was alpine grassland under which Cab-Gel-Sandic Entisols had developed (Chinese Soil Taxonomy, Gong et al. 1999). About 70% of the ground was covered by the dominant plants such as *Avena fatua*, *Kobresia pygmaea*, *Aster asteroides*, *Astragalus melilotoides*, and *Saussurea arenaria*. The parent material of the soil at 0–100 cm was aeolian sand and at the 100–140 cm depth, alluvial sand over red residual of the Tertiary at 140–180 cm. The contents of CaCO₃ and clay along the profile illustrated CaCO₃ moved downward slightly, but the clay did not, reflecting unintensive soil water movement. The high clay content at the 140–160 cm layer should be ascribed to the parent material. There was no groundwater at the 0–180 cm depth when soil sampling.

Experimental design

CO₂ concentrations at different layers in the soil were examined thrice (1 d) a month from January 2006 to January 2007. On each sampling day, CO₂ concentrations were measured between 10:00 and 16:00. At each depth, three

samples were taken by sampling pipes. All gas samples were taken with polypropylene syringes equipped with three-way stopcocks into 12 mL polyethylene vacuum vials for CO₂ concentration analyses (Maljanen et al. 2001). The samples were transported to the lab frozen, and were analyzed using gas chromatography.

We gathered the soil gas samples at the depths of 0.1, 0.2, 0.4, 0.6, 0.8, 1.0, 1.2, 1.4, 1.6, and 1.8 m from the soil through soil gas samplers, which were similar to Burton's facilities (Burton & Beauchamp 1994). Our gas samplers were made of stainless steel tubes. The outside tube has an exterior diameter of 16 mm, and the diameter of the inside pipes was 8 mm. The tops of the inside pipes were tightened by three-way stopcocks, thereby separating the inner soil gases from the outer atmosphere. The sampling plots were selected on typical plant community and coverage of the study area, and the example wells were dug on January 2006. Samplers were put in each well osculated to the soil profiles in order to get the exact CO₂ concentrations at different soil layers. Gas samples were gathered from each of the airtight pipes with polypropylene syringes into 12 mL polyethylene vacuum vials. Furthermore, the soil temperature and moisture content were also measured using temperature and moisture content probes during the experimental time.

Sample analyses

The Total Soil Organic Carbon (TOC) was analyzed using a Shimadzu 5000A, and its standard analytical procedure for TOC was adopted. The Microbial Biomass Carbon (MB-C) was measured by extracting 20 g of defrosted soil with 40 ml K₂SO₄ solution for 1 h under shaking at 200 rpm. After extraction, the soil suspensions were filtered. MB-C was measured by directly determining TOC using the Shimadzu 5000A at 680°C. The Water Dissolved Organic Carbon (WDOC) was measured by the method described by Wu et al. (2003). CO₂ concentrations were analyzed within 30 days by a gas chromatography (GC) (Type: Hewlett-Packard 6890), which was equipped with a flame-ionization detector (FID).

Results and Discussion

Soil carbon characteristics

Soil moisture increased gradually with depth from values of about 3.61% at the surface to 13.75% at 1.5 m. The root system here was stronger than the plain area due to the frigid climate.

The TOC content in the soil profiles decreased as the depth increased, and the trends could be described as exponential processes. It decreased dramatically in the 0–60 cm depths and then slowly in the lower layers with the depth increasing.

The TOC mass (0–180 cm) in the soil was 69.64 Mg C ha⁻¹, of which 66.11 Mg C ha⁻¹ was in the 0–100 cm depth. About 94.4% of TOC in the solum was in the upper 0–100 cm layers and only a little below the layers. Even though the solum of this site was composed of loam or sandy loam which favor water percolation, the soil moisture in the layers below

100 cm were saturant the whole year and it was near saturant in the 50–100 cm layers most of a year, due to the permafrost layer beneath 180 cm (Zhao et al. 2000). The excess water prohibited root growth, and thus nearly all of the TOC was located in the upper 60 cm layer. The distribution of root residual along the profile was both a reflection of the soil water regime and an explanation of the TOC distribution in the layers: totally 9.23 Mg C ha⁻¹ as root residual and all of it was in the 0–40 cm layers. Beside the soil water regime, the high content of pebble or particles larger than 2 mm in the layers below 40 cm definitely influenced the root growth and therefore the TOC distribution along the profile.

The WDOC contents declined dramatically with depth increasing, and it was significantly higher in the 0–40 cm layers than the lower layers. Also, in the soils MB-C was detected only in the 0–20 cm layers, and it was much higher in the 0–10 cm layer than the 10–20 cm layer.

CO₂ concentration in soil profile

Soil CO₂ concentrations increased gradually with depth, and the highest CO₂ concentration was found at the depth of 150 cm; the lowest CO₂ concentration occurred at the 10 cm, which is similar to the researches at the agriculture (Burton & Beauchamp 1994). In general, the mean concentrations in the atmosphere were all much lower than the CO₂ concentrations in the soil, which introduced a CO₂ emission from the alpine grassland soil to the atmosphere in our study area. Furthermore, the standard deviations of CO₂ concentrations in the atmosphere were all much lower than those in the soil. The ranges of CO₂ concentrations changed successively from 1138 to 3162 ppm in soil, which are less than the range in Chinese Loutu soil and the soil under alpine grassland in the Wudaoliang region of the Tibetan Plateau, and is less than the range in soil of farmland and grassland that has been reported.

The particle size distribution of soil has been described as the dominant independent variable determining CO₂ concentrations. It has been clearly demonstrated that CO₂ in soils is produced by microbe processes. But things are more complex than this, because the amount of CO₂ produced by either transfer processes or the activity and amount of microbe depends on the prevailing oxygen conditions; maximum yields of the gas occur only in a narrow range of low oxygen concentrations (Bange 2000). Some previous

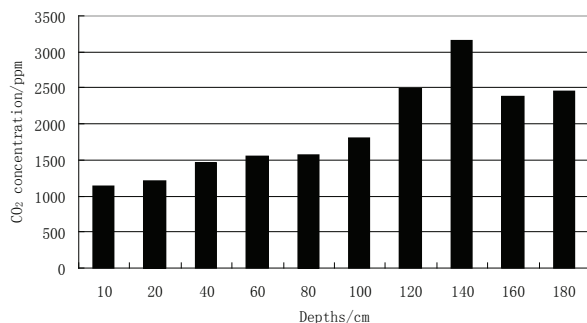


Figure 1. The average CO₂ concentration in soil depths.

studies suggested that higher CO₂ concentrations were caused by increased CO₂ production from aerobic conditions rather than by increased production from anaerobic conditions in soils (Dowrick 1999). At the same time, the soil aperture, which is produced by particle size heterogeneity, controls the amount of CO₂ in soil.

Temporal variations of CO₂ concentrations

Over the one-year measurement period, concentrations tended to be positively correlated with the active layer freezing-thawing processes, with highest CO₂ levels occurring in thawing conditions, and lowest values in frozen, soil temperature also exerted an important control.

Soil CO₂ concentrations varied significantly during the study period, both temporally and with depth. Seasonal variation of CO₂ concentrations in the soil during the sampling period were the greatest at superstratum depths (Fig. 2). This was quite different and provided an interesting contrast to some previous studies (Bouton & Beauchamp 1994). Their experiments were carried out in the areas with strong human impacts. Production of CO₂ at topsoil changed widely with human activities including fertilizer application, farming, and land-use changes (Hadietal. 2000, Pathak & Nedwell 2001). But our study site was located at a remote plateau with little human activities. CO₂ concentrations in the surface layers kept a more stable state than those in the deeper layers, whereas the diffusion of CO₂ in deeper layers was lacking efficient pathways. The seasonal variation of CO₂ concentrations in soil showed a very clear pattern, with the higher CO₂ concentration occurring at the thawing period (from summer mid-autumn to the mid-autumn) and the lower concentrations during the frozen period (spring and winter). During the experimental period, variations of

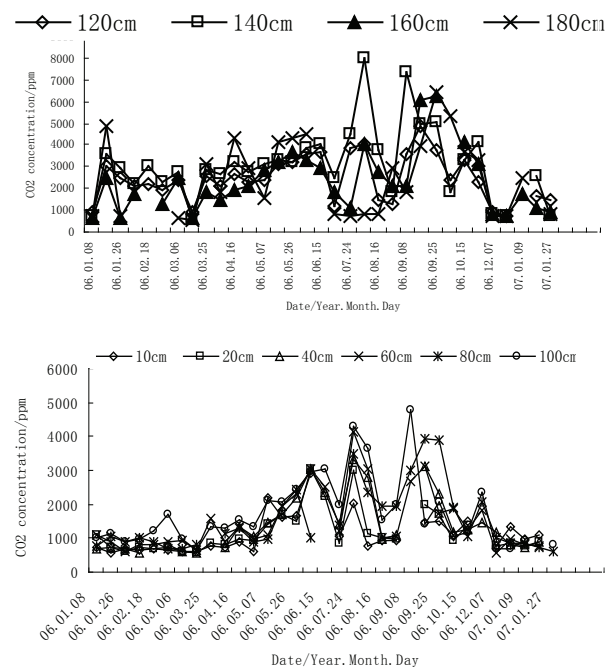


Figure 2. Variation of CO₂ concentrations at different depths in the soil.

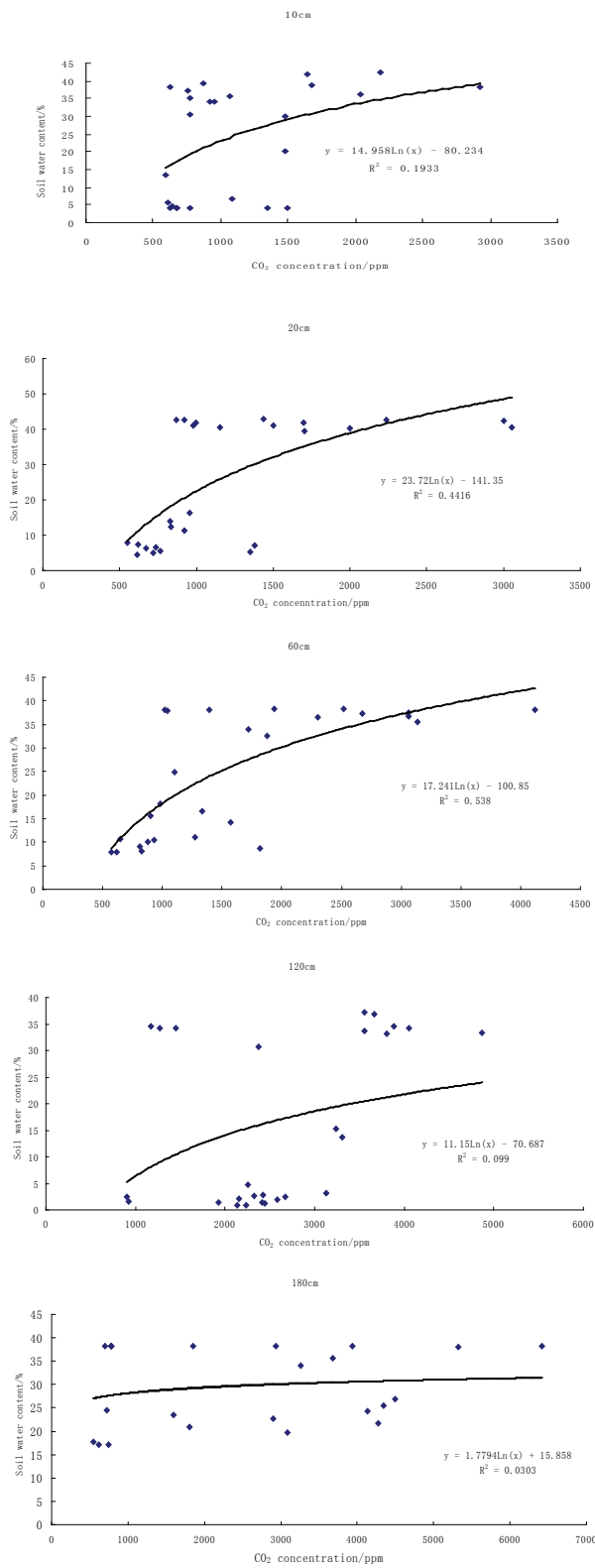


Figure 3. Correlations between CO₂ concentrations and soil water content at different depths in the soil.

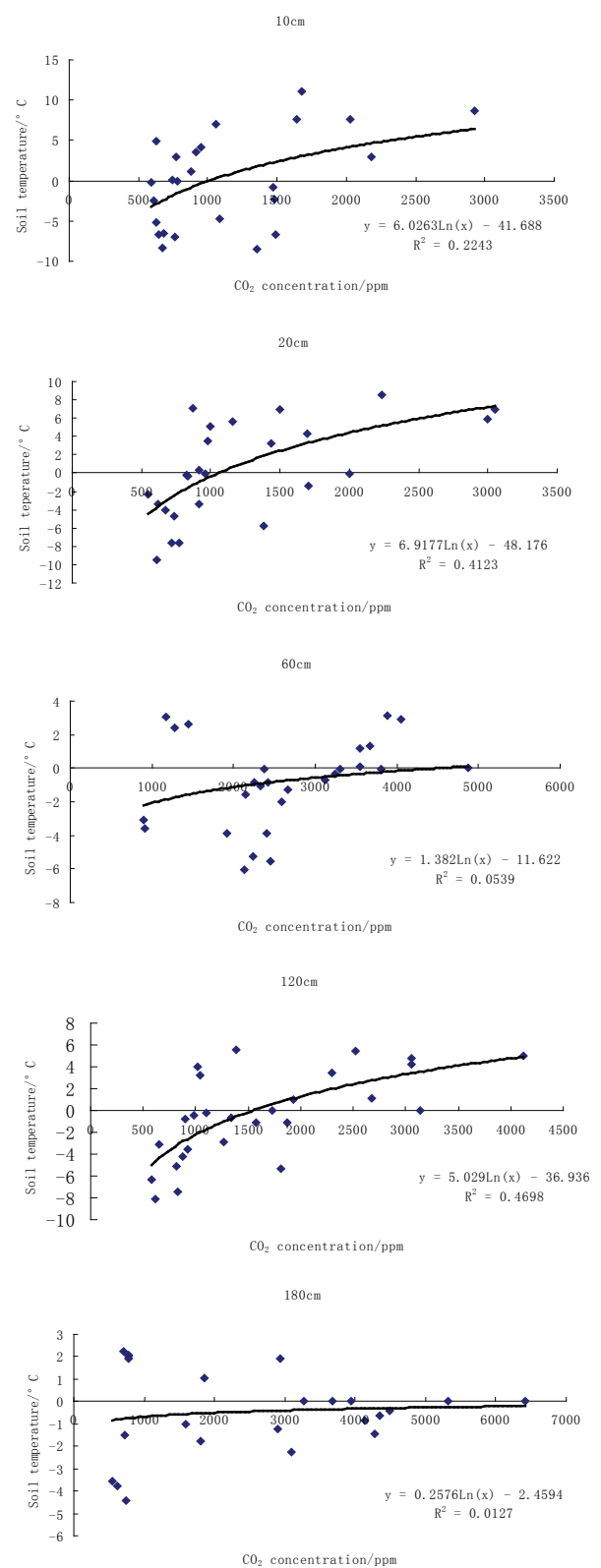


Figure 4. Correlations between CO₂ concentrations and soil temperature at different depths in the soil.

CO₂ concentrations in soil showed different ranges at all depths: the ranges of deeper layers (120–180 cm) larger than which in topsoils (10–100 cm). It may be caused by the variations of particle size distribution and unfrozen-water content in the bottom of active layers. The highest ranges occurred in the 140 cm depth layer, which was the pebble layer in the soil. It is well known that CO₂ concentrations in soil was the direct lie on the CO₂ producing processes and the storage conditions, so the CO₂ concentrations and its variability in the pebble layer were large.

Although mean CO₂ concentrations varied widely with depth in the soil, the seasonal variations of concentrations showed significant correlation between soil water contents in surface soil (10–60 cm). The most interesting result is the correlation between CO₂ concentrations at surface layers increased with depth, and the most significant correlation ($R^2=0.54$, $P<0.01$) (Fig. 3) was found at 60 cm depth layers where the greater mass of WDOC was measured. The WDOC, which have effect on CO₂ production and transportation procedures, were easily disturbed by the soil water contents at soil surface; on the contrary, the soil water contents showed more stable state at deeper layers relatively because of unfrozen-water content was near saturation.

Furthermore, the soil temperature has influences on CO₂ concentrations at the soil surface layers, but we can find influences 1.2 m deep in the soil. The situation in the surface layers in soil is relatively simpler than the soil deeper layers, so the CO₂ procedures here were only dominated by the temperature. That is the reason why the correlation between CO₂ concentration variations at surface layers was more significant than that at bottom layers. A significant correlation ($R^2= 0.47$, $P<0.01$) was also found between CO₂ concentrations and soil temperature at 1.2 m in depth during the study period (Fig. 4). This implied that the variation of CO₂ concentrations in the layer was the most direct driving force of soil particle size distribution (sandy loam). It is known that the terrestrial C cycles are driven by the activities of microorganisms. The frozen water in the form of an ice layer represents a diffusion barrier which reduces CO₂ supply to the microorganisms and partly prevents the release of the CO₂.

Conclusions

CO₂ concentrations increase gradually from 0 to 140 cm depth in soil, and feebly decrease from 140 cm to 180 cm. The ranges changed successively from 1138 to 3162 ppm. Seasonal variations in the 0 to 100 cm depth soil showed almost the same seasonal pattern, with the highest concentrations occurring in the active layer thawing period and lowest concentrations occurring in the active layer thawing period. The seasonal variations of CO₂ concentrations in the 100–180 cm layers did not show clear trends, but it can be explained by temperature and unfrozen-water content in soil. There was a significant correlation between CO₂ concentrations changing and active layer unfrozen-water content.

Acknowledgments

This study is financially supported by the projects of National Foundation for Sciences (40701033) and (40471025). The efforts of Mr. Zhixue Ma and Mr. Zesheng Gao are appreciated for their help in locating study sites. Ms. Yuemei Li and Ms. Donghui Wang are appreciated for their assistance in laboratory analyses. Dr. Guojun Sun is sincerely appreciated for his efforts in identification of plant species. This study was conducted at the Beiluhe Experimental Station and Germud Experimental Station of Chinese Academy of Sciences.

References

- Actuat, B. *Chem* 81: 42-48.
- Andersen, K., Kjar, T. & Revsbech, N.P. 2001. An oxygen insensitive microsensor for nitrous oxide. *Sensor*.
- Bange, G.W. 2000. It's not a gas. *Nature* 408: 301-302.
- Bouma, T.J. & Bryla, D.R. 2000. On the assessment of root and soil respiration for soils of different textures: interactions with soil moisture contents and soil CO₂ concentrations. *Plant Soil* 227: 215-221.
- Brooks, P.D., Williams, M.W. & Schmidt, S.K. 1998. Inorganic nitrogen and microbial biomass dynamics before and during spring snowmelt. *Biogeochemistry* 43: 1-15.
- Crowley, T.J. 2000. Causes of climate change over the past 1000 years. *Science* 298: 270-277.
- DeLuca, T.H. & Keeney, D.R. 1992. Effect of freeze-thaw events on mineralization of soil nitrogen. *Biology and Fertility of Soils* 14: 116-120.
- Fang, C. & Moncrieff, J.B. 2001. The dependence of soil CO₂ efflux on temperature. *Soil Biol. Biochem.* 33: 155-165.
- Grogan, P. & Jonasson, S. 2003. Controls on annual nitrogen cycling in the understorey of a sub-arctic birch forest. *Ecology* 84: 202–218.
- Hamada, Y. & Tanaka, 2001. Dynamics of carbon dioxide in soil profiles based on long-term field observation. *Hydrol. Process* 15: 1829-1845.
- Lipson, D.A. & Monson, R.K. 1998. Plant-microbe competition for soil amino acids in the alpine tundra: effects of freeze-thaw and dry-rewet events. *Oecologia* 113: 406-414.
- Lipson, D.A., Schmidt, S.K. & Monson, R.K., 1999. Links between microbial population dynamics and nitrogen availability in an alpine ecosystem. *Ecology* 80: 1623-1631.
- Maestre, F.T. & Cortina, J., 2003. Small-scale spatial variation in soil CO₂ efflux in a Mediterranean semiarid steppe. *Appl. Soil Ecol.* 23: 199-209.
- Muller, C., Martin, M., Stevens, R.J., Laughlin, R.J. & Kammann, C. 2002. Processes leading to N₂O emissions in grassland soil during freezing and thawing. *Soil Biology & Biochemistry* 34: 1325-1331.

- Pangle, R.E. & Seiler, J. 2002. Influence of seedling roots, environmental factors and soil characteristics on soil CO₂ efflux rates in a 2-year-old loblolly pine (*Pinus taeda* L.) plantation in the Virginia Piedmont. *Environ. Pollut.* 116: 85-96.
- Rayment, M.B. & Jarvis, P.G. 2000. Temporal and spatial variation of soil CO₂ efflux in a Canadian boreal forest. *Soil Biol. Biochem.* 32: 35-45.
- Skogland, T., Lomeland, S. & Goksoyr, J. 1988. Respiratory burst after freezing and thawing of soil: experiments with soil bacteria. *Soil Biology & Biochemistry* 20: 851-856.
- Stoyan, H., De-Polli, H., Bohm, S. et al. 2000. Spatial heterogeneity of soil respiration and related properties at the plant scale. *Plant Soil* 222: 203-214.
- Teepe, R., Brumme, R. & Beese, F. 2000. Nitrous oxide emissions from frozen soils under agricultural, fallow and forest land. *Soil Biol Biochem* 32:1807-1810.
- Zhao, L., Cheng, G.D., Li, S.X. et al. 2000. Freezing and thawing process of active layer in permafrost region near Wu Dao Liang on Qinghai-Tibetan Plateau. *Chinese Science Bulletin* 45(11): 1205-1211.

Cost Impact of Climate Change-Induced Permafrost Degradation on Building Foundations in Inuvik, Northwest Territories

F. Zhou, A. Zhang

*Canada Centre for Remote Sensing, Enhancing Resilience in a Changing Climate Program,
Natural Resources of Canada, Ottawa, Canada*

E. Hoeve

EBA Engineering Consultants Ltd., Yellowknife, Canada

Abstract

Permafrost degradation due to climate warming can impact buildings supported on permafrost. This paper describes a methodology used to evaluate impacts and costs for adaptation, considering soil profile, geothermal response, foundation type, mode of deformation, and building age, type, and service life to determine if and when foundation adaptation would be warranted, and at what likely cost. As Inuvik is predicted to experience the largest impact in the Northwest Territories, with 40 to 75% of existing buildings potentially impacted during their remaining service life, this case is described. The estimated cost without adaptation ranges from \$52M, under a moderate climate warming scenario, to \$121M, under an aggressive climate warming scenario. "Informed adaptation" (where the costs of remedial measures are considered in the context of the remaining service life and value of the building) was the most economical approach, reducing the cost impacts to about two-thirds of these costs.

Keywords: climate change; cost assessment; foundations; permafrost degradation.

Introduction

The stability of building foundations in many northern communities relies on the strength of the underlying permafrost. The Intergovernmental Panel on Climate Change (IPCC) projected that by 2100, air temperature will likely increase globally by 2.0°C to 4.5°C, based on a range of greenhouse gas emission scenarios (Solomon et al. 2007). Temperature increases in the north are predicted to be higher than the global average. Air temperature increases can be expected to bring about permafrost degradation, thereby impacting foundation systems in northern communities.

The impact of climate warming on foundation systems was recognized as a community issue in the Canadian north, and a lack of specific information was identified as a concern (Eamer et al. 2003). Studies of the climate change impacts on community housing, especially quantitative assessments, have been very limited and adaptation cost estimates are rare.

In Canada, the only previous studies (Robinson et al. 2001, Couture et al. 2002) dealt with the compilation and documentation of the infrastructure, geotechnical, and borehole data for two of the 32 communities in the Northwest Territories (Norman Wells, Tuktoyaktuk). While these studies identified permafrost degradation to have potential negative impacts on the foundation systems of these communities, no follow-up investigations or analyses were undertaken.

Khrustalev (2000, 2001) indicated that temperature increases could result in a significant decrease in the service life and potential failure of foundations. Nelson et al. (2001, 2002) mapped the hazard potential associated with thawing permafrost under global warming. The maps were created using a dimensionless thaw-settlement index, computed using the projected percentage change in active-layer thickness and

the ground ice content. The resulting maps depicted areas of "low," "moderate," and "high" hazard potential. They then superimposed the locations of existing infrastructure on the hazard map to obtain a general assessment of the susceptibility of engineered works to thaw-induced damage. However, the spatial resolution of this mapping was rather coarse (0.5° by 0.5°), thus producing only a macro-view, which could not be used for foundation impact assessment at the community level.

This paper summarizes an approach to obtain quantitative estimates of the potential physical and cost impacts of climate change, and the associated timeframe, on existing building foundations in the Northwest Territories, using Inuvik as an example. This represents a portion of a broader project by Natural Resources Canada, which developed similar estimates for five communities. The overall objective of the study summarized in this paper was to take science and engineering-based information and put it into a form that could be considered at the planning and policy level to assist in determining the resources to be expended towards mitigation.

Methodology

A multiple accounts analysis (MAA) of the 32 communities in the Northwest Territories was used to rank the sensitivity of building foundation infrastructure in these communities to climate change. MAA is well suited to situations where a variety of factors affect an outcome, and it provides an overall framework in which such factors, described quantitatively or qualitatively, may be taken into account. MAA has been previously used fully or in part to identify most acceptable options in various development projects (e.g., Robertson & Shaw 2004).

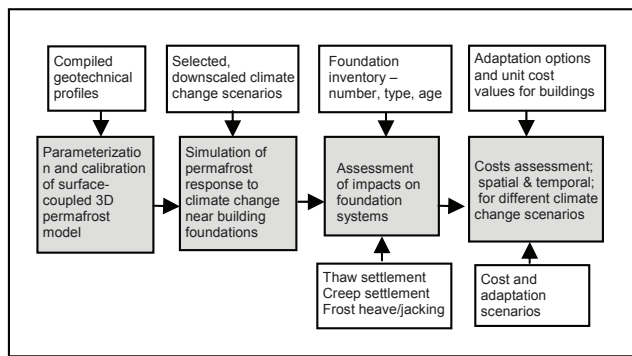


Figure 1. Methodology for foundation impact assessment.

In this case, thermal, physical, and infrastructure sensitivities were considered. The Inuvik region in general, and the community of Inuvik in particular, were determined to have the highest overall sensitivities (EBA 2005, Hoeve 2005).

Based on the MAA assessment, five representative communities were selected among the 32 for a more detailed analysis: Inuvik, Tuktoyaktuk, and Paulatuk in the continuous permafrost zone and Norman Wells and Tulita in the extensive, discontinuous permafrost zone. The selection was designed to represent a range of sensitivities, geographic regions, and population sizes. Only the results from Inuvik are summarized in this paper.

Figure 1 illustrates the methodological framework of the overall study leading to the cost assessment for the selected case communities.

Geotechnical profiles

Generalized geotechnical profiles were compiled to represent areas within which the subsurface was assumed to have geotechnical properties, such as soil texture, hydraulic and thermal properties, water/ice content, and the thickness of each layer, that are horizontally uniform or vary within only a narrow range. The impacts of permafrost degradation were assessed for each sub-area, considering the temporal and spatial distribution of foundation systems.

Climate change scenarios selection and downscaling

From among the many scenarios produced with the aid of General Circulation Models (GCMs) (IPCC 2001), three were chosen (CGCM 1 GHG + aerosol, HadCM3 SRES A2 and B2) that roughly represent an upper, a middle, and a lower level of the impact of greenhouse gases emissions on future air temperature trends. Thus, with these scenarios, the simulated geothermal dynamics should accordingly have an upper and lower bound as well as a middle range.

In this study, the selected GCMs were downscaled by using the Statistical Downscaling Model (SDSM) tool (Wilby & Dawson 2004). Six climatic variables were downscaled—air temperature, precipitation, solar shortwave and longwave radiation, wind speed, and water vapour pressure—for input into the model.

Surface-coupled three-dimensional geothermal model

A physical, process-based, surface-coupled, three-dimensional finite-element geothermal model (SC3D) was developed. Driven by climate variables, and constrained by ground surface condition, geothermal gradient, and geotechnical profile characteristics, the model transforms the changes in climate variables into ground surface temperature dynamics by computing surface energy and water balance including snow. The model mimics the three-dimensional flux of heat and water that occurs around and underneath the building. The model also represents the building's effects on these processes through dynamically differentiating the solar radiation, precipitation, and snow cover received by the ground surface at different locations underneath and around the building, and it reflects the modification of the natural geothermal regime by the building. Zhou et al. (2006) provides a detailed description of the model, the required input data, and results of its validation.

Modeling of permafrost changes

The modeling space was specified as a cube, 22 m by 18 m in plan and 100 m deep. The “building” was specified as a typical residential house, with an enclosed area of 14 m by 10 m, and a height of 5 m with a 0.5 m high air space under the floor.

The finite-element mesh was uniform in both X and Y directions, on a 2 m grid. To capture the details of heat and water transfer near the ground surface and to achieve computational efficiency, the vertical cell size was 10 cm for upper layers, and it increased downward to 4 m at the bottom of the modeling space.

Following the protocol recommended in IPCC-TGIA (1999), the period of 1961–1990, with actual data, served as a benchmark, and the projected period 2010–2069 was used to assess the changes due to climate warming with respect to the benchmark. The IPCC recommended three assessment periods: 2010–2039, 2040–2069, and 2070–2099. The period of 2010–2069, representing two of these recommended periods, was chosen because it covers the expected service life of all the existing buildings (constructed before 2005).

The simulation employed a daily time step. From recorded vertical temperature profiles, two indices of permafrost condition were computed: mean annual ground temperature and active layer thickness.

Impact of permafrost degradation on building foundations

The rate of permafrost degradation determines the degree of soil deformation in response to climate change. In this study, three types of terrain instability due to permafrost degradation were taken into account in the estimation of the impacts: thaw settlement and creep settlement, and frost-jacking. The rate of permafrost degradation was quantified through increasing mean annual ground temperature and deepening active layer thickness. The former was considered mainly in creep settlement analysis, and the latter is used for the calculation of thaw settlement and frost-jacking.

For pile foundations, the assessment took into account all

the three types of terrain instability. Only thaw and creep settlements were involved in estimating the impact on shallow foundations, which would include surface footings or buried spread footings.

Differential settlements were obtained as a result of the varying geothermal response below various portions of the building. The ground below the centre of the building was coldest and the ground at the south corners/side was the warmest.

A critical part of the physical impact assessment concerns the thresholds at which damage to building systems is considered to occur. The maximum allowable total settlement of a building was set at 30 mm, and allowable differential settlement between adjacent foundation supports at 10 mm over a 3 m span during the service life of the building (CFEM 1992). Thus, if settlement of a building is 30 mm or higher or if differential creep settlement is more than 10 mm over the horizontal distance of 3 m, the building was regarded to be at risk.

For pile foundations, the frost-jacking and resisting forces were evaluated. If at any location under the building, the frost-jacking force exceeded the resisting force (sum of pile resistance and dead load), the building was considered at risk of frost-jacking.

Cost assessment

Typical building sizes, foundation configurations and unit costs for the most appropriate rehabilitation technique applicable to each foundation type were determined (EBA 2006, Hoeve et al. 2006).

Foundation inventories were prepared to characterize individual buildings within each geotechnical profile area by age (grouped at 5-year intervals), replacement cost and present value. A depreciation factor of 5% per year was used to determine present value. The age distribution was determined by examination of historical air photos. It should be noted that the compilation of inventories was office-based, incorporating assumptions based on experience and judgment, and not including site visits, except as documented by Robinson et al. (2001) and Couture et al. (2002) for Tuktoyaktuk and Norman Wells.

Commercial/institutional buildings were considered to have a longer service life (65 years) than residential buildings (50 years). If the age of a building reached these thresholds, the building was considered to retire “maturely.” If a younger building was assessed at risk due to permafrost degradation, it would either be forced to retire prematurely or to undergo an adaptation.

The cost study considered three responses (Fig. 2):

Response 1 – mature retirement: a building will reach the end of its service life without detrimental impact induced by climate warming. In this scenario, no action will be needed and no cost will be incurred. As no cost would occur in Response 1, it is not considered further.

Response 2 – no action: a building is assessed to be at risk, but no action will be taken. The building will be forced to retire early and cost of the premature retirement would

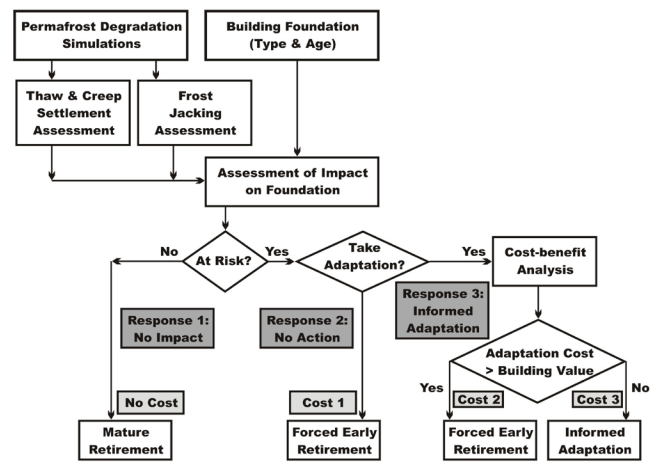


Figure 2. Procedures for impact and cost assessment.

be incurred, equal to the residual value of the building. Therefore, the cost will be the total asset value of all impacted buildings at the age when the buildings would be assessed at risk.

Response 3 – informed-adaptation: when a building is assessed to be at risk, a cost-benefit analysis is conducted to determine what actions should be taken and when. The cost-benefit analysis thus compares the adaptation cost and asset value of the building under consideration when it is assessed at risk.

If a building at risk is approaching the end of its service life, the cost of the impact (forced premature retirement) would be relatively low. Conversely, if a building is at risk in its early service life, the cost of the impact would be relatively high and adaptation may be warranted. The cost-benefit analysis thus aims to minimize total costs of the climate change impacts, i.e., the sum of Cost 2 and Cost 3 is less than Cost 1.

The foregoing procedure was applied to each category of building/foundation type in each geotechnical profile, over each time increment and for each case community. Details are presented in Zhou et al. (2007).

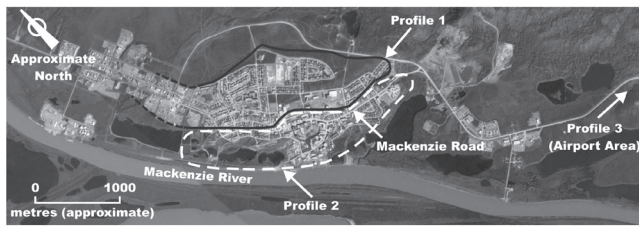
Assessment Results for Inuvik

Inuvik is located on the East Channel of Mackenzie Delta, approximately 100 km from the Arctic Ocean, at latitude 68°19'N and longitude 133°29'W. In 2003, it had a population of 3688.

Typical geotechnical profiles

Geotechnical data from 17 evaluations was reviewed to develop typical subsurface soil profiles in the Inuvik area. The community was divided into two sub-areas of generally similar subsurface stratigraphy. The extent of Profiles 1 and 2 within the community are shown on Figure 3. Profile 3 was developed for the area located west of town along the Dempster Highway out to and including the Inuvik airport.

The soil profiles and associated thermal properties were described in EBA (2004) and are summarized in Figure 4.



NOTE: Background image provided courtesy of Google Earth and is for visual presentation purposes only.

Figure 3. Location of geotechnical profiles for Inuvik.

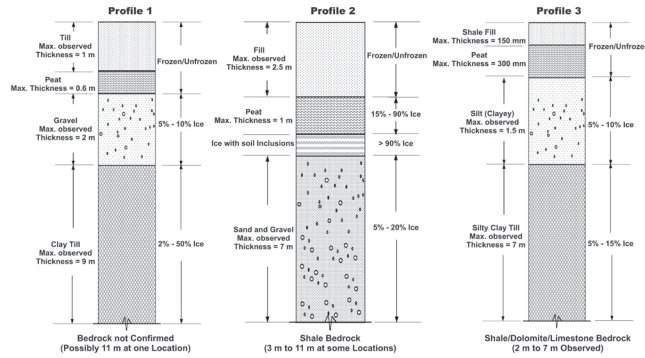


Figure 4. Geotechnical profiles for Inuvik.

Building age distribution

The temporal distribution of buildings over about 5-year increments were compiled by examining air photos. The majority of the buildings are located in the Profile 1 and Profile 2 areas. The area of Profile 1 has about 600 residential and 60 commercial buildings and encompasses the newer development areas. Profile 2 is in a mature area of the community and the number of buildings has remained stable since the late 1970s, with about 400 residential and 40 commercial/institutional buildings. The area of soil Profile 3 has exhibited growth, but only has about 30 commercial/institutional buildings and negligible residential buildings.

Ground temperature trends under climate change scenarios

The model was calibrated with ground temperature data from a power station in Inuvik, a site within the Profile 2 area. Cables were installed in 1995, extending under the building, at the perimeter of the building and away from the building (EBA 1996). Regular data were available for four years, with sporadic data available for another six years. The model was initialized and run from 1961 through the period where measurements were available.

Permafrost simulations were conducted for the baseline period (1961–1990) and two projected periods (2010–2039, 2040–2069). The simulations through the baseline period were driven by actual climate data, and the simulations during the projected periods were driven by the downscaled GCM data.

The intervening period, 1991–2009, was not modeled, because it was not called for in the IPCC-TGIA (1999) protocol and because the input data, either actual or projected, were not complete.

Figure 5 shows the mean annual ground temperature response (average for depths 1 m to 10 m) at three locations,

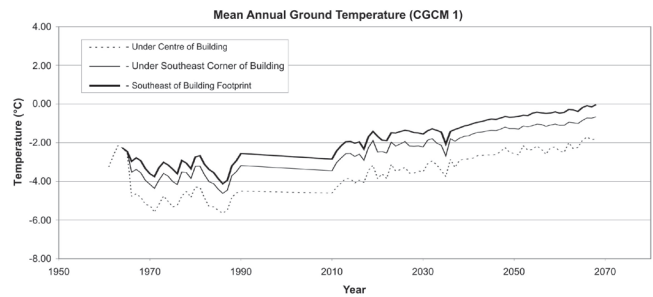


Figure 5. Mean annual ground temperatures for Inuvik, Profile 1.

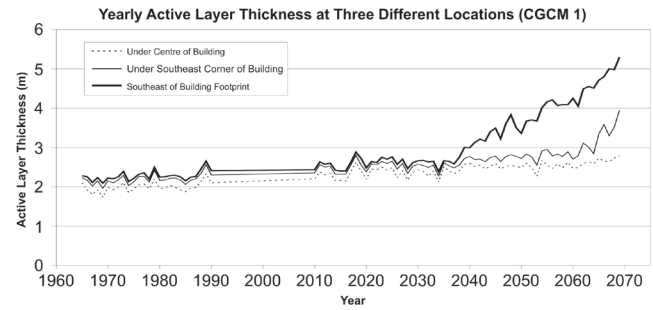


Figure 6. Active layer thickness response for Inuvik, Profile 1.

derived from the CGCM 1 scenario, which is the most severe. The locations for which results are plotted range from the maximum mean annual ground temperature at a point outside the building footprint to the minimum mean annual ground temperature under the centre of the building. The intermediate point represents the warmest under the building, with the southeast and southwest corners being approximately the same.

The simulation began in 1961, and the building effect was introduced in 1965. The building caused an immediate and substantial change in the temperature regime, and this effect was strongest underneath in the centre of the building. Figure 5 also suggests that the temperature differential did not increase over time. Once the thermal regime stabilized, the building exerted an approximately constant additional effect on the near-surface temperature profile.

Figure 6 shows the change in active layer thickness derived from the CGCM 1 scenario. It indicates that the projected active layer thickness did not change substantially between 2010 and 2040 for all the locations. However, the active layer thickness became deeper at a faster rate away from the building after about 2040, at the south corner around 2065, and there was little change under the centre of the building during the modeling period.

The results in Figure 6 seem to suggest that the shading effect of a building, on solar radiation and snow cover, has a more dominant effect on active layer thickness than increasing air temperature.

The analyses indicate that, over the long term, ground temperature changes more or less in step with air temperature but changes in the active layer lag behind changes in ground temperature. This is attributable to the latent heat that must be overcome for an active layer response in ice-rich soil.

Table 1. Summary of impacted buildings in Inuvik.

	Profile 1	Profile 2	Profile 3	Inuvik Overall				
Total Buildings	659	448	34	1141				
Scenario	Buildings Impacted						#	%
	#	%	#	%	#	%		
CGCM1	393	60	441	98	16	47	850	74
HadCM3 A2	5	1	441	98	5	14	451	40
HadCM3 B2	5	1	441	98	14	42	460	40

Table 2. Cost impacts in Inuvik for three climate scenarios.

Climate Change Scenario	Response 3 (2005 C\$M)					Response 2 (2005 C\$M) (Cost 1)
	Premature Retirement (Cost 2)		Adaptation (Cost 3)		Total	
	Res.	Com.	Res.	Com.		
	CGCM1	15.3	5.4	4.0	55.3	80.0
HadCM3 A2	9.0	4.1	1.3	21.5	36.0	52.3
HadCM3 B2	9.0	4.9	1.3	24.5	40.0	56.3

Impacts on building foundations

Table 1 summarizes the number of buildings impacted for the three climate change scenarios and within the three geotechnical profiles. Among the 1141 buildings in Inuvik (as of 2005), 659 buildings are located in Profile 1, 448 in Profile 2, and 34 in Profile 3. The buildings in Profile 2 are most severely affected. This is because the baseline (1961–1990) active layer in Profile 2 is deeper, at about 3 m, compared to about 2.5 m and 1.5 m for Profiles 1 and 3.

The fraction of buildings in Profiles 1 and 3 that would be affected ranged from around 15% (Profile 3 with HadCM3 A2) to 60% (Profile 1 with CGCM1 GHG+aerosol). Buildings in Profile 3 would be the least impacted due to a shallower active layer and lower mean annual ground temperature. These results reflect the importance of the geotechnical conditions on the susceptibility of building foundations, the impact being modulated by the climate change scenario employed.

The differences between climate change scenarios (CGCM1 GHG+aerosol and HadCM3 A2 or HadCM3 B2) are rather strong: about 74% of all buildings would be impacted under CGCM1 scenario, compared to approximately 40% for the two HadCM3 scenarios. This difference represents about 400 buildings, mostly located in Profile 1.

Cost impacts

Table 2 summarizes the distribution of costs to community buildings for the three climate scenarios. Results of Responses 2 and 3 are shown. Based on the Response 3 (informed adaptation, Fig. 2), cost-benefit analysis was used to determine whether or not adaptation measures were warranted for each impacted building. The results show that CGCM1 scenario would bring about the highest cost

of approximately C\$80M, and HadCM3 A2 and HadCM3 B2 would result in the cost about C\$36M and C\$40M, respectively. The costs were also broken down to the costs due to premature retirement (Cost 2) or costs for adaptation (Cost 3). The results show that, under CGCM1 scenario, about 74% of the total cost would be for adaptation. Under climate change scenarios HadCM3 A2 and HadCM3 B2, about 64% of the total cost would be due to adaptation.

Under all climate change scenarios, the higher adaptation costs are associated with commercial/institutional buildings. The highest premature retirement costs are associated with residential buildings. This is partially attributable to the longer service life of commercial/institutional buildings, but is also a result of the magnitude of adaptation costs relative to residential building value. Commercial/institutional buildings are more likely to warrant adaptation than residential buildings.

The table also lists the costs of the no action scenario in which impacted buildings are assumed to retire prematurely with no attempt at adaptation (Cost 1, Response 2). Although the total number of impacted buildings in Responses 2 and 3 are the same, the total cost of informed adaptation (\$80M) is only about two-thirds of the no-adaptation scenario (\$121M) under CGCM 1 scenario. This relationship held true for the HadCM3 A2 and B2 scenarios.

To help put these costs into perspective, the total replacement cost of the building infrastructure in Inuvik was calculated to be about \$1.2 billion and the present value of the buildings was calculated to be about \$250 million, in 2005 dollars.

The analysis shows that “informed adaptation” is the preferable management response to dealing with impacts of climate change on building foundations in Inuvik.

Acknowledgments

The authors are grateful to Josef Cihlar for his advice on the study and for his guidance. Thanks also go to Yu Zhang and Fred Wright for advice on permafrost modeling and Richard Fernandes’ research group for providing climate data; the NWT Housing Corporation, the Government of the NWT, and Departments of Public Works and Services and Municipal and Community Affairs who contributed community infrastructure data. Funding was by the Climate Change Impact and Adaptation Directorate with support by the Earth Sciences Sector, Natural Resources Canada.

References

Canadian Foundation Engineering Manual. 1992. Third Edition. Canadian Geotechnical Society, Technical Committee on Foundations, 512 pp.

Couture R., Robinson, S.D., Burgess, M.M. & Solomon, S. 2002. *Climate change, permafrost, and community infrastructure: A compilation of background material form a pilot study of Tuktoyaktuk, Northwest Territories*. Geological Survey of Canada, Open File 3867, May 2002.

- Eamer C., Johnson, P.G. & Love, C. 2003. C-CIARN North online workshop on Climate Change and Infrastructure: summary report. *Weathering Change Vol. 1, No. 4*, 2003.
- EBA Engineering Consultants Ltd. 1996. *Geotechnical Investigation, Volcano Boiler Foundation Improvements*. Report submitted to the Northwest Territories Power Corporation, January 1996.
- EBA Engineering Consultants Ltd. 2004. *Geotechnical Characterization for Inuvik, NWT*. Report submitted to Natural Resources Canada, November 2004.
- EBA Engineering Consultants Ltd. 2005. *Assessment of foundation sensitivity to climate change in the Northwest Territories*. Report submitted to Natural Resources Canada, January 2005.
- EBA Engineering Consultants Ltd. 2006. *Estimated Costs for Foundation Adaptation in the Northwest Territories—Draft*. Report submitted to Natural Resources Canada, January 2006.
- Hoeve, E., Zhou, F. & Zhang, A. 2005. *Assessment of Building Foundation Sensitivity to Climate Change in the Northwest Territories*. Presentation at Adapting to Climate Change in Canada 2005, Montreal, Quebec. PowerPoint summary available at: http://adaptation2005.ca/abstracts/hoeve_e.html
- Hoeve E., Zhou, F. & Zhang, A. 2006. Potential Cost Impacts for Adaptation of Building Foundation Infrastructure in the Northwest Territories. *Engineering Institute of Canada—Climate Change Technology Conference, Ottawa, Canada, May 2006*.
- Intergovernmental Panel on Climate Change (IPCC). 2001. *Climate change 2001: Synthesis Report*. Geneva, Switzerland: Intergovernmental Panel on Climate Change, 84 pp.
- IPCC-TGCI. 1999. *Guidelines on the Use of Scenario data for Climate Impact and Adaptation Assessment. Version 1*. Prepared by T.R. Carter, M. Hulme & M. Lal. Intergovernmental Panel on Climate Change, Task Group on Scenarios for Climate Impact Assessment, 69 pp.
- Khrustalev, L.N. 2000. Allowance for climate change in designing foundations on permafrost grounds. *International Workshop on Permafrost Engineering, Longyearbyen, Norway, 18–21 June, 2000*. Tapir Publishers, 25–36.
- Khrustalev, L.N. 2001. Problems of permafrost engineering as related to global climate warming. In: R. Paepe & V.P. Melnikov (eds.), *NATO Advanced Workshop on Permafrost Response on Economic Development, Environmental Security and Natural Resources, Novosibirsk, Russia, 12–16 November 1998*. Kluwer Academic Publishers, 407–423.
- National Research Council (NRC). 1962. *Engineering site information for Inuvik, NWT*. Technical Paper No. 135. Division of Building Research.
- Nelson, F.E., Anisimov, O.A. & Shiklomanov, N.I. 2001. Subsidence risk from thawing permafrost. *Nature* 410: 889-890.
- Nelson, F.E., Anisimov, O.A. & Shiklomanov, N. I. 2002. Climate change and hazard zonation in the circum-arctic permafrost regions. *Natural Hazards* 26(3): 203-225.
- Robertson, A. & Shaw, S. 2004. Use of multiple accounts analysis process for sustainability optimization. *Proceedings of the SME Annual Meeting, February 23-25, Denver, CO: 7pp*.
- Robinson, S.D., Couture, R. & Burgess, M.M. 2001. *Climate change, permafrost, and community infrastructure: A compilation of background material from a pilot study of Norman Wells, Northwest Territories*. Geological Survey of Canada, Open File 3913. January 2001.
- Solomon, S., Qin, D., Manning, M., Alley, R.B., Berntsen, T., Bindoff, N.L., Chen, Z., Chidthaisong, A., Gregory, J.M., Hegerl, G.C., Heimann, M., Hewitson, B., Hoskins, B.J., Joos, F., Jouzel, J., Kattsov, V., Lohmann, U., Matsuno, T., Molina, M., Nicholls, N., Overpeck, J., Raga, G., Ramaswamy, V., Ren, J., Rusticucci, M., Somerville, R., Stocker, T.F., Whetton, P., Wood, R.A. & Wratt, D. 2007. 2007: Technical Summary. In: *Climate Change 2007: The Physical Science Basis. Contribution of Working Group I to the Fourth Assessment Report of the Intergovernmental Panel on Climate Change*. Cambridge, United Kingdom, and New York, NY, USA: Cambridge University Press.
- Wilby, R.L. & Dawson, C.W. 2004. *Using SDSM version 3.1 - A Decision Support Tool for the Assessment of Regional Climate Change Impacts*. User Manual.
- Zhou, F., Zhang, A., & Li, R. 2006. *Surface-coupled 3-D permafrost model for impact assessment on building foundations in Northern Canada due to permafrost degradation*. Presented at the first Asian Conference on Permafrost, Lanzhou, China, 2006.
- Zhou, F., Zhang, A., Li, R., Hoeve, E. & Majid, A. 2007. *Potential climate change-induced permafrost degradation and building foundations: An assessment of impacts and costs for five communities in the Northwest Territories*. Report (V.3) distributed to stakeholders for feedback, September 2007.

Iron-Oxides and Pedogenesis of Modern Gelisols and Paleosols of the Southern Lena Delta, Siberia, Russia

Sebastian Zubrzycki

University of Hamburg, Hamburg, Germany

Sebastian Wetterich

Alfred Wegener Institute for Polar and Marine Research, Potsdam, Germany

Lutz Schirrmeister

Alfred Wegener Institute for Polar and Marine Research, Potsdam, Germany

Anastasia Germogenova

Moscow State University, Moscow, Russia

Eva-Maria Pfeiffer

University of Hamburg, Hamburg, Germany

Abstract

Five exposures on two arctic islands in southern Lena Delta, Russia, were investigated in order to determine the development of iron-oxides under different pedogenic conditions in permafrost-affected paleosols and to prove their application for describing environmental conditions during pedogenesis of buried soils and the predominant paleoclimate during their development. The samples were collected from the active layer on Samoylov Island as well as from Late Pleistocene and Holocene paleosols on Kurungnakh Island. The amounts of iron extractable by dithionite (Fe_d) and by oxalate (Fe_o) were determined for all samples. The extracts were conducted to determine the forming conditions of paleosols and their iron-oxide contents and to compare them with modern permafrost-affected soils. The iron-oxide amounts characterize well the sedimentation conditions and the paleoclimate of the investigated paleosols. As contributing factors, the organic matter content and the inundation were identified. Additionally, in modern soils, translocation processes within the polygon affect the conditions of the different Fe-fractions.

Keywords: environmental and climate change; Gelisols; iron-oxides; Lena Delta; paleosols; Siberia.

Introduction

Permafrost-affected soils (Gelisols or Cryosols) cover nearly one-fourth of the terrestrial surface in the northern hemisphere. Studies have been conducted for more than 100 years (Goryachkin et al. 2004). The first studies were exploratory in nature in order to find land for agriculture. Pedoscientists study permafrost-affected soils to learn more of their active physico-chemical processes (Tarnocai 2004). Spatial distribution, genesis and properties of different Cryosols are presented in details by Kimble 2004. However, this does not imply that these soils have been sufficiently investigated.

Pedogenesis in permafrost regions takes place in the active layer above the permafrost table only during the short summer period. On one hand, the cold conditions hinder strong pedogenesis; on the other hand, permafrost preserves records of former soil conditions.

Spatial distribution and genesis of soils in the southern Lena Delta provide a basis for evaluation of the impact of environmental and climate change on permafrost landscapes.

The objective of this study was to prove if crystallized iron-oxides are a useful criterion for estimating environmental conditions of pedogenesis of buried soils and paleoclimate during their development.

Morphological and analytical data are taken into account

to understand both properties and genesis of buried soils in ice rich permafrost sediments (so called ice complex) and modern soils in the southern Lena Delta.

Identifying different forms of iron-oxides helps to understand the environment in which active pedogenesis took place. In general paleosols are often characterized by their iron-oxides fractions, and this data facilitates an estimate of the relative age of a given soil-sequence (Arduino et al. 1984, Arduino et al. 1986, Bäumler 2001).

During expeditions to the Lena Delta in 2002 and 2007 investigation of several soil profiles were carried out to determine the development of iron-oxides under different pedogenic conditions in permafrost-affected paleosols and to prove their application for description of environmental conditions of pedogenesis of buried soils and predominant paleoclimate during their development. For understanding the processes of modern pedogenesis, from the active layer of young soils were investigated.

Investigation Area

The study sites are located on Samoylov Island (72°22'N, 126°28'E) and Kurungnakh Island (72°20'N, 126°18'E). The islands are situated at one of the main Lena River channels, the Olenyokskaya Channel in the southern part of Lena Delta (Fig. 1). The Lena Delta is located in northeastern Siberia, where the Lena River cuts through the Verkhoyansk

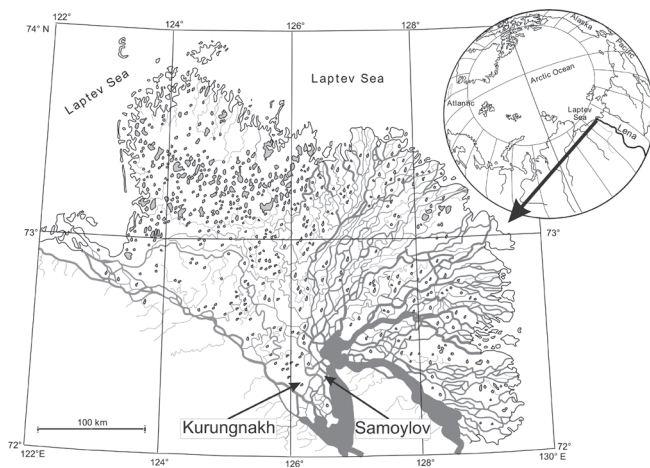


Figure 1. Map of the Lena Delta with study sites.

Mountains Ridge and discharges into the Laptev Sea, which is part of the Arctic Ocean.

Samoylov Island can be divided into two major geomorphological units (Akhmadeeva et al. 1999): the relative young floodplain (0 to 4 m a.r.l. [about river level]) in the western part which is flooded annually in spring, and the higher-elevated (1 to 12 m a.r.l.) river terrace of Late Holocene age, the “first” terrace in the eastern part (Pavlova & Dorozhkina 1999). The first terrace is flooded only during extreme high-water events (Kutzbach 2005).

Kurungnakh Island belongs to the third river terrace complex (up to 55 m a.r.l.) of the Lena Delta. The third terrace is the oldest terrace in the delta. It was formed in Middle and Late Pleistocene (Schwamborn et al. 2002, Kuzmina et al. 2003). This terrace forms autonomous islands along the Olenyokskaya and Bykovskaya Channels. The Kurungnakh Island is located at the southeastern part of Olenyokskaya Channel (Schwamborn et al. 2002).

The climate in the Lena Delta is high-arctic with continental influence and characterized by low temperatures and low precipitation. The mean annual air temperature, measured by the meteorological station in Tiksi located about 110 km (68 stat. mi.) to the southeast directly at the coast of the Laptev Sea, was -13.6°C (7.5°F) during the 30-year period 1961–1990; the mean annual precipitation in the same period was 319 mm. The average temperatures of the warmest month August and the coldest month January were 7.1°C (44.8°F) and -32.4°C (-26.3°F), respectively (ROSHYDROMET 2007), demonstrating the extreme climatic contrasts between polar day and polar night for continental Polar Regions.

Material and Methods

The main soil unit of the first terrace above the floodplains of Samoylov Island is covered mainly by polygonal wet sedge tundra with soil-plant-complexes which consist of ice rich ground, wet and cryoturbated Gelisols (Glacic Aquiturbels) and very wet organic rich Gelisols (Typic Historthels). Typic Historthels are Gelisols that have more than 40%, by volume,

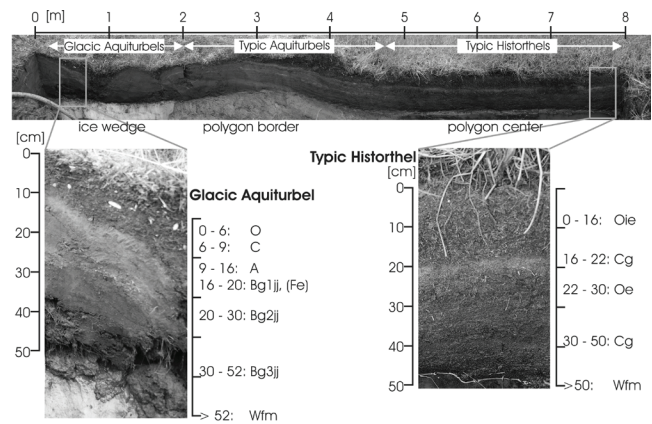


Figure 2. Soil-cross-section of a half of a low-centered polygon on Samoylov Island with the soil-complex of Glacic Aquiturbel and Typic Historthel, according to U.S. Soil Taxonomy.

organic materials from the surface to a depth of 50 cm (Soil Survey Staff 2006). According the WRB-Classification the Gelisols were classified as Glacic Turbic Cryosols and Haplic Histic Cryosols (Food and Agriculture Organisation, 2006). Typic Historthels were formed in depressed centers of low-centered ice-wedge polygons characterized by high water saturation to the soil surface and high organic matter accumulation due to anaerobic conditions.

Glacic Aquiturbels formed at the elevated borders of the polygons are characterized by prolonged inundation but with less organic matter accumulation and pronounced cryoturbation. Thus Glacic Aquiturbels are Gelisols that have one or more horizons showing cryoturbation in the form of irregular, broken or distorted horizon boundaries, involutions, and accumulation of organic matter on top of the permafrost and ice wedges. They have within 50 cm of the mineral soil surface redox depletions and also aquic conditions during normal years and a glacic layer with its upper boundary within 100 cm of the mineral soil surface (Soil Survey Staff 2006).

Beside these wet and organic rich soils various sandy soil complexes such as Psammorthels and Psammoturbels are typical along the eroded cliffs. They are drier than the Aquiturbels and Historthels (Pfeiffer et al. 1999, Pfeiffer et al. 2000, Pfeiffer et al. 2002). Psammorthels and Psammoturbels are soils that have less than 35%, by volume, rock fragments and a texture of loamy fine sand or coarser in all layers within the particle-size control section (Soil Survey Staff 2006). In the erosional cliff area thermal erosion results in formation of high-centred polygons which are often covered with eolian sands.

Glacic Aquiturbels and Aquic Histurbels are common on Kurungnakh Island as on Samoylov Island. These modern soils are compared with paleosols such as Histels of different degree of decomposition, iron-rich Aquorthels and Aquiturbels of exposures on both islands.

For investigations of paleosols three exposures of 2.1, 2, and 1.2 m thickness were selected on the third terrace of Lena Delta on Kurungnakh Island. The samples were taken during the expedition “LENA 2002” (Kuzmina et al. 2003).

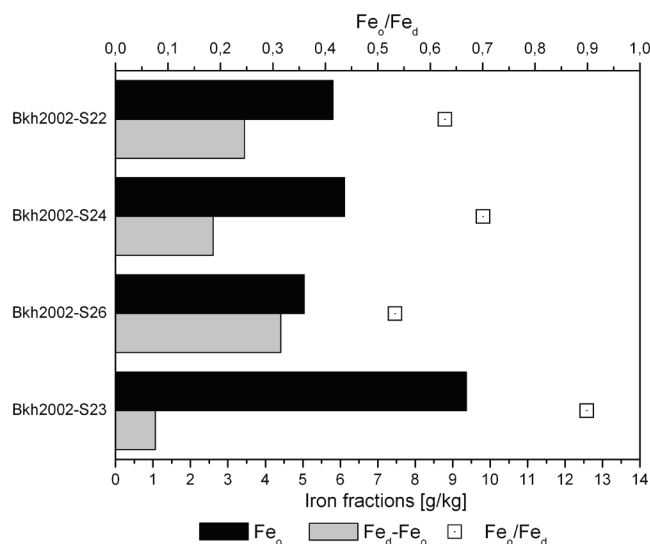


Figure 3. Values of Fe_0 , Fe_d-Fe_0 , and Fe_0/Fe_d in different soil horizons of profile Bkh2002-S22 to S26. Late Pleistocene paleosol, Kurungnakh Island.

The third terrace was formed in Middle and Late Pleistocene (Schwamborn et al. 2002). We collected samples of different ages from 5.8 to 40 ky BP (Schirrmeister et al. 2003, Wetterich et al. *subm.*).

Samples of modern soils have been taken on Samoylov Island during the expedition 'LENA – New Siberian Islands – 2007' in summer 2007 from the active layer of a low-centered polygon (Fig. 2).

Samples were collected from each layer of individual exposures. Pedological descriptions including Munsell soil color, fresh weight and other morphological remarks were made in the field. All analyses were done on the <2mm fraction and data are expressed on an oven-dry basis (105°C).

For pH determination a soil suspension with 0.01 M $CaCl_2$ was prepared and measured after an equilibration time of one hour with pH-Meter Schott CG820.

Total organic carbon (TOC) and nitrogen (N) were determined by VarioMax Elementaranalysator (Elementar Analyse Systeme GmbH).

A special consideration is given to different pedogenically formed iron-oxides to compare recently formed cryosols with paleosols of deeper sediment layers of both islands.

Oxalate-extractable iron (Fe_0) was determined by the method of Schwertmann (1964) at room temperature, in dark with acid ammonium oxalate at pH 3.25. Dithionite-extractable iron (Fe_d) was determined by the DCB method of Mehra & Jackson (1960) with dithionite-citrate buffered by bicarbonate at pH 7.3. Iron in all extracts was determined by Atomic-Absorption-Spectrometer.

To make an estimation of the degree of pedogenesis and relative age of a soil-horizon using analysis of different forms of Fe the following fractions were used: Fe_0 as "active" Fe-oxides, probably ferrihydrite, ($Fe_d - Fe_0$) as Fe-oxides in less "active" well crystallized form, probably goethite and the ratio Fe_0/Fe_d as a degree of activity and pedogenesis.

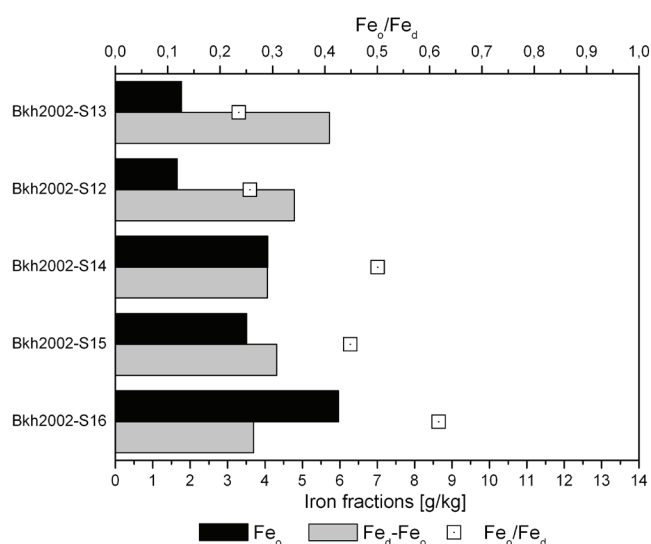


Figure 4. Values of Fe_0 , Fe_d-Fe_0 , and Fe_0/Fe_d in different soil horizons of profile Bkh2002-S12 to S16. Late Glacial paleosol, Kurungnakh Island.

Results and Discussion

Bkh2002-soil-sample series, Kurungnakh Island (Expedition 2002)

This sample collection represents the paleosols of the third terrace of Lena Delta. The lowest part of the third terrace consists of fluvial sands with low organic matter content (Schwamborn et al. 2002, Wetterich et al. *subm.*). The accumulation conditions were shallow water similar to the modern flood plains (Schirrmeister et al. 2003). The pedogenesis was characterized by hydromorphic conditions scarce vegetation and a cold dry climate. The unit was radiocarbon dated to >57 ky BP (Schirrmeister et al. 2003). The sand unit is covered by ice complex deposits (17 – 29.5 m a.r.l.). The profile Bkh2002-S22 to S26 (24 – 26.1 m a.r.l.) belongs to the ice complex sequence that was formed during the Late Pleistocene regression (Schwamborn et al. 2002). It is composed of fine grained poorly sorted sediments, thick peaty paleosols and large ice wedges (about 5 m wide and 20 m high). The thick peat layers were found in the lower part of the ice complex. They are thinner in the upper part where sand lenses were often observed. According to radiocarbon ages the entire ice complex sequence was formed between 44 and 17 ky BP in connection with niveo-eolian and slope processes (Schirrmeister et al. 2003, Wetterich et al. *subm.*). Pedogenesis during this time mirrors relatively warm and wet interstadial climate with tundra-steppe vegetation. Climate conditions with high production of organic matter are clearly recognizable in the extracted iron-oxide values that vary from 5 to 9.4 g/kg for active not crystallized oxides (Fe_0) and 1.1 to 4.4 g/kg for crystallized oxides (Fe_d-Fe_0) (Fig. 3).

High amounts of organic matter as they were found in the peaty paleosols with TOC values from 3.5 to 7.1% (Tab. 1) hinders the transformation of active iron-oxides to more crystallized oxides or even leads to formation of Fe-organic complexes (Cornell & Schwertmann 2004).

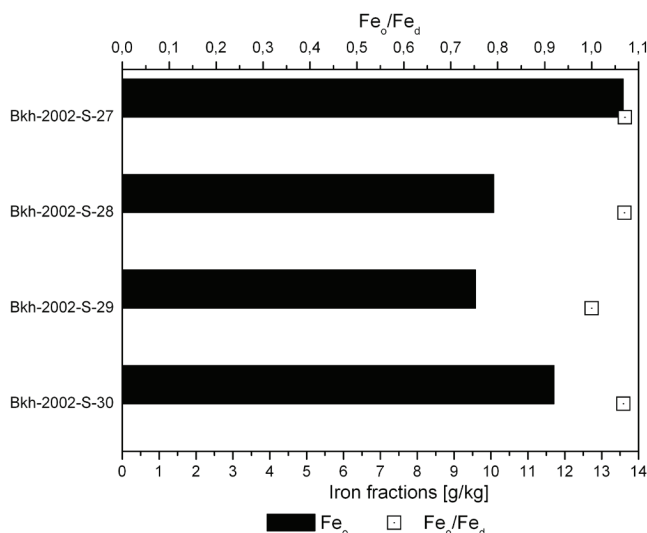


Figure 5. Values of Fe_o and Fe_o/Fe_d in different soil horizons of profile Bkh2002-S27 to S30. Early Holocene paleosol, Kurungnakh Island.

According to the high amount of Fe_o -fraction the Fe_o/Fe_d ratio is relatively high with amounts from 0.5 to 0.9. The highest ratio was measured in the Bkh2002-S23 sample of a peat layer (TOC – 7.1%) that was formed during the wettest and warmest conditions that existed between ca. 44 and 38 ky BP (Schirrmeister et al. 2003).

The pH values vary from 6.9 to 5.5 whereby the moderate acid one was found in the peat horizon with the highest Fe_o/Fe_d ratio.

The ice complex is covered by two younger units dated to 17 – 8 ky BP and 6 – 3 ky BP respectively. The first one (29.5 – 33.5 m a.r.l.) was formed under very cold and dry climate with scarce steppe-like vegetation and dry soil conditions (Schirrmeister et al. 2003, Wetterich et al. subm.). It consists of poorly sorted silt deposits with low organic matter content. In this unit Bkh2002-S12 to S16 were sampled (29 – 31 m a.r.l.).

Values of the extracted iron-oxides vary from 1.7 to 6 g/kg and 3.7 to 5.7 g/kg for Fe_o -oxides and Fe_d-Fe_o -oxides respectively (Fig. 4). The Fe_o/Fe_d ratio is relatively low in the samples Bkh2002-S13 and S12 with 0.24 and 0.26. With increasing altitude the ratio decreases. The highest ratio of 0.62 was found in Bkh2002-S16 (29 m a.r.l.) sampled of a mixed horizon of sand and peat. Under dry and cold late glacial climate conditions with scarce vegetation and low organic matter content pedogenesis can progress but less intense well-expressed by relatively low iron activity ratio and high amounts of better crystallized iron-oxides indicating dry soil conditions with distinct iron-oxide crystallization.

The TOC values vary from 1.1 to 4.7% and pH values show low variability in the sandy horizons (7.4–7.3). In the mixed horizon there are weakly acid conditions (6.7) corresponding to higher content of organic matter (TOC–4.7%) similar to the last sample of the ice complex profile (Bkh2002-S23).

Samples of the last profile were taken from the youngest unit that was formed in Mid Holocene (6 ky BP). It comprises of 4 samples (Bkh2002-S27 - S30) taken from

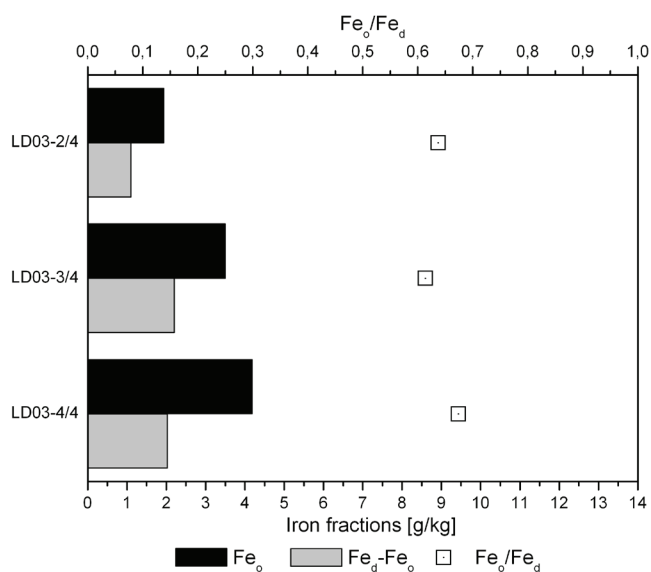


Figure 6. Values of Fe_o , Fe_d-Fe_o , and Fe_o/Fe_d in different soil horizons of profile LD03-2/4 to 4/4. Modern Gelisol Typic Historthel, Samoylov Island.

the 33.5 to 34.7 m a.r.l. The values of not crystallized active iron-oxides and Fe-organic complexes are very high and vary from 9.6 to 13.6 g/kg (Fig. 5). Crystallized iron-oxides were not verifiable, because of negative Fe_o-Fe_d values.

The Fe_o/Fe_d ratio is about 1 and the highest described in this paper. The pH values are acid (4.4 to 4.9) and correspond to the high organic matter content (TOC 3 to 4.6%) throughout the entire profile that consists of grey silt sediments with peat lenses. These sediments with high amounts of organic matter developed because of warmer climate, which caused a vegetation change to tundra-like. According to paleoenvironmental reconstructions (Wetterich et al. subm.) the pedogenesis took place under wet local conditions during this period.

LD-soil-sample series, Samoylov Island (Expedition 2007)

This sample collection which is composed of two active layer profiles represents recent pedogenesis on the first terrace of Lena Delta. The first terrace is of Holocene age and the young floodplains are assumed to represent the active part of Lena Delta. Maximum altitude is 12 m a.r.l. representing the oldest parts of the first terrace. The first terrace is formed by fluvial sediments that change from organic-rich sands at the bottom to silty-sandy peats towards the surface including several layers of eolian sands (Akhmadeeva et al. 1999, Schwamborn et al. 2002). This terrace is characterized by active ice wedge growth, low- and high-centered polygons, and thermokarst lakes.

The investigated profiles were sampled at a cross-section of a typical low-centered polygon (Fig. 2). These modern soils were classified by using U.S. Soil Taxonomy (Soil Survey Staff 2006).

In the polygon center a Typic Historthel (LD03-2/4 – 4/4) (11.85 – 11.5 m a.r.l.) and at polygon rim a Glacial

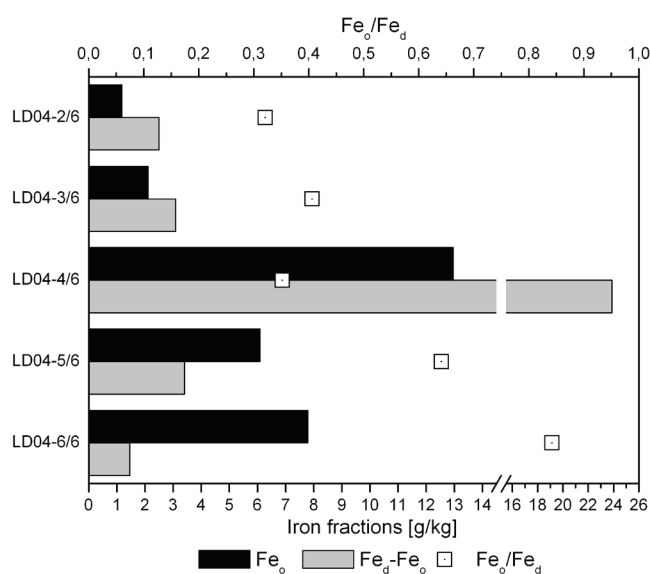


Figure 7. Values of Fe_0 , Fe_a-Fe_0 , and Fe_0/Fe_a in different soil horizons of profile LD04-2/6 to 6/6. Modern Gelisol Glacic Aquiturbel, Samoylov Island.

Aquiturbel (LD04-2/6–6/6) (11.95–11.5 m a.r.l.) were selected (Figs. 6, 7).

In the polygon center the values of the oxalate extractable iron-oxides (Fe_0) vary from 1.9 to 4.2 g/kg and for crystallized iron-oxides from 1.1 to 2.2 g/kg where the lowest values (Fe_0 - 1.9 g/kg, Fe_a-Fe_0 - 1.1 g/kg) were found in C-horizon (sample LD03-2/4) containing an eolian sand band at the altitude of 11.85 m a.r.l. (Fig. 6) with very slightly decomposed organic matter with C/N of 25. (Table 1). All horizons of this profile are rich in organic matter (TOC values from 1.8 to 5.5 %) and high C/N values from 23 to 25.2. Due to the organic matter the Fe_0/Fe_a ratio is relatively high. The pH values are strongly acid (4.5 – 4.8) and show low variability (Table 1).

The Fe_0 values of the investigated Glacic Aquiturbel (LD04-2/6–6/6) vary from 1.18 to 12.96 g/kg and values of less active iron-oxides vary from 1.1 to 23.87 g/kg. The particularly high values were extracted from the Bg1jj-horizon (sample LD04-4/6) containing an iron band (Figs. 2, 7). This iron band can probably be considered as an enrichment horizon due to element redistribution among recent soil profiles by downward-translocation of mobile iron (Fiedler et al. 2004).

Relatively low values of iron-oxides in C- and A-horizon (samples LD04-2/6 and 3/6) support this hypothesis (Fig. 7) when they are regarded as eluvial horizons. The Fe_0/Fe_a ratio is low in the upper part of the profile. The value increases with increasing depth below ground surface. The upper horizons are first aerated during the slow process of thawing in spring and summer. This leads to the transformation of active iron-oxides to more crystallized oxides in the upper part. The pH values vary from 4.6 to 5.8 with strongly acid values in horizons Bg2jj and Bg3jj (samples LD04-5/6 and 6/6). The organic matter content (TOC) is lower than in the polygon center and shows values from 1.5 to 2.3% (Tab. 1).

Table 1. Analysis data of different soil horizons. Bkh2002: paleosol samples, Kurungnakh Island. LD: modern soil samples, Samoylov Island.

Soil sample	Altitude [m]	pH [CaCl ₂]	TOC [%]	C/N
Bkh2002 - S27	34.70	4.9	4.6	18.1
Bkh2002 - S28	34.50	4.4	3.6	17.9
Bkh2002 - S29	34.00	4.6	3.8	19.7
Bkh2002 - S30	33.50	4.5	3.0	17.6
Bkh2002 - S13	31.00	7.4	1.7	10.9
Bkh2002 - S12	30.50	7.4	1.1	8.3
Bkh2002 - S14	30.00	7.4	1.4	10.1
Bkh2002 - S15	29.50	7.3	1.6	10.6
Bkh2002 - S16	29.00	6.7	4.7	12.7
Bkh2002 - S22	26.10	6.8	4.3	12.8
Bkh2002 - S24	25.00	6.4	4.2	13.4
Bkh2002 - S26	24.50	6.9	3.5	11.7
Bkh2002 - S23	24.00	5.5	7.1	15.1
LD04-2/6	11.95	5.8	1.6	15.9
LD04-3/6	11.90	5.8	2.3	15.9
LD04-4/6	11.85	4.6	2.1	14.6
LD04-5/6	11.80	4.7	1.9	14.0
LD04-6/6	11.70	4.8	1.5	15.4
LD03-2/4	11.85	4.5	1.8	25.2
LD03-3/4	11.80	4.8	5.5	24.5
LD03-4/4	11.70	4.8	4.2	23.0

Conclusions

The differences in values and ratios of extractable iron-oxides suggest that changes in forms of iron-oxides depend on the main soil material and water conditions. The influence of organic matter on iron-oxide transformation from young and active to more crystallized oxides is in evidence.

Paleosols show clear differentiation according to their stratigraphic position and paleoenvironmental conditions.

Soils that developed under relatively warm and wet interstadial climate (44–38 ky BP) and during the Early Holocene Climatic Optimum (8–6 ky BP) are characterized by relatively low values of well crystallized iron-oxides due to climatically caused high production of vegetation and the negative effect of the organic matter on the crystallization progress. Dry stadial climatic conditions as they were predominant at the end of Late Pleistocene (about 17 ky BP) associated with lower production of biomass and higher aeration of soil horizons principally lead to the formation of varying iron-oxides with relatively high values of the well crystallized fraction.

The results of the investigated modern soils from the active layer are comparable with those of the paleosols. The organic matter content and the seasonal inundation play a major role for Fe-transformation in modern soils. Further elements of modern soils are affected by translocation processes within the polygon. Detailed considerations of processes taking place in polygons during thawed periods have to be included in further investigations.

This approach promises to be more effective when applied to iron-oxides. The identification of texture and minerals and

the radiocarbon dating of all samples will be finished. The analysis is still in progress.

Acknowledgments

This paper is based on the joint Russian-German science cooperation "System Laptev Sea" supported by the German Ministry of Education and Research. We thank the University of Hamburg and the Alfred Wegener Institute for Polar and Marine Research for financial support. We thank all Russian and German colleagues who helped us during fieldwork and laboratory studies. In addition, we thank Leon von Below for English language correction as well as two anonymous reviewers for their helpful comments.

References

- Ahmadeeva, I., Becker, H., Friedrich, K., Wagner, D., Pfeiffer, E.-M., Quass, W., Zhurbenko, M. & Zöllner, E. 1999. Investigation site 'Samoylov'. *Reports on Polar and Marine Research* 315: 19-21.
- Arduino, E., Barberis, E., Carraro, F. & Foro, M.G. 1984. Estimating relative Ages from Iron-Oxide/Total-Iron Ratios of Soil in the Western Po Valley. Italy. *Geoderma* 33: 39-52.
- Arduino, E., Barberis, E., Ajmone Marsan, F., Zanini, E. & Franchini, M. 1986. Iron Oxides and Clay Minerals within Profiles as Indicators of Soil Age in Northern Italy. *Geoderma* 37: 45-55.
- Bäumler, R. 2001. *Vergleichende bodenkundliche Untersuchungen in Hochasien und Kamtschatka*. Berlin: Gebr. Borntraeger. 215 pp.
- Cornell, R.M. & Schwertmann, U. 2004. *The Iron Oxides*. Weinheim: Wiley-VCH, 663 pp.
- Fiedler, S., Wagner, D., Kutzbach, L. & Pfeiffer, E.-M. 2004. Element Redistribution along Hydraulic and Redox Gradients of Low-Centered Polygons. Lena Delta. Northern Siberia. *Soil Science Society of America Journal* 68: 1002-1011
- Food and Agriculture Organisation. 2006. *World reference base for soil resources 2006*. FAO, Rom. 128 pp.
- Goryachkin, S.V., Karavaeva, N.A. & Makeev, O.V. 2004. The History of Research of Euroasian Cryosols. In: Kimble, J.M. (ed.). *Cryosols. Permafrost-Affected Soils*. Berlin: Springer Verlag, 17-28.
- Kimble, J.M. (ed.) 2004. *Cryosols. Permafrost-Affected Soils*. Berlin: Springer Verlag, 726 pp.
- Kutzbach, L. 2005. *The Exchange of Energy. Water and Carbon Dioxide between Wet Arctic Tundra and the Atmosphere at the Lena River Delta, Northern Siberia*. (PhD Thesis) Hamburg: University of Hamburg. 141 pp.
- Kuzmina, S., Wetterich, S. & Meyer, H. 2003. Paleoecological and sedimentological studies of Permafrost deposits in the Central Lena Delta (Kurungnakh and Samoylov Islands). *Reports on Polar and Marine Research* 466: 71-81.
- Mehra, O.P. & Jackson, M.L. 1960. Iron oxide removal from soils and clays by dithionite-citrate systems buffered with sodium bicarbonate. *7th National Conference on Clays and Clay Minerals*: 317-327.
- Munsell. 1975. *Soil Color Chart*. Baltimore: Kollmogen Corporation.
- Pavlova, E. & Dorozhkina, M. 1999. Geological-geomorphological studies in the northern Lena river delta. *Reports on Polar and Marine Research* 315: 112-126.
- Pfeiffer, E.-M., Akhmadeeva, I., Becker, H., Friedrich, K., Wagner, D., Quass, W., Zhurbenko, M. & Zöllner, E. 1999. Modern processes in permafrost affected soils. *Reports on Polar and Marine Research* 315: 19-79.
- Pfeiffer, E.-M., Wagner, D., Becker, H., Vlasenko, A., Kutzbach, L., Boike, J., Quass, W., Kloss, W., Schulz, B., Kurchatova, A., Pozdnyakov, V. & Akhmadeeva, I. 2000. Modern processes in permafrost affected soils. *Reports on Polar and Marine Research* 354: 22-54.
- Pfeiffer, E.-M., Wagner, D., Kobabe, S., Kutzbach, L., Kurchatova, A., Stoof, G. & Wille, C. 2002. Modern processes in permafrost affected soils. *Reports on Polar and Marine Research* 426: 21-41.
- ROSHYDROMET. 2007.10.10. Russian Federal Service for Hydrometeorology and Environmental Monitoring. Weather Information for Tiksi. <http://www.worldweather.org/107/c01040.htm>.
- Schirrmeyer, L., Grosse, G., Schwamborn, G., Andreev, A.A., Meyer, H., Kunitsky, V.V., Kuznetsova, T.V., Dorozhkina, M.V., Pavlova, E.Y., Bobrov, A.A. & Oezen, D. 2003. Late Quaternary History of the Accumulation Plain North of the Chekanovsky Ridge (Lena Delta, Russia): A Multidisciplinary Approach. *Polar Geography* 27(4): 277-319.
- Schwamborn, G., Rachold, V. & Grigoriev, M.N. 2002. Late quaternary sedimentation history of the Lena Delta. *Quaternary International* 89: 119-134.
- Schwertmann, U. 1964. Differenzierung der Eisenoxide des Bodens durch photochemische Extraktion mit saurer Ammoniumoxalat-Lösung. *Zeitschrift für Pflanzenernährung, Düngung und Bodenkunde* 105: 194-202.
- Soil Survey Staff. 2006. *Keys to Soil Taxonomy*. 10th ed. Washington, DC: U.S. Department of Agriculture & Natural Resources Conservation Service. 332 pp.
- Tarnocai, C. 2004. Northern Soil Research in Canada. In: Kimble, J.M. (ed.). *Cryosols. Permafrost-Affected Soils*. Berlin: Springer Verlag, 29-43.
- Wetterich, S., Kuzmina, S., Kuznetsova, T., Andreev, A.A., Kienast, F., Meyer, H., Schirrmeyer, L. & Sierralta, M. 2008. (subm.). Paleoenvironmental dynamics inferred from late Quaternary permafrost deposits on Kurungnakh Island (Lena Delta, Northeast Siberia, Russia). Submitted to *Quaternary Science Reviews*.

Author Index

- Aalto, R., 613
Abliazina, D., 1131
Abnizova, A., 2003
Abramenko, O., 971
Abramov, A., 993, 1251
Aðalgeirsdóttir, G., 1705
Adam, J.C., 177
Adams, P.C., 1845
Addison, J., 95
Affleck, R.T., 1
Aguirre, A., 7
Akagawa, S., 13, 327, 895, 1573
Akerman, H.J., 19, 851
Aksenov, V.I., 25
Alexeev, S.V., 31
Alexeeva L.P. 31
Allard, M., 591
Allen, S., 37
Amils, R., 523
Andersen, D.T., 43
Anderson, S.L., 49
Andreev, A., 1191
Anisimov, O., 779
Anisimova, N.P., 55
Arena, L., 1781
Arenson, L.U., 59, 89, 1261, 1411, 1685
Argunov, R.N., 983
Arnold, F., 1131
Atkinson, D.E., 65
Aubé-Maurice, B., 457
Aus der Beek, T., 71
Avian, M., 77, 343, 1505
Azelton, M.T., 83
Azmatch, T.F., 59, 89

Bach, M., 675
Bakulina, N.T., 1681
Barbour, E.M., 1893
Barnet, C., 1981
Barrett, J.E., 529
Battogtokh, D., 821
Bauer, A., 77
Bayasan, R.M., 1787
Beget, J.E., 95
Bellefleur, G., 101
Belova, N.G., 107, 1671
Bennett, P.C., 1327
Benowitz, J., 95
Beutel, J., 669
Biggar, K.W., 89, 815
Bing, H., 113

Bjella, K.L., 119
Blaks M.R., 1369
Blanco, J.J., 1463, 1839
Blanco-Chao, R., 1799
Blikra, L.H., 789
Bo, H., 839
Bockheim, J.G., 125
Bode, J.A., 131
Bodin, X., 137, 343
Böhlert, R., 143
Boike, J., 149, 155, 1549, 1589
Bolton, W.R., 155
Bommer, C., 159
Boschi, D., 569
Boudreau, L. D., 1405
Bowden, W.B., 165
Bowen, R.G., 171
Bowling, L.C., 177
Bradford, J., 165
Brandová, D., 143
Bray, M.T., 183, 889
Brent, T., 101
Brewer, M.C., 189
Broll, G., 195, 1717, 1751
Brosten, T., 165
Brown, J., 7, 199, 1267, 1273, 1369, 1647,
Brunstein, D., 493
Bubier, J., 649
Bubnov, N.G., 25
Buhanov, B.A., 205
Buldovich, S., 211
Burgess, M.M., 1665
Burn, C.R., 901, 907, 1363
Busey, R.C., 215
Butzbach, R., 773
Bykhovets, S., 993

Caline, F., 1005
Callaghan, T.V., 851
Campbell, I.B., 125, 221
Cannone, N., 227
Cao, W., 1921
Caplan-Auerbach, J., 747
Caranti, G., 1781
Carey, S.K., 233
Carpenter, G.W., 1481
Carreau, R., 285
Carrera-Gómez, P., 1799
Casais, M.C., 1381
Cassano, E., 215
Cassano, J.J., 215

Cassie, J.W., 285
Chan, E., 469
Chang, X., 1921
Chehina, I.V., 1493
Chen, J., 1049, 1179
Chen, W., 2055
Chen, Y., 845
Cheng, G., 239
Cherkauer, K.A., 177
Chernyadyev, V., 1775
Chestnykh, O., 1155
Christensen, J.H., 247, 1705
Christensen, T.R., 251, 851
Christiansen, H.H., 257, 877, 1005, 1149, 1369, 1933
Christl, M., 143
Chuvilin, E.M., 205, 263
Clague, J.J., 269
Claridge, G.G.G., 221
Clark, E., 1
Clark, M.H., 275
Clarke, J., 279
Claypool, G., 285
Cleall, P., 919
Collett, T.S., 291
Collins, C.M., 1
Coronato, A., 1381
Costard, F., 297, 391, 493
Côté, M.M., 171
Couture, N.J., 303, 1025, 1433
Cremonese, E., 1427
Croll, J.G.A., 309
Crossen, K.J., 1993
Cuchí, J.A., 1621
Cuomo, C.J., 415
Cysewski, M., 315

D'Agata, C., 569
Daanen, R., 321, 1519, 1705
Dallimore, S.R., 101, 171, 1757
Darrow, M.M., 327
Dashtseren, A., 821
Davies, M., 663
Davydov, S.P., 333, 481
Davydova, A.I. 333
De Pascale, G.P., 337
DeBeer, C.M., 233
Dech, S., 947
Delaloye, R., 343, 699, 1019, 1233, 1505
Deline, P., 143, 349
Demitroff, M., 355

- Derevyagin, A.Y., 1595
Diekmann, B., 1601
Dietrich, R., 1589
DiFurio, S., 469
Dillon, M., 361
Ding, Y., 1061, 1975, 2071
Dobinski, W., 367
Doolittle, J.A., 355
Dorjgotov, B., 795
Dorthe, J., 1233
Dou, F., 1197
Douglas, T.A., 373, 1887
Drozdov, D.S., 379, 1511
Duchesne, C., 385, 403
Duguay, C., 591
Dupeyrat, L., 391
Durán, J.J., 1621
Dutilleul, P., 639
Dutta, U., 1227
- Easton, N.A., 1993
Ebohon, B., 397
Ednie, M., 385, 403
Efremov, V.N., 409
Egli, M., 143
Eiken, T., 789, 1311
Eisner, W.R., 415
Ellis-Evans, C., 569
Etzelmüller, B., 421, 427, 1627
Everts, J.R., 1339
- Fang, J., 1049
Farbrot, H., 421, 427, 789
Fedorov, A.N., 433, 493, 1077
Fedorov, G., 1601
Feklistov, V.N., 1173
Feng, W., 113
Fenton, C., 279
Fernández-Remolar, D.C., 523, 1445
Fernández-Sampedro, M., 523, 1445
Ferris, G.F. 1327
Fiencke, C., 1567
Fischer, L., 439
Foged, N., 445, 773
Font, M., 297, 663
Förster, A., 1601
Fortier, D., 361, 451, 889
Fortier, R., 457
Frape, S., 469
Frauenfelder, R., 463
Freifeld, B.M., 469
French, H.M. 199, 475
Friborg, T., 251
Fukuda, M., 645
Fuller, C.C., 649
Fyodorov-Davydov, D.G., 333, 481, 993
- Gaboury, M.N., 1015
Gailhardis, E. C., 391
Gasselt, S., 487, 1531
Gattinger, A., 1875
Gautier, E., 493
Gavriliev, P.P., 499
Gavriliev, R., 505
Gaylord, A., 7
Gens, A., 279
Georgiadi, A.G., 511
Gerasimov, E.Y., 983, 1077
Germogenova, A., 2095
Gevorkyan, S.G., 25
Gex, P., 1583
Giardino, J.R., 1857
Giardino, M., 1427
Giebels, M., 1549
Gieck, R.E., 711, 883
Gilichinsky, D.A., 517, 993
Goldberg, M., 1981
Gómez Ortiz, A., 1321
Gómez, F., 523, 1445
Gómez-Elvira, J., 523, 1445
Gómez-Ortiz, D., 1445
Gooseff, M.N., 165, 529
Gorelik, J.B., 535
Gorshkov, S., 1769
Goryachkin, S.V., 1093
Goulden, C.E., 1627
Grebenets, V.I., 541, 2037
Grechishchev, S.E., 1105
Greenwald, M.J., 165
Grigoriev, M.N., 1345
Groisman, P.Y., 1643
Grom, J.D., 545
Grosse, G., 551, 1239, 1595
Gruber, S., 143, 557, 597, 669, 723, 747, 1293, 1427, 1463, 1839
Guan, X.J., 1951
Gubarkov, A.A., 563, 1037
Gubin, S.V., 1083, 1827
Guðmundsson, Á., 421
Guenther, K.P., 947
Günzel, F.K., 581
Guggenberger, G., 1077
Guglielmin, M., 125, 227, 569
Gugolj, D., 575
Guo, Y., 1921
Guodong, C., 199
Guryanov, I.E., 587
Guryeva, O.M., 205, 263
- Hachem, S., 591
Haerberli, W., 143, 597, 607, 1505
Hagedorn, B., 149, 613
Hallégouët, B., 619
Hallet, B., 613, 625, 631
- Haltigin, T.W., 639
Hamilton, T.D., 1255
Hammadi, J., 493
Hao, J., 845, 1639
Harada, K., 645, 809
Harden, J.W., 649
Harris, C., 655, 663, 919
Hartikainen, J., 1833
Hasler, A., 669
Hatano, R., 1077
Hauber, E., 487, 1531
Hauck, C., 463, 675, 699, 1293, 1463, 1839
Hausmann, H., 343
Hayley, D.W., 681
Haywood, H., 1143
He, J., 687
He, P., 113
He, R., 693, 845, 1939
Head, J.W., 1043
Hegdal, L.A., 857
Heggem, E.S.F., 1627
Hiasa, S., 13
Hibsch, C., 619
Hidalgo, M.A., 1463
Hilbich, C., 463, 675, 699, 1293
Hinkel, K.M., 415, 705, 1267, 1273, 1647
Hinzman, L.D., 65, 215, 711, 883, 1613
Hjort, J., 717, 1137
Hoelzle, M., 463, 557, 699, 723, 1293
Hoeve, E., 2089
Hohmann, R., 607
Holden, B., 469
Hollister, R.D., 729
Holubec, I., 735
Hoque, M.A., 303, 741
Horne, B., 681
Huang, S.L., 13, 327, 941, 1179
Huggel, C., 37, 439, 747
Humbolt, D., 1857
Humlum, O., 257, 753, 877
- Iijima, Y., 761, 795, 821
Ikard, S., 529
Ikeda, A., 343, 767, 1733, 1933
Ingeman-Nielsen, T., 445, 773, 865
Instanes, A., 779, 785
Instanes, B., 785
Iospa, A.V., 25
Isaev, V., 971
Isaksen, K., 427, 655, 789, 1311
Ishii, T., 1733
Ishikawa, M., 795, 809, 821
Istratov, V., 1221

- Ivanova, L.D., 801
 Ivanova, R.N., 805
 Ivy-Ochs, S., 143
 Iwahana, G., 327, 809
 Iwakun, O., 815
- Jaillet, S., 137, 349
 Jambaljav, Y., 821
 Janowicz, J.R., 827
 Jardine, J., 735
 Jardine, R., 279
 Jenkins, R.E.L., 833, 965
 Ji, C., 839
 Ji, Y., 845, 1939
 Jin, H., 189, 845, 1055, 1921, 1939, 2009
 Johansen, B., 789
 Johansson, M., 251, 851
 Johnson, A., 469
 Johnson, E.R., 857
 Jonasson, C., 851
 Jones, A., 1717
 Jones, B.M., 415
 Jørgensen, A.S., 773, 865
 Jorgenson, M.T., 373, 869, 1087, 1197, 1423
 Jorgenson, T., 889
 Juliussen, H., 877
- Kääb, A., 343, 1505
 Kadota, T., 795, 821
 Kalling, K., 1745
 Kane, D.L., 711, 883, 1067
 Kanevskiy, M., 361, 373, 451, 889, 1423, 1721
 Kanie, S., 13, 895, 1573
 Kanigan, J.C.N., 833, 901
 Karelin, D., 2021
 Karunaratne, K.C., 907
 Kashutina, E.A., 511
 Katamura, F., 809
 Kaufmann, V., 343, 1505
 Kellerer-Pirklbauer, A., 77, 343, 913
 Kern-Luetschg, M., 663, 919
 Kershaw, G.P., 925
 Keusen, H.R., 159
 Kholodov, A.L., 481, 993, 1511
 Khomutov, A., 1037
 Kidd, J.G., 931
 Kienast, F., 937
 Kienholz, H., 1209
 Kim, K., 941
 Kirschke, S., 947
 Kizyakov, A., 1037
 Klene, A.E., 705, 953, 1727
 Klinova, G.I., 25
 Kneisel, C., 463, 959
- Koch, K., 1875
 Koemle, N.I., 113
 Kokelj, S.V., 833, 901, 907, 965, 1763
 Kolisoja, P., 1299
 Komarov, I., 971
 Kondratiev, V.G., 977
 Kononov, A.M., 31
 Konstantinov, P.Y., 433, 983
 Korobova, E.M., 987
 Kotov, A., 2021
 Kotov, P.I., 205
 Kraev, G.N., 481, 993, 1499
 Krainer, K., 343
 Krautblatter, M., 999
 Kristensen, L., 877, 1005
 Krummenacher, B., 1209
 Krzewinski, T.G., 49
 Kubik, P.W., 143
 Kuhry, P., 247, 1493
 Kunitsky, V.V., 1595
 Kurchatova, A.N., 1659
 Kutvitskaya, N.B., 1105
 Kutzbach, L., 1549
 Kuzmin, G.P., 1011
 Kuznetsova, T.V., 1595
- LaDouceur, M., 321
 Lagarde, J.L., 297
 Lai, A., 1015
 Lambiel, C., 343, 1019, 1505, 1583
 Lantuit, H., 551, 1025
 Layer, P., 95
 Lehmkuhl, F., 1031, 1701
 Leibman, M.O., 563, 1037, 1815
 Levy, J., 1043
 Li, D., 1049, 1179
 Li, G., 845, 1055, 1639
 Li, R., 1061
 Li, S., 1969
 Li, Y., 919
 Lilly, M.R., 1067
 Lin, Z., 1287
 Lipski, A., 1875
 Liu, J., 1049
 Liu, X., 1981
 Liu, Y., 1921, 1963
 Long, E.L., 1073
 Lopez, L., 1077
 López-Martínez, J., 125, 1621, 1839
 Lorenson, T.D., 171
 Lü, L., 845, 1055
 Lugon, R., 1019
 Luo, T., 687
 Luoto, M., 717, 1137
 Lupachev, A.V., 993, 1083
 Lynn, L.A., 1087, 1197, 1423
 Lyuri, D.I., 1093
- Ma, W., 239, 1099, 1917, 2077
 Ma, X., 2043
 Maddy, E., 1981
 Magomedgadzhieva, M.A., 1105
 Maier, H.A., 1255, 1893
 Maisch, M., 143
 Majhi, I., 1109
 Majorowicz, J.A., 1113
 Malkova, G.V., 379, 1119, 1155, 1375, 1511
 Mamykin, V., 993
 Marchant, D.R., 1043
 Marchenko, Sergei, 1125
 Marchenko, Sergey, 1131, 1705
 Marchenko, S.S., 1511, 1519, 2061
 Margreth, S., 1417
 Marmion, M., 1137
 Marsh, P., 1143
 Martín Redondo, M.P., 1445
 Martin, C., 279
 Matsuoka, N., 1149, 1733, 1933
 Maximov, T.C., 761
 Mazhitova, G., 1155, 1493
 McGraw, M., 1161
 McHattie, R.L., 1167
 McKay, C.P., 43
 McNamara, J.P., 165
 Melnikov, V.P., 379, 1173
 Meng, Q., 1049, 1179
 Meng, X., 1921
 Merekalova, A.A., 481
 Mesquita, P.S., 1185
 Meyer, H., 1191, 1595, 1945
 Michaelson, G.J., 1087, 1197, 1423
 Michel, F.A., 1203
 Mihajlovic, D., 343, 1209
 Mikami, T., 1573
 Mikhailov, V.M., 1215
 Milanovskiy, S., 1221
 Milyukova, I.P., 511
 Mink, S., 1621
 Miranda, R., 1227
 Mölders, N., 1351
 Molnia, B.F., 747
 Montanarella, L., 1717
 Moorman, B.J., 131, 575, 1711, 1881
 Morard, S., 1233
 Morgenstern, A., 551, 1239
 Morra Di Cella, U., 1427
 Moskalenko, N.G., 1245, 1511, 1815
 Motenko, R.G., 1251
 Munger, C.A., 1255
 Murton, J., 663, 1905
 Muslimov, A.V., 1607
 Myers-Smith, I., 649
- Narita, K., 645

- Näslund, J.O., 1833
Nater, P., 1261
Navas, A., 1621
Neff, J.C. 333
Neill, I., 469
Nelson, F.E., 355, 475, 705, 729, 953,
1267, 1273, 1633, 1647, 1727
Nesterov, A.N., 1173
Nethercot, D., 279
Neukum, G., 487, 1531
Nicolosky, D.J., 1281
Nikitina, N.M., 801
Nishimura, S., 279
Niu, F., 1287, 2049
Noetzli, J., 1293, 1869
Northcott, M., 529
Nurmikolu, A., 1299
Nussbaum, A., 1209
- Oberman, N.G., 1305, 1511
Ødegård, R.S., 1025, 1311
Ogorodov, S.A., 1317
Ohata, T., 761, 795
Okamoto, H., 895
Okoemova, A.P., 1787
Oliva, M., 1321
Olivella, S., 279
Omelon, C.R., 1327
Onclin, C., 1143
Onstott, T.C., 469
Osadetz, K., 1113
Osinski, G.R., 639
Osterkamp, T.E., 869, 1333
Ostroumov, V.E., 481, 993
Oswell, J.M., 1339
Overduin, P.P., 155, 1025, 1345,
1369
Owens, I., 37
- Paetzold, R.F., 1067
PaiMazumder, D., 1351
Panda, S.K., 1357
Pang, Q., 1969
Panin, V.N., 1011
Parameswaran, V.R., 1363
Park, H., 761
Parmuzin, I.S., 1493
Parsons M.A., 1369
Parviainen, M., 1137
Pavlov, A.V., 1375
Pavlova, N.A., 55
Perez-Alberti, A., 1381, 1799
Perlshtein, G.Z., 1387, 1391
Perruchoud, E., 343
Peterson, R.A., 1399
Petrone, R.M. 1405
Pfeiffer, E.M., 1567, 2095
- Pfiffner, S.M., 469
Pham, H.N., 1411
Phillips, M., 159, 1417
Ping, C.L., 1087, 1197, 1423
Pogliotti, P., 1427
Pollard, W.H., 43, 303, 337, 545, 639,
741, 1327, 1433
Pondrelli, M., 1531
Ponomareva, O., 1439
Popova, A.P., 1493
Postigo Cacho, M., 523
Prakash, A., 1357
Pratt, L.M., 469
Prieto-Ballesteros, O., 523, 1445
Prowse, T.D., 1185, 1763
Pu, Y., 2077
Pustovoit, G.P., 1787
Putkonen, J., 631, 1451
- Qi, J., 1055, 1457
- Rabassa, J., 1381
Rabatel, A., 349
Rachold, V., 1345
Raetzo, H., 1019
Ramachandran, K., 101
Ramos, M., 1463, 1839
Randriamazaoro, R., 391
Ravanel, L., 349
Raynolds, M.K., 1469
Razzhivin, V., 2021
Regmi, D., 1475
Regmi, N.R., 1857
Reifen, C., 279
Reshetnikov, A.M., 1173
Reynard, E., 1583
Riddle, C.H., 1481, 1525
Riedel, M., 101
Riseborough, D.W., 1487, 1665,
2055
Rivkin, F.M., 1493
Rivkina, E., 1499
Rodríguez-Manfredi, J.A., 523, 1445
Roer, I., 343, 1505, 1869
Romanenko, F.A., 107
Romanovskiy, N., 211
Romanovsky, V.E., 211, 247, 321,
373, 551, 1125, 1267, 1281, 1369,
1511, 1519, 1633, 1705
Rooney, J.W., 1481, 1525
Rossi, A.P., 487, 1531
Roth, K., 149, 2009
Roujanski, V.E., 1537
Rouse, W.R., 1405
Ruskeeniemi, T., 469
Russell, M., 1143
Rutter, P., 279
- Saarelainen, S.M.I., 1543
Sachs, T., 947, 1549
Safanda, J., 1113
Saito, K., 1555
Saito, T., 1561
Sanders, T., 1567
Saruulzaya, A., 821
Sato, M., 895, 1573
Sawada, Y., 645, 809, 1577
Scapozza, C., 1583
Scheller, S., 1589
Scheritz, M., 1589
Schirrmeyer, L., 937, 1191, 1239,
1595, 1601, 1945, 2095
Schneider, W., 1589
Schoeneich, P., 137
Schrott, L., 397
Schuler, T.V., 421
Schulte, L., 1321
Schwamborn, G., 1601
Schwindt, D., 959
Seaquist, J.W., 639
Sedov, B.M., 1607
Seelen, S.J., 1613
Sego, D.C., 59, 89, 815, 1411
Sekulich, I.R., 1617
Sergeev, D.O., 211, 1511, 1519,
1695
Serrano, E., 1621, 1839
Shangin, M., 2027
Sharkhuu, A., 1627, 1633
Sharkhuu, N., 795, 1627, 1633, 2061
Sheng, Y., 845, 1055, 1639
Sherstyukov, A.B., 1643
Sherstyukov, B.G., 1643
Shiklomanov, N.I., 333, 953, 1267,
1273, 1369, 1633, 1647, 1727,
2037
Shimazaki, K., 1573
Shoop, S.A., 1
Shur, Y., 315, 361, 373, 451, 869,
889, 1423, 1439
Siegert, C., 1595, 1945
Skachkov, Y.B., 1653
Skryabin, P.N., 1653
Slagoda, E.A., 1659
Sletten, R.S., 613, 631
Slider, R.T., 729
Smith, F., 663
Smith, S.L., 1369, 1665
Solie, D.N., 1357
Sollid, J.L., 789, 1311
Solomatin, V.I., 107, 1671
Solomon, S.M., 131, 1675, 1711
Solongo, D., 821
Sone, T., 809
Sorensen, S., 2027

- Sorokovikov, V.A., 481, 993
 Spektor, V.B., 1681
 Spektor, V.V., 1681
 Spieck, E., 1567
 Springman, S.M., 1261, 1685
 Stanilovskaya, J., 1695
 Staub, B., 343, 1209
 Stauch, G., 1701
 Stendel, M., 247, 1705
 Stevens, C.W., 131, 1675, 1711
 Stolbovoy, V., 1717
 Stone, D., 95
 Stotler, R., 469
 Strasser, F., 279
 Streletskaya, I.D., 1721
 Streletskiy, D.A., 953, 1267, 1647,
 1727, 1957, 2037
 Strozzi, T., 1019
 Sueyoshi, T., 809, 1733
 Surkov, V.V., 987
 Swendseid, J., 49

 Tahirkheli, S.N., 1739
 Tait, M.P., 575
 Talzi, I., 669
 Tammiksaar, E., 1745
 Tarnocai, C., 195, 1717, 1751
 Taylor, A.E., 1675, 1757
 Teichert, E., 71
 Thibert, E., 343
 Thomas, H., 919
 Thompson, D.K., 1951
 Thompson, M.S., 965, 1763
 Tikhmenev, P.E., 1607
 Tikhonova, E.P., 1251
 Tipenko, G., 211, 1125, 1281, 1387
 Tishkova, M., 1769
 Titkov, S., 1775
 Tomé, D., 1463
 Torres Redondo, J., 523, 1445
 Toumi, R., 279
 Trainor, T., 1613
 Trombotto Liaudat, D., 1781
 Trumbore, S.E., 649
 Tschudin, C., 669
 Tseeva, A.N., 1787
 Tsvetkova, M., 1775
 Tweedie, C.E., 7, 729

 Ugarov, I.S., 983
 Ukhova, J., 1695
 Ukraintseva, N.G., 987, 1793
 Utkina, I., 1695

 Valcarcel-Diaz, M., 1381, 1799
 Vanshtein, B., 1037
 Varlamov, S.P., 1653

 Vasil'chuk, A.C., 1803, 1809
 Vasil'chuk, Y.K., 1803, 1809
 Vasiliev, A.A., 1511, 1721, 1815
 Vasiliev, I.S., 1821
 Védie, E., 297
 Velikin, S., 1221
 Veremeeva, A., 1827
 Vesbach, C., 529
 Vidstrand, P., 1833
 Vieira, G., 1463, 1839
 Viereck, L.A., 1845
 Vinson, T.S., 1167, 1851
 Vitek, J.D., 1857
 Vlasova, J.V., 1493
 Vliet-Lanoë, B. Van 619
 Volokhov, S.S., 1863
 Vonder Mühlh, D.S., 1869

 Wagner, D., 1875
 Wainstein, P.A., 1881
 Wake, T., 1927
 Waldrop, M.P., 1887
 Walker, D.A. 321, 1255, 1281, 1469,
 1519, 1893
 Walker, H.J., 1899
 Waller, R., 1905
 Walsh, J., 247, 1911
 Walter, K., 551
 Wang, D., 1917
 Wang, G., 1921
 Wang, L., 1987
 Wang, P., 1287
 Wang, S., 2049
 Watanabe, K., 1927
 Watanabe, T., 1933
 Watt, B., 735
 Webber, P.J., 729
 Wei, Z., 845, 1939
 Wen, Z., 1639, 1917
 Werdin-Pfisterer, N.R., 1845
 Wessels, R.L., 747
 Wetterich, S., 937, 1595, 1945, 2095
 White III, R., 1887
 Whitehead, K., 1881
 Whiteman, C., 1905
 Wille, C., 1549
 Wilmking, M., 649
 Wisskirchen, K., 947
 Woo, M., 1951
 Wood, K.R., 1957
 Worland, M.R., 569
 Wright, J.F., 171, 385, 403, 1757
 Wrona, F.J., 1185, 1763
 Wu, Q., 239, 1099, 1963
 Wu, T., 1969, 1975, 2061, 2071,
 2083
 Wu, W., 845, 1639

 Xie, C., 1969, 1975, 2071
 Xiong, X., 1981
 Xu, A., 839, 1179
 Xu, J., 1287
 Xu, X., 1987

 Yabuki, H., 761, 795, 821
 Yamazaki, T., 761
 Yang, C., 1921
 Yang, D., 493, 1109
 Yang, S., 1939
 Yang, Z., 1227
 Yarmak, E. Jr., 1073
 Yesner, D.R., 1993
 Yoshikawa, K., 373, 767, 1191, 1267,
 1561, 1613, 1633, 1845, 1997
 Young, K.L., 1951, 2003
 Yu, F., 1921
 Yu, H., 1963
 Yu, L., 1987
 Yu, Q., 839, 845, 1921, 2009
 Yu, S., 839, 1939
 Yu, W., 1055

 Zabolotnik, S.I., 2015
 Zajdlik, B., 965
 Zamolodchikov, D., 1155, 2021
 Zarling, J.P., 2027
 Zarnetske, J.P., 165
 Zegers, T., 1531
 Zeglin, L., 529
 Zemskova, A.M., 2033
 Zepalov, F.N., 2037
 Zhang T., 1369
 Zhang, A., 2089
 Zhang, Jianming, 845, 1457, 1921,
 1939, 2043
 Zhang, Jinzhao, 2049
 Zhang, L., 1099
 Zhang, W., 1969
 Zhang, Y., 795, 821, 2055
 Zhao, L., 1061, 1969, 1975, 2061,
 2071, 2083
 Zhao, S., 2077
 Zhao, Y., 845, 2049, 2083
 Zheleznyak, M.N., 1511
 Zheng, B., 2043
 Zheng, J., 2077
 Zhou, F., 2089
 Zhou, W., 941
 Zhuang, Q., 687
 Zimov, N., 993
 Zimov, S., 551
 Zimova, G., 993
 Zubrzycki, S., 2095
 Zufelt, J.E., 83

Subject Index

- Active layer, 155, 221, 257, 321, 385, 409, 481, 529, 625, 645, 711, 729, 761, 795, 809, 821, 865, 877, 919, 931, 983, 993, 1061, 1077, 1083, 1125, 1155, 1203, 1267, 1273, 1451, 1463, 1487, 1519, 1627, 1647, 1665, 1727, 1815, 1839, 1845, 1869, 1975, 2037, 2083
thickness (ALT), 333, 481, 529, 729, 931, 983, 1647, 2021, 2037
- Agricultural landscape, 499, 805, 1093, 1627, 2021
- Alas depression, 937
- Alaska, 7, 65, 83, 95, 189, 291, 415, 705, 711, 747, 767, 857, 869, 883, 889, 931, 953, 1015, 1067, 1073, 1087, 1161, 1191, 1197, 1255, 1267, 1281, 1333, 1357, 1423, 1445, 1525, 1613, 1727, 1845, 1887, 1899, 1993, 2027
- Anabar shield, 31
- Anchor, 159
- Antarctica, 125, 149, 221, 227, 529, 569, 631, 1043, 1463, 1621, 1839
- Anthropogenic impact, 221, 587, 693, 705, 805, 987, 1245, 1439, 1617, 1627
- Arctic, 149, 177, 251, 291, 613, 947, 1025, 1087, 1423, 1469, 1911
ecology, 19, 805
storms, 65, 83
- Argentina, 1381, 1781, 1799
- Astrobiology, 43, 517, 523, 523, 1445
- Aufeis (naleds), 1543, 1881
- Austrian Alps, 77, 397
- Bearing capacity, 159, 1787
- Beaufort Sea, 7, 303, 741
- Bibliography, 1739
- Biogeochemistry, 165
- Biological activity, 1185, 1327, 1567, 1945
- Boreal, 649, 1845
- Borehole, 469, 655, 723, 993, 1005, 1267, 1333, 1463, 1561, 1577, 1633, 1695
- Brine, 31, 1345
- CALM, 257, 1155, 1273, 1647, 1727, 1815, 2021, 2037
- Canada, 291, 681
High Arctic, 43, 639, 1327, 1433, 1881, 1951, 2003
Manitoba, 925, 1405
northwestern, 101, 337, 815, 827, 907, 1143, 1339, 1363, 1665
Nunavut, 285, 1537
- Carbon
budget, 1493
content, 1751
dioxide, 251, 2083
dissolved organic (DOC), 333
processes, 687
sequestration, 687
stocks, 195, 649, 1751
- Cations, 327
- Chemical thaw, 25, 31
- China, northeast, 693, 839, 1639, 1939
- Climate, 753, 1405, 1439, 1653, 2015
change, 95, 171, 189, 211, 215, 269, 279, 337, 403, 433, 439, 469, 493, 597, 607, 655, 681, 711, 779, 947, 965, 993, 1113, 1119, 1203, 1209, 1245, 1255, 1273, 1317, 1531, 1685, 1705, 1717, 1751, 1763, 1769, 1793, 1815, 1939, 1957, 2003, 2055, 2061, 2089, 2095
controls, 1037
global, 247, 511, 1093, 1555
reconstruction, 1191
scenarios, 65, 71, 1351, 1705, 1833
warming, 239, 385, 457, 499, 901, 1073, 1077, 1155, 1305, 1333, 1375, 1525, 1733, 1781, 1827, 2071
- Coastal, 1037, 1317, 1345
erosion, 7, 83, 303, 1025, 1087, 1197, 1317, 1423
- Colorado, 1857
- Confining pressure, 1917
- Contaminants, 815, 833, 987
- Continental Shelf, 1345
- Convective
cooling, 83
natural, 113, 557, 1215, 1233, 1411
- Cost assessment, 2089
- Cracks, 59, 309, 631, 925, 1131, 1149, 1863
- Creep, 119, 227, 343, 463, 999, 1019, 1417, 1531, 1863, 1869
- Crude oil, 857
- Cryogenic
processes, 379, 433, 535, 541, 563, 1375, 1391, 1601
structure, 183, 355, 361, 451, 889, 1659
- Cryolithology, 1595, 1681, 2009
- Cryopegs, 25, 31, 517
- Cut-off wall, 49
- Dam, 1221, 1607
design, 49
seepage, 1601, 1757
- Dansgaard-Oeschger events, 1809
- Data management (archiving), 1369, 1647
- Debris flow, 297, 1839
- DEM, 77, 131, 137, 1589
- Diffusion, 505
- Earthquakes, 619, 1227
- Ecological survey, 275, 587
- Effective pressure, 13
- Electrical freezing potential, 1363
- Embankment, 239, 445, 839, 977, 1049, 1055, 1099, 1543, 1963, 2043, 2049
orientation, 247, 1099
- Energy balance, 1405
- Engineering, 279, 285, 475, 693, 735, 779, 785, 857, 1015, 1049, 1167, 1227, 1287, 1573, 1787, 1921, 2049
geology, 845, 1227, 1391, 1685, 1851
- Eurasia, 795, 1643
- Europe, 655
- European Alps, 343, 439, 1031, 1505
- Finland, 717, 1137, 1543
- Foundation, 159, 315, 735, 779, 785, 1417, 1481, 1787, 1921, 1987, 2089
pile, 1787, 1851
- Freeze-back, 285
- Freezing, 1917
axial, 2077
one-sided, 663
point depression, 445
radial, 2077
two-sided, 663, 919

- Freezing index, 591, 1463, 1821, 1969, 2015
- French Alps, 137
- Frost
- action, 1537
 - blister, 1997
 - boils, 613
 - bulb, 895
 - heave, 13, 59, 89, 535, 541, 575, 625, 845, 941, 1055, 1105, 1281, 1299, 1399, 1439, 1481, 1519, 1543
 - number, 71
 - seasonal, 1711
 - susceptibility, 59, 89, 845, 1299
- Frozen fringe, 13, 59
- Fungi, 1887
- Gas
- flux, 251, 1499, 1549
 - hydrates, 101, 171, 205, 263, 291, 1113, 1173
 - seep, 171
 - trace, 1197
- GCM, 71, 681
- Geoarchaeology, 1993
- Geochemistry, 987, 1613
- Geocryological, 821, 1493
- Geomorphology, 625, 753, 1893
- Geophysics, 675, 959, 1221, 1583
- model, 675
- Geotechnical investigation, 49, 779, 785, 1685
- Geothermal, 469, 1005, 1757
- GIS, 379, 415, 493, 767, 1025, 1239, 1255, 1893
- Glacial maximum, 107
- Glacial tectonics, 1905
- Glacier, 607, 1701, 1881
- mass wasting, 269
- Grassland, 2083
- Greenland, 613, 773, 865, 1705
- Ground
- frozen, 199, 409, 625, 1179, 1227, 1261, 1369, 1381, 1387, 1391, 1555, 1561
 - ice, 7, 337, 451, 1025, 1191, 1203, 1451, 1681, 1775, 2033
 - patterned, 227, 309, 569, 613, 625, 631, 639, 925, 1043, 1087, 1131, 1137, 1255, 1281, 1399, 1519, 1537, 1589, 1775, 1857, 1933, 1997, 2009
 - subsidence (settlement), 131, 575, 833, 845, 977, 1155, 1273, 1639, 1665, 1727, 1963
 - thermal regime, 65, 421, 433, 711, 729, 773, 789, 821, 851, 901, 925, 983, 1067, 1125, 1215, 1221, 1233, 1267, 1487, 1511, 1665, 1775, 1799, 1815, 1957, 2055
- Groundwater, 211, 801, 1387, 1613, 1833
- chemistry, 55, 1613
 - infiltration, 1613
 - mineralized, 25
 - springs, 43
 - subpermafrost, 801
- Gullies, 297, 1043
- Hazards, 597, 1287, 1375, 1921
- Heat
- balance, 391, 795, 1215
 - latent, 1113
 - pipes, 2027
 - storage, 983
 - transfer, 149, 557, 877, 971, 1411, 1481, 1927
- Heinrich events, 1803
- History, 199, 475, 1525, 1739, 1745, 1957
- Holocene, 1945
- Hydraulic conductivity, 155, 1105, 1927
- Hydrochemistry, 1951
- Hydrograph recession, 233
- Hydrology, 19, 177, 233, 711, 1109, 1881, 1951, 1975, 2003
- effects, 1975
 - evapotranspiration, 761, 883
 - modeling, 155, 177
 - processes, 563
 - rainfall, 761, 883
 - runoff, 233, 827, 883, 1143
 - surface storage, 883
- Hyporheic zone, 165
- Ice, 1173
- age, 1745
 - avalanche, 747
 - basal, 361
 - blister, 1997
 - bottom-fast, 1675, 1711
 - classification, 1671
 - genesis, 1671
 - glacial, 361, 1781
 - ground, 177, 303, 1037
 - lens, 59, 89, 1399
 - massive, 107, 119, 337, 545, 1433, 1721, 1775
 - mechanics, 999
 - nearshore, 1675, 1711
 - segregation, 451, 575, 1863
 - sheet, 107, 1905
 - strength, 581
 - types, 1671
 - wedge, 119, 131, 741, 1131, 1149, 1161, 1721, 1803, 1809, 1887, 1899, 1933
 - wedge casts, 95, 619
- Iceland, 421
- Indigenous knowledge, 415
- Infiltration, 211
- Infrastructure, 1921, 1987, 2027
- Instrumentation (methods)
- aerial balloon, 1589
 - atmospheric infrared sounder, 1981
 - centrifuge, 919
 - closed chamber, 1549
 - ground penetrating radar, 131, 337, 355, 865, 1711, 1881
 - nuclear magnetic resonance (NMR), 327
 - particle image velocimetry, 89
 - radiocarbon dating, 1577
 - radiowave impedance, 409
 - reflectance spectroscopy, 143
 - refraction seismic, 675, 747, 959, 999
 - resistivity, 337, 367, 373, 463, 645, 675, 699, 767, 773, 959, 999, 1293
 - Schmidt-hammer, 913
 - Self-potential, 1583
 - TDR, 1927
 - terrestrial laser scanning, 349
 - thermostabilizer, 1787
 - tomography, 101, 361, 367, 463, 699, 1293, 1445
 - ultrasonic velocity, 1179
 - wireless sensor, 669
 - x-ray, 361
- Insulation, 1481
- International Permafrost Association, 199, 1369
- International Polar Year, 199, 1369, 1511, 1957, 2033
- IPCC, 1911
- projections, 215, 1911
- ITEX, 729
- Japan, 809, 1577
- Kara Sea, 107, 1317
- Lake (pond), 551, 901, 965, 1143, 1161, 1185, 1239, 1363, 1405, 1445, 1757, 1763, 1899, 1945, 1951, 2003

- Landscapes, 1245, 1493, 1653, 1695, 1827, 2033
- Landslides, 269, 563, 1793
- Laptev Sea, 1345, 1875
- Last Glacial Maximum, 1701
- Lena
Delta, 1239, 1567, 2095
River, 55, 493
- LIDAR, 77, 137, 349
- Little Ice Age, 269
- Mackenzie
Delta, 131, 171, 833, 901, 965, 1113, 1675, 1763
River, 385, 901
Valley, 403
- Mars, 43, 297, 487, 517, 631, 639, 971, 1043, 1531
- Methane, 251, 263, 947, 1173, 1197, 1499, 1549, 1875, 1981
methanogenesis, 1875
- Microbiology, 469, 517, 523, 1567
- Mining, 815
- Modeling, 753, 947, 971, 1487, 1511, 1757
erosion, 303
forecast, 1939
GCM, 71, 279, 1555
hydroclimate, 1555
limitations, 247
numerical, 211, 215, 385, 403, 1049, 1125, 1281, 1387, 1399, 1411, 1685, 1733, 1833, 1987
permafrost, 247, 215, 397, 421, 569, 1939, 2055
physical, 297, 663, 895, 1555
regional climate, 1705, 1911
thermal, 279, 575, 747, 901, 1049, 1293, 1451
- Mongolia, 1627, 2061
- Monitoring, 257, 333, 373, 379, 655, 699, 753, 789, 809, 821, 977, 1119, 1149, 1209, 1221, 1267, 1305, 1311, 1339, 1391, 1487, 1601, 1633, 1647, 1653, 1695, 1727, 1815, 1857, 1869, 1963, 1969, 2071
- Mountains, 597, 607
- NDVI, 1469, 1893
- Nepal, 1475
- New Zealand, 37
- N-Factor, 315, 705, 907, 953, 2027
- Nitrogen cycle, 1567
- Non-sorted circles, 321
- Norway, 427, 789, 1311
- Nutrients, 165
- Off-road (trails), 415, 1067
- Paleoenvironment, 1595, 1601, 1701
- Paleogeography, 107
- Peat (peatland), 649, 907, 1665, 1751
- Periglacial, 199, 227, 391, 487, 569, 619, 625, 631, 717, 753, 1031, 1149, 1381, 1475, 1531, 1621
morphology, 309, 619, 717, 1031, 1137, 1621
- Permafrost
affected soils, 195, 805, 1093, 2061, 2071
aggrading, 1363
alpine, 137, 143, 397, 723, 1261, 1293, 1311, 1417, 1427, 1775, 1799, 1869
bluffs, 7, 1423
cold, 189, 1433, 2015
dating, 1191, 1577
degradation, 1499, 1643, 1733, 1769, 1839, 1845, 1851, 2071, 2089
discontinuous, 211, 233
distribution, 37, 71, 1621
dry-frozen, 125
fossil, 367
ground surface temperature, 591, 953, 1209
ice content, 183, 535
ice-cemented, 125
ice-rich, 1167, 2043
mapping, 125, 427, 457, 889, 1137, 1273, 1357, 1469, 1827, 1851
mountain, 37, 159, 557, 669, 699, 809
paleo, 427
planetary, 487
process, 499, 1511
publications, 1739
retrogressive thaw slumps, 545, 741, 965, 1185, 1433, 1763
science, 475
sensitivity, 1769
strength, 183, 1167, 1261, 1639
subsea (submarine), 1005, 1345, 1875
temperature, 257, 529, 541, 655, 669, 699, 729, 851, 971, 993, 1119, 1305, 1463, 1633, 1643, 1653, 1727, 1821, 1869, 1911
thawing, 269, 373, 457, 541, 869, 1125, 1161, 1167, 1511, 1981
thermal state, 993, 1633, 1695, 2061
tunnel, 119, 451, 1887
type, 1659
warm, 239, 779, 785, 795, 833, 1209, 1457, 1733, 2043
- Phase change, 391, 941, 1011
- Pipeline, 845, 857, 895, 941, 1015, 1105, 1391, 1573, 1639, 2027
pipe-in-pipe, 1573
- Pleistocene, 1659, 1905, 1993
- Pollen, 1803
- Pore-water pressure, 13
- Qinghai-Tibet, 113, 239, 687, 1061, 1099, 1287, 1963, 1969, 1975, 2009, 2043, 2049, 2061, 2071, 2083
- Quaternary, 95, 1191, 1721, 2033
- Radiation
global, 1061
reflective surface, 865
solar, 865, 1061
- Railroad, 113, 239, 977, 1299, 1963, 2043
- Reclamation, 681
- Remote sensing, 355, 551, 591, 1019, 1239, 1357, 1893
- Road, 977, 1049, 1055, 1543, 2049
- Rock
falls (avalanches), 349, 747, 999
glaciers, 77, 137, 343, 463, 487, 557, 767, 877, 913, 1019, 1031, 1209, 1475, 1505, 1583, 1781, 1799, 1869
joints, 581
motion, 343
slopes, 581
stability, 37, 143, 349, 439, 581
surface age, 143, 913
wall, 439, 767, 1427
weathering, 1327, 1601
- Runoff, 511
- Russia, northeast, 2021
- Rutting, 1
- Sea ice, 19
- Sea water, 25
- Seasonal terrain, 1
- Sediments
frozen, 205
hydrate-bearing, 205, 263

- Seismic data, 101
- Shear, 1863
- Siberia, 511, 761, 937, 983, 1109, 1131, 1245, 1351, 1439, 1549, 1589, 1659, 1695, 1701, 1745, 1769, 1793, 1809, 1815, 2033, 2037, 2095
- Slope
- scree (talus), 959, 1233, 1583
 - stability, 597, 607, 1505
- Snow, 321, 505, 557, 705, 789, 851, 925, 953, 1073, 1109, 1519, 1543, 1643, 1821, 2055
- ablation, 391
- Socio-economic changes, 1093
- Soil, 221, 481, 2095
- biocoenoses, 195
 - carbon, 649, 1197, 1751
 - classification, 1423, 1717
 - clay, 13
 - components, 1005
 - crushed rock, 1099, 1299
 - cryoturbation, 1087
 - development, 2095
 - gravel, 113, 119
 - loess, 119
 - marine, 1721, 1793
 - moisture, 1067
 - organics, 1083
 - properties, 1179, 1457, 1917
 - saline, 25, 445, 773, 1055, 1077
 - sand, 83, 107
 - saturated, 2077
 - seasonally frozen, 195, 1055, 1321
 - sensitivity, 275
 - silt, 89
 - surveys, 275, 321, 1717
 - unsaturated, 1927, 2077
 - volcanic, 1251
 - wedge, 1381, 1933
- Solifluction, 663, 919, 1321
- Spain, 1321
- Spatial analysis, 639
- Stable isotope, 1809, 1997
- Streams/rivers, 165, 1215
- erosion, 1015, 1899
- Stress/strain, 895, 1105, 1457
- Structural bending, 1573
- Svalbard, 19, 257, 785, 877, 1005, 1149, 1933
- Sweden, 367, 851
- Swiss Alps, 463, 669, 959, 1019, 1233, 1293, 1417, 1583
- Switzerland, 723, 1209
- Talik, 101, 285, 385, 801, 1215, 1221, 1305, 1487, 1833
- open, 55
 - suprapermafrost, 55
 - thaw bulb, 165, 1757
- Thaw settlement, 25
- Thaw weakening, 1055
- Thawing condition, 1, 189
- Thawing index, 591, 1155, 1969
- Thermal
- analysis, 681, 1351, 1647
 - conductivity, 113, 205, 315, 839, 971
 - diffusivity, 1427
 - erosion, 391, 493, 563, 889, 1037
 - mitigation, 1339
 - offset, 557, 723, 907, 1519
 - processes, 149
 - properties, 1251
- Thermokarst, 355, 415, 433, 457, 499, 545, 551, 649, 869, 925, 931, 937, 1239, 1333, 1433, 1439, 1617, 1775, 1827, 1839, 1945
- Thermosyphon, 681, 735, 1073, 1987
- flat-looped, 735
- Transitional layer, 333, 1083
- Unfrozen water, 327, 675, 1451
- Upfreezing, 625
- Vapor flux, 505
- Vegetation, 227, 373, 937, 1245, 1255, 1469, 1617, 1627, 1793, 1893, 1951, 2009
- mapping, 1469
 - recovery (and disturbance), 1, 373, 1617
- Vehicle disturbance, 1
- Volcanoes, 517, 1251
- Water
- balance, 511, 883
 - migration, 2077
 - quality, 1763
 - soil-water, 149, 1927
- Water supply, 1525
- WaterGap, 71
- Water-heat coupling, 1975
- Wetland, 177, 931, 1951, 1981, 2003
- Wildfire, 645, 1077, 1845
- Woolly mammoths, 1745
- Yakutsk (Yakutia), 481, 587, 1681, 1803, 1821, 1945, 2015
- Yedoma, 333, 551, 937, 1595
- Zero Curtain, 1451